INSTITUTE OF PHYSICS
SERIES IN PLASMA PHYSICS

THE INTERACTION OF HIGH-POWER LASERS WITH PLASMAS

SHALOM ELIEZER

IoP

The Interaction of High-Power Lasers with Plasmas

Series in Plasma Physics

Series Editors:

Other books in the series

Introduction to Dusty Plasma Physics
P K Shukla and A A Mamum

The Theory of Photon Acceleration
J T Mendonça

Laser Aided Diagnostics of Plasmas and Gases
K Muraoka and M Maeda

Reaction-Diffusion Problems in the Physics of Hot Plasmas
H Wilhelmsson and E Lazzaro

The Plasma Boundary of Magnetic Fusion Devices
P C Stangeby

Non-Linear Instabilities in Plasmas and Hydrodynamics
S S Moiseev, V N Oraevsky and V G Pungin

Collective Modes in Inhomogeneous Plasmas
J Weiland

Transport and Structural Formation in Plasmas
K Itoh, S-I Itoh and A Fukuyama

Tokamak Plasmas: A Complex Physical System
B B Kadomstev

Forthcoming titles in the series

Microscopic Dynamics of Plasmas and Chaos
Y Elskens and D Escande

Nonlinear Plasma Physics
P K Shukla

Series in Plasma Physics

The Interaction of High-Power Lasers with Plasmas

Shalom Eliezer

Plasma Physics Department, Soreq N.R.C.,
Yavne, Israel
and
Institute of Nuclear Fusion,
Madrid Polytechnic University, Madrid, Spain

IoP
Institute of Physics Publishing
Bristol and Philadelphia

British Library Cataloguing-in-Publication Data

A catalogue record of this book is available from the British Library.

ISBN 0 7503 0747 1

Library of Congress Cataloging-in-Publication Data are available

Commissioning Editor: John Navas
Production Editor: Simon Laurenson
Production Control: Sarah Plenty
Cover Design: Victoria Le Billon
Marketing: Nicola Newey and Verity Cooke

Published by Institute of Physics Publishing, wholly owned by
The Institute of Physics, London

Institute of Physics Publishing, Dirac House, Temple Back,
Bristol BS1 6BE, UK

US Office: Institute of Physics Publishing, The Public Ledger Building,
Suite 929, 150 South Independence Mall West, Philadelphia,
PA 19106, USA

Typeset by Academic + Technical, Bristol
Printed in the UK by J W Arrowsmith Ltd, Bristol

Preface

This book covers the physics of high-power laser interaction with plasmas, a subject related to both fundamental physics and the applied sciences. The book covers high-power laser irradiation, from low-laser intensity $I_L \approx 10^9\,W/cm^2$ up to extremely high intensities $I_L \approx 10^{20}\,W/cm^2$, and for laser pulse duration between $\tau_L \approx 10$ nanoseconds to as short as $\tau_L \approx 10$ femtoseconds. The plasma medium varies from low densities (dilute gases) to very high densities (highly-compressed solid state). The relevant temperatures can change over many orders of magnitude, and electric and magnetic fields can reach enormously high values.

The interaction of high-power lasers with matter should be of interest to people from different branches of science who may be unfamiliar with plasma science. Therefore, the relevant basic plasma physics is developed and explained in detail. Three basic approaches to plasma physics are considered, namely the two fluids model, the Boltzmann–Vlasov equations and the particle simulation method.

This book is not a summary of research results, but rather it is a pedagogical presentation where the basic physics issues are addressed and simple models are used wherever appropriate. The material covered could serve as a good foundation on which the undergraduate as well as the graduate student can build an understanding of the past and present research in this field. For the experienced researcher, I hope that this book is a comprehensive and useful presentation of laser–plasma interaction.

The book describes the laser absorption and propagation by a plasma medium, the electron transport phenomenon and the analysis of the relevant plasma waves. The physics of the electric and magnetic fields in a laser-induced plasma medium is comprehensively described. The subjects of laser-induced shock waves, rarefaction waves, heat waves and the related hydrodynamic instabilities (Rayleigh–Taylor, Richtmyer–Meshkov and Kelvin–Helmholtz) are developed and discussed. The very important subject of applications was purposely omitted as it merits a volume of its own.

A prerequisite in plasma physics is to know and master both systems of units: the m.k.s., known as the SI (International System) units, and the c.g.s.–Gaussian units. Furthermore, one of the most useful physical quantities is the laser intensity (energy flux) I_L, which is usually given in mixed units (Watts/cm^2). Although most of the time the c.g.s.–Gaussian units are chosen, both systems of units are used, in addition to the practical units such as electron-volt (eV) for energy or temperature.

I would like to thank my colleagues from the plasma physics department at Soreq in Yavne, Israel, and from the Institute of Nuclear Fusion at the Polytechnic University in Madrid, Spain, for the fruitful discussions which were very inspiring, stimulating and useful. I am grateful to D. Fisher for his critical reading of the manuscript and to Y. Paiss for the valuable discussions regarding the first chapter of this book. I greatly acknowledge the help from A. Borowitz, E. Dekel and M. Fraenkel for their help with the technical problems in preparing the manuscript. My thanks are also extended to R. Naem for the preparation of the figures. Last, but not least, my deep appreciation to my wife Yaffa for her encouragement to write the book and to bear with me to its successful completion.

Contents

1 High Power Lasers, from Nanoseconds to Femtoseconds **1**
1.1 Basics 2
1.2 A Stroll through a Glass Laser System 7
1.2.1 The oscillator 8
1.2.2 The amplifiers 9
1.2.3 Spatial filters 10
1.2.4 Isolators 10
1.2.5 Diagnostics 10
1.3 Highlights of the Femtosecond Laser 11

2 Introduction to Plasma Physics for Electrons and Ions **14**
2.1 Ionization 14
2.2 Cross Section, Mean Free Path and Collision Frequency 17
2.3 Transport Coefficients 22
2.3.1 Electrical conductivity 22
2.3.2 Thermal conductivity 23
2.3.3 Diffusion 24
2.3.4 Viscosity 26
2.4 Radiation Conductivity 27
2.4.1 Bound–bound (bb) transitions 27
2.4.2 Bound–free (bf) transitions 28
2.4.3 Free–free (ff) transitions 28
2.4.4 Energy transport 28
2.5 Debye Length 33
2.6 Plasma Oscillations and Electron Plasma Waves 36
2.7 The Dielectric Function 40
2.8 The Laser-Induced Plasma Medium 42

3 The Three Approaches to Plasma Physics **47**
3.1 Fluid Equations 47
3.1.1 Mass conservation 47

3.1.2 Momentum conservation 48
3.1.3 Energy conservation 49
3.2 Eulerian and Lagrangian Coordinates 51
3.3 'Femtosecond' Laser Pulses 54
3.4 Boltzmann–Vlasov Equations 55
3.4.1 Liouville's theorem 55
3.4.2 Vlasov equation 56
3.4.3 Boltzmann equation 57
3.4.4 The moment equations 58
3.5 Particle Simulations 61

4 The Ponderomotive Force 65
4.1 The Landau–Lifshitz Ponderomotive Force 65
4.2 The Single-Particle Approach to Ponderomotive Force in Plasma 68
4.3 The Effect of Ponderomotive Force on Wave Dispersion 69
4.3.1 The electron wave dispersion 69
4.3.2 The ion wave dispersion 71

5 Laser Absorption and Propagation in Plasma 74
5.1 Collisional Absorption (Inverse Bremsstrahlung) 74
5.2 The Electromagnetic Wave Equation in a Plasma Medium 79
5.3 Slowly Varying Density—the WKB Approximation 81
5.4 Linear Varying Density—the Airy Functions 84
5.5 Obliquely Incident Linearly Polarized Laser 88
5.5.1 s-polarization 90
5.6 p-Polarization: the Resonance Absorption 91
5.7 Femtosecond Laser Pulses 96

6 Waves in Laser-Produced Plasma 105
6.1 Foreword to Parametric Instabilities 105
6.2 The Forced Harmonic Oscillator 110
6.3 Landau Damping 112
6.4 Parametric Decay Instability 115
6.5 Stimulated Brillouin Scattering 120
6.6 A Soliton Wave 124
6.6.1 A historical note 124
6.6.2 What is a soliton? 126
6.6.3 What is a solitary wave? 126
6.6.4 The wave equation 126
6.6.5 Ion plasma wave and the KdV equation 127

7 Laser-Induced Electric Fields in Plasma 134
7.1 High- and Low-Frequency Electric Fields 134

7.2 Expansion of Plasma into the Vacuum 135
7.3 Double Layers 138
7.4 Charged Particle Acceleration 140
7.4.1 A static model 140
7.4.2 A dynamic model 141

8 Laser-Induced Magnetic Fields in Plasma 144
8.1 The $\nabla n \times \nabla T$ Toroidal Magnetic Field 145
8.2 Magneto-Hydrodynamics and the Evolution of the Magnetic Field 146
8.2.1 The generalized Ohm's law 147
8.2.2 The magnetic Reynolds number 151
8.2.3 Magnetic Reynolds numbers $R_m \ll 1$ 151
8.2.4 Magnetic Reynolds numbers $R_m \gg 1$ 152
8.3 Faraday and Inverse Faraday Effects 153
8.3.1 The Faraday effect 153
8.3.2 The inverse Faraday effect 157
8.3.3 Angular momentum considerations 159
8.4 Waves in the Presence of the Steady-State Magnetic Field 162
8.4.1 Ordinary and Extraordinary Waves 162
8.4.2 Electromagnetic waves propagating parallel to $\mathbf{B}_0$ 165
8.4.3 Alfvén waves 168
8.5 Resonance Absorption in a Magnetized Plasma 169

9 Thermal Conduction and Heat Waves 175
9.1 The Scenario 175
9.2 The Rocket Model 180
9.3 Relaxation Rates 183
9.4 The Fokker–Planck Equation 189
9.5 The Spitzer–Härm Conductivity 195
9.6 Hot Electrons 198
9.7 Heat Waves 205

10 Shock Waves and Rarefaction Waves 213
10.1 A Perspective 213
10.2 Sound Waves 216
10.3 Rarefaction Waves 219
10.4 Shock Waves 221
10.5 Shock Waves in the Presence of Magnetic Fields 233
10.6 The Study of High-Pressure Physics 237
10.7 Studies of Equations of State 241
10.8 Studies of Dynamic Strength of Materials 249

11 Hydrodynamic Instabilities **254**
11.1 Background 254
11.2 Rayleigh–Taylor Instability, Linear Analysis 260
11.3 Ablation-Surface Instability 264
11.4 The Magnetic Field Effect 266
11.5 Bubbles from Rayleigh–Taylor Instability 269
11.6 Richtmyer–Meshkov Instability 272
11.6.1 The differential equation for the pressure in regions 1 and 2 275
11.6.2 The boundary conditions on the interface 276
11.6.3 The boundary conditions at the shock-wave surfaces 276
11.7 Kelvin–Helmholtz Instability 279

Appendix A: Maxwell Equations **284**

Appendix B: Prefixes **290**

Appendix C: Vectors and Matrices **291**

Appendix D: A Note on the Maxwell Distribution **297**

Bibliography **300**

Index **309**

Chapter 1

High Power Lasers, from Nanoseconds to Femtoseconds

This chapter is an introduction to high power lasers and it is intended to present the principles and the parameters of such systems. **Lasers** (acronym of **l**ight **a**mplification by **s**timulated **e**mission of **r**adiation) are devices that generate or amplify electromagnetic radiation, ranging from the long infrared region up through the visible region and extending to the ultraviolet and recently even to the x-ray region (Ross 1968, Sargent *et al*. 1974, Svelto 1976, Thyagarajan and Ghatak 1981, Siegman 1986, Elton 1990, Diels and Rudolph 1996 and Robieux 2000). The 1964 Nobel Prize for physics was shared between Charles Townes, Nikolai Basov and Alexander Prokhorov for their fundamental work in the 1950s that led to the construction of the laser.

Maiman demonstrated the first laser in 1960; the lasing medium was a ruby crystal, pumped by xenon flash discharge, and the pulse duration was between 1 ms and 1 μs (Maiman 1960). In 1961 Hellwarth invented the concept of **Q switching** and put it into practice with a ruby laser by using a Kerr cell shutter. Hellwarth reported (Hellwarth 1961) a pulse duration of about 10 nanoseconds (1 nanosecond = 1 ns = 10^{-9} s).

The first **active mode locking** was achieved in 1964 for a helium–neon laser yielding a laser with pulse duration above 1 ns. The mode locking was achieved by modulating the index of refraction acoustically at the period that the light travels (a round trip) in the cavity (Hargrove *et al*. 1964). Using a saturable absorber, the idea of **passive mode locking** was suggested (Mocker and Collins 1965), and in 1966 a neodymium glass laser pulse shorter than a nanosecond was first obtained (DeMaria *et al*. 1966). Today pulses of the order of 10 picosecond (1 picosecond = 1 ps = 10^{-12} s) duration are common in many laboratories around the world. In the past decade 10 femtosecond (1 femtosecond = 1 fs = 10^{-15} s) pulses were achieved from a Ti–sapphire laser (Zhou *et al*. 1994, Glezer 1997). The **chirped pulse amplification** technique (used in microwave devices for many years) was first suggested for the lasers in 1985 (Strickland and Mourou 1985) in

order to amplify short laser pulses. In this scheme the femtosecond laser pulse is first stretched in time (chirped in frequency), then amplified and finally recompressed (Perry and Mourou 1994, Gibbon and Forster 1996, Backus *et al.* 1997). An interesting brief review of how the development of laser pulse duration, from nanosecond to femtosecond, has changed many fields of science and technology is given by Bloembergen (Bloembergen 1999).

1.1 Basics

Although it is assumed that the reader is familiar with the basics of laser physics, it is inconceivable not to mention the Einstein coefficients. In 1917 Einstein postulated that an atom in an excited level (2) could decay to lower energetic level (1) either **spontaneously** or by **stimulated emission**. In order to prove this statement, Einstein studied a system of atoms at a temperature T in **thermal equilibrium** with electromagnetic radiation (Einstein 1917).

Let n_1 and n_2 represent the number of atoms per unit volume of levels 1 and 2 having energies E_1 and E_2 respectively. Regarding these two levels, an atom can emit or absorb a photon with an energy $h\nu$ ($\omega = 2\pi\nu$), given by

$$\hbar\omega = E_2 - E_1. \tag{1.1}$$

h is the Plank constant and $\hbar = h/2\pi$.

The spectral distribution of the photons in thermal equilibrium is given by **black body radiation**, as suggested by Planck's law,

$$U_{\mathrm{p}}(\omega) = \left(\frac{\hbar\omega^3}{\pi^2 c^3}\right)\left[\exp\left(\frac{\hbar\omega}{k_{\mathrm{B}}T}\right) - 1\right]^{-1} \tag{1.2}$$

where c is the speed of light, k_{B} is Boltzmann's constant and $U_{\mathrm{p}}(\omega)\,\mathrm{d}\omega$ is the radiation energy per unit volume within the frequency interval $[\omega, \omega + \mathrm{d}\omega]$. $U_{\mathrm{p}}(\omega)$ is in $\mathrm{J \cdot s/m^3}$ in m.k.s. (note that $U_{\mathrm{p}}(\nu) = 2\pi U_{\mathrm{p}}(\omega)$ since $U_{\mathrm{p}}(\nu)\,\mathrm{d}\nu = U_{\mathrm{p}}(\omega)\,\mathrm{d}\omega$).

The populations of the upper level 2 and the lower level 1 obey the following **rate equations**:

$$\begin{aligned} \frac{\mathrm{d}n_2}{\mathrm{d}t} &= -An_2 - B_{21}U_{\mathrm{p}}(\omega)n_2 + B_{12}U_{\mathrm{p}}(\omega)n_1 = 0 \\ \frac{\mathrm{d}n_1}{\mathrm{d}t} &= +An_2 + B_{21}U_{\mathrm{p}}(\omega)n_2 - B_{12}U_{\mathrm{p}}(\omega)n_1 = 0. \end{aligned} \tag{1.3}$$

The quantities A (in $\mathrm{s^{-1}}$), B_{12} and B_{21} [in $\mathrm{m^3/(J \cdot s^2)}$] are known as Einstein coefficients, and in thermal equilibrium the populations are constant, implying $\mathrm{d}n_1/\mathrm{d}t = 0$, $\mathrm{d}n_2/\mathrm{d}t = 0$. An_2 is the rate of spontaneous emission of photons from the upper level, $B_{21}n_2U_{\mathrm{p}}(\omega)$ is the rate of stimulated emission from the upper level to the lower level, and $B_{12}n_1U_{\mathrm{p}}(\omega)$ is the rate of stimulated absorption from the lower level to the upper level.

In thermal equilibrium the levels 1 and 2 are related by the **Boltzmann distribution**

$$\frac{n_2}{n_1} = \frac{g_2}{g_1} \exp\left(-\frac{\hbar(E_2 - E_1)}{k_B T}\right) \tag{1.4}$$

where g_1 and g_2 are the degeneracy of the atomic levels 1 and 2 accordingly. Equations (1.1)–(1.4) yield

$$B_{12}\left(\frac{g_1}{g_2}\right) = B_{21} \equiv B, \qquad \frac{A}{B} = \frac{\hbar\omega^3}{\pi^2 c^3}, \qquad \frac{A}{BU_p(\omega)} = \exp\left(\frac{\hbar\omega}{k_B T}\right) - 1. \tag{1.5}$$

From the last equation of (1.5) and the rate equations (1.3), one can see that for $\hbar\omega \ll k_B T$ the number of stimulated emissions is much larger than the number of spontaneous emissions, while for $\hbar\omega \gg k_B T$ the number of spontaneous emissions exceeds the number of stimulated emissions. For example, for typical light sources the temperature is less than $T \approx 3000\,\mathrm{K}$, implying $k_B T/\hbar < 4 \times 10^{14}\,\mathrm{s}^{-1}$, and for the optical spectrum $\omega \approx 4 \times 10^{15}\,\mathrm{s}^{-1}$; therefore, the emission in the optical spectrum from usual light sources is incoherent (i.e. it is due mainly to spontaneous emissions, $A/(BU_p) \approx e^{10}$).

The Einstein coefficients can also be understood by analysing the rate equations (1.3). A^{-1} and $(BU_p)^{-1}$ have dimensions of time; therefore, one can define the spontaneous emission lifetime τ_{sp} (of the excited level, denoted above by 2) and the induced emission lifetime τ_i of the excited level by

$$\tau_{sp} = \frac{1}{A}, \qquad \tau_i = \frac{1}{BU_p}, \qquad \frac{1}{\tau} = \frac{1}{\tau_{sp}} + \frac{1}{\tau_i}. \tag{1.6}$$

The physical quantity $1/\tau$ is the transition probability per unit time for the excited state under consideration.

It is important to note that the ratio A/B given in the first two relations of (1.5) is correct not only in thermal equilibrium but is valid in general. A and B are describing atomic physics, and atomic physics does not depend on temperature. The ratio between the probabilities of induced transitions and spontaneous transitions as given by (1.5) is independent of the particular case for which it was calculated.

Einstein's genius idea, as described above, shows how dynamic physical quantities, such as 'lifetimes', transport coefficients, etc., can be related from analysing a system in thermodynamic equilibrium.

In the above analysis only one laser frequency was considered, the **resonant frequency**, with the energy difference between the two levels $(E_2 - E_1)$. In general, the atom transition from the exited level to the lower level (from level 2 to level 1) can be induced by radiation over a range of frequencies around the resonant frequency. The probability of the interaction is a function of frequency. Therefore, the laser beam is not a

delta function in frequency (i.e. one single frequency) but a function $g(\omega)$, known as the **line shape function**, normalized by

$$\int g(\omega)\,\mathrm{d}\omega = 1. \tag{1.7}$$

The change in the total number of stimulated emissions per unit time per unit volume is changed according to the following (using (1.5) and (1.6)):

$$B_{21}U_{\mathrm{p}}(\omega)n_2 \Rightarrow n_2 \int B_{21}U_{\mathrm{p}}(\omega)g(\omega)\,\mathrm{d}\omega = \frac{\pi^2 c^3 n_2}{\hbar\tau_{\mathrm{sp}}}\int \frac{U_{\mathrm{p}}(\omega)g(\omega)\,\mathrm{d}\omega}{\omega^3}. \tag{1.8}$$

The **natural line shape** is given by a **Lorentzian profile**

$$g_{\mathrm{n}}(\omega) = \frac{2\tau_{\mathrm{sp}}}{\pi}\left(\frac{1}{1+4\tau_{\mathrm{sp}}^2(\omega-\omega_0)^2}\right), \qquad (\Delta\omega)_{\mathrm{FWHM}} = \frac{1}{\tau_{\mathrm{sp}}} \tag{1.9}$$

where τ_{sp} is the natural lifetime of the excited state, $\omega_0 = (E_2 - E_1)/\hbar$ is the centre frequency, the normalization (1.7) is satisfied for $\omega_0\tau_{\mathrm{sp}} \gg 1$, and the natural full width at half maximum of $g(\omega)$ is $(\Delta\omega)_{\mathrm{FWHM}} = (\tau_{\mathrm{sp}})^{-1}$.

The line shape changes because of **collisions**. In a **solid**, the interaction of the atom with the lattice causes line broadening. In a **gas**, the collisions are between the atoms; in **plasma**, there are collisions between ions (not fully ionized) and other ions or electrons. For example, in a gas medium, random collisions occur and an atom sees an electromagnetic field that changes its phase at each collision. If the average time between two collisions is τ_{c}, the line shape broadening due to collisions is also of a **Lorentzian profile**

$$\begin{aligned} g_{\mathrm{c}}(\omega) &= \frac{\tau_{\mathrm{c}}}{\pi}\left(\frac{1}{1+(\omega-\omega_0)^2\tau_{\mathrm{c}}^2}\right) \\ (\Delta\omega)_{\mathrm{FWHM}} &= \frac{2}{\tau_{\mathrm{c}}} = \frac{1}{P4\pi^3R^2}\left(\frac{\pi M k_{\mathrm{B}}T}{16}\right)^{1/2}. \end{aligned} \tag{1.10}$$

The normalization condition (1.7) is satisfied for $\omega_0\tau_{\mathrm{c}} \gg 1$. The right-hand side of the second equation is satisfied for an ideal gas with a temperature T and pressure P, and this medium contains atoms of mass M and radius R. For the general case this expression is considerably more complicated.

The **Doppler effect** also changes the line shape, since resonance absorption at ω_0 is possible even for a non-resonant frequency ω, if the atom moving with a velocity v satisfies

$$\omega[1 \pm (v/c)] = \omega_0 \tag{1.11}$$

where c is the speed of light.

The **Doppler broadening** produces a **Gaussian profile**, given by

$$g_{\mathrm{D}}(\omega) = \frac{1}{\omega_0}\left(\frac{Mc^2}{2\pi k_{\mathrm{B}}T}\right)^{1/2} \exp\left[-\frac{Mc^2}{2k_{\mathrm{B}}T}\left(\frac{(\omega-\omega_0)^2}{\omega_0^2}\right)\right]$$
$$(\Delta\omega)_{\mathrm{FWHM}} = 2\omega_0\left(\frac{2k_{\mathrm{B}}T\ln 2}{Mc^2}\right). \tag{1.12}$$

Equations (1.9), (1.10) and (1.12) consider the broadening produced by different mechanisms separately. In general, all mechanisms may be present simultaneously. In this case the line shape is a convolution of the different line shapes.

The various spectral line-broadening mechanisms are also classified as homogeneous and inhomogeneous. If the spectrum of each atom is broadened in the same way, like the natural and the collisional broadening, then it is considered as **homogeneous broadening**. On the other hand, if local inhomogeneities, as in Doppler broadening or inhomogeneities in a laser medium (for example, the inhomogeneity in a solid crystal lattice), produce the broadening then it is considered as **inhomogeneous broadening**. If the effects which cause the inhomogeneous broadening are occurring at random then the broadened line has a Gaussian shape. On the other hand, in homogeneous broadening there is a Lorentzian profile. The **propagation**, in the x direction, of a monochromatic electromagnetic beam in a medium is described to a good approximation by the following equation for the energy flux $I(\omega)$ (dimension of energy/area second)

$$\frac{\mathrm{d}I(\omega)}{\mathrm{d}x} = (G-\kappa)I(\omega), \qquad G = \frac{\pi^2 c^2 \tilde{n}(n_2-n_1)g(\omega)}{\omega^2\tau_{\mathrm{sp}}} \tag{1.13}$$

where $\tilde{n}$ is the refractive index of the medium, so that $c/\tilde{n}$ is the phase velocity of the electromagnetic field in this medium. G is the **gain** for a system with **population inversion** satisfying $n_2 > n_1$, and κ is the **dissipation** (losses) due mainly to collisions. In order to achieve a population inversion it is required to **pump energy** into the laser medium. However, pumping is necessary but not sufficient. In thermal equilibrium the Boltzmann distribution does not permit population inversion, independent of the power of the pump. Therefore, population inversion is required 'to violate' thermodynamic equilibrium. For example, this is possible for three (or more) atomic levels where the pumping excites atoms from level 1 (ground level) to level 2, which is energetically higher than some level 3. In this case it might be possible to achieve a population inversion between levels 3 and 2.

There are various ways to insert energy into the laser medium. For example, a solid state laser can be pumped with flash lamps or with other laser devices such as a laser diode. A gas laser can receive its energy from various electrical discharges and also from different particle beams. One of the important issues for a large laser system is the quality and the uniformity

of the energy input, and for some applications the overall efficiency of the laser pumping is crucial (e.g. for the use of inertial confining fusion in an energy reactor).

Assuming that $n_1 - n_2$ is independent of $I(\omega)$, i.e. the laser intensity is not very large, and G and κ do not change with x, then the solution of (1.13) is

$$I(\omega; x) = I(\omega; 0) \exp[(G - \kappa)x]. \tag{1.14}$$

If the medium is in thermal equilibrium, i.e. $n_1 > n_2$, there are fewer atoms in the excited level than in the lower level (see (1.4)), then the energy of the radiation beam decreases exponentially as it propagates through the medium. On the other hand, if there are more atoms in the excited level than in the lower level, $n_2 > n_1$ (population inversion), and also $G > \kappa$, then the intensity of the radiation increases exponentially. This is the effect of **light amplification**.

In the **oscillator**, the medium is placed between two mirrors. Defining the energy reflectivity of the mirrors by R_1 and R_2 and the medium length by L, then the laser oscillation begins if the following relation is satisfied:

$$R_1 R_2 \exp[2L(G - \kappa)] \geq 1. \tag{1.15}$$

In comparison with other **radiation sources** the laser is characterized by the following properties: the laser is monochromatic, coherent in time and in space, is directional and has a high brightness.

The laser is **monochromatic** since the amplification is done for frequencies satisfying equation (1.1). Moreover, the two mirrors form a resonant cavity, causing the natural line-width (of the spontaneous transition 2 to 1) to be narrowed by many orders of magnitude.

The **spatial coherence** of the laser is defined by the phase change of the electric field (and magnetic field) of two separated points in space. If the phase difference of two points separated at a distance L is constant in time, then these two points are coherent. The maximum value of L, denoted by L_{coh}, is the laser coherent length.

The **temporal coherence** is defined by the phase change of the electric field (and magnetic field) in time at a point in space. If the phase of this point is equal at time t and at time $t + \tau$ for all times t, then this point is coherent during the time τ. The maximum value of τ, denoted by τ_{coh}, is the temporal coherence of the laser.

In general, the spatial coherence and the temporal coherence are independent concepts. The above definitions are only qualitative. For a more accurate definition of coherence, one has to analyse the appropriate **correlation functions**: $\langle \mathbf{F}(\mathbf{r}, t + \tau)\mathbf{F}(\mathbf{r}, t)\rangle$ for temporal coherence and $\langle \mathbf{F}(\mathbf{r} + \mathbf{L}, t)\mathbf{F}(\mathbf{r}, t)\rangle$ for spatial coherence, where $\mathbf{F}$ denotes the laser electric or magnetic field.

The small **divergence** of the laser beam is due to the fact that only a propagating wave along the cavity direction can be sustained. However,

due to diffraction from a finite aperture there is always a beam divergence. For a perfect spatial coherent wave, with a wavelength λ and a beam diameter D, the **diffraction limited** divergence θ_d is given by

$$\theta_d = \frac{\beta\lambda}{D} \tag{1.16}$$

where β is a numerical coefficient of order 1. For example, $\beta = 1.22$ for a plane wave beam with a constant intensity over its circular cross section.

Last but not least, the laser is a very bright light source. The **brightness**, defined as the power emitted per unit surface area per unit solid angle, of the laser is usually many orders of magnitude brighter than any conventional sources.

There are two classes of **high power lasers**: solid state lasers (Nakai *et al.* 1995) and **gas lasers** (Key *et al.* 1995). The term **solid state laser** is usually used for the lasers having an insulating crystal or a glass as their medium. These lasers use impurity ions as their active medium. The neodymium doped glass (Nd:glass) lasers are the most popular type of solid state laser. Neodymium lasers can oscillate on several lines; the strongest and therefore the most commonly used have a wavelength of $\lambda = 1.06\,\mu m$.

At present there are five different laser media which are of interest to high power laser interactions: the **neodymium glass** with a wavelength $\lambda = 1.06\,\mu m$, the **CO_2** with $\lambda = 10.6\,\mu m$, the **iodine** (I_2) with $\lambda = 1.3\,\mu m$, **KrF** with $\lambda = 0.249\,\mu m$ and **titanium sapphire** with $\lambda = 0.8\,\mu m$. In the following section the glass laser (Holzrichter 1980) is schematically discussed.

1.2 A Stroll through a Glass Laser System

The laser–target interaction system consists of oscillator, amplifiers, propagation and isolator devices, a target system and diagnostics. The purpose of this system is to deposit energy in an appropriate time interval on various targets. The laser input to the target must be well controlled, repeatable and predictable, in order to study the laser–target interaction physics or to operate laser-induced plasma devices. To investigate the laser–target interaction the 'target response' parameters such as plasma density and temperature, x-ray productions, nuclear reaction yields, particle accelerations, shock waves, heat waves, etc. are measured.

The components of the laser system are:

1. The **oscillator** creates the laser pulse with output energy of about 10^{-3}–10^{-1} J. The output energy of the oscillator is kept small in order to control the laser pulses.
2. The **telescope** system magnifies the laser beam radius emerging from the oscillator and projects it into the amplifiers.

Table 1.1. Orders of magnitude for an Nd:glass laser.

Laser on target energy	$10–10^5$ J
Laser pulse duration	$10^{-10}–10^{-8}$ s (0.1–10 ns)
Laser medium pumping time	$10^{-6}–10^{-3}$ s
Capacitor charging time	$1–10^2$ s
Beam diameters	5–50 cm
Laser energy fluency (limited by breakdown thresholds and self-focusing)	1–20 J/cm^2
Typical beam intensities (before focusing on the target)	$10^9–10^{10}$ W/cm^2
Beam (peak) electric field (before focusing on the target)	$10^6–3 \times 10^6$ V/cm
Beam (peak) magnetic field (before focusing on the target)	3000–9000 Gauss

3. The **amplifiers** amplify the oscillator pulse to energies in the domain of $10–10^5$ J. Thus the amplifier gains are in the range of $10^4–10^8$. In order to obtain maximum energy one requires about 10 amplifiers in a series. The diameter of the amplifiers increases from about 1 cm to about 50 cm, in order to avoid glass damage, while increasing the energy in the beam. Using state of the art technology and design, megajoule lasers are now under construction in the USA and France.
4. The **isolating elements** prevent target reflections returning and damaging the oscillator. These isolators also prevent the amplifiers from self-oscillating off the target (i.e. precluding an undesired resonance between the target and one of the optical surfaces). With a gain of $10^4–10^8$ even the smallest reflection from the target through the amplifiers can totally damage the oscillator and many other small optical components at the beginning of the laser line. To avoid destruction, isolation is a necessity.
5. The **mirror** and **focusing lens** system directs the laser light along the line into the target.
6. The **target**.
7. Last but not least, the **diagnostics** that analyse the laser beam and measure the parameters of the laser–target interaction.

To comprehend and get a feeling for such laser systems the relevant orders of magnitude are summarized in table 1.1.

In order to build a laser system, it is necessary to understand the physical constraints and the performance of the individual components.

1.2.1 The oscillator

The oscillator must generate the desired pulse shape in space and in time with the appropriate bandwidth.

Consider a volume (V) of the laser medium that has a constant gain for frequencies $\nu \pm \Delta\nu/2$. The number of electromagnetic modes N in the laser

medium is

$$\frac{N}{V} = \frac{8\pi\nu^2\Delta\nu}{c^3} \tag{1.17}$$

where c is the velocity of light. The number of possible modes available for a laser with wavelength $\lambda = 1\,\mu m$ is obtained from (1.17) using the typical values of $\nu = 3 \times 10^{14}\,s^{-1}$, $\Delta\nu = 3 \times 10^{10}\,s^{-1}$, yielding $N/V = 2.5 \times 10^9$ modes/cm^3. For an oscillator with a rod of 10 cm long and 1 cm diameter, the number of free space modes are $N = 2.5 \times 10^{10}$. The purpose of the oscillator is to select only a few modes for amplification and propagation.

The mirrors are added around the gain medium to form a 'cavity' in order to limit the spatial direction of the oscillation and to obtain standing waves in the cavity. Due to the mirrors, stable electric field modes occur only at frequency intervals $\Delta\nu = n(c/2L)$, where $n = 1, 2, 3, \ldots$, and L is the cavity length of the oscillator. Furthermore, an aperture is added in order to obtain the lowest transverse mode (called TEM_{00}) which is Gaussian in its spatial profile.

Finally, a stationary mode is obtained in the oscillator when the desired field builds up relative to all transient modes. This is obtained with the help of a time-variable loss element. By modulating the loss element at a rate equal to the round trip cavity time $2L/c$, the build-up of the pulses that cycle through the oscillator are forced to follow the periodicity of the time-dependent loss. Modes that are very close in frequency are 'locked' together and therefore this is called '**mode-locking**'.

Another technique that allows the generation of high-power laser is called '**Q switching**'. An electro-optical shutter (e.g. a **Pockels cell** or a **Kerr cell** which change their index of refraction when a suitable voltage is applied) is opened in a short time compared with the build-up time of the laser pulse, after the cavity has gained energy in excess of the losses. This technique is called 'Q switching' since it switches the cavity **Q factor** (the ratio of stored energy in a volume to the dissipated energy in that volume, during a round trip of the photons in the cavity) from a high to a low value so that the accumulated energy in the cavity is released in a short time.

The oscillator pulse, Q switched or mode locked, can be coherently amplified through a set of amplifiers to very high energies (as given in table 1.1). In addition, the oscillator pulse can be shaped in time in order to achieve the desired time-dependent profile (Jackel *et al*. 1982).

1.2.2 The amplifiers

Amplifiers increase the beam radiance from the oscillator to the level required for target experimentation or for suitable application. They operate on the principle that their medium has been pumped and a population inversion was created before the oscillator output enters the medium of the

amplifier. The medium gain should have a good optical quality in order to get phase uniformity and gain uniformity.

The Nd:glass laser is based on the lasing properties of neodymium in an amorphous glass host. The concentration of the Nd ion in the glass is about 2%. The Nd:glass is excited by photons from broadband xenon flash-lamps. The energy storage time of this medium is long, about 300 μs, thus allowing the use of electrical pulse discharge technology (flash lamps). The pumping is done from the periphery of the medium and the Nd population that can be excited is limited by the radiance of the xenon flash lamps. The efficiency of the conversion of energy from flash lamps to stored energy and finally to laser energy is about 1–2%, thus making it a low-efficiency conversion device. However, new technology pumping with diode lasers increases this efficiency up to about 40%.

1.2.3 Spatial filters

Spatial filters are needed in order to 'clean' the laser beam front from the diverging modes caused by the inhomogeneity of the optical system. In a laser chain of amplifiers the diameters of the laser beams are increasing through the line, and therefore imaging elements, such as 'astronomical telescopes', are required to control the divergence and the diameter of the laser beam. When an aperture is added to the focus between two lenses, the system behaves as a spatial filter relay. In constructing the filter, one has to avoid the creation of plasma in a pinhole. This is usually achieved by inserting the aperture into a vacuum system.

1.2.4 Isolators

Optical isolators act as 'diodes', allowing the laser light to pass only in one direction. The isolators are used to prevent back-reflected light from destroying the 'source' from which the laser originally came. The main optical isolators are based on either the Faraday effect or the Pockels effect. In the Faraday rotation system, the polarization plane of the laser is rotated by an amount proportional to the magnetic field applied along the direction of propagation. For example, linear polarized light can be rotated 45° with respect to the magnetic field so that the back-reflected light will be perpendicular to the original beam and therefore rejected by a polarizer.

1.2.5 Diagnostics

The laser beam diagnostics should provide a complete description of the laser input on target in order to define the initial conditions in laser–plasma interaction. Measurements are made to determine the oscillator pulse-shape in space and time, its intensity and output energy. The amplifier performance

is known by measuring the input and output energies and beam profiles. Finally, the laser incident on target is diagnosed by directly imaging a fraction of the incoming beam and analysing it spatially and temporally. The input energy on target, the pulse shape and the existence of pre-pulses are checked routinely. Besides the laser beam diagnostics, a comprehensive set of spectrometers, optical and x-ray streak cameras, charge particle collectors, etc. is used to measure the laser–target interaction.

1.3 Highlights of the Femtosecond Laser

Usually a 'femtosecond laser' is a laser with a pulse duration less than 1 ps, and a state of the art laser can be as short as a few femtoseconds ($1\,\text{fs} = 10^{-15}\,\text{s}$). What is so exciting about these 'femtosecond' lasers? First, their short duration; second the extremely high power achieved today, about petawatt ($= 10^{15}\,\text{W}$); and last but not least is the fact that a terawatt ($10^{12}\,\text{W}$) laser can be a tabletop system and available also to small laboratories. By focusing these lasers, power flux densities up to $10^{20}\,\text{W/cm}^2$ were attained.

The first constraint on the femtosecond laser medium is the requirement of a large bandwidth, $\Delta\nu_\text{L}$. Since $\Delta\nu_\text{L}\tau_\text{L} \approx 1$ (the uncertainty principle), one requires a laser wavelength bandwidth of $\Delta\lambda_\text{L} \approx 18\,\text{nm}$ ($1\,\text{nm} = 10^{-9}\,\text{m}$) for a laser with $\lambda_\text{L} = 0.8\,\mu\text{m}$ to have a pulse duration $\tau_\text{L} \approx 100\,\text{fs}$ ($\tau_\text{L} \approx \lambda_\text{L}^2/(c\Delta\lambda_\text{L})$). Since the temporal and spectral behaviour of the electromagnetic fields are related through the Fourier transform, the laser bandwidth $\Delta\nu_\text{L}$ and the laser pulse duration τ_L are related by

$$\Delta\nu_\text{L}\tau_\text{L} \geq K. \tag{1.18}$$

The equality in (1.18) is known as 'bandwidth limited' or 'Fourier limited' and is satisfied for pulses without frequency modulation (such as chirping). K is a numerical constant depending on the field pulse shape, for example (Diels and Rudolph 1996)

$$\begin{aligned}
&\text{Gaussian pulse:} && E \propto \exp[-1.385(t/\tau_\text{L})^2] && K = 0.44 \\
&\text{Lorentzian pulse:} && E \propto [1 + 1.656(t/\tau_\text{L})^2]^{-1} && K = 0.14 \\
&\text{sech-pulse:} && E \propto \operatorname{sech}[1.763(t/\tau_\text{L})] && K = 0.32.
\end{aligned} \tag{1.19}$$

One of the most practical media for very short laser pulses is the Ti–sapphire crystal. The spectrum emission of this crystal is very broad with a maximum at about 800 nm. Taking the optics of the cavity into account, a Ti–sapphire oscillator output can achieve a wavelength band [at full width half maximum (FWHM)] of about 25 nm. The Ti–sapphire crystal can produce 'spontaneous' mode locking without using a saturable absorber (Spence *et al.* 1991). The nonlinear index of refraction $\tilde{n}_2$ (note that $\tilde{n}$ and $\tilde{n}_0$ are dimensionless while

$\tilde{n}_2$ is in cm^2/W) causes self-focusing with the increasing of the laser irradiance I_L (dimensions of power/area):

$$\tilde{n} = \tilde{n}_0 + \tilde{n}_2 I_\mathrm{L}. \tag{1.20}$$

This effect, together with a suitable aperture, increases the round trip gain when the laser is focused to pass through the aperture in the resonator. In order to obtain the very short pulses it is also necessary to compensate for the dispersion of the group velocity. The Ti–sapphire femtosecond oscillators are today available in many laboratories around the world.

The dramatic increase in power of the femtosecond laser pulses became possible (Strickland and Mourou 1985) thanks to the **chirped pulse amplification** (CPA) technique (developed more than 40 years ago for radar devices). In a chirped pulse the frequency of the electromagnetic wave varies with time. The time-dependence of the laser electric field E can be described by

$$E(t) = \tfrac{1}{2}\{E_\mathrm{env}(t)\exp[\mathrm{i}\varphi(t)]\exp(\mathrm{i}\omega_\mathrm{L} t) + \mathrm{c.c.}\} \tag{1.21}$$

where E_env is the field envelope, c.c. is the complex conjugate, $\omega_\mathrm{L} = 2\pi\nu_\mathrm{L} = 2\pi c/\lambda_\mathrm{L}$ is the angular frequency at the peak of the laser pulse, and $\varphi(t)$ is the time-dependent phase so that the time-dependent laser frequency ω is

$$\omega(t) = \omega_\mathrm{L} + \frac{\mathrm{d}\varphi(t)}{\mathrm{d}t} \equiv \omega_\mathrm{L} + f(t). \tag{1.22}$$

If $f(t) \neq$ constant, then the laser pulse is **frequency modulated**, or in other words it is **chirped**. For example, consider a Gaussian pulse with a linear chirp, i.e. $f(t) = at$, then the laser electric field is given by

$$E(t) = E_0 \exp\left\{-(1 + \mathrm{i}a)\left(\frac{t\sqrt{2\ln 2}}{\tau_\mathrm{L}}\right)^2\right\} \tag{1.23}$$

and the product of τ_L with the bandwidth is

$$\Delta\nu_\mathrm{L}\tau_\mathrm{L} = \frac{2\ln 2}{\pi}\sqrt{1 + a^2}. \tag{1.24}$$

Without chirp ($a = 0$), the bandwidth times the pulse duration is equal to the Fourier limited value, $2\ln 2/\pi = 0.44$ (see (1.19)), while with chirping this value is increased by a factor of $\sqrt{1 + a^2}$.

In the CPA scheme, the output femtosecond laser pulse from the oscillator is first stretched in time (chirped in frequency), then amplified and finally recompressed (see figure 1.1).

Before the oscillator output is injected into the amplifier it is stretched in time by a factor $\sim 10^4$. The pulse duration is increased in order to avoid damage to the crystal and to the optics, and to avoid nonlinear distortions to the spatial and temporal beam profile (maximum $10\,\mathrm{GW/cm}^2$). The intensity dependent index of refraction, equation (1.20), creates a nonlinear

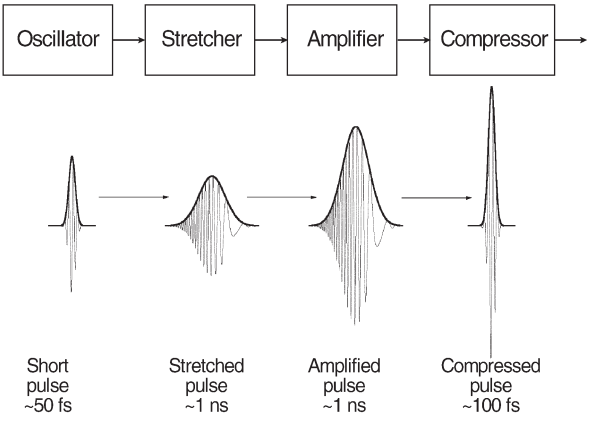

Figure 1.1. Principle of chirped pulse amplification.

phase retardation given by the B integral

$$B = \frac{2\pi}{\lambda} \int_{z=0}^{\mathrm{L}} \tilde{n}_2 I_{\mathrm{L}}(z)\, \mathrm{d}z \tag{1.25}$$

where $I_{\mathrm{L}}(z)$ is the peak value of $I_{\mathrm{L}}(z, t)$ and L is the propagation length of the beam. The nonlinear index of refraction for sapphire is $\tilde{n}_2 \approx 2.5 \times 10^{-16}\,\mathrm{cm}^2/\mathrm{W}$. For $B > 1$, this nonlinear phase retardation causes wave-front distortion and filamentation that can damage the amplifiers' medium.

A frequency-chirped pulse could be easily obtained by propagating it through an optical fibre. However, the high-order phase terms introduced by a fibre make it unsuitable for stretching and compressing a femtosecond pulse. The stretching and the compression are obtained by using a pair of gratings (or prisms). The grating pairs can be arranged to separate the output pulse spectrum from the oscillator in such a way that the different wavelengths follow different paths through the optical system. This enables pulse compression by using the reverse procedure.

The sub-nanojoule output from the oscillator is stretched in time by a factor of 10^4, and then its energy is amplified by a factor of 10^6 in a smaller system and up to 10^{10} in the larger systems. After that the laser pulse duration is recompressed to almost its initial value. In this way one can achieve a table-top laser system with peak power $>10^{12}\,\mathrm{W}$ (terawatts = TW) and for larger systems (Wharton *et al.* 1998, Norreys *et al.* 1999 and Perry *et al.* 1999) a peak power $>10^{15}\,\mathrm{W}$ (petawatts = PW) was obtained. By focusing the lasers, power flux densities up to $10^{20}\,\mathrm{W/cm}^2$ were attained. These laser systems have opened up many scientific fields and new technological possibilities, and in particular it became possible to investigate a domain of plasma physics not available before in the laboratory.

Chapter 2

Introduction to Plasma Physics for Electrons and Ions

This chapter reviews the important features of a plasma medium and sets the background for the next chapters. An introductory and popular book on plasma physics is by Eliezer and Eliezer (2001). For more serious studies of basic plasma physics, books by the following authors are recommended: Ginzburg (1961), Spitzer (1962), Schmidt (1966), Shkarofsky *et al*. (1966), Clemmow and Dougherty (1969), Krall and Trivelpiece (1973), Chen (1974), Nicholson (1983), Kruer (1988), Tajima (1989), Stix (1992), Dendy (1993), Ichimaru (1994), Goldston and Rutherford (1995), Hazeltine and Waelbroeck (1998), Salzmann (1998) and Hora (2000).

2.1 Ionization

The word **ion**, in Greek 'to go', was introduced by the famous English scientist Michael Faraday in 1830 to describe the state of an electrically charged particle. Ionization is the process where a neutral atom becomes an ion, or more generally, an atom that lost j (= 0, 1, 2, ...) electrons (denoted by A_j) is converted to an atom that lost $j+1$ electrons (A_{j+1}). In thermal dynamic equilibrium this process is described by

$$A_j \leftrightarrow A_{j+1} + e^-, \qquad j = 0, 1, 2 \ldots \tag{2.1}$$

$$\delta N_j = -\delta N_{j+1} = -\delta N_e \tag{2.2}$$

where N is the number of particles per unit mass of the ions A_j, A_{j+1} and the electrons accordingly and δ is the appropriate variation on the number of particles. The thermodynamic state can be described by the free energy F (dimension energy/mass). The variables of F are the plasma temperature T, the specific volume V and the number of particles N. V is related to the density ρ by

$$V = \frac{1}{\rho}. \tag{2.3}$$

In a thermal dynamic equilibrium the free energy $F(T, V, N)$ is minimized:

$$F(T, V, N) = -\sum_j N_j k_B T \ln \frac{eQ_j}{N_j} - N_e k_B T \ln \frac{eQ_e}{N_e} \tag{2.4}$$

$$\delta F = \sum_j \frac{\delta F}{\delta N_j} \delta N_j + \frac{\delta F}{\delta N_e} \delta N_e = 0. \tag{2.5}$$

k_B is the **Boltzmann constant** and Q_j and Q_e are the **partition functions** for the ions and electrons appropriately, defined by

$$Q = \sum_i \exp\left(-\frac{\varepsilon_i}{k_B T}\right) \tag{2.6}$$

where ε_i are the energy eigenstates of the Hamiltonian describing the plasma system. Solving equations (2.2), (2.4) and (2.5) yields

$$\frac{N_{j+1} N_e}{N_j} = \frac{Q_{j+1} Q_e}{Q_j}, \qquad j = 0, 1, 2 \ldots \tag{2.7}$$

implying the famous **Saha equations**

$$\frac{n_{j+1} n_e}{n_j} = \frac{2U_{j+1}}{U_j} \left(\frac{2\pi m_e k_B T}{h^2}\right)^{3/2} \exp\left(-\frac{I_j - \Delta I_j}{k_B T}\right), \qquad j = 1, 2, \ldots, (Z-1) \tag{2.8}$$

where $n = N/V$, i.e. n_{j+1} and n_j are the densities of the $(j+1)$th and jth ionization state and n_e is the electron density, U_{j+1} and U_j are the internal parts of the ionic partition function, m_e is the electron mass and h is Planck's constant, I_j is the **ionization energy** of the ground state and $I_j = \varepsilon_{j+1,0} - \varepsilon_{j,0}$. ΔI_j is the reduction of the ionization potential due to local electrostatic fields in the plasma. The density of the ionization states n_j includes all possible excited states, whose partial densities n_{jm} satisfy

$$n_j = \sum_m n_{jm}. \tag{2.9}$$

The sum over m extends over all bound levels for which $\varepsilon_{jm} < I_j - \Delta I_j$. Equation (2.8) is subject to the following constraints:

$$n_t = \sum_{j=0}^{Z} n_j \tag{2.10}$$

$$n_e = \sum_{j=0}^{Z} j n_j = Z_i n_t \tag{2.11}$$

where n_t is the total ion number density, Z is the atomic number and Z_i is the average degree of ionization.

Table 2.1. A few examples of the approximation (2.12) in comparison with the exact results (Cowan 1981). The last column is the absolute difference between the approximation and the exact result divided by the exact result (in %). H is hydrogen, He is helium, Li is lithium, etc.

		Z_i	n	Equation (2.12) (eV)	Cowan (1981) (eV)	Accuracy (%)
$Z = 13$, Al	H-like	12	1	2298	2304	0.26
$Z = 13$, Al	He-like	11	1	1958	2086	6
$Z = 13$, Al	Li-like	10	2	411	442	7
$Z = 13$, Al	Be-like	9	2	340	399	14.8
$Z = 26$, Fe	H-like	25	1	9194	9277.7	0.9
$Z = 26$, Fe	He-like	24	1	8500	8828	3.7
$Z = 26$, Fe	Li-like	23	2	1958	2045	4.2
$Z = 26$, Fe	Be-like	22	2	1799	1950	7.7
$Z = 26$, Fe	B-like	21	2	1646	1799	8.5
$Z = 26$, Fe	C-like	20	2	1499	1689	11.2
$Z = 26$, Fe	Ar-like	8	3	122.4	233.6	47.6

The ionization energy I of a partial ionized atom can be estimated by the 'hydrogen-like' model

$$I(\text{eV}) \approx \frac{13.6(Z_\text{i} + 1)^2}{n^2} \tag{2.12}$$

where n is the principal quantum number of the outermost bound electron (see table 2.1).

The Saha equations are satisfied for plasma in **local thermodynamic equilibrium** (LTE). LTE is characterized by the fact that the dynamic properties of the plasma particles, such as electron and ion velocities, population partition among the excited atomic states and ionization state densities, follow **Boltzmann distributions**

$$n_{jm} \propto \exp\left(-\frac{\varepsilon_{jm}}{k_\text{B} T}\right) \tag{2.13}$$

where ε_{jm} is the level energy above the ground state.

In contrast to complete thermodynamic equilibrium, in LTE the radiation may escape from the plasma; therefore the radiation is not necessarily in equilibrium with the plasma particles. More generally, in this case all laws of thermodynamic equilibrium are valid except Planck's radiation law. LTE may also be valid when there are temperature gradients in the plasma, i.e. $\nabla T \neq 0$, in which case complete thermodynamic equilibrium cannot occur.

LTE is valid mainly for high-density plasmas, where the frequent collisions between electrons and ions or between the electrons themselves

produce equilibrium. For this to happen it is necessary that the electron and ion densities must be high enough for collisional processes to be more important than the dissipative radiative processes.

As a simple example of the Saha equation (2.8) consider the case $j = 0$ in (2.1), i.e. the first ionization of a neutral atom. Denoting the degree of ionization in this case by Z_1,

$$Z_1 = \frac{n_e}{n_0} = \frac{n_1}{n_0} \tag{2.14}$$

the Saha equation (2.8) can be written as (Zeldovich and Raizer 1966)

$$\frac{Z_1^2}{1 - Z_1} \approx \frac{2}{n_0} \left(\frac{2\pi m_e k_B T}{h^2} \right)^{3/2} \exp\left(-\frac{I}{k_B T} \right). \tag{2.15}$$

For $I/(k_B T) \gg 1$, one gets $Z_1 \ll 1$; that is, most of the atoms are neutral and only a few have been ionized. Moreover, in this case n_0 is proportional to the density ρ, and therefore equation (2.15) yields

$$Z_1 \propto \frac{1}{\sqrt{\rho}} \exp\left(-\frac{I}{2k_B T} \right) \tag{2.16}$$

implying that the degree of ionization increases very rapidly with increasing temperature and increases slowly with decreasing density. The first ionization energy, I, for the majority of atoms and molecules varies between 7 and 15 eV (an exception is the alkali metals, which have a lower I). For example, the ionization of an oxygen atom, an oxygen molecule, a nitrogen atom and a nitrogen molecule are accordingly: $I_O = 13.6\,\text{eV}$, $I_{O_2} = 12.1\,\text{eV}$, $I_N = 13.6\,\text{eV}$ and $I_{N_2} = 12.1\,\text{eV}$. For air at standard density ($\rho_0 = 1.29 \times 10^{-3}\,\text{g/cm}^3$), the Saha equation yields $n_e/n_0 \approx 0.24$ for $T \approx 20\,000\,\text{K}$, $n_e/n_0 \approx 1.5$ for $T \approx 50\,000\,\text{K}$ and $n_e/n_0 \approx 5.0$ for $T \approx 250\,000\,\text{K}$.

The Saha equations, which are valid only in LTE, were derived using general thermodynamic consideration without considering the dynamics of ionization. However, if LTE is not satisfied then one has to write in general a complete set of rate equations for all ions and their respective quantum levels, taking into account all possible collision processes causing ionization and recombination (opposite of ionization). In this case one has to know the different cross sections and collision frequencies for the relevant processes.

2.2 Cross Section, Mean Free Path and Collision Frequency

The cross section is one of the most important concepts of basic physics. A simple explanation of this concept is now described. Consider a beam of particles a, such as electrons, ions or photons, with a flux of F_a particles

per unit area per unit time (the dimension of F_a is in $\mathrm{cm}^{-2}\,\mathrm{s}^{-1}$ in c.g.s.). These particles collide with the particles of a medium b of density n_b (in cm^{-3}). The beam flux crossing a thickness $\mathrm{d}l$ of the medium, containing $n_b\,\mathrm{d}l$ particles per unit area, is attenuated by an amount $\mathrm{d}F_a$, that is proportional to F and $n\,\mathrm{d}l$,

$$\mathrm{d}F_a = -\sigma_{ab} F_a n_b\,\mathrm{d}l. \tag{2.17}$$

The proportionality factor σ_{ab} has the dimension of area and is called the **cross section** for the collision between a and b. From the geometrical picture of this collision one can see that σ_{ab} is the effective area of one collision.

The integration of (2.17) for constant σ_{ab} and n_b yields

$$F_a(l) = F_a(0)\exp(-n_b\sigma_{ab}l) \tag{2.18}$$

where $F_a(0)$ is the incident flux and l is the thickness of the medium b that a has traversed. Equation (2.18) is not always correct since σ_{ab} can be effectively a function of the distance l and therefore the integration of (2.17) is not as simple as above. This usually happens when the particles lose energy during collisions, and in general the cross section is a function of the energy.

The physical quantity μ_a (in cm^{-1}), defined as the absorption coefficient, is given by

$$\mu_a = \sum_b n_b\sigma_{ab} = \frac{1}{l_a} \tag{2.19}$$

where the sum is over all species of the medium. The reciprocal of μ_a, sometimes defined as the attenuation, is the mean free path l_a. If (2.18) is not correct then it is necessary to define the absorption coefficient and the mean free path in a more sophisticated way (for example, by making appropriate averages with respect to the energy of the projectile).

The cross section is not only a function of energy but it may also depend on the direction in which the particles are scattered. When $\sigma_{ab}(E,\theta,\phi)$ is a function of the centre of mass energy E of the colliding particles and the direction in spherical coordinates (θ,ϕ) of the scattered particle, one has to define the **differential scattering cross section**, $\mathrm{d}^2\sigma_{ab}/(\mathrm{d}E\,\mathrm{d}\Omega)$, where $\mathrm{d}\Omega$ is the infinitesimal solid angle in the direction (θ,ϕ). In this case, equation (2.17) for the flux change of the particles due to collisions $\mathrm{d}F_a$ is replaced by

$$\begin{aligned}&\mathrm{d}F_a\ [\text{into } \mathrm{d}\Omega \text{ in direction } (\theta,\phi),\ \text{in energy interval } \mathrm{d}E]\\ &= \left(\frac{\mathrm{d}^2\sigma_{ab}}{\mathrm{d}E\,\mathrm{d}\Omega}\,\mathrm{d}E\,\mathrm{d}\Omega\right) F_a n_b\,\mathrm{d}l\end{aligned} \tag{2.20}$$

and the total cross section σ_{ab} is

$$\sigma_{ab} = \iint \mathrm{d}E\,\mathrm{d}\Omega\,\frac{\mathrm{d}^2\sigma_{ab}}{\mathrm{d}E\,\mathrm{d}\Omega}. \tag{2.21}$$

The cross section for elastic scattering between an electron (not very energetic) and a neutral atom (or molecule) in a gas, σ_{e0}, can be described in good approximation by the effective area of the atom (or the molecule). Denoting by R_0 the radius of the neutral particle, the cross section is

$$\sigma_{e0} \approx \pi R_0^2. \tag{2.22}$$

For most atoms and molecules in a gas, σ_{e0} is in the range 10^{-16}–$10^{-15}\,\mathrm{cm}^2$. The **mean free path**, i.e. the average length between two collisions of a particle (electron, ion, photon, etc.) with the background particles, was introduced by Clausius as early as 1858. The concept of the mean free path is useful for irreversible processes and is also important for problems where ordinary thermodynamics is not applicable. As one can see from (2.19), the information obtained from the mean free path is equivalent to the information contained in the appropriate total cross section.

The **collision frequency** ν_{ab} between a particle a with a velocity $\mathbf{v}_a$ and the background is defined as the number of collisions per second of the particle under consideration (sometimes called the test particle) with the background particles b:

$$\nu_{ab} = n_b \sigma_{ab} v_a = \frac{v_a}{l_{ab}}. \tag{2.23}$$

ν_{ab} is also the **probability per unit time** for the collision to occur.

For the air density, $n_0 \approx 3 \times 10^{19}\,\mathrm{cm}^{-3}$, the mean free path of an electron at room temperature ($v_e \approx 6.7 \times 10^6\,\mathrm{cm/s}$) is about 3 μm (for a cross section of $10^{-16}\,\mathrm{cm}^2$) and its collision frequency is about $2 \times 10^{10}\,\mathrm{s}^{-1}$.

In ionized plasma the Coulomb forces dominate the trajectory of the charged particles. The famous **Rutherford differential scattering cross section** describes the collision between an electron and an ion (with a charge Ze) possessing an infinite mass, as described in figure 2.1.

This cross section is given by

$$\frac{\mathrm{d}\sigma_{ei}}{\mathrm{d}\Omega} = \left(\frac{1}{4}\right)\left(\frac{Ze^2}{m_e v^2}\right)^2 \frac{1}{\sin^4(\theta/2)} \tag{2.24}$$

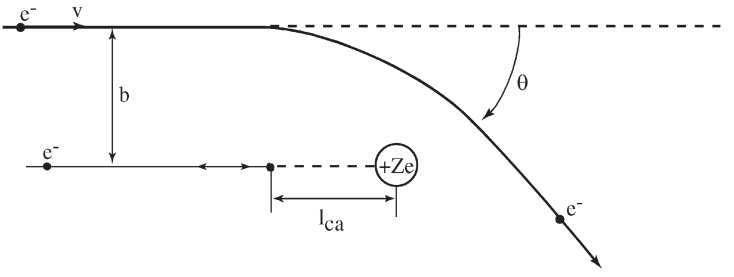

Figure 2.1. Orbit of an electron colliding with a positive ion of charge Ze. b is the impact parameter, l_{ca} is the closest approach for $b = 0$ and θ is the scattering angle.

where m_e and v are the mass and the velocity of the electron accordingly, θ is the scattering angle and $d\Omega$ is the differential solid angle. In spherical coordinates with an azimuthal symmetry, $d\Omega$ is related to the scattering angle θ by

$$d\Omega = 2\pi \sin\theta \, d\theta. \tag{2.25}$$

The impact parameter b, defined asymptotically before the Coulomb interaction is effective, is related to the scattering angle θ by

$$b \tan\frac{\theta}{2} = \frac{Ze^2}{m_e v^2}. \tag{2.26}$$

Although equations (2.24)–(2.26) are given for an electron–ion collision in the laboratory system of reference, these equations are also valid for the collision of any two charged particles with masses m_1 and m_2 and charges q_1 and q_2 appropriately. For this general collision the following changes are to be done in the above equations to be valid in the centre of mass:

(a) $-Ze^2$ is replaced by $q_1 q_2$.
(b) The electron mass is replaced by the reduced mass m_r defined by

$$\frac{1}{m_r} = \frac{1}{m_1} + \frac{1}{m_2}. \tag{2.27}$$

(c) v is the relative velocity between the colliding particles.
(d) The scattering angle θ is given in the centre of mass of the colliding particles.

The (total) cross section σ_{ei} is defined by

$$\sigma_{ei} = \int d\Omega \frac{d\sigma_{ei}}{d\Omega} = \frac{\pi}{2}\left(\frac{Ze^2}{m_e v^2}\right)^2 \int_0^{\pi} d\theta \frac{\sin\theta}{\sin^4(\theta/2)}. \tag{2.28}$$

The above integral diverges at $\theta = 0$, or equivalently (using equation (2.26)) for $b \to \infty$. However, the very distant interactions are screened by the surrounding charged particles so that there is an effective b_{max} instead of $b \to \infty$. In general b_{max} is taken as the Debye length (section 2.4).

In calculating the collision frequency in (2.23) for electron–ion collisions, one has to take into account the velocity distribution of the particles, i.e. $\sigma_{ab} v_a$ has to be replaced by $\langle \sigma_{ab} v_a \rangle$, an average over all possible velocities. For ions at rest and electrons in LTE (for $T_i = 0$ and an electron temperature T_e), the electron velocity distribution $f(\mathbf{v})$ is given by the **Maxwell distribution**,

$$f(v) = \frac{1}{(\sqrt{\pi} v_T)^3} \exp\left(-\frac{v^2}{v_T^2}\right), \qquad \int_0^{\infty} dv \frac{4\pi v^2}{(\sqrt{\pi} v_T)^3} \exp\left(-\frac{v^2}{v_T^2}\right) = 1. \tag{2.29}$$

The distribution is isotropic, $f(v)$ has the dimension $(\mathrm{cm/s})^{-3}$ and the thermal velocity (v_T) is defined by

$$v_\mathrm{T}^2 = \frac{2k_\mathrm{B}T}{m_\mathrm{e}}. \tag{2.30}$$

The $\sigma_{ab}v_a$ in (2.23) is replaced by

$$\begin{aligned}\sigma_{ab}v_a \to \langle\sigma_{ab}v_a\rangle &\equiv \int_0^\infty \sigma_{ab}vf(v)4\pi v^2\,\mathrm{d}v \\ &= \frac{4\pi}{\pi^{3/2}v_\mathrm{T}^3}\int_{b_\mathrm{min}}^{b_\mathrm{max}} \exp\left(-\frac{v^2}{v_\mathrm{T}^2}\right)\sigma_{ab}(v)v^3\,\mathrm{d}v.\end{aligned} \tag{2.31}$$

For Coulomb interaction, e.g. using the Rutherford scattering (2.28), the above integral diverges logarithmically at $b = 0$. $\sigma_\mathrm{ei}(v)$ is proportional to $1/v^4$ and therefore one also has an integral over $\mathrm{d}v/v$ (integrating by parts, or just equating the exponent to 1 for very small v). Using the screening effect as discussed above, $b = \infty$ is replaced by b_max and $b = 0$ is replaced by b_min equal to the **closest approach** l_ca (see figure 2.1), defined by

$$\frac{Ze^2}{l_\mathrm{ca}} = k_\mathrm{B}T_\mathrm{e}. \tag{2.32}$$

In the plasma literature one can find that if the electron **de Broglie wavelength** l_dB is larger than the closest approach one has to take $b_\mathrm{min} = l_\mathrm{dB}$:

$$l_\mathrm{dB} = \frac{\hbar}{m_\mathrm{e}v_\mathrm{T}} = \frac{\hbar}{(2m_\mathrm{e}k_\mathrm{B}T_\mathrm{e})^{1/2}}. \tag{2.33}$$

However, in this case the entire classical approach is not appropriate (Lifshitz and Pitaevskii 1981) and one has to calculate the cross section correctly according to quantum mechanics (Landau and Lifshitz 1965). Therefore for the classical approximation l_min is always given by (2.32).

A simple order of magnitude estimate for the electron ion collision frequency can be obtained by taking the cross section

$$\sigma_\mathrm{ei} \approx \pi l_\mathrm{ca}^2 \propto T_\mathrm{e}^{-2}. \tag{2.34}$$

The proportionality is derived from (2.32). Using this equation together with equations (2.23) and (2.30), one gets an estimate for the electron ion collision frequency

$$\nu_\mathrm{ei} \approx \frac{\sqrt{2}\pi Z^2e^4n_\mathrm{i}}{\sqrt{m_\mathrm{e}}(k_\mathrm{B}T_\mathrm{e})^{3/2}}. \tag{2.35}$$

A more accurate calculation (see section 9.3) yields

$$\nu_\mathrm{ei} = \frac{4(2\pi)^{1/2}Z^2e^4n_\mathrm{i}\ln\Lambda}{3\sqrt{m_\mathrm{e}}(k_\mathrm{B}T_\mathrm{e})^{3/2}} \approx 2.9\times10^{-6}\frac{Z^2n_\mathrm{i}(\mathrm{cm}^{-3})\ln\Lambda}{[T_\mathrm{e}(\mathrm{eV})]^{3/2}} \quad [\mathrm{s}^{-1}] \tag{2.36}$$

$$\Lambda = \frac{b_{\max}}{b_{\min}}. \tag{2.37}$$

In the right-hand side of (2.36), n_i is the ion density in cm^{-3} and T_e(eV) is the electron temperature in electronvolt (eV).

2.3 Transport Coefficients

2.3.1 Electrical conductivity

The **Drude model** is used to get a simple estimate on the electrical conductivity of a plasma gas. The same formalism is a good approximation for solids (Ashcroft and Mermin 1976). The definition of the electrical conductivity is given by

$$\mathbf{j}_e = -n_e e \mathbf{v}_e = \sigma_E \mathbf{E} \tag{2.38}$$

where $\mathbf{v}_e$ is the electron velocity, $\mathbf{j}_e$ is the electric current, n_e is the electron density and σ_E is the electric conductivity. The relation between the electric current and the electric field is known as Ohm's law. Due to the local electric field $\mathbf{E}$, assumed constant (d.c.) in this model, an electron is accelerated between any two collisions with the background particles. Newton's law yields

$$\frac{d\mathbf{v}_e}{dt} = -\frac{e\mathbf{E}}{m_e}. \tag{2.39}$$

It is assumed that the collisions are instantaneous and suddenly alter the electron velocity. In this picture the electrons are bumping from particle to particle. Denoting by t the time that passed since the last collision of the electron, the solution of (2.39) is $\mathbf{v}_{(t=0)} - e\mathbf{E}t/m_e$. Since in this model an electron emerges from a collision in a random direction, $\mathbf{v}_{(t=0)}$ does not contribute to the average velocity. Therefore, assuming that the average time between collisions is the relaxation time τ, the velocity in (2.38) is

$$\mathbf{v}_e = -\frac{e\mathbf{E}\tau}{m_e}, \qquad \tau = \frac{1}{\nu_{ei}}. \tag{2.40}$$

An electron in the plasma collides with the ions, the other electrons and if the plasma is not fully ionized it collides also with the neutral atoms. In equation (2.40) it is assumed that this frequency is dominated by electron–ion collisions. Substituting the velocity from (2.40) into (2.38) one gets the electrical conductivity

$$\sigma_E = \frac{n_e e^2}{m_e \nu_{ei}} \tag{2.41}$$

where σ_E is in s^{-1} in c.g.s. units, $(\Omega\,m)^{-1}$ in m.k.s. (standard units) and the relation between the units is: $1\,(\Omega\,m)^{-1} = 9 \times 10^9\,s^{-1}$. Using equation (2.36), in (2.41) the electrical conductivity can be written as

$$\sigma_E(\text{ei}) = 2.7 \times 10^{17} Z \left(\frac{T_e}{\text{keV}}\right)^{3/2} \quad [s^{-1}] \tag{2.42}$$

where the electron temperature is in keV. It is worthwhile to compare this numerical result (equation (2.42)) with the conductivity of a very good conductor such as copper, $\sigma_E(\text{copper}) = 5.5 \times 10^{17}\,s^{-1}$.

For comparison between plasma (known as a good conductor) and a gas (known as a very bad conductor), it is interesting to calculate the d.c. electrical conductivity of air. The first question is how many free electrons are in air at standard conditions. Using the Saha equation (2.16) one gets $n_e \approx \exp(-I/(2T_{(\text{eV})}))$; $I \approx 15\,\text{eV}$ and the room temperature is $T \approx 1/40\,\text{eV}$, therefore the exponential factor is $\exp(-300)$, implying practically a zero n_e. However, due to cosmic radiation the number of induced electrons is of the order $\sim \frac{1}{2}(\text{statcoulomb})/(\text{year}\,\text{cm}^3) \approx 30$ electrons/$(\text{cm}^3\,\text{s})$ (this number changes for different locations on Earth). These free electrons are attached to the air molecules; taking a lifetime of about 10 ns for these electrons, one gets a steady state number of free electrons about $n_e \approx 3 \times 10^{-7}\,\text{cm}^{-3}$. Using this electron density, the electron cross section for colliding with a neutral molecule (2.22), and using the collision frequency (2.23), in (2.41) one gets $\sigma_E(\text{air}) \approx 3 \times 10^{-9}\,s^{-1}$, a number that is about 26 orders of magnitude smaller than the electrical conductivity of copper.

2.3.2 Thermal conductivity

Consider a medium in which the temperature is not uniform, i.e. T is a function of space $T = T(\mathbf{r})$. The tendency to reach equilibrium requires a flow of heat from the region of higher temperature to that of lower temperature. Defining $\mathbf{q}_H$ as the energy crossing a unit area per unit time in the direction orthogonal to this area, the heat flux (in $\text{erg}/(\text{cm}^2\,\text{s})$) can be defined by

$$\mathbf{q}_H = -\kappa \nabla T. \tag{2.43}$$

The value of κ can be easily estimated in a simple model. We assume that the temperature is a function of x, the particles have an average energy $\varepsilon(x)$, a density n and a velocity v. This simplification does not affect the calculations since κ does not depend on the model that is calculated. The flux of the particles in the $+x$ direction, normal to the y–z plane, is $\frac{1}{6}(nv)$ (the factor $\frac{1}{6}$ can be understood by considering three dimensions x–y–z and each dimension has two directions). The heat flux $q_H(x)$ in the direction of $+x$ is

$$q_H = \frac{1}{6}(nv)[\varepsilon(x-l) - \varepsilon(x+l)] \approx -\frac{1}{3} nvl \frac{\partial \varepsilon}{\partial x} = -\frac{1}{3} nvl \frac{\partial \varepsilon}{\partial T} \frac{\partial T}{\partial x} \tag{2.44}$$

where l is the mean free path discussed in the previous section. Since the energy derivative with respect to the temperature is the heat capacity (at constant volume for a process that the density is constant), one gets

$$q_{\mathrm{H}} = -\frac{1}{3} n v l c_{\mathrm{V}} \frac{\partial T}{\partial x}. \tag{2.45}$$

l is the mean free path of the particles that are transporting the heat (for example, the molecules in a gas and the electrons in a plasma), c_{V} is the heat capacity per particle at constant volume, and assuming that v equals the thermal velocity v_{T}, one gets

$$\kappa = \frac{1}{3} n c_{\mathrm{V}} l v_{\mathrm{T}} = \frac{n_{\mathrm{e}} c_{\mathrm{Ve}} v_{\mathrm{T}}^2}{3\nu_{\mathrm{ei}}} \propto T_{\mathrm{e}}^{5/2} \quad [\mathrm{erg}/(\mathrm{cm} \cdot \mathrm{s} \cdot \mathrm{K})]. \tag{2.46}$$

The second equality was obtained using (2.23). For the last proportionality it was assumed that the electrons are transporting the heat, $\nu_{\mathrm{ei}} \approx T_{\mathrm{e}}^{-3/2}$, $v_{\mathrm{T}}^2 \approx T_{\mathrm{e}}$, and taking for the plasma under consideration a constant c_{V}.

It is worth mentioning that the heat transport in a gas is done by the gas molecules; and in this case (to a first approximation) the cross section is temperature-independent, the collision frequency is proportional to the temperature square root, and therefore

$$\kappa(\mathrm{gas}) \propto T^{1/2} \tag{2.47}$$

where T is the gas temperature.

Comparing the electrical conductivity σ_{E}, equation (2.41), with the thermal conductivity κ (2.46) and using the ideal gas equation of state (Eliezer *et al*. 1986), $c_{\mathrm{V}} = \frac{3}{2} k_{\mathrm{B}}$ and (2.30) we get the **Wiedemann and Franz law**

$$\frac{\kappa}{\sigma_{\mathrm{E}}} = \frac{3}{2} \left(\frac{k_{\mathrm{B}}}{e} \right)^2 T. \tag{2.48}$$

2.3.3 Diffusion

In equilibrium the electrons are distributed uniformly throughout the plasma so that n_{e} is independent of position. Suppose that a disturbance causes the electron density to depend on position $n_{\mathrm{e}}(\mathbf{r})$. In this case the electrons will move in such a way as to restore equilibrium. This motion is described by the diffusion equation

$$\frac{\partial n_{\mathrm{e}}}{\partial t} = \nabla \cdot (D \nabla n_{\mathrm{e}}) \tag{2.49}$$

where D is the diffusion coefficient, defined by the relation

$$\mathbf{j}_{\mathrm{n}} = -D \nabla n. \tag{2.50}$$

$\mathbf{j}_{\mathrm{n}} = n\mathbf{v}$ is the particle current density.

The diffusion coefficient can be calculated using the simple model used above (to calculate the thermal conductivity coefficient). The density is a function of one space dimension, $n(x)$, and the particle flux in the $+x$ direction is

$$j_{\mathrm{n}} = \frac{1}{6}[v_{\mathrm{T}} n_{\mathrm{e}}(x-l) - v_{\mathrm{T}} n_{\mathrm{e}}(x+l)] \approx -\frac{1}{3} v_{\mathrm{T}} l \frac{\partial n_{\mathrm{e}}}{\partial x}. \tag{2.51}$$

The right-hand side of the equation was obtained by the first-order Taylor expansion. From this equation the diffusion coefficient is

$$D = \frac{1}{3} v_{\mathrm{T}} l \propto \frac{T_{\mathrm{e}}^{5/2}}{n_{\mathrm{e}}} \quad [\mathrm{cm}^2/\mathrm{s}]. \tag{2.52}$$

In the presence of a magnetic field in a fully ionized plasma the diffusion coefficient in a direction perpendicular to the magnetic field, $D_\perp$, is a function of the magnetic field. In this case, for a steady-state plasma the Ohm law (2.38) (in c.g.s. units) is generalized to

$$\mathbf{j} = \sigma_{\mathrm{E}} \left(\mathbf{E} + \frac{\mathbf{v} \times \mathbf{B}}{c} \right) \tag{2.53}$$

where c is the speed of light. The magnetic force (force/volume) $\mathbf{J} \times \mathbf{B}/c$ is balanced by the pressure gradient (force/volume) ∇P

$$\frac{\mathbf{j} \times \mathbf{B}}{c} = \nabla P. \tag{2.54}$$

The plasma velocity in the perpendicular direction to the magnetic field is obtained by taking the cross-product of the generalized Ohm's law with the magnetic field [(2.53) $\times$ **B**] and using (2.54) for an ideal gas pressure with constant temperature, $\nabla P = k_{\mathrm{B}} T \nabla n$. The derived perpendicular velocity $\mathbf{v}_\perp$ is

$$\mathbf{v}_\perp = \frac{c\mathbf{E} \times \mathbf{B}}{B^2} - \frac{c^2 k_{\mathrm{B}} T}{\sigma_{\mathrm{E}} B^2} \nabla n \equiv \mathbf{v}_{\mathrm{drift}} + \mathbf{v}_{\mathrm{diffusion}}. \tag{2.55}$$

Therefore, the diffusion coefficient $D_\perp$ is $(-n v_{\mathrm{diffusion}}/\nabla n)$

$$D_\perp = \frac{c^2 n k_{\mathrm{B}} T}{\sigma_{\mathrm{E}} B^2} \quad [\mathrm{cm}^2/\mathrm{s}]. \tag{2.56}$$

This value for $D_\perp$ is known as the **classical diffusion**. However, it appeared in many experiments that the $1/B^2$ scaling law of $D_\perp$ is not satisfied and instead a $1/B$ dependence was derived (Bohm *et al* 1949). Bohm, Burhop and Massey, who were using an arc discharge in the presence of a magnetic field for uranium isotope separation, first noted this **anomalous diffusion** in 1946. Bohm suggested the semi-empirical formula

$$D_\perp = \frac{c k_{\mathrm{B}} T_{\mathrm{e}}}{16 e B} \equiv D_{\mathrm{B}} \quad [\mathrm{cm}^2/\mathrm{s}]. \tag{2.57}$$

The diffusion following this law is called the **Bohm diffusion**. Note that D_B, unlike $D_\perp$, does not depend on the density. It was found that (2.57) is satisfied in a surprisingly large number of experiments.

2.3.4 Viscosity

The pressure is in general a tensor P_{ij}, the first index designating the orientation of the plane and the second index the component of the force exerted across this plane. In Cartesian coordinates, i or j is equal to x, y, z. Viscosity arises when adjacent fluid elements flowing with different velocities exchange momentum. The tensor P_{ij} is given by

$$P_{ij} = P\delta_{ij} + \rho v_i v_j - \eta\left(\frac{\partial v_i}{\partial x_j} + \frac{\partial v_j}{\partial x_i} - \frac{2}{3}\sum_{k=1}^{3}\frac{\partial v_k}{\partial x_k}\delta_{ij}\right) - \varsigma\sum_{k=1}^{3}\frac{\partial v_k}{\partial x_k}\delta_{ij}. \tag{2.58}$$

The **Navier–Stokes** equation of ordinary fluid dynamics can be written in the form (Landau and Lifshitz 1987)

$$\frac{\partial(\rho v_i)}{\partial t} = -\sum_{k=1}^{3}\frac{\partial P_{ik}}{\partial x_k}. \tag{2.59}$$

In general the coefficients of viscosity η (the first coefficient) and ζ (the second coefficient) are positive numbers that are functions of temperature and density. P is the scalar pressure given by the equation of state (Eliezer *et al.* 1986)

$$P = P(\rho, T) \tag{2.60}$$

where ρ is the density of the plasma fluid. For an incompressible fluid the divergence of the velocity vanishes, $\nabla \cdot \mathbf{v} = 0$, and the second coefficient of viscosity ζ does not contribute to the pressure tensor. In many plasma systems the effects of viscosity are negligible since the first two terms in (2.58) are much larger than the viscous terms. However, we shall estimate the coefficients of viscosity η in a simple model, as described above for the coefficients of diffusion and conductivity. We take an x dependence only and a flow velocity $\mathbf{v} = (0, 0, v_z)$, so that the only off-diagonal tensor element of the pressure is

$$P_{xz} = -\eta\frac{\partial v_z}{\partial x}. \tag{2.61}$$

P_{xz}, known as the **stress**, is the mean increase of the momentum flux in the z direction transported by the fluid particles per unit time and per unit area in the x direction (the y–z plane). In this model P_{xz} is defined by

$$P_{xz} = \tfrac{1}{6}(nv_T)m[v_z(x-l) - v_z(x+l)] \tag{2.62}$$

where m is the mass of the particle fluid under consideration. A first-order Taylor expansion of v_z yields

$$P_{xz} = -\left(\frac{1}{3}nmv_T l\right)\frac{\partial v_z}{\partial x} \equiv -\eta\frac{\partial v_z}{\partial x}. \tag{2.63}$$

In the calculation of the transport coefficients derived above, the coefficient factors are not to be taken too seriously. However, the scaling laws with the mass m, the mean free path l, the density n and the average velocity (denoted by v_T) of the particles under consideration give a reasonable approach for the behaviour of the transport coefficients: σ_E, κ, D and η.

2.4 Radiation Conductivity

In high-power laser interaction with plasma medium, x-ray radiation is produced (Gauthier 1989, Kauffman 1991, More 1991). Laser-produced plasmas achieved the highest brightness of x-ray source in the laboratory. The x-rays are produced by the different electron transitions, shown schematically in figure 2.2. In this figure three classes of transitions are described: **bound–bound (bb)**, **bound–free (bf)** and **free–free (ff)**.

2.4.1 Bound–bound (bb) transitions

A photon is emitted when an electron jumps from a higher to a lower energetic quantum state of the ion, or a photon is absorbed when an electron is excited to a higher energetic state. The emission is in the form of a line and is denoted by LE (line emission) in figure 2.2, while the absorption in this case

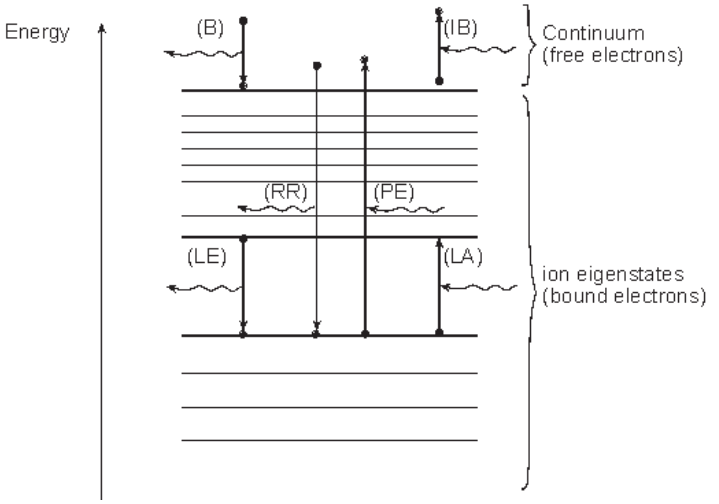

Figure 2.2. Electron transitions in an ion (or atom) associated with radiation emission or absorption. The notation is B = bremsstrahlung, IB = inverse bremsstrahlung, RR = radiative recombination, PE = photoelectric effect (known also as photoionization), LE = line emission and LA = line absorption.

is denoted by LA (line absorption). This can be described by

LE (line emission): $i_1 \rightarrow i_2 + \gamma$,
LA (line absorption): $\gamma + i_2 \rightarrow i_1$,

where i states for an ion, 1 and 2 describe the quantum numbers of the ion states, and γ is the photon.

It should be noted that for high-Z atoms there are many possible configurations of LE so that this fact together with line broadening (e.g. Doppler) changes the discrete line emission with an effective energy band (Bauche *et al.* 1988).

2.4.2 Bound–free (bf) transitions

A photon is emitted when a free electron is caught by an ion, known as the radiative recombination (RR) process, while in the inverse process the absorption of a photon is associated with the release of a bound electron. This later process is the famous **photoelectric effect** (PE), known also as **photoionization**. These processes can be described by

RR (radiative recombination): $e^- + i_1 \rightarrow i_2 + \gamma$,
PE (photoelectric effect): $\gamma + i_2 \rightarrow i_1 + e^-$,

where e^- denotes a free electron, i_1 and i_2 are different charge ion states and γ is the photon.

2.4.3 Free–free (ff) transitions

In the bremsstrahlung effect a free electron collides with an ion and emits a photon, while in the inverse process a photon is absorbed. This last transition plays a major role in laser absorption by plasma. These processes can be described by

B (bremsstrahlung): $e^- + i \rightarrow e^- + i + \gamma$,
IB (inverse bremsstrahlung): $e^- + i + \gamma \rightarrow i + e^-$.

2.4.4 Energy transport

The production of x-rays is a superposition of lines and continuous energies according to the above processes. The derived spectrum depends on the medium characteristics such as atomic number Z, degree of ionization, density and temperature. Most of the x-rays are produced in the domain of high electron density, as the probability of the above processes is proportional to the square of the plasma density. Since shorter laser wavelengths penetrate with higher electron density, the x-ray conversion efficiency increases with the decrease of the laser wavelength.

Detailed studies of the conversion of laser light into x-rays were performed for a wide parameter range of laser intensity, wavelength and pulse duration for targets of various atomic numbers. The x-ray generation efficiency (x-ray energy/absorbed laser energy) for soft x-rays, between 0.1 to 1 keV of energy, reaches the high value of 80% for a gold target irradiated with a 263 nm laser pulse of the order of 1 ns duration.

Since for high-Z materials a significant part of the laser energy is converted into x-rays, the transport of these x-rays plays an important role in these plasma media. In this section the transport of energy by radiation is analysed. The radiation can be treated classically by electromagnetic fields or quantum mechanically by the description of particles called photons. The equation of radiative transfer can be generally stated as the conservation of a physical quantity X (such as the number of photons or the energy density) with a given frequency ν and direction Ω in an arbitrary volume V bounded by a closed surface Σ. Schematically this statement can be written in the following way:

$$\begin{aligned}\text{change of } X(\nu,\mathbf{\Omega}) = {} & X(\text{flow out of volume } V \text{ via surface } \Sigma)\\ & + X(\text{absorption in the volume } V)\\ & + X(\text{scattering 'out' from } (\nu,\mathbf{\Omega}) \text{ to } (\nu',\mathbf{\Omega}') \text{ within } V)\\ & + X(\text{scattering 'in' from } (\nu',\mathbf{\Omega}') \text{ to } (\nu,\mathbf{\Omega}) \text{ within } V).\end{aligned} \tag{2.64}$$

There are many ways to formulate quantitatively this statement of radiation transport (Zeldovich and Raizer 1966, Pomraning 1973, Mihalas and Mihalas 1984, Minguez 1993). We shall follow the simplest approach given by Zeldovich and Raizer. For this purpose we introduce a variety of quantities usually used to describe the radiation energy transport.

The wavelength λ or the frequency ν (at which the electromagnetic fields oscillate) characterizes the radiation that can also be considered as photon particles with energy E_ν and momentum p_ν. λ, ν, p_ν and E_ν are related by the Planck constant h and the speed of light c:

$$\lambda = \frac{c}{\nu}, \qquad E_\nu = h\nu, \qquad p_\nu = \frac{h\nu}{c}. \tag{2.65}$$

The **distribution function of the photon particles** f ([cm^{-3} s]), where f is a function of the photon frequency ν, the photon position $\mathbf{r}$ and direction Ω at a time t, is described by

$$f(\nu,\mathbf{r},\mathbf{\Omega},t)\,\mathrm{d}\nu\,\mathrm{d}^3r\,\mathrm{d}\Omega = \text{number of photons with frequency } \nu \text{ at } (\mathbf{r},t) \tag{2.66}$$

The speed of light in the plasma medium is equal to c/n_R, where n_R is the index of refraction for photons with a frequency ν and is given by

$$n_\mathrm{R} = \left(1 - \frac{\nu_\mathrm{pe}^2}{\nu^2}\right)^{1/2} \tag{2.67}$$

where ν_{pe} is the electron oscillation frequency in the plasma. In the domain of the critical density, where the incident laser beam is reflected because it cannot penetrate into higher densities, one has for a laser with photon energy ~1 eV and an x-ray photon ~100 eV a refractive index $n_R \approx 0.99995$. Therefore, it is conceivable to assume that in the domain of the critical density and lower densities the x-ray photons move with the speed of light in vacuum. Hence, one can define the **spectral radiation intensity** I_ν [erg/cm^2] as the radiation energy per frequency between ν and $\nu + d\nu$, crossing a unit area per unit time in the direction Ω, within the solid angle $d\Omega$, by

$$I_\nu(\mathbf{r}, \mathbf{\Omega}, t)\, d\nu\, d\Omega = h\nu c f(\mathbf{r}, \mathbf{\Omega}, t)\, d\nu\, d\Omega, \qquad I\left[\frac{\text{erg}}{\text{cm}^2 \cdot \text{s}}\right] = \int I_\nu(\mathbf{r}, \mathbf{\Omega}, t)\, d\nu. \tag{2.68}$$

The radiation field is defined either by f or by I_ν (both scalar quantities). Two more useful functions are defined in order to describe the radiation transport, the **spectral energy density scalar** U_ν [erg · s/cm^3] and the **spectral energy flux vector** $\mathbf{S}_\nu$ [erg · s/cm^2]

$$\begin{aligned} U_\nu(\mathbf{r}, t) &= \frac{1}{c}\int I_\nu\, d\Omega, \qquad U[\text{erg/cm}^3] = \int_0^\infty U_\nu(\mathbf{r}, t)\, d\nu \\ \mathbf{S}_\nu(\mathbf{r}, t) &= \int I_\nu \mathbf{\Omega}\, d\Omega, \qquad \mathbf{S}[\text{erg/cm}^3] = \int_0^\infty \mathbf{S}_\nu(\mathbf{r}, t)\, d\nu, \qquad \int d\Omega = 4\pi \end{aligned} \tag{2.69}$$

where $\mathbf{\Omega}$ is the unit vector in the direction of the photon motion.

In a state of **thermodynamic equilibrium**, the number of photons in a unit volume emitted per unit time by the medium in the interval ($d\nu$, $d\Omega$) is equal to the number of absorbed photons in the same interval. The equilibrium radiation field is isotropic and depends only on frequency and the medium temperature T. In this case the Planck functions are given for the **spectral radiation intensity** $I_{\nu p}$ [erg/cm^2] and the **spectral energy density scalar** $U_{\nu p}$ [erg · s/cm^3]:

$$\begin{aligned} I_{\nu p} &= \frac{cU_{\nu p}}{4\pi} \\ U_{\nu p} &= \left(\frac{8\pi h\nu^3}{c^3}\right)\left[\exp\left(\frac{h\nu}{k_B T}\right) - 1\right]^{-1} \\ U_p[\text{erg/cm}^3] &= \int_0^\infty U_{\nu p}\, d\nu = \left(\frac{4\sigma_{SB}}{c}\right) T^4 \\ \sigma_{SB} &= \frac{2\pi^5 k_B^4}{15h^3c^2} = 5.6705 \times 10^{-5} \quad [\text{ergï/(cm}^2 \cdot \text{s} \cdot \text{deg}^4)] \end{aligned} \tag{2.70}$$

where σ_{SB} is the Stefan–Boltzmann constant. The Planck function $U_{\nu p}$, which describes the energy distribution for radiative equilibrium, has a maximum at a photon energy $h\nu_{max} = 2.822k_B T$. The isotropic equilibrium radiation implies that the **spectral energy flux vector** $\mathbf{S}_\nu$ is zero. However, it is possible to define the **one-sided** spectral energy flux $S_{\nu p}$, by integrating $I_{\nu p}\cos\theta$ (see (2.69) and (2.70)) over a hemisphere, where θ is the angle between $\mathbf{\Omega}$ and the flux vector direction:

$$\begin{aligned} S_{\nu p} &\equiv \int_0^{2\pi} d\phi \int_0^{\pi/2} d\theta \sin\theta (I_{\nu p}\cos\theta) = \pi I_{\nu p} = \frac{cU_{\nu p}}{4} \\ S_p[\text{erg}/(\text{cm}^2\cdot\text{s})] &= \int_0^{\infty} S_{\nu p}\, d\nu = \sigma_{SB} T^4. \end{aligned} \tag{2.71}$$

Before writing the transport equation, a few more variables have to be defined. The **emissivity** j_ν (erg/cm^3) describes the spontaneous emission of the medium, and it depends on the medium atoms, the degree of ionization and the temperature, but it is independent of the existence of radiation. The spontaneous emission is defined by

$$j_\nu\, d\nu\, d\mathbf{\Omega} = [\text{energy}/(\text{volume}\times\text{time})] \text{ of spontaneous emission.} \tag{2.72}$$

In order to calculate the total emission of the medium one has to add the **induced emission**, given by

$$j_\nu\left(\frac{c^2 I_\nu}{2h\nu^3}\right) d\nu\, d\Omega = [\text{energy}/(\text{volume}\times\text{time})] \text{ of induced emission.} \tag{2.73}$$

The term in the brackets is the number of photons in the same phase space cell as the emitted photon (with a definite polarization). The total emission is given by the sum of (2.72) and (2.73).

A transport equation in the form of (2.64) requires the knowledge of absorption and scattering. This can be written in the form

$$\begin{aligned} \kappa_\nu I_\nu\, d\nu\, d\Omega &= [\text{energy}/(\text{volume}\times\text{time})] \text{ absorbed or scattered} \\ &\quad \text{by the medium} \\ \kappa_\nu &= \frac{1}{l_\nu} = \sum_j n_j \sigma_{\nu j} \end{aligned} \tag{2.74}$$

where κ_ν(cm^{-1}) is **the opacity** (occasionally in the literature, the value κ_ν/ρ(cm^2/g) where ρ = density is defined as the opacity), the appropriate **mean free path** is l_ν(cm), n_j(cm^{-3}) is the density of particles of type j and $\sigma_{\nu j}$ is the appropriate cross section for absorption or scattering of the processes under consideration, as described in figure 2.2. For example

(More 1991), the inverse bremsstrahlung cross-section is given by

$$\begin{aligned}\sigma_{\mathrm{ff}}^{\mathrm{IB}}(\nu) &= \left(\frac{2^8\pi\alpha}{3\sqrt{3}}\right)(n_{\mathrm{e}}a_{\mathrm{B}}^3)\left(\frac{I_{\mathrm{H}}}{k_{\mathrm{B}}T}\right)^{1/2}\left(\frac{I_{\mathrm{H}}}{h\nu}\right)^3 Z_{\mathrm{i}}^2 a_{\mathrm{B}}^2 \\ \alpha &\equiv \frac{2\pi e^2}{hc} \cong \frac{1}{137.036} \\ a_{\mathrm{B}} &\equiv \frac{h^2}{4\pi e^2 m_{\mathrm{e}}} \cong 0.529\times 10^{-8}\,\mathrm{cm} \\ I_{\mathrm{H}} &\equiv \frac{e^2}{2a_{\mathrm{B}}} \cong 13.6\,\mathrm{eV}\end{aligned} \tag{2.75}$$

where Z_{i} is the effective ion charge. For $h\nu = k_{\mathrm{B}}T = 100\,\mathrm{eV}$ and $n_{\mathrm{e}} = 10^{20}\,\mathrm{cm}^{-3}$ one gets a cross section of $4.34\times 10^{-25}Z_{\mathrm{i}}^2\,(\mathrm{cm}^2)$.

For a hydrogen-like atom the photoelectric cross-section is given by (Zeldovich and Raizer 1966)

$$\sigma_{\mathrm{bf}}^{\mathrm{PE}}(\nu) = \begin{cases} \left(\dfrac{64\pi^4 e m_{\mathrm{e}} Z_{\mathrm{i}}^4}{3\sqrt{3}h^6 c n^5}\right)\dfrac{1}{\nu^3} \approx 7.9\times 10^{-18}\left(\dfrac{n}{Z_{\mathrm{i}}^2}\right)\left(\dfrac{I_{\mathrm{n}}}{h\nu}\right)^3\,[\mathrm{cm}^2] & \text{for } h\nu > I_{\mathrm{n}} \\ 0 & \text{for } h\nu < I_{\mathrm{n}} \end{cases} \tag{2.76}$$

where $I_{\mathrm{n}} \equiv I_{\mathrm{H}}/n^2$ and n is the quantum level of the electron.

Finally, combining equations (2.72), (2.73) and (2.74) with 'the change' (in an equation like (2.64)) given by the total derivative of the intensity with respect to time, one gets the **transport equation**

$$\frac{1}{c}\left(\frac{\partial I_\nu}{\partial t} + c\boldsymbol{\Omega}\cdot\nabla I_\nu\right) = j_\nu\left(1 + \frac{c^2 I_\nu}{2h\nu^3}\right) - \kappa_\nu I_\nu. \tag{2.77}$$

Since the value of j_ν does not depend on the character of the radiation, but is a property of the medium under consideration, one can estimate this quantity in a thermal equilibrium system. In thermal equilibrium the ratio of the spontaneous emission to the absorption is a universal function of the frequency and temperature and is given by (see section 1.1)

$$\begin{aligned}\frac{j_\nu}{\kappa_\nu} &= \frac{2h\nu^3}{c^2}\exp\left(-\frac{h\nu}{k_{\mathrm{B}}T}\right) = I_{\nu\mathfrak{p}}\left[1 - \exp\left(-\frac{h\nu}{k_{\mathrm{B}}T}\right)\right] \\ j_\nu &= \kappa'_\nu I_{\nu\mathfrak{p}} \\ \kappa'_\nu &\equiv \kappa_\nu\left[1 - \exp\left(-\frac{h\nu}{k_{\mathrm{B}}T}\right)\right].\end{aligned} \tag{2.78}$$

Equation (2.78), known as Kirchhoff's law, is based on the general law of detailed balance between emission and absorption of a physical process,

where T is the temperature of the medium. For this equation to be valid, it is not mandatory for the radiation to be in equilibrium with the matter, but it is required that a local temperature can be defined for the atoms and ions of the medium.

Substituting (2.70) into (2.78), one finds that the right-hand side of (2.77) equals $j_\nu - \kappa_\nu\{1 - \exp[-h\nu/(k_B T)]\}I_\nu$. Using again the relations (2.78), the transport equation (2.77) can be rewritten as

$$\frac{\partial I_\nu}{c\,\partial t} + \mathbf{\Omega} \cdot \nabla I_\nu = \kappa'_\nu (I_{\nu \mathrm{p}} - I_\nu). \tag{2.79}$$

Integrating this equation over the solid angle and using the relations (2.69) and (2.71), one gets another equivalent form of the transport equation

$$\frac{\partial U_\nu}{\partial t} + \nabla \cdot \mathbf{S}_\nu = c\kappa'_\nu (U_{\nu \mathrm{p}} - U_\nu). \tag{2.80}$$

This transport equation describes the radiation energy conservation of a frequency ν. In order to use this equation the matter of the medium should be in local thermodynamic equilibrium (LTE).

2.5 Debye Length

In plasma the Coulomb interaction range is reduced due to the **screening effect**. In order to calculate the screening scale length, called the Debye length and denoted by λ_D, imagine a charge Ze at rest at the origin of the coordinates surrounded by plasma electrons. The vector position from the ion is given by $\mathbf{r}$. The plasma system is neutral, i.e. one can look at the ions as a neutralizing background for the plasma electrons having a temperature T_e.

The equation of motion of the electron fluid in this case is given by

$$n_e e\mathbf{E} + \nabla P_e = 0 \tag{2.81}$$

where $\mathbf{E}$ is the electric field and P_e the electronic pressure. Assuming an ideal gas equation of state

$$P_e = n_e k_B T_e \tag{2.82}$$

with a constant electron temperature, T_e, and defining the electrostatic potential φ, $\mathbf{E} = -\nabla\varphi$, one gets from the electron equation of motion (2.81)

$$n_e e \nabla\varphi = k_B T_e \nabla n_e \tag{2.83}$$

the following electron distribution

$$n_e = n_{0e} \exp\left(\frac{e\varphi}{k_B T_e}\right) \tag{2.84}$$

where n_{0e} is initial uniform density of the electrons. The electron potential φ is obtained by solving the Poisson equation (in c.g.s. units):

$$\nabla^2\varphi = -4\pi Ze\delta(\mathbf{r}) + 4\pi e(n_e - n_{0e}) \tag{2.85}$$

where $\delta(\mathbf{r})$ is the Dirac function and it takes care that for $r \to 0$, $\varphi \to Ze/r$.

Substituting (2.84) into (2.85) and expanding the exponential for $e\varphi/(k_B T_e) \ll 1$, one gets the differential equation

$$\left(\nabla^2 - \frac{1}{\lambda_{De}^2}\right)\varphi + 4\pi Ze\,\delta(r) = 0 \tag{2.86}$$

where the electron Debye length λ_{De} is

$$\lambda_{De} = \left(\frac{k_B T_e}{4\pi e^2 n_{0e}}\right)^{1/2} \approx 743\left(\frac{T_e(\text{eV})}{n_{0e}(\text{cm}^{-3})}\right)^{1/2}. \tag{2.87}$$

The solution of equation (2.86) is

$$\varphi = \frac{Ze}{r}\exp\left(-\frac{r}{\lambda_{De}}\right). \tag{2.88}$$

This solution shows that the screening effect, namely the Coulomb interaction $1/r$ law of the electrostatic potential, is changed according to equation (2.88), implying that the effective infinite range of the Coulomb interaction is shortened to a distance of the order of λ_{De}.

At this stage let us compare the characteristic lengths of a plasma medium with the Debye length λ_{De}. In discussing the binary collisions between charged particles, the closest approach was introduced, i.e. (2.32). For an ion with a charge $Z = 1$ one has

$$l_{ca}(\text{cm}) \approx \frac{1.44 \times 10^{-7}}{T(\text{eV})}. \tag{2.89}$$

The cross section for close collisions between charged particles is of the order of πl_{ca}^2; therefore the mean free path l, equation (2.19), is of the order of

$$l(\text{cm}) = \frac{1}{n\sigma} = \frac{1}{n\pi l_{ca}^2} \approx 4.89 \times 10^{12}\frac{T(\text{eV})^2}{n(\text{cm}^{-3})}. \tag{2.90}$$

Taking the scale of length as the average distance between charged particles, $a_0 = n^{-1/3}$, we get

$$\frac{\lambda_{De}}{a_0} \approx 0.29\left(\frac{l_{ca}}{a_0}\right)^{-1/2} \approx 0.50\left(\frac{l}{a_0}\right)^{1/4}. \tag{2.91}$$

For example, for a laser plasma interaction with $n = 10^{21}\,\text{cm}^{-3}$, $T = 100\,\text{eV}$, one gets $a_0 = 10.0 \times 10^{-8}$ cm, $\lambda_D/a_0 = 2.37$, $l_{ca}/a_0 = 0.014$ and $l/a_0 = 490$, so that in this case $l > \lambda_D > a_0 > l_{ca}$.

Another scale length is introduced by the gyro motion of charged particles in the presence of a magnetic field B. The electron gyroradius r_e, known as the **Larmor radius**, is given by

$$r_e = \frac{m_e v_e c}{eB} \approx 2.38 \frac{T_e(\text{eV})^{1/2}}{B(\text{gauss})} \quad [\text{cm}]. \tag{2.92}$$

The evaluation of the right-hand side of (2.92) was done with v_e equal to the thermal velocity. In the above numerical example, the gyroradius r_e is of the order of the mean free path l for a magnetic field of about 0.5 megagauss (MG), a value achieved easily in laser plasma interactions. For r_e to be equal to the Debye length, a magnetic field of 100 MG is needed.

Assume that, in a plasma with dimension L large in comparison to λ_{De}, a local charge fluctuation is created or an external potential is introduced. In this case the created electric fields are shielded for a distance smaller than L. However, within dimensions of the order of λ_{De} the plasma is not neutral and the electric forces do not vanish there, although the plasma is neutral on the large scale, $L \gg \lambda_{De}$. This situation is described by saying that the plasma is **quasineutral**.

The Debye shielding is effective only if the number of electrons in the cloud surrounding the ion is large enough. If on average there are only one or two electrons in a sphere with a radius λ_{De}, known as a **Debye sphere**, then the Debye shielding is not a statistically valid concept. Therefore, defining the number of electrons, N_{De}, in a sphere with a radius λ_{De} by

$$N_{De} = \tfrac{4}{3}\pi n_e \lambda_{De}^3 \tag{2.93}$$

the effective Debye shielding requires $N_{De} \gg 1$. N_{De} is usually called the **plasma parameter**.

For example, in a typical plasma created in laser solid interaction with an electron temperature of 1 keV and an electron density of $10^{21}\,\text{cm}^{-3}$, one has $\lambda_{De} = 7.5 \times 10^{-8}$ cm and $N_{De} = 170$. Note that the typical laser wavelength λ_L, of the order of 1 μm, is about 10^3 larger than λ_{De}.

For plasmas where the ion temperature, T_i, is not zero the ions also contribute to the Debye shielding. The ion fluid equation of motion, similar to equation (2.81), is

$$Zen_i\mathbf{E} - \nabla P_i = 0 \tag{2.94}$$

and the ion pressure, P_i, is given by the ideal gas equation of state

$$P_i = n_i k_B T_i. \tag{2.95}$$

Similarly, to the derivation of (2.84) for the ion distribution; one gets

$$n_i = n_{i0} \exp\left(-\frac{Ze\varphi}{k_B T_i}\right). \tag{2.96}$$

The initial uniform ion density n_{i0} is related to the electron undisturbed density n_{e0} by

$$n_{e0} = Zn_{i0}. \tag{2.97}$$

Instead of (2.86), the Poisson equation (2.85) yields the equation

$$\left(\nabla^2 - \frac{1}{\lambda_{De}^2} - \frac{1}{\lambda_{Di}^2}\right)\varphi + 4\pi Ze\delta(r) = 0 \tag{2.98}$$

where $Ze\varphi/(k_B T_e) \ll 1$ has been assumed and the ion Debye length is defined by

$$\lambda_{Di} = \left(\frac{k_B T_i}{4\pi e^2 n_{i0}}\right)^{1/2}. \tag{2.99}$$

In the solution of the Poisson equation (2.88) one has to substitute λ_{De} with λ_D defined by

$$\frac{1}{\lambda_D^2} = \frac{1}{\lambda_{De}^2} + \frac{1}{\lambda_{Di}^2}. \tag{2.100}$$

2.6 Plasma Oscillations and Electron Plasma Waves

In this section the equations describing the plasma oscillations and the electron plasma waves are derived from a set of very simple equations, based on the hydrodynamic theory without a magnetic field in the plasma. The plasma is assumed to be cold, that is, the plasma temperature is zero, and therefore the thermal velocities of the electrons and the ions vanish. In hydrodynamic theory this means that no pressure forces exist in the plasma. Also, as is usually done with the simplest models, it is assumed that the ions are a stationary background of charge which neutralizes the unperturbed plasma at each point. In this case a perturbation is applied in space only to the electrons and due to this disturbance an electric field is created in the plasma. The question is how the electrons move in this case.

Although the mathematics of this model are quite simple, the solution illustrates a general behaviour of the plasma. For this problem the following Maxwell equation is of interest (in c.g.s.):

$$\nabla \cdot \mathbf{E} = 4\pi\rho_e \tag{2.101}$$

where ρ_e is the electric charge density related to the local current density $\mathbf{j}_e$, given in (2.38). The equation of charge conservation is given by (see appendix A)

$$\nabla \cdot \mathbf{j}_e + \frac{\partial \rho_e}{\partial t} = 0. \tag{2.102}$$

Substituting into (2.102) the density current from (2.38), taking the time derivative of this equation and using (2.101), one gets the following equation for ρ_e:

$$\frac{\partial^2 \rho_e}{\partial t^2} + \left(\frac{4\pi e^2 n_e}{m_e}\right)\rho_e = 0. \tag{2.103}$$

The quantity in the brackets of (2.103) has the dimensions of the square of an angular frequency known as the **plasma frequency** ω_{pe}:

$$\omega_{pe} = \left(\frac{4\pi e^2 n_e}{m_e}\right)^{1/2} \approx 5.64 \times 10^4 \sqrt{n_e} \quad \text{(rad/s)} \tag{2.104}$$

where the electron density n_e is given in cm^{-3}. This result can be easily understood in one dimension by considering a slab of plasma. A perturbation is set up to displace the electrons through a small distance x in a direction normal to the slab, while the positive ions are fixed and at rest (i.e. assuming an infinite mass for the positive ions). This translation of the electrons induces an effective surface charge density $+n_e ex$ on the faces of the original slab and $-n_e ex$ on the faces of the shifted electrons. The charge separation creates a uniform electric field equal to $4\pi e n_e x$ that applies a restoring force on each electron. Newton's law of motion gives a simple harmonic motion of the electrons at the plasma frequency. From this picture one can conclude that the mechanism of plasma oscillations is an expression of the plasma to preserve its electrical neutrality.

Equation (2.103) does not describe a wave, that is, the oscillations do not propagate. In order to get a wave the plasma should have a nonzero temperature. We shall analyse the case where the electrons have a temperature T_e and the ions are at rest, i.e. $T_i = 0$. The two hydrodynamic equations in this case are the mass conservation

$$\frac{\partial n_e}{\partial t} + \nabla \cdot (n_e \mathbf{v}_e) = 0 \tag{2.105}$$

and the momentum conservation

$$m_e n_e \left[\frac{\partial \mathbf{v}_e}{\partial t} + (\mathbf{v}_e \cdot \nabla)\mathbf{v}_e\right] = -e n_e \mathbf{E} - \nabla P_e \tag{2.106}$$

where n_e and $\mathbf{v}_e$ are the electron density and velocity respectively, $-e$ and m_e are the appropriate charge and mass of the electron, $\mathbf{E}$ is the electric field in the plasma and P_e is the electronic pressure. The relation between the pressure and the temperature is known as the equation of state. The ideal gas equation of state for the electrons in the plasma is

$$P_e = n_e k_B T_e. \tag{2.107}$$

Moreover, an isentropic (constant entropy) equation for the ideal gas is assumed with constant specific heats and a constant number of electrons

$$P_e = Cn_e^{\gamma} \tag{2.108}$$

where C is a function of the entropy and is constant for the isentropic process. The adiabatic exponent γ is defined by

$$\gamma = \frac{c_P}{c_V} = \frac{g+2}{g} \tag{2.109}$$

where c_P and c_V are the specific heats at constant pressure and volume respectively and g is the **number of degrees of freedom**. In one dimension $\gamma = 3$ ($g = 1$) while in three dimensions $\gamma = 5/3$ ($g = 3$) for free moving particles. From (2.107) and (2.108) one gets

$$\nabla P_e = P_e \gamma \left(\frac{\nabla n_e}{n_e} \right) = \gamma k_B T_e \nabla n_e. \tag{2.110}$$

Equations (2.106), (2.107) and (2.110) are to be solved together with the Maxwell equation

$$\nabla \cdot \mathbf{E} = 4\pi e(n_i - n_e). \tag{2.111}$$

These equations are nonlinear and therefore it is not easy to get a solution in the general case. However, if all the amplitudes of oscillations are small and higher-order terms of the amplitude factors can be neglected, then the equations can be easily solved by the procedure of **linearization**. We denote the equilibrium part by a subscript 0 and the oscillating amplitudes by the subscript 1:

$$n_e = n_{e0} + n_{e1}, \qquad \mathbf{v}_e = \mathbf{v}_{e0} + \mathbf{v}_{e1}, \qquad \mathbf{E} = \mathbf{E}_0 + \mathbf{E}_1. \tag{2.112}$$

The equilibrium conditions for the simple model discussed here is

$$n_{e0} = n_i = \text{const.}, \qquad \mathbf{v}_{e0} = 0, \qquad \mathbf{E}_0 = 0, \qquad \frac{\partial}{\partial t}\{n_{e0}, \mathbf{v}_{e0}, \mathbf{E}_0\} = 0. \tag{2.113}$$

As already mentioned, the linearization approach requires $(n_{e1}/n_{e0})^2 \ll (n_{e1}/n_{e0})$, $(\mathbf{v}_{e1} \cdot \nabla)\mathbf{v}_{e1} \ll \partial v_{e1}/\partial t$, etc., therefore reducing equations (2.105), (2.106), (2.110) and (2.111) to

$$\begin{aligned} \frac{\partial n_{e1}}{\partial t} + n_{e0} \nabla \cdot \mathbf{v}_{e1} &= 0 \\ m_e \frac{\partial \mathbf{v}_{e1}}{\partial t} &= -e\mathbf{E}_1 - \gamma k_B T_e \nabla n_{e1}, \\ \nabla \cdot \mathbf{E}_1 &= -4\pi e n_{e1}. \end{aligned} \tag{2.114}$$

For further simplicity a one-dimension model is assumed so that all variables are functions of time t and space x, and the adiabatic exponent is $\gamma = 3$.

Substituting a monochromatic wave solution with a **frequency** ω and a **wave number** $k = 2\pi/\lambda$ where λ is the **wavelength**

$$\begin{aligned} n_{e1} &= n \exp[\mathrm{i}(kx - \omega t)] \\ v_{e1} &= v \exp[\mathrm{i}(kx - \omega t)] \\ E_1 &= E \exp[\mathrm{i}(kx - \omega t)] \end{aligned} \tag{2.115}$$

into (2.114), a set of linear algebraic equations is obtained

$$\begin{aligned} \omega n - n_{e0} k v &= 0 \\ -\mathrm{i}\omega m_e v + eE + 3\mathrm{i}k k_B T_e n &= 0 \\ \mathrm{i}kE + 4\pi e n &= 0. \end{aligned} \tag{2.116}$$

The solution of (2.116) is the following **dispersion relation** for the electron plasma wave, known also as a **plasmon**:

$$\omega^2 = \omega_p^2 + 3k^2 v_{th}^2. \tag{2.117}$$

The thermal velocity v_{th} in the one-dimension model is

$$v_{th} = \sqrt{\frac{k_B T_e}{m_e}}. \tag{2.118}$$

The two velocities related to the wave, the phase velocity v_ϕ and the group velocity v_g (the velocity that energy is transferred), defined by

$$v_\phi = \frac{\omega}{k}, \qquad v_g = \frac{\mathrm{d}\omega}{\mathrm{d}k} \tag{2.119}$$

are connected to the thermal velocity by the dispersion relation (2.117)

$$v_g v_\phi = 6 v_{th}^2. \tag{2.120}$$

Laser light can interact directly with the plasma particles and also with the plasma waves (Kruer 1988, Liu and Tripathi 1995). The plasma waves may be of an electromagnetic nature, i.e. **transverse waves**, or of an electrostatic or acoustic nature, i.e. **longitudinal waves**, like the one described above (the plasmon).

In the presence of magnetic fields a large zoo of plasma waves are possible (Stix 1992).

In a plasma state of equilibrium it is important to know what happens if one of the plasma parameters is slightly disturbed. If the disturbance grows, the plasma is unstable, while if the small disturbance decays and disappears, the plasma is in a stable equilibrium. **Plasma instabilities** are classified in two large categories: **macroinstabilities** are associated with a departure from equilibrium of a large part of the plasma system, and **microinstabilities** are

associated with small disturbances in the velocity of the plasma particles, which can increase and cause the plasma to be unstable.

It is worth mentioning some of the colourful descriptive names given to plasma wave instabilities: sausage, kink, banana, firehose, flute, interchange, **two-stream**, tearing, loss-cone, mirror, **ion-acoustic**, **Brillouin**, **Raman**, **parametric**, **two-plasmon**, **Rayleigh–Taylor**, **Richtmyer–Meshkov**, **Kelvin–Helmholtz**, etc. We shall encounter some of these instabilities (in bold letters) in the following chapters.

Every wave has its own dispersion relation, namely a relation between the wave number k and the frequency ω described by some function $F(\omega, k) = 0$. Denoting the plasma wave amplitude for any parameter (such as density, temperature, electric field, magnetic field, pressure, etc.) by ψ, one can write

$$\psi \propto \exp[\mathrm{i}(kx - \omega t)]. \tag{2.121}$$

There are two ways to analyse the different domains of the dispersion relation in ω–k space:

(a) The wave instability in time at a given x. The solution of the dispersion relation $F(\omega, k) = 0$ may yield a complex frequency $\omega = \omega_\mathrm{R} + \mathrm{i}\omega_\mathrm{I}$, where ω_R and ω_I are the real and imaginary values of ω. If $\omega^2 < 0$ then $\omega_\mathrm{I} \neq 0$, and from (2.121) one gets

$$\psi \propto \exp(\omega_\mathrm{I} t). \tag{2.122}$$

For $t \to \infty$ the amplitude ψ goes to infinity for $\omega_\mathrm{I} > 0$, namely the domain in ω–k space where $\omega_\mathrm{I} > 0$ is unstable, and if the wave is 'allowed' to be there by the dispersion relation then we get an instability.

The nonzero imaginary part of the frequency, ω_I, plays an important role in the physical phenomenon of collisionless damping, known also as **Landau damping**. This effect describes the damping of a plasma wave as it propagates away from its point of origination, even though there are no binary collisions in the plasma.

(b) If instead we want to know how a disturbance develops in space for a fixed frequency, then one must solve $F(\omega, k) = 0$ for k in terms of ω. A complex $k = k_\mathrm{R} + \mathrm{i}k_\mathrm{I}$ implies

$$\psi \propto \exp(-k_\mathrm{I} x) \tag{2.123}$$

and for a very large plasma system with $k_\mathrm{I} < 0$ the amplitude ψ goes to infinity for $x \to \infty$, and an instability arises.

2.7 The Dielectric Function

In this section it is shown that the plasma medium can also be described as a dielectric medium with a scalar function ε. In the general case ε is a tensor.

The Maxwell equations are summarized in Appendix A. The plasma is described there as a vacuum with electromagnetic sources, given by the electric charge density ρ_e and electric current density $\mathbf{J}_e$. In Gaussian units the two Maxwell equations that include the sources are

$$\nabla \cdot \mathbf{E} = 4\pi\rho_e, \qquad \nabla \cdot \mathbf{B} = \frac{1}{c}\frac{\partial \mathbf{E}}{\partial t} + \frac{4\pi}{c}\mathbf{J}_e. \tag{2.124}$$

These equations are equivalent to the following two equations of a dielectric medium:

$$\nabla \cdot (\varepsilon \mathbf{E}) = 0, \qquad \nabla \cdot \mathbf{B} = \frac{1}{c}\frac{\partial(\varepsilon \mathbf{E})}{\partial t}. \tag{2.125}$$

The other two Maxwell equations are identical in vacuum and in a dielectric medium. For simplicity we shall prove the equivalence of equations (2.124) and (2.125) for the following sources:

$$\rho_e = -en_e + qn_0, \qquad \mathbf{J}_e = -en_e\mathbf{v}_e. \tag{2.126}$$

Equations (2.126) assume that the ions are stationary and serve as a charge-neutralizing background (i.e. $qn_0 =$ constant) to the electron motion. Moreover, we assume a monochromatic electromagnetic field

$$\mathbf{E}(\mathbf{r}, t) = \mathbf{E}(\mathbf{r})\exp(-i\omega t), \qquad \mathbf{B}(\mathbf{r}, t) = \mathbf{B}(\mathbf{r})\exp(-i\omega t). \tag{2.127}$$

The electron velocity $\mathbf{v}_e$ in the electric current is calculated from Newton's law:

$$\frac{\partial \mathbf{v}_e}{\partial t} + \nu_e\mathbf{v}_e = -\frac{e}{m_e}\mathbf{E}(r)\exp(-i\omega t) \tag{2.128}$$

where ν_e is the electron collision frequency, for example the electron–ion collision frequency. The solution of (2.128) for constant ν_e is

$$\mathbf{v}_e(\mathbf{r}, t) = \frac{-ie\mathbf{E}(\mathbf{r}, t)}{m_e(\omega + i\nu_e)}. \tag{2.129}$$

Substituting this solution into the electric current density (2.126), one gets

$$\mathbf{J}_e(\mathbf{r}, t) = \sigma_E\mathbf{E}(\mathbf{r}, t), \qquad \sigma_E = \frac{i\omega_{pe}^2}{4\pi(\omega + i\nu_e)} \tag{2.130}$$

where σ_E is the (complex) electrical conductivity and ω_{pe} is the plasma angular frequency as defined in (2.104). Substituting $\mathbf{J}_e$ and using $\partial/\partial t = -i\omega$ (note that this relation is correct only for linear equations) into the second equation of (2.124), one gets the second equation of (2.125) if the dielectric function of the plasma medium is defined by

$$\varepsilon = 1 - \frac{\omega_{pe}^2}{\omega(\omega + i\nu)} = 1 + \frac{i4\pi\sigma_E}{\omega}. \tag{2.131}$$

The proof of the equivalence of the first equation of (2.124) and (2.125) is given as

$$\begin{aligned}\nabla\cdot(\varepsilon\mathbf{E}) &= \nabla\cdot\mathbf{E}+\nabla\cdot[(\varepsilon-1)\mathbf{E}] = 4\pi\rho_{\mathrm{e}}+\nabla\cdot[(\varepsilon-1)\mathbf{E}]\\ &= 4\pi\rho_{\mathrm{e}}-\frac{4\pi e^2}{\omega(\omega+\mathrm{i}\nu_{\mathrm{e}})m_{\mathrm{e}}}\nabla\cdot(n_{\mathrm{e}}\mathbf{E}) = 4\pi\rho_{\mathrm{e}}-\frac{4\pi}{\mathrm{i}\omega}\nabla\cdot(-en_{\mathrm{e}}\mathbf{v}_{\mathrm{e}})\\ &= 4\pi\rho_{\mathrm{e}}-\frac{4\pi}{\mathrm{i}\omega}\nabla\cdot\mathbf{J}_{\mathrm{e}} = -\frac{4\pi}{\mathrm{i}\omega}\left(\frac{\partial\rho_{\mathrm{e}}}{\partial t}+\nabla\cdot\mathbf{J}_{\mathrm{e}}\right)=0. \qquad (2.132)\end{aligned}$$

In the third equality, equation (2.131) and $\omega_{\mathrm{pe}}^2\propto n_{\mathrm{e}}$ were used; the fourth equality was obtained with the help of equation (2.129); the next equality uses the current density definition; and the last step is the continuity equation.

In summary, we have seen that a plasma can be described as a dielectric medium with a dielectric function, as given in equation (2.131) (for the electromagnetic sources of (2.126)).

Assuming a spatial dependence $\exp(\mathrm{i}\mathbf{k}\cdot\mathbf{r})$ for the electric and magnetic fields, one gets from Maxwell equations the following dispersion relation for the electromagnetic field:

$$k^2=\frac{\omega^2\varepsilon}{c^2}\Leftrightarrow\omega^2=\omega_{\mathrm{pe}}^2+k^2c^2. \qquad (2.133)$$

In this case, the index of refraction for the electromagnetic wave propagating in the plasma medium is given by

$$\tilde{n}=\sqrt{\varepsilon}=\tilde{n}_{\mathrm{R}}+\mathrm{i}\tilde{n}_{\mathrm{I}}. \qquad (2.134)$$

2.8 The Laser-induced Plasma Medium

The purpose of this section is to define some of the nomenclature used in the following chapters and to get some orders of magnitude for the plasma systems to be discussed. In this book we consider high-power laser irradiation, from $I_{\mathrm{L}}\approx 10^9\,\mathrm{W/cm^2}$ up to $I_{\mathrm{L}}\approx 10^{20}\,\mathrm{W/cm^2}$, with laser pulse duration between $\tau_{\mathrm{L}}\approx 10\,\mathrm{ns}$ and as short as $\tau_{\mathrm{L}}\approx 10\,\mathrm{fs}$. Practically, up to about $I_{\mathrm{L}}\lambda_{\mathrm{L}}^2\approx 10^{16}\,(\mathrm{W/cm^2})\,\mu\mathrm{m}^2$ has been experimentally achieved with the long laser pulse duration ($\tau_{\mathrm{L}}\approx 1\,\mathrm{ns}$), while values as high as $I_{\mathrm{L}}\lambda_{\mathrm{L}}^2\approx 10^{20}\,(\mathrm{W/cm^2})\,\mu\mathrm{m}^2$ have been achieved with the so-called femtosecond lasers (τ_{L} between 10 and 500 fs).

The maximum electric ($E_{\max}$) and magnetic ($B_{\max}$) fields of the laser in vacuum are related to the laser irradiance I_{L} (in Gaussian units) by

$$I_{\mathrm{L}}=\frac{cE_{\max}^2}{8\pi}=\frac{cB_{\max}^2}{8\pi} \qquad (2.135)$$

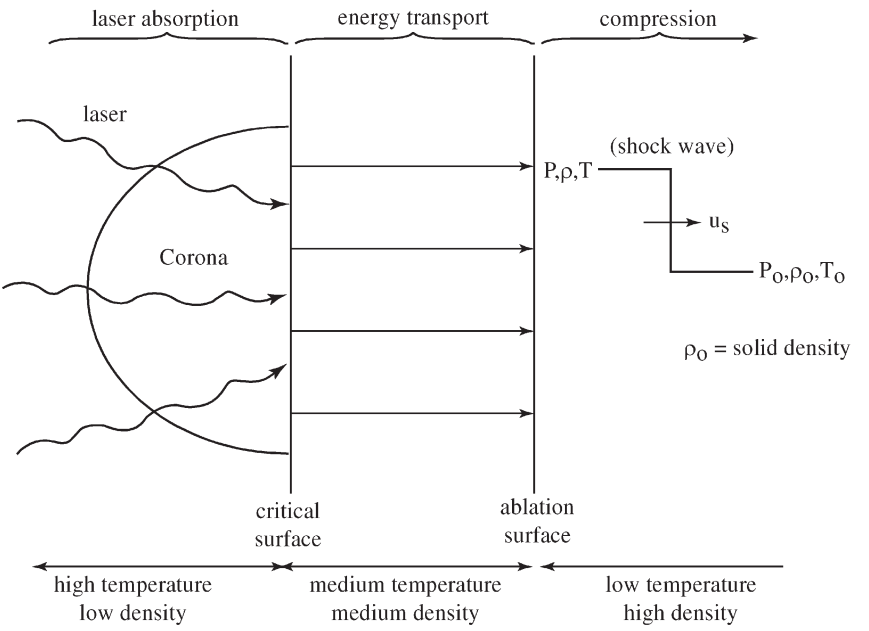

Figure 2.3. A schematic description of laser–plasma interaction.

and in practical units one has

$$E_{\max}\left[\left(\frac{V}{\mathrm{cm}}\right)\right] \cong 2.75\times 10^{9}\left(\frac{I_{\mathrm{L}}}{10^{16}\,\mathrm{W/cm^2}}\right)^{1/2}$$
$$B_{\max}[\mathrm{Gauss}] \cong 9.2\times 10^{6}\left(\frac{I_{\mathrm{L}}}{10^{16}\,\mathrm{W/cm^2}}\right)^{1/2}. \tag{2.136}$$

For the long laser pulses a corona is created, while the laser–plasma system is described schematically in figure 2.3. This figure is relevant for the long laser pulses (typically $\sim$1 ns). As an order of magnitude for low and high densities in figure 2.3, the following values can give an indication about the plasma systems: **absorption domain**: density $<0.01\,\mathrm{g/cm^3}$, temperature $\sim$1000 eV (in energy units); **transport domain**: density between $\sim 0.01\,\mathrm{g/cm^3}$ and the solid target density ρ_0, temperature $\sim$30 eV to 1000 eV; **compression domain**: density $\sim \rho_0$ up to $10\rho_0$, temperature $\sim$1 eV to 30 eV.

The laser propagates up to the critical density n_{c}, about $10^{21}\,\mathrm{cm^{-3}}$ for a laser with a wavelength of 1 μm. Note that the critical density is inversely proportional to the square of the laser wavelength

$$n_{\mathrm{c}}[\mathrm{cm^{-3}}] = 1.1\times 10^{21}\left(\frac{1\,\mu\mathrm{m}}{\lambda_{\mathrm{L}}}\right)^{2}. \tag{2.137}$$

The plasma system from the critical density outwards (towards the laser irradiation) is defined as the **corona**. The electrons in the corona absorb the laser. The absorbed energy is transported from the critical density to the area where the plasma is created, defined as the ablation surface in figure 2.3. The blow-off velocity of the plasma (towards the laser) is about equal to the sound speed c_T (at constant temperature) at the critical density

$$u_{\text{blow-off}}[\text{cm/s}] \approx c_T = \left(\frac{Zk_B T_e}{m_i}\right)^{1/2} \approx 3 \times 10^7 \left[\left(\frac{Z}{A}\right)^{1/2} \left(\frac{T_e}{\text{keV}}\right)^{1/2}\right] \quad (2.138)$$

and the size of the corona is about few times $c_T \tau_L$. Therefore, for the femtosecond laser pulses the corona is extremely small, and practically it does not exist. In this case the laser is absorbed in the **skin depth** δ of the solid target

$$\delta = \frac{c}{\omega_p} \approx 1.68 \times 10^{-6} \left(\frac{10^{23}\,\text{cm}^{-3}}{n_e}\right)^{1/2} \quad [\text{cm}]. \quad (2.139)$$

For high laser irradiance, $I_L \lambda_L^2 > 10^{14}\,(\text{W/cm}^2)\,\mu\text{m}^2$, two (or more) types of electrons are produced: the **'cold' electrons**, with a temperature T_e of the order of 1 keV; and the **'hot' electrons**, with a typical temperature $T_H > 10\,\text{keV}$. Occasionally the situation is more complicated since a local thermodynamic equilibrium for the electrons cannot be defined for the two species of electrons ('cold' and 'hot'). The 'cold' electrons carry energy away from the point of absorption by the diffusion process (thermal conduction). The 'hot' electrons deposit their energy ahead of the **thermal conduction** front induced by the 'cold' electrons, causing 'hot' electron **preheating**. For $I_L \lambda_L^2 > 10^{14}\,(\text{W/cm}^2)\,\mu\text{m}^2$ the **transport of energy** inside the undisturbed target seems to be inhibited in comparison with the classical diffusion process.

There are a few kinds of pressure in laser produced plasma. First, the **light pressure** P_L caused by the direct laser radiation

$$P_L = \frac{I_L}{c}(1 + R) \approx 3.3\,\text{Mbar}\left(\frac{I_L}{10^{16}\,\text{W/cm}^2}\right)(1 + R) \quad (2.140)$$

where R is the laser reflectivity ($0 < R < 1$) and c is the speed of light. One can see that for very high laser irradiance, of the order of $3 \times 10^{18}\,\text{W/cm}^2$, one can get a radiation pressure of 1 Gbar, an extremely high pressure. One of the effects of P_L is to steepen the density gradient near the critical density.

The second kind of pressure in the corona is the thermal pressure of plasma particles: the **'cold' electron pressure** P_e, the **'hot' electron pressure** P_H and the **ion pressure** P_i, associated with the different temperatures T_e, T_H and T_i accordingly. The two electron temperatures are obtained if the electrons in the corona have two distinct velocity distributions. To a good

approximation, the ideal gas equations of state may be used, namely

$$\begin{aligned} P_{\mathrm{e}} &= n_{\mathrm{e}} k_{\mathrm{B}} T_{\mathrm{e}} \approx 1.6\,\mathrm{Mbar}\left(\frac{n_{\mathrm{e}}}{10^{21}\,\mathrm{cm}^{-3}}\right)\left(\frac{T_{\mathrm{e}}}{\mathrm{keV}}\right) \\ P_{\mathrm{H}} &= n_{\mathrm{H}} k_{\mathrm{B}} T_{\mathrm{H}} \\ P_{\mathrm{i}} &= n_{\mathrm{i}} k_{\mathrm{B}} T_{\mathrm{i}}. \end{aligned} \tag{2.141}$$

The third kind of pressure is the **ablation pressure** $\boldsymbol{P_{\mathrm{a}}}$ associated with the flow of heated plasma from the solid target. The ablation pressure drives a **shock wave** into the solid target and causes it to **compress**. The **inhibition** of energy transport and the creation of 'hot' electrons reduce the value of the ablation pressure. A very important feature related to the ablation pressure is related to **hydrodynamic instability**. Since the ablation pressure acts by a lower density (hot plasma) on a higher density (cold plasma), the **Rayleigh–Taylor instability** occurs.

Between the critical and the ablation surfaces the plasma might be **strongly coupled**. In **ideal plasma**, like in the corona, the Coulomb interactions are weak in comparison with the thermal energy. Defining the ratio between the Coulomb and thermal energies by Γ,

$$\begin{aligned} \Gamma &= \frac{\text{Coulomb interaction energy}}{\text{Thermal interaction energy}} \\ &\Rightarrow \left\{ \begin{array}{l} \Gamma > 1 \text{ for strongly coupled plasmas} \\ \Gamma < 1 \text{ for ideal plasmas} \end{array} \right\}. \end{aligned} \tag{2.142}$$

It is convenient to use the mean spacing between particles by the radius of the sphere that each particle occupies:

$$a_{\mathrm{k}} = \left(\frac{3}{4\pi n_{\mathrm{k}}}\right)^{1/3}, \qquad \mathrm{k} = \mathrm{e} \text{ or } \mathrm{i}. \tag{2.143}$$

The strongly coupled parameters, Γ_{ii} for ions (with a charge Ze), Γ_{ee} for electrons and Γ_{ei} for the electron–ion coupling, can be defined by

$$\Gamma_{\mathrm{ii}} = \frac{Z^2 e^2}{a_{\mathrm{i}} k_{\mathrm{B}} T_{\mathrm{i}}}, \qquad \Gamma_{\mathrm{ee}} = \frac{e^2}{a_{\mathrm{e}} k_{\mathrm{B}} T_{\mathrm{e}}}, \qquad \Gamma_{\mathrm{ei}} = \frac{Ze^2}{a_{\mathrm{e}} k_{\mathrm{B}} T_{\mathrm{e}}}. \tag{2.144}$$

In ideal plasma, unlike in strongly coupled plasma, a large number of particles participate in the screening, namely many particles are in the Debye sphere. In a strongly coupled plasma the electrons are degenerate (like in a solid) so that the **Fermi–Dirac distribution** describes the electrons, while the ideal electrons in plasma are described by the **Maxwell distribution**. A good review of strongly coupled plasma can be found in More (1986).

Last but not least, for very high laser irradiances relativistic effects might become important. In the relativistic regime, the relativistic factor γ is related to the quiver energy E_{q} and the quiver velocity v_{q} of the electrons (in the

electromagnetic field of the laser) by

$$\begin{aligned} E_q &= \gamma m_e c^2 = [(\gamma m_e v_q)^2 c^2 + m_e^2 c^4]^{1/2} \\ v_q &= \frac{eE_L}{\gamma m_e \omega_L} \\ \omega_L &= \frac{2\pi\lambda_L}{c}. \end{aligned} \tag{2.145}$$

Using (2.135) we get

$$\begin{aligned} \gamma &= \left(1 + \frac{I_L \lambda_L^2}{\Phi_0}\right)^{1/2} \approx \left(1 + \frac{I_L \lambda_L^2}{1.4 \times 10^{18}\,(\mathrm{W/cm^2})\,\mu\mathrm{m}^2}\right)^{1/2} \\ \Phi_0 &= \left(\frac{\pi}{2}\right)\frac{m_e^2 c^5}{e^2} \quad [\mathrm{erg/s}]. \end{aligned} \tag{2.146}$$

Therefore, the relativistic effects for the electrons are important for $I_L \lambda_L^2 > 10^{18}\,(\mathrm{W/cm^2})\,\mu\mathrm{m}^2$.

Chapter 3

The Three Approaches to Plasma Physics

There are three basic approaches to plasma physics: the **hydrodynamic theory**, the **kinematic theory** and the **particle theory**. The particle theory approach is using the equations of motion for the individual plasma particles, and with the help of particle simulation codes and appropriate averages the plasma physics is analysed. The kinematic theory is based on a set of equations for the distribution functions of the plasma particles, together with Maxwell equations. In the hydrodynamic model the conservation laws of mass, momentum and energy are coupled to Maxwell equations. In addition, for a fluid model, a local thermodynamic equilibrium is assumed and the knowledge of the equations of state (relations between pressure, temperature, energy, entropy, etc.) is mandatory for solving the problem.

3.1 Fluid Equations

3.1.1 Mass conservation

We define $\rho(\mathbf{r}, t)$ as the mass density and $\mathbf{u}(\mathbf{r}, t)$ its velocity for a mass element positioned at $\mathbf{r}$ at time t. Denoting the differential volume and surface vector by $\mathrm{d}V$ and $\mathrm{d}\mathbf{A}$ accordingly, the mass conservation can be written in an integral form by

$$\frac{\partial}{\partial t}\int_{\Gamma} \rho \,\mathrm{d}V + \oint_{S} \rho \mathbf{u} \cdot \mathrm{d}\mathbf{A} = 0. \tag{3.1}$$

The first term, the change of mass in a volume Γ, is balanced by the mass flow across surface S enclosing the volume Γ (the second term). Using Gauss' theorem, one gets for equation (3.1)

$$\frac{\partial}{\partial t}\int_{\Gamma} \rho \,\mathrm{d}V + \int_{\Gamma} \nabla \cdot (\rho \mathbf{u}) \,\mathrm{d}V = 0. \tag{3.2}$$

Since the last relation is true for any arbitrary volume Γ, one obtains the following equation (known also as the **equation of continuity**) which describes the **conservation of mass**:

$$\frac{\partial \rho}{\partial t} + \nabla \cdot (\rho \mathbf{u}) = 0. \tag{3.3}$$

3.1.2 Momentum conservation

It is convenient to consider the frame of reference of a moving volume whose surface encloses a constant amount of fluid. This fluid mass $\rho \, \mathrm{d}V$, called a **'fluid particle'**, has a vector velocity $\mathbf{u}$. $\mathrm{D}/\mathrm{D}t$ describes the change in time (**total derivative**) of a moving fluid volume and is related to the partial time derivative by

$$\frac{\mathrm{D}}{\mathrm{D}t} = \frac{\partial}{\partial t} + \mathbf{u} \cdot \nabla. \tag{3.4}$$

Denoting the **surface forces** by a tensor $\mathbf{f}$, with dimension of (force/area), and the **volume forces** by a vector $\mathbf{F}$, with dimensions of (force/volume), one can write Newton's second law as

$$\int_\Gamma \rho \frac{\mathrm{D}\mathbf{u}}{\mathrm{D}t} \, \mathrm{d}V = \oint_S \mathbf{f} \cdot \, \mathrm{d}\mathbf{A} + \int_\Gamma \mathbf{F} \, \mathrm{d}V. \tag{3.5}$$

Neglecting viscosity, the tensor $\mathbf{f}$ is given by

$$f_{ij} = -P\delta_{ij} \tag{3.6}$$

where P is the pressure and $i, j = 1, 2, 3$ denotes three orthogonal directions in space, e.g. x–y–z directions. The first term on the right-hand side of (3.5) can be transformed into a volume integral by using Gauss' theorem

$$\oint_S \sum_{j=1}^{3} f_{ij} \, \mathrm{d}A_j = -\oint_S P \, \mathrm{d}A_i = -\int_\Gamma \frac{\partial P}{\partial x_i} \, \mathrm{d}V. \tag{3.7}$$

Using this relation in (3.5), one gets

$$\int_\Gamma \rho \frac{\mathrm{D}\mathbf{u}}{\mathrm{D}t} \, \mathrm{d}V = -\int_\Gamma \nabla P \, \mathrm{d}V + \int_\Gamma \mathbf{F} \, \mathrm{d}V. \tag{3.8}$$

Since the last equation is satisfied for any arbitrary volume Γ, the following differential equation is valid:

$$\rho \frac{\mathrm{D}\mathbf{u}}{\mathrm{D}t} = -\nabla P + \mathbf{F}. \tag{3.9}$$

Using (3.4) the **momentum conservation** equation is derived in the form suggested by **Euler**:

$$\rho \frac{\partial \mathbf{u}}{\partial t} + \rho(\mathbf{u} \cdot \nabla)\mathbf{u} = -\nabla P + \mathbf{F}. \tag{3.10}$$

The volume forces **F** are acting on the fluid and differ from one problem to another. For example, the electromagnetic force due to the motion of free charges is equal to (in m.k.s. units)

$$\mathbf{F} = \rho_e \mathbf{E} + \mathbf{J} \times \mathbf{B} \tag{3.11}$$

where **E** and **B** are the electric and magnetic fields respectively, **J** is the sum of the current flow due to the transport of charges and ρ_e is the electric charge density. In a similar way, the polarization force, the magnetization force, the gravitational force or any other force acting on the volume elements can be taken into account.

3.1.3 Energy conservation

The energy conservation (units of [energy/second]) in the frame of reference of the moving fluid element is

$$\int_\Gamma \rho \frac{\mathrm{D}(u^2/2)}{\mathrm{D}t}\,\mathrm{d}V + \int_\Gamma \rho \frac{\mathrm{D}\varepsilon}{\mathrm{D}t}\,\mathrm{d}V = Q_{\mathrm{ext}} + Q_{\mathrm{H}} + W_{\mathrm{F}} + W_{\mathrm{f}}. \tag{3.12}$$

The first term and the second term on the left-hand side of the equation are the rate of change of the **kinetic energy** and the **internal energy** accordingly. ε is the energy of the fluid per unit mass (energy/mass). The increase of the fluid particle energy (left-hand side of the equation) is balanced by the external energy sources Q_{ext}, the heat conduction Q_{H}, the work per unit time done by the volume forces W_{F}, and the surface forces W_{f}. The rate of work done by the surface forces is obtained by integrating $\mathbf{u} \cdot \mathbf{f}$ over the surface of the fluid particle. Neglecting viscosity, one gets

$$W_{\mathrm{f}} = \oint_{\mathrm{S}} \mathbf{u} \cdot \mathbf{f} \cdot\, \mathrm{d}\mathbf{A} = -\oint_{\mathrm{S}} P\mathbf{u} \cdot\, \mathrm{d}\mathbf{A} = -\int_\Gamma \nabla \cdot (P\mathbf{u})\,\mathrm{d}V. \tag{3.13}$$

Again, Gauss' theorem was applied in the last equality. The rate of work done by the volume forces is

$$W_{\mathrm{F}} = \int_\Gamma \mathbf{F} \cdot \mathbf{u}\,\mathrm{d}V. \tag{3.14}$$

The energy entering the fluid particle per unit time by heat conduction is

$$Q_{\mathrm{H}} = \int_\Gamma q_{\mathrm{H}}\,\mathrm{d}V = -\int_\Gamma \nabla \cdot (\kappa \nabla T)\,\mathrm{d}V. \tag{3.15}$$

The rate at which external energy enters the fluid particle depends on the system under consideration. In particular for the electric (Ohm) deposition of energy

$$Q_{\mathrm{ext}} = \int_\Gamma q_{\mathrm{ext}}\,\mathrm{d}V = \int_\Gamma \mathbf{E} \cdot \mathbf{J}\,\mathrm{d}V. \tag{3.16}$$

Substituting (3.13)–(3.16) into (3.12), one gets

$$\rho\frac{\mathrm{D}}{\mathrm{D}t}(\varepsilon+\tfrac{1}{2}u^2)+\nabla\cdot(P\mathbf{u}) = \mathbf{F}\cdot\mathbf{u}-\nabla\cdot(\kappa\nabla T)+\mathbf{E}\cdot\mathbf{J} \quad \left(\frac{\text{energy}}{\text{volume}\times\text{second}}\right). \tag{3.17}$$

Using (3.4), the first term on the left-hand side of (3.17) is

$$\begin{aligned}\rho\frac{\mathrm{D}}{\mathrm{D}t}(\varepsilon+\tfrac{1}{2}u^2) &= \rho\frac{\partial}{\partial t}(\varepsilon+\tfrac{1}{2}u^2)+\rho\mathbf{u}\cdot\nabla(\varepsilon+\tfrac{1}{2}u^2)\\ &= \frac{\partial}{\partial t}(\rho\varepsilon+\tfrac{1}{2}\rho u^2)-(\varepsilon+\tfrac{1}{2}u^2)\frac{\partial\rho}{\partial t}+\nabla\cdot[\rho\mathbf{u}(\varepsilon+\tfrac{1}{2}u^2)]\\ &\quad -(\varepsilon+\tfrac{1}{2}u^2)\nabla\cdot(\rho\mathbf{u})\\ &= \frac{\partial}{\partial t}[\rho(\varepsilon+\tfrac{1}{2}u^2)]+\nabla\cdot[\rho\mathbf{u}(\varepsilon+\tfrac{1}{2}u^2)].\end{aligned} \tag{3.18}$$

The mass conservation (3.3) was used to obtain the last relation. Substituting (3.18) into (3.17), the differential equation that describes the energy conservation is derived in its known form:

$$\frac{\partial}{\partial t}[\rho(\varepsilon+\tfrac{1}{2}u^2)]+\nabla\cdot[\rho\mathbf{u}(\varepsilon+\tfrac{1}{2}u^2)+P\mathbf{u}] = \mathbf{F}\cdot\mathbf{u}-\nabla\cdot(\kappa\nabla T)+\mathbf{E}\cdot\mathbf{J}. \tag{3.19}$$

The differential equations describing a fluid system are: **mass conservation** (3.3), **momentum conservation** (3.10) and the **energy conservation** (3.19). For these equations one has to define initial conditions and boundary values. Moreover, it is necessary to know the relations between ρ–P–T–ε, known as the equations of state. Furthermore, the knowledge of the transport coefficients such as κ is required. Last but not least, for a plasma system the fluid equations are coupled to the Maxwell equations (given in Appendix A) since the volume forces $\mathbf{F}$ and also the pressure may be a function of the electromagnetic fields. For the external energy deposition we took the Ohmic heating term, $\mathbf{E}\cdot\mathbf{J}$; however, for a laser plasma system this source of energy might need a 'special treatment'.

The fluid equations for the laser-induced plasma system are given below. We consider the general case where the electron temperature T_e is not equal to the ion temperature T_i. The ideal equations of state are taken separately for the ion fluid and the electron fluid, i.e.

$$\begin{aligned}P_\mathrm{e} &= n_\mathrm{e}k_\mathrm{B}T_\mathrm{e}, \qquad P_\mathrm{i} = n_\mathrm{i}k_\mathrm{B}T_\mathrm{i}\\ E_\mathrm{e} &= \tfrac{3}{2}n_\mathrm{e}k_\mathrm{B}T_\mathrm{e}, \qquad E_\mathrm{i} = \tfrac{3}{2}n_\mathrm{i}k_\mathrm{B}T_\mathrm{i}\end{aligned} \tag{3.20}$$

where m_e, m_i and v_e, v_i are the masses and the velocities of the electron and the ion accordingly, and n_j and E_j (j = e or i) are the particle and the energy densities. The fluid equations (3.3), (3.10) and (3.19) for the electrons and the

ions are obtained by using the definitions of the densities $\rho_j = m_j n_j$ and $\varepsilon_j = E_j/\rho_j$ for $j = \mathrm{e}$ or i for the ideal equations of state.

Moreover, the following assumptions are used in deriving the two fluid energy equations:

(a) The electron fluid is coupled to the ion fluid through the electron–ion collisions described by the term $\gamma(T_\mathrm{e} - T_\mathrm{i})$.
(b) The volume force is given only by the electric field in the plasma $\mathbf{E}$.
(c) As usually happens the external source term (energy/(volume · time)), denoted by q_L, contributes only to the electron fluid, i.e. the electrons absorb the laser energy.
(d) Since the ion is much heavier than the electron only the electrons do the heat transport.
(e) Ideal gas equations of state were taken for both fluids (see (3.20)).

The two temperature fluid equations are

$$\frac{\partial n_\mathrm{e}}{\partial t} + \nabla \cdot (n_\mathrm{e}\mathbf{v}_\mathrm{e}) = 0, \qquad \frac{\partial n_\mathrm{i}}{\partial t} + \nabla \cdot (n_\mathrm{i}\mathbf{v}_\mathrm{i}) = 0 \tag{3.21}$$

$$\begin{aligned} m_\mathrm{e} n_\mathrm{e}\left(\frac{\partial \mathbf{v}_\mathrm{e}}{\partial t} + (\mathbf{v}_\mathrm{e}\cdot\nabla)\mathbf{v}_\mathrm{e}\right) &= -\nabla P_\mathrm{e} - e n_\mathrm{e}\mathbf{E} \\ m_\mathrm{i} n_\mathrm{i}\left(\frac{\partial \mathbf{v}_\mathrm{i}}{\partial t} + (\mathbf{v}_\mathrm{i}\cdot\nabla)\mathbf{v}_\mathrm{i}\right) &= -\nabla P_\mathrm{i} + Z e n_\mathrm{i}\mathbf{E} \end{aligned} \tag{3.22}$$

$$\begin{aligned} &\frac{\partial}{\partial t}\left[n_\mathrm{e}\left(\frac{3}{2}k_\mathrm{B}T_\mathrm{e} + \frac{m_\mathrm{e}v_\mathrm{e}^2}{2}\right)\right] + \nabla\cdot\left[n_\mathrm{e}\mathbf{v}_\mathrm{e}\left(\frac{5}{2}k_\mathrm{B}T_\mathrm{e} + \frac{m_\mathrm{e}v_\mathrm{e}^2}{2}\right)\right] \\ &\quad = q_\mathrm{L} - \gamma(T_\mathrm{e} - T_\mathrm{i}) - e n_\mathrm{e}\mathbf{E}\cdot\mathbf{v}_\mathrm{e} - \nabla\cdot(\kappa\nabla T_\mathrm{e}) \\ &\frac{\partial}{\partial t}\left[n_\mathrm{i}\left(\frac{3}{2}k_\mathrm{B}T_\mathrm{i} + \frac{m_\mathrm{i}v_\mathrm{i}^2}{2}\right)\right] + \nabla\cdot\left[n_\mathrm{i}\mathbf{v}_\mathrm{i}\left(\frac{5}{2}k_\mathrm{B}T_\mathrm{i} + \frac{m_\mathrm{i}v_\mathrm{i}^2}{2}\right)\right] \\ &\quad = \gamma(T_\mathrm{e} - T_\mathrm{i}) + e n_\mathrm{i}\mathbf{E}\cdot\mathbf{v}_\mathrm{i}. \end{aligned} \tag{3.23}$$

Equations (3.21) describe the mass conservation, (3.22) the momentum conservation and (3.23) the energy conservation. It is worth mentioning that both m.k.s. and c.g.s. units can be used (in a consistent way) in equations (3.23). If a magnetic field is introduced, e.g. in the momentum equation, then $\mathbf{E} \to \mathbf{E} + \mathbf{v}\times\mathbf{B}$ in m.k.s. and $\mathbf{E} \to \mathbf{E} + \mathbf{v}\times\mathbf{B}/c$ in c.g.s. units. The fluid equations are coupled to the electromagnetic Maxwell equations.

3.2 Eulerian and Lagrangian Coordinates

The fluid equation variables (velocity, pressure, energy, entropy, etc.), described by functions of space coordinates and time, are called the **Eulerian coordinates**. In contrast to the Eulerian coordinates, which determine the

fluid variables at a given point in space for all times, the **Lagrangian coordinates** describe in time the fluid variables of a given fluid particle. Mathematically the time derivative in Lagrangian coordinates is equal to the total derivative $\mathrm{D}/\mathrm{D}t$, which is related to the usual Eulerian time derivative $\partial/\partial t$ by equation (3.4) (∇ is the usual Eulerian space derivative). The Lagrangian coordinates are useful in general for problems with plane, cylindrical or spherical symmetry. The fluid particle is described either by its position at time $t = 0$ or by the total mass from the first particle to the particle under consideration. In a one-dimensional plane geometry with **Eulerian coordinates** (x, t), the **Lagrangian coordinate** a or m is defined by

$$m \equiv \rho_0 a = \int_{x_1}^{x} \rho \, \mathrm{d}x, \qquad \frac{\partial}{\partial x} = \rho \frac{\partial}{\partial m} = \frac{\rho}{\rho_0} \frac{\partial}{\partial a}. \tag{3.24}$$

The following notation is used here: u is the fluid velocity, ρ is the density related to the specific volume $V = 1/\rho$, m is the mass of a column of fluid of unit cross-section in plane geometry and P is the pressure. The first fluid particle is located at x_1 and the fluid particle under consideration is located at x. The initial density is defined by $\rho_0 = \rho(x, t = 0)$. For the following Eulerian mass and momentum conservation (Newton second law) the appropriate Lagrangian equations are given:

$$\begin{aligned} &\text{Eulerian:} && \frac{\partial \rho}{\partial t} + \frac{\partial}{\partial x}(\rho u) = 0, && \frac{\partial u}{\partial t} + u \frac{\partial u}{\partial x} = -\frac{1}{\rho} \frac{\partial P}{\partial x} \\ &\text{Lagrangian:} && \frac{\partial V}{\partial t} = \frac{\partial u}{\partial m}, && \frac{\partial u}{\partial t} = -\frac{\partial P}{\partial m}. \end{aligned} \tag{3.25}$$

Note that in one dimension with a planar geometry, m has the dimensions of (mass/area). The x coordinate does not enter explicitly in the Lagrangian equations and therefore the Eulerian position x of the particle is obtained from the Lagrangian solution $V(m, t)$:

$$x(m, t) = \int_0^m V(m, t) \, \mathrm{d}m + x_1. \tag{3.26}$$

We end this section with a set of equations (a model) in a Lagrangian coordinate describing the laser–plasma interactions with two temperatures, the electron temperature T_e and the ion temperature T_i, where $T_\mathrm{e} \neq T_\mathrm{i}$. The density of the fluid is $\rho = n_\mathrm{i} m_\mathrm{i}$ (since $n_\mathrm{e} m_\mathrm{e} \ll n_\mathrm{i} m_\mathrm{i}$) and its velocity is u. The two temperatures $(T_\mathrm{e}, T_\mathrm{i})$, the two appropriate pressures $(P_\mathrm{e}, P_\mathrm{i})$ and their associated energies $(E_\mathrm{e}, E_\mathrm{i})$ (energy/mass) are related by the equations of state, e.g. (3.20). In this model we have one equation for the mass conservation, one equation for the momentum conservation and two energy equations, one for electrons and one for ions. The electrons absorb the laser energy and they also transport the heat energy. The two physical quantities describing these phenomena are the I_L and the heat energy flux I_e, both with dimension of (energy/(area · time)). There is a coupling

energy term between the ions and the electrons proportional to $T_e - T_i$. The fluid equations of this model, in Lagrangian coordinates, are

$$\begin{aligned} \frac{\partial V}{\partial t} - \frac{\partial u}{\partial m} &= 0 \\ \frac{\partial u}{\partial t} + \frac{\partial (P_e + P_i)}{\partial m} &= 0 \\ \frac{\partial E_e}{\partial t} + P_e \frac{\partial u}{\partial m} &= \frac{\partial I_L}{\partial m} - \frac{\partial I_e}{\partial m} - g(T_e - T_i) \\ \frac{\partial E_i}{\partial t} + P_i \frac{\partial u}{\partial m} &= g(T_e - T_i). \end{aligned} \tag{3.27}$$

The dimensions of the above equations are: (energy/(mass · second)) for the energy equations, (length/second^2) for the momentum equation and (length^3/(mass · second)) for the continuity equation. The energy equations in (3.23) have the dimension of (energy/(volume · second)) and therefore have to be divided by the density ρ in order to obtain the energy equations in (3.27). For example, the values of the electron ion energy coupling in (3.23) and (3.27) are related by $g = \gamma/\rho$.

We end this section with a generalization of equations (3.25) for problems with plane, cylindrical or spherical symmetry. One fluid is assumed where the body forces, heat conduction and energy sources are absent. In the following equations, r denotes the spatial coordinate: $r = x$ for plane symmetry, $r^2 = x^2 + y^2$ for cylindrical symmetry, and $r^2 = x^2 + y^2 + z^2$ for the spherical symmetry, and $u = \partial r/\partial t$.

$$\begin{aligned} &\text{Eulerian:} \quad \frac{\partial \rho}{\partial t} + u\frac{\partial \rho}{\partial r} + \frac{\rho}{r^{k-1}}\frac{\partial (r^{k-1}u)}{\partial r} = 0, \quad \frac{\partial u}{\partial t} + u\frac{\partial u}{\partial r} + \frac{1}{\rho}\frac{\partial P}{\partial \rho} = 0 \\ &\text{Lagrangian:} \quad \frac{\partial V}{\partial t} - \frac{\partial (r^{k-1}u)}{\partial m} = 0, \qquad \frac{\partial u}{\partial t} + r^{k-1}\frac{\partial P}{\partial m} = 0. \end{aligned} \tag{3.28}$$

Equations (3.28) describe the mass conservation and the momentum conservation for the following cases: $k = 1$ for plane symmetry; $k = 2$ for cylindrical symmetry; and $k = 3$ for spherical symmetry.

The energy equation for the above fluid is

$$\begin{aligned} &\text{Eulerian:} \quad \frac{\partial E}{\partial t} + u\frac{\partial E}{\partial r} + \frac{P}{\rho r^{k-1}}\frac{\partial (r^{k-1}u)}{\partial r} = 0 \\ &\text{Lagrangian:} \quad \frac{\partial E}{\partial t} + P\frac{\partial V}{\partial t} = 0 \end{aligned} \tag{3.29}$$

and as usual, the knowledge of the equations of state $P = P(E, \rho)$ is needed in order to solve the problem.

3.3 'Femtosecond' Laser Pulses

The word 'femtosecond' stands for very short laser pulse duration or, more accurately, the laser–target interaction is during a time so short that the hydrodynamics are not important. For example, for a 50 fs laser pulse the plasma motion is about $\Delta r \approx c_s \Delta t \approx 10^6\,(\mathrm{cm/s}) \cdot 5 \times 10^{-14}\,(\mathrm{s}) = 5\,\mathrm{A}$, which is much smaller than the laser penetration (skin) depth $\delta \approx c/\omega_p \approx 100\,\mathrm{A}$ (where $1\,\mathrm{A} = 10^{-8}\,\mathrm{cm}$). c_s and c are the speed of sound and the speed of light accordingly and ω_p is the plasma frequency for a solid density. It is conceivable to assume in this case that during the laser–target interaction the solid target density does not change and the flow velocity is negligible. Therefore, during this short time the system is described mainly by the energy equations.

In a metal irradiated by fs-laser pulse the temperature T_e of the electrons in the conduction band and the temperature T_i of the ion lattice (i.e. of the phonons) can differ by orders of magnitude. The reason for this effect is that the electrons absorb the laser energy and the relaxation time for electron–ion collision is much larger than the laser pulse duration. This happens because the heat capacity of electrons is significantly smaller than the heat capacity of the lattice. In the following we assume that T_e and T_i are well defined. If the laser spot (x–y direction on the target) dimension is much larger than the energy deposition (z direction) depth, then one has a one-dimensional problem and the energy equation (3.19) for the electrons and the ions are (Anisimov *et al*. 1974)

$$\begin{aligned} C_e(T_e)\frac{\partial T_e}{\partial t} &= \frac{\partial}{\partial z}\left(\kappa(T_e)\frac{\partial T_e}{\partial z}\right) - U(T_e, T_i) + Q(z,t) \\ C_i(T_i)\frac{\partial T_i}{\partial t} &= U(T_e, T_i). \end{aligned} \tag{3.30}$$

The dimension of these equations in c.g.s. units is (erg/(cm^3 s)). C_e and C_i are the electron and ion heat capacities (dimension (erg/(cm^3 K))), κ is the electron heat conductivity (dimension (erg/(cm s))), U is the energy transfer rate from electrons to ions and can also be written as

$$U = \gamma(T_e - T_i) \tag{3.31}$$

and Q is the laser energy deposition rate that can be approximated by

$$Q(z,t) = AI_L(t)\frac{2}{\delta}\exp\left(-\frac{2z}{\delta}\right) \tag{3.32}$$

where AI_L is the absorbed laser irradiance (dimension erg/(cm^2 s)), A is the absorption coefficient and δ is the skin depth.

C_e and C_i are derived from knowledge of the equations of state (Eliezer *et al*. 1986):

$$\begin{aligned} C_e(\text{low}) &= \frac{\pi^2 n_e k_B^2 T_e}{2E_F} \quad \text{for } k_B T_e \ll E_F \\ C_e(\text{high}) &= 1.5 k_B n_e \qquad \text{for } k_B T_e \gg E_F \end{aligned} \tag{3.33}$$

where E_F is the Fermi energy (equals about 11.7 eV for aluminium), k_B is the Boltzmann constant and n_e is electron density (equals about 1.8×10^{23} cm^{-3} for solid aluminium). C_i can be approximated by the Dulong–Petit law

$$C_i = 3k_B n_i \tag{3.34}$$

where the ion density satisfies $n_i = n_e/Z$, and Z is the number of ionized electrons, including the number of electrons in the conduction band ($Z = 3$ for aluminium).

In order to calculate U and κ as functions of T_e and T_i, one has to take into account the electron–phonon interactions, as explained in section 5.7.

3.4 Boltzmann–Vlasov Equations

The fluid theory given in previous sections, which is considered to be the simplest description of a plasma system, is a good approximation for many phenomena in laser–plasma interaction. However, the fluid model is not always adequate. All the variables (including the fluid velocity) in the fluid equations are functions of time and position, and each species in an LTE plasma has a Maxwellian distribution of the velocities everywhere. Physical quantities such as temperature and pressure can be defined only in local thermal equilibrium (LTE). Systems that are not in LTE cannot be described by fluid equations. For example, in a laser plasma corona LTE is not always satisfied, and in this case the fluid model is not suitable.

3.4.1 Liouville's theorem

For a very large number of interacting particles, as in a plasma system, a statistical description is required. In this case the starting point is the **phase space** of the particles: q_k, p_k, $k = 1, \ldots, K$, where the q_k are the coordinates for all the degrees of freedom and the p_k are the corresponding momenta. N identical particles with s degrees of freedom for each one satisfy $K = sN$. The fundamental physical quantity is the **probability density** $F(q_k, p_k, t)$, where $F\,\mathrm{d}q_1, \ldots, \mathrm{d}q_K\,\mathrm{d}p_1, \ldots, \mathrm{d}p_K$ is the probability of finding the system at time t in the phase space domain $(q_1, q_1 + \mathrm{d}q_1), (p_1, p_1 + \mathrm{d}p_1), \ldots, (q_K, q_K + \mathrm{d}q_K), (p_K, p_K + \mathrm{d}p_K)$. By analogy with the continuity equation in

the fluid theory, the conservation equation for the probability density is

$$\frac{\partial F}{\partial t}+\sum_{k=1}^{K}\frac{\partial(Fq_{k,t})}{\partial q_k}+\sum_{k=1}^{K}\frac{\partial(Fp_{k,t})}{\partial p_k}=0 \tag{3.35}$$

where $q_{k,t}$ and $p_{k,t}$ are the time derivative of q_k and p_k accordingly. The system is described by a **Hamiltonian** $H(q_k,p_k,t)$, satisfying the following equations of motion:

$$q_{k,t}=\frac{\partial H}{\partial p_k},\qquad p_{k,t}=-\frac{\partial H}{\partial q_k}. \tag{3.36}$$

From these equations one gets $\partial q_{k,t}/\partial q_k=-\partial p_{k,t}/\partial p_k$ $(=\partial^2 H/\partial p_k\,\partial q_k)$. Using this result in (3.35), the **Liouville theorem** is obtained:

$$\frac{\partial F}{\partial t}+\sum_{k=1}^{K}q_{k,t}\frac{\partial F}{\partial q_k}+\sum_{k=1}^{K}p_{k,t}\frac{\partial F}{\partial p_k}\equiv\frac{\mathrm{D}F}{\mathrm{D}t}=0 \tag{3.37}$$

where $\mathrm{D}/\mathrm{D}t$ is the time derivative in the frame of the appropriate phase space element (i.e. moving with the phase space element). From the Liouville theorem one can conclude that F is invariant (i.e. $F=$ constant) on a phase space trajectory of the system. From this theorem the basic assumption of statistical mechanics is justified, namely that equal volumes of phase space have equal *a priori* probability. However, for non-LTE processes a general solution is equivalent to solving the equations of motion for all the particles (i.e. solving (3.36)), a task that is usually impossible (and if possible it is useless) for an extremely large number of particles, e.g. of the order of Avogadro's number ($\sim 10^{23}$). In this case approximations of the Liouville equation are required.

3.4.2 Vlasov equation

For identical particles the phase space of a single particle is considered instead of the phase space of all the particles. We use the Cartesian coordinates $[\mathbf{x}=(x,y,z),\mathbf{v}=(v_x,v_y,v_z)]$, where $\mathbf{x}$ and $\mathbf{v}$ are respectively the position and the velocity of a particle. A function $f(\mathbf{x},\mathbf{v},t)$ is defined to replace the probability density of the whole phase space F. In this approach, $f\,\mathrm{d}^3x\,\mathrm{d}^3v$ is equal to the number of particles in the domain $[(\mathbf{x},\mathbf{x}+\mathrm{d}\mathbf{x}),(\mathbf{v},\mathbf{v}+\mathrm{d}\mathbf{v})]$. For the electron and ion particles in the plasma, two (or more, if there are many species of ions) distribution functions f_j, for $j=$ e or i, are defined to describe the electrons and the ions accordingly. In analogy with the Liouville theorem (3.37) the distribution functions f_j satisfy the equations

$$\frac{\partial f_j}{\partial t}+(\mathbf{v}\cdot\nabla)f_j+(\mathbf{a}\cdot\nabla_{\mathrm{V}})f_j=0 \tag{3.38}$$

$$\nabla=\left(\frac{\partial}{\partial x},\frac{\partial}{\partial y},\frac{\partial}{\partial z}\right)\equiv\frac{\partial}{\partial\mathbf{x}},\qquad \nabla_{\mathrm{V}}=\left(\frac{\partial}{\partial v_x},\frac{\partial}{\partial v_y},\frac{\partial}{\partial v_z}\right)\equiv\frac{\partial}{\partial\mathbf{v}} \tag{3.39}$$

where **v** is the velocity and **a** is the acceleration. For an electromagnetic field the equations of motion are (in c.g.s.)

$$\mathbf{v} = \frac{\mathrm{d}\mathbf{x}}{\mathrm{d}t}, \qquad \mathbf{a} = \frac{\mathrm{d}\mathbf{v}}{\mathrm{d}t} = \frac{q}{m}\left(\mathbf{E} + \frac{\mathbf{v}\times\mathbf{B}}{c}\right) \tag{3.40}$$

where q and m are the charge and mass of e or i. Equations (3.38) coupled to Maxwell equations are known as the **Vlasov equations**. The statistical content of the Vlasov equations is expressed by assuming that f_j is a smooth function (i.e. differentiable) describing an average quantity over a phase space volume $\mathrm{d}^3x\,\mathrm{d}^3v$ containing a large number of particles. The electromagnetic fields, **E** and **B**, are also 'local' smooth averaged quantities. In this picture f_j is regarded as a density of a continuous 'fluid' in phase space. The force acting on any plasma particle, describing the effect of all the other particles, is assumed to be a continuous and slowly varying function of space. This is a good approximation only if the collective effect is larger than the 'direct' collisions with nearby particles; therefore, the Vlasov equations are considered to be '**collisionless**'. If the 'direct' collisions are important then the Vlasov equations (3.38) are replaced by the Boltzmann equations.

3.4.3 Boltzmann equation

Taking short-range collisions into account, equations (3.38) are replaced by

$$\frac{\partial f_j}{\partial t} + (\mathbf{v}\cdot\nabla)f_j + (\mathbf{a}\cdot\nabla_{\mathrm{V}})f_j = \left(\frac{\partial f_j}{\partial t}\right)_{\mathrm{c}}. \tag{3.41}$$

The collisions are described formally by the term $(\partial f_j/\partial t)_{\mathrm{c}}$. One of the simplest models for the collision term, known as the BGK (Bhatnagar, Gross and Krook 1956) model, is given by

$$\left(\frac{\partial f_j}{\partial t}\right)_{\mathrm{c}} = \sum_k \nu_{jk}(f_j - f_{jk}) \tag{3.42}$$

where f_j is assumed to be a Maxwellian distribution in velocity space and ν_{jk} is an empirical collision frequency taken as a constant in the simplest model. $-\nu_{jk}f_{jk}$ represents the rate of loss of particles in the phase space under consideration described by f_j, while $\nu_{jk}f_j$ is the rate of gain. ν_{jk} is proportional to the particle density n_k, therefore $\nu_{jk} = C_{jk}n_k$ and $C_{jk} = C_{kj}$.

The BGK model is appropriate for collisions between charged and neutral particles. However, this model is not a good approximation for collisions between charged particles (the Coulomb interactions) since the collisions are not predominantly binary. In the Coulomb interactions, the cumulative effect of many small collisions between particles at large distances is more important than a nearby binary collision. The major

contribution to $(\partial f_j/\partial t)_c$ comes from electron and ion collisions within the Debye sphere (radius λ_D) and not from the collision of nearby particles (at the distance $n_j^{-1/3}$), for plasmas where $\lambda_D \gg n_j^{-1/3}$. Suppressing the subscript j of the distribution function, the following Fokker–Planck collision term is appropriate (see section 9.4):

$$\left(\frac{\partial f}{\partial t}\right)_c = \sum_{i=1}^{3} \frac{\partial}{\partial v_i}\left[-F_i f + \frac{1}{2}\sum_{k=1}^{3}\frac{\partial}{\partial v_k}(D_{ik} f)\right] \tag{3.43}$$

where F_i and D_{ik} are the friction and diffusion 'coefficients' respectively. The subscripts i and k denote the x–y–z components in Cartesian coordinates. In general, these 'coefficients' are not only functions of $(\mathbf{x}, \mathbf{v}, t)$ but also of f itself. For simplicity it can be assumed that

$$F_i = -\nu(v_i - u_i), \qquad D_{ik} = D\delta_{ik} \tag{3.44}$$

where $\mathbf{u}$ is the local drift velocity, D is the diffusion coefficient and ν is a constant describing the effective collision frequency.

3.4.4 The moment equations

In this section we suppress the subscript j on the distribution f_j; however, it is understood that the following equations and relations are obtained for each species of the plasma particles (e.g. electrons and ions). The moment $\langle Q \rangle$ is defined by

$$\langle Q \rangle = \int Q(v) f(x, v, t)\, \mathrm{d}^3 v \tag{3.45}$$

where the distribution function $f(\mathbf{x}, \mathbf{v}, t)$ is given by the Boltzmann equation, which we rewrite in the following way (equations (3.40) and (3.41)):

$$\frac{\partial f}{\partial t} + \mathbf{v}\cdot\frac{\partial f}{\partial \mathbf{x}} + \frac{q}{m}\left(\mathbf{E} + \frac{\mathbf{v}\times\mathbf{B}}{c}\right)\cdot\frac{\partial f}{\partial \mathbf{v}} = \left(\frac{\partial f}{\partial t}\right)_c. \tag{3.46}$$

For example, for $Q = 1$, $\mathbf{v}$ and v^2, the moments correspond to the macroscopic quantities of density, momentum and energy respectively. For $Q =$ equation (3.46), the zero moment, one has to average the equation over the velocity in order to obtain the continuity equation (mass conservation). The integral over $\mathrm{d}^3 v$ of the first term of (3.46) gives $\partial n/\partial t$. The integral of the second term gives the space derivative of the integral of $\mathbf{v}f$. One can see that the integral of the third term vanishes after integration by parts and using the property that f goes to zero as v tends to infinity. Last but not least, the integral of $(\partial f/\partial t)_c$ vanishes since the collisions do not change the number of particles. This last statement is not correct if there is ionization

or some other process, e.g. fusion, such that the collision can change the number of particles of the species under consideration. Thus, the zero moment of the Boltzmann equation yields the following continuity equation (mass conservation):

$$\frac{\partial n}{\partial t} + \frac{\partial}{\partial \mathbf{x}} \cdot (n\mathbf{u}) = 0 \tag{3.47}$$

where n is the particle density and $\mathbf{u}$ is the average velocity defined by

$$n = \int f(\mathbf{x}, \mathbf{v}, t)\, \mathrm{d}^3 v, \qquad n\mathbf{u} = \int \mathbf{v} f(\mathbf{x}, \mathbf{v}, t)\, \mathrm{d}^3 v\,. \tag{3.48}$$

Taking the first moment of the Boltzmann equation (3.46), one gets the momentum equation. The first term gives

$$\int \mathrm{d}^3 v \mathbf{v} \frac{\partial f}{\partial t} = \frac{\partial}{\partial t}(n\mathbf{u}). \tag{3.49}$$

The integral of the second term yields

$$\begin{aligned} \int \mathrm{d}^3 v \mathbf{v} \cdot \frac{\partial f}{\partial x} &= \frac{\partial}{\partial \mathbf{x}} \cdot \int \mathrm{d}^3 v \mathbf{v} \mathbf{v} f \equiv \frac{\partial}{\partial \mathbf{x}} \cdot \int \mathrm{d}^3 v (\mathbf{v} - \mathbf{u} + \mathbf{u})(\mathbf{v} - \mathbf{u} + \mathbf{u}) f \\ &= \frac{\partial}{\partial \mathbf{x}} \cdot \int \mathrm{d}^3 v (\mathbf{v} - \mathbf{u})(\mathbf{v} - \mathbf{u}) f + \frac{\partial}{\partial \mathbf{x}} \cdot \int \mathrm{d}^3 v \mathbf{u} \mathbf{u} f \\ &\equiv \frac{\partial}{\partial \mathbf{x}} \cdot \frac{\Pi}{m} + \frac{\partial}{\partial \mathbf{x}} \cdot n\mathbf{u}\mathbf{u} \end{aligned} \tag{3.50}$$

where Π (with components Π_{jk}) is the pressure tensor, and we have used (3.48) to calculate the $(v - u)f$ integral. The integral of the third term gives, after integrating by parts,

$$\int \mathrm{d}^3 v \mathbf{v} \frac{q}{m} \left(\mathbf{E} + \frac{\mathbf{u} \times \mathbf{B}}{c} \right) \cdot \frac{\partial f}{\partial \mathbf{v}} = -\frac{nq}{m} \left(\mathbf{E} + \frac{\mathbf{u} \times \mathbf{B}}{c} \right). \tag{3.51}$$

Using the following procedure:

(a) assuming the pressure to be isotropic, $\Pi_{jk} = P\delta_{jk}$,
(b) defining

$$\int \mathrm{d}^3 v \mathbf{v} \left(\frac{\partial f}{\partial t} \right)_{\mathrm{c}} = \left(\frac{\partial (n\mathbf{u})}{\partial t} \right)_{\mathrm{c}} \tag{3.52}$$

(c) collecting (3.49)–(3.52),
(d) using the continuity equation, and
(e) introducing the subscripts e and i for electrons and ions,

the following momentum conservation equations are derived (a generalization of the momentum equations (3.22)):

$$
\begin{aligned}
n_e \frac{\partial \mathbf{u}_e}{\partial t} + n_e \mathbf{u}_e \cdot \frac{\partial \mathbf{u}_e}{\partial \mathbf{x}} &= -\frac{e n_e}{m_e}\left(\mathbf{E} + \frac{\mathbf{u}_e \times \mathbf{B}}{c}\right) - \frac{1}{m_e}\frac{\partial P_e}{\partial \mathbf{x}} + \left(\frac{\partial (n_e \mathbf{u}_e)}{\partial t}\right)_{i \to e} \\
n_i \frac{\partial \mathbf{u}_i}{\partial t} + n_i \mathbf{u}_i \cdot \frac{\partial \mathbf{u}_i}{\partial \mathbf{x}} &= \frac{Z e n_i}{m_i}\left(\mathbf{E} + \frac{\mathbf{u}_i \times \mathbf{B}}{c}\right) - \frac{1}{m_i}\frac{\partial P_i}{\partial \mathbf{x}} + \left(\frac{\partial (n_i \mathbf{u}_i)}{\partial t}\right)_{e \to i} \\
\left(\frac{\partial (n_i \mathbf{u}_i)}{\partial t}\right)_{e \to i} &= -\left(\frac{\partial (n_e \mathbf{u}_e)}{\partial t}\right)_{i \to e}
\end{aligned}
\tag{3.53}
$$

where Ze is the ion charge and $-e$ the electron charge. The last equation of (3.53) represents the conservation of the momentum exchange by collisions between electrons and ions. The momentum equations for electrons and ions can be combined together to yield an equation for one species by using the following relations:

$$
\begin{aligned}
\mathbf{U} &= \frac{n_i m_i \mathbf{u}_i + n_e m_e \mathbf{u}_e}{n_i m_i + n_e m_e} && \text{[centre of mass velocity]} \\
\rho &= n_i m_i + n_e m_e \cong n_i m_i && \text{[mass density]} \\
\mathbf{J} &= e(Z n_i \mathbf{u}_i - n_e \mathbf{u}_e) && \text{[current density]} \\
\rho_e &= e(Z n_i - n_e) && \text{[charge density].}
\end{aligned}
\tag{3.54}
$$

In a similar way as above, by taking the moment of $Q = v^2$ times the Boltzmann equation (3.46), the following energy equation is derived:

$$
\frac{\partial}{\partial t}(n\langle v^2 \rangle) + \frac{\partial}{\partial \mathbf{x}} \cdot (n\langle v^2 \mathbf{v} \rangle) - \frac{2nq}{m}\mathbf{E} \cdot \mathbf{u} = \left(\frac{\partial}{\partial t}(n\langle v^2 \rangle)\right)_c \tag{3.55}
$$

where $\langle v^2 \rangle$ and $\langle v^2 \mathbf{v} \rangle$ are defined in (3.45) for $Q = v^2$ and $Q = v^2 \mathbf{v}$ respectively.

In taking the moment of $Q = v^k$ times the Boltzmann equation (3.46), a v^{k+1} term is introduced. For $k = 0$ the mean velocity appears (a $k = 1$ term), for $k = 1$ the pressure tensor (a $k = 2$ term) is introduced, for $k = 2$ a tensor of rank 3 appears (i.e. a $k = 3$ term) describing the energy flow, etc. Therefore, the moment equations are an infinite set of equations and a truncation is required in order to solve these equations. For example, by using the equations of motion, defining the pressure and assuming an isotropic process, then the energy equation is no longer required and the moment equations are truncated in such a way that the mass and momentum fluid equations are practically derived. If the diffusion and the heat transport are important, then the moment equations have to be truncated after the energy equation is considered. In this case a knowledge of the transport

coefficients is necessary besides the full equations of state. However, the equations of state are well defined only in local thermodynamic equilibrium, so if LTE is not satisfied other ideas of truncation are required.

3.5 Particle Simulations

The particle theory approach uses the equations of motion for the individual plasma particles, and with the help of particle simulation codes (some known as 'particle in cell' (PIC) codes) the plasma physics is analysed. In this approach the plasma is described by electrons and ions moving under the influence of the electric and magnetic fields due to their own charge, and of the laser fields (Dawson 1962, Hockney and Eastwood 1981, Adam 1982, Birdsall and Langdon 1985, Evans 1986, Kruer 1988, Pert 1989). The equations of motion for the particles are

$$\begin{aligned}
&\frac{\mathrm{d}\mathbf{r}_j}{\mathrm{d}t} = \mathbf{v}_j \\
&\frac{\mathrm{d}(\mathbf{v}_j)}{\mathrm{d}t} = \frac{q_j}{m_j}\left(\mathbf{E} + \frac{\mathbf{v}_j \times \mathbf{B}}{c}\right) \\
&\oplus \text{ Maxwell equations, where} \\
&\rho_\mathrm{e} = \sum_j \mathrm{q}_j \delta(\mathbf{r}_j - \mathbf{r}) \\
&\mathbf{J} = \sum_j q_j \mathbf{v}_j \delta(\mathbf{r}_j - \rho)
\end{aligned} \tag{3.56}$$

where q_j, m_j, $\mathbf{r}_j$, $\mathbf{v}_j$ are respectively the charge, mass, position and velocity for a particle denoted by index j. c is the speed of light, δ is the Dirac delta function, and $\mathbf{E}$, $\mathbf{B}$, ρ_e and $\mathbf{J}$ are the electric field, the magnetic field, the charge density and the electric current respectively.

Defining the positions and velocities of the particles at a given time, the electric charge and current are determined on a spatial grid. Using these electric charges and currents in the Maxwell equations, the self-consistent electric and magnetic fields are calculated. The electric and magnetic fields are inserted into Lorentz's equation of motion (the first two equations of (3.56)) to calculate the new positions and velocities of the particles, where they are used to calculate the electric charge and current, and so on. The basic cycle of a particle code is described schematically by

$$\{\mathbf{r}_j, \mathbf{v}_j\} \rightarrow (\rho_\mathrm{e}, \mathbf{J}) \rightarrow (\mathbf{E}, \mathbf{B}) \rightarrow \{\mathbf{r}_j, \mathbf{v}_j\} \rightarrow \text{etc.} \tag{3.57}$$

The time step of this procedure should be small enough in order to resolve the shortest time scale in the problem. This time scale, Δt, in many cases is

determined by the plasma frequency

$$\Delta t \approx \frac{2\pi}{\omega_p} = \left(\frac{\pi m_e}{e^2 n}\right)^{1/2} \tag{3.58}$$

where e and m_e are the charge and the mass of the electron accordingly and n is the particle density.

The spatial grid Δx should be small enough to resolve the collective behaviour of the plasma. This scale length is of the order of the electron Debye length λ_{De} rather than the smaller-scale length determined by direct particle collisions. The large-angle collisions can be ignored in collisionless plasmas, i.e. when the number of particles in a Debye sphere is much larger than one. If the plasma is not collisionless then the particle simulation approach is not realistic since it is extremely difficult to use a grid with a dimension smaller than the spacing between the particles.

For practical reasons, computer simulation of plasma using particle codes is limited to $\sim 10^6$ particles $= N_C$ (equal also to the number of cells). In a real plasma there are $N = nV$ particles, where n is the particle density and V the plasma volume. For some typical laboratory laser–plasma systems one has $n \approx 10^{20}\,\mathrm{cm}^{-3}$ and $V \approx 10^{-5}\,\mathrm{cm}^3$, implying $N \approx 10^{15}$. Therefore, each simulation particle represents a large number of real electrons and ions. In the above example the simulation mass and charge of 'a particle' is 10^9 times that of an electron (or an ion). However, in the simulation it is necessary to keep the mass-to-charge ratio of the 'electron particle' equal to e/m_e (and similarly for the ions), although the mass of each electron can be equal to $10^9 m_e$. Moreover, the plasma frequency in the simulation must be equal to the real plasma frequency. Therefore, from equation (3.58), if the charge and mass of the 'electron' is $10^9 e$ and $10^9 m_e$ accordingly, then the electron density in the simulation is $10^{-9} n_e$. In a particle in cell (PIC) simulation,

$$q_e = \left(\frac{N}{N_C}\right)e, \qquad m_e = \left(\frac{N}{N_C}\right)m_e, \qquad n_e = \left(\frac{N}{N_C}\right)^{-1} n_e. \tag{3.59}$$

Let us consider now a one-dimensional problem. In this case the particles are surfaces of charge in the y–z plane (sheets) and the ions are positioned at a grid defined by $x_k = k\Delta x$ $(k = 1, 2, 3, \ldots)$.

For the one-dimensional problem, Maxwell equations are reduced to the Poisson equation

$$\frac{\partial E}{\partial x} = 4\pi\rho_e. \tag{3.60}$$

The grid spacing Δx is chosen to be uniform and the indices k, j and n denote the cell, the particle and the order of the numerical time step respectively. The finite-difference approach to the Poisson equation (3.60) gives

$$E^n_{k+1/2} = E^n_{k-1/2} + 4\pi\rho^n_k \Delta x, \qquad E^n_k = \tfrac{1}{2}(E^n_{k+1/2} + E^n_{k-1/2}). \tag{3.61}$$

The second equation of (3.61) gives the electric field on the grid points. The electric field E_j at the particle position x_j and the electric charge density ρ_k at the grid position x_k ($= k\Delta x$) are given by interpolation with a shape function $\delta_k(\mathrm{x}_j)$:

$$E_j^n = \sum_k E_k^n \delta_k(x_j^n), \qquad \rho_k^n = \sum_k n_e e \delta_k(x_j^n). \tag{3.62}$$

Two shape functions that are popular in these simulations are the 'nearest grid point' model

$$\delta_k(x_j) = \begin{cases} 1 & \text{if } |x_j - x_k| < \Delta x/2 \\ 0 & \text{otherwise} \end{cases} \tag{3.63}$$

and the 'cloud in cell' model

$$\delta_k(x_j) = \begin{cases} 1 - |x_j - x_k|/\Delta x & \text{if } |x_j - x_k|/\Delta x < 1 \\ 0 & \text{otherwise.} \end{cases} \tag{3.64}$$

The position and velocity of the particles are advanced in time by using Newton's law (3.56):

$$v_j^{n+1/2} = v_j^{n-1/2} + \frac{eE_j^n \Delta t}{m_e}, \qquad x_j^{n+1} = x_j^n + v_j^{n+1/2}\Delta t. \tag{3.65}$$

The numerical equations (3.61), (3.62), (3.63) (or (3.64)) and (3.65) are started by defining the grid and by giving the particles a random Gaussian velocity distribution (or an average zero velocity with a mean squared velocity equal to the thermal velocity). The numerical stability of these equations requires a time step $\Delta t < 2/\omega_{\mathrm{p}}$, while a reasonable time accuracy for the plasma wave motion implies $\omega_{\mathrm{p}}\Delta t < 0.2$. The high-frequency spatial modes cannot be distinguished because of the finite grid spacing, i.e. the Fourier components (of x_j) k_j and $k_j + 2\pi/\Delta x$ are identical (aliasing). Therefore, it is necessary to damp the high-frequency spatial modes. This is done by Landau damping $k_j\lambda_{\mathrm{De}} > 0.2$ and choosing a grid spacing $\Delta x < \lambda_{\mathrm{De}}$.

Table 3.1. The dimensionality and the appropriate variables for the particle simulations.

Dimension	Particle position	Particle velocity	Electric field	Magnetic field	Notes
3D	$\mathbf{r} = (x, y, z)$	$\mathbf{v} = (v_x, v_y, v_z)$	$\mathbf{E} = (E_x, E_y, E_z)$	$\mathbf{B} = (B_x, B_y, B_z)$	–
2.5D	$\mathbf{r} = (x, y, 0)$	$\mathbf{v} = (v_x, v_y, v_z)$	$\mathbf{E} = (E_x, E_y, E_z)$	$\mathbf{B} = (B_x, B_y, B_z)$	$\partial/\partial z = 0$
2D	$\mathbf{r} = (x, y, 0)$	$\mathbf{v} = (v_x, v_y, 0)$	$\mathbf{E} = (E_x, E_y, 0)$	$\mathbf{B} = (B_x, B_y, B_z)$	$\partial/\partial z = 0$
1.5D	$\mathbf{r} = (x, 0, 0)$	$\mathbf{v} = (v_x, v_y, 0)$	$\mathbf{E} = (E_x, E_y, 0)$	$\mathbf{B} = (0, 0, B_z)$	$\partial/\partial z = 0$, $\partial/\partial y = 0$
1D	$\mathbf{r} = (x, 0, 0)$	$\mathbf{v} = (v_x, 0, 0)$	$\mathbf{E} = (E_x, 0, 0)$	$\mathbf{B} = (0, 0, 0)$	$\partial/\partial z = 0$, $\partial/\partial y = 0$

The general problem described by equations (3.56) is three-dimensional; however, since the computer programs in this case are very large and complex, simpler systems with lower dimensionality are used, as described in table 3.1.

The step time for solving these numerical equations is very small ($\sim 10^{-15}$ s) and therefore the particle theory simulation can be done only for periods of time much shorter than the typical laser plasma lifetime. Moreover, this approach is suitable only for plasmas where the ratio between the plasma dimension (L) and the Debye length (λ_{De}) is not very large. Nevertheless, it turns out that the particle computer simulation of plasma is a very useful and enlightening tool to study and understand nonlinear plasma effects.

Chapter 4

The Ponderomotive Force

For normal laser light incidence on plasma the **ponderomotive force** $\mathbf{f}_p$ per unit volume is given by (the proof of this equation is given at the end of section 4.1 and in section 4.2)

$$\mathbf{f}_p = -\frac{\omega_p^2}{16\pi\omega_L^2}\nabla E_s^2 = -\frac{\omega_p^2}{8\pi\omega_L^2}\nabla\langle E^2\rangle \tag{4.1}$$

where $\omega_p^2 = 4\pi n_e e^2/m_e$ is the plasma frequency, ω_L is the angular laser frequency, $\mathbf{E}_s$ is the space-dependent electric field of $\mathbf{E}$, given by

$$\mathbf{E} = \mathbf{E}_s(\mathbf{r})\cos\omega_L t \tag{4.2}$$

and the time average over one laser oscillating period (i.e. over one wavelength) is denoted by $\langle\ \rangle$. The ponderomotive force is a **nonlinear force** where a high-frequency electromagnetic laser field induces a slow time scale force. This force is involved in many physical phenomena, such as:

(a) momentum transfer to the target (Hora 1969, Arad *et al.* 1980, Hora 1981);
(b) self-focusing and filamentation of the laser beam (Kaw *et al.* 1973, Max 1976);
(c) plasma profiles density changes such as the formation of cavitons and solitons (Morales and Lee 1977, Mulser and van Kessel 1977, Evely and Morales 1978);
(d) parametric instabilities (Chen 1977);
(e) second harmonic generation (Jackel *et al.* 1981);
(f) magnetic field generation (Stamper and Tidman 1973, Lehner 1994, Horovitz *et al.* 1997, Horovitz *et al.* 1998).

4.1 The Landau–Lifshitz Ponderomotive Force

More than 150 years ago the ponderomotive force, $\mathbf{f}_{Kelv}$, was introduced by Kelvin in order to describe the force applied by a static electric field $\mathbf{E}$ on a

dielectric medium with a polarization **p**:

$$\mathbf{f}_{\mathrm{Kelv}} = (\mathbf{p} \cdot \nabla)\mathbf{E}. \tag{4.3}$$

One hundred and twenty years ago Helmholtz (Helmholtz 1881) used thermodynamics to obtain the ponderomotive force, $\mathbf{f}_{\mathrm{Helm}}$, exerted on a dielectric material with permittivity ε and density ρ:

$$\mathbf{f}_{\mathrm{Helm}} = -\frac{E^2 \nabla \varepsilon}{8\pi} + \nabla\left(\frac{\rho E^2}{8\pi}\frac{\partial \varepsilon}{\partial \rho}\right). \tag{4.4}$$

Equations (4.3) and (4.4) are given in c.g.s. units. At the turn of the last century it was realized that these two equations are wrong (Pavlov 1979, Kentwell and Jones 1987). Landau and Lifshitz (Landau and Lifshitz 1975) achieved the correct expression only in the 1950s. For a homogeneous medium, without free electric charges and current ($\mathbf{J} = 0, \rho_{\mathrm{e}} = 0$) with time-independent dielectric function ε and magnetic permeability μ, the two Maxwell equations relevant for this discussion are

$$\nabla \times \mathbf{E} = -\frac{\mu}{c}\frac{\partial \mathbf{H}}{\partial t}, \qquad \nabla \times \mathbf{H} = \frac{\varepsilon}{c}\frac{\partial \mathbf{E}}{\partial t}. \tag{4.5}$$

Using these Maxwell equations, Landau and Lifshitz calculated the force per unit volume **f** from the derivative of the **stress tensor** σ_{jk}:

$$f_j = \sum_{k=1}^{3} \frac{\partial \sigma_{jk}}{\partial x_k} - \frac{1}{4\pi c}\frac{\partial (\mathbf{E} \times \mathbf{H})_j}{\partial t} \quad j \text{ and } k = (x, y, z). \tag{4.6}$$

The last term on the right-hand side of (4.6) is the rate of change of the electromagnetic field momentum per unit volume. This term is subtracted from the derivative of the stress tensor since σ_{jk} includes the momentum of both the medium and the electromagnetic field, while **f** is the force per unit volume on the medium only. The stress tensor for the above medium is

$$\begin{aligned}
\sigma_{jk} &= -P_0(\rho, T)\delta_{jk} + \sigma_{jk}^{\mathrm{E}} + \sigma_{jk}^{\mathrm{H}} \\
\sigma_{jk}^{\mathrm{E}} &= -\frac{E^2}{8\pi}\left[\varepsilon - \rho\left(\frac{\partial \varepsilon}{\partial \rho}\right)_{\mathrm{T}}\right]\delta_{jk} + \frac{\varepsilon E_j E_k}{4\pi} \\
\sigma_{jk}^{\mathrm{H}} &= -\frac{H^2}{8\pi}\left[\mu - \rho\left(\frac{\partial \mu}{\partial \rho}\right)_{\mathrm{T}}\right]\delta_{jk} + \frac{\mu H_j H_k}{4\pi}
\end{aligned} \tag{4.7}$$

where $P_0(\rho, T)$ is the pressure as a function of density ρ and temperature T that exists in the medium in the absence of the electromagnetic fields $(\mathbf{E}, \mathbf{H})$. Substituting equations (4.7) into equation (4.6) and using the Maxwell equations (4.5), one gets the total force acting on the medium **f** per unit

volume:

$$\begin{aligned}\mathbf{f} &= -\nabla P_0 + \mathbf{f}_\mathrm{p}\\ \mathbf{f}_\mathrm{p} &= -\frac{E^2\nabla\varepsilon}{8\pi} + \nabla\left[\rho\left(\frac{\partial\varepsilon}{\partial\rho}\right)_\mathrm{T}\left(\frac{E^2}{8\pi}\right)\right] - \frac{H^2\nabla\mu}{8\pi}\\ &\quad +\nabla\left[\rho\left(\frac{\partial\mu}{\partial\rho}\right)_\mathrm{T}\left(\frac{H^2}{8\pi}\right)\right] + \frac{(\varepsilon\mu-1)}{4\pi c}\frac{\partial(\mathbf{E}\times\mathbf{H})}{\partial t}\end{aligned} \tag{4.8}$$

where $\mathbf{f}_\mathrm{p}$ is the correct (Landau and Lifshitz) ponderomotive force acting on the medium defined above.

Assuming a dielectric medium with $\mu = 1$, relevant for plasma physics, and an ε as in a plasma without collisions,

$$\varepsilon = 1 - \frac{\omega_\mathrm{p}^2}{\omega_\mathrm{L}^2} = 1 - \frac{\rho(\mathbf{r})}{\rho_\mathrm{c}} \tag{4.9}$$

then $\rho\,\partial\varepsilon/\partial\rho = -\rho/\rho_\mathrm{c} = \varepsilon - 1$ and equation (4.8) yields the ponderomotive force given in equation (4.1). In general, for a dielectric medium satisfying

$$\varepsilon = \alpha + \beta\rho \tag{4.10}$$

one gets that the first term on the right-hand side of (4.8) is equal to $(\varepsilon - \alpha)\nabla(E^2/8\pi)$. The second term on the right-hand side of (4.8) vanishes for $\mu = 1$. Regarding the third term on the right-hand side of (4.8), we assume an electric field given by (4.2), and using the Maxwell equation (4.5) the magnetic field is

$$\mathbf{H} = -\left(\frac{c}{\mu\omega_\mathrm{L}}\right)(\nabla\times\mathbf{E}_\mathrm{s})\sin\omega_\mathrm{L}t \equiv \mathbf{H}_\mathrm{s}\sin\omega_\mathrm{L}t. \tag{4.11}$$

Thus, the third term on the right-hand side of (4.8) is zero because its time average over a laser period time scale is proportional to

$$\left\langle \frac{\partial}{\partial t}(\cos\omega_\mathrm{L}t\sin\omega_\mathrm{L}t)\right\rangle = \omega_\mathrm{L}(-\langle\sin^2\omega_\mathrm{L}t\rangle + \langle\cos^2\omega_\mathrm{L}t\rangle) = 0 \tag{4.12}$$

where the relations $\langle\sin^2\omega_\mathrm{L}t\rangle = \langle\cos^2\omega_\mathrm{L}t\rangle = \frac{1}{2}$ have been used. Therefore, in a dielectric medium satisfying equations (4.9) or (4.10), the ponderomotive force is

$$\begin{aligned}\mathbf{f}_\mathrm{p} &= -\frac{\omega_\mathrm{p}^2}{\omega_\mathrm{L}^2}\left[\frac{\nabla E_\mathrm{s}^2}{16\pi}\right] \quad \text{for } \varepsilon \text{ given by (4.9)}\\ \mathbf{f}_\mathrm{p} &= (\varepsilon-\alpha)\left[\frac{\nabla E_\mathrm{s}^2}{16\pi}\right] \quad \text{for } \varepsilon \text{ given by (4.10).}\end{aligned} \tag{4.13}$$

4.2 The Single-Particle Approach to Ponderomotive Force in Plasma

The ponderomotive force per unit volume is related to the gradient of the radiation pressure P_L. If the laser propagates in vacuum with irradiance I_L and hits a sharp boundary, then the radiation pressure is

$$P_L = \frac{I_L}{c}(1+R) \tag{4.14}$$

where R is the reflection from the boundary. However, for a laser in inhomogeneous plasma this relation is meaningless, since the electromagnetic field in the plasma cannot be determined only from knowledge of I_L, and therefore the light pressure is not known. In this case, knowledge of the electromagnetic fields in the plasma is required in order to calculate the radiation pressure, related directly to the ponderomotive force per unit volume.

In this section we calculate the ponderomotive force, analysing the motion of a single particle in a given electromagnetic field in the plasma (Schmidt 1966, Chen 1974). Assuming a monochromatic electric field as in (4.2) and a plasma with a magnetic permeability $\mu = 1$, we have (see (4.11)) in c.g.s. units ($\mathbf{H} = \mathbf{B}$, etc.)

$$\begin{aligned} \mathbf{E}(\mathbf{r},t) &= \mathbf{E}_s(\mathbf{r})\cos\omega t \\ \mathbf{B}(\mathbf{r},t) &= \mathbf{B}_s(\mathbf{r})\sin\omega t = -\frac{c}{\omega}\nabla\times\mathbf{E}_s(\mathbf{r})\sin\omega t. \end{aligned} \tag{4.15}$$

The electromagnetic angular frequency ω in the plasma medium, as derived from the dispersion relation, can differ from the laser frequency ω_L in vacuum. The equation of motion (Lorentz equation) for an electron moving in these fields is

$$m_e\frac{d\mathbf{v}}{dt} = -e\left(\mathbf{E}_s\cos\omega t + \frac{\mathbf{v}}{c}\times\mathbf{B}_s\sin\omega t\right), \qquad \mathbf{v} = \frac{d\mathbf{r}}{dt}. \tag{4.16}$$

For non-relativistic electrons the $\mathbf{v}\times\mathbf{B}/c$ term is smaller than the $\mathbf{E}$ term; therefore, to first order ($\mathbf{v} = \mathbf{v}_1$, $\mathbf{r} = \mathbf{r}_1$), the electron oscillates in the direction of $\mathbf{E}_s$ and in this case one has to solve

$$m_e\frac{d\mathbf{v}_1}{dt} + e\mathbf{E}_s(\mathbf{r}_0)\cos\omega t = 0, \qquad \mathbf{v}_1 = \frac{d\mathbf{r}_1}{dt}. \tag{4.17}$$

The solution of these equations is

$$\mathbf{v}_1 = -\frac{e\mathbf{E}_s(\mathbf{r}_0)\sin\omega t}{m_e\omega}, \qquad \mathbf{r}_1 = \frac{e\mathbf{E}_s(\mathbf{r}_0)\cos\omega t}{m_e\omega^2}. \tag{4.18}$$

To second order one has to consider

$$\mathbf{v} = \mathbf{v}_1 + \mathbf{v}_2, \qquad \mathbf{E}_s = \mathbf{E}_s(\mathbf{r}_0) + (\mathbf{r}_1\cdot\nabla)\mathbf{E}_s(\mathbf{r}=\mathbf{r}_0), \qquad \mathbf{B}_s = \mathbf{B}_s(\mathbf{r}_0). \tag{4.19}$$

Substituting (4.17) and (4.19) into (4.16), we get the second order equation:

$$m_e \frac{d\mathbf{v}_2}{dt} = -e\left[(\mathbf{r}_1 \cdot \nabla)\mathbf{E}_s(\mathbf{r}_0)\cos\omega t + \frac{\mathbf{v}_1 \times \mathbf{B}_s(\mathbf{r}_0)\sin\omega t}{c}\right]. \tag{4.20}$$

The nonlinear force $\mathbf{F}_{NL}$ acting on an electron is given by substituting (4.18) and (4.15) into (4.20) and averaging over time (note that $\langle \sin^2 \omega t\rangle = \langle \cos^2 \omega t\rangle = \frac{1}{2}$ and $\langle \sin \omega t \cos \omega t\rangle = 0$):

$$\mathbf{F}_{NL} = m_e\left\langle \frac{d\mathbf{v}_2}{dt} \right\rangle = -\frac{e^2}{2m_e\omega^2}[(\mathbf{E}_s \cdot \nabla)\mathbf{E}_s + \mathbf{E}_s \times (\nabla \times \mathbf{E}_s)]. \tag{4.21}$$

The first term on the right-hand side of (4.21) is the force which causes the electron to move in a linear trajectory, while the second term on the right-hand side is the $\mathbf{E} \times \mathbf{B}$ force acting on the electron and distorts the linear motion into a figure 8 trajectory. Using the identity

$$\mathbf{E}_s \times (\nabla \times \mathbf{E}_s) = (\nabla \mathbf{E}_s) \cdot \mathbf{E}_s - (\mathbf{E}_s \cdot \nabla)\mathbf{E}_s = \tfrac{1}{2}\nabla \cdot \mathbf{E}_s^2 - (\mathbf{E}_s \cdot \nabla)\mathbf{E}_s \tag{4.22}$$

in (4.21) and multiplying with the electron density n_e to get the ponderomotive force per unit volume, the following equation is obtained:

$$\mathbf{f}_p = n_e\mathbf{F}_{NL} = -\frac{n_e e^2}{4m_e\omega^2}\nabla \mathbf{E}_s^2 = -\frac{\omega_p^2}{16\pi\omega^2}\nabla \mathbf{E}_s^2. \tag{4.23}$$

This equation is identical to (4.1).

From equation (4.23) one can see that the ratio of the ponderomotive force exerted on the ions, $\mathbf{f}_{pi}$, to that applied on the electrons, $\mathbf{f}_{pe} \equiv \mathbf{f}_p$, is equal to $f_{pi}/f_{pe} = m_e/m_i$, where m_i is the ion mass; therefore, the ponderomotive force on the ions is negligible. However, the ponderomotive force exerted on the electrons is transmitted to the ions by the electric fields in the plasma. Due to the force described in (4.23) the electrons are separated from the ions, and an electric charge separation is created in the plasma which induces an extra electric field $\mathbf{E}_{cs}$ between the ion and the electrons, so that

$$\mathbf{f}_e = \mathbf{f}_p - en_e\mathbf{E}_{cs}, \qquad \mathbf{f}_i = q_i n_i \mathbf{E}_{cs}, \qquad q_i n_i = en_e \Rightarrow \mathbf{f}_e + \mathbf{f}_i = \mathbf{f}_p \tag{4.24}$$

where $\mathbf{f}_e$ and $\mathbf{f}_i$ are the forces (due to the above interactions) applied on the electron and ion fluids accordingly, and the last equation in (4.24) is due to the charge neutrality of the plasma, which is correct on a scale length larger than the above charge separation length (or in any case larger than the Debye length).

4.3 The Effect of Ponderomotive Force on Wave Dispersion

4.3.1 The electron wave dispersion

The dispersion relation for electron plasma waves was derived in chapter 2 (section 2.6) without taking into account the ponderomotive force. We

shall repeat that derivation with an added ponderomotive force. It is assumed that:

(a) the problem is one-dimensional;
(b) the ions are immobile;
(c) the ponderomotive force in (4.23) is denoted by f; and
(d) the charge separation electric field is E.

The electron is assumed to be an ideal gas where the oscillations are adiabatic, so that the electron pressure P_e and the electron density n_e are related through the following equations of state:

$$P_e n_e^{-3} = \text{const.}, \qquad P_e = n_e k_B T_e. \tag{4.25}$$

The electron continuity and momentum equations are

$$\frac{\partial n_e}{\partial t} + \frac{\partial (n_e v)}{\partial x} = 0, \qquad m_e n_e \left(\frac{\partial v}{\partial t} + v \frac{\partial v}{\partial x} \right) = -\frac{\partial P_e}{\partial x} - e n_e E + n_e f \tag{4.26}$$

and the appropriate Maxwell equations are reduced to the following Gauss equation (sometimes referred to as Poisson's equation):

$$\frac{\partial E}{\partial x} = -4\pi e (n_e - n_0). \tag{4.27}$$

From equation (4.25) the pressure derivative is calculated, $\partial P_e / \partial x = 3(P_e/n_e)\partial n_e / \partial x = 3 k_B T_e \partial n_e / \partial x$. Equations (4.26) and (4.27) are solved by using the linearization procedure about the steady state $n_e = n_0$, $v_0 = 0$, $E_0 = 0$. Assuming first-order variations of the form $n_e = n_0 + n_1$, $v = v_1$ and $E = E_1$, where

$$\left.\begin{matrix} n_1 \\ v_1 \\ E_1 \end{matrix}\right\} \propto \exp[\mathrm{i}(kx - \omega t)] \tag{4.28}$$

the following first-order equations are derived:

$$\begin{aligned} -\mathrm{i}\omega n_1 + \mathrm{i} n_0 k v_1 &= 0 \\ (\mathrm{i}3 k_B T_e k - f) n_1 - \mathrm{i} m_e n_0 \omega v_1 + e n_0 E_1 &= 0 \\ 4\pi e n_1 + \mathrm{i} k E_1 &= 0. \end{aligned} \tag{4.29}$$

Note that for a constant density n_0, one has $f = 0$ (since in this case $\nabla E_s^2 = 0$); therefore, the ponderomotive force in this notation is $(n_e - n_0)f$. A solution for (n_1, v_1, E_1) is possible only if the determinant of the coefficients of equations (4.29) vanishes, i.e.

$$\begin{vmatrix} -\mathrm{i}\omega & \mathrm{i} n_0 k & 0 \\ 3\mathrm{i} k_B T_e k - f & -\mathrm{i} m_e n_0 \omega & e n_0 \\ 4\pi e & 0 & \mathrm{i} k \end{vmatrix} = 0. \tag{4.30}$$

Equation (4.30) gives the dispersion relation for the electron wave (known also as plasmon)

$$\omega^2 = \omega_p^2 + \frac{3k_B T_e k^2}{m_e} + \frac{ifk}{m_e}. \tag{4.31}$$

The last term on the right-hand side of (4.31) gives the ponderomotive force contribution to the wave dispersion. Due to this term ω^2 is complex, so that wave growth, fed by the imposed ponderomotive force, is possible. In the limit of zero T_e, or when the ponderomotive force dominates the plasma pressure, the real (ω_R) and the imaginary (ω_I) parts of ω are

$$\omega_R = \left(\omega_p^2 + \frac{f^2k^2}{4m_e^2\omega_p^2}\right)^{1/2}, \qquad \omega_I = \frac{fk}{2m_e\omega_R}. \tag{4.32}$$

It is interesting that even for $T_e = 0$ wave propagation occurs, unlike in the case without ponderomotive force. The phase velocity (v_ϕ) and the group velocity (v_g) for a zero electron temperature are given by

$$v_\phi = \frac{\omega}{k} = \sqrt{\frac{\omega_p^2}{k^2} + \frac{if}{m_e k}}, \qquad v_g = \frac{\partial\omega}{\partial k} = \frac{if}{2m_e}\left(\omega_p^2 + \frac{ifk}{m_e}\right)^{-1/2}. \tag{4.33}$$

In the usual case of no imposed ponderomotive force, the group velocity vanishes for a zero electron temperature and wave propagation ceases.

4.3.2 The ion wave dispersion

Next we consider ion waves. In this case we are looking for a solution that the electrons and the ions oscillate together with an angular frequency ω. The system is specified by the electron continuity and momentum equations, the ion continuity and momentum equations, the Poisson equation, and an isothermal ($T_e = \text{const.}$) electron equation of state:

$$\begin{aligned}
\frac{\partial n_e}{\partial t} + \frac{\partial(n_e v_e)}{\partial x} &= 0 \\
m_e\frac{dv_e}{dt} = 0 &= -\frac{\partial P_e}{\partial x} - en_eE + n_e f \\
\frac{\partial n_i}{\partial t} + \frac{\partial(n_i v_i)}{\partial x} &= 0 \\
m_i\frac{\partial v_i}{\partial t} &= eZE \\
\frac{\partial E}{\partial x} &= 4\pi e(Zn_i - n_e) \\
P_e = n_e k_B T_e, &\quad T_e = \text{const.}
\end{aligned} \tag{4.34}$$

where m_i and Z are the ion mass and charge accordingly and quasineutrality $n_{i0} = Zn_{e0}$ is assumed. Electron inertia has been neglected in the electron momentum equation and ion pressure has been ignored in the ion momentum equation. The linearization approximation is

$$\begin{aligned} n_e &= n_{e0} + n_{e1} \\ n_i &= n_{i0} + n_{i1} \\ v_e &= v_{e1}, \qquad v_i = v_{i1}, \qquad E = E_1. \end{aligned} \tag{4.35}$$

We are looking for a wave where the electrons and ions have a common angular frequency of oscillations, i.e. the perturbations behave like

$$\left.\begin{matrix} n_{e1} \\ n_{i1} \\ v_{e1} \\ v_{i1} \\ E_1 \end{matrix}\right\} \propto \exp[\mathrm{i}(kx - \omega t]. \tag{4.36}$$

Substituting (4.35) and (4.36) into (4.34), one gets the following set of equations, written in matrix form:

$$\begin{pmatrix} -\mathrm{i}\omega & \mathrm{i}n_{e0}k & 0 & 0 & 0 \\ -\mathrm{i}kk_B T_e + f & 0 & 0 & 0 & -en_{e0} \\ 0 & 0 & -\mathrm{i}\omega & \mathrm{i}n_{i0}k & 0 \\ 0 & 0 & 0 & -\mathrm{i}\omega m_i & -eZ \\ 4\pi e & 0 & -4\pi eZ & 0 & \mathrm{i}k \end{pmatrix} \begin{pmatrix} n_{e1} \\ v_{e1} \\ n_{i1} \\ v_{i1} \\ E_1 \end{pmatrix} = \begin{pmatrix} 0 \\ 0 \\ 0 \\ 0 \\ 0 \end{pmatrix}. \tag{4.37}$$

A solution is possible only if the determinant of the matrix in (4.37) is zero, implying the following dispersion relation:

$$\omega^2 = \left(\frac{Z}{m_i}\right)\left(\frac{(k_B T_e k^2 + \mathrm{i}kf)}{1 - \dfrac{(k_B T_e k^2 + \mathrm{i}kf)}{4\pi e^2 n_{e0}}}\right) \approx \left(\frac{Z}{m_i}\right)(k_B T_e k^2 + \mathrm{i}kf). \tag{4.38}$$

The approximate equality in (4.38) is obtained for

$$\frac{(k_B T_e k^2 + \mathrm{i}kf)}{4\pi e^2 n_{e0}} = \frac{v_{Te}^2 k^2 + \mathrm{i}kfm_e}{\omega_{pe}^2} \ll 1. \tag{4.39}$$

If the ponderomotive pressure is much smaller than the thermal electron pressure, then the ratio of (4.39) is about $[(v_{Te}/\lambda)/\nu_{pe}]^2 \approx [\nu_{ion}/\nu_{pe}]^2 \ll 1$. $v_{Te}^2 \approx k_B T_e/m_e$, $\lambda = 2\pi/k$ is the wavelength of the ion wave, ν_{ion} is of the order of the oscillation frequency of the ion wave under consideration and $\nu_{pe} = \omega_{pe}/2\pi$ is the electron plasma oscillation frequency, which is of the

order of the electron wave frequency. Since the ion wave frequency is much smaller than the electron wave frequency the above approximation is justified.

For $f = 0$ the approximated equation (4.38) gives the standard dispersion relation for an ion wave, while for $T_e = 0$ the real and imaginary part of ω are

$$\omega_R = \sqrt{\frac{Z|fk|}{2m_i}}, \qquad \omega_I = \frac{Zfk}{2m_i\omega_R}. \tag{4.40}$$

Here too, ion waves (also called acoustic waves) can propagate even for a zero temperature, unlike in the case without the ponderomotive force.

Considering the imaginary parts of the dispersion relations of equations (4.32) and (4.40), one can see that the dependence of the perturbations $(n_{e1}, n_{i1}, v_{e1}, v_{i1}, E_1) \approx \exp(-i\omega t) = \exp(\omega_I t)$ implies that the growth of both electron waves and ion waves occurs for $\omega_I > 0$. From these equations one gets that $\omega_I > 0$ corresponds to waves with $k > 0$, $\omega_R > 0$, i.e. propagating out of the plasma (towards the laser beam). In this case the inward propagating ($k < 0$) waves are damped and therefore do not build up out of any initially present noise.

In the examples given in this section, the wave growth can occur only at times and domains where the imposed ponderomotive force exists. In these cases the wave energy is taken from the electromagnetic wave energy through the work done by the ponderomotive force. This may limit or dampen the ponderomotive force.

With the invention of very high power lasers, in particular the femtosecond lasers, the radiation pressure, as expressed by the ponderomotive force, plays an important role not only in astrophysics but also in laboratory plasmas.

Chapter 5

Laser Absorption and Propagation in Plasma

5.1 Collisional Absorption (Inverse Bremsstrahlung)

The radiation emitted by a charged particle during the collision with another particle is customarily called **bremsstrahlung** (in German 'braking radiation') because it was first detected when high-energy electrons were stopped in a thick metallic target. **Inverse bremsstrahlung** is the process in which an electron absorbs a photon while colliding with an ion or with another electron. A rigorous calculation of the inverse bremsstrahlung absorption can be made by using the kinetic theory (e.g. the Vlasov equation) to take into account the distribution function of the electrons and the positions of the ions (Dawson 1968). In this case the absorption coefficient depends on the correlation function of the ions.

Here we consider a simple model where the plasma is infinite and homogeneous, the ions are infinitely heavy (i.e. their motion is neglected) and no static magnetic or electric fields interfere. Since the electromagnetic waves have a phase velocity much higher than the thermal velocity of the electrons it is justifiable to neglect their thermal motion. Thus the equation of motion for the electrons is

$$\frac{\mathrm{d}\mathbf{v}}{\mathrm{d}t} = -\frac{e\mathbf{E}}{m_\mathrm{e}} - \frac{\mathbf{v}}{\tau_\mathrm{c}} \tag{5.1}$$

where $-e$, m_e and $\mathbf{v}$ are the electron charge, mass and velocity, respectively, $\mathbf{E}$ is the electric field and τ_c is the effective time between electron–ion collisions (we neglect here the electron–electron collisions). τ_c^{-1} is equal to the electron–ion collision frequency ν_ei, which in general depends on ion density n_i, the degree of the plasma ionization, Z_i, and the electron temperature, T_e (Spitzer 1962), and is given by (see sections 2.2 and 9.3)

$$\tau_\mathrm{c} = \nu_\mathrm{ei}^{-1} = \frac{3}{4}\frac{(k_\mathrm{B}T_\mathrm{e})^{3/2}m_\mathrm{e}^{1/2}}{(2\pi)^{1/2}Z_\mathrm{i}^2e^4n_\mathrm{i}\ln\Lambda} \cong 3.44\times10^5\frac{T_\mathrm{e}(\mathrm{eV})^{3/2}}{Z_\mathrm{i}^2n_\mathrm{i}\ln\Lambda}\ [\mathrm{s}], \qquad \Lambda \equiv \frac{\lambda_\mathrm{D}}{l_\mathrm{min}} \tag{5.2}$$

where λ_D is the Debye length and l_{min} is the minimum impact parameter, defined by the classical distance of closest approach between an electron and an ion l_{ca} (see section 2.2).

In order to get the dispersion relation in the simple plasma model, one has to solve equation (5.1), together with the Maxwell equations in free space containing the electric charge and the electric current:

$$\nabla \times \mathbf{E} = -\frac{1}{c}\frac{\partial \mathbf{B}}{\partial t} \tag{5.3}$$

$$\nabla \times \mathbf{B} = \frac{1}{c}\frac{\partial \mathbf{E}}{\partial t} - \frac{4\pi e n_e \mathbf{v}}{c} \tag{5.4}$$

$$\nabla \cdot \mathbf{E} = -4\pi e n_e \tag{5.5}$$

$$\nabla \cdot \mathbf{B} = 0. \tag{5.6}$$

The above equations are given in Gaussian units. Since the above model is described by charges and currents imbedded in free space, there is no distinction between the magnetic field strength $\mathbf{H}$ and the magnetic induction $\mathbf{B}$; $\mathbf{H} = \mathbf{B}$ and also the electric field strength $\mathbf{E}$ equals the electric induction (displacement) $\mathbf{D}$; $\mathbf{E} = \mathbf{D}$.

Solving equations (5.1) and (5.3)–(5.6) for a monochromatic wave (constant ω) with a frequency ω_L, propagating in a homogeneous medium (i.e. the wave number k is constant), one can substitute in these equations

$$\begin{Bmatrix} \mathbf{E}(\mathbf{r},t) \\ \mathbf{B}(\mathbf{r},t) \\ \mathbf{v}(\mathbf{r},t) \end{Bmatrix} = \begin{Bmatrix} \mathbf{E} \\ \mathbf{B} \\ \mathbf{v} \end{Bmatrix} \exp \mathrm{i}(\mathbf{k}\cdot\mathbf{r} - \omega_L t). \tag{5.7}$$

The following set of algebraic equations are obtained

$$\mathrm{i}\omega_L \mathbf{v} = \frac{e\mathbf{E}}{m_e} + \nu_{ei}\mathbf{v} \tag{5.8}$$

$$\mathrm{i}\mathbf{k} \times \mathbf{E} = \frac{1}{c}\mathrm{i}\omega_L \mathbf{B} \tag{5.9}$$

$$\mathrm{i}\mathbf{k} \times \mathbf{B} = -\frac{1}{c}\mathrm{i}\omega_L \mathbf{E} - \frac{4\pi}{c} n_e e \mathbf{v} \tag{5.10}$$

$$\mathrm{i}\mathbf{k} \cdot \mathbf{E} = -4\pi n_e e \tag{5.11}$$

$$\mathrm{i}\mathbf{k} \cdot \mathbf{B} = 0. \tag{5.12}$$

Multiplying equation (5.9) by '$\times\mathbf{k}$' and using equations (5.8)–(5.12), one gets

$$(\mathbf{k}\cdot\mathbf{E})\mathbf{k} - \left[k^2 - \frac{\omega_L^2}{c^2} + \frac{\omega_p^2 \omega_L^2}{c^2(\omega_L + \mathrm{i}\nu_{ei})}\right]\mathbf{E} = 0 \tag{5.13}$$

where the electron plasma frequency ω_p is defined by

$$\omega_p^2 = \frac{4\pi e^2 n_e}{m_e}. \tag{5.14}$$

For transverse waves (**E** orthogonal to **k**) $\mathbf{k} \cdot \mathbf{E} = 0$, equation (5.13) yields the dispersion relation

$$k^2 = \frac{\omega_L^2}{c^2} - \frac{\omega_p^2 \omega_L}{c^2(\omega_L + i\nu_{ei})}. \tag{5.15}$$

For longitudinal waves (**E** parallel to **k**) $\mathbf{k} \times \mathbf{E} = 0$, equation (5.13) yields the dispersion relation

$$\omega^2 + i\nu_{ei}\omega = \omega_p^2. \tag{5.16}$$

Since the transverse waves couple directly to the laser field in vacuum we shall now consider only the dispersion relation (5.15). For ν_{ei} much smaller than ω_L, typical of the plasma in the corona, a first-order Taylor expansion (in ν_{ei}/ω) of equation (5.15) is permitted, yielding

$$k^2 \cong \frac{\omega_L^2}{c^2}\left(1 - \frac{\omega_p^2}{\omega_L^2} + \frac{i\nu_{ei}\omega_p^2}{\omega_L^3}\right). \tag{5.17}$$

Solving this equation for k, by expanding the square root of the right-hand side of (5.17) for $\nu_{ei}/\omega_L \ll 1$ and $\omega_L^2 - \omega_p^2 \gg (\nu_{ei}/\omega_L)\omega_p^2$, one gets

$$k \cong \pm\frac{\omega_L}{c}\left(1 - \frac{\omega_p^2}{\omega_L^2}\right)^{1/2}\left\{1 + i\left(\frac{\nu_{ei}}{2\omega_L}\right)\left(\frac{\omega_p^2}{\omega_L^2}\right)\frac{1}{1 - \omega_p^2/\omega_L^2}\right\}. \tag{5.18}$$

The spatial damping rate of the laser energy by inverse bremsstrahlung, κ_{ib}, is given by twice the imaginary part of k:

$$\kappa_{ib} = 2\,\mathrm{Im}\,k = \left(\frac{\nu_{ei}}{c}\right)\left(\frac{\omega_p^2}{\omega_L^2}\right)\left(1 - \frac{\omega_p^2}{\omega_L^2}\right)^{-1/2}. \tag{5.19}$$

Using equation (5.2) and the definition of the critical density n_c,

$$n_c = \frac{m_e\omega_L^2}{4\pi e^2} \cong 1.1 \times 10^{21}\left(\frac{1\,\mu m}{\lambda_L^2}\right)\mathrm{cm}^{-3} \tag{5.20}$$

one gets for equation (5.19)

$$\kappa_{ib} = \frac{\nu_{ei}(n_c)}{c}\left(\frac{n_e}{n_c}\right)^2\left(1 - \frac{n_e}{n_c}\right)^{-1/2} \propto \frac{Z_i n_e^2}{T_e^{3/2}}\left(1 - \frac{n_e}{n_c}\right)^{-1/2} \tag{5.21}$$

where $\nu_{ei}(n_c)$ is the collision frequency evaluated at the critical density and $\lambda_L = 2\pi c/\omega_L$ is the laser wavelength in vacuum.

The change in laser intensity I, passing through a slab of plasma in the z direction, is given by

$$\frac{\mathrm{d}I}{\mathrm{d}z} = -\kappa_{\mathrm{ib}} I. \tag{5.22}$$

For a slab of plasma of length L, the absorption coefficient α_{abs} is given by

$$\alpha_{\mathrm{abs}} = \frac{I_{\mathrm{in}} - I_{\mathrm{out}}}{I_{\mathrm{in}}} = 1 - \exp\left(- \int_0^L \kappa_{\mathrm{ib}} \, \mathrm{d}z \right) \tag{5.23}$$

where I_{in} and I_{out} (I is proportional to the square of the electric field amplitude) are the incoming and the outgoing laser intensities respectively. For weak absorption, $\kappa_{\mathrm{ib}} L \ll 1$ and therefore $\alpha_{\mathrm{abs}} \cong \kappa_{\mathrm{ib}} L$, while for strong absorption $\alpha_{\mathrm{abs}} \to 1$.

For inhomogeneous plasma the solution of (5.22) is more complicated since κ_{ib} is a function of n_{e}, T_{e} and $\ln \Lambda$ which may all depend on position. In general the problem is even more difficult since all these quantities might depend also on time. For long laser pulse duration (pulse duration of the order of 1 ns or more) with intermediate intensities (smaller than $10^{14}\,\mathrm{W/cm^2}$), it is conceivable to assume that T_{e} and $\ln \Lambda$ are constant and the dominant spatial dependence comes from n_{e}.

Solving (5.22) for a linear density profile (Ginzburg 1961)

$$n_{\mathrm{e}} = n_{\mathrm{c}} \left(1 - \frac{z}{L} \right) \qquad 0 \le z \le L \tag{5.24}$$

and using equation (5.21), where the laser propagates from $n_{\mathrm{e}} = 0$ to $n_{\mathrm{e}} = n_{\mathrm{c}}$ and back to $n_{\mathrm{e}} = 0$, the absorption coefficient is given by solving the integral of (5.23):

$$\alpha_{\mathrm{abs}} = 1 - \exp\left\{ -\frac{32}{15} \frac{\nu_{\mathrm{ei}}(n_{\mathrm{c}}) L}{c} \right\}. \tag{5.25}$$

In this equation the collision frequency is evaluated at the critical density.

Similarly, solving (5.22) for an exponential profile (Kruer 1988)

$$n_{\mathrm{e}} = n_{\mathrm{c}} \exp(-z/L) \tag{5.26}$$

the absorption coefficient is

$$\alpha_{\mathrm{abs}} = 1 - \exp\left\{ -\frac{8}{3} \frac{\nu_{\mathrm{ei}}(n_{\mathrm{c}}) L}{c} \right\}. \tag{5.27}$$

The dependence of κ_{ib} on $n_{\mathrm{e}}/n_{\mathrm{c}}$ in equation (5.21) shows that a significant fraction of the inverse bremsstrahlung absorption is from the region near the critical density, $n_{\mathrm{e}}/n_{\mathrm{c}} \approx 1$. If for some reason the exponential density profile becomes steeper at the critical surface, for example due to the action of the high radiation pressure obtained at high laser intensity, then one can describe this situation by the density profile

$$n_{\mathrm{e}} = \beta n_{\mathrm{c}} \exp(-z/L) \qquad \beta < 1 \tag{5.28}$$

then the factor $\frac{8}{3}$ in equation (5.27) is changed to $\frac{4}{3}[1-(1+\beta/2)(1-\beta)^{1/2}]$. For $\beta=0.5$ the factor $\frac{8}{3}$ is changed to 0.15, reducing significantly the inverse bremsstrahlung absorption.

At high laser intensities, e.g. $I > 10^{15}\,\mathrm{W/cm^2}$, the large electric field of the laser will distort the thermal distribution of the electrons, thus changing the electron–ion collision frequency, ν_{ei}. In this case it has been shown (Rand 1964, Silin 1965, Osborn 1972, Brysk 1975, Schlessinger and Wright 1979, Langdon 1980) that the spatial damping rate, κ_{ib}, depends on the laser intensity, I. Therefore, in this domain of intensities the collision absorption is known as nonlinear bremsstrahlung.

The electron oscillatory velocity in the laser electromagnetic field E_L is given by

$$v_E = \frac{eE_L}{m_e\omega_L} \tag{5.29}$$

and for laser intensities at which the energy of oscillation of the electrons in the electric field is comparable with their thermal energy, the electron mean square thermal velocity, v_{Te}^2, is effectively changed to

$$v_{eff}^2 = v_{Te}^2 + v_E^2. \tag{5.30}$$

Since the spatial damping rate of the laser energy by inverse bremsstrahlung, κ_{ib} in equation (5.21), scales as $T_e^{-3/2} \propto [(v_{eff}^2)^{1/2}]^{-3}$, at high laser intensities κ_{ib} is replaced by

$$\kappa_{ib} \rightarrow \frac{\kappa_{ib}}{[1+(v_E^2/v_{Te}^2)]^{3/2}} \propto \frac{1}{E_L^3} \propto \frac{1}{I_L^{3/2}} \tag{5.31}$$

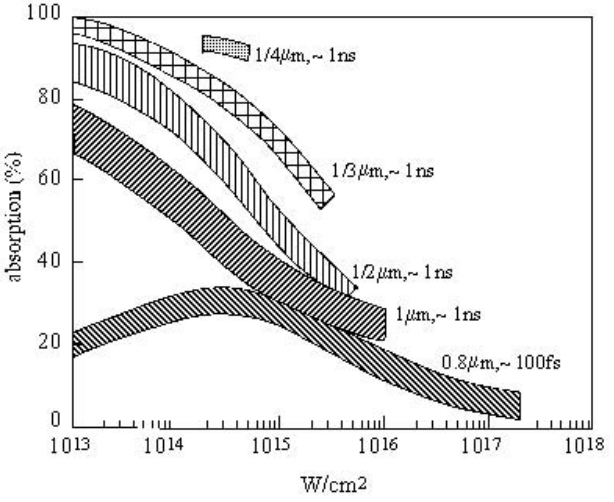

Figure 5.1. The domain of experimental data of laser absorption by solid targets with a low atomic number. The laser is irradiated perpendicular to the target.

for $v_E/v_{Te} > 1$, and one obtains (a Taylor expansion of the denominator of (5.31))

$$\kappa_{ib} \to \frac{\kappa_{ib}}{1 + \frac{3}{2}(v_E^2/v_{Te}^2)} \tag{5.32}$$

for $v_E/v_{Te} < 1$.

The experimental absorption coefficient for a solid with a low atomic number Z (e.g. aluminium) versus the incident laser intensity I_L is given in figure 5.1. One can see the different behaviour between the long pulse duration (of the order of 1 ns) for different laser wavelength (1 μm, $\frac{1}{2}$ μm, $\frac{1}{3}$ μm, $\frac{1}{4}$ μm) and short laser pulses (of about 100 fs) with a wavelength of 0.8 μm.

5.2 The Electromagnetic Wave Equation in a Plasma Medium

In the previous section we considered the propagation of the electromagnetic field in a homogeneous medium. In the following sections the laser absorption in inhomogeneous plasmas are analysed. For this purpose the electromagnetic wave equations have to be written and solved. From knowledge of the electromagnetic fields entering and exiting the plasma medium the absorption is easily calculated (Ginzburg 1961, Kruer 1988).

The electromagnetic wave equations are now developed for a plasma medium where the ions are stationary and serve only as a charge-neutralizing background to the electron motion. This is justified since the laser angular frequency ω_L (larger than or equal to the electron plasma frequency ω_{pe}) and the electron plasma frequency ω_{pe} are much larger than the ion plasma frequency ω_{pi}, $\omega_L \geq \omega_{pe} \gg \omega_{pi}$.

The wave equations for the electromagnetic fields are first derived. Gaussian units are used. In this chapter we consider a monochromatic electric field $\mathbf{E}(\mathbf{r}, t)$ and magnetic field $\mathbf{B}(\mathbf{r}, t)$ defined by

$$\mathbf{E}(\mathbf{r}, t) = \mathbf{E}(\mathbf{r}) \exp(-i\omega t), \qquad \mathbf{B}(\mathbf{r}, t) = \mathbf{B}(\mathbf{r}) \exp(-i\omega t). \tag{5.33}$$

The electric current $\mathbf{J}_e$ in the plasma

$$\mathbf{J}_e = -en_e\mathbf{v}_e \tag{5.34}$$

is calculated from the electron momentum fluid equation by neglecting the second-order terms $[(\mathbf{v}_e \cdot \nabla)\mathbf{v}_e$ and $\mathbf{v}_e \times \mathbf{B}]$, i.e. by the linear Newton's law for the electron motion

$$\frac{\partial \mathbf{v}_e}{\partial t} = -\frac{e}{m_e}\mathbf{E}(\mathbf{r}) \exp(-i\omega t). \tag{5.35}$$

Integrating this equation and substituting into (5.34), one gets

$$\mathbf{J}_e(\mathbf{r}, t) = \frac{ie^2 n_e(\mathbf{r})\mathbf{E}(\mathbf{r}) \exp(-i\omega t)}{m_e \omega} \equiv \sigma_E \mathbf{E}(\mathbf{r}, t) \tag{5.36}$$

where the electrical conductivity coefficient σ_E (a tensor in the general case) is

$$\sigma_E = \frac{i\omega_{pe}^2}{4\pi\omega}. \tag{5.37}$$

Substituting $\mathbf{J}_e$ from (5.36) into Maxwell equations and using $\partial/\partial t = -i\omega$ yields

$$\nabla \times \mathbf{E}(\mathbf{r}) = -\frac{1}{c}\frac{\partial \mathbf{B}}{\partial t} = \frac{i\omega \mathbf{B}(\mathbf{r})}{c} \tag{5.38}$$

$$\nabla \times \mathbf{B}(\mathbf{r}) = \frac{1}{c}\frac{\partial \mathbf{E}}{\partial t} + \frac{4\pi \mathbf{J}_e}{c} = \frac{-i\omega\varepsilon \mathbf{E}(\mathbf{r})}{c} \tag{5.39}$$

where ε is the dielectric function of the plasma equal to

$$\varepsilon = 1 - \frac{\omega_{pe}^2}{\omega^2} = 1 - \frac{n_e(\mathbf{r})}{n_{ec}} \tag{5.40}$$

where n_{ec} is the critical density ($\cong 1.1 \times 10^{21}\,\mathrm{cm}^{-3}/\lambda_L\,\mu\mathrm{m}^2$, where λ_L is the laser wavelength in vacuum). Taking $\nabla \times$ equation (5.38) and using (5.39), one gets **the wave equation for the electric field in the plasma medium**

$$\nabla^2 \mathbf{E}(\mathbf{r}) + \left(\frac{\omega^2 \varepsilon}{c^2}\right)\mathbf{E}(\mathbf{r}) - \nabla[\nabla \cdot \mathbf{E}(\mathbf{r})] = 0. \tag{5.41}$$

In a similar way, taking $\nabla \times$ equation (5.39) and using (5.38) **the wave equation for the magnetic field in the plasma medium** is obtained:

$$\nabla^2 \mathbf{B}(\mathbf{r}) + \left(\frac{\omega^2 \varepsilon}{c^2}\right)\mathbf{B}(\mathbf{r}) + \left(\frac{\nabla \varepsilon}{\varepsilon}\right) \times [\nabla \times \mathbf{B}(\mathbf{r})] = 0. \tag{5.42}$$

For a homogeneous plasma (i.e. $n_e = \text{const.}$) one has a constant ε (equation (5.40)) and therefore $\nabla\varepsilon = 0$ and $\nabla \cdot \mathbf{E} = 0$. The last relation is obtained from the Maxwell equation

$$\nabla \cdot \mathbf{E} = 4\pi(n_e - n_{i0}) = 0 \tag{5.43}$$

since the constant electron density equals the ion background density in order to keep charge neutrality of the medium. Therefore, for homogeneous plasmas the wave equations for $\mathbf{E}$ and $\mathbf{B}$ are identical:

$$\left(\nabla^2 + \frac{\omega^2 \varepsilon}{c^2}\right)\mathbf{E}(\mathbf{r}) = 0, \qquad \left(\nabla^2 + \frac{\omega^2 \varepsilon}{c^2}\right)\mathbf{B}(\mathbf{r}) = 0. \tag{5.44}$$

The solutions of these equations are

$$\mathbf{E}(\mathbf{r}, t) = \mathbf{E}_0 \exp[i(\mathbf{k} \cdot \mathbf{r} - \omega t)], \qquad \mathbf{B}(\mathbf{r}, t) = \mathbf{B}_0 \exp[i(\mathbf{k} \cdot \mathbf{r} - \omega t)] \tag{5.45}$$

where the wave vector k is defined by

$$k^2 = \frac{\omega^2 \varepsilon}{c^2} = \frac{1}{c^2}(\omega^2 - \omega_{pe}^2). \tag{5.46}$$

These solutions for **E** and **B** were assumed in the previous section (equation (5.7)). k is imaginary for $\omega/\omega_{pe} < 1$, i.e. for $n_{ec}/n_e < 1$. In this case the electric and magnetic fields decay exponentially. Therefore, the electromagnetic wave cannot propagate into a plasma medium with a density larger than the critical density.

5.3 Slowly Varying Density—the WKB Approximation

We consider an electromagnetic wave normally incident onto a plasma medium, containing from $z = 0$ to infinity. It is assumed that the physical quantities depend only on one space coordinate z, namely $n_e(z)$, $\varepsilon(z;\omega)$ and $\mathbf{E}(\mathbf{r}) = \mathbf{E}(z)$. Since in Cartesian coordinates

$$\nabla^2\mathbf{E}(z) - \nabla[\nabla \cdot \mathbf{E}(z)] = \left(\frac{\mathrm{d}^2E_x}{\mathrm{d}z^2}, \frac{\mathrm{d}^2E_y}{\mathrm{d}z^2}, 0\right) \tag{5.47}$$

the wave equation (5.41) for the electric field $\mathbf{E}(z)$ is

$$\begin{pmatrix} \dfrac{\mathrm{d}^2}{\mathrm{d}z^2} + \dfrac{\omega^2\varepsilon}{c^2} & 0 & 0 \\ 0 & \dfrac{\mathrm{d}^2}{\mathrm{d}z^2} + \dfrac{\omega^2\varepsilon}{c^2} & 0 \\ 0 & 0 & \varepsilon \end{pmatrix} \begin{pmatrix} E_x(z) \\ E_y(z) \\ E_z(z) \end{pmatrix} = \begin{pmatrix} 0 \\ 0 \\ 0 \end{pmatrix}. \tag{5.48}$$

Similarly, since

$$\nabla\varepsilon \times [\nabla \times \mathbf{B}(z)] = \left(-\frac{\mathrm{d}\varepsilon}{\mathrm{d}z}\frac{\mathrm{d}B_x}{\mathrm{d}z}, -\frac{\mathrm{d}\varepsilon}{\mathrm{d}z}\frac{\mathrm{d}B_x}{\mathrm{d}z}, 0\right) \tag{5.49}$$

the wave equation (5.42) for the magnetic field $\mathbf{B}(z)$ is

$$\begin{pmatrix} \dfrac{\mathrm{d}^2}{\mathrm{d}z^2} - \dfrac{1}{\varepsilon}\dfrac{\mathrm{d}\varepsilon}{\mathrm{d}z}\dfrac{\mathrm{d}}{\mathrm{d}z} + \dfrac{\omega^2\varepsilon}{c^2} & 0 & 0 \\ 0 & \dfrac{\mathrm{d}^2}{\mathrm{d}z^2} - \dfrac{1}{\varepsilon}\dfrac{\mathrm{d}\varepsilon}{\mathrm{d}z}\dfrac{\mathrm{d}}{\mathrm{d}z} + \dfrac{\omega^2\varepsilon}{c^2} & 0 \\ 0 & 0 & \dfrac{\mathrm{d}^2}{\mathrm{d}z^2} + \dfrac{\omega^2\varepsilon}{c^2} \end{pmatrix} \begin{pmatrix} B_x(z) \\ B_y(z) \\ B_z(z) \end{pmatrix} = \begin{pmatrix} 0 \\ 0 \\ 0 \end{pmatrix}. \tag{5.50}$$

Equations (5.48) and (5.50) are solved for an orthogonal incidence of a linearly polarized laser, as described in figure 5.2. The direction of the electric field is chosen along the x-axis, $\mathbf{E} = (E_x(z) \equiv E(z), 0, 0)$, the magnetic field oscillates along the y-axis, $\mathbf{B} = (0, B(z), 0)$, while these fields propagate in the z direction, $\mathbf{k} = (0, 0, k)$. Equations (5.48) reduce to

$$\frac{\mathrm{d}^2E}{\mathrm{d}z^2} + \frac{\omega^2\varepsilon}{c^2}E = 0. \tag{5.51}$$

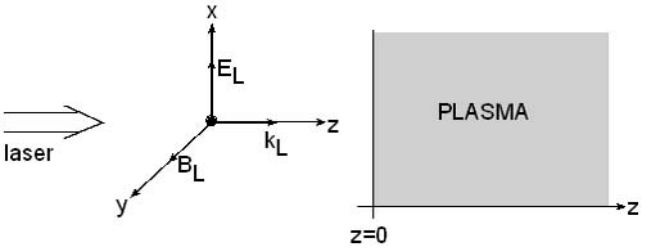

Figure 5.2. Linearly polarized electromagnetic wave normally incident onto a plasma medium.

In the WKB (Wentzel, Kramers and Brillouin, who used this approximation to solve the Schrödinger equation) approximation one looks for a solution of the form

$$E(z) = E_0(z) \exp\left(\frac{\mathrm{i}\omega}{c}\int^z \psi(\zeta)\,\mathrm{d}\zeta\right) \tag{5.52}$$

where E_0 and ψ are slowly-varying functions of z. In this approximation the local wave number $k(z)$ in the plasma is defined by

$$k(z) = \frac{\omega\psi(z)}{c}. \tag{5.53}$$

Substituting the solution (5.52) into the wave equation (5.51) gives the differential equation

$$\frac{\mathrm{d}^2E_0}{\mathrm{d}z^2} + \left[\frac{\mathrm{i}\omega}{c}\left(2\psi\frac{\mathrm{d}E_0}{\mathrm{d}z} + E_0\frac{\mathrm{d}\psi}{\mathrm{d}z}\right)\right] + \left[\frac{\omega^2E_0}{c^2}(\varepsilon - \psi^2)\right] = 0. \tag{5.54}$$

In the WKB approximation the second derivative is negligible, i.e. one takes $\mathrm{d}^2E_0/\mathrm{d}z^2 = 0$. Moreover, this approximation requires that the zeroth-order derivatives vanish and the first-order derivative terms vanish. That is, the last equation is reduced to

$$\varepsilon - \psi^2 = 0, \qquad 2\psi\frac{\mathrm{d}E_0}{\mathrm{d}z} + E_0\frac{\mathrm{d}\psi}{\mathrm{d}z} = 0. \tag{5.55}$$

The solution of (5.55) is

$$\psi = \sqrt{\varepsilon}, \qquad E_0(z) = \frac{\text{const.}}{\sqrt{\psi}} = \frac{\text{const.}}{\varepsilon^{1/4}}. \tag{5.56}$$

The plasma–vacuum interface is taken at $z = 0$. Substituting (5.56) into (5.52) and denoting the electric field in vacuum by E_L, one gets the WKB solution for the electric field in the plasma medium

$$E(z) = \frac{E_\mathrm{L}}{\varepsilon^{1/4}}\exp\left[\frac{\mathrm{i}\omega}{c}\int^z \sqrt{\varepsilon(\omega,\zeta)}\,\mathrm{d}\zeta\right]. \tag{5.57}$$

Thus, the amplitude of the electric field in the plasma is (using (5.40))

$$E_0(z) \equiv \frac{E_L}{\varepsilon^{1/4}} = \frac{E_L}{(1-(n_e(z)/n_{ec}))^{1/4}}. \tag{5.58}$$

From the last equation it is evident that the amplitude increases at higher electron density.

For the WKB approximation to be valid one requires that the second derivative of the amplitude is much smaller than the first derivatives

$$\frac{d^2E_0}{dz^2} \ll \frac{\omega E_0}{c}\frac{d\psi}{dz} = E_0\frac{dk(z)}{dz}, \qquad \frac{d^2E_0}{dz^2} \ll \frac{\omega\psi}{c}\frac{dE_0}{dz} = k(z)\frac{dE_0(z)}{dz}. \tag{5.59}$$

Adding the two equations of (5.59) and integrating, one obtains the following necessary condition for the WKB solution to be valid:

$$\frac{dE_0}{dz} \ll k(z)E_0(z) = \frac{\omega\psi E_0}{c}. \tag{5.60}$$

Substituting (5.58) into (5.60), one gets the WKB approximation requirement that the plasma density should vary slowly with the coordinate

$$\frac{dn_e}{dz} \ll \frac{8\pi n_{ec}}{\lambda(z)}\left(1-\frac{n_e(z)}{n_{ec}}\right) = \frac{8\pi n_{ec}\varepsilon(\omega,z)}{\lambda(z)}. \tag{5.61}$$

We shall now solve the magnetic field in the WKB approximation. In this case the laser magnetic field is in the y direction, and therefore the wave equation for the magnetic field is given by the y component of equation (5.50). However, it is not necessary to solve this equation since the magnetic field is easily derived by using equation (5.38):

$$B(z) = -\frac{ic}{\omega}\frac{dE(z)}{dz} = \left[E_0(z)\psi - \frac{ic}{\omega}\frac{dE_0(z)}{dz}\right]\exp\left[\frac{i\omega}{c}\int^z d\zeta\sqrt{\varepsilon(\omega,\zeta)}\right]. \tag{5.62}$$

Using the WKB validity condition, as given by equation (5.60), one can neglect the second term in (5.62). Now using $E_0(z)$ and $\psi(z)$ from (5.56) and (5.58), we get the solution for the magnetic field in the plasma medium

$$B(z) = E_L\varepsilon^{1/4}\exp\left[\frac{i\omega}{c}\int^z d\zeta\sqrt{\varepsilon(\omega,\zeta)}\right]. \tag{5.63}$$

From equations (5.57), (5.58) and (5.63) one can see that while the electric field increases at higher electron densities the magnetic field decreases accordingly.

The WKB approximation is not valid at the critical surface (where $\varepsilon = 0$, $k = 0$ and $\lambda = \infty$). In laser–plasma interaction the critical surface plays a very important role; part of the laser beam is absorbed there and the other part is reflected from this surface. Therefore, the WKB solution is mainly of pedagogical importance rather than of practical use. In the next section we discuss an analytic solution (Ginzburg 1961) relevant also in the region of the critical density.

5.4 Linear Varying Density—the Airy Functions

In this section we choose the same geometry as given in the previous section and described in figure 5.2. The plasma–vacuum interface is as before at $z = 0$, but the plasma density profile is given by

$$n_e(z) = n_{ec}\frac{z}{L}. \tag{5.64}$$

Using this density profile with equation (5.40) into the electric field wave equation (5.51), one gets (Ginzburg 1961, Landau and Lifshitz 1975)

$$\frac{d^2E(z)}{dz^2} + \frac{\omega^2}{c^2}\left(1 - \frac{z}{L}\right)E(z) = 0. \tag{5.65}$$

Changing now the variable z with the dimensionless quantity defined by

$$\zeta = \left(\frac{\omega^2}{c^2 L}\right)^{1/3}(z - L) \tag{5.66}$$

one obtains

$$\frac{d^2E(\zeta)}{d\zeta^2} - \zeta E(\zeta) = 0. \tag{5.67}$$

This equation is known as the Stokes differential equation. The solution to this differential equation is given by the **Airy functions** Ai(ζ) and Bi(ζ) (Abramowitz and Stegun 1964):

$$E(\zeta) = a\,\mathrm{Ai}(\zeta) + b\,\mathrm{Bi}(\zeta). \tag{5.68}$$

The coefficients a and b are determined by matching the solution at the plasma boundaries. The functions Ai, derivative of Ai and Bi, are given in figure 5.3. From equations (5.64) and (5.66) one gets that at $\zeta = 0$ the density is equal to the critical density, and $\zeta = -(\omega L/c)^{2/3}$ is the vacuum–plasma interface. The electron density is thus given by

$$\begin{aligned}
&\textbf{vacuum}: \quad n_e(z < 0) = n_e\left[\zeta \le -\left(\frac{\omega L}{c}\right)^{2/3}\right] = 0 \\
&\textbf{plasma}: \quad n_e(z \ge 0) = n_e\left[\zeta > -\left(\frac{\omega L}{c}\right)^{2/3}\right] > 0 \\
&\textbf{critical surface}: \quad n_e(z = L) = n_e(\zeta = 0) = n_{ec}.
\end{aligned} \tag{5.69}$$

The electromagnetic wave cannot propagate for $n_e > n_{ec}$, or equivalently for $\zeta > 0$. Since the Airy function Bi diverges for $\zeta \to \infty$ one has to exclude the Bi solution, namely $b = 0$ in equation (5.68). Therefore, the electric field in the plasma is given by the Airy function Ai(ζ).

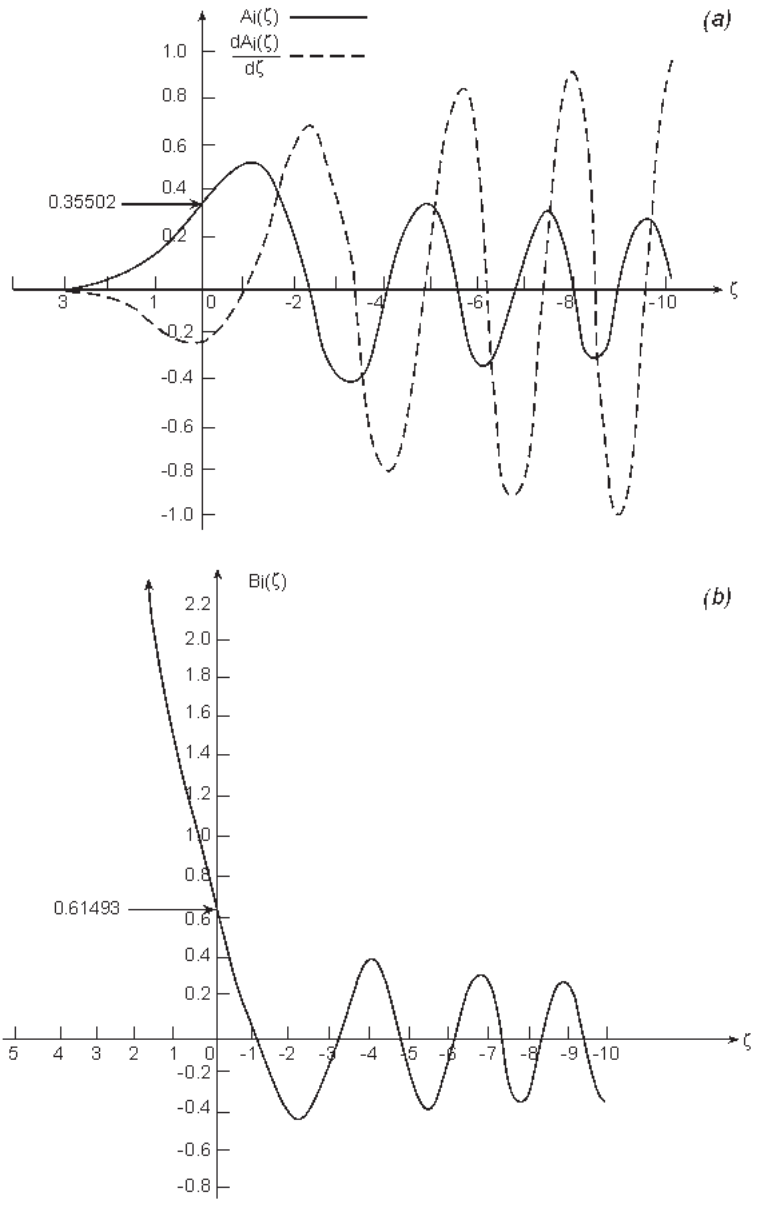

Figure 5.3. The Airy functions Ai, its derivative and Bi.

It is assumed that the dimension of the plasma L, from the vacuum to the critical surface, is large in comparison with the electromagnetic wavelength λ_L. On the other hand, L is of the order of the product of the laser time duration τ_L and the expansion (towards the vacuum) plasma

velocity $u_{\exp}$:

$$L \gg \frac{c}{\omega} = \frac{\lambda_L}{2\pi}, \qquad \tau_L(ps) \gg 1.6\left(\frac{\lambda_L}{\mu m}\right)\left(\frac{10^7\ cm/s}{u_{\exp}}\right). \tag{5.70}$$

From this relation one can see that the approximation of this section is not relevant for the femtosecond lasers.

The plasma vacuum interface is at $|\zeta| = (\omega L/c)^{2/3} \gg 1$ (see (5.70)); therefore, we can use the asymptotic expansion (Abramowitz and Stegun 1964) of the Airy function Ai(z) for $|\zeta| \gg 1$:

$$\mathrm{Ai}(-\zeta) = \frac{1}{\sqrt{\pi}\zeta^{1/4}} \cos\left(\frac{2}{3}\zeta^{3/2} - \frac{\pi}{4}\right) \tag{5.71}$$

in order to describe the electric field near the plasma–vacuum interface. Therefore, the electric field at $z = 0$, from the plasma side, can be approximated by the expression

$$\begin{aligned} E(z=0, \text{plasma}) &= \frac{a}{\sqrt{\pi}}\left(\frac{c}{\omega L}\right)^{1/6} \cos\left(\frac{2\omega c}{3L} - \frac{\pi}{4}\right) \\ &= \frac{a}{2\sqrt{\pi}}\left(\frac{c}{\omega L}\right)^{1/6} \\ &\quad \times \left\{\exp\left[\mathrm{i}\left(\frac{2\omega c}{3L} - \frac{\pi}{4}\right)\right] + \exp\left[-\mathrm{i}\left(\frac{2\omega c}{3L} - \frac{\pi}{4}\right)\right]\right\}. \end{aligned} \tag{5.72}$$

Looking from the vacuum side, one has at $z = 0$ the incident laser field E_L and a reflected wave given by $E_L \exp(\mathrm{i}\phi)$:

$$E(z=0, \text{vacuum}) = E_L[1 + \exp(\mathrm{i}\phi)]. \tag{5.73}$$

The requirement that the solution is continuous at the plasma–vacuum interface (i.e. equating equations (5.72) and (5.73)) yields

$$\begin{aligned} a &= 2\sqrt{\pi}\left(\frac{\omega L}{c}\right)^{1/6} E_L \exp\left[-\mathrm{i}\left(\frac{2\omega L}{3c} - \frac{\pi}{4}\right)\right] \\ \phi &= \frac{4\omega L}{3c} - \frac{\pi}{2} = \frac{4}{3}[-\zeta(z=0)]^{3/2} - \frac{\pi}{2}. \end{aligned} \tag{5.74}$$

Substituting $b = 0$ and a from (5.74) into (5.68), one gets the solution for the electric field in the plasma:

$$E(\zeta) = 2\sqrt{\pi}\left(\frac{\omega L}{c}\right)^{1/6} E_L \exp\left[-\mathrm{i}\left(\frac{2\omega L}{3c} - \frac{\pi}{4}\right)\right] \mathrm{Ai}(\zeta). \tag{5.75}$$

Ai(ζ) has a maximum at $\zeta = -1$ (see figure 5.3); therefore, the ratio between the maximum value of the electric field in the plasma and the laser electric

field in vacuum is

$$\left|\frac{E_{\max}}{E_{\mathrm{L}}}\right| \approx 1.90\left(\frac{\omega L}{c}\right)^{1/6}. \tag{5.76}$$

For example, for a laser-produced plasma with a dimension $L = 100\,\mu\mathrm{m}$ and a laser wavelength of $\lambda_{\mathrm{L}} = 1\mu\mathrm{m}$, one gets (using (5.70)) $E_{\max}/E_{\mathrm{L}} \cong 5.57$.

The solution for the magnetic field is easily derived by using (5.38),

$$B(z) = -\frac{\mathrm{i}c}{\omega}\frac{\partial E(z)}{\partial z} \tag{5.77}$$

the solution for E as given by (5.75), and the relation (5.66),

$$B(\zeta) = -\mathrm{i}2\sqrt{\pi}\left(\frac{c}{\omega L}\right)^{1/6} E_{\mathrm{L}} \exp\left[-\mathrm{i}\left(\frac{2\omega L}{3c} - \frac{\pi}{4}\right)\right]\frac{\mathrm{d}\,\mathrm{Ai}(\zeta)}{\mathrm{d}\zeta}. \tag{5.78}$$

It is interesting to point out that when E is maximum, B is zero. At the critical surface, $\zeta = 0$, one has ($E_{\mathrm{L}} = B_{\mathrm{L}}$ in Gaussian units)

$$\begin{aligned}\left|\frac{E(\text{critical surface})}{E_{\mathrm{L}}}\right| &\cong 1.26\left(\frac{\omega L}{c}\right)^{1/6}\\ \left|\frac{B(\text{critical surface})}{E_{\mathrm{L}}}\right| &\cong 0.92\left(\frac{\omega L}{c}\right)^{-1/6}.\end{aligned} \tag{5.79}$$

Note that the energy conservation (as expressed by the Poynting theorem, see Appendix A) does not require the conservation of $\mathbf{E} \times \mathbf{B}$.

So far we have discussed in this section the propagation of the electromagnetic field without absorption. For absorption to occur, a damping of energy is required. This is possible only if the equations of wave propagation include collision processes, such as particle–particle and/or wave–particle. Taking into account electron–ion collisions, the dielectric function is

$$\varepsilon = 1 - \frac{\omega_{\mathrm{pe}}^2}{\omega(\omega + \mathrm{i}\nu_{\mathrm{ei}})} = 1 - \frac{z}{L[1 + \mathrm{i}(\nu_{\mathrm{ei}}/\omega)]} \tag{5.80}$$

where a linear density profile is assumed for the second equality in this equation. For a wave propagating in the z direction with an electric field in the x direction, $E(z)$, one has to solve the wave equation (5.51) with the dielectric function of (5.80). Assuming in this equation that the electron–ion collision frequency is a constant equal to its value at the critical surface, i.e. $\nu_{\mathrm{ei}} = \nu_{\mathrm{ei}}(n_{\mathrm{ec}}) = \nu_{\mathrm{c}}$, equation (5.51) then takes the form

$$\frac{\mathrm{d}^2E(z)}{\mathrm{d}z^2} + \frac{\omega^2}{c^2}\left[1 - \frac{z}{L[1 + (\nu_{\mathrm{c}}/\omega)]}\right]E(z) = 0. \tag{5.81}$$

Change of variables

$$\zeta = \left[\frac{\omega^2}{c^2 L[1 + \mathrm{i}(\nu_{\mathrm{c}}/\omega)]}\right]^{1/3}\left[z - L\left(1 + \mathrm{i}\frac{\nu_{\mathrm{c}}}{\omega}\right)\right] \tag{5.82}$$

yields the Stokes equation (5.67) for a complex variable. Note that for $\nu_c = 0$ the change of variables is identical to that of equation (5.66). The solution to the differential equation is, as before, $E(\zeta, \text{plasma}) = aEi(\zeta)$ and

$$\begin{aligned} E(z=0, \text{vacuum}) &= E_L[1 + \exp(i\phi)] = E_{in} + E_{out} \\ \phi &= \frac{4}{3}\left[\frac{\omega L}{c}\left(1 + i\frac{\nu_c}{\omega}\right)\right] - \frac{\pi}{2} \equiv \phi_R + i\phi_I \end{aligned} \tag{5.83}$$

where $E_{in} = E_L$ is the incoming electric field and E_{out} is the outgoing electric field from the plasma. Since ϕ is complex we not only get a phase shift (as before, in (5.74)), but also a damping of the wave determined by the imaginary value of ϕ ($\phi_I = 4\nu_c L/3c$). The absorbed fraction f_a of the input laser energy is

$$f_a = \frac{|E_{in}|^2 - |E_{out}|^2}{|E_{in}|^2} = \frac{E_L^2 - E_L^2 \exp(-2\phi_I)}{E_L^2}. \tag{5.84}$$

Using the value of ϕ_I, one gets the absorption coefficient

$$f_a = 1 - \exp\left(-\frac{8\nu_c L}{3c}\right). \tag{5.85}$$

In comparing this result with the one obtained in (5.25) (both cases with the same density profile), one can see that the absolute value of the coefficient in the exponent of equation (5.85) is larger than the one in (5.25) by a factor of 5/4, implying a larger absorption coefficient. This can be understood since in that deriving the last equation we assumed a constant collision frequency larger than or equal to the real collision frequency. The larger the collision frequency the larger is the absorption coefficient.

5.5 Obliquely Incident Linearly Polarized Laser

Without any loss of generality we choose the coordinates in such a way that the laser propagates in the y–z plane, i.e. the wave vector $\mathbf{k}$ is in this plane. The vacuum–plasma interface is chosen at $z = 0$ and the electromagnetic wave is obliquely incident at an angle θ_0 to the normality of this surface.

The electron density $n_e(z)$ is assumed to be linear as in the previous section. θ is the angle between the electron density gradient and the wave vector $\mathbf{k}$. The electric field is in the x direction for s-polarization and in the y–z plane for the p-polarization (see figure 5.4). Therefore, the components of the electromagnetic fields are

$$\begin{aligned} &\textbf{the wave vector:} \quad \mathbf{k} = [0, k_y = (\omega/c)\sin\theta, k_z = (\omega/c)\cos\theta] \\ &\textbf{s-polarization:} \quad \mathbf{E} = [E_x(y,z), 0, 0]; \mathbf{B} = [0, B_y(y,z) B_z(y,z)] \\ &\textbf{p-polarization:} \quad \mathbf{E} = [0, E_y(y,z), E_z(y,z)]; \mathbf{B} = [B_x(y,z), 0, 0]. \end{aligned} \tag{5.86}$$

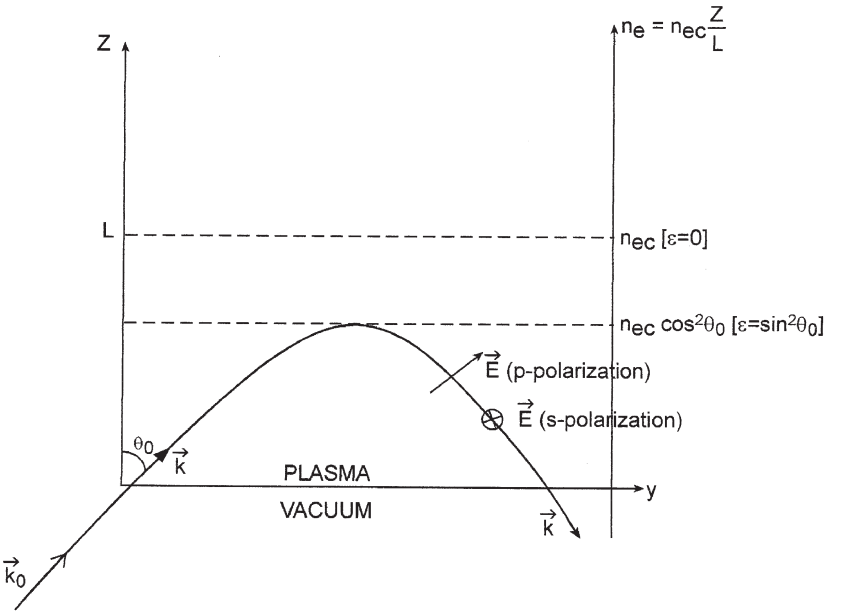

Figure 5.4. A linearly polarized laser propagating in the y–z plane.

The dispersion relation (5.46) is

$$\omega^2 = \omega_{\mathrm{pe}}^2 + (k_y^2 + k_z^2)c^2. \tag{5.87}$$

Since we have only a z-dependence in the electron density, one has a constant k_y:

$$k_y = \frac{\omega}{c}\sin\theta_0 \tag{5.88}$$

while k_z is a function of z. The relation (5.88) can be seen as the photon momentum ($= h\mathbf{k}$, h is Planck's constant) conservation in the y direction.

The reflection of the laser occurs at the surface where $k_z = 0$, i.e. where $\theta = 90^\circ$. Using the linear density relation (5.64) and equations (5.40), (5.87) and (5.88), one gets

$$\begin{aligned} n_{\mathrm{e}}(k_z = 0) &= n_{\mathrm{ec}}\cos^2\theta_0, \qquad n_{\mathrm{ec}} = \frac{m_{\mathrm{e}}\omega^2}{4\pi e^2} \\ \omega_{\mathrm{pe}}(k_z = 0) &= \omega\cos\theta_0 \\ z(k_z = 0) &= L\cos^2\theta_0 \\ \varepsilon(k_z = 0) &= \sin^2\theta_0. \end{aligned} \tag{5.89}$$

Solving the wave equations for the electromagnetic fields, one finds that there is no sharp cut-off as might appear from the geometrical optics (figure 5.4), but an exponential decay of the field amplitudes for $z > L\cos^2\theta_0$.

5.5.1 s-polarization

In this case the electric field is in the x direction and the wave equation for the x-component of the electric field, $E_x(z)$, is

$$\frac{\partial^2 E_x}{\partial y^2} + \frac{\partial^2 E_x}{\partial z^2} + \frac{\omega^2 \varepsilon(z)}{c^2} E_x = 0. \tag{5.90}$$

The electric field is a function of z and the phase $\exp[\mathrm{i}(k_y y + k_z z)]$. Since $k_z z$ is a function of z it can be included in the amplitude and using (5.88) the electric field can be written in the form

$$E_x = E(z) \exp\left(\frac{\mathrm{i}\omega y \sin\theta_0}{c}\right). \tag{5.91}$$

Substituting (5.91) into (5.90) and using $\varepsilon = 1 - z/L$ yields

$$\frac{\mathrm{d}^2 E(z)}{\mathrm{d}z^2} + \frac{\omega^2}{c^2}\left(1 - \frac{z}{L} - \sin^2\theta_0\right) E(z) = 0. \tag{5.92}$$

Changing the variable z to ζ defined by

$$\zeta = \left(\frac{\omega^2}{c^2 L}\right)^{1/3} (z - L\cos^2\theta_0) \tag{5.93}$$

one gets the Stokes differential equation (5.67) with the solution (5.75).

We shall now calculate the absorption of the s-polarized laser with oblique incidence. The dielectric function given in equation (5.80) is taken, but unlike in the previous section the electron–ion collision frequency is not a constant. For the linear electron density profile the electron–ion collision frequency is

$$\nu_{\mathrm{ei}} = \nu_{\mathrm{c}} \frac{n_{\mathrm{e}}}{n_{\mathrm{ec}}} = \nu_{\mathrm{c}} \frac{z}{L}. \tag{5.94}$$

The dispersion relation (5.87) can be written as

$$k_z^2 = \frac{\omega^2}{c^2}[\varepsilon(z) - \sin^2\theta_0]. \tag{5.95}$$

Using (5.80) and (5.94), one gets

$$k_z = \frac{\omega}{c}\left[\cos^2\theta_0 - \frac{z}{L[1 + \mathrm{i}(\nu_{\mathrm{c}} z/\omega L)]}\right]^{1/2} \equiv k_{\mathrm{R}} + \mathrm{i}k_{\mathrm{I}}. \tag{5.96}$$

We shall assume that $\nu_{\mathrm{ei}}/\omega \ll 1$ and use the WKB approximation to calculate the absorption coefficient defined by (5.84). Using equation (5.57), where

$$\sqrt{\varepsilon} = \frac{ck_z}{\omega} \tag{5.97}$$

one gets

$$|E(z)|^2 \propto \exp\left[-2\int^{z} k_{\mathrm{I}}(\zeta)\,\mathrm{d}\zeta\right]. \tag{5.98}$$

Expanding (5.96) for $\nu_{\mathrm{c}}/\omega \ll 1$, and taking the integral in (5.98) twice from 0 to $L\cos^2\theta_0$ (the 'turning' surface where the laser is reflected), i.e. from the plasma–vacuum boundary to the 'turning' surface and back to the plasma–vacuum boundary, one gets

$$\frac{|E_{\mathrm{out}}(z=0)|^2}{|E_{\mathrm{in}}(z=0)|^2} = \exp\left\{\frac{4\omega}{c}\,\mathrm{Im}\int_0^{L\cos^2\theta_0} \mathrm{d}\zeta\left[\left(\cos^2\theta_0 - \frac{\zeta}{L}\right) + \mathrm{i}\frac{\nu_{\mathrm{c}}}{\omega}\frac{\zeta^2}{L^2}\right]^{1/2}\right\} \tag{5.99}$$

where Im stands for the imaginary part. Doing the integral and taking the imaginary part, one gets for the absorption coefficient

$$f_{\mathrm{a}} = 1 - \frac{|E_{\mathrm{out}}|^2}{|E_{\mathrm{in}}|^2} = 1 - \exp\left(-\frac{32\nu_{\mathrm{c}}L\cos^5\theta_0}{15c}\right). \tag{5.100}$$

This result for $\theta_0 = 0$ is identical to the one obtained in equation (5.25) for the same electron density profile. Equation (5.100) is frequently used in the literature in order to understand the experimental results for the inverse bremsstrahlung absorption in laser–plasma interactions.

5.6 p-Polarization: the Resonance Absorption

Laser light might be absorbed by resonance absorption in the plasma. The solution of Maxwell's equations show (Denisov 1957, Ginsburg 1961, Friedberg *et al*. 1972, Speziale and Catto 1977) that p-polarized light incident on a steeply rising plasma density at an angle different from zero from normal incidence has a singularity in the magnitude of the oscillating electric field in the plasma. This electric field resonantly drives an electron plasma wave (see next chapter). The damping of this wave is possible either by collision or collisionless processes, so that resonance absorption is effective even when the electron–ion collision frequency, ν_{ei}, is very small. The resonance absorption is larger than the inverse bremsstrahlung for the following variables: high plasma temperatures, i.e. high laser intensities; longer laser wavelength, i.e. lower values of n_{c}; and short plasma scale length, L. For high laser intensities, e.g. $I_{\mathrm{L}}\lambda_{\mathrm{L}}^2 > 10^{15}\,(\mathrm{W/cm^2})\,\mu\mathrm{m}^2$, at the right laser polarization (p-polarization) and angle of incidence, up to about 50% absorption may occur by resonance absorption. The main feature of the resonant absorption is the creation of hot electrons, since only a minority of the plasma electrons acquires most of the absorbed energy in contrast to collision absorption (inverse bremsstrahlung), which heats all of the electrons.

For the p-polarization obliquely incident laser it is convenient to solve the equation for the magnetic field, which is in the x direction. Similar to the arguments leading to equation (5.91), the magnetic field can be presented by

$$B_x = B(z)\exp\left(\frac{\mathrm{i}\omega y \sin\theta_0}{c}\right). \tag{5.101}$$

Substituting (5.101) into the wave equation (5.50) for the magnetic field, one has to solve the differential equation

$$\frac{\mathrm{d}^2B(z)}{\mathrm{d}z^2} - \frac{1}{\varepsilon}\frac{\mathrm{d}\varepsilon}{\mathrm{d}z}\frac{\mathrm{d}B(z)}{\mathrm{d}z} + \frac{\omega^2}{c^2}(\varepsilon - \sin^2\theta_0)B(z) = 0. \tag{5.102}$$

Using ε from (5.80) for $\nu_{\mathrm{ei}} = 0$, equation (5.102) can be rewritten as

$$\frac{\mathrm{d}^2B(z)}{\mathrm{d}z^2} + \frac{1}{(z-L)}\frac{\mathrm{d}B(z)}{\mathrm{d}z} - \left(\frac{\omega^2}{Lc^2}\right)[(z-L) + L\sin^2\theta_0]B(z) = 0. \tag{5.103}$$

Substituting

$$\zeta = \left(\frac{\omega^2}{Lc^2}\right)^{1/3}(z-L), \qquad \tau = \left(\frac{\omega L}{c}\right)^{1/3}\sin\theta_0 = \left(\frac{2\pi L}{\lambda_{\mathrm{L}}}\right)^{1/3}\sin\theta_0 \tag{5.104}$$

equation (5.103) takes the form

$$\frac{\mathrm{d}^2B}{\mathrm{d}\zeta^2} - \frac{1}{\zeta}\frac{\mathrm{d}B}{\mathrm{d}\zeta} - (\zeta + \tau^2) = 0. \tag{5.105}$$

Note that τ and ζ are dimensionless. The differential equation (5.105) depends on a single parameter τ. This equation is singular at $\zeta = 0$, i.e. at the critical surface. Near the critical surface, where $\zeta \ll \tau^2$, one has the equation

$$\frac{\mathrm{d}^2B}{\mathrm{d}\zeta^2} - \frac{1}{\zeta}\frac{\mathrm{d}B}{\mathrm{d}\zeta} - \tau^2 = 0. \tag{5.106}$$

The solution of this differential equation is (one can easily check the solution by direct substitution into (5.106))

$$B(\zeta) = B_0(1 + \tfrac{1}{2}\tau^2\zeta^2\ln\zeta) \tag{5.107}$$

where B_0 is a constant. The magnetic field $B_x(y,z)$ is thus given near the critical surface from (5.101), (5.104) and (5.107):

$$B_x(z \to L, y) = B_0\left\{1 + \frac{\tau^2}{2}\left(\frac{\omega^2}{Lc^2}\right)^{2/3}(z-L)^2\left[\frac{1}{3}\ln\left(\frac{\omega^2}{Lc^2}\right) + \ln(z-L)\right]\right\} \times \exp\left(\frac{\mathrm{i}\omega y\sin\theta_0}{c}\right). \tag{5.108}$$

The electric field in the critical surface region is calculated by using equation (5.39) (note that $\partial/\partial x = 0$ in our choice of coordinates):

$$\mathbf{E}(z \to L, y) = \frac{\mathrm{i}cL}{\omega(L-z)} \nabla \times \mathbf{B} = \frac{\mathrm{i}cL}{\omega(L-z)} \left(0, \frac{\partial B_x(y,z)}{\partial z}, \frac{\partial B_x(y,z)}{\partial y}\right)$$
$$\Rightarrow \left(0, \ln(z-L), \frac{1}{(L-z)}\right). \tag{5.109}$$

While the magnetic field goes to a constant the electric field has a singularity, i.e. a resonance, at the critical surface. This singularity disappears by including a small damping of the wave, i.e. including collisions (electron–ion or Landau electron–wave). The collisions introduce an imaginary part in the dielectric function ε (see (5.80) that moves the singularity off the z axis. A schematic solution for the electric field is given in figure 5.5.

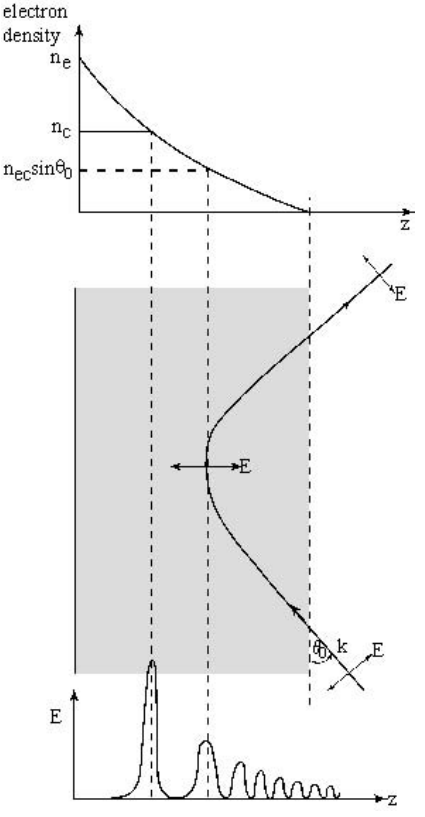

Figure 5.5. A schematic solution for the electric field in the p-polarization case.

The existence of the singularity in the electric field at the critical surface can be recognized immediately by considering the following Maxwell equation in the dielectric plasma medium:

$$0 = \nabla \cdot (\varepsilon \mathbf{E}) = \varepsilon \nabla \cdot \mathbf{E} + (\nabla \varepsilon) \cdot \mathbf{E}. \tag{5.110}$$

Therefore, for $\varepsilon = \varepsilon(z)$ one has

$$\nabla \cdot \mathbf{E} = -\frac{1}{\varepsilon} \frac{\partial \varepsilon}{\partial z} E_z. \tag{5.111}$$

The resonance is only for the p-polarization where the electric field in the z direction does not vanish, but the dielectric function can vanish there ($\varepsilon = 0$ at $\omega = \omega_{pe}$). When the p-polarized laser is reflected (when $\theta = 90^\circ$) the electric field has a component parallel to the density gradient. This field causes charge separation as the electron oscillates along the gradient. The electron density wave variations (δn) due to this effect are given by

$$\delta n \approx \nabla \cdot \mathbf{E} = -\frac{1}{\varepsilon} \frac{\partial \varepsilon}{\partial z} E_z \tag{5.112}$$

where $\nabla \cdot \mathbf{E}$ from (5.111) was substituted into (5.112). One can see that for a plasma frequency equal to the laser frequency (where ε vanishes) one has a resonance in the plasma wave. Therefore, the electron plasma wave is excited resonantly at the critical density for the p-polarized laser radiation.

Let us check the consistency of this analysis with the solution of the electric field near the critical surface (equation (5.109)). From this equation one gets

$$\begin{aligned} E(z \to L) &\approx \frac{1}{(z - L)} \\ \delta n_e \approx \nabla \cdot E(z \to L) &\approx \frac{1}{(z - L)^2} \approx \frac{E(z \to L)}{\varepsilon(z \to L)} \end{aligned} \tag{5.113}$$

as predicted in the above picture by equation (5.111). Therefore, the charge separation near the critical surface oscillates with the plasma frequency and excites the plasma wave resonantly.

No laser absorption is possible without damping. The dissipation of the laser energy is possible by electron–ion or electron–wave collisions, or any other mechanism that makes the dielectric function complex. The absorbed energy flux I_{abs} [dimension of energy/(area time)] can also be presented as

$$I_{abs} = \int \nu_{eff} \left(\frac{E^2}{8\pi} \right) \mathrm{d}z \tag{5.114}$$

where ν_{eff} is the effective collision frequency and the integral is along the electromagnetic ray path. The fraction f_a of the absorbed energy is therefore

given by

$$f_a = \frac{I_{abs}}{I_L} = \frac{\int \nu_{eff} E^2 \, dz}{cE_L^2}. \tag{5.115}$$

For the linear density profile and a p-polarized laser it has been calculated (Ginzburg 1961, Pert 1978) that the laser absorption is

$$f_a \cong 36\tau^2 \frac{[\mathrm{Ai}(\tau)]^3}{|\mathrm{d}\,\mathrm{Ai}(\tau)/\mathrm{d}(\tau)|} \tag{5.116}$$

where Ai is the Airy function and τ is defined in equation (5.104). f_a vanishes at $t = 0$, goes to zero for $\tau \approx 2$, and has a maximum value at about $\tau \approx 0.8$ with a maximum absorption of about 50%, i.e.

$$f_a(\tau \approx 0.8) \cong 0.5. \tag{5.117}$$

It has been shown (Forslund *et al*. 1975) that for ions at rest the absorption is practically unchanged up to electron temperatures of 100 keV.

Substituting for $\tau = 0.8$ in equation (5.104) yields $\sin\theta_0 = 0.42\lambda_L/L$. For a plasma dimension $L \gg \lambda_L$, the resonant absorption is confined to a light incident almost perpendicular ($\theta_0 \approx 0^\circ$). However, for large laser irradiances $I_L > 10^{16}\,\mathrm{W/cm^2}$, the ponderomotive force steepens the plasma density and in this case $L \approx \lambda_L$ is possible. Also for small laser pulse duration, $\tau_L < 20\,\mathrm{ps}$, the plasma dimension is smaller than the laser wavelength in vacuum. These small plasma dimensions have peak resonance absorption at about 25° (see figure 5.6). The high electric field near the critical surface in these cases can accelerate electrons to energies much higher than the plasma temperature.

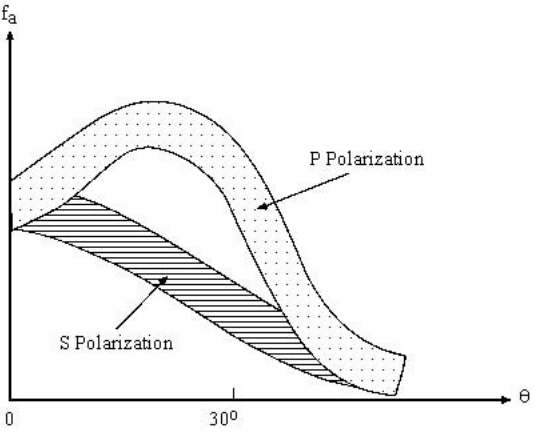

Figure 5.6. Schematic absorption fraction for a p-polarized laser in comparison with an s-polarized laser for a given laser intensity.

5.7 Femtosecond Laser Pulses

For this class of lasers the solid target is heated faster than the time scale for hydrodynamic expansion. The plasma medium in this case has a density equal to its initial solid density during the laser pulse duration. The typical laser pulse duration is of the order of $\tau_L \sim 100\,\text{fs}$. During this time the laser is absorbed and heats the target along a skin depth $\delta \approx 200\,\text{Å}$, a value much larger than the surface expansion $\sim 10\,\text{Å}$. For a laser spot much larger than the skin depth one can assume a one-dimensional problem.

We assume that the laser is radiated in the z direction and is normally incident on a solid target (positioned in the x–y plane) at $z = 0$. The wave equation of the electric field for a linearly polarized monochromatic wave at normal incidence is (see (5.51))

$$\frac{\partial^2 E(z)}{\partial z^2} + \frac{\varepsilon(\omega, z)\omega^2 E(z)}{c^2} = 0. \tag{5.118}$$

This equation is also known as the **Helmholtz equation** (Milchberg and Freeman 1989). $\varepsilon(\omega, z)$ is the dielectric permittivity of the target related to the electrical conductivity σ_E by (see section 2.7)

$$\varepsilon = 1 + \frac{\mathrm{i}4\pi\sigma_E}{\omega}. \tag{5.119}$$

For a constant ε and a vanishing electric field at infinity, the solution of equation (5.118) is

$$E(z) = E(0)\exp\left(-\frac{z}{\delta}\right) \tag{5.120}$$

where $E(z)$ is the electric field **transmitted** into the solid target. Denoting by E_i and E_r the **incident** and **reflected** electric field accordingly, one can write

$$E_i = E(0)\exp[\mathrm{i}(kz - \omega t)], \qquad E_r = \sqrt{R}E(0)\exp[\mathrm{i}(-kz - \omega t)] \tag{5.121}$$

where R is the reflection coefficient. The **absorption coefficient** A is given by (Landau and Lifshitz 1975, Born and Wolf 1980)

$$A = 1 - R, \qquad R = \left|\frac{1-\sqrt{\varepsilon}}{1+\sqrt{\varepsilon}}\right|^2 = \frac{(n_R - 1)^2 + n_I^2}{(n_R + 1)^2 + n_I^2} \tag{5.122}$$

where the complex index of refraction is defined as

$$\sqrt{\varepsilon} = n_R + \mathrm{i}n_I. \tag{5.123}$$

Substituting the solution (5.120) into (5.118) yields the **skin depth** δ:

$$\delta = \frac{\mathrm{i}}{\sqrt{\varepsilon}}\frac{c}{\omega}. \tag{5.124}$$

Substituting for the dielectric function (see section 2.7),

$$\varepsilon = 1 - \frac{\omega_{pe}^2}{\omega(\omega + i\nu)} \tag{5.125}$$

where ω_{pe} is the plasma frequency and ν is the electron effective collision frequency (e.g. $\nu = \nu_{ei}$), one gets (More *et al.* 1988)

$$\begin{aligned}\delta &= \frac{c}{\omega_{pe}}\left(\frac{1 + i(\nu/\omega)}{1 - (\omega^2/\omega_{pe}^2) - i(\nu\omega/\omega_{pe}^2)}\right)^{1/2} \\ &\approx \frac{c}{\omega_{pe}}\left(1 + i\frac{\nu}{\omega}\right)^{1/2} \quad \text{for } \omega_{pe} \gg \omega.\end{aligned} \tag{5.126}$$

In our plasma medium (solid target) $\omega_{pe} \gg \omega$ and therefore the last approximation is justified. The skin depth is therefore given by

$$\delta = \begin{cases} \dfrac{c}{\omega_{pe}} & \text{for } \dfrac{\nu}{\omega} \ll 1 \text{ and } \dfrac{\omega}{\omega_{pe}} \ll 1 \\ \dfrac{c}{\omega_{pe}}\left(\dfrac{\nu}{2\omega}\right)^{1/2} & \text{for } \dfrac{\nu}{\omega} \gg 1 \text{ and } \dfrac{\omega}{\omega_{pe}} \ll 1. \end{cases} \tag{5.127}$$

For the last stage the following algebraic relation was used:

$$\begin{aligned}\sqrt{a + ib} = \frac{1}{\sqrt{2}}(a^2 + b^2)^{1/4} \\ \times \left[\left(1 + \frac{a}{\sqrt{a^2 + b^2}}\right)^{1/2} + i\left(1 - \frac{a}{\sqrt{a^2 + b^2}}\right)^{1/2}\right].\end{aligned} \tag{5.128}$$

Using the dielectric function from (5.125) into the absorption coefficient A in (5.122), one gets

$$A = \begin{cases} \dfrac{2\nu}{\omega_{pe}} & \text{for } \dfrac{\nu}{\omega} \ll 1 \text{ and } \dfrac{\omega}{\omega_{pe}} \ll 1 \\ \dfrac{2\nu}{\omega_{pe}}\sqrt{\dfrac{\omega}{\nu}} & \text{for } \dfrac{\nu}{\omega} \gg 1 \text{ and } \dfrac{\omega}{\omega_{pe}} \ll 1. \end{cases} \tag{5.129}$$

For the above analysis it was assumed that the dielectric function ε is a constant in space and time. However, in general this is a very crude approximation, since during the (time-dependent) laser pulse duration, the dielectric function ε is not constant due to the change of electron and ion temperatures as well as possible change of the electron number density. The electron collision frequency ν and the electrical conductivity σ_E are functions of T_e, T_i and n_e, which are functions of space and time. In this case the following approach is more suitable.

The Joule heating gives the laser power deposition into the target per unit volume:

$$Q(z, t) = \tfrac{1}{2}\mathrm{Re}\{\sigma_E(z, t)\}|E|^2. \tag{5.130}$$

Note that $\sigma_E(\omega, z)$ and $\varepsilon(\omega, z)$ vary with time t on a time scale much longer than $2\pi/\omega$. Both σ_E and ε depend on z and t through $T_e(z,t)$ and $T_i(z,t)$, while Q and $E(z)$ also depend on t via the laser pulse temporal intensity profile, $I_L(t)$. A good approximation for the intensity profile is

$$\begin{aligned} I_L &\approx I_0 \sin^2\left(\frac{\pi t}{2\tau_L}\right) \quad \text{for } 0 \le t \le 2\tau_L \\ I_L &\approx 0 \qquad\qquad\qquad\quad \text{for } t \le 0, t \ge 2\tau_L \end{aligned} \tag{5.131}$$

where τ_L is the FWHM pulse duration. The absorption coefficient A measured at a given location (x, y) on the target surface $(z = 0)$ is averaged over the temporal pulse profile:

$$A = \frac{\displaystyle\int_0^{2\tau_L} \mathrm{d}t \int_0^{\infty} Q(z,t)\,\mathrm{d}z}{\displaystyle\int_0^{2\tau_L} I_L(t)\,\mathrm{d}t}. \tag{5.132}$$

In order to calculate the absorption coefficient A in (5.132) one has to use the heat deposition $Q(z,t)$ given in (5.130), which requires knowledge of the electric field E and electric conductivity σ_E inside the target.

Since the interaction of the femtosecond laser has a solid state of matter during the laser pulse duration, a knowledge of **quantum solid state physics** is required (Ziman 1960, Ashcroft and Mermin 1976, Gantmakher and Levinson 1987, Peierls 2001). In the following we shall outline the ingredients and some approximated formulas for the calculation of the absorption of femtosecond lasers by solid targets. The dielectric permittivity ε, or equivalently the electrical conductivity σ_E (equation (5.119)), contains the contribution from both the inter-band and intra-band absorption mechanism:

$$\sigma_E = \sigma_{bb} + \sigma_D. \tag{5.133}$$

The subscript bb and D stand for inter-band (band–band transition) absorption and intra-band absorption, known as the Drude contribution (the inverse bremsstrahlung absorption) given by

$$\sigma_D = \frac{n_e e^2}{m_{eff}}\left(\frac{\nu + \mathrm{i}\omega}{\nu^2 + \omega^2}\right). \tag{5.134}$$

Regarding the band–band transitions there are two distinct possibilities. One transition can occur between the Bloch-electron bands (between the lower (e.g. first band) and the upper (e.g. second band) one-electron bands in the first Brillouin zone), as in aluminium metal (Ashcroft and Sturm 1971). The other possibility is the transition between the occupied atomic states and the Fermi surface. The bb transitions will not be further discussed

here, although they can contribute significantly to the absorption of femtosecond lasers (Fisher *et al.* 2001).

The electric conductivity in equation (5.134) is a function of the electron collision frequency ν, which in our case is the total momentum relaxation rate for electrons in the solid. This collision frequency has two contributions,

$$\nu = \nu_{\text{e-ph}}(T_\text{e}, T_\text{i}) + \nu_{\text{e-e}}(T_\text{e}) \tag{5.135}$$

where $\nu_{\text{e-ph}}$ and $\nu_{\text{e-e}}$ are the electron momentum relaxation rates due to electron–phonon and electron–electron collisions, respectively. Since ν is a function of T_e and T_i it is necessary to solve the energy equations (as given in section 3.3):

$$\begin{aligned} C_\text{e}(T_\text{e})\frac{\partial T_\text{e}}{\partial t} &= \frac{\partial}{\partial z}\left(\kappa(T_\text{e})\frac{\partial T_\text{e}}{\partial z}\right) - U(T_\text{e}, T_\text{i}) + Q(z,t) \\ C_\text{i}(T_\text{i})\frac{\partial T_\text{i}}{\partial t} &= U(T_\text{e}, T_\text{i}) \end{aligned} \tag{5.136}$$

where C_e and C_i are the electron and ion heat capacities at constant volume (dimension [erg/(cm^3 K)]), κ is the electron heat conductivity (dimension [erg/(cm s)]) and U is the energy transfer rate from electrons to ions and can also be written by

$$U = \gamma(T_\text{e} - T_\text{i}). \tag{5.137}$$

To calculate κ, U and σ_E as functions of T_e and T_i, knowledge of the phonon spectrum (i.e. the dispersion relation) and the electron–phonon interaction matrix element is required (Kaganov *et al.* 1957).

The phonon spectrum $\omega_\text{ph}(q)$ for longitudinal phonons, where q is the phonon wave vector, can be approximated by (Dederichs *et al.* 1981)

$$\begin{aligned} \omega_\text{ph}(q) &= qs \quad \text{for } q \le q_\text{b} \\ \omega_\text{ph}(q) &= q_\text{b}s \quad \text{for } q \ge q_\text{b} \end{aligned} \tag{5.138}$$

where s is the longitudinal sound velocity (e.g. $s = 6.4 \times 10^5$ cm/s for aluminium) and q_b is a parameter determined by fitting the d.c. electrical conductivity data.

Since electron–phonon scattering in metals occurs primarily via a single longitudinal phonon absorption or emission (by an electron), the following matrix element squared is assumed (Gantmakher and Levinson 1987):

$$|M(\mathbf{k} \to \mathbf{k}' \pm \mathbf{q})|^2 = \begin{cases} \dfrac{\hbar w_0^2 q}{2V\rho s}\delta_{\mathbf{k}'-\mathbf{k},\mp\mathbf{q}} & \text{for } q \le q_\text{b} \\ \dfrac{\hbar w_0^2 q_\text{b}}{2V\rho s}\delta_{\mathbf{k}'-\mathbf{k},\mp\mathbf{q}} & \text{for } q \ge q_\text{b} \end{cases} \tag{5.139}$$

where w_0 is the deformation potential constant, ρ and V are the medium density and volume and $\hbar\mathbf{q}$ is the quasi-momentum of the absorbed (or emitted) phonon as the electron wave vector has changed from $\mathbf{k}$ to $\mathbf{k}'$. The δ in (5.139) takes care of the momentum conservation in these processes. The transition probability is given by

$$W(\mathbf{k} \to \mathbf{k}' \pm \mathbf{q}) = \frac{2\pi}{\hbar} |M(\mathbf{k} \to \mathbf{k}' \pm \mathbf{q})|^2 (N_\mathrm{q} + \tfrac{1}{2} \pm \tfrac{1}{2}) \delta(E_\mathrm{k} - E_{\mathrm{k}'} \mp \hbar\omega_\mathrm{ph}(q)) \tag{5.140}$$

where $E_\mathrm{k} = E_\mathrm{F} + \hbar^2\{k_\mathrm{F}(|k| - |k_\mathrm{F}|)/2m_\mathrm{eff}\}$ and the δ describes the energy conservation. N_q is the population of longitudinal phonon mode in the first Brillouin zone with the reduced momentum $q_\mathrm{red} = \mathbf{q} - \mathbf{K}$, where $\mathbf{K}$ is a corresponding vector of the reciprocal lattice. $\mathbf{q}$ may lie outside the first Brillouin zone (Umklapp process) but q_b is inside the first Brillouin zone. N_q is the Bose–Einstein distribution function given by

$$N_\mathrm{q} = \left\{ \exp\left[\frac{\hbar\omega_\mathrm{ph}(q_\mathrm{red})}{k_\mathrm{B} T_\mathrm{i}} \right] - 1 \right\}^{-1}. \tag{5.141}$$

The rate of electron–phonon (i.e. electron–ion) energy exchange U is calculated by the method described by Kaganov *et al.* (Kaganov *et al.* 1957, Allen 1987, Fisher *et al.* 2001):

$$U = \frac{1}{(2\pi)^3} \int \left(\frac{\mathrm{d}N_\mathrm{q}}{\mathrm{d}t} \right) \hbar\omega_\mathrm{q} 4\pi q^2 \, \mathrm{d}q. \tag{5.142}$$

Using the phonon dispersion relation (5.138) and the matrix element (5.139), we get equation (5.143). Note that $U(T_\mathrm{e} = T_\mathrm{i}) = 0$ as required from physical consideration. For aluminium with ion temperatures larger than 300 K equation (5.143) yields a γ value in the domain $(3.7\text{–}3.9) \times 10^{18}$ erg/(cm^3 s K). This value is in very good agreement with Wang and Downer (Wang and Downer 1992) and is by a factor of 1.5–3 larger than the empirical values of Eidman *et al.* (Eidman *et al.* 2000):

$$\begin{aligned} U &= \gamma(T_\mathrm{e} - T_\mathrm{i}) \\ &= \frac{s w_0^2 m_\mathrm{eff}^2}{4\pi^3 \hbar^2 \rho} \\ &\quad \times \left\{ \begin{array}{l} \left(\dfrac{\hbar s}{k_\mathrm{B} T_\mathrm{e}} \right)^{-5} \displaystyle\int_0^{(\hbar q_\mathrm{b} s / k_\mathrm{B} T_\mathrm{e})} \frac{x^4 \, \mathrm{d}x}{e^x - 1} - \left(\frac{\hbar s}{k_\mathrm{B} T_\mathrm{i}} \right)^{-5} \int_0^{(\hbar q_\mathrm{b} s / k_\mathrm{B} T_\mathrm{i})} \frac{x^4 \, \mathrm{d}x}{e^x - 1} \\ + \dfrac{q_\mathrm{b}^3}{2} (4k_\mathrm{F}^2 - q_\mathrm{b}^2) \left\{ \left[\exp\left(\dfrac{\hbar q_\mathrm{b} s}{k_\mathrm{B} T_\mathrm{e}} \right) - 1 \right]^{-1} - \left[\exp\left(\dfrac{\hbar q_\mathrm{b} s}{k_\mathrm{B} T_\mathrm{i}} \right) - 1 \right]^{-1} \right\} \end{array} \right\}. \end{aligned} \tag{5.143}$$

The electron heat conductivity is given by

$$\kappa(T_e, T_i) \approx \frac{C_e}{3\nu}\left(v_F^2 + \frac{3k_B T_e}{m_e}\right) \tag{5.144}$$

where $v_F = \hbar k_F / m_{eff}$ is the Fermi velocity, m_{eff} is the effective mass of the electron in the solid and $\hbar = 2\pi h$, where h is the Planck constant. The Fermi momentum k_F is related to the Fermi energy $E_F = (\hbar k_F)^2/2m_e$, where m_e is the (free) electron mass. ν is given by (5.135) and it has two contributions, one from the electron–electron collisions and the second from the electron–phonon collisions defined by

$$\nu_{e\text{-}ph} = \sum_{k'} W(\mathbf{k} \to \mathbf{k}' \pm \mathbf{q})\left[\frac{(\mathbf{k} - \mathbf{k}') \cdot \mathbf{k}}{k^2}\right]\left[\frac{1 - f(k', T_e)}{1 - f(k, T_e)}\right]. \tag{5.145}$$

$f(k, T_e)$, the Fermi–Dirac distribution, describes the electron population

$$f(k, T_e) = \left\{\exp\left[\frac{E_k - \mu(T_e)}{k_B T_e}\right] + 1\right\}^{-1} \tag{5.146}$$

where μ is the free electron chemical potential. One can see from (5.145) that ν is the electron momentum relaxation rate due to collisions with phonons. For temperatures higher than the Fermi temperature the $\nu_{e\text{-}ph}$ has to be changed to the plasma frequency collisions ν_{ei} (see section 2.2).

We do not give here a detailed calculation of $\nu_{e\text{-}ph}$, but point out that for temperature lower than the Fermi temperature the electron–phonon collision frequency is independent of T_e and the following approximation is valid:

$$\nu_{e\text{-}ph} \approx B_1 T_i \quad \text{for } T_i \le T_F = \frac{E_F}{k_B} \tag{5.147}$$

where B_1 is a constant. If solid–liquid phase transition takes place then the approximation (5.147) is valid for $T_e = T_i < T_m$ (T_m is the melting temperature) and for $T_F > T_e = T_i > T_m$, and $\nu_{e\text{-}ph}$ is expected to have a jump at T_m. However, on the femtosecond time scale T_e is not equal to T_i and it is conceivable that the solid–liquid transition time is longer than the laser pulse duration, so that in this case equation (5.147) might be a good approximation. For $T_e > T_F$ this dependence on T_i is no longer satisfied. However, in this domain $\nu_{e\text{-}ph}$ is significantly smaller than the momentum relaxation rate in electron–electron collisions $\nu_{e\text{-}e}$, given by

$$\nu_{e\text{-}e} \approx \begin{cases} \dfrac{E_F}{\hbar}\left(\dfrac{T_e}{T_F}\right)^2 \equiv B_2 T_e^2 & \text{for } T_e < T_F \\ \dfrac{E_F}{\hbar}\left(\dfrac{T_e}{T_F}\right)^{-3/2} & \text{for } T_e > T_F. \end{cases} \tag{5.148}$$

In the second approximation of (5.148) the logarithmic factor in T_e was ignored. The values of w_0 and q_b in the above equations are determined by

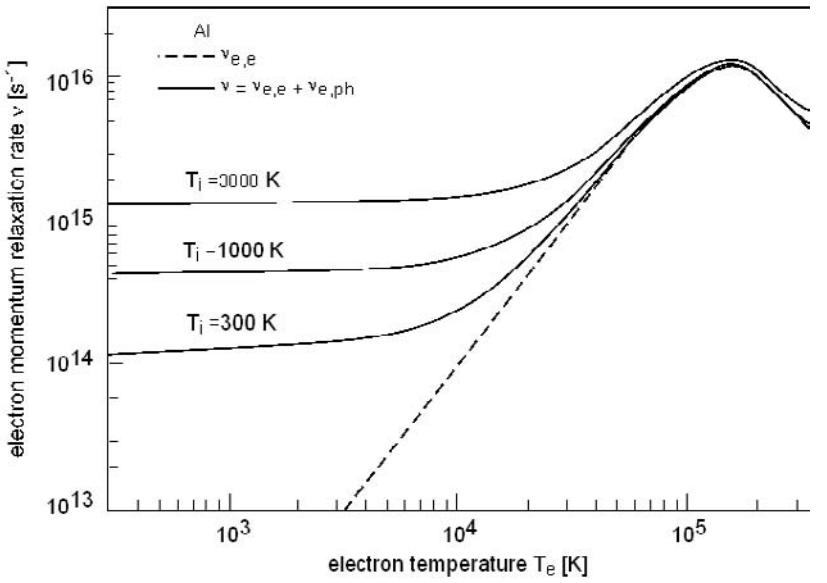

Figure 5.7. Calculated collision frequency $\nu(T_e, T_i)$ for several values of ion temperature T_i.

fitting the d.c. electrical conductivity with the experimental data (Zinovev 1996) as a function of temperature. Using (5.134), (5.147) and (5.148), one has to fit the following expression in order to obtain the values of w_0 and q_b:

$$\begin{aligned} \sigma_E(\text{d.c.}) &\equiv \sigma_E(\omega = 0) = \frac{n_e e^2}{m_{\text{eff}}\nu} \\ \nu(T_e = T_i = T < T_m) &= B_1 T + B_2 T^2. \end{aligned} \tag{5.149}$$

For example, for aluminium with an electron effective mass $m_{\text{eff}} = 1.20 m_e$ one gets $w_0 = 5.16\,\text{eV}$ and $q_b = 4.77 \times 10^7\,\text{cm}^{-1}$. Figure 5.7 shows the calculated values of the collision frequency $\nu(T_e, T_i)$ as a function of the electron temperature for several values of ion temperatures.

In order to solve the energy equations (5.136) one has to know also the electron and ion heat capacities at constant volume C_e and C_i. C_e can be approximated by

$$\begin{aligned} C_e(\text{low}) &= \frac{\pi^2 n_e k_B^2 T_e}{2E_F} && \text{for } k_B T_e \ll E_F \\ C_e(\text{high}) &= 1.5 k_B n_e && \text{for } k_B T_e \gg E_F \\ C_e &= \frac{C_e(\text{low}) C_e(\text{high})}{\sqrt{C_e(\text{low})^2 + C_e(\text{high})^2}} && \text{for } k_B T_e \approx E_F. \end{aligned} \tag{5.150}$$

The ion heat capacity at constant volume is given by

$$C_i = \left(\frac{\partial E_i}{\partial T_i}\right)_V \approx \begin{cases} 3k_B n_i & \text{for } T_i \geq 300\,\text{K} \\ \sim T_i^3 & \text{for } T_i \ll 300\,\text{K} \end{cases}$$
$$E_i = \sum_{\text{phonon modes}} \int_0^{q_{\max}} \frac{dq\, 4\pi q^2 \hbar\omega(q)}{(2\pi)^3 \left[\exp\left(\frac{\hbar\omega(q)}{k_B T_i}\right) - 1\right]} \tag{5.151}$$

where E_i is the phonon energy per unit volume and plasma neutrality requires $n_e = Zn_i$, where Z is the degree of ionization (including the electrons in the conduction band). Last input to the energy equations (5.136) is the electron heat conductivity, given by

$$\kappa(T_e, T_i) \approx \frac{C_e}{3\nu}\left(v_F^2 + \frac{3k_B T_e}{m_e}\right) \tag{5.152}$$

where $v_F = \hbar k_F / m_{\text{eff}}$ is the Fermi velocity.

The characteristic time scale for electron **momentum relaxation** τ_{ke} is

$$\tau_{ke} = \frac{1}{\nu(T_e, T_i)}. \tag{5.153}$$

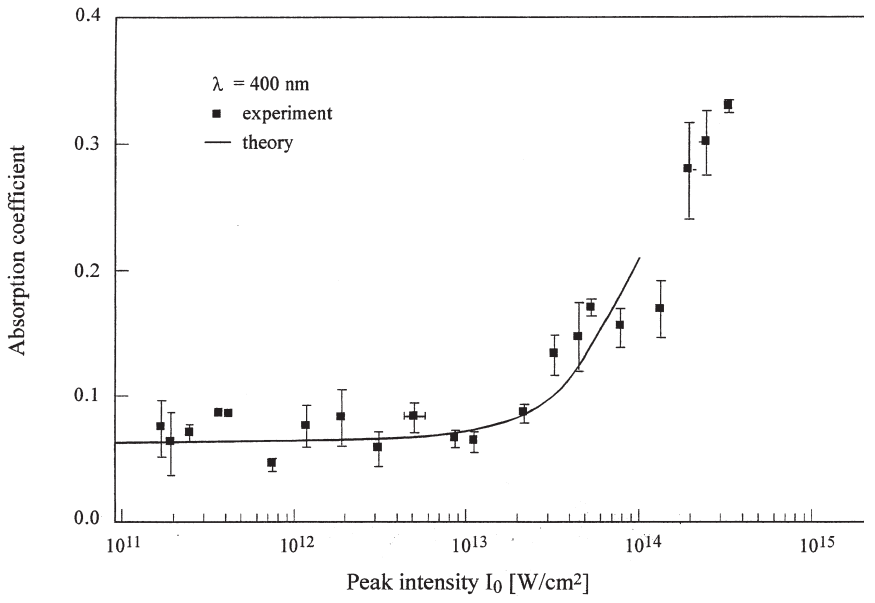

Figure 5.8. Absorption of a 50 fs titanium–sapphire laser ($\lambda_L = 0.800\,\mu$m), doubled in frequency ($\lambda_L = 0.4\,\mu$m), by an aluminium target (Fisher *et al.* 2001).

For aluminium at room temperature this characteristic time scale is dominated by electron–phonon collisions and equals $\tau_k = 8\,\text{fs}$, while at the Fermi temperature ($T_F = 0.135 \times 10^6\,\text{K}$) the electron–electron collisions dominate and $\tau_k = 0.1\,\text{fs}$.

The characteristic times of **electron energy relaxation** (cooling) τ_{Ee}, and **ion** (i.e. lattice) **energy relaxation** (heating) τ_{Ei}, are defined by

$$\tau_{Ee} = \frac{C_e(T_e - T_i)}{U} = \frac{C_e}{\gamma}, \qquad \tau_{Ei} = \frac{C_i}{\gamma}. \tag{5.154}$$

For aluminium the electron energy relaxation time increases from $\tau_{Ee}(T_e = 300\,\text{K}) \approx 100\,\text{fs}$ to $\tau_{Ee}(T_e = T_F) \approx 10\,\text{ps}$ mainly due to the increase in $C_e(T_e)$, while $\tau_{Ei}(T_e > 300\,\text{K}) \approx 6\,\text{ps}$ since both C_i and γ are nearly constant in T_e and T_i at room temperature and above.

We end this chapter with figure 5.8, showing the detailed results of the above calculations for a titanium–sapphire laser ($\tau_L = 50\,\text{fs}$, $\lambda_L = 0.800\,\mu\text{m}$) interacting with an aluminium target. The experimental data for a doubled frequency ($\lambda_L = 0.4\,\mu\text{m}$) indicate the domain where the above approximations are relevant.

Chapter 6

Waves in Laser-Produced Plasma

6.1 Foreword to Parametric Instabilities

The dispersion relation for electron plasma waves is developed in section 2.6. Some changes in the dispersion relation of electron and ion waves due to ponderomotive force are given in section 4.3. In this chapter we discuss mainly the parametric instabilities in laser–plasma interactions.

All material substances, including plasma, interact nonlinearly with high-power lasers leading to parametric instabilities. A **parametric instability** is defined in general by the nonlinear phenomenon where a periodic variation in the medium induces growing oscillations at a different frequency. In solids, liquids and gases these instabilities arise due to the nonlinear polarizability of the material. In a plasma medium the nonlinear effects are caused by such terms as $\mathbf{v} \times \mathbf{B}$, $\mathbf{v} \cdot \nabla \mathbf{v}$, $\nabla \cdot (n\mathbf{v})$, ponderomotive forces, changes of mass due to relativistic velocities, velocity-dependent collision frequency, etc. These terms can cause a large amplitude wave, called the **pump wave**, which provides the driving force to excite other wave modes in the plasma.

In the absence of a pump wave and a magnetic field, three modes of propagation are possible in plasma:

(a) **electromagnetic wave**;
(b) **electron wave**, known as **plasmon** or **Langmuir wave** (sometimes denoted by '**high frequency electrostatic plasma wave**'); and
(c) **ion wave**, also called **acoustic wave** (sometimes denoted by '**low frequency electrostatic ion-acoustic wave**').

Neglecting the ponderomotive forces, the dispersion relations of these waves are

$$\textbf{electromagnetic wave}: \quad \omega^2 = \omega_{\mathrm{pe}}^2 + c^2 k^2 \tag{6.1}$$

$$\textbf{electron wave} = \textbf{plasmon}: \quad \omega^2 = \omega_{\mathrm{pe}}^2 + 3k^2 v_{\mathrm{e}}^2 \tag{6.2}$$

$$\textbf{ion wave} = \textbf{acoustic wave}: \quad \omega = kc_s = k\left(\frac{Zk_B T_e}{m_i}\right)^{1/2} \tag{6.3}$$

where ω and k are the wave frequency and wave number respectively and $\omega_{pe} = (4\pi e^2 n_e/m_e)^{1/2}$ is the electron plasma frequency. m_e and m_i are the electron and ion mass respectively, Z is the degree of ionization, c is the speed of light and c_s is the sound velocity, T_e, v_e and n_e are the electron temperature, velocity and density respectively, and k_B is the Boltzmann constant. T_e much larger than the ion temperature is assumed. Equations (6.1) and (6.2) were derived in sections 2.7 and 2.6 respectively, while equation (6.3) is developed in section 6.6 of this chapter (the soliton section).

A high-power laser wave (denoted by the incoming 'photon'), serving as a pump, can induce the following parametric instabilities in plasma:

Wave–wave interaction

photon → photon + acoustic	(stimulated Brillouin scattering = SBS)
photon → photon + plasmon	(stimulated Raman scattering = SRS)
photon → acoustic + plasmon	(decay instability)
photon → plasmon + plasmon	(two-plasmon instability)

Wave–particle interaction

photon + particle → photon + particle	(stimulated Compton scattering)
photon + particle → plasmon + particle	(stimulated Compton scattering)
photon + particle → acoustic + particle	(stimulated Compton scattering)

(6.4)

In (6.4) 'photon', 'acoustic' and 'plasmon' mean electromagnetic, ion and electron waves respectively. The **energy and momentum conservation** in the wave–wave interaction is described by

$$\omega_0 = \omega_1 + \omega_2, \qquad \mathbf{k}_0 = \mathbf{k}_1 + \mathbf{k}_2 \tag{6.5}$$

where ω_0 and $\mathbf{k}_0$ are the frequency and wave number of the pumping laser field that decays into two waves (ω_1, $\mathbf{k}_1$) and (ω_2, $\mathbf{k}_2$). Using these conservation laws and the dispersion relations (6.1), (6.2) and (6.3), the wave–wave interactions are induced in the following domain:

1. A laser pump with frequency near the plasma frequency, $\omega_0 \approx \omega_{pe}$, may decay into a plasmon and an ion wave, resulting in absorption of the laser. This effect happens near the critical surface since $\omega_0 \approx \omega_{pe}$ implies $n_e \approx n_{ec}$, where n_{ec} is the critical density.
2. A laser pump with frequency $\omega_0 > 2\omega_{pe}$ may decay into a photon and a plasmon (SRS), leading to laser scattering, including backscattering.

This instability reduces the laser absorption. $\omega_0 > 2\omega_{pe}$ implies that this instability occurs at $n_e < \frac{1}{4}n_{ec}$.

3. A laser pump with frequency $\omega_0 > \omega_{pe}$ may decay into a photon and an acoustic wave (SBS), resulting in backscattering and thus reduced laser

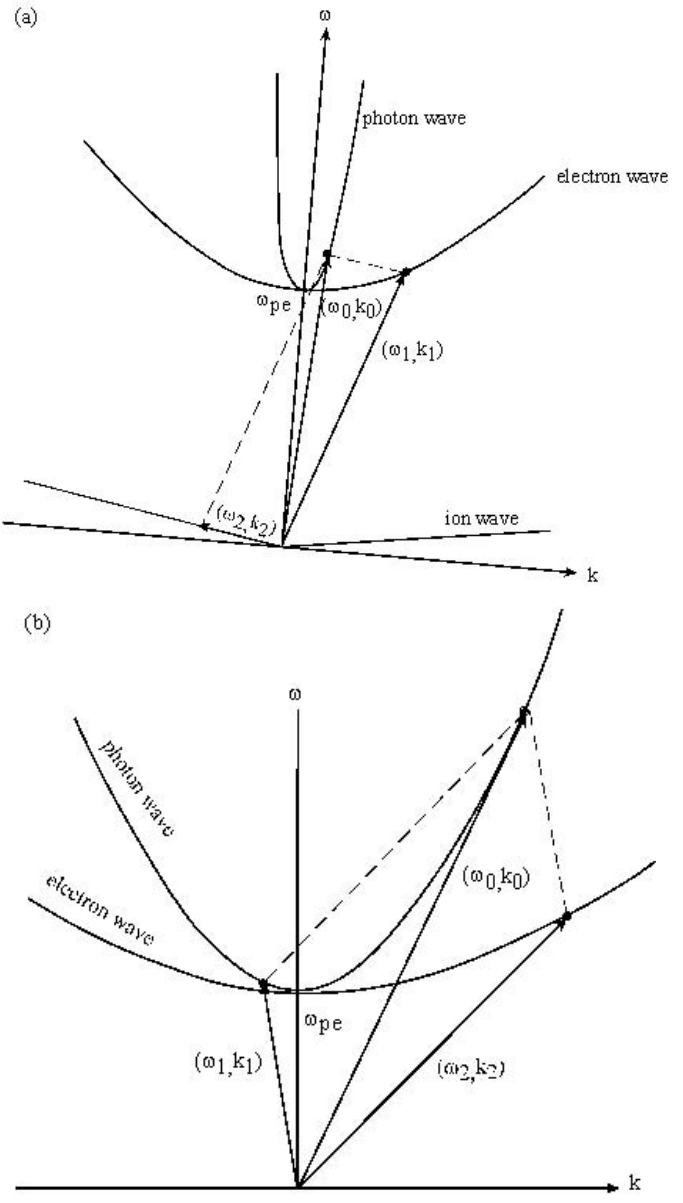

Figure 6.1—continues.

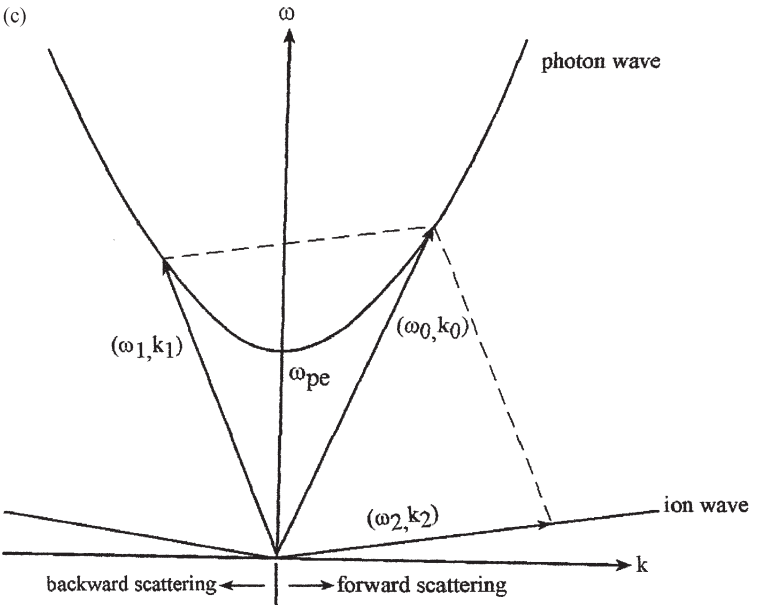

Figure 6.1. Schematic description in the ω-k space of the conservation laws given in equations (6.5), taking into account the dispersion relations (6.1), (6.2) and (6.3) for (a) decay instability, (b) stimulated Raman instability and (c) stimulated Brillouin instability.

absorption. SBS contains a low-energy ion wave that takes only a small fraction of the laser energy, while the rest of the energy can be scattered out of the plasma. $\omega_0 > \omega_{pe}$ implies that this instability occurs at $n_e < n_{ec}$.

4. A laser pump with frequency $\omega_0 = 2\omega_{pe}$ may decay into two plasmons, inducing laser absorption. This phenomenon happens at an electron density $n_e = \frac{1}{4} n_{ec}$.

A schematic description of the conservation laws given in equations (6.5) are given in figure 6.1 (Hughes 1980), taking into account the dispersion relations (6.1), (6.2) and (6.3) for (a) decay instability, (b) stimulated Raman instability and (c) stimulated Brillouin instability. The wave is described by a point vector on the appropriate dispersion relation line in the ω-k space and equations (6.5) are satisfied by adding the vectors according to the decay under consideration.

The possible absorption mechanisms and the domain of wave–wave interactions are summarized in figure 6.2 along a density profile typical of laser–plasma interaction.

Parametric instabilities in plasma have been studied for the past 40 years. Since the first analytic analysis (Dubois and Goldman 1965, Silin

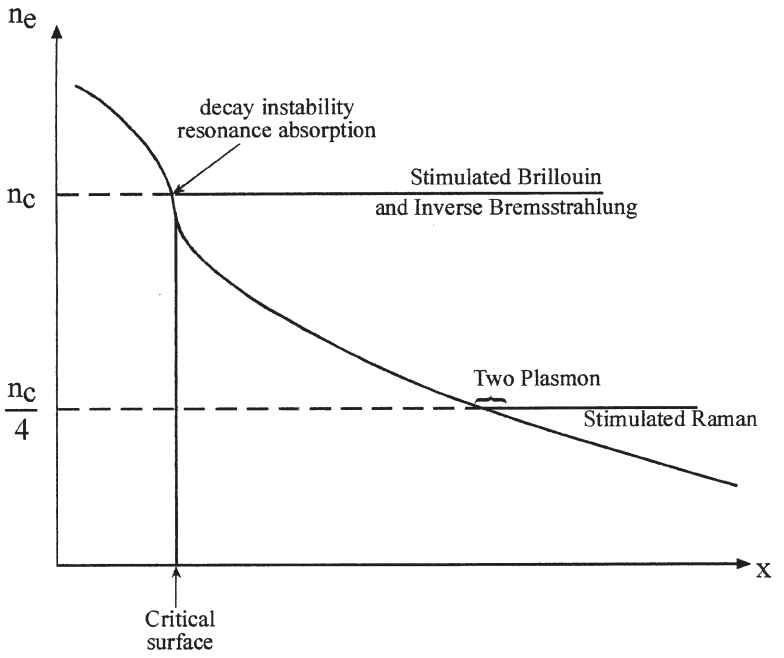

Figure 6.2. Possible absorption mechanisms and the domain of wave–wave interactions along the density profile.

1965a), general treatment of the parametric instabilities were developed (Nishikawa 1968, Rosenbluth 1972, Chen 1974, Dawson and Lin 1974, Kaw *et al.* 1976, Hughes 1980, Cairns 1983, Kruer 1988) and the experimental status summarized (Baldis *et al.* 1991). Since the 1960s at almost every conference on high-power laser–plasma interactions, the subject of parametric instabilities has been on the agenda.

In section 6.2 the forced harmonic oscillator is summarized in an elementary introduction (Crawford 1968) to the general formalism of parametric instabilities. As is demonstrated in this section, energy cannot be absorbed by a wave without the existence of damping. In non-relativistic plasma the electromagnetic wave suffers only collisional damping. However, the electron and ion waves experience in addition to collision the collisionless damping due to wave particle interactions. In order to clarify this physically important phenomenon, discovered by Landau (Landau 1946), a physical picture of Landau damping (Stix 1992, Kruer 1988) is given in section 6.3. In section 6.4 the formalism of the parametric decay instability is given and in section 6.5 the stimulated Brillouin scattering is developed. We end this chapter with section 6.6, where the soliton equation is obtained for ion plasma waves.

6.2 The Forced Harmonic Oscillator

In this section the harmonic motion of a point mass oscillating in the x direction is summarized (Crawford 1968). This is instructive for understanding the more complex problem of parametric instabilities. The displacement from equilibrium is denoted by $x(t)$. The forces acting on the mass m are:

(a) The return force, $-m\omega_0^2 x(t)$, due to a spring constant $K = m\omega_0^2$.
(b) A frictional drag force, $-m\Gamma(\mathrm{d}/\mathrm{d}t)x$, where Γ is the damping constant per unit mass (Γ has the dimension of s^{-1}).
(c) An external force $F(t)$.

First, the special case where $F = 0$ is considered. The equation describing the motion for the displacement from equilibrium $x_1(t)$ is

$$\frac{\mathrm{d}^2 x_1}{\mathrm{d}t^2} + \Gamma \frac{\mathrm{d}x_1}{\mathrm{d}t} + \omega_0^2 x_1 = 0. \tag{6.6}$$

The solution of (6.6) with the initial conditions $x_1(0)$ and $v_1(0) = (\mathrm{d}/\mathrm{d}t)x_1(0)$ is

$$x_1(t) = \exp\left(-\frac{\Gamma t}{2}\right)\left\{x_1(0)\cos\omega_1 t + \left[\frac{v_1(0) + 0.5\Gamma x_1(0)}{\omega_1}\right]\sin\omega_1 t\right\} \tag{6.7}$$

$$\omega_1^2 = \omega_0^2 - \tfrac{1}{4}\Gamma^2.$$

The oscillations are weakly damped if $\frac{1}{2}\Gamma \ll \omega_0$. The oscillations are critically damped if $\frac{1}{2}\Gamma \approx \omega_0$, in this case $\omega_1 \to 0$, $\cos\omega_1 t \to 1$ and $(1/\omega)\sin\omega_1 t \to t$. If $\frac{1}{2}\Gamma > \omega_0$ the oscillations are over-damped, $\omega_1 = \pm\mathrm{i}|\omega_1|$ and $\cos\omega_1 t \to \cosh\omega_1 t$, $\sin\omega_1 t \to \sinh\omega_1 t$.

Next, the forced oscillation is introduced by taking $F(t) = F_0\cos\omega t$. This case is representative for functions that can be described by Fourier transform. Therefore, the equation of motion in this case is given by

$$\frac{\mathrm{d}^2 x}{\mathrm{d}t^2} + \Gamma\frac{\mathrm{d}x}{\mathrm{d}t} + \omega_0^2 x = \left(\frac{F_0}{m}\right)\cos\omega t. \tag{6.8}$$

The **steady-state** solution of this equation describes the motion of the oscillator after the harmonic driving force has been applied for a very long time compared with the free oscillation mean decay time $\tau_\mathrm{f} = 1/\Gamma$. In this case the harmonic oscillations are at frequency ω. The steady-state solution of equation (6.8) is

$$\begin{aligned} x_\mathrm{s} &= X_\mathrm{ab}\sin\omega t + X_\mathrm{el}\cos\omega t \\ X_\mathrm{ab} &= \left(\frac{F_0}{m}\right)\left\{\frac{\Gamma\omega}{(\omega_0^2-\omega^2)^2 + \Gamma^2\omega^2}\right\} \\ X_\mathrm{el} &= \left(\frac{F_0}{m}\right)\left\{\frac{\omega_0^2-\omega^2}{(\omega_0^2-\omega^2)^2 + \Gamma^2\omega^2}\right\}. \end{aligned} \tag{6.9}$$

It is important to point out that $X_{ab}(\Gamma = 0) = 0$. One can see that X_{ab} is the amplitude of power absorption. On the other hand, X_{el} does not contribute to the power absorption (see equation (6.10)) but contributes only to the energy of the system; thus it describes an elastic amplitude.

The time-averaged input power $P(\omega)$ into the oscillator is

$$P(\omega) = \left\langle F(t)\frac{dx}{dt}\right\rangle = \frac{1}{2}F_0\omega X_{ab}$$
$$= \left(\frac{F_0^2}{2m\Gamma}\right)\frac{\Gamma^2\omega^2}{(\omega_0^2-\omega^2)^2+\Gamma^2\omega^2} \tag{6.10}$$

where $\langle\ \rangle$ denotes time average, and $\langle\cos^2\omega t\rangle = \frac{1}{2}$, $\langle\cos\omega t\sin\omega t\rangle = 0$ was used. We emphasize again that $P = 0$ if $\Gamma = 0$.

The frequencies $\omega(\pm\frac{1}{2})$, where the power decreases to half its value, are

$$\omega(\pm\tfrac{1}{2}) = \sqrt{\omega^2+\frac{\Gamma^2}{4}} \pm \frac{\Gamma}{2}. \tag{6.11}$$

The frequency interval between the two half-power points, $\Delta\omega_{res} = \omega(+\frac{1}{2}) - \omega(-\frac{1}{2})$ is defined as the 'full-frequency width at half maximum' and equals Γ. Therefore, one has the following very important relation between the resonance 'full-width' for forced oscillations and the mean decay time for free oscillations τ_f:

$$\Delta\omega_{res}\tau_f = 1, \qquad \Delta\omega_{res} = \Gamma, \qquad \tau_f = \frac{1}{\Gamma}. \tag{6.12}$$

It is important to note that even for a system with many degrees of freedom the resonant width and the free decay time for each mode satisfy equation (6.12), assuming that the resonances are well separated, i.e. they do not overlap.

The time-averaged stored energy $W(\omega)$ is given by

$$W(\omega) = \frac{1}{2}m\left\langle\left(\frac{dx}{dt}\right)^2\right\rangle + \frac{1}{2}m\omega_0^2\langle x^2\rangle = \frac{1}{4}m(\omega_0^2+\omega^2)(X_{ab}^2+X_{el}^2)$$
$$= \left(\frac{F_0^2}{4m}\right)\frac{(\omega_0^2+\omega^2)}{(\omega_0^2-\omega^2)^2+\Gamma^2\omega^2}. \tag{6.13}$$

The general solution of equation (6.8) is

$$x(t) = x_1(t) + x_s(t)$$
$$= \exp\left(-\frac{\Gamma t}{2}\right)(X_1\sin\omega_1 t + X_2\cos\omega_1 t) + X_{ab}\sin\omega t + X_{el}\cos\omega t \tag{6.14}$$

where X_1 and X_2 are arbitrary constants fixed by the initial conditions of displacement and velocity. Taking $x(0) = 0$, and $v(0) = 0$ the solution

(6.14) can be rewritten

$$x(t) = X_{\mathrm{ab}}\left[\sin\omega t - \exp\left(-\frac{\Gamma t}{2}\right)\sin\omega_1 t\right] + X_{\mathrm{el}}\left[\cos\omega t - \exp\left(-\frac{\Gamma t}{2}\right)\cos\omega_1 t\right]. \tag{6.15}$$

Two special solutions are of interest, one at the eigenvalue frequency,

$$x(t, \omega = \omega_1) = \left[1 - \exp\left(-\frac{\Gamma t}{2}\right)\right] x_{\mathrm{s}}(t) \tag{6.16}$$

(note that for $t \gg 1/\Gamma$ one gets the steady-state solution as given above) and the second, more important, is the resonance solution (for $\Gamma = 0$)

$$x(t, \omega = \omega_0) = \left(\frac{F_0}{2m\omega_0}\right) t \sin\omega_0 t. \tag{6.17}$$

In the resonant case the amplitude of oscillations is unbounded as $t \to \infty$ because the oscillator continuously absorbs energy from periodic external force. This system is in resonance with the external force.

6.3 Landau Damping

Landau damping is discussed in almost every book on plasma physics. However, in most of the literature this collisionless damping appears in an abstract mathematical formalism. An electron or ion wave can be damped without collisions. Since this phenomenon is not a mathematical trick, but has a concrete physical reality, it is also important to explain it in a physical picture supported by mathematics. We shall follow a picture suggested by Stix (Kruer 1988, Stix 1992).

In the simplest one-dimensional model, the motion of the particles (electrons or ions) in an electric field are described by Newton's law:

$$\frac{\mathrm{d}^2 x}{\mathrm{d}t^2} = \frac{\mathrm{d}v}{\mathrm{d}t} = \frac{qE}{m}\sin(kx - \omega t) \tag{6.18}$$

where x is the coordinate of the particle, q and m are the charge and mass of the particle, and E, k and ω are the amplitude, the wave number and the angular frequency of the electric field. Equation (6.18) is nonlinear and very complex.

Following the previous section it seems that without damping it is impossible to damp energy into (or out) of the particles. This statement is correct only for one particle, or for a system of particles whose velocity distribution is constant. However, by considering a non-constant velocity distribution of the particles, one can divide the particles into two groups: one with velocity v significantly different from the wave phase velocity

ω/k, and the second with a velocity in the range of the electric field phase velocity, $v \approx \omega/k$. For v very different from ω/k, equation (6.18) implies that these particles oscillate without any gain or loss of energy. However, particles with a velocity $v \approx \omega/k$ feel a nearly constant electric field and therefore can be accelerated or decelerated. If the velocity distribution of the particles is not constant in the surrounding $v \approx \omega/k$, then the wave can exchange energy with the particles.

Equation (6.18) is solved using the iteration method, by expanding the solutions for $x(t)$ about a position x_0 and a free streaming velocity v_0 ($\approx \omega/k$):

$$x(t) = x_0 + v_0 t + x_1(t) + x_2(t), \qquad v(t) = \frac{\mathrm{d}x}{\mathrm{d}t} = v_0 + v_1 + v_2. \tag{6.19}$$

The zeroth-order solution of (6.18) is obtained by taking $E = 0$:

$$x(t, E = 0) = x_0 + v_0 t. \tag{6.20}$$

Substituting (6.20) into (6.18), one obtains the first-order contributions v_1 and x_1:

$$\begin{aligned} v_1 &= \frac{qE}{m\alpha}[\cos(kx_0 - \alpha t) - \cos kx_0] \\ x_1 &= -\frac{qE}{m\alpha^2}[\sin(kx_0 - \alpha t) - \sin kx_0 + \alpha t \cos kx_0] \\ \alpha &\equiv \omega - kv_0 \end{aligned} \tag{6.21}$$

where the initial conditions $v_1(0) = 0$ and $x_1(0) = 0$ were chosen. Substituting $x = x_0 + v_0 t + x_1$ into the right-hand side of equation (6.18), one gets $(\mathrm{d}/\mathrm{d}t)v_1 + (\mathrm{d}/\mathrm{d}t)v_2$ on the left-hand side of this equation. Using v_1 and x_1 from (6.21) yields

$$\begin{aligned} \frac{\mathrm{d}v_2}{\mathrm{d}t} &= \frac{qE}{m}\{\sin[(kx_0 - \alpha t) + kx_1] - \sin(kx_0 - \alpha t)\} \\ &= \frac{2qE}{m}\left\{\cos\left(kx_0 - \alpha t + \frac{kx_1}{2}\right)\sin\left(\frac{kx_1}{2}\right)\right\} \\ &\approx \frac{qE}{m}\{kx_1 \cos(kx_0 - \alpha t)\} \\ &= \frac{kq^2E^2}{m^2\alpha^2}\cos(kx_0 - \alpha t)[\sin(kx_0 - \alpha t) - \sin(kx_0) + \alpha t \cos kx_0]. \end{aligned} \tag{6.22}$$

Now the formulae are available to calculate the rate of change of the particle energy, $P(t)$. Denoting by $\langle\ \rangle_{x_0}$ the average over the initial positions and assuming that the particles are initially at random (i.e. $\langle \cos kx_0 \rangle_{x_0} = \langle \sin kx_0 \rangle_{x_0} = 0$, $\langle \cos^2 kx_0 \rangle_{x_0} = \frac{1}{2}$, etc.), one gets for $P(t; v_0)$:

$$P(t; v_0) = \left\langle \frac{\mathrm{d}}{\mathrm{d}t}\left(\frac{1}{2}mv^2\right)\right\rangle_{x_0} = m\left(\left\langle v_0 \frac{\mathrm{d}v_2}{\mathrm{d}t}\right\rangle_{x_0} + \left\langle v_1 \frac{\mathrm{d}v_1}{\mathrm{d}t}\right\rangle_{x_0}\right). \tag{6.23}$$

The term $\langle v_0 v_1 \rangle_{x_0} = 0$, while terms with a higher order than E^2 were neglected. Substituting (6.21) and (6.22) into (6.23) and averaging over the initial positions of the particles, one gets

$$P(t; v_0) = \frac{q^2 E^2}{2m} \left[\frac{\sin \alpha t}{\alpha} + k v_0 \left(\frac{\sin \alpha t}{\alpha^2} - \frac{t \cos \alpha t}{\alpha} \right) \right]$$
$$= \frac{q^2 E^2}{2m} \left[\frac{\sin \alpha t}{\alpha} - \frac{\partial}{\partial \alpha} \left(\frac{\sin \alpha t}{\alpha} \right) \right]. \tag{6.24}$$

We are interested in the vicinity of $\omega - k v_0 = \alpha \approx 0$, therefore the main contribution to the power given above is achieved for very large times. Therefore, it seems justifiable to take the limit $t \to \infty$ (Kruer 1988) in equation (6.24). Using in (6.24) the following representation for the Dirac delta function:

$$\delta(\alpha) = \frac{1}{\pi} \lim_{t \to \infty} \frac{\sin \alpha t}{\alpha} \tag{6.25}$$

and the identity

$$\delta(\alpha) = \delta(\omega - k v_0) = \frac{1}{|k|} \delta \left(v_0 - \frac{\omega}{k} \right) \tag{6.26}$$

one gets

$$P(v_0) = \frac{\pi q^2 E^2}{2m|k|} \frac{\partial}{\partial v_0} \left[v_0 \delta \left(v_0 - \frac{\omega}{k} \right) \right]. \tag{6.27}$$

The last step is to average over the initial velocity distribution of the particles $f(v_0)$, in order to obtain the desired energy rate exchange between the wave and the particles:

$$\langle P(v_0) \rangle_{v_0} = \int_{-\infty}^{+\infty} \mathrm{d}v_0 f(v_0) P(v_0) = -\frac{\pi q^2 E^2}{2m|k|} \left(\frac{\omega}{k} \right) \left[\frac{\partial f(v_0)}{\partial v_0} \right]_{(v_0 = \omega/k)}. \tag{6.28}$$

Note that $\langle P(v_0) \rangle_{v_0}$ is the average power given to the particles. For positive values the particles gain energy, while for negative values the particles lose energy, and all this without collisions between the particles. From this result one can see that the collisionless energy exchange between the wave and the particles occurs for particles having a velocity almost equal to the wave phase velocity. Particles with $v_0 < \omega/k$ (but in the vicinity of ω/k) gain energy from the wave, while particles with $v_0 > \omega/k$ (but in the vicinity of ω/k) lose energy to the wave. If $f(v_0)$ decreases with increasing velocity, i.e. the slope of $f(v_0)$ is negative at ω/k, then the wave loses energy to the particles. If $f(v_0)$ increases with increasing velocity, i.e. the slope of $f(v_0)$ is positive at ω/k, then the wave gains energy from the particles.

The power density balance (energy given by the wave = energy taken by the particles) between the wave and the particles can be written by

$$n\langle P(v_0)\rangle_{v_0} = -\frac{\mathrm{d}}{\mathrm{d}t}\left(\frac{E^2}{8\pi}\right) = -\frac{\Gamma_{\mathrm{EM}}E^2}{4\pi} \tag{6.29}$$

where n is the particle density, $E \propto \cos(\omega t)$, and Γ_{EM} (the wave damping constant) is the imaginary part of ω. Using (6.28) and (6.29), one gets

$$\frac{\Gamma_{\mathrm{EM}}}{\omega} = \frac{\pi\omega_{\mathrm{pe}}^2}{2n_{\mathrm{e}}k^2}\left[\left(\frac{\partial f(v_0)}{\partial v_0}\right)_{v_0=\omega/k}\right]. \tag{6.30}$$

In the last equation an electron wave is assumed, where ω_{pe} is the electron plasma frequency and $n = n_{\mathrm{e}}$ is the electron density. Landau has derived equation (6.30) by using the Vlasov equation (see section 3.4). Using a Maxwellian distribution for the electrons, $f(v) \approx \exp(-v^2/2v_{\mathrm{e}}^2)$, where $mv_{\mathrm{e}}^2 = k_{\mathrm{B}}T_{\mathrm{e}}$ (T_{e} = the electron temperature), equation (6.30) yields

$$\frac{\Gamma_{\mathrm{EM}}}{\omega} = -\sqrt{\frac{\pi}{8}}\,\frac{\omega_{\mathrm{pe}}^2\omega}{k^2|k|v_{\mathrm{e}}^3}\exp\left(-\frac{\omega^2}{2k^2v_{\mathrm{e}}^2}\right). \tag{6.31}$$

6.4 Parametric Decay Instability

The energy-momentum conservation of an electromagnetic wave decaying into a plasma wave is described schematically in figure 6.1(a). This decay is called the parametric decay instability. This instability is described in a formalism (Nishikawa 1968) of two harmonic oscillators with damping (see section 6.1), where the electromagnetic wave times the 'other oscillator' are acting as a driving force. The electromagnetic wave is the pump, where A_0 and ω_0 denote its amplitude and frequency:

$$A_0 = E_0\cos\omega_0 t = \frac{E_0}{2}[\exp(\mathrm{i}\omega_0 t) + \exp(-\mathrm{i}\omega_0 t)]. \tag{6.32}$$

The electron and ion density fluctuation amplitudes are A_1 and A_2; their appropriate frequencies are ω_1 and ω_2 and $\omega_1 > \omega_2$. More explicitly, the equations of motion describing the electron wave (denoted by index 1) and the ion wave (denoted by index 2) are

$$\begin{aligned}\frac{\mathrm{d}^2A_1}{\mathrm{d}t^2} + \Gamma_1\frac{\mathrm{d}A_1}{\mathrm{d}t} + \omega_1^2A_1 &= c_1A_2A_0\\ \frac{\mathrm{d}^2A_2}{\mathrm{d}t^2} + \Gamma_2\frac{\mathrm{d}A_2}{\mathrm{d}t} + \omega_2^2A_2 &= c_2A_1A_0.\end{aligned} \tag{6.33}$$

The coefficients Γ_j ($j = 1$ or 2) describe the collision plus collisionless (Landau) damping, ω_j ($j = 1$ or 2) are the eigenvalue of equations (6.33) with the neglect of damping and coupling ($c_1 = c_2 = 0$), and it is assumed

that the pump amplitude A_0 is unaffected by the decay waves 1 and 2. These nonlinear equations are transformed to algebraic equations by Fourier transform:

$$A(\omega) = \frac{1}{2\pi}\int \mathrm{d}t \exp(\mathrm{i}\omega t)A(t). \tag{6.34}$$

Note that in the case of nonlinear equations it is not permitted to make the substitution $(\partial/\partial t) \to -\mathrm{i}\omega$. For example, using (6.32) and (6.34) one gets

$$\begin{aligned}\frac{1}{2\pi}\int \mathrm{d}t\, A_0(t)\exp(\mathrm{i}\omega t)A_2(t) &= \frac{E_0}{4\pi}\int \mathrm{d}t[\exp(\mathrm{i}\omega_0 t) + \exp(-\mathrm{i}\omega_0 t)]\exp(\mathrm{i}\omega t)A_2(t)\\ &= \frac{E_0}{2}[A_2(\omega+\omega_0) + A_2(\omega-\omega_0)].\end{aligned} \tag{6.35}$$

Assuming constant damping rates, the Fourier transform of equations (6.33) yields the following algebraic equations:

$$\begin{aligned} D_1(\omega)A_1(\omega) + \frac{c_1E_0}{2}[A_2(\omega+\omega_0) + A_2(\omega-\omega_0)] &= 0\\ D_2(\omega-\omega_0)A_2(\omega-\omega_0) + \frac{c_2E_0}{2}[A_1(\omega) + A_1(\omega-2\omega_0)] &= 0\\ D_2(\omega+\omega_0)A_2(\omega+\omega_0) + \frac{c_2E_0}{2}[A_1(\omega) + A_1(\omega+2\omega_0)] &= 0\end{aligned} \tag{6.36}$$

where $D_j(\omega)$ is defined by

$$D_j(\omega) = \omega^2 - \omega_j^2 + \mathrm{i}\omega\Gamma_j \quad \text{for } j = 1, 2. \tag{6.37}$$

In the first equation of (6.36) one can see that mode 1 at a frequency $\omega[A_1(\omega)]$ couples with mode 2 $[A_2]$ at $\omega+\omega_0$ and $\omega-\omega_0$, as demonstrated in (6.35). Therefore, in order to obtain $A_2(\omega+\omega_0)$ and $A_2(\omega-\omega_0)$, one has to take a Fourier transform like (6.35) for modes 1 at frequencies ω, $\omega+2\omega_0$ and $\omega-2\omega_0$, leading to the second and third equations of (6.36). Assuming that mode 1 is resonant only near ω, one can neglect $A_1(\omega+2\omega_0)$ and $A_1(\omega-2\omega_0)$ in equations (6.36), yielding three algebraic equations with three unknowns $A_1(\omega)$, $A_2(\omega-\omega_0)$ and $A_2(\omega+\omega_0)$, written in matrix form:

$$\begin{pmatrix} D_1(\omega) & c_1E_0/2 & c_1E_0/2\\ c_2E_0/2 & D_2(\omega-\omega_0) & 0\\ c_2E_0/2 & 0 & D_2(\omega+\omega_0)\end{pmatrix}\begin{pmatrix} A_1(\omega)\\ A_2(\omega-\omega_0)\\ A_2(\omega+\omega_0)\end{pmatrix} = \begin{pmatrix}0\\0\\0\end{pmatrix}. \tag{6.38}$$

A solution is obtained only if the determinant of the coefficients vanish. Since A_1 describes the electron wave, where $\omega_0 \approx \omega \approx \omega_1$, one can neglect the parametric decay instability for the off-resonance amplitude $A_2(\omega+\omega_0)$. In

this case the zero determinant of the coefficients of (6.38) yields

$$D_1(\omega)D_2(\omega-\omega_0)-\frac{c_1c_2E_0^2}{4}$$
$$\approx -4\omega_1\omega_2\left(\omega-\omega_1+\mathrm{i}\frac{\Gamma_1}{2}\right)\left(\omega-\omega_0+\omega_2+\mathrm{i}\frac{\Gamma_2}{2}\right)-\frac{c_1c_2E_0^2}{4}=0 \quad (6.39)$$

where the following relations have been used: $\omega_0-\omega\approx\omega_2$, $\omega+\omega_1\approx 2\omega_1$ and $\Gamma_1\omega\approx\Gamma_1\omega_1$. Defining the real and complex parts of ω by ω_R and Γ respectively,

$$\omega=\omega_\mathrm{R}+\mathrm{i}\Gamma. \quad (6.40)$$

Equation (6.39) yields two equations (the first by equating the real part to zero and the second by equating the imaginary part to zero):

$$\begin{aligned}(\omega_\mathrm{R}-\omega_1)(\omega_\mathrm{R}-\omega_1-\delta)+\alpha E_0^2&=(\Gamma+\tfrac{1}{2}\Gamma_1)(\Gamma+\tfrac{1}{2}\Gamma_2)\\ \omega_\mathrm{R}&=\omega_1+\frac{(\Gamma+\frac{1}{2}\Gamma_1)\delta}{2\Gamma+\frac{1}{2}\Gamma_1+\frac{1}{2}\Gamma_2}\\ \delta&\equiv\omega_0-\omega_1-\omega_2\\ \alpha&\equiv\frac{c_1c_2}{4\omega_1\omega_2}.\end{aligned} \quad (6.41)$$

Substituting the second equation of (6.41) into the first one we get

$$E_0^2=\frac{1}{\alpha}\left\{(\Gamma+\tfrac{1}{2}\Gamma_1)(\Gamma+\tfrac{1}{2}\Gamma_2)\left[1+\frac{\delta^2}{(2\Gamma+\frac{1}{2}\Gamma_1+\frac{1}{2}\Gamma_2)^2}\right]\right\}. \quad (6.42)$$

Note that $E_0^2/(8\pi)$ is the (time-averaged) laser field energy density, i.e. the pump energy density in our case. For E_0 defined in (6.32) the laser irradiance I_L (erg cm^{-2} s^{-1}) is $cE_0^2/(8\pi)$. The pump energy can be invested into the electron and ion waves only if the damping Γ is positive, $\Gamma\geq 0$. The threshold pumping, i.e. the threshold laser field $E_{0,\mathrm{th}}$, is obtained by substituting $\Gamma=0$ in equation (6.42):

$$E_{0,\mathrm{th}}^2=\frac{\omega_1\omega_2\Gamma_1\Gamma_2}{c_1c_2}\left[1+\frac{4\delta^2}{(\Gamma_1+\Gamma_2)^2}\right]. \quad (6.43)$$

The threshold energy of the pump goes to zero when the damping (collisional or Landau) of either the electron wave or the ion wave goes to zero. The minimum pumping amplitude $E_{0,\mathrm{min}}$ is obtained for the exact resonance condition, i.e. $\delta=0$:

$$E_{0,\mathrm{min}}^2=\frac{\omega_1\omega_2\Gamma_1\Gamma_2}{c_1c_2}. \quad (6.44)$$

The maximum growth rate $\Gamma_{\max}$ of the parametric instability is given from (6.42), by substituting in this equation $\Gamma_1 = \Gamma_2 = 0$ and $\delta = 0$:

$$\Gamma_{\max} = \left(\frac{c_1 c_2}{4\omega_1 \omega_2} \right)^{1/2} E_0. \tag{6.45}$$

At this stage it is important to point out that the vanishing of the 3×3 determinant of (6.38) also has an imaginary eigenvalue

$$\omega = \mathrm{i}\Gamma. \tag{6.46}$$

In this case one of the modes has a zero frequency and the second mode has the pump frequency ω_0. This instability is known as the **oscillating two-stream** instability. This phenomenon acquired this name because the electrons (or the ions) have a time-averaged particle distribution function with two peaks, as in the two-stream instabilities. The following scenario can explain this instability (Chen 1974) if the pump frequency is smaller than the plasma frequency: an ion density fluctuation causes a charge separation, which induces an electric field oscillating with the pump frequency. Even if the pump is homogeneous in space, the induced electric field is not homogeneous and thus applies a ponderomotive force on the electrons, which are moving from the low-density to the high-density region. The created d.c. (low frequency) electric field drags the ions and the ion density perturbation grows. The density ripple does not propagate since $\mathrm{Re}\,\omega = 0$.

We now calculate the values of c_1 and c_2 in the above equations by analysing the more (algebraic) simple oscillating two-stream instability. Note that in Gaussian units the dimension of $[c_j]$ is $[\mathrm{s}^{-1}\,(\mathrm{cm/g})^{1/2}]$. Since c_1 and c_2 are model-independent, we can choose the simplest relevant model. In particular, the Poisson equation and the fluid equations for ions and electrons are used; where the collision frequencies are neglected, $\Gamma_1 = \Gamma_2 = 0$, the electron and ion temperatures also vanish, $T_\mathrm{e} = T_\mathrm{i} = 0$, and the degree of ionization is taken as $Z = 1$.

The electron motion is described by a superposition of a high-frequency motion and a low-frequency motion. The high-frequency motion is independent of the ion motion, while the low-frequency motion describes electrons and ions moving together in a quasi-neutral motion. The induced electric field, as explained above, also has low- and high-frequency components. The indices l and h are used for low- and high-frequency components, while the index 0 is used for the pump component or the zeroth-order approximation. The electric field E, the ion and electron densities n_i and n_e, and the fluid ion and electron velocities v_i and v_e have the components

$$\begin{gathered} E = E_0 + E_\mathrm{h} + E_\mathrm{l}, \qquad n_\mathrm{i} = n_0 + n_\mathrm{l}, \\ n_\mathrm{e} = n_0 + n_\mathrm{l} + n_\mathrm{h}, \qquad v_\mathrm{i} = v_\mathrm{l}, \qquad v_\mathrm{e} = v_0 + v_\mathrm{l} + v_\mathrm{h}. \end{gathered} \tag{6.47}$$

It is assumed that the space perturbation is oscillatory, of the form $\exp(\mathrm{i}kx)$, and the equations are linearized, so that in the equations describing the plasma one can use the Fourier transform result for linear equations:

$$\frac{\partial}{\partial x} = \mathrm{i}k. \tag{6.48}$$

The equations describing the plasma system under consideration are:

(a) The ion force (momentum) and continuity equations

$$\frac{\partial v_\mathrm{l}}{\partial t} = \frac{eE_\mathrm{l}}{m_\mathrm{i}}, \qquad \frac{\partial n_\mathrm{l}}{\partial t} + n_0 \frac{\partial v_\mathrm{l}}{\partial x} = 0. \tag{6.49}$$

(b) The electron force (momentum) and continuity equation

$$\frac{\partial v_\mathrm{e}}{\partial t} + v_\mathrm{e} \frac{\partial v_\mathrm{e}}{\partial x} = -\frac{e}{m_\mathrm{e}}(E_0 + E_\mathrm{h} + E_\mathrm{l}), \qquad \frac{\partial n_\mathrm{e}}{\partial t} + n_\mathrm{e} \frac{\partial v_\mathrm{e}}{\partial x} = 0. \tag{6.50}$$

(c) The Poisson equation

$$\frac{\partial E}{\partial x} = -4\pi e n_\mathrm{h} \;\Rightarrow \mathrm{i}kE_\mathrm{h} = -4\pi e n_\mathrm{h}. \tag{6.51}$$

Taking the time derivative of the continuity ion equation and using the force equation, both of (6.49) and using (6.48), one gets

$$\frac{\partial^2 n_\mathrm{l}}{\partial t^2} = -\frac{\mathrm{i}ken_0 E_\mathrm{l}}{m_\mathrm{i}}. \tag{6.52}$$

Note that E_l is induced by the ponderomotive force, proportional to $\nabla(E_0 + E_\mathrm{h})^2 \approx 2E_0 \nabla E_\mathrm{h}$. Therefore, E_l is determined by the knowledge of E_h. Linearizing the electron force equation in (6.50) about the zeroth-order electron velocity, and using a Poisson equation, one gets for the fast and low frequency components

$$-\mathrm{i}\omega_0 v_\mathrm{h} = \frac{4\pi e^2 n_\mathrm{h}}{\mathrm{i}km_\mathrm{e}}, \qquad \mathrm{i}k\left(\frac{eE_0 \cos\omega_0 t}{\mathrm{i}\omega_0 m_\mathrm{e}}\right) v_\mathrm{h} = -\frac{eE_\mathrm{l}}{m_\mathrm{e}}. \tag{6.53}$$

From these last two equations one gets the low-frequency electric field E_l, which is substituted into (6.52) to get the ion (i.e. low-frequency) driven equation:

$$\frac{\partial^2 n_\mathrm{l}}{\partial t^2} = c_2 n_\mathrm{h} E_0 \cos\omega_0 t, \qquad c_2 \equiv -\frac{\mathrm{i}ek}{m_\mathrm{i}}\left(\frac{\omega_\mathrm{pe}^2}{\omega_0^2}\right) \approx -\frac{\mathrm{i}ek}{m_\mathrm{i}}. \tag{6.54}$$

Equation (6.54) describes how a high-frequency density (n_h) times the pump drives a low-frequency (n_l) density with a coupling c_2.

The electron continuity equation of (6.50), with the use of (6.48) and (6.51), yields

$$\frac{\partial n_\mathrm{h}}{\partial t} + \mathrm{i}kn_0 v_\mathrm{h} + \mathrm{i}kv_0 n_\mathrm{l} = 0. \tag{6.55}$$

Taking the time derivative of this equation, neglecting $\partial n_l/\partial t$, and using

$$\frac{\partial v_0}{\partial t} = -\frac{eE_0 \cos \omega_0 t}{m_e}, \qquad \frac{\partial v_h}{\partial t} = -\frac{4\pi e^2 n_h}{ikm_e} \tag{6.56}$$

one obtains the high-frequency (electron) wave equation driven by the low-frequency (ion) density times the pump:

$$\frac{\partial^2 n_h}{\partial t^2} + \omega_{pe}^2 n_h = c_1 n_l E_0 \cos \omega_0 t, \qquad c_1 = \frac{ike}{m_e}. \tag{6.57}$$

Substituting c_2 and c_1 from (6.54) and (6.57) into (6.43), (6.44) and (6.45), we get for the **parametric decay instability** the threshold and minimum pump amplitudes, as well as the maximum possible growth of the instability:

$$\begin{aligned} E_{0,th}^2 &= \frac{m_e m_i \omega_1 \omega_2 \Gamma_1 \Gamma_2}{e^2 k^2} \left[1 + \frac{4\delta^2}{(\Gamma_1 + \Gamma_2)^2}\right] \\ E_{0,min}^2 &= \frac{m_e m_i \omega_1 \omega_2 \Gamma_1 \Gamma_2}{e^2 k^2} \\ \Gamma_{max} &= \left(\frac{1}{m_e m_i \omega_1 \omega_2}\right)^{1/2} \frac{ekE_0}{2} \\ I_0 &= \frac{cE_0^2}{8\pi} \end{aligned} \tag{6.58}$$

where I_0 is the pump (laser) energy flux (in erg s^{-1} cm^{-2}).

6.5 Stimulated Brillouin Scattering

The general equations (6.33) can also be used to analyse the stimulated Brillouin or Raman instabilities. However, in this section we are using a different approach (Cairns 1983). The formalism of this section is sometimes more easily generalized to inhomogeneous systems, and occasionally the physics is more transparent. Neglecting damping and couplings, the solutions of (6.33) amplitudes and the unaffected pump amplitude can be written as

$$A_j = a_j \exp(i\omega_j t) + \text{c.c.} \quad \text{for } j = 1, 2, 3 \tag{6.59}$$

where a_j are constants and c.c. denotes complex conjugate. It is assumed that by the introduction of damping and couplings the amplitudes can still be presented by (6.59) but with a_j ($j = 1, 2$) functions of time, but the time variation scale of these functions is small in comparison with the oscillation frequency time. This implies that d^2a_j/dt^2 and $\Gamma\, da_j/dt$ ($j = 1, 2$) can be neglected when substituting (6.59) into (6.33). The pump amplitude a_0 is not affected by the instability. In this approximation the following equations

are derived from (6.33):

$$2\omega_1 \frac{\mathrm{d}a_1}{\mathrm{d}t} + \omega_1 \Gamma_1 a_1 = -\mathrm{i}c_1 a_0 a_2, \qquad 2\omega_2 \frac{\mathrm{d}a_2}{\mathrm{d}t} + \omega_2 \Gamma_2 a_2 = \mathrm{i}c_2 a_0 a_1. \tag{6.60}$$

First-order differential equations of the form of (6.60) are now directly derived for the stimulated Brillouin scattering (Dawson and Lin 1974). The following notation is used: E_0 is the (laser) pump amplitude; E is the scattered electromagnetic field moving in the opposite direction to the pump wave (i.e. reflection out of the plasma); T_e is the electron temperature, assumed to be much larger than the ion temperature; n_ia is the ion density perturbation associated with the acoustic wave; and n_0 is the background plasma density. Plasma charge neutrality requires that the electron density associated with the acoustic wave n_ea equals the ion density perturbation, defined by

$$n_\mathrm{ea} = n_\mathrm{ai} = n_\mathrm{a} \cos k_\mathrm{a} x \tag{6.61}$$

where k_a is the wave number of the acoustic wave. The electron energy density is $k_\mathrm{B} T_\mathrm{e} n_\mathrm{ei}$ and a fraction n_ai/n_0 (n_0 is the background density) of this energy is acquired by the ion acoustic wave. The (space average) energy density conservation of the Brillouin process (i.e. photon wave $\rightarrow$ photon wave + ion acoustic wave) is

$$\frac{E_0^2}{8\pi} = \frac{E^2}{8\pi} + \frac{1}{2} k_\mathrm{B} T_\mathrm{e} n_\mathrm{a} \left(\frac{n_\mathrm{a}}{n_0} \right). \tag{6.62}$$

The momentum density Π in the wave is related to the energy density of a wave W by

$$\Pi = \left(\frac{W}{\omega} \right) \mathbf{k}. \tag{6.63}$$

The simplest proof of (6.63) is in the quantum picture, $W = \hbar \omega n$, where $\hbar = h/2\pi$ and h is the Planck constant, ω is the (angular) wave frequency and n is the appropriate density. $\Pi = \hbar \mathbf{k} n$, where $\mathbf{k}$ is the wave number vector. The ratio of Π to W gives (6.63). Therefore, the momentum density conservation of the Brillouin process is

$$\left(\frac{E_0^2}{4\pi} \right) \left(\frac{\mathbf{k}_0}{\omega_0} \right) = \left(\frac{E^2}{4\pi} \right) \left(\frac{\mathbf{k}}{\omega} \right) + \left(\frac{k_\mathrm{B} T_\mathrm{e} n_\mathrm{a}^2}{n_0} \right) \left(\frac{\mathbf{k}_\mathrm{a}}{\omega_\mathrm{a}} \right). \tag{6.64}$$

Substituting (6.62) into (6.64), one gets

$$\frac{E^2}{4\pi} \left(\frac{\mathbf{k}_0}{\omega_0} - \frac{\mathbf{k}}{\omega} \right) = \frac{k_\mathrm{B} T_\mathrm{e} n_\mathrm{a}^2}{n_0} \left(\frac{\mathbf{k}_\mathrm{a}}{\omega_\mathrm{a}} - \frac{\mathbf{k}_0}{\omega_0} \right). \tag{6.65}$$

Since $(\mathbf{k}, \omega)$ describes a backscatter electromagnetic wave, and $\omega_\mathrm{a} \ll \omega_0$, one can use

$$\mathbf{k} \approx -\mathbf{k}_0, \qquad \omega \approx \omega_0, \qquad \frac{k}{\omega} \approx \frac{k_0}{\omega_0} = \frac{1}{c}, \qquad \frac{k_\mathrm{a}}{\omega_\mathrm{a}} = \frac{1}{v_\mathrm{a}} = \sqrt{\frac{m_\mathrm{i}}{k_\mathrm{B} T_\mathrm{e}}} \gg \frac{1}{c} \tag{6.66}$$

into (6.65) to obtain

$$E = \left(\frac{2\pi c}{n_0}\sqrt{m_i k_B T_e}\right)^{1/2} n_a = \sqrt{2\pi n_0 m_i c v_a}\left(\frac{n_a}{n_0}\right). \tag{6.67}$$

From energy and momentum conservation the important result has been obtained that an ion acoustic wave induces an electromagnetic field; this field is proportional to the ion density wave amplitude. In order to calculate the rate of growth of E as a function of n_{ia} (and vice versa), the dynamical equations, i.e. Maxwell's equations and the fluid (or Vlasov–Boltzmann) plasma equations, must be used.

The electric wave equation, derived from Maxwell's equations (see Appendix A), is

$$\nabla^2 \mathbf{E} - \frac{1}{c^2}\frac{\partial^2 \mathbf{E}}{\partial t^2} - \nabla(\nabla \cdot \mathbf{E}) = \frac{4\pi}{c^2}\frac{\partial \mathbf{J}}{\partial t}. \tag{6.68}$$

For the Brillouin instability the source current $\mathbf{J}$ is given by

$$\mathbf{J} = -e n_{ea} \mathbf{v}_e = -e \mathbf{v}_e n_a \cos k_a x \tag{6.69}$$

where (6.61) was used in the second equality. The zeroth-order equation for the electron velocity $\mathbf{v}_e$, induced by the pump wave E_0, is

$$\frac{\partial v_e}{\partial t} = -\frac{eE_0}{m_e}\cos(k_0 x - \omega_0 t). \tag{6.70}$$

Taking the solution of (6.70), i.e. $v_e = -v_0 \sin(k_0 x - \omega_0 t)$, $v_0 = eE_0/(m_e\omega_0)$, and inserting it into (6.69) yields a source current

$$J = \frac{n_a e^2 E_0}{2m_e\omega_0}\{\sin[(k_0 + k_a)x - \omega_0 t] + \sin[(k_0 - k_a)x - \omega_0 t]\}. \tag{6.71}$$

The electromagnetic backscattered wave is described by the second term of the source current, $\mathbf{k}_0 - \mathbf{k}_a = \mathbf{k} \approx -\mathbf{k}_0$, and therefore only the second term is kept for further analysis. From (6.68), the back-reflected electromagnetic wave equation is derived by using the second term of (6.71):

$$\frac{\partial}{\partial t}\sin[(k_0 - k_a)x - \omega_0 t] = -\omega_0 \cos[(k_0 - k_a)x - \omega_0 t] \approx -\omega_0 \cos(-k_0 x - \omega t)$$

$$= -\omega_0 \cos(k_0 x + \omega t)$$

$(\partial^2/\partial x^2)E = -k^2 E$, and the transversal property ($\mathbf{k} \cdot \mathbf{E} = 0$) of the electromagnetic wave

$$\frac{\partial^2 E}{\partial t^2} + k^2 c^2 E = \frac{\omega_{pe}^2 n_a E_0}{2n_0}\cos(k_0 x + \omega_0 t) \tag{6.72}$$

where ω_{pe} is the electron plasma frequency. For the resonant case, $kc = \omega = \omega_0$, equation (6.72) has the solution (6.17):

$$E = E(t)\sin(k_0 x + \omega_0 t), \qquad E(t) = \frac{\omega_{pe}^2 E_0 t}{4\omega_0}\left(\frac{n_a}{n_0}\right). \tag{6.73}$$

Taking the time derivative of the amplitude $E(t)$,

$$\frac{dE(t)}{dt} = \left(\frac{\omega_{pe}^2}{4\omega_0 n_0}\right) E_0 n_a \tag{6.74}$$

and substituting n_a/n_0 from (6.67), one gets

$$\frac{dE}{dt} = \left(\frac{\omega_{pe}^2 E_0}{4\omega_0\sqrt{2\pi n_0 m_i c v_a}}\right) E \equiv \Gamma_{Bril} E, \qquad E(t) = \exp(\Gamma_{Bril} t). \tag{6.75}$$

Using the values of the energy flux of the pump, $I_0 = cE_0^2/(8\pi)$, we get for the growth rate of the backscattered wave amplitude, Γ_{Bril},

$$\Gamma_{Bril} = \frac{1}{\sqrt{2}}\,\frac{\omega_{pe}^2}{\omega_0}(n_0 m_i c^2 v_a)^{-1/2}(I_0)^{1/2}. \tag{6.76}$$

Generalizing (6.74) to include damping due to electron–ion collisions Γ_{EM}, one has the following equation for the backscattered wave amplitude:

$$\frac{dE(t)}{dt} + \Gamma_{EM} E(t) = \frac{\omega_{pe}^2}{4n_0\omega_0} E_0 n_a. \tag{6.77}$$

This equation has the structure generally developed in (6.60). Γ_{EM} can be related to the electron–ion collision frequency ν_{ei}, by assuming that the coherent oscillations of the electrons are converted to thermal motion at the rate of electron–ion collisions. The energy conservation rate in this case implies the relation between Γ_{EM} and ν_{ei}:

$$\Gamma_{EM}\frac{E^2}{8\pi} = \nu_{ei}\left[\frac{1}{2} n_e m_e \left(\frac{eE}{m_e\omega}\right)^2\right] \;\Rightarrow\; \Gamma_{EM} = \nu_{ei}\left(\frac{\omega_{pe}^2}{\omega^2}\right). \tag{6.78}$$

A similar equation to (6.77) for dn_a/dt has to be developed in order to solve the problem.

From equation (6.67) one has that $dn_a/dt \propto dE/dt$ and from (6.75) that $dE/dt \propto E_0 E$, thus implying the desired equation $dn_a/dt \propto E_0 E$. Substituting explicitly (6.75) into (6.67) gives

$$\frac{dn_a}{dt} = \frac{\omega_{pe}^2}{8\pi\omega_0 m_i c v_a} E_0 E. \tag{6.79}$$

Including collisional and Landau damping in this equation, one gets

$$\frac{dn_a}{dt} + \Gamma_a n_a = \frac{\omega_{pe}^2}{8\pi\omega_0 m_i c v_a} E_0 E. \tag{6.80}$$

This is the second equation with a structure as in (6.60). Using the relationship $\mathrm{d}n_a/\mathrm{d}t = \Gamma_{Bril} n_a$ and $\mathrm{d}E/\mathrm{d}t = \Gamma_{Bril} E$, the differential equations (6.77) and (6.80) yield the algebraic equations:

$$\begin{pmatrix} \Gamma_{Bril} + \Gamma_{EM} & -\dfrac{\omega_{pe}^2 E_0}{4 n_0 \omega_0} \\ -\dfrac{\omega_{pe}^2 E_0}{8\pi\omega_0 m_i c v_a} & \Gamma_{Bril} + \Gamma_a \end{pmatrix} \begin{pmatrix} E \\ n_a \end{pmatrix} = \begin{pmatrix} 0 \\ 0 \end{pmatrix}. \tag{6.81}$$

A solution of these equations is possible only if the determinant of the coefficients vanish, which implies

$$\Gamma_{Bril} = \frac{1}{2}\left\{ -(\Gamma_{EM} + \Gamma_a) \pm \left[(\Gamma_{EM} + \Gamma_a)^2 + \left(\frac{\omega_{pe}^4 I_0}{\omega_0^2 n_0 m_i c^2 v_a} - 4\Gamma_{EM}\Gamma_a \right) \right]^{1/2} \right\} \tag{6.82}$$

where $(\Gamma_{EM}\Gamma_a)^2$ was neglected. The threshold for the pump irradiance I_0 is obtained by taking $\Gamma_{Bril} = 0$:

$$I_0 \geq I_{0,th} = \frac{4\Gamma_{EM}\Gamma_a \omega_0^2 n_0 m_i c^2 v_a}{\omega_{pe}^4}. \tag{6.83}$$

For pump intensities large compared with threshold, (6.82) and (6.83) give

$$\Gamma_{Bril}(I_0 \gg I_{0,th}) = \frac{\omega_{pe}^2}{2\omega_0}\sqrt{\frac{I_0}{n_0 m_i c^2 v_a}}. \tag{6.84}$$

A similar formalism for stimulated Raman instability yields

$$\begin{aligned} \Gamma_{Ram}(I_0 \gg I_{0,th}) &= \frac{\omega_{pe}^2}{2\omega_0}\sqrt{\frac{I_0}{2 n_0 m_e c^2 v_p}} \\ I_{0,th} &= \frac{4\Gamma_{EM}\Gamma_p \omega_0^2 n_0 m_e c^2 v_p}{\omega_{pe}^4} \end{aligned} \tag{6.85}$$

where $v_p = \omega_p/k_p$; v_p, ω_p and k_p are the phase velocity, the angular frequency and wave number of the plasmon (electron) wave respectively. Γ_p is the collisional and Landau damping for the plasmon wave.

6.6 A Soliton Wave

6.6.1 A historical note

J. Scott Russell, who made observations on water waves on the Edinburgh to Glasgow canal, first realized the phenomenon of solitary wave in 1834. These observations together with laboratory experiments, where solitary waves

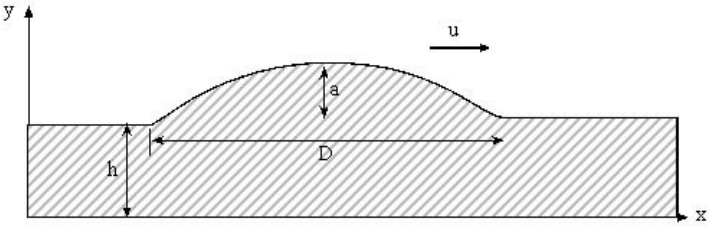

Figure 6.3. A solitary wave moving with a steady velocity u. h is the height of the undisturbed water, a is the amplitude of the wave and g is the gravitational acceleration constant, satisfying $D \gg h \gg a$.

were generated by dropping a weight at one end of a shallow water channel, were published (Russell 1844) in 1844 before the British Association for the Advancement of Science. Russell suggested the following empirical formula in order to explain the steady state velocity u of the solitary wave:

$$u^2 = g(h + a) \tag{6.86}$$

where h is the height of the undisturbed water, a is the amplitude of the wave (figure 6.3) and g is the gravitational acceleration constant. Equation (6.86) was later deduced by Boussinesq in 1871 (Boussinesq 1871) and independently by Rayleigh (Rayleigh 1876), by using the equations of motion for an incompressible fluid and assuming a wavelength $\sim D$ much greater than the height h of the water in the channel. They also derived the displacement $(y - h)$ of the wave above the level h:

$$y(x, t) - h = a\,\mathrm{sech}^2\left[\frac{(x - ut)}{D}\right], \qquad D^2 = \frac{4h^2(h + a)}{3a}. \tag{6.87}$$

In 1895 Korteweg and de Vries (**KdV**) developed (Korteweg and de Vries 1895) the equation

$$\frac{\partial y}{\partial t} = \frac{3}{2}\sqrt{\frac{g}{h}}\left[\left(y - h + \frac{2\alpha}{3}\right)\frac{\partial y}{\partial x} + \frac{\beta}{3}\frac{\partial^3 y}{\partial x^3}\right] \tag{6.88}$$

in order to describe the motion of weakly nonlinear long transversal waves. In equation (6.88), α is a small arbitrary parameter and β is given by

$$\beta = \frac{h^3}{3} - \frac{\sigma_{\mathrm{st}} h}{g\rho} \tag{6.89}$$

where σ_{st} is the surface tension and ρ is the density of the liquid. Equation (6.87) is a solution of the KdV equation (6.88).

The modern development in the theory of the KdV equation starts with the work of Fermi, Pasta and Ulam in 1955 (Fermi *et al*. 1955). They studied a nonlinear discrete mass string, and to their surprise the thermalization of the energy in such a nonlinear system could not be achieved. Kruskal and

Zabusky (1965) solved this paradox by modelling the nonlinear spring with the KdV equation, yielding (numerically) the soliton solution. The Fermi–Pasta–Ulam problem suggests that a nonlinear interaction does not necessarily cause the destruction of oscillations, causing randomization. This type of phenomenon and the KdV equation have since been derived in many physical problems, such as an ion acoustic wave in plasma (Washimi and Taniuti 1966).

6.6.2 What is a soliton?

A soliton is a localized nonlinear wave of steady-state form. If it interacts with other solitons, after the interaction these structures separate in such a way that their original structure is preserved and their velocities are unchanged. The positions of the solitons are slightly shifted from where they would have been without the existence of the interaction. The solitons are solitary waves but the solitary waves are not necessarily solitons (Eliezer 1985).

6.6.3 What is a solitary wave?

The solitary waves are a one-parameter family of shaped pulses, moving with a velocity u proportional to the wave amplitude a, and their width D is inversely proportional to the square root of the amplitude (see figure 6.3). Therefore, the larger the amplitude the faster is their velocity and the narrower is their width.

6.6.4 The wave equation

The wave equation in one space dimension is

$$\frac{1}{u^2}\frac{\partial^2\psi}{\partial t^2} - \frac{\partial^2\psi}{\partial x^2} = 0. \tag{6.90}$$

This equation describes the propagation of waves in homogeneous media with a constant velocity u. In deriving this equation, one has to make three main assumptions:

(a) There is no **dissipation**.
(b) The amplitude of oscillation ψ is small so that one can **neglect nonlinear terms**.
(c) There is no **dispersion**, i.e. the velocity of the wave propagation does not depend on the frequency of the wavelength.

If one does not assume the absence of dissipation, nonlinearity and dispersion, then the universal wave equation (6.90) is not applicable and each medium has to be described by a different system of equations.

If the initial value of ψ and its time derivative are given, i.e. $\psi(x,0)$ and $(\partial/\partial t)\psi(x,0)$ are known, then the wave equation (6.90) is a well-defined initial value problem. This equation, like any other linear differential equation, obeys the **superposition principle**. That is, if $f(x-ut)$ and $g(x+ut)$ solve equation (6.90), then $\psi(x,t)=f(x-ut)+g(x+ut)$ is also a solution of this equation. $f(x-ut)$ and $g(x+ut)$ represent waves of fixed shape, travelling to the right and left respectively. The general solution $\psi=f+g$ describes two waves that can pass through each other without changing their shape. In general, this superposition principle does not occur in physical systems described by nonlinear differential equations. However, a number of nonlinear differential equations have been discovered which allow waves to pass through each other without changing their shapes and velocities. Moreover, some principle of superposition can be defined for these nonlinear equations. These equations are called 'solitary wave equations', and the KdV equation belongs to this class of equations.

Next we show that an ion plasma wave with a wavelength much larger than the Debye length satisfies the KdV equation; thus a soliton solution exits in laser–plasma interaction.

6.6.5 Ion plasma wave and the KdV equation

We consider the fluctuation in the ion density of two component plasma (electrons and ions), i.e. the ion acoustic waves. This problem is described by the following fluid-Poisson equations:

$$\begin{aligned}
\frac{\partial n_\mathrm{i}}{\partial t}+\frac{\partial(n_\mathrm{i}v_\mathrm{i})}{\partial x}&=0\\
n_\mathrm{i}m_\mathrm{i}\frac{\mathrm{d}v_\mathrm{i}}{\mathrm{d}t}&=Zen_\mathrm{i}E\\
n_\mathrm{e}m_\mathrm{e}\frac{\mathrm{d}v_\mathrm{e}}{\mathrm{d}t}&=-en_\mathrm{e}E-\frac{\partial(n_\mathrm{e}k_\mathrm{B}T_\mathrm{e})}{\partial x}\approx 0\\
\frac{\partial E}{\partial x}&=4\pi e(Zn_\mathrm{i}-n_\mathrm{e})
\end{aligned}\tag{6.91}$$

where n_i is the ion density and v_i their velocity, n_e is the electron density and v_e the electron fluid velocity, m_i and m_e are the ion mass and the electron mass, and Z is the charge ionization of the ions. The electron pressure is $n_\mathrm{e}k_\mathrm{B}T_\mathrm{e}$. The electron temperature is much larger than the ion temperature, and in this case for simplicity one can take a zero ion temperature, $T_\mathrm{i}=0$. In the third equation of (6.91), the right-hand side is taken as zero by neglecting the inertia of the electrons relative to that of the ions. Since $m_\mathrm{i}\gg Zm_\mathrm{e}$, the inertia term $(n_\mathrm{e}m_\mathrm{e}\,\mathrm{d}v_\mathrm{e}/\mathrm{d}t)$ in the electron momentum equation can be neglected when $\mathrm{d}v_\mathrm{e}/\mathrm{d}t\approx\mathrm{d}v_\mathrm{i}/\mathrm{d}t$, i.e. when the high-frequency plasma oscillations are neglected. Since we are interested in the regime of density and

velocity fluctuations near the ion plasma frequency, the above approximation is justified.

In solving equations (6.91) we introduce the dimensionless variables

$$\begin{aligned}
&\xi = \frac{x}{\lambda_D}, \qquad \lambda_D = \left(\frac{k_B T_e}{4\pi e^2 Z n_0}\right)^{1/2}, \qquad \tau = \omega_{pi} t \\
&\omega_{pi} = \left(\frac{4\pi n_0 Z^2 e^2}{m_i}\right)^{1/2}, \qquad v = \frac{v_i}{\omega_{pi}\lambda_D}, \qquad F = \frac{e\lambda_D E}{k_B T_e} \\
&N = \frac{n_i}{n_0}, \qquad N_e = \frac{n_e}{Z n_0}, \qquad \Omega = \frac{\omega}{\omega_{pi}} \\
&\kappa = k\lambda_D, \qquad k = \frac{2\pi}{\lambda}
\end{aligned} \tag{6.92}$$

where n_0 and Zn_0 are the ion and electron initial (undisturbed) densities accordingly, and k is the wave number. The fluid-Poisson equations (6.91) in these dimensionless variables are

$$\begin{aligned}
\frac{\partial N}{\partial \tau} + \frac{\partial (Nv)}{\partial \xi} &= 0 \\
\frac{\partial v}{\partial \tau} + v\frac{\partial v}{\partial \xi} - F &= 0 \\
\frac{1}{N_e}\frac{\partial N_e}{\partial \xi} + F &= 0 \\
\frac{\partial F}{\partial \xi} + N_e - N &= 0.
\end{aligned} \tag{6.93}$$

At this stage it is convenient to define the Fourier modes:

$$\begin{aligned}
N_e &= 1 + \delta N_e \exp[\mathrm{i}(\kappa\xi - \Omega\tau)] \\
N &= 1 + \delta N \exp[\mathrm{i}(\kappa\xi - \Omega\tau)] \\
v &= \delta v \exp[\mathrm{i}(\kappa\xi - \Omega\tau)] \\
F &= \delta F \exp[\mathrm{i}(\kappa\xi - \Omega\tau)].
\end{aligned} \tag{6.94}$$

Substituting (6.94) into (6.93) and linearizing the equations (i.e. neglecting powers of δ greater than one), one gets

$$\begin{pmatrix} -\mathrm{i}\kappa & 0 & 0 & -1 \\ 0 & -\Omega & \kappa & 0 \\ 0 & 0 & -\mathrm{i}\Omega & -1 \\ 1 & -1 & 0 & \mathrm{i}\kappa \end{pmatrix} \begin{pmatrix} \delta N_e \\ \delta N \\ \delta v \\ \delta F \end{pmatrix} = \begin{pmatrix} 0 \\ 0 \\ 0 \\ 0 \end{pmatrix}. \tag{6.95}$$

A non-trivial solution of (6.95) requires the vanishing of the determinant of the coefficients, yielding the dispersion relation

$$\kappa = \frac{\Omega}{\sqrt{1-\Omega^2}} \qquad \text{for } \Omega \ll 1: \quad \kappa \approx \Omega + \tfrac{1}{2}\Omega^3, \quad \Omega \approx \kappa \approx \frac{\lambda_D}{\lambda}. \tag{6.96}$$

As can be seen from this dispersion relation, one has an ion wave with large wavelength (in comparison with the Debye length) if $\Omega \ll 1$. It is worth mentioning that to the lowest order one has for the ion wave the dispersion relation

$$\kappa = \Omega \;\Rightarrow\; \frac{\omega}{k} = \left(\frac{Zk_B T_e}{m_i}\right)^{1/2} = v_a \tag{6.97}$$

where v_a is the phase velocity. The dispersion relation given in equation (6.97) was used in (6.66) for $Z = 1$ and throughout the book for (the linear) ion acoustic phase velocity.

The soliton solution is obtained by taking into account the nonlinear dispersion relation (6.96). The phase term in the Fourier transform of equations (6.94) is

$$\mathrm{i}(\kappa\xi - \Omega\tau) = \mathrm{i}[\Omega(\xi - \tau) + \tfrac{1}{2}\Omega^3\xi]. \tag{6.98}$$

The term $\frac{1}{2}\Omega^3\xi$ is called the dispersive term. It is convenient to introduce new variables that incorporate this effect:

$$\zeta = \Omega(\xi - \tau), \qquad \eta = \Omega^3\xi. \tag{6.99}$$

We rewrite equations (6.93) in terms of these variables. For this purpose we use

$$\frac{\partial}{\partial\xi} = \Omega\frac{\partial}{\partial\zeta} + \Omega^3\frac{\partial}{\partial\eta}, \qquad \frac{\partial}{\partial\tau} = -\Omega\frac{\partial}{\partial\zeta} \tag{6.100}$$

so that the fluid-Poisson equations to be solved are

$$\begin{aligned}
\frac{\partial N}{\partial\zeta} + \frac{\partial(Nv)}{\partial\zeta} + \Omega^2\frac{\partial(Nv)}{\partial\eta} &= 0 \\
\Omega\frac{\partial N_e}{\partial\zeta} + \Omega^3\frac{\partial N_e}{\partial\eta} + FN_e &= 0 \\
-\Omega\frac{\partial v}{\partial\zeta} + \Omega v\left(\frac{\partial v}{\partial\zeta} + \Omega^2\frac{\partial v}{\partial\eta}\right) - F &= 0 \\
\Omega\frac{\partial F}{\partial\zeta} + \Omega^3\frac{\partial F}{\partial\eta} + N_e - N &= 0.
\end{aligned} \tag{6.101}$$

Equations (6.101) are solved by the following perturbation series:

$$\begin{aligned} N &= 1 + \Omega^2 N_1 + \Omega^4 N_2 + \cdots \\ N_e &= 1 + \Omega^2 N_{e1} + \Omega^4 N_{e2} + \cdots \\ v &= \Omega^2 v_1 + \Omega^4 v_2 + \cdots \\ F &= \Omega^3 F_1 + \Omega^5 F_2 + \cdots . \end{aligned} \tag{6.102}$$

The leading terms of the expansion are evident from equations (6.101). The Ω^2 expansion of N and N_e is necessary in order to have a consistent perturbation theory in the small parameter Ω. Equations (6.101) to lowest order in Ω are (first and last equations to order Ω^2 and second and third equations to order Ω^3)

$$\begin{aligned} -\frac{\partial N_1}{\partial \zeta} + \frac{\partial v_1}{\partial \zeta} &= 0 \\ \frac{\partial v_1}{\partial \zeta} - F_1 &= 0 \\ \frac{\partial N_{e1}}{\partial \zeta} + F_1 &= 0 \\ N_1 &= N_{e1}. \end{aligned} \tag{6.103}$$

The solution of these equations is

$$N_1 = N_{e1} = v_1 = \phi(\zeta, \eta), \qquad F_1 = -\frac{\partial \phi}{\partial \zeta}. \tag{6.104}$$

An arbitrary function of η was neglected by integrating the first equation of (6.103). In the next order in Ω, equations (6.101) are (first and last equations to order Ω^4 and second and third equations to order Ω^5)

$$\begin{aligned} -\frac{\partial N_2}{\partial \zeta} + \frac{\partial}{\partial \zeta}(v_2 + \phi^2) + \frac{\partial \phi}{\partial \eta} &= 0 \\ -\frac{\partial v_2}{\partial \zeta} + \phi \frac{\partial \phi}{\partial \zeta} - F_2 &= 0 \\ \frac{\partial N_{e2}}{\partial \zeta} + \frac{\partial \phi}{\partial \eta} + \phi F_1 + F_2 &= 0 \\ \frac{\partial F_1}{\partial \zeta} - N_2 + N_{e2} &= 0. \end{aligned} \tag{6.105}$$

Equations (6.105) are linearly combined ($\partial/\partial\zeta$ [last eq.] + [second eq.] − [first eq.] − [third eq.] = 0) and F_1 is substituted by using (6.104) to yield

an equation for ϕ:

$$\frac{\partial \phi}{\partial \eta} + \phi \frac{\partial \phi}{\partial \zeta} + \frac{1}{2} \frac{\partial^3 \phi}{\partial \zeta^3} = 0. \tag{6.106}$$

This equation is the famous **KdV equation** describing a **soliton**. Equation (6.106) admits a solution of a solitary wave that is a single pulse, which retains its shape as it propagates with a velocity u^* in (ζ, η) space. Thus we are looking for a solution of the variable $(\zeta - u^*\eta)$, or equivalently in the usual space (x, t) the solution is a function of $(x - ut)$, where u is the speed of the solitary wave. The following relations between the coordinates

$$\zeta = \Omega\xi - \Omega\tau = \Omega\lambda_D^{-1}x - \Omega\omega_{pi}t, \qquad \eta = \Omega^3\xi = \Omega^3\lambda_D^{-1}x \tag{6.107}$$

imply

$$x - ut = K(\zeta - u^*\eta) \;\Rightarrow\; \begin{cases} u^* = \dfrac{1}{\Omega^2}\left(1 - \dfrac{\omega_{pi}\lambda_D}{u}\right) \\ u = \dfrac{\omega_{pi}\lambda_D}{1 - \Omega^2 u^*} \\ K = \dfrac{u}{\Omega\omega_{pi}} \end{cases}. \tag{6.108}$$

Looking now for a solution of equation (6.106) in the variable z,

$$z = \zeta - u^*\eta \tag{6.109}$$

one gets from (6.106)

$$-u^* \frac{\partial \phi}{\partial z} + \phi \frac{\partial \phi}{\partial z} + \frac{1}{2} \frac{\partial^3 \phi}{\partial z^3} = 0. \tag{6.110}$$

This equation can be integrated to yield

$$u^*\phi - \frac{1}{2}\phi^2 - \frac{1}{2}\frac{\mathrm{d}^2\phi}{\mathrm{d}z^2} = 0 \tag{6.111}$$

where the constant of integration is assumed to vanish. Multiplying equation (6.111) by $\mathrm{d}\phi/\mathrm{d}z$ and integrating once more (again with a zero constant of integration), one has

$$\left(\frac{\mathrm{d}\phi}{\mathrm{d}z}\right)^2 = \frac{2}{3}\phi^2(3u^* - \phi). \tag{6.112}$$

The solution of this equation is

$$\phi(z) = 3u^* \operatorname{sech}^2\left[\left(\sqrt{\frac{u^*}{2}}\right)z\right]. \tag{6.113}$$

One can verify the solution (6.113) by direct substitution into (6.111) by using the identities

$$\frac{\mathrm{d}(\operatorname{sech} z)}{\mathrm{d}z} = -(\operatorname{sech} z)(\tanh z), \qquad \operatorname{sech}^2 z + \tanh^2 z = 1. \tag{6.114}$$

The solution ϕ of (6.113) has a peak at $z = 0$ with a maximum $\phi_{\max} = 3u^*$. ϕ vanishes at $z = \pm\infty$, it moves with a velocity u^* in (ζ, η) coordinates, and it has a width of $\sqrt{2/u^*}$. This solution has only one parameter, u^*, and has the characteristic properties of a solitary wave, i.e. the larger the speed the greater is the amplitude and the narrower is the width.

Recalling that $\phi = v_1 = N_1 = N_{e1}$, we return to the dimensional variables $x - t$. From (6.92), (6.102) and (6.113) one gets

$$n_i - n_0 = \Omega^2 n_0 N_1 = (\delta n) \operatorname{sech}^2\left(\frac{x - ut}{D}\right), \qquad \delta n = 3\Omega^2 n_0 u^*. \tag{6.115}$$

Using (6.108) and (6.115) yields

$$u = \frac{\omega_{pi}\lambda_D}{1 - \Omega^2 u^*} = \frac{\omega_{pi}\lambda_D}{1 - (\delta n/3n_0)} \approx \omega_{pi}\lambda_D\left(1 + \frac{\delta n}{3n_0}\right). \tag{6.116}$$

Using the relations (6.108), the solution (6.113) and δn from (6.115), one gets the width of the soliton wave D,

$$D = \sqrt{\frac{2}{u^*}}\,\frac{u}{\Omega\omega_{pi}} = \frac{\lambda_D}{1 - (\delta n/3n_0)}\sqrt{\frac{6n_0}{\delta n}} \approx \lambda_D\sqrt{\frac{6n_0}{\delta n}}. \tag{6.117}$$

The standard properties of a solitary wave can be seen from equations (6.116) and (6.117):

(a) The width of the solitary wave D decreases with increasing δn.
(b) The velocity of the solitary wave u increases with increasing δn.

We end this section with a note on the KdV equation. Equation (6.106) is a special case of the general KdV equation

$$\frac{\partial\phi}{\partial t} + \mu\phi\frac{\partial\phi}{\partial x} + \nu\frac{\partial^3\phi}{\partial x^3} = 0 \tag{6.118}$$

where μ and ν are two coefficients. The solution of the KdV equation is

$$\begin{aligned} \phi &= \phi_0 \operatorname{sech}^2[(x - ut)/D] \\ D &= 2\sqrt{\frac{3\nu}{\phi_0\mu}} \\ u &= \frac{\phi_0\mu}{3}. \end{aligned} \tag{6.119}$$

In our equation (6.106) the coefficients are $\mu = 1$ and $\nu = \frac{1}{2}$, implying $\phi_0 = 3u$ and $D = (2/u)^{1/2}$ (see equation (6.113)).

The soliton concept has also attracted interest and speculation in laser–plasma interactions. In particular the solitary waves were associated with the ponderomotive force. Cavity structures, measured experimentally near the critical surface, were related to solitary waves. However, it seems that the very interesting phenomena of the soliton have not yet been fully and successfully investigated in laser–plasma interactions.

Chapter 7

Laser-Induced Electric Fields in Plasma

7.1 High- and Low-Frequency Electric Fields

In laser–plasma interaction the electric field, or rather the various macroscopic electric fields, plays a major role in defining the properties of the plasma system. First, the laser electric field, $E_L \cos \omega_L t$, is propagating into the plasma, where part of it is reflected and the other part is absorbed. The laser electric field amplitude and its frequency are given by

$$\begin{aligned} E_L\,(\mathrm{V/cm}) &= 2.75 \times 10^9 \left(\frac{I_L}{10^{16}\,\mathrm{W/cm^2}} \right)^{1/2} \\ \omega_L\,(\mathrm{s^{-1}}) &= \frac{2\pi c}{\lambda_L} = 1.88 \times 10^{15} \left(\frac{\mu\mathrm{m}}{\lambda_L} \right) \end{aligned} \tag{7.1}$$

where I_L is the laser energy flux and λ_L is the laser wavelength. ω_L sets the scale for high-frequency phenomena and the period of one laser oscillation $(2\pi/\omega_L)$ is about 3.3 fs for a 1 μm laser wavelength.

The propagating and reflected electric fields in different plasma media were calculated in chapter 5. The electric fields associated with the possible waves in the plasma were calculated in chapter 6. Two classes of electric fields were derived: the high-frequency one, of the order of the laser frequency or the electron–plasma frequency, $\omega \approx \omega_{pe} \approx 10^{15}\,\mathrm{s^{-1}}$ (for electron density $\sim 10^{21}\,\mathrm{cm^{-3}}$), and the low-frequency electric field of the order of the ion–plasma frequency $\omega \approx 10^{12}\,\mathrm{s^{-1}}$. The appropriate time scales are about 1 fs for the high-oscillation fields and about 1 ps for the low-oscillation fields.

Another interesting case of a slowly-varying (in time) electric field is the one induced by the ponderomotive force and developed in chapter 4. This 'd.c.' (i.e. very slow varying in time) electric field E is in the direction of the gradient of E_L^2 and the magnitude of this electric field (E) is of

the order

$$en_e E \approx \left(\frac{\omega_{pe}^2}{\omega_L^2}\right)\frac{E_L^2}{16\pi r_L}$$

$$\Rightarrow\ E\,(\mathrm{V/cm}) \approx 1.0\times 10^7\left(\frac{I_L}{10^{16}\,\mathrm{W/cm^2}}\right)\left(\frac{10^{21}\,\mathrm{cm^{-3}}}{n_{ec}}\right)\left(\frac{100\,\mu\mathrm{m}}{r_L}\right) \qquad (7.2)$$

where n_e is the electron density, n_{ec} is the electron critical density, r_L is the laser radius defined by $I_L \approx \exp(-r^2/2r_L^2)$, and it is assumed that $\mathrm{grad}\, E_L^2 \approx E_L^2/r_L$. As discussed in chapter 6, an electric field can also be induced by the ponderomotive forces associated with the wave–wave instabilities.

In general, the electric field in laser–plasma interactions is discussed in the previous three chapters. In this chapter we shall add two cases of slowly varying electric fields: in section 7.2 the electric field of an expanding plasma into the vacuum is calculated and in section 7.3 an electric field in the double layers is calculated. An example of charge particle acceleration due to these electric fields is given in section 7.4.

7.2 Expansion of Plasma into the Vacuum

A laser-created plasma is expanding into the vacuum, towards the laser irradiation (Gurevich *et al.* 1965, 1968, 1969, Crow *et al.* 1975, Anisimov *et al.* 1979, Sigel 1979). When a laser irradiates a target, the electrons are heated and they expand towards the vacuum. The ions follow the electrons that expand towards the vacuum. In this section the hydrodynamic problem of plasma expansion is calculated, by assuming that the electrons and the ions are treated as separate fluids with different temperatures.

We assume the simplest one-dimensional problem with plane geometry. For a laser spot on target $2r_L = D$ (r_L, the laser radius, is defined in the previous section), this approximation is valid as long as $D \gg v_i t$, where v_i is the streaming velocity of the ions and t is the expansion time. The continuity equation for the ions and the momentum equations for the electrons and ions are

$$\begin{aligned}\frac{\partial n_i}{\partial t} + \frac{\partial (n_i v_i)}{\partial x} &= 0\\ \frac{\partial P}{\partial x} + en_e E &= 0\\ m_i n_i\left(\frac{\partial v_i}{\partial t} + v_i\frac{\partial v_i}{\partial x}\right) &= eZn_i E\end{aligned} \qquad (7.3)$$

where E is the electric field in the expanding plasma, n_i and n_e are the ion and electron densities accordingly, m_i is the ion mass and Ze is the ion charge.

Neglecting the ion temperature in comparison with the electron temperature T_e, the plasma pressure P is given by

$$P = n_e k_B T_e. \tag{7.4}$$

In the electron momentum equation, the second equation of (7.3), the inertia term of the electrons ($m_e \, dv_e/dt$, where v_e is the electron fluid velocity) is neglected. This is justified when adding the two inertia terms of the electrons and the ions, since $m_e \ll m_i$, and neglecting the high-frequency oscillations (not relevant to this problem) one has $dv_e/dt \approx dv_i/dt$. Assuming charge neutrality $n_e = Zn_i$, adding the electron and ion momentum equations of (7.3), one gets

$$\frac{\partial v_i}{\partial t} + v_i \frac{\partial v_i}{\partial x} = -\frac{1}{m_i n_i} \frac{\partial P}{\partial x}. \tag{7.5}$$

Using the definition of the sound velocity, $n_e = Zn_i$, and equation (7.4), one gets

$$c_s^2 = \frac{1}{m_i} \frac{\partial P}{\partial n_i} = \frac{Z k_B T_e}{m_i} \tag{7.6}$$

where the electron temperature is assumed constant, a reasonable assumption for the plasma corona under investigation. Implying the identity $\partial P/\partial x = (\partial P/\partial n)(\partial n/\partial x)$ into the right-hand side of equation (7.5) and using (7.6), we obtain

$$\frac{\partial v_i}{\partial t} + v_i \frac{\partial v_i}{\partial x} + c_s^2 \left(\frac{1}{n_i} \frac{\partial n_i}{\partial x} \right) = 0. \tag{7.7}$$

One has to solve (7.7) together with the continuity equation (first of equations (7.3)). For this purpose we define the dimensionless variables

$$\begin{aligned} &\xi = \frac{x}{c_s t}, \qquad v = \frac{v_i}{c_s}, \qquad n = \frac{n_i}{n_0} \\ &\frac{\partial}{\partial x} = \frac{1}{c_s t} \frac{\partial}{\partial \xi}, \qquad \frac{\partial}{\partial t} = -\frac{\xi}{t} \frac{\partial}{\partial \xi} \end{aligned} \tag{7.8}$$

where n_0 is the background density. Substituting (7.8) into the first equation of (7.3) and (7.7), we get

$$\begin{pmatrix} v - \xi & 1 \\ 1 & v - \xi \end{pmatrix} \begin{pmatrix} d \ln n/d\xi \\ dv/d\xi \end{pmatrix} = \begin{pmatrix} 0 \\ 0 \end{pmatrix}. \tag{7.9}$$

The determinant of the 2×2 matrix should vanish in order to get a nonzero solution, yielding

$$v = \xi + 1 \;\Rightarrow\; v_i = \frac{x}{t} + c_s \tag{7.10}$$

where we choose the positive x axis in the direction of the plasma expansion. The density profile is obtained from one of the equations of (7.9) by using (7.10):

$$n_i = n_0 \exp(-\xi - 1) \tag{7.11}$$

where the boundary condition $n = n_0$ was taken for $\xi = -1$. The plasma is expanding in the $+x$ direction with a velocity v_i, but at the same time a disturbance (a rarefaction wave—see chapter 10) moving with the speed of sound c_s in the $-x$ direction is taking place. This rarefaction arrives at a position $x = -c_s t$ at time t, or equivalently at $\xi = -1$ in the dimensionless variable. For this reason one has to choose $n_i = n_0$ at $\xi = -1$.

The electric field is obtained from the second equation of (7.3) by using (7.6) and (7.11), yielding

$$E = -\frac{k_B T_e}{e n_e}\frac{\partial n_e}{\partial x} = -\frac{k_B T_e}{e c_s t}\frac{\partial \ln n}{\partial \xi} = \frac{k_B T_e}{e c_s t}. \tag{7.12}$$

From (7.12) one can see that the electric field is uniform (i.e. constant) in space: it goes to zero for $t \to \infty$, but has a singularity at $t = 0$. At $t = 0$ this solution is not relevant. The self-similar solution developed above (i.e. where the two variables x and t can be combined into one variable, x/t) is not permitted at very small t, small compared with the time scale defining the problem. In our case the time defining the laser–plasma interaction is the laser pulse duration; therefore, the above self-similar solution is relevant only for $t \gg \tau_L$ (the laser pulse duration). The electric field in the expanding plasma corona as given by (7.12) is about 10^4 V/cm at $t \approx 3\tau_L$, for a laser pulse duration of about 1 ns and a typical electron temperature (in energy units) of 1 keV ($c_s \approx 3 \times 10^7$ cm/s for $T_e = 1$ keV).

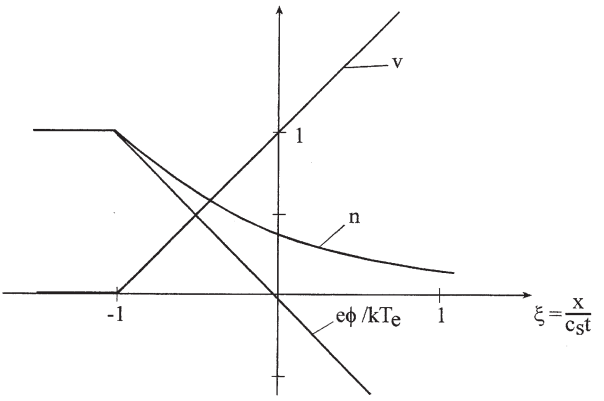

Figure 7.1. Self-similar solution—the plasma expansion into vacuum. v and n are the dimensionless ion velocity and density respectively and $x = \xi c_s t$, where c_s is the isothermal speed of sound. ϕ is the electric potential and T_e is the electron temperature.

The electric potential ϕ is given by

$$\phi = -\int E\,\mathrm{d}x = -\left(\frac{k_B T_e}{e}\right)\frac{x}{c_s t} = -\frac{k_B T_e}{e}\,\xi \tag{7.13}$$

where the boundary condition $\phi = 0$ for $\xi = 0$ was taken.

The self-similar solution, as developed in this section for v, n and $e\phi/k_B T_e$, is given in figure 7.1.

7.3 Double Layers

In a static model, the double layer (DL) consists of two adjacent regions of opposite electric charge, which induce a potential drop and an electric field. The plasma within the DL is not locally neutral, but over the entire DL region it maintains space charge neutrality (global neutrality). A characteristic distance of the order of Debye length separates these layers of positive and negative charges, although in many cases the distance may be many times the Debye length. The potential jump across these layers is of the order of magnitude of the electron thermal temperature (where both the potential and the temperature are in energy units).

In high-power laser–plasma interaction, the electric fields inside the DL are no longer static, and therefore the nomenclature 'dynamic electric fields' was introduced (Eliezer and Hora 1989). According to two-fluid simulations (Lalousis 1983, Hora *et al*. 1984) these fields act deep inside plasmas and are oscillating and damped.

The first research on DL was conducted by Langmuir (1929). A condition for DL formation was given by Bohm (1949). Although DLs have been studied since the early days of plasma physics, this phenomenon is still a subject of active research. The DL phenomenon is a highly nonlinear effect of great interest in basic plasma physics, as well as in many plasma applications. DL solutions have been obtained theoretically by using the Vlasov equation (Bernstein *et al*. 1957), by solving fluid models coupled by the Poisson equation where space charge quasi-neutrality is not assumed (Lalousis 1983, Lalousis and Hora 1983, Hora 2000), and by performing computer simulations (Smith 1987).

Electrostatic DLs are now a well-known phenomenon in laboratory plasmas (Saeki *et al*. 1980, Hatakeyama *et al*. 1983, Chan *et al*. 1984, Hershkowitz 1985). The experiments have shown the existence of various types of DLs that can arise under different plasma conditions, including both magnetized and non-magnetized plasmas. Dynamic DLs in laser–plasma interactions were also measured experimentally (Eliezer and Ludmirsky 1983, Ludmirsky *et al*. 1984).

A schematic potential $\phi(x)$, defining an electric field $E(x)$ and a space–charge density $\rho_e(x)$, are given in figure 7.2. The following three conditions

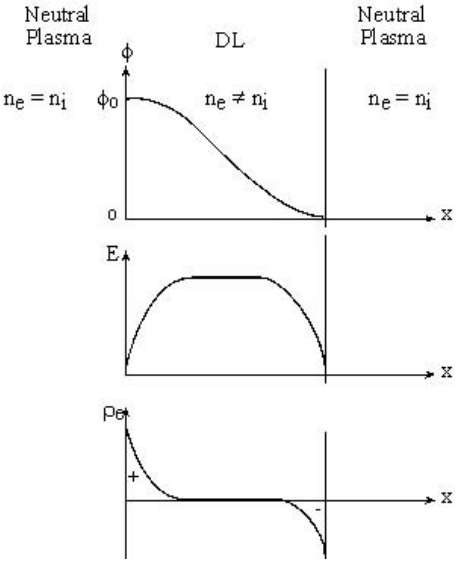

Figure 7.2. Schematic of the potential ϕ, the electric field E and the charge density ρ_e in a static DL.

must be fulfilled for the existence of a DL:

1. The potential drop ϕ_0 through the DL obeys the relation

$$\phi_0 \geq \frac{k_B T}{e} \tag{7.14}$$

   where T is the temperature of the coldest plasma bordering the layer, k_B is the Boltzmann constant and e is the electron charge.
2. Quasi-neutrality is locally violated in both space charge layers.
3. Global neutrality, i.e. zero net charge of the DL, is required.

The last constraint implies that the electric field is much stronger inside the DL than outside. The DL potential divides the plasma particles into four classes: free and trapped or reflected electrons and ions. The free electrons and ions have a kinetic energy larger than the potential barrier, and therefore they can move from one side of the DL to the other side. The particles with a kinetic energy smaller than the potential barrier are reflected or trapped at the DL borders and cannot move from one side of the DL to the other side. The charge separation in the DL is maintained by flux continuity of the free-streaming particles. The free particles are the streaming electrons from $\phi = 0$ towards $\phi = \phi_0$ and the ions are streaming in the opposite direction. Outside the DL, trapped or reflected ions on the low-potential side and trapped or reflected electrons on the high-potential end maintain charge neutrality.

In the next section it is shown how these DLs can accelerate electrons and ions.

7.4 Charged Particle Acceleration

7.4.1 A static model

Laser-produced plasma experiments have shown that high-energy ions are emitted and carry away a large fraction of the absorbed laser energy. X-ray emission measurements at laser intensities $I_L\lambda_L^2 > 10^{14}\,\mathrm{W\,\mu m^2/cm^2}$ (the laser irradiance I_L is measured in $\mathrm{W/cm^2}$ and the laser wavelength λ_L in μm) have shown non-Maxwellian electron velocity distribution (Haines 1979, Ahlstrom 1982). Two distinct electron temperatures, the so-called thermal (or cold) and supra-thermal (or hot) temperatures, usually characterize this distribution. These electron distributions are associated with the existence of fast ions. We shall now describe a very simple model showing how DLs accelerate ions.

A high-power laser irradiates a spherical pellet of radius R. The fast electrons emitted from the spherical plasma leave the sphere until an electrostatic potential is set up to stop the outgoing electrons. The thermal electrons then traverse this field (i.e. the DL), decelerate and accelerate back towards the sphere. The same field will accelerate positive ions from the outer surface of the plasma. The fast ions are field-extracted from the plasma and therefore they can be used to measure the electric field and the potential of the DL under consideration. For simplicity, monochromatic fast electrons and protons (the ions) species are assumed. The protons, with a mass M, are emitted from the DL with velocity v, so that

$$\tfrac{1}{2}Mv^2 = e\phi \tag{7.15}$$

where ϕ is the DL potential drop. Assuming that the fast protons have a total energy W and a total charge Q, one can write

$$W = Q\phi. \tag{7.16}$$

The charge of the proton q present at any moment inside the DL (defined by the potential drop ϕ and charge separation d) is given by

$$q = \frac{Qd}{v\tau_L} = \frac{Wd}{\phi v\tau_L} \tag{7.17}$$

where τ_L is the laser pulse duration. For the geometry under consideration, the DL can be modelled by a capacitor with a capacity C:

$$C = \frac{4\pi R^2}{d}. \tag{7.18}$$

The capacitor is charged with a charge greater than q (the momentary charge of the protons inside the DL) and with a voltage equal to ϕ; therefore

$$\phi > \frac{q}{C} = \frac{Wd^2}{4\pi R^2 \phi v \tau_L}. \tag{7.19}$$

This relation implies that the electric field created by the charge separation (i.e. the DL) is

$$E = \frac{\phi}{d} \geq \left(\frac{W}{4\pi R^2 v \tau_L} \right)^{1/2}. \tag{7.20}$$

The velocity of the ions is measured from the time of flight and the number of ions is measured with charge collectors, and from these their energy is deduced. Using a typical experiment where $W = 10\,\text{J}$, $v = 10^8\,\text{cm/s}$, $\tau_L = 1\,\text{ns}$, $R = 50\,\mu\text{m}$, one gets an electric field $E > 5 \times 10^8\,\text{V/cm}$.

From this simple model we can conclude that the fast electrons transfer their energy to the electrostatic field in order to create a DL, while the fast ions take their energy from the electric field of the DL. This mechanism can lead to very high electric fields, as is obtained above.

7.4.2 A dynamic model

DL solutions have been obtained theoretically by solving a two-fluid model coupled by the Poisson equation, where space-charge quasi-neutrality is not assumed. For example, in the simulation (Hora *et al.* 1984) of the interaction between a plasma with a highly bent parabolic initial density profile of 25 wavelengths thickness and a neodymium glass laser radiation of $10^{17}\,\text{W/cm}^2$ intensity, the following results were achieved:

(a) a caviton (i.e. a minimum in the density) is created,
(b) the plasma is accelerated towards the vacuum with a velocity of about $10^8\,\text{cm/s}$,
(c) a dynamic (time-dependent) DL is created with a maximum electric field about $10^9\,\text{V/cm}$ and
(d) electrons were accelerated to energies $\sim$140 keV.

The following simple dynamical model has been suggested in order to explain how dynamical DL accelerates electrons (Eliezer *et al.* 1995).

We assume that a DL is created at time $t = 0$ during a very short time interval, described by the Dirac delta function, $\delta(t)$. The Poisson equation gives

$$\frac{dE}{dx} = -4\pi e[n_e(x,t) - n_i(x,t)] = f(x)\delta(t). \tag{7.21}$$

Integrating this equation yields

$$E = \delta(t) \int f(x)\,\mathrm{d}x = F(x)\delta(t). \tag{7.22}$$

For example, from a 'quadrupole' type (two DL in a sequence) of interaction defined by a charge density

$$f(x) = K\left[\frac{2x}{\sigma^4}\left(1 - \frac{2x^2}{\sigma^2}\right)\right] \exp\left(-\frac{x^2}{\sigma^2}\right) \tag{7.23}$$

one gets a space-dependent electric field

$$F(x) = \frac{K}{\sigma^2}\left(1 + \frac{2x^2}{\sigma^2}\right) \exp\left(-\frac{x^2}{\sigma^2}\right). \tag{7.24}$$

The Newton equation for the electron

$$\frac{\mathrm{d}v}{\mathrm{d}t} = -\frac{eE}{m} = -\frac{e}{m} F(x)\delta(t) \tag{7.25}$$

has the solution

$$\begin{aligned} &\frac{\mathrm{d}x}{\mathrm{d}t} = v(t) = -\frac{e}{m} F(x)\theta(t) + v_0 = (v_1 - v_0)\theta(t) + v_0 \\ &\theta(t) = \begin{cases} 1 & \text{for } t > 0 \\ 0 & \text{for } t < 0 \end{cases} \end{aligned} \tag{7.26}$$

where v_0 is the initial velocity and v_1 the final velocity, after the acceleration. If the electron is at the position x when the force is applied (at $t = 0$ in this example), then the final velocity is achieved according to the value of $-eF(x)/m$.

The position of the electron is given by integrating (7.26):

$$x(t) = v_0 t + (v_1 - v_0)\theta(t)t \tag{7.27}$$

where the identity $\delta(t)t = 0$ was used.

Substituting (7.26) into (7.25), the electric field can be written

$$E(x,t) = F(x)\delta(t) = -\frac{m}{e}(v_1 - v_0)\delta(t). \tag{7.28}$$

The energy given to the particle by the electric field is given by using (7.26) and (7.28):

$$\begin{aligned} -e \int E(x,t)\,\mathrm{d}x = &-e \int_{-\infty}^{+\infty} E[x(t),t]\frac{\mathrm{d}x}{\mathrm{d}t}\,\mathrm{d}t \\ &= m(v_1 - v_0) \int_{-\infty}^{+\infty} \delta(t)[(v_1 - v_0)\theta(t) + v_0]\,\mathrm{d}t \\ &= \tfrac{1}{2}m(v_1^2 - v_0^2) \end{aligned} \tag{7.29}$$

where in the last stage we have used the identity

$$\int \theta(t)\delta(t)\,\mathrm{d}t = \tfrac{1}{2} \tag{7.30}$$

which can be easily proven by integrating by parts.

Equation (7.29) is the energy conservation, which shows that a particle can be accelerated or decelerated by E, depending on the value of the electric field at the particle position, at the time that the DL is created. It has been shown that under the right configuration a charged particle can be accelerated to high energies even when the electric field is changing very fast in time.

In summary, it has been demonstrated that a dynamic DL can accelerate charged particles, as was suggested in astrophysics (Fälthammer 1987, Alfvén 1988, Raadu 1989). The existence of DL in laser-produced plasma in the outer corona was detected directly by the deflection of a probing beam (Ehler 1975, Mendel and Olsen 1975) and by using Rogowski coils (Eliezer and Ludmirsky 1983). Therefore, similar to DL in astrophysics, the DL might play an important role in laser–plasma interactions.

Chapter 8

Laser-Induced Magnetic Fields in Plasma

When a laser irradiates a medium, the laser magnetic field $B_L \cos \omega_L t$ (together with the associated electric field) is propagating into the plasma, part of it is reflected and the other part is absorbed. The laser magnetic field amplitude and its frequency are given by

$$\begin{aligned} B_L(\text{Gauss}) &= 9.2 \times 10^6 \left(\frac{I_L}{10^{16}\,\text{W/cm}^2} \right)^{1/2} \\ \omega_L\,(\text{s}^{-1}) &= \frac{2\pi c}{\lambda_L} = 1.88 \times 10^{15} \left(\frac{\mu\text{m}}{\lambda_L} \right) \end{aligned} \tag{8.1}$$

where I_L is the laser energy flux and λ_L is the laser wavelength. ω_L sets the scale for high-frequency phenomena. The period of one laser oscillation $(2\pi/\omega_L)$ is about 3.3 fs for a laser with a wavelength of 1 μm. The propagation of electromagnetic field in plasma was calculated in chapter 5. There are also high-frequency magnetic fields associated with the stimulated Brillouin and Raman scattering discussed in chapter 6.

In this chapter we are interested only in the slowly-varying (on the time scale of the laser pulse duration) magnetic fields, approximated as d.c. magnetic fields. The generation of d.c. mega-Gauss magnetic fields in laser-produced plasmas is well-documented (Stamper *et al.* 1971, Boyd and Cooke 1988, Horovitz *et al.* 1998). In this chapter we discuss the mechanisms proposed to explain the generation of the d.c. magnetic fields and some theoretical consequences.

In section 8.1, the $\nabla n \times \nabla T$ toroidal magnetic field (Raven *et al.* 1978, Bobin 1985, Stamper 1991) is derived. In section 8.2, the magneto-hydrodynamic equations are derived (Braginskii 1965, Nicholson 1983, Parks 1991). Using the generalized Ohm's law together with the Maxwell equations, a generalized equation for the d.c. magnetic field is obtained. In particular the magnetic Reynolds number is defined and the dynamo effect is described (Briand *et al.* 1983, Dragila 1987). Section 8.3 describes the Faraday effect

and the magnetic field created by the inverse Faraday effect (Steiger and Woods 1972, Eliezer *et al*. 1992, Lehner 1994, 2000, Sheng and Meyer-ter-Vehn 1996, Haines 2001). In section 8.4 we develop the dispersion relation for waves in the presence of the d.c. magnetic field. In particular, ordinary, extraordinary and Alfvén waves are analysed. We conclude this chapter with section 8.5, showing the effect of resonance absorption in the presence of the d.c. magnetic field (Woo *et al*. 1978, David and Pellat 1980).

8.1 The $\nabla n \times \nabla T$ Toroidal Magnetic Field

One can see from the Maxwell equation (in Gaussian units)

$$\nabla \times \mathbf{E} = -\frac{1}{c}\frac{\partial B}{\partial t} \tag{8.2}$$

that a magnetic field is generated if the electric field E does not have a vanishing curl, i.e. the electric field in the plasma is not derivable from a potential. As discussed in the previous chapter, the electric field in the plasma is required in order to keep quasi-neutrality on a large scale (compared with the Debye length) during long periods of time (compared with the inverse plasma frequency). From the electron momentum equation (see section 3.1), on the long time scale it is justifiable to neglect the inertia of the electrons, implying

$$0 = -\nabla P_{\mathrm{e}} - e n_{\mathrm{e}} \mathbf{E}. \tag{8.3}$$

This equation is equivalent to the assumption that the volume forces due to the free electrical charges balance the electron pressure gradient. In equation (8.3), the charge motion is neglected. Substituting the ideal gas equation of state

$$P_{\mathrm{e}} = n_{\mathrm{e}} k_{\mathrm{B}} T_{\mathrm{e}} \tag{8.4}$$

into equation (8.3), one gets the electric field E for equation (8.2), yielding

$$\frac{\partial \mathbf{B}}{\partial t} = \frac{c k_{\mathrm{B}}}{e n_{\mathrm{e}}} \nabla T_{\mathrm{e}} \times \nabla n_{\mathrm{e}}. \tag{8.5}$$

From this equation an estimate of the magnitude of the magnetic field B is obtained by the substitution of

$$\frac{\partial}{\partial t} \approx \frac{1}{\tau_{\mathrm{L}}}, \qquad \frac{\nabla n_{\mathrm{e}}}{n_{\mathrm{e}}} \approx \frac{1}{L_{\mathrm{n}}}, \qquad \nabla T_{\mathrm{e}} \approx \frac{T_{\mathrm{e}}}{L_{\mathrm{T}}} \tag{8.6}$$

into equation (8.5), implying

$$B\,(\mathrm{MGauss}) \approx 10 \left(\frac{\tau_{\mathrm{L}}}{1\ \mathrm{ns}}\right)\left(\frac{k_{\mathrm{B}} T_{\mathrm{e}}}{1\ \mathrm{keV}}\right)\left(\frac{30\ \mu\mathrm{m}}{L_{\mathrm{n}}}\right)\left(\frac{30\ \mu\mathrm{m}}{L_{\mathrm{T}}}\right) \tag{8.7}$$

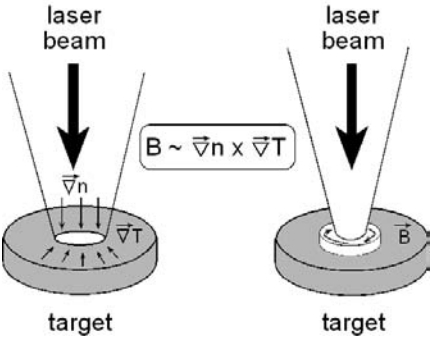

Figure 8.1. Magnetic field is generated from non-parallel density and temperature gradients.

where τ_L is the laser pulse duration or the characteristic loss time due to ablation and diffusion.

Thus a magnetic field is generated from non-parallel density and temperature gradients, as shown in figure 8.1. It turns out that this is the dominant phenomenon for the generation of a toroidal magnetic field, although there are other terms that contribute to the generation of d.c. toroidal magnetic fields, as proven in the following section.

8.2 Magneto-Hydrodynamics and the Evolution of the Magnetic Field

In this section the evolution equation of the magnetic field is developed. For this purpose the plasma is described as a magnetic fluid and the equations include the generalized Ohm's law, together with Maxwell equations. The following equations describe the mass conservation and the momentum conservation for the ion and electron fluids (in Gaussian units):

$$\begin{aligned}
&\frac{\partial n_i}{\partial t} + \nabla \cdot (n_i \mathbf{v}_i) = 0 \\
&\frac{\partial n_e}{\partial t} + \nabla \cdot (n_e \mathbf{v}_e) = 0 \\
&m_i n_i \frac{\partial \mathbf{v}_i}{\partial t} + m_i n_i (\mathbf{v}_i \cdot \nabla)\mathbf{v}_i = -\nabla P_i + Z e n_i \left(\mathbf{E} + \frac{\mathbf{v}_i \times \mathbf{B}}{c} \right) + \mathbf{R}_i \\
&m_e n_e \frac{\partial \mathbf{v}_e}{\partial t} + m_e n_e (\mathbf{v}_e \cdot \nabla)\mathbf{v}_e = -\nabla P_e - e n_e \left(\mathbf{E} + \frac{\mathbf{v}_e \times \mathbf{B}}{c} \right) + \mathbf{R}_e
\end{aligned} \tag{8.8}$$

where m_i, m_e and n_i, n_e are the ion and electron masses and densities, $\mathbf{v}_i$ and $\mathbf{v}_e$ are the ion and electron fluid velocities, P_i and P_e are the appropriate pressures, $\mathbf{E}$ and $\mathbf{B}$ are the electric and magnetic fields in the plasma

medium and c is the light velocity. $\mathbf{R}_e(\mathbf{r})$ represents the change in electron momentum at position $\mathbf{r}$ due to collisions with ions and $\mathbf{R}_i(\mathbf{r})$ is the change in ion momentum at $\mathbf{r}$ due to collisions with electrons. Therefore

$$\mathbf{R}_e = -\mathbf{R}_i. \tag{8.9}$$

We combine the ion and the electron equations to obtain the equations for one fluid. This fluid is described by the mass density $\rho(\mathbf{r})$, charge density $\rho_e(\mathbf{r})$, a centre of mass fluid flow $\mathbf{u}$ and an electrical current $\mathbf{J}$, defined by

$$\begin{aligned} \rho &= m_i n_i + m_e n_e \cong m_i n_i \\ \rho_e &= Z e n_i - e n_e \\ \mathbf{u} &= \frac{1}{\rho}(m_i n_i \mathbf{v}_i + m_e n_e \mathbf{v}_e) \\ J &= Z e n_i \mathbf{v}_i - e n_e \mathbf{v}_e \end{aligned} \tag{8.10}$$

and a total pressure

$$P = P_e + P_i\,. \tag{8.11}$$

Multiplying the first equation of (8.8) by m_i and the second equation by m_e and adding, one gets the one-fluid continuity equation (i.e. the mass conservation):

$$\frac{\partial \rho}{\partial t} + \nabla \cdot (\rho \mathbf{u}) = 0. \tag{8.12}$$

Multiplying the first equation of (8.8) by Ze and the second equation by $-e$ and adding, one gets the charge continuity, or the charge conservation law:

$$\frac{\partial \rho_e}{\partial t} + \nabla \cdot \mathbf{J} = 0. \tag{8.13}$$

It is assumed that $\mathbf{v}_e$, $\mathbf{v}_i$, $\partial n_e/\partial t$ and $\partial n_i/\partial t$ are small quantities and second-order terms, such as $(\mathbf{v} \cdot \nabla)\mathbf{v}$, are neglected. Adding the third equation of (8.8) with the fourth equation and using the definitions (8.10) and (8.11), one gets the one-fluid force equation (or the momentum conservation):

$$\rho \frac{\partial \mathbf{u}}{\partial t} = -\nabla P + \rho_e \mathbf{E} + \frac{1}{c}\,\mathbf{J} \times \mathbf{B}. \tag{8.14}$$

8.2.1 The generalized Ohm's law

We assume charge neutrality

$$n_e = Z n_i \tag{8.15}$$

and neglect the second-order terms (in $\mathbf{v}_e$, $\mathbf{v}_i$, $\partial n_e/\partial t$ and $\partial n_i/\partial t$) and $1/m_i \ll 1/m_e$. Adding the third equation of (8.8) multiplied by Ze/m_i with

the fourth equation multiplied by $-e/m_e$, and using the definitions (8.10), one gets

$$\frac{\partial \mathbf{J}}{\partial t} = \frac{e}{m_e}\nabla\left[\left(1+\frac{T_i}{ZT_e}\right)^{-1}P\right] + \frac{Ze^2\rho}{m_e m_i}\left(\mathbf{E}+\frac{1}{c}\,\mathbf{u}\times\mathbf{B}\right) - \frac{e}{m_e c}\,\mathbf{J}\times\mathbf{B} + \frac{e}{m_e}\,\mathbf{R}_i\,. \tag{8.16}$$

Algebraic relations such as the following were used in order to derive equation (8.16):

$$\frac{e^2 n_e}{m_e} = \frac{e^2 Z n_i}{m_e} = \frac{e^2 Z}{m_e m_i}(m_i n_i) \cong \frac{e^2 Z}{m_e m_i}(m_i n_i + m_e n_e) = \frac{e^2 Z\rho}{m_e m_i} \tag{8.17}$$

$$\frac{e^2 n_e \mathbf{v}_e}{m_e c} = \frac{e}{m_e c}(e n_e \mathbf{v}_e - Z e n_i \mathbf{v}_i) + \frac{Ze^2 n_i m_i \mathbf{v}_i}{m_e m_i c}$$

$$\cong -\frac{e}{m_e c}\mathbf{J} + \frac{Ze^2}{m_e m_i c}(n_i m_i \mathbf{v}_i + n_e m_e \mathbf{v}_e) = -\frac{e}{m_e c}\mathbf{J} + \frac{Ze^2}{m_e m_i c}\,\rho\mathbf{u} \tag{8.18}$$

$$\frac{Ze}{m_i}\,\mathbf{R}_i - \frac{e}{m_e}\,\mathbf{R}_e = \left(\frac{Ze}{m_i}+\frac{e}{m_e}\right)\mathbf{R}_i \cong \frac{e}{m_e}\,\mathbf{R}_i \tag{8.19}$$

$$\frac{P_e}{P} = \frac{n_e k_B T_e}{n_e k_B T_e + n_i k_B T_i} = \frac{Z n_i T_e}{Z n_i T_e + n_i T_i} = \left(1+\frac{T_i}{ZT_e}\right)^{-1} \tag{8.20}$$

where $\mathbf{R}_i$ in equation (8.16) is the change in the ion momentum due to collisions with electrons. Therefore, one can expand $\mathbf{R}_i$ as a Taylor series in the relative velocity between the ions and the electrons. Keeping only the first term in the Taylor expansion, one gets

$$\mathbf{R}_i = C_1(\mathbf{v}_i - \mathbf{v}_e). \tag{8.21}$$

Using charge neutrality and the definition of the electric current, equations (8.10) and (8.15), into equation (8.21) gives

$$\mathbf{R}_i = C_2\mathbf{J}. \tag{8.22}$$

Since the value of C_2 does not depend on the general structure of equation (8.16), one can consider this equation for the following special case: steady state, no pressure (or temperature) gradients and without magnetic field. Substituting (8.22) into (8.16) for this special case, one obtains

$$\frac{Ze\rho}{m_i}\,\mathbf{E} + C_2\mathbf{J} = 0. \tag{8.23}$$

Using now the simple Ohm's law for this case (see section 2.3), where σ_E is the electrical conductivity coefficient,

$$\mathbf{J} = \sigma_E\mathbf{E} \tag{8.24}$$

one gets the value of C_2, implying

$$\mathbf{R}_\mathrm{i} = C_2\mathbf{J} = -\frac{Ze\rho}{m_\mathrm{i}\sigma_\mathrm{E}}\,\mathbf{J}. \tag{8.25}$$

Substituting (8.25) into (8.16), we get the **generalized Ohm's law**:

$$\left(\frac{m_\mathrm{e}m_\mathrm{i}}{Ze^2\rho}\right)\frac{\partial\mathbf{J}}{\partial t} = \left(\frac{m_\mathrm{i}}{Ze\rho}\right)\nabla\left[\left(1+\frac{T_\mathrm{i}}{ZT_\mathrm{e}}\right)^{-1}P\right] + \mathbf{E} + \left(\frac{1}{c}\right)\mathbf{u}\times\mathbf{B} - \left(\frac{m_\mathrm{i}}{Zec\rho}\right)\mathbf{J}\times\mathbf{B} - \left(\frac{1}{\sigma_\mathrm{E}}\right)\mathbf{J}. \tag{8.26}$$

The magneto-hydrodynamic equations are (8.12), (8.13), (8.14) and (8.26), together with the following Maxwell equations:

$$\nabla\times\mathbf{E} = -\left(\frac{1}{c}\right)\frac{\partial\mathbf{B}}{\partial t}, \qquad \nabla\times\mathbf{B} = \left(\frac{4\pi}{c}\right)\mathbf{J} + \left(\frac{1}{c}\right)\frac{\partial\mathbf{E}}{\partial t}. \tag{8.27}$$

One therefore has 14 equations with 14 unknowns: ρ, ρ_E, $\mathbf{u}$, $\mathbf{J}$, $\mathbf{E}$ and $\mathbf{B}$. This is correct only if the temperatures T_e and T_i are known, otherwise the (electron and ion) energy conservation equations are also necessary. Moreover, knowledge of the equations of state, $P_\mathrm{e} = P_\mathrm{e}(\rho, T_\mathrm{e})$ and $P_\mathrm{i} = P_\mathrm{i}(\rho, T_\mathrm{i})$, is necessary. For not very dense plasmas ($\rho \ll \rho_\mathrm{solid}$), the ideal gas equations of state are suitable (such as those we have used in equation (8.20)).

In this chapter we are interested in calculating the steady-state magnetic field. Therefore, the generalized Ohm's law given in equation (8.26) is assumed, together with the assumption $\partial\mathbf{J}/\partial t = 0$, yielding an electric field

$$\mathbf{E} = \left(\frac{1}{\sigma_\mathrm{E}}\right)\mathbf{J} - \left(\frac{m_\mathrm{i}}{Ze\rho}\right)\nabla\left[\left(1+\frac{T_\mathrm{i}}{ZT_\mathrm{e}}\right)^{-1}P\right] - \left(\frac{1}{c}\right)\mathbf{u}\times\mathbf{B} + \left(\frac{m_\mathrm{i}}{Zec\rho}\right)\mathbf{J}\times\mathbf{B}. \tag{8.28}$$

From this equation we see that the electric field in the plasma has four contributions:

1. The $\mathbf{J}\times\mathbf{B}$ term, which is the Hall effect.
2. $\mathbf{u}\times\mathbf{B}$ is the convective (plasma flow) term.
3. ∇P is the pressure gradient contribution.
4. The $\mathbf{J}/\sigma_\mathrm{E}$ term is the (standard Ohm's law) voltage drop on plasma-active resistance.

Using for the electrical conductivity the value obtained in section 2.3 (Drude model),

$$\sigma_\mathrm{E} = \frac{e^2 n_\mathrm{e}}{m_\mathrm{e}\nu_\mathrm{ei}} \tag{8.29}$$

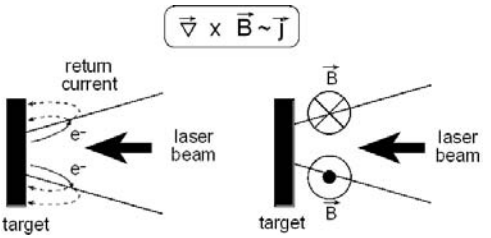

Figure 8.2. A toroidal magnetic field created by a return current.

and substituting (8.28) into the first equation of (8.27), one gets for $T_i \ll T_e$

$$\frac{\partial \mathbf{B}}{\partial t} = -\frac{m_e c \nu_{ei}}{e^2} \nabla \times \left(\frac{\mathbf{J}}{n_e} \right) + \frac{c k_B}{e n_e} \nabla T_e \times \nabla n_e + \nabla \times (\mathbf{u} \times \mathbf{B}) - \frac{1}{e} \nabla \times \left(\frac{\mathbf{J} \times \mathbf{B}}{n_e} \right). \tag{8.30}$$

The first term in (8.30) may contribute a toroidal magnetic field, as described in figure 8.2. The second term is the one given in the previous section and described schematically in figure 8.1.

The current **J** is substituted into (8.30) from the second equation of (8.27), and using the first equation of (8.27) one obtains a complex equation for the magnetic field generated in laser–plasma interaction. We consider now some special cases.

Case 1

It is assumed that the second and third terms of equation (8.30) are dominant. Looking for a d.c. solution ($\partial B/\partial t = 0$), one gets from equation (8.30):

$$\frac{c}{e n_e} \nabla P_e + \mathbf{u} \times \mathbf{B} = 0. \tag{8.31}$$

Taking $\nabla \approx 1/L$ and $u \approx c_s$, where L is the scale length of the electron pressure gradient and c_s is the speed of sound, and using the ideal gas equation of state for the electron pressure (equation (8.4)), one gets from equation (8.31):

$$B \approx \left(\frac{c}{c_s} \right) \frac{(k_B T_e/e)}{L} \approx \frac{(m_i c^2 k_B T_e)^{1/2}}{eL} \approx \left(\frac{m_i}{m_p} \right)^{1/2} \left(\frac{T_e}{\text{keV}} \right)^{1/2} \left(\frac{30\,\mu\text{m}}{L} \right) \quad [\text{MGauss}] \tag{8.32}$$

where m_i and m_p are the ion and the proton masses respectively. For an electron temperature of 1 keV and a pressure scale length of 30 μm one gets a d.c. magnetic field of 1 MG.

Case 2

It is now assumed that the first and third terms of equation (8.30) are dominant.

Moreover, a constant electrical conductivity is taken so that equation (8.30) can be rewritten as (after using equation (8.29))

$$\frac{\partial \mathbf{B}}{\partial t} = -\frac{c}{\sigma_{\mathrm{E}}} \nabla \times \mathbf{J} + \nabla \times (\mathbf{u} \times \mathbf{B}). \tag{8.33}$$

Substituting into this equation the second equation of (8.27) with $\partial E/\partial t = 0$, one obtains the equation for the magnetic field:

$$\frac{\partial \mathbf{B}}{\partial t} = -\frac{c^2}{4\pi\sigma_{\mathrm{E}}} \nabla \times (\nabla \times \mathbf{B}) + \nabla \times (u \times \mathbf{B}). \tag{8.34}$$

Using the identity

$$\nabla \times (\nabla \times \mathbf{B}) = -\nabla^2 \mathbf{B} + \nabla(\nabla \cdot \mathbf{B}) = -\nabla^2 \mathbf{B} \tag{8.35}$$

(where the Maxwell equation $\nabla \cdot \mathbf{B} = 0$ is used), one gets from equation (8.34):

$$\frac{\partial \mathbf{B}}{\partial t} = \left(\frac{c^2}{4\pi\sigma_{\mathrm{E}}}\right) \nabla^2 \mathbf{B} + \nabla \times (\mathbf{u} \times \mathbf{B}). \tag{8.36}$$

8.2.2 The magnetic Reynolds number

The first term on the right-hand side of (8.36) describes the diffusion of the magnetic field, while the second term is the convection of the plasma fluid moving with a velocity **u** (relative to a fixed observer, the laboratory frame of reference). The ratio between the convective and the diffusion terms defines the magnetic Reynolds number R_{m}:

$$R_{\mathrm{m}} = \left[\frac{uB/L}{(c^2 B)/(4\pi\sigma_{\mathrm{E}} L^2)}\right] = \left(\frac{4\pi}{c^2}\right) \sigma_{\mathrm{E}} L u \tag{8.37}$$

where L is the macroscopic scale length and u is the characteristic flow velocity. Note that R_{m} is dimensionless (in the Gaussian units used here the electrical conductivity coefficient σ_{E} has dimensions of s^{-1}). $c^2/(4\pi\sigma_{\mathrm{E}})$ is equivalent to the kinematic viscosity in defining the Reynolds number for a fluid flow (= inertial force/viscous force).

8.2.3 Magnetic Reynolds numbers $R_{\mathrm{m}} \ll 1$

For $R_{\mathrm{m}} \ll 1$ the convective term is negligible and equation (8.36) describes the diffusion of the magnetic field

$$\frac{\partial B}{\partial t} = \eta \nabla^2 B, \qquad \eta \equiv \frac{c^2}{4\pi\sigma_{\mathrm{E}}}. \tag{8.38}$$

This equation is similar to the heat diffusion equation

$$\frac{\partial T}{\partial t} = \kappa \nabla^2 T \tag{8.39}$$

where T is the temperature and κ is the coefficient of heat conduction. Similarly, in a viscous fluid flow the vorticity Ω satisfies a similar equation:

$$\frac{\partial \Omega}{\partial t} = \nu \nabla^2 \Omega, \qquad \Omega \equiv \nabla \times \mathbf{u} \tag{8.40}$$

where ν is the kinematic viscosity. Note that η, κ and ν have the dimension of cm^2/s in c.g.s. and m^2/s in m.k.s.

We now analyse equation (8.38). Assuming at $t = 0$ (initial condition) a magnetic field $B_{\mathrm{i}}(r, 0)$ in Cartesian coordinates ($i = x, y, z$), then at $t > 0$ the magnetic field is given by

$$B_i(\mathbf{r}, t) = \int \mathrm{d}^3 r' G(\mathbf{r} - \mathbf{r}', t) B_i(\mathbf{r}', 0) \tag{8.41}$$

where $G(\mathbf{r} - \mathbf{r}', t)$ is Green's function:

$$G(\mathbf{r} - \mathbf{r}', t) = \frac{1}{(4\pi\eta t)^{3/2}} \exp\left[-\frac{(\mathbf{r} - \mathbf{r}')^2}{4\eta t} \right]. \tag{8.42}$$

This solution shows that the magnetic field at an initial position $\mathbf{r}'$ diffuses in time with a Gaussian profile which has the width $(4\eta t)^{1/2}$, i.e. the width increases with the square root of time. An estimate of the magnetic field diffusion time is derived by taking $\nabla^2 \approx 1/L^2$ in equation (8.38), yielding

$$\frac{\partial \mathbf{B}}{\partial t} \approx \pm \frac{\eta}{L^2} B. \tag{8.43}$$

The solution of this equation is

$$B = B_0 \exp\left(\pm \frac{t}{\tau_{\mathrm{m}}} \right), \qquad \tau_{\mathrm{m}} = \frac{L^2}{\eta} = \frac{4\pi\sigma_{\mathrm{E}} L^2}{c^2} = \frac{R_{\mathrm{m}} L}{u}. \tag{8.44}$$

The $+$ or $-$ sign refer to 'gain' or 'loss' (with time) of the magnetic field.

For example, in a typical laser-produced plasma where diffusion is dominant, one has $L \approx 100\,\mu\mathrm{m}$ and $u \approx 10^6$ cm/s, implying a magnetic Reynolds number $R_{\mathrm{m}} \approx 0.1$ and a diffusion relaxation time $\tau_{\mathrm{m}} \approx 1\,\mathrm{ns}$.

8.2.4 Magnetic Reynolds numbers $R_{\mathrm{m}} \gg 1$

For $R_{\mathrm{m}} \gg 1$ the diffusion term is negligible and equation (8.36) describes the convection of the magnetic field:

$$\frac{\partial \mathbf{B}}{\partial t} = \nabla \times (\mathbf{u} \times \mathbf{B}). \tag{8.45}$$

In this case it is important to notice that if initially there is a magnetic field in the x–y plane, $\mathbf{B} = (B_x, B_y, B_z = 0)$, then equation (8.45) implies that for $t > 0$ a magnetic field perpendicular to the x–y plane is induced. For example,

$$\begin{aligned} t = 0: &\qquad \mathbf{B} = (B_x, B_y, 0), \qquad \mathbf{u} = (0, 0, u) \\ t > 0: &\qquad \frac{\partial B_z}{\partial t} = \frac{\partial (u B_y)}{\partial x} \;\Rightarrow\; B_z(t > 0) \approx \frac{tu}{L} B_y(t = 0). \end{aligned} \tag{8.46}$$

Assuming that in laser–plasma interactions ripples are created of the order of $L = 10\,\mu\text{m}$ and the plasma flow towards the laser is $u = 10^6\,\text{cm/s}$, then at a time $t \approx \tau_\text{L}$, where $\tau_\text{L} \approx 1\,\text{ns}$ is the laser pulse duration, one gets from (8.46)

$$B_z(t \approx \tau_\text{L}) \approx B_y(t = 0). \tag{8.47}$$

This phenomenon, where a magnetic field in the x–y plane develops into a magnetic field in the z direction, is called the **dynamo effect**. Therefore, we have seen that for a large magnetic Reynolds number the toroidal magnetic field may develop into a large axial magnetic field. However, for this phenomenon to happen fluctuations of small-scale L are necessary. Thus, this effect is a random process.

In the next section we shall see how an axial magnetic field (by definition, in the direction of the laser irradiation, or normal to the plane target) can be created in a controllable way for any magnetic Reynolds numbers.

8.3 Faraday and Inverse Faraday Effects

8.3.1 The Faraday effect

Michael Faraday discovered in 1845 that when plane-polarized light passed through lead glass in the direction of a magnetic field, the plane of polarization was rotated. The linear polarized electric field rotates when propagating along the magnetic field in a dielectric or a plasma medium. A linear polarized wave can be resolved into the sum of left- and right-circularly polarized waves, and the rotation arises due to the difference in the index of refraction between the two waves. The angle of rotation is proportional to the magnitude of the magnetic field.

We now calculate the angle of rotation for a linearly polarized light propagating in plasma or a dielectric media. Since there is an analogy between a dielectric medium and plasma, the Faraday effect is developed simultaneously for both media. The m.k.s. (SI) units are used in this section.

The equations of motion for the electrons in the presence of the laser electric field $\mathbf{E}_\mathrm{L}$ and the d.c. magnetic field $\mathbf{B}$ are (the $\mathbf{B}_\mathrm{L} \times \mathbf{v}$ force, where $\mathbf{B}_\mathrm{L}$ is the magnetic field of the laser that is negligible and therefore neglected)

$$\begin{aligned} \textbf{dielectric}: \quad & m_\mathrm{e}\frac{\mathrm{d}^2\mathbf{r}}{\mathrm{d}t^2} + m_\mathrm{e}\omega_0^2\mathbf{r} = -e\left(\mathbf{E}_\mathrm{L} + \frac{\mathrm{d}\mathbf{r}}{\mathrm{d}t}\times\mathbf{B}\right) \\ \textbf{plasma}: \quad & m_\mathrm{e}\frac{\mathrm{d}^2\mathbf{r}}{\mathrm{d}t^2} = -e\left(\mathbf{E}_\mathrm{L} + \frac{\mathrm{d}\mathbf{r}}{\mathrm{d}t}\times\mathbf{B}\right). \end{aligned} \tag{8.48}$$

$m_\mathrm{e}\omega_0^2\mathbf{r}$ is the restoring force of the center of charge of the electrons (q_e) of one atom in the dielectric medium. The dipole moment $\mathbf{p}$ of a single atom in the presence of a d.c. electric field $\mathbf{E}$ can be approximated by $\mathbf{p} = q_\mathrm{e} \simeq q_\mathrm{e}^2\mathbf{E}/(m_\mathrm{e}\omega_0^2)$. The laser electric field is in the x–y plane and propagates in the z direction, parallel to the d.c. magnetic field. Therefore, the electron motion is in the x–y plane and the following notation can be used in Cartesian coordinates:

$$\begin{aligned} \mathbf{B} &= (0,0,B), \qquad \mathbf{E} = (E_x, E_y, 0), \qquad \mathbf{r} = (x,y,0) \\ E_\pm &= E_x \pm \mathrm{i}E_y = E_0\exp[\mathrm{i}(k_\pm z - \omega t)] \\ E_x &= \frac{E_0}{2}\{\exp[\mathrm{i}(k_+ z - \omega t)] + \exp[\mathrm{i}(k_- z - \omega t)]\} \\ E_y &= -\mathrm{i}\frac{E_0}{2}\{\exp[\mathrm{i}(k_+ z - \omega t)] - \exp[\mathrm{i}(k_- z - \omega t)]\} \\ r_\pm &= x \pm \mathrm{i}y = r_0\exp[\mathrm{i}(k_\pm z - \omega t)] \end{aligned} \tag{8.49}$$

where r_0 and E_0 are real and $E_\pm$ describe circularly-polarized monochromatic lasers. One defines E_+ as right-handed circular polarization (RHCP) and E_- as left-handed circular polarization (LHCP). Using the notation of equations (8.49), one can write the solution of equations (8.48) in the following form:

$$\begin{aligned} \textbf{dielectric}: \quad & r_\pm = \frac{-(e/m_\mathrm{e})E_\pm}{\omega_0^2 \mp (eB/m_\mathrm{e})\omega - \omega^2} \\ \textbf{plasma}: \quad & r_\pm = \frac{-(e/m_\mathrm{e})E_\pm}{\mp\omega_\mathrm{c}\omega - \omega^2} \end{aligned} \tag{8.50}$$

where the electron cyclotron frequency is defined by

$$\omega_\mathrm{c} = \frac{eB}{m_\mathrm{e}}. \tag{8.51}$$

Using Maxwell equations, one obtains the following wave equations for the two appropriate media (see Appendix A):

$$\begin{aligned}
&\textbf{dielectric}: \quad \nabla^2\mathbf{E} - \frac{1}{c^2}\frac{\partial^2\mathbf{E}}{\partial t^2} - \mu_0\frac{\partial^2\mathbf{P}}{\partial t^2} = 0, \qquad \mathbf{P} = -en_e\mathbf{r} \\
&\textbf{plasma}: \quad \nabla^2\mathbf{E} - \frac{1}{c^2}\frac{\partial^2\mathbf{E}}{\partial t^2} - \mu_0\frac{\partial\mathbf{J}}{\partial t} = 0, \qquad \mathbf{J} = -en_e\frac{\mathrm{d}\mathbf{r}}{\mathrm{d}t}
\end{aligned} \tag{8.52}$$

where μ_0 is the magnetic permeability in vacuum, $\mathbf{P}$ is the polarization of the dielectric medium and $\mathbf{J}$ is the electric current in the plasma. Using equations (8.49) and (8.50) in (8.52), the following dispersion relations are derived:

$$\begin{aligned}
&\textbf{dielectric}: \quad k_\pm^2 = \frac{\omega^2}{c^2}\left[1 - \frac{\omega_{pe}^2}{\omega^2 \mp (eB/m_e)\omega - \omega_0^2}\right], \qquad \omega_{pe}^2 = \frac{e^2 n_e}{\varepsilon_0 m_e} \\
&\textbf{plasma}: \quad k_\pm^2 = \frac{\omega^2}{c^2}\left[1 - \frac{\omega_{pe}^2}{\omega^2 \mp \omega_c\omega}\right], \qquad \frac{1}{\varepsilon_0} = \mu_0 c^2
\end{aligned} \tag{8.53}$$

where ω_{pe} is the electron plasma frequency in the dielectric or the plasma medium.

The appropriate indices of refraction for the RHCP and LHCP are

$$n_\pm = \frac{ck_\pm}{\omega}. \tag{8.54}$$

At $z = 0$ one has a linearly polarized laser, given by

$$E_x(z=0) = E_0\cos\omega t = \frac{E_0}{2}[\exp(\mathrm{i}\omega t) + \exp(-\mathrm{i}\omega t)], \qquad E_y(z=0) = 0. \tag{8.55}$$

In order to obtain the values of $E_\pm$ at $z = l$ we define

$$\varphi(z) = \tfrac{1}{2}[z(k_+ + k_-)] - \omega t, \qquad \theta(z) = \tfrac{1}{2}[z(k_+ - k_-)]. \tag{8.56}$$

Using the identity

$$k_\pm = \tfrac{1}{2}(k_+ + k_-) \pm \tfrac{1}{2}(k_+ - k_-) \tag{8.57}$$

together with equations (8.49) and (8.56), one obtains the electric field (at $z = l$), after propagating along the d.c. magnetic field a distance l:

$$\begin{aligned}
E_\pm(z=l) &= E_0\exp[\mathrm{i}\varphi(l)]\exp[\pm\mathrm{i}\theta(l)] \\
E_x &= E_0\exp[\mathrm{i}\varphi(l)]\cos\theta(l) \\
E_y &= E_0\exp[\mathrm{i}\varphi(l)]\sin\theta(l).
\end{aligned} \tag{8.58}$$

From these equations one can see that φ is a phase of the amplitude and θ is the angle of rotation. At $z = 0$ the angle θ is zero (i.e. by definition of the linearly polarized light $E_y = 0$). From the definition of θ in (8.56) one gets at $z = l$:

$$\theta(l) = \frac{l}{2}(k_+ - k_-). \tag{8.59}$$

The values of $k_\pm$ are obtained from the dispersion relation (8.53). For constant electron density n_e and magnetic field B, and neglecting B^2 terms (i.e. $\omega_c/\omega \ll 1$), one gets

dielectric: $\theta = VlH, \qquad H = B/\mu_0$

$$V = \left(\frac{\mu_0 e}{2nm_e c}\right)\frac{\omega^2\omega_{pe}^2}{(\omega^2-\omega_0^2)^2}, \qquad n = \tfrac{1}{2}(n_+ + n_-) \tag{8.60}$$

plasma: $\theta = l\left(\frac{eB}{m_e c}\right)\left(\frac{\omega_{pe}^2}{\omega^2}\right) \approx 3.4\left(\frac{B}{\text{Tesla}}\right)\left(\frac{l}{100\,\mu\text{m}}\right)\left(\frac{\omega_{pe}^2}{\omega^2}\right)$ degrees.

For the dielectric medium case the coefficient V is called the Verdet constant.

For the plasma medium, one can see that close to the critical density ($\omega_{pe} \approx \omega$) the angle of rotation is 3.4° per Tesla for a laser propagating along $l = 100\,\mu$m. Equation (8.60) is valid if $n_e =$ constant and B is small (we neglected B^2) on the scale defined by

$$\omega_c \ll \omega \;\Rightarrow\; \frac{B}{B_c} \ll 1, \qquad B_c \equiv \frac{m_e\omega}{e} \approx \frac{1.07\times 10^8}{\lambda_L\,(\mu\text{m})}\ \text{Gauss}. \tag{8.61}$$

For most experiments in laser–plasma interactions the constraint (8.61) is satisfied. However, the electron density is not constant in these experiments. For a non-constant electron density the angle θ in equation (8.59) is modified to

$$\theta = \frac{1}{2}\int_0^l \mathrm{d}z(k_+ - k_-). \tag{8.62}$$

Using the dispersion relation (8.53) in the plasma medium for $\omega_c \ll \omega$, one can use the approximations

$$\begin{aligned} k_+ - k_- = \frac{k_+^2 - k_-^2}{k_+ + k_-} &\approx \frac{(\omega_{pe}/\omega)^2(1+\omega_c/\omega) - (\omega_{pe}/\omega)^2(1-\omega_c/\omega)}{2(\omega/c)\sqrt{1-(\omega_{pe}/\omega)^2}} \\ &= \left(\frac{eBc}{m_e\omega^2}\right)\left(\frac{n_e}{n_{ec}}\right)\left[1-\left(\frac{n_e}{n_{ec}}\right)\right]^{-1/2} \end{aligned} \tag{8.63}$$

where n_{ec} is the electron critical density and ω is the angular frequency of the laser ('probe') beam:

$$\omega = \frac{2\pi c}{\lambda_p}. \tag{8.64}$$

Substituting (8.63) into (8.62), one obtains the angle of rotation (in practical units) for a plasma medium:

$$\theta(\text{deg}) = 3.02\left(\frac{\lambda_p}{\mu\text{m}}\right)^2\int_0^l\left(\frac{\mathrm{d}z}{\mu\text{m}}\right)\left(\frac{n_e}{10^{21}\,\text{cm}^{-3}}\right)\left(\frac{B}{\text{MGauss}}\right)\left(1-\frac{n_e}{n_{ec}}\right)^{-1/2}. \tag{8.65}$$

The Faraday effect is used in laser–plasma interactions to measure the magnetic field (Raven *et al.* 1978, Horovitz *et al.* 1997). For this purpose it is also necessary to know the electron density. At the critical density there is a singularity in equation (8.65), but this is not a problem since the laser cannot propagate along a critical density. Using this equation, megagauss (d.c.) magnetic fields were measured in laser–plasma interactions.

8.3.2 The inverse Faraday effect

The inverse Faraday effect is the phenomenon where a magnetic field is created in a medium due to the rotation of the electromagnetic field. In particular, a circularly-polarized laser can induce a magnetic field in the plasma. The magnetic field arises because the electrons quiver with the oscillating electric field of the incoming laser light, and if the laser is circularly polarized then the electrons describe a circular motion. The net effect of this is a circular current on the edge of the plasma, which generates the magnetic field (see figure 8.3).

A simple (order of magnitude) calculation for the magnetic field created by the inverse Faraday effect in cold plasma is now developed. The motion of the electrons in an applied electric field is, according to linearized law,

$$\frac{\partial \mathbf{v}}{\partial t} = -\frac{e}{m_e}\mathbf{E} \tag{8.66}$$

where $\mathbf{v}$ is the electron velocity and $\mathbf{E}$ is the applied electric field in the plasma, as a result of the absorbed laser energy. The ions are considered immobile. The electric field is incident in the z direction and is circularly polarized in the x–y plane:

$$\mathbf{E} = E_0\left(\frac{\hat{\mathbf{x}} + \mathrm{i}\hat{\mathbf{y}}}{\sqrt{2}}\right)\exp[-\mathrm{i}(\omega t - kz)] \tag{8.67}$$

where $\hat{\mathbf{x}}$ and $\hat{\mathbf{y}}$ are unit vectors in the x and y directions respectively.

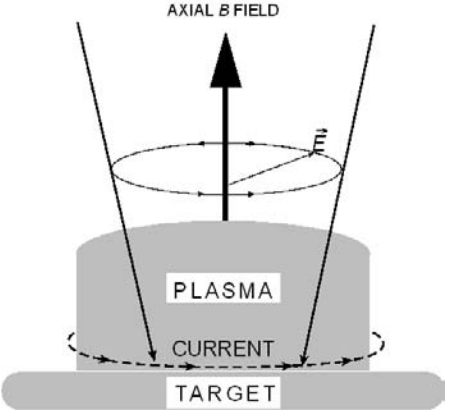

Figure 8.3. A schematic presentation of the inverse Faraday effect.

Substituting (8.67) into (8.66), one gets the solution for the electron (fluid) velocity:

$$\mathbf{v} = v_0\left(\frac{-\mathrm{i}\hat{\mathbf{x}} + \hat{\mathbf{y}}}{\sqrt{2}}\right)\exp[-\mathrm{i}(\omega t - kz)], \qquad v_0 = \frac{eE_0}{m_\mathrm{e}\omega}. \tag{8.68}$$

The electrons also satisfy the continuity equation

$$\frac{\partial n_\mathrm{e}}{\partial t} = -\nabla\cdot(n_\mathrm{e}\mathbf{v}). \tag{8.69}$$

The density is assumed to consist of a background (n_0) and perturbed (n_1) components

$$n_\mathrm{e} = n_0 + n_1, \qquad n_0 \gg n_1 \tag{8.70}$$

where n_0 does not depend on time and $n_1 \approx \exp(-\mathrm{i}\omega t)$. Since $\nabla\cdot\mathbf{v} = 0$, the continuity equation (8.69) yields

$$\mathrm{i}\omega n_1 = \mathbf{v}\cdot(\nabla n_0). \tag{8.71}$$

The electric current, which in this approximation is a second-order perturbed value, is obtained by using (8.68) and (8.71):

$$\mathbf{J} = -e\langle n_1\mathbf{v}\rangle = \left\langle \frac{\mathrm{i}e}{\omega}(\mathbf{v}\cdot\nabla n_0)\mathbf{v}\right\rangle = \frac{e^3E_0^2}{2m_\mathrm{e}\omega^3}\nabla n_0\times\hat{\mathbf{z}} \tag{8.72}$$

where $\langle\ \rangle$ is a time average over the fast oscillations and $\hat{\mathbf{z}}$ is the unit vector in the z direction. Note that the wave number vector $\mathbf{k}$ of the electromagnetic field is parallel to $\hat{\mathbf{z}}$. From equation (8.72) one can see that the electric current $\mathbf{J}$ has a contribution from the density gradient in the x–y plane (mainly from the edge of the plasma) and it points in the toroidal direction. This current produces an axial magnetic field (i.e. in the z direction) according to Maxwell's equation (we are using again Gaussian units):

$$\nabla\times\mathbf{B} = \frac{4\pi}{c}\mathbf{J}. \tag{8.73}$$

Substituting (8.72) into (8.73) yields the following order of magnitude estimate:

$$\mathbf{B} = B\hat{\mathbf{z}}, \qquad \frac{B}{B_\mathrm{c}} = \left(\frac{\omega_\mathrm{pe}^2}{2\omega^2}\right)\left(\frac{eE_0}{m_\mathrm{e}\omega c}\right)^2, \qquad B_\mathrm{c} \equiv \frac{m_\mathrm{e}\omega c}{e} = \frac{1.07\times10^8}{\lambda(\mu\mathrm{m})}\ \text{Gauss}. \tag{8.74}$$

Assuming that all of the laser energy is absorbed,

$$I_\mathrm{L} = c\,\frac{E_0^2}{8\pi} \tag{8.75}$$

where I_L is the laser peak intensity (power/area). In this case the axial magnetic field given in (8.74) can be written, in practical units, as

$$B_z\,(\text{Gauss}) = 6.0 \times 10^4 \left(\frac{n_e}{n_{ec}}\right)\left(\frac{\lambda_L}{\mu m}\right)\left(\frac{I_L}{10^{14}\,\text{W/cm}^2}\right) \tag{8.76}$$

where λ_L is the laser wavelength and n_{ec} is the critical density.

Using ponderomotive forces (Lehner 1994), it was suggested that the induced magnetic field is not linear with I_L, as given by the classical inverse Faraday effect (equations (8.74) or (8.76)), but B is proportional to the square root of I_L. Moreover, the constant of proportionality is significantly larger than in the classical approach. In this formalism the electric current is a first-order effect rather than a second-order perturbation value. In the non-relativistic domain the axial magnetic field, as developed by Lehner, can be written as

$$B = B_c\left(\frac{\omega_{pe}}{\omega}\right)\left(\frac{eE_0}{m_e\omega c}\right) \approx 6.5 \times 10^5 \left(\frac{n_e}{n_{ec}}\right)^{1/2}\left(\frac{I_L}{10^{14}\,\text{W/cm}^2}\right)^{1/2}. \tag{8.77}$$

This formula fits some experiments (Horovitz *et al.* 1998) in the domain of $I_L \approx 10^{10}$ W/cm^2 to 10^{13} W/cm^2. However, for $\sim 10^{14}$ W/cm^2 the experimental values are larger than those estimated by equation (8.77).

8.3.3 Angular momentum considerations

In a circularly-polarized laser beam the spins of the photons are aligned (each photon has a spin $\hbar = h/(2\pi)$, where h is the Planck constant), so that the laser beam has an angular momentum. Denoting the number density of the photons by n_γ, and the angular momentum density parallel to the z axis for a laser beam moving in the z direction by L_z (Eliezer *et al.* 1992, Haines 2001), one has

$$L_z = n_\gamma \hbar. \tag{8.78}$$

Every photon has an energy $h\nu$ ($\omega = 2\pi\nu$); therefore, the laser pulse energy density W in the plasma medium is

$$W = n_\gamma \hbar\omega = \frac{|E|^2}{8\pi} = \frac{I}{c} \tag{8.79}$$

where I is the intensity of the electromagnetic field in the plasma. From (8.78) and (8.79) one can write for photons moving in the z direction:

$$I = n_\gamma \hbar\omega c = L_z \omega c. \tag{8.80}$$

This relation is globally correct for a uniform distribution of photons, or equivalently it is locally correct at any domain in space. For an axisymmetric

beam of a circularly polarized laser defined by

$$I = \begin{cases} I(r), & r < r_0 \\ 0, & r \geq 0 \end{cases} \tag{8.81}$$

one can write (Haines 2001)

$$L_z = -\frac{r}{2\omega c}\left(\frac{\partial I}{\partial z}\right). \tag{8.82}$$

One can easily check the validity of this equation by integrating it from $r = 0$ to $r = r_0$, where r_0 is the edge of the laser beam:

$$\int_0^{r_0} \mathrm{d}r\, 2\pi r L_z = -\frac{2\pi}{\omega c}\left\{\left[\frac{r^2 I(r)}{2}\right]_{r=0}^{r=r_0} - \int_0^{r_0} I(r) r\, \mathrm{d}r\right\} = \frac{2\pi}{\omega c}\int_0^{r_0} I(r) r\, \mathrm{d}r. \tag{8.83}$$

This is derived by using the laser beam profile defined by (8.81) and integrating by parts. Equation (8.83) shows that equation (8.80) is locally correct, thus justifying the classical equation (8.82).

Using cylindrical coordinates (r, θ, z), the angular momentum conservation equation for the electrons can be written by

$$\frac{\mathrm{d}L_z\,(\text{electrons})}{\mathrm{d}t} + \frac{\mathrm{d}L_z\,(\text{photons})}{\mathrm{d}t} = \left(\mathbf{r} \times \sum \mathbf{F}\right)_z. \tag{8.84}$$

The angular momentum of the absorbed photons is transferred to the electrons. The rate of change of the electron angular momentum is

$$\frac{\mathrm{d}L_z\,(\text{electrons})}{\mathrm{d}t} = n_\mathrm{e} m_\mathrm{e} r \frac{\mathrm{d}v_\theta}{\mathrm{d}t} + \nu_\mathrm{ei} n_\mathrm{e} m_\mathrm{e} r v_\theta \tag{8.85}$$

where v_θ is the toroidal electron velocity, $m_\mathrm{e} v_\theta$ is the linear momentum of one electron in the θ direction and $r m_\mathrm{e} v_\theta$ is the angular momentum of one electron in the z direction. The second term in the right-hand side of the last equation is due to electron–ion collisions, where ν_ei is the collision frequency.

The rate of change in the photon angular momentum is obtained using equation (8.82). The electromagnetic intensity I is equal to the laser absorption coefficient f_a times the laser intensity I_L. One can also write

$$\frac{\mathrm{d}I}{\mathrm{d}t} \approx \frac{cI}{l} \tag{8.86}$$

where l is the axial distance that the laser is absorbed by the fraction f_a. Therefore, one can approximate the second term of the left-hand side of equation (8.84) by

$$\frac{\mathrm{d}L_z\,(\text{photons})}{\mathrm{d}t} = \frac{f_\mathrm{a} r}{2l\omega}\left(\frac{\partial I_\mathrm{L}}{\partial r}\right). \tag{8.87}$$

The torque $(\mathbf{r} \times \sum \mathbf{F})_z$ applied on the electrons is

$$\left(\mathbf{r} \times \sum \mathbf{F}\right)_z = -en_e r\left[E_\theta + \frac{1}{c}(v_z B_r - v_r B_z)\right] \tag{8.88}$$

where E_θ is the toroidal electric field induced by the toroidal electron motion in such a way as to oppose the generation of the axial magnetic field. The electron velocity, electric field and magnetic field components are accordingly: $\mathbf{v} = (v_r, v_\theta, v_z)$, $\mathbf{E} = (E_r, E_\theta, E_z)$, $\mathbf{B} = (B_r, B_\theta, B_z)$. Substituting equations (8.85), (8.87) and (8.88) into (8.84), one gets the angular momentum conservation in the z direction (Haines 2001):

$$n_e m_e r\left(\frac{\mathrm{d}v_\theta}{\mathrm{d}t}\right) = -en_e r E_\theta - \frac{f_a r}{2l\omega}\left(\frac{\partial I_L}{\partial r}\right) - \frac{en_e r}{c}(v_z B_r - v_r B_z) - n_e m_e r \nu_{ei} v_\theta. \tag{8.89}$$

Assuming a steady state, $\mathrm{d}v_\theta/\mathrm{d}t = 0$ and, neglecting the last two terms on the right-hand side of equation (8.89), the following simplified equation is obtained:

$$E_\theta \approx -\frac{f_a}{en_e \omega l}\left(\frac{\partial I_L}{\partial r}\right). \tag{8.90}$$

Using now the Faraday–Maxwell equation (in cylindrical coordinates),

$$\frac{\partial B_z}{\partial t} = -\frac{c}{r}\frac{\partial}{\partial r}(rE_\theta) \tag{8.91}$$

and assuming a parabolic laser profile beam,

$$I_L = I_0\left(1 - \frac{r^2}{r_0^2}\right) \quad \text{for } r \le r_0 \text{ and zero otherwise} \tag{8.92}$$

one gets from (8.90), (8.91) and (8.92) the following solution for the axial magnetic field:

$$B_z = \frac{4c}{\omega l e r_0^2}\int \frac{f_a I_0}{n_e}\,\mathrm{d}t. \tag{8.93}$$

It is worth noting that this equation does not have a singularity at $n_e = 0$ since $f_a = 0$ in this case.

As one can see from this calculation of the inverse Faraday effect, the axial magnetic field apparently looks in complete disagreement with the previously derived equation (8.76). In particular, in (8.76) the magnetic field is proportional to the electron density, while in (8.93) B is inversely proportional to n_e. However, one has to be careful because the absorption coefficient f_a may be proportional to n_e^2. In section 5.1 we derived the inverse

bremsstrahlung absorption coefficient:

$$\frac{f_a}{l} \approx \kappa_{ib} = \frac{\nu_{ei}(n_{ec})}{c}\left(\frac{n_e}{n_{ec}}\right)^2\left(1-\frac{n_e}{n_{ec}}\right)^{-1/2}. \tag{8.94}$$

In summary of this section, we have derived two apparently different equations ((8.76) and (8.93)) for the axial magnetic field induced by the inverse Faraday effect (see also (8.77)). So far there are not enough experiments of the inverse Faraday effect in order to check the different theories. Furthermore, it seems that the theory of this phenomenon and the relevant numerical simulations have not yet been performed comprehensively in order to clarify this subject.

8.4 Waves in the Presence of the Steady-State Magnetic Field

In the previous sections of this chapter we have seen that non-negligible steady-state magnetic fields are created in laser–plasma interaction. These magnetic fields can be present only in configurations that do not possess an exact spherical symmetry. **No magnetic field can exist in a spherical symmetry.** However, most of the experiments done so far in laser–plasma interaction have a planar or cylindrical geometry rather than a spherical one. Even for the large laser systems with a 'perfect' spherical laser irradiance of spherical shells (with the purpose of achieving inertial confinement fusion), local spherical symmetry breaking can be induced by hydrodynamic instabilities. Therefore, large local magnetic fields might be created even in these cases. It seems that steady-state magnetic fields are always associated with laser–plasma interactions. In this section we analyse the dispersion relation for some plasma waves in the presence of a d.c. magnetic field.

8.4.1 Ordinary and Extraordinary Waves

We analyse now the behaviour of an electromagnetic wave that propagates in uniform and magnetized plasma. A constant magnetic field $\mathbf{B}_0$ in the z direction is present in the plasma medium considered here. For simplicity, a cold plasma is considered, i.e. $T_e = 0$. Since the electromagnetic waves have a high frequency, one can ignore the ion motion. The electromagnetic wave is described by the Maxwell equations, where the electric current is calculated from the electron momentum equation. Denoting the electromagnetic fields by $\mathbf{E}$ and $\mathbf{B}$, the linearized equations to be solved are (Gaussian units are used here)

$$\begin{aligned} \nabla\times\mathbf{E} &= -\frac{1}{c}\frac{\partial\mathbf{B}}{\partial t}, \qquad \nabla\times\mathbf{B} = \frac{1}{c}\frac{\partial\mathbf{E}}{\partial t}+\frac{4\pi}{c}\mathbf{J} \\ \mathbf{J} &= -en_e\mathbf{v}, \qquad m_e n_e\frac{\partial\mathbf{v}}{\partial t} = -en_e\mathbf{E}-\frac{en_e}{c}\mathbf{v}\times\mathbf{B}_0 \end{aligned} \tag{8.95}$$

where $\mathbf{v}$ is the electron (fluid) velocity, and $-e$, m_e and n_e are the charge, the mass and the density of the electrons respectively. Equations (8.95) are 12 equations with 12 unknowns: $\mathbf{E}$, $\mathbf{B}$, $\mathbf{v}$ and $\mathbf{J}$; so one has the same number of unknowns as equations (caution should be exercised not to add, during the algebra manipulations, new equations for these unknowns).

We now analyse waves that propagate perpendicularly to $\mathbf{B}_0$. Since $\mathbf{B}_0$ is parallel to $\hat{\mathbf{z}}$ (the unit vector in the z direction), the wave vector $\mathbf{k}$ is chosen in the x direction in Cartesian coordinates. In this case one has two possibilities:

(a) $\mathbf{E}$ parallel to $\mathbf{B}_0$, which is called **ordinary wave**, and
(b) $\mathbf{B}$ parallel to $\mathbf{B}_0$, which is called **extraordinary wave**.

$$\begin{aligned} &\mathbf{B}_0 = (0,0,B_0), \qquad \mathbf{k} = (0,0,k) \\ \textbf{ordinary wave}: \quad &\mathbf{E} = (0,0,E), \qquad \mathbf{B} = (0,B,0) \\ \textbf{extraordinary wave}: \quad &\mathbf{E} = (E_x,E_y,0), \qquad \mathbf{B} = (0,0,B). \end{aligned} \tag{8.96}$$

For an ordinary wave (defined also as O-mode) the electric field, in the z direction, induces an electron velocity in the z direction; therefore, the $\mathbf{v} \times \mathbf{B}_0$ term in the last of equations (8.95) vanishes. Therefore, equations (8.95) are identical to those obtained in the unmagnetized plasma (see section 2.7), where the following dispersion relation was obtained:

$$\omega^2 = \omega_{pe}^2 + k^2 c^2 \tag{8.97}$$

where ω_{pe} is the electron plasma frequency. This dispersion relation describes an electromagnetic wave that propagates in the plasma as if there is not a d.c. magnetic field (B_0). This may be the reason that it acquired the name of **ordinary wave**.

For **extraordinary wave** (defined also as **X-mode**) the electric field is perpendicular to $\mathbf{B}_0$, and therefore the electric field induces an electron velocity in the x–y plane. As a result the force $\mathbf{v} \times \mathbf{B}_0$ introduces another velocity term in this plane. Since in this case there is no velocity component in the z direction, one can write $\mathbf{v} = (v_x, v_y, 0)$. Assuming a uniform plasma, the following substitution can be made in the linear equations (8.95):

$$\nabla \Rightarrow \mathrm{i}\mathbf{k}, \qquad \frac{\partial}{\partial t} \Rightarrow -\mathrm{i}\omega. \tag{8.98}$$

(c) Using the geometry defined by (8.96) and the Fourier transform as expressed (for the linear equations) in (8.98), one gets from (8.95) the following five algebraic equations with five unknowns (v_x, v_y, E_x, E_y, B):

$$\begin{aligned} -\mathrm{i}\omega m_e v_x &= -eE_x - \frac{eB_0}{c} v_y, \qquad -\mathrm{i}\omega m_e v_y = -eE_y + \frac{eB_0}{c} v_x, \\ \mathrm{i}kE_y &= \frac{\mathrm{i}\omega}{c} B, \qquad -\mathrm{i}kB = -\frac{4\pi e n_e}{c} v_y - \frac{\mathrm{i}\omega}{c} E_y, \\ 0 &= -\frac{4\pi e n_e}{c} v_x - \frac{\mathrm{i}\omega}{c} E_x. \end{aligned} \tag{8.99}$$

Using the definitions of the plasma frequency ω_{pe} and the cyclotron frequency ω_{ce},

$$\omega_{pe}^2 = \frac{4\pi e^2 n_e}{m_e}, \qquad \omega_{ce}^2 = \frac{eB_0}{m_e c} \tag{8.100}$$

we rewrite equations (8.99) in matrix form:

$$\begin{pmatrix} 1 & i\Omega & 0 & 0 & i \\ -i\Omega & 1 & 0 & i & 0 \\ 0 & 0 & 1 & -A & 0 \\ 0 & -iC & -A & 1 & 0 \\ -iC & 0 & 0 & 0 & 1 \end{pmatrix} \begin{pmatrix} (\omega m_e/e)v_x \\ (\omega m_e/e)v_y \\ B \\ E_y \\ E_x \end{pmatrix} = \begin{pmatrix} 0 \\ 0 \\ 0 \\ 0 \\ 0 \end{pmatrix} \tag{8.101}$$

$$\Omega \equiv (\omega_{ce}/\omega), \qquad A \equiv (kc/\omega), \qquad C \equiv (\omega_{pe}^2/\omega_{ce}^2).$$

Note that all the variables have the same dimensional form (Gaussian units), so that all the elements of the matrix are dimensionless. In order to get a non-zero solution for the variables, it is necessary that the determinant of the matrix in (8.101) is zero. The vanishing determinant gives the following **dispersion relation** for the **extraordinary** electromagnetic wave:

$$n^2 = \frac{k^2 c^2}{\omega^2} = 1 - \left(\frac{\omega_{pe}^2}{\omega^2}\right)\left(\frac{\omega^2 - \omega_{pe}^2}{\omega^2 - \omega_{uh}^2}\right) \tag{8.102}$$

where n is the index of refraction and ω_{uh} is called the **upper hybrid** frequency, given by

$$\omega_{uh}^2 = \omega_{pe}^2 + \omega_{ce}^2. \tag{8.103}$$

It is worth mentioning that the extraordinary wave is a **superposition** of a **transverse wave** (electromagnetic), $\mathbf{k} = (k_x, 0, 0)$, $\mathbf{E} = (0, E_y, 0)$, $\mathbf{B} = (0, 0, B)$, and a **longitudinal wave**, $\mathbf{k} = (k_x, 0, 0)$, $\mathbf{E} = (E_x, 0, 0)$. Solving for E_x and E_y, one gets that at a given point in space the vector $\mathbf{E}$ rotates as a function of time ($E_x \approx \exp[i(kx - \omega t)]$ and $E_y \approx \exp[i(kx - \omega t)]$), and since E_x and E_y are not equal one gets an elliptical rotation of the electric field.

Analysing the dispersion relation (8.102), one can see that the index of refraction can attain zero values, called **cutoff**, and infinite values, called **resonance**. Since the phase velocity of the wave is

$$v_\phi = \frac{c}{n} = \frac{\omega}{k} \tag{8.104}$$

one defines

$$\begin{aligned} &\textbf{cutoff}: \quad n = 0,\ k = 0 \ \Rightarrow\ v_\phi(k = 0) = \infty \\ &\textbf{resonance}: \quad n = \infty,\ k = \pm\infty \ \Rightarrow\ v_\phi(k = \pm\infty) = 0. \end{aligned} \tag{8.105}$$

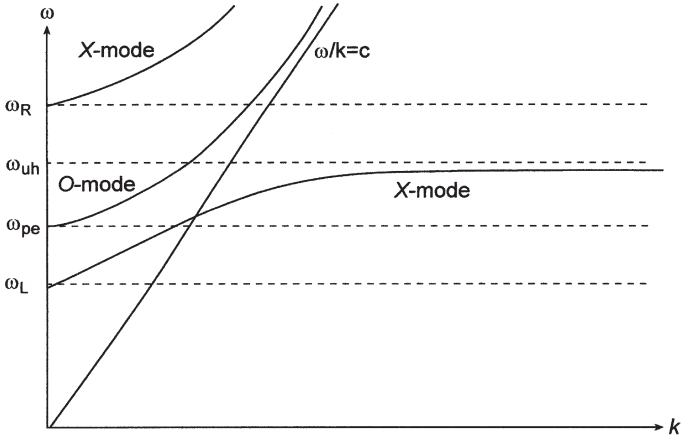

Figure 8.4. A schematic presentation of the dispersion relation $\omega = \omega(k)$ for extraordinary (X-mode) and ordinary (O-mode) waves.

From the dispersion relation, equation (8.102), the resonances for the X-mode (the extraordinary wave) are at

$$\textbf{X-mode resonances}: \quad \omega = 0, \quad \omega = \omega_{\mathrm{uh}} \tag{8.106}$$

and the cutoffs are the solution of the following quadratic equation:

$$\omega^4 - (\omega_{\mathrm{pe}}^2 + \omega_{\mathrm{uh}}^2)\omega^2 + \omega_{\mathrm{pe}}^4 = 0. \tag{8.107}$$

Denoting the two solutions of this quadratic equation by ω_{L} and ω_{R}, and using (8.103), one gets

$$\omega_{\pm} = \pm\frac{\omega_{\mathrm{ce}}}{2} + \sqrt{\omega_{\mathrm{pe}}^2 + \tfrac{1}{4}\omega_{\mathrm{ce}}^2}, \qquad \omega_{+} \equiv \omega_{\mathrm{R}}, \qquad \omega_{-} \equiv \omega_{\mathrm{L}}. \tag{8.108}$$

The notations R and L are used because these solutions describe right- and left-handed circular polarization. The right-hand rotation of the electric field is defined by the 'right-hand rule'. If the thumb is along k then the fingers of the right hand are in the direction of the rotation of the electric field for the R-wave. In the L-wave, E rotates in the opposite direction.

A schematic presentation of the dispersion relation $\omega = \omega(k)$ for extraordinary (X-mode) and ordinary (O-mode) waves, according to equations (8.102) and (8.97) respectively, is given in figure 8.4.

8.4.2 Electromagnetic waves propagating parallel to $\mathbf{B_0}$

In this case the following geometry is considered in Cartesian coordinates:

$$\begin{aligned} &\mathbf{B}_0 = (0, 0, B_0), \qquad \mathbf{k} = (0, 0, k), \qquad \mathbf{E} = (E_x, E_y, 0) \\ &\mathbf{B} = (B_x, B_y, 0), \qquad \mathbf{v} = (v_x, v_y, 0) \end{aligned} \tag{8.109}$$

Linearization and Fourier transform of equations (8.95) yields

$$\begin{aligned} \mathrm{i}\mathbf{k}\times\mathbf{E}-\frac{\mathrm{i}\omega}{c}B&=0\\ \mathrm{i}\mathbf{k}\times\mathbf{B}+\frac{\mathrm{i}\omega}{c}\mathbf{E}+\frac{4\pi e n_{\mathrm{e}}}{c}\mathbf{v}&=0\\ -\mathrm{i}\omega m_{\mathrm{e}}\mathbf{v}+e\mathbf{E}+\frac{e}{c}\mathbf{v}\times\mathbf{B}_0&=0. \end{aligned} \tag{8.110}$$

Writing this equation explicitly, for the configuration defined in (8.109), in matrix form we obtain

$$\begin{pmatrix} 1 & \mathrm{i}\Omega & 0 & 0 & \mathrm{i} & 0\\ \mathrm{i}\Omega & 1 & 0 & 0 & 0 & \mathrm{i}\\ 0 & 0 & 1 & 0 & 0 & A\\ 0 & 0 & 0 & 1 & -A & 0\\ -\mathrm{i}K & 0 & 0 & -A & 1 & 0\\ 0 & -\mathrm{i}K & A & 0 & 0 & 1 \end{pmatrix} \begin{pmatrix} (m_{\mathrm{e}}\omega/e)v_x\\ (m_{\mathrm{e}}\omega/e)v_y\\ B_x\\ B_y\\ E_x\\ E_y \end{pmatrix} = \begin{pmatrix} 0\\0\\0\\0\\0\\0 \end{pmatrix} \tag{8.111}$$

$$\Omega\equiv\frac{\omega_{\mathrm{ce}}}{\omega},\qquad A\equiv\frac{kc}{\omega},\qquad K\equiv\frac{\omega_{\mathrm{pe}}^2}{\omega^2}.$$

The dispersion relations are obtained by setting the determinant of this matrix equal to zero:

$$n_{\pm}^2=\frac{k^2c^2}{\omega_{\pm}^2}=1-\frac{\omega_{\mathrm{pe}}^2/\omega^2}{1\mp\omega_{\mathrm{ce}}/\omega} \tag{8.112}$$

where $+$ and $-$ denote right (R) and left (L) circular polarization, and n_+ and n_- are the indices of refraction for R and L waves propagating parallel to B_0 respectively. See equations (8.53) and (8.54).

From this dispersion relation we see that there is one resonance at $\omega=\omega_{\mathrm{ce}}$, and this is satisfied only for the R-wave. The cutoffs are derived by equating k to zero in (8.112), implying the same results as those of the X-mode in equation (8.108).

Figure 8.5 shows the schematic dispersion relation $\omega=\omega(k)$ of an electromagnetic wave propagating parallel to B_0 for two cases: (a) $\omega_{\mathrm{L}}<\omega_{\mathrm{pe}}<\omega_{\mathrm{ce}}$, (b) $\omega_{\mathrm{pe}}>\omega_{\mathrm{L}}>\omega_{\mathrm{ce}}$. As can be seen from these figures, there are two R-mode branches (as in the X-mode, figure 8.4) but only one L-mode, where $\omega>\omega_{\mathrm{L}}$ is satisfied. The low-frequency branch of the R-wave is also known as the electron–cyclotron wave.

The dispersion relation (8.112) shows that the index of refraction for the right-hand and left-hand polarization are not equal, as already derived in section 8.3 (equations (8.53) and (8.54)). Moreover, the index of refraction is complex (i.e. $n^2<0,\omega^2<0$) in the domain $\omega_{\mathrm{ce}}<\omega<\omega_{\mathrm{R}}$ for the R-wave

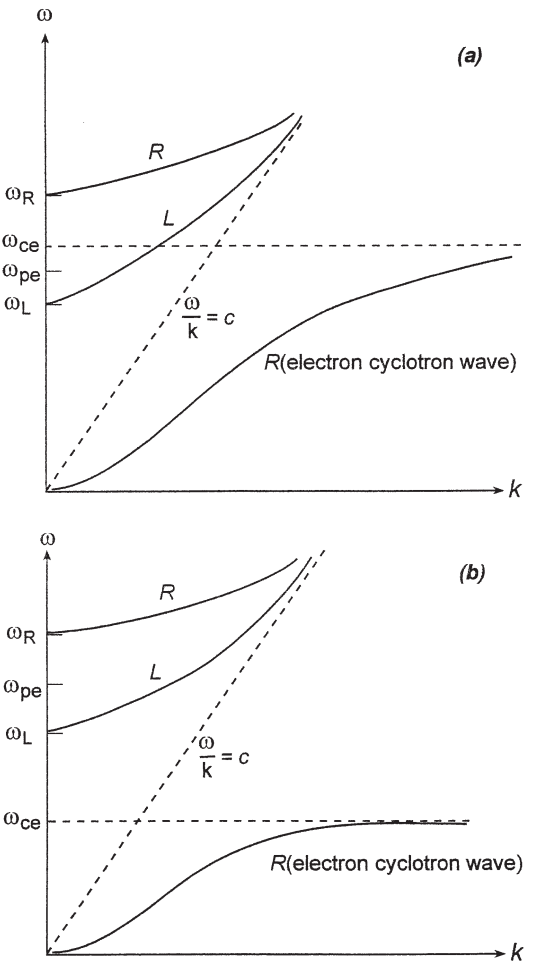

Figure 8.5. Schematic dispersion relation $\omega = \omega(k)$ for an electromagnetic wave propagating parallel to B_0: (a) $\omega_L < \omega_{pe} < \omega_{ce}$, (b) $\omega_{pe} > \omega_L > \omega_{ce}$.

and in the region $0 < \omega < \omega_L$ for the L-wave. Appropriate waves with these frequencies cannot propagate along B_0 in plasma.

The plasma and cyclotron frequencies can be expressed in practical units for typical laser-induced magnetic fields and densities:

$$\begin{aligned} \omega_{ce}\,[\mathrm{rad/s}] &= \frac{eB_0}{m_e c} = 1.76 \times 10^{13}\left(\frac{B_0}{\mathrm{MGauss}}\right) \\ \omega_{pe}\,[\mathrm{rad/s}] &= \left(\frac{4\pi e^2 n_e}{m_e}\right)^{1/2} = 5.64 \times 10^{14}\left(\frac{n_e}{10^{20}\,\mathrm{cm}^{-3}}\right)^{1/2}. \end{aligned} \tag{8.113}$$

Therefore, for figure 8.5(a) to be relevant for laser–plasma interactions, one requires

$$\omega_{ce} > \omega_{pe} \;\Rightarrow\; \left(\frac{B_0}{\text{MGauss}}\right) > 32.0\left(\frac{n_e}{10^{20}\,\text{cm}^{-3}}\right)^{1/2} \tag{8.114}$$

while for figure 8.5(b) it is necessary that the opposite inequality is satisfied, which in general is more realistic for laser–plasma interactions.

Last but not least, from figure 8.5 at high frequencies (for typical laser intensities and B_0, one usually has $\omega > \omega_{ce}$), one can see that the phase velocity ω/k is larger for an R-wave than for an L-wave. If a plane wave (i.e. linearly polarized) is propagating along B_0, then this wave can be described as a linear combination of an R-wave and an L-wave. These waves (R and L) propagate with different phase velocity; therefore, the plane of polarization of the wave rotates as it travels along B_0. This is the Faraday effect, as explained in section 8.3.

8.4.3 Alfvén waves

So far, in this section, the ion motion was ignored. Now we combine the ion motion with the electromagnetic equations (Maxwell equations). If an electromagnetic wave propagates along the d.c. magnetic field, i.e. the wave vector $\mathbf{k}$ is parallel to the magnetic field in the plasma B_0, one gets the famous Alfvén waves.

The following configuration is considered in Cartesian coordinates:

$$\begin{aligned} &\mathbf{k} = (0,0,k), \qquad \mathbf{B}_0 = (0,0,B_0), \qquad \mathbf{E} = (E,0,0) \\ &\mathbf{B} = (0,B,0), \qquad \mathbf{v}_e = (v_{ex}, v_{ey}, 0), \qquad \mathbf{v}_i = (v_{ix}, v_{iy}, 0) \end{aligned} \tag{8.115}$$

where $\mathbf{v}_e$ and $\mathbf{v}_i$ are the electron and ion velocities, and $\mathbf{E}$ and $\mathbf{B}$ are the electromagnetic fields propagating in the plasma. It is assumed that the plasma is neutral and cold (Z is the ion charge):

$$n_e = Zn_i = n_0, \qquad T_e = T_i = 0 \tag{8.116}$$

where n_e and n_i are the electron and ion densities, and T are appropriate temperatures. Moreover, it is assumed that the electron inertia can be neglected in the momentum equation. In this case the relevant linearized Fourier transform fluid equations, together with Maxwell's equations, are

$$\begin{aligned} 0 &= -e\mathbf{E} - (e/c)\mathbf{v}_e \times \mathbf{B}_0 \\ -\mathrm{i}\omega m_i v_i &= Ze\mathbf{E} + (Ze/c)\mathbf{v}_{ie} \times \mathbf{B}_0 \\ \mathrm{i}\mathbf{k} \times \mathbf{E} &= (\mathrm{i}\omega/c)\mathbf{B} \\ \mathrm{i}\mathbf{k} \times \mathbf{B} &= -(\mathrm{i}\omega/c)\mathbf{E} + (4\pi/c)n_0(\mathbf{v}_i - \mathbf{v}_e) \end{aligned} \tag{8.117}$$

where m_i is the ion mass. Using similar algebra as before, one gets from these equations the Alfvén dispersion relation

$$\omega^2 = \frac{k^2 v_A^2}{1 + (v_A^2/c^2)}$$
$$v_A = \left(\frac{B_0^2}{4\pi n_0 m_i}\right)^{1/2} \approx 2.18 \times 10^7 \left(\frac{m_p}{m_i}\right)\left(\frac{B_0}{\text{MGauss}}\right)\left(\frac{10^{20}\,\text{cm}^{-3}}{n_i}\right)^{1/2} \left[\frac{\text{cm}}{\text{s}}\right] \tag{8.118}$$

where v_A is the Alfvén wave velocity and m_p is the proton mass. In deriving this dispersion relation one must also assume that $\omega < \omega_{ci}$, where the ion cyclotron frequency is given by

$$\omega_{ci} = \frac{ZeB_0}{m_i c} \approx 9.58 \times 10^9 \left(\frac{Zm_p}{m_i}\right)\left(\frac{B_0}{\text{MGauss}}\right). \tag{8.119}$$

The condition $\omega < \omega_{ci}$ is nonrealistic for typical laser–plasma interactions. Moreover, using equation (8.118), one gets a time scale ($\sim 2\pi/\omega$) larger by many orders of magnitude than any high-power laser pulse duration. Therefore, it seems that the Alfvén waves do not play any important role in laser–plasma interactions.

8.5 Resonance Absorption in a Magnetized Plasma

Resonance absorption was considered in section 5.6. In this section we analyse how the absorption is modified due to the presence of a steady-state (d.c.) magnetic field. As in the previous section, we consider the electron momentum equation together with Maxwell equations for cold plasma. In this case one is interested in the effects of the density gradient, where the electric and magnetic fields in the plasma can be written for a monochromatic wave:

$$\mathbf{E}(\mathbf{r}, t) = \mathbf{E}(\mathbf{r}) \exp(-i\omega t), \qquad \mathbf{B}(\mathbf{r}, t) = \mathbf{B}(\mathbf{r}) \exp(-i\omega t). \tag{8.120}$$

Therefore, one cannot use the relation $\nabla \to i\mathbf{k}$ when taking the Fourier transform of the linear equations. However, the substitution $\partial/\partial t \to -i\omega$ is permitted for the class of solutions given by (8.120). The linearized equations to be solved are

$$\begin{aligned} \nabla \times \mathbf{E}(\mathbf{r}) &= \frac{i\omega}{c}\mathbf{B}(\mathbf{r}) \\ \nabla \times \mathbf{B}(\mathbf{r}) &= -\frac{i\omega}{c}\mathbf{E}(\mathbf{r}) - \frac{4\pi e n_e}{c}\mathbf{v} \\ -i\omega\mathbf{v} &= -\frac{e}{m_e}\left(\mathbf{E}(\mathbf{r}) + \frac{1}{c}\mathbf{v} \times \mathbf{B}_0(\mathbf{r})\right) \end{aligned} \tag{8.121}$$

where $\mathbf{v}$ is the average velocity of the electrons, and the d.c. magnetic field is taken parallel to the z axis but is not necessarily a constant in space. The third of these equations can be written in matrix form as

$$\begin{pmatrix} v_x \\ v_y \\ v_z \end{pmatrix} = \begin{pmatrix} -\mathrm{i}\omega\Delta & \omega_{\mathrm{ce}}\Delta & 0 \\ \omega_{\mathrm{ce}}\Delta & -\mathrm{i}\omega\Delta & 0 \\ 0 & 0 & -\mathrm{i}/\omega \end{pmatrix} \begin{pmatrix} (e/m_{\mathrm{e}})E_x \\ (e/m_{\mathrm{e}})E_y \\ (e/m_{\mathrm{e}})E_z \end{pmatrix} \qquad (8.122)$$

$$\Delta \equiv \frac{1}{\omega^2 - \omega_{\mathrm{ce}}^2}$$

where the electron cyclotron frequency is defined in (8.100). Substituting $\mathbf{v}$ from (8.122) into the second equation of (8.121), one gets

$$\nabla \times \mathbf{B}(\mathbf{r}) = -\frac{\mathrm{i}\omega}{c}\,\boldsymbol{\varepsilon} \cdot \mathbf{E}(\mathbf{r}) \qquad (8.123)$$

where this equation defines the **dielectric tensor** $\boldsymbol{\varepsilon}$, given by

$$\boldsymbol{\varepsilon} = \begin{pmatrix} \dfrac{\omega^2 - \omega_{\mathrm{uh}}^2}{\omega^2 - \omega_{\mathrm{ce}}^2} & \dfrac{\mathrm{i}\omega_{\mathrm{pe}}^2}{(\omega^2 - \omega_{\mathrm{ce}}^2)} & 0 \\ \dfrac{-\mathrm{i}\omega_{\mathrm{pe}}^2\omega_{\mathrm{ce}}}{\omega(\omega^2 - \omega_{\mathrm{ce}}^2)} & \dfrac{\omega^2 - \omega_{\mathrm{uh}}^2}{\omega^2 - \omega_{\mathrm{ce}}^2} & 0 \\ 0 & 0 & 1 - \dfrac{\omega_{\mathrm{pe}}^2}{\omega^2} \end{pmatrix} \qquad (8.124)$$

where the plasma frequency is given in (8.100) and the upper hybrid frequency ω_{uh} is defined in (8.103). Note that the elements of the dielectric tensor are dimensionless.

In order to get the electromagnetic field, one has to solve equation (8.123) and the first equation of (8.121). The equation for the electric field $\mathbf{E}$ is derived by taking $\nabla\times$[first equation of (8.121)] and using (8.123), yielding

$$\nabla^2\mathbf{E}(\mathbf{r}) + \frac{\omega^2}{c^2}\,\boldsymbol{\varepsilon} \cdot \mathbf{E}(\mathbf{r}) = 0 \qquad (8.125)$$

where the tensor $\boldsymbol{\varepsilon}$ is given in (8.124). In deriving this equation it was assumed that $\nabla \cdot \mathbf{E} = 0$, i.e. the plasma is neutral.

For the equation of the magnetic field $\mathbf{B}(\mathbf{r})$ it is convenient to use the inverse matrix $\boldsymbol{\varepsilon}^{-1}$ of the dielectric tensor $\boldsymbol{\varepsilon}$. The inverse matrix is defined by

$$\boldsymbol{\varepsilon}^{-1} \cdot \boldsymbol{\varepsilon} = \boldsymbol{\varepsilon} \cdot \boldsymbol{\varepsilon}^{-1} = \mathbf{1} \qquad (8.126)$$

where $\mathbf{1}$ is the unit matrix

$$\mathbf{1} = \begin{pmatrix} 1 & 0 & 0 \\ 0 & 1 & 0 \\ 0 & 0 & 1 \end{pmatrix}. \qquad (8.127)$$

Using the tensor $\boldsymbol{\varepsilon}^{-1}$, equation (8.123) can be rewritten by

$$\boldsymbol{\varepsilon}^{-1} \cdot \nabla \times \mathbf{B} = -\frac{\mathrm{i}\omega}{c}\,\mathbf{E}. \tag{8.128}$$

Using equations (8.124) and (8.126), one gets the inverse tensor of $\boldsymbol{\varepsilon}$ (David and Pellat 1980):

$$\begin{aligned}
\boldsymbol{\varepsilon}^{-1} &= \begin{pmatrix} \varepsilon_{\mathrm{e}}^{-1} & -\mathrm{i}\beta & 0 \\ \mathrm{i}\beta & \varepsilon_{\mathrm{e}}^{-1} & 0 \\ 0 & 0 & \varepsilon_0^{-1} \end{pmatrix} \\
\varepsilon_{\mathrm{e}} &= \left[\left(1 - \frac{\omega_{\mathrm{pe}}^2}{\omega^2}\right)^2 - \frac{\omega_{\mathrm{ce}}^2}{\omega^2}\right]\left(1 - \frac{\omega_{\mathrm{uh}}^2}{\omega^2}\right)^{-1} \\
\varepsilon_0 &= \left(1 - \frac{\omega_{\mathrm{pe}}^2}{\omega^2}\right)^2 \\
\beta &= \frac{\omega_{\mathrm{pe}}^2 \omega_{\mathrm{ce}}}{\omega^3}\left[\left(1 - \frac{\omega_{\mathrm{pe}}^2}{\omega^2}\right)^2 - \frac{\omega_{\mathrm{ce}}^2}{\omega^2}\right]^{-1}.
\end{aligned} \tag{8.129}$$

One can define ε_0 and ε_{e} as the square of the ordinary and extraordinary index of refraction respectively (see previous section).

The wave equation for the magnetic field $\mathbf{B}$ is derived by taking $\nabla \times$ (8.128) and using the first equation of (8.121), together with the Maxwell equation $\nabla \cdot \mathbf{B} = 0$, implying

$$\nabla \times (\boldsymbol{\varepsilon}^{-1} \cdot \nabla \times \mathbf{B}) - \frac{\omega^2}{c^2}\,\mathbf{B} = 0. \tag{8.130}$$

For the extraordinary mode the electric field $\mathbf{E}$ is perpendicular to the d.c. magnetic field $\mathbf{B}_0$. Choosing $\mathbf{B}_0$ to be in the z direction, the plane of the laser incidence is x–y, then the following configuration is defined (a p-polarization):

$$\begin{aligned}
\mathbf{B}_0 &= (0, 0, B_0), \qquad & \mathbf{k} &= (k\cos\theta, k\sin\theta, 0) \\
\mathbf{E} &= (E_x, E_y, 0), \qquad & \mathbf{B} &= (0, 0, B_z).
\end{aligned} \tag{8.131}$$

In this configuration the equation for B_z (the extraordinary mode) is derived from equation (8.130):

$$\nabla^2 B_z + \left(-\frac{\nabla\varepsilon_{\mathrm{e}}}{\varepsilon_{\mathrm{e}}} + i\varepsilon_{\mathrm{e}}\boldsymbol{\gamma}\right) \cdot \nabla B_z + k^2 \varepsilon_{\mathrm{e}} B_z = 0, \qquad \boldsymbol{\gamma} \equiv \hat{\mathbf{x}}\,\frac{\partial\beta}{\partial y} - \hat{\mathbf{y}}\,\frac{\partial\beta}{\partial x}. \tag{8.132}$$

For an ordinary wave the electric field $\mathbf{E}$ is parallel to the d.c. magnetic field $\mathbf{B}_0$ (chosen in the z direction) and equation (8.125) in this case is

$$\nabla^2 E_z + k^2 \varepsilon_0 E_z = 0. \tag{8.133}$$

The ordinary wave, i.e. the s-polarization wave in our case, is not modified by an external magnetic field $B_0\hat{\mathbf{z}}$, and this wave does not drive the resonance absorption mechanism.

The p-polarization wave described above describes an extraordinary wave and can drive the resonance absorption mechanism (see section 5.5). It is convenient to describe this case by the equation of the magnetic field (equation (8.132)). From this equation one gets a resonance for B_z, due to $\varepsilon_e = 0$, at

$$\textbf{resonance}: \quad \omega^2 = \omega_{uh}^2. \tag{8.134}$$

This resonance is responsible for the excitation of an electrostatic wave that is the origin of the resonant absorption phenomenon. Two other singularities of equation (8.132), where ε_e is zero and β becomes infinite, are derived from solving

$$1 - \frac{\omega_{pe}^2}{\omega^2} = \pm\frac{\omega_{ce}}{\omega}. \tag{8.135}$$

However, B_z is regular at these points and these two singularities describe the turning points of the WKB solution (see section 5.4).

It is assumed that the laser is incident at $x = -L$, in the x–y plane with a positive x component (the domain $x < -L$ is vacuum and $x > -L$ is plasma), and that the incident p-polarized wave is obliquely incident at an angle θ_0 with the density gradient. For a constant (in space and time) external magnetic field and a linear density profile, described by

$$\frac{n_e}{n_{ec}} = \begin{cases} 0 & \text{for } x < -L \\ 1 + (x/L) & \text{for } x > -L \end{cases} \Rightarrow \varepsilon_0 = \begin{cases} 1 & \text{for } x < -L \\ -(x/L) & \text{for } x > -L \end{cases} \tag{8.136}$$

equation (8.132) takes the form (David and Pellat 1980)

$$\frac{d^2B}{d\xi^2} + \left(\frac{1}{\xi} - \frac{1}{\xi - \sigma} - \frac{1}{\xi + \sigma}\right)\frac{dB}{d\xi} + \left(\frac{\sigma^2}{\xi} - \xi - \tau^2 + \frac{\tau}{\xi - \sigma} - \frac{\tau}{\xi + \sigma}\right)B = 0. \tag{8.137}$$

The following change of variables is used in equation (8.132) in order to get equation (8.137):

$$\begin{aligned} B_z &= B(x)\exp(\mathrm{i}ky\sin\theta_0) \\ \xi &= x\left(\frac{k^2}{L}\right)^{1/3} \\ \tau &= (kL)^{1/3}\sin\theta_0 \\ \sigma &= (kL)^{2/3}\left(\frac{\omega_{ce}}{\omega}\right). \end{aligned} \tag{8.138}$$

Moreover, equation (8.137) is derived only for $\omega_{ce}/\omega \ll 1$ (i.e. we neglect $(\omega_{ce}/\omega)^2$ and higher-order terms), an assumption satisfied in most laser–plasma experiments.

As we have seen in chapter 5, without a dissipation mechanism such as electron ion–collisions or Landau damping, all of the laser light is reflected (or transferred, if the plasma density is smaller than the critical density everywhere) out of the plasma (i.e. no absorption). In order to obtain a laser absorption one requires an effective collision frequency ν_{eff}. If the mechanism of the damping of electrostatic waves is known then it is possible to include ν implicitly in the dielectric constant, e.g. changing equation (8.136) to

$$\varepsilon_0 = \begin{cases} 1 & \text{for } x < -l \\ -(x/L) + \mathrm{i}(\nu_{\text{eff}}/\omega) & \text{for } x > -L. \end{cases} \tag{8.139}$$

However, it turns out that in most cases the collision frequency determines the magnetic (or electric) field strength at resonance and its spatial structure there, but does not modify the qualitative values of the absorption coefficient. The amplitude ratio square between the outgoing and incoming wave (at $x = -L$ in our above example) gives the reflection coefficient R ($1 - R$ is the absorption coefficient). This value does not depend on ν_{eff} as long as it is not zero. In this case equation (8.137) is solved numerically by integrating

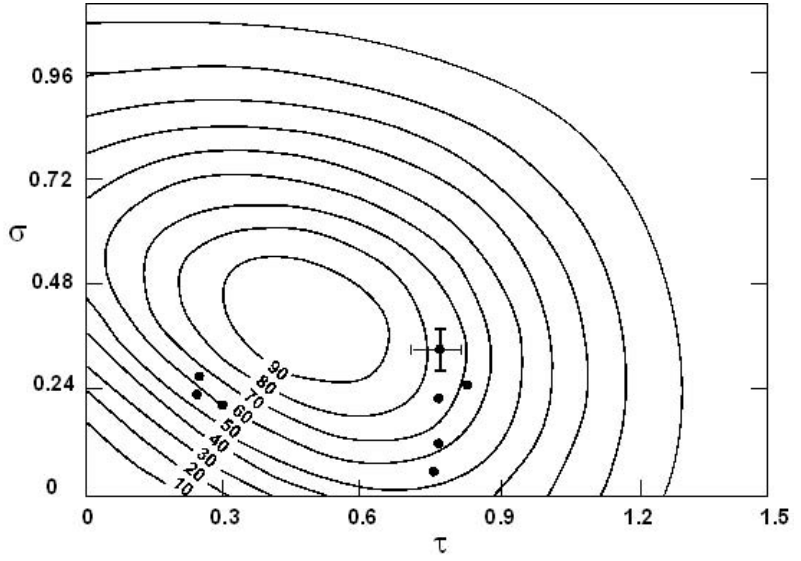

Figure 8.6. Absorption of p-polarized laser at oblique incidence in magnetized plasma. τ and σ are defined in equation (8.138). The dots are experimental points (Horovitz *et al.* 1998) of τ and σ. The measured absorption at these points fits within 10% of the theoretical values given in this figure.

it along a path in the complex plane (of ξ), where the singularities are avoided by taking a 'detour' from the x axis (i.e. the real ξ axis). The solution for the laser absorption, as given in figure 8.6 (Woo *et al*. 1978, David and Pellat 1980), shows that a p-polarized laser at oblique incidence in magnetized plasma can be almost 100% absorbed.

It turns out that the laser absorption depends only on two parameters, τ and σ, defined in equation (8.138). τ is related to the density gradient (scaling as L) and to the incidence angle θ_0, while σ is related both to the density gradient and the magnetic field. It is interesting to point out that even at normal incidence ($\theta_0 = 0$), the absorption can be as high as 50% for $\sigma \approx 0.5$. Using practical units for laser–plasma interactions, one can write

$$\sigma \approx 0.148 \left[\left(\frac{\lambda_L}{1\,\mu\text{m}} \right) \left(\frac{L}{10\,\mu\text{m}} \right)^2 \right]^{1/3} \left(\frac{B_0}{\text{MGauss}} \right) \tag{8.140}$$

so that $\sigma \approx 0.5$ for a magnetic field $\sim 3\,\text{MG}$ and a density scale length $\sim 10\,\mu\text{m}$, values measured experimentally in many plasmas created by lasers.

Chapter 9

Thermal Conduction and Heat Waves

9.1 The Scenario

Thermal conduction or, in more general terms, the energy transport in laser-produced plasma, is related to basic plasma physics in a wide range of parameters, such as density and temperature. This subject is of great interest because it plays a very important role in major applications, such as inertial confinement fusion (ICF), the production of x-ray sources and x-ray lasers. For example, the acceleration of shell targets for ICF relies not only on the energy absorbed by the plasma, but also on the efficient coupling between this energy and the solid shell. In section 9.2 we calculate this efficiency in a simple model.

A high intensity laser radiation ($>10^{11}\,\mathrm{W/cm^2}$), with pulse duration τ_L larger than 100 ps, is incident on a solid target. Plasma is created instantaneously (on a time scale shorter than τ_L by many orders of magnitude); it is heated to a high temperature and this plasma expands into the vacuum to create a low-density corona. Once the plasma corona is created, the laser radiation no longer reaches the solid since it cannot penetrate beyond the critical surface, with an electron density $n_{ec} = 10^{21}(\lambda_L/\mu\mathrm{m})^{-2}\,\mathrm{cm^{-3}}$, where λ_L is the laser wavelength. At the critical surface, part of the laser beam is absorbed and the other part is reflected into the corona. We have seen in chapter 5 that most of the absorption is done in the domain near the critical surface. Moreover, as has been shown in chapter 6, waves are created in the plasma-corona.

Figure 9.1 describes schematically the temperature and the electron density in laser-produced plasma. The temperature has a maximum in the region of the critical surface, where most of the laser energy is absorbed. The temperature decreases sharply towards the cold solid, and to a good approximation it is constant throughout the corona. The density is decreasing towards the vacuum and, for laser radiation intensities larger than about $10^{15}\,\mathrm{W/cm^2}$, there is a steep density gradient at the critical

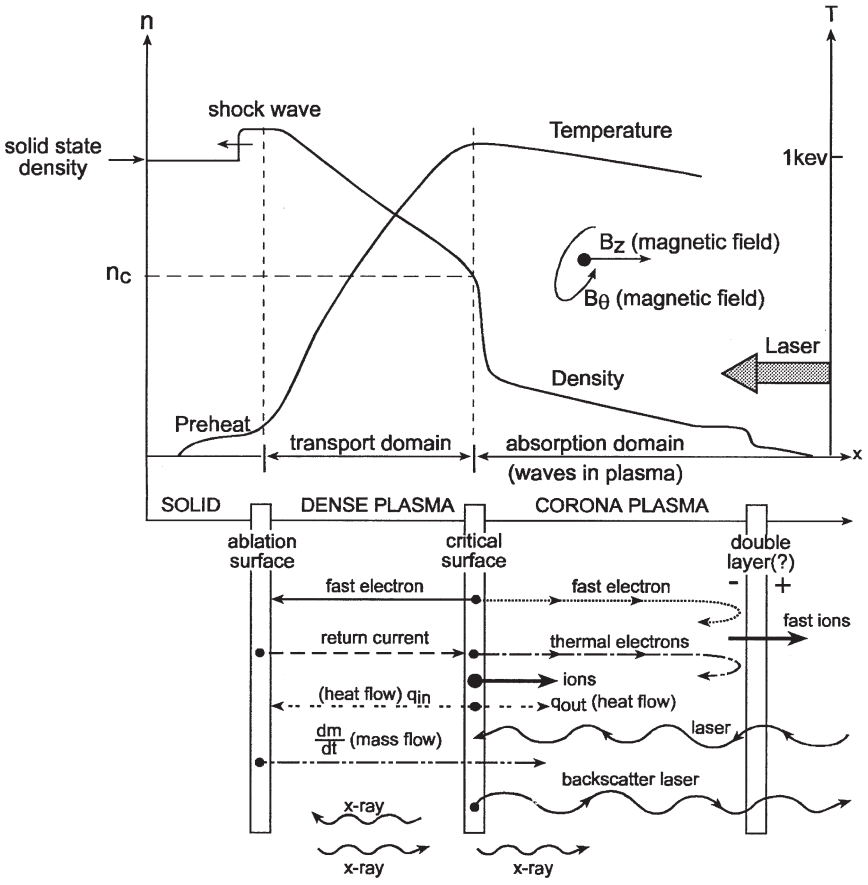

Figure 9.1. Schematic diagram of the temperature and density profile in a laser-induced plasma. A scenario is given for plasma particle streams, currents, heat flow, laser and laser-induced x-ray propagation, a possible double layer formation and the creation of axial and toroidal magnetic fields.

surface. The density and pressure rise towards the solid surface and the pressure (ablation pressure) reaches a maximum at the ablation surface, where plasma is created and the flow velocity is zero.

The energy absorbed at the critical surface domain is transported beyond the critical surface towards the solid target, either by (x-ray) radiation or by electron thermal conduction (figure 9.1). Most of the electrons in the plasma have a Maxwellian velocity distribution, with a temperature usually denoted by T_c (c stands for 'cold', which can be of the order of $k_B T_c \approx 1\,\mathrm{keV}$). For high laser intensities I_L, satisfying

$I_L\lambda_L^2 > 10^{14}\,(\mathrm{W/cm^2})\,\mu\mathrm{m}^2$, the electron velocity distribution may be described by two (or more) Maxwellian distributions with a second temperature T_h, much larger than T_c. In this case the fast electrons with a temperature T_h, which are created in the critical surface domain, transport part of their energy into the solid, causing preheating of the target. This is easily understood since the electron mean free path λ_e (for 90° deflection in multiple Coulomb collisions with ions, see section 9.3) is proportional to the square electron temperature,

$$\lambda_e(\mathrm{cm}) = 5.71 \times 10^4 \frac{T_e^2}{Zn_e \ln \Lambda} \tag{9.1}$$

where T_e, in degrees Kelvin, stands for the electron (cold or hot) temperature, Z is the charge of the ion, n_e is the electron density and $\ln \Lambda$ is the Coulomb logarithmic factor. For example, for $T_e = 10^7\,\mathrm{K} \approx 1\,\mathrm{keV}$, $Z = 10$, $\ln \Lambda = 10$ and $n_e = 10^{20}\,\mathrm{cm}^{-3}$, one gets $\lambda_e \approx 5.7\,\mu\mathrm{m}$. When $T_h/T_c \approx 10$, the energy of the hot electrons is deposited 100 times deeper into the target than the energy deposited by the cold electrons. Furthermore, if the cold electron mean free path is smaller than the temperature density gradient, then the thermal conduction is diffusive (see section 9.4) and the heat flux $\mathbf{q}$ (erg/(s·cm^2)) is given by (see section 2.3)

$$\mathbf{q} = -\tfrac{1}{3}\lambda_e v_e n_e k_B \nabla T_e = \kappa \nabla T_e \tag{9.2}$$

where v_e is the electron velocity and k_B is Boltzmann's constant. Substituting (9.1) into (9.2), one gets the classical result of Spitzer and Härm, denoted by SH theory (see section 9.5) for the conductivity κ:

$$\kappa(\mathrm{erg \cdot s^{-1} \cdot cm^{-1} \cdot K^{-1}}) = 1.77 \times 10^{-6} \frac{T_e^{5/2}}{Z \ln \Lambda}. \tag{9.3}$$

The heat flow is possible due to the distortion of the Maxwellian velocity distribution. For example, in one dimension the Gaussian form of the electron velocity distribution is changed in such a way that more electrons have a suitable velocity and energy to carry heat to the cold region. This effect creates an electric field $\mathbf{E}$. In order to keep charge neutrality, an electric current $\sigma_E\mathbf{E}$ (σ_E is the electrical conductivity coefficient), called 'return current', is created from the cold target towards the critical surface (see figure 9.1). The electrons in the return current have low energy. The thermal flux of electrons, from the critical surface towards the ablation surface, has a higher energy than the electrons in the return current, so the target is heated.

The temperature gradient between the critical surface and the ablation surface induces a thermoelectric effect. This phenomenon reduces the classical

heat flow according to the relation

$$\mathbf{J} = \sigma_E \mathbf{E} - \alpha \nabla T, \qquad \mathbf{q} = \beta \mathbf{E} - \kappa \nabla T \tag{9.4}$$

where $\mathbf{J}$ is the total electrical current, and the coefficients α, β, σ_E and κ are not independent (Onsager relations in irreversible thermodynamics). Assuming only a net heat flow transport, $\mathbf{J} = 0$, one gets from (9.4):

$$\mathbf{q} = -\kappa \left(1 - \frac{\alpha\beta}{\sigma_E \kappa}\right) \nabla T_e \tag{9.5}$$

where a reduction factor due to the thermoelectric effect shows up, which may reduce the heat transport by a factor of about 2.

Furthermore, the heat transport of the cold electrons for very steep temperature gradients does not satisfy the diffusion approach. The SH theory is valid only if the electron velocity distribution function f is slightly perturbed from its equilibrium distribution (f_0 is the Maxwell distribution), namely $f = f_0 + f_1$ where $f_0 \gg f_1$. The validity of the diffusion approximation (SH model) depends strongly on the ratio λ_e / L_T, where λ_e is the electron mean free path (see (9.1)) and L_T is the temperature density scale length:

$$L_T = \frac{T}{(\mathrm{d}T/\mathrm{d}x)}. \tag{9.6}$$

The diffusion approximation is valid for $\lambda_e \ll L_T$. It has been shown (Gray and Kilkenny 1980) that the diffusion approximation is valid only for $\lambda_e / L_T < 10^{-2}$. For $\lambda_e / L_T > 10^{-2}$ the energy transport is significantly reduced, and it is necessary to introduce an inhibition factor f in order to get agreement with experiments. The inhibition factor f is defined as the ratio between the actual heating flux q and the free streaming flux q_f, the maximum possible flux, defined by

$$q_f = n_e k_B T_e \left(\frac{k_B T_e}{m_e}\right)^{1/2}. \tag{9.7}$$

The free streaming is the heat flow carried by the electrons if they stream freely at their thermal velocity along the temperature gradient. For high laser irradiance, $I_L > 10^{15}\,\mathrm{W/cm^2}$, where $\lambda_e / L_T \approx 1$, the agreement with experiments are obtained when using an electron thermal flux

$$\mathbf{q} = f \mathbf{q}_f \approx 0.03 \mathbf{q}_f \tag{9.8}$$

instead of the diffusion flux given by (9.2) (see, for example, Rosen 1984).

As we have seen in chapter 8, magnetic fields of the order of few megagauss are easily created in the corona of laser-produced plasma (see

figure 9.1). Magnetic fields significantly affect the electron transport if

$$\omega_{ce}\tau_e > 1, \qquad \omega_{ce} = \frac{eB}{m_e c} \tag{9.9}$$

where τ_e is the angular scattering time of the electron and ω_{ce} is the Larmor angular frequency. Assuming that the main contribution to τ_e is from electron–ion collisions, then (see section 2.2)

$$\tau_e[\mathrm{s}] \approx \tau_{ei} = 3.44 \times 10^{-16}\left[\left(\frac{10}{Z}\right)\left(\frac{10^{22}\,\mathrm{cm}^{-3}}{n_e}\right)\left(\frac{10}{\ln\Lambda}\right)\left(\frac{T_e}{100\,\mathrm{eV}}\right)^{3/2}\right] \tag{9.10}$$

and using

$$\omega_{ce}[\mathrm{s}^{-1}] = 1.76 \times 10^{13}\left(\frac{B}{\mathrm{MGauss}}\right) \tag{9.11}$$

one gets in practical units

$$\omega_{ce}\tau_e = 6.05 \times 10^{-3}\left(\frac{10}{Z}\right)\left(\frac{10^{22}\,\mathrm{cm}^{-3}}{n_e}\right)\left(\frac{10}{\ln\Lambda}\right)\left(\frac{T_e}{100\,\mathrm{eV}}\right)^{3/2}\left(\frac{B}{\mathrm{MGauss}}\right). \tag{9.12}$$

The megagauss magnetic fields were measured in the corona, where the electron density is much smaller than $10^{22}\,\mathrm{cm}^{-3}$ and the temperature can be much larger than 100 eV. In this case $\omega_{ce}\tau_e$ can be larger than one, and therefore in the corona the electron transport in a magnetized plasma might be relevant. However, in the more important domain of the energy transport, between the critical surface and the ablation surface, $\omega_{ce}\tau_e$ is in general smaller than one even if the large magnetic field penetrates from the corona into the solid. Thus the electron transport between the critical surface and the ablation surface seems not to be affected significantly by the magnetic field. We shall not further discuss in this chapter the transport in magnetized plasma.

Electron transport also plays an important role in spreading the absorbed laser energy uniformly around the solid target. It is well known that a high-laser-intensity beam does not have a uniform spatial distribution, and even for the same laser system the spatial intensity distribution changes from shot to shot. Therefore, a major difficulty in high-intensity laser–plasma experiments is the non-uniformity of the laser beams. This can cause irreproducible and uncontrollable experiments, and therefore is difficult to analyse and use in various applications (such as ICF). However, after a corona with a dimension much larger than the laser wavelength has been formed, the energy transport in the lateral direction (in the plasma) can redistribute the energy uniformly around the solid surface. Electron

conduction reduces the temperature within 'hot spots' and thus decreases the possible creation of hot and narrow filaments in the plasma.

Regarding the scenario in the corona, it is interesting to point out the possible existence of a double layer (DL) (see figure 9.1). The creation of hot electrons, also known as suprathermal electrons (see section 9.6), with a temperature higher by a factor of 10 or more than the cold temperature (the thermal electrons) may be associated with the formation of this DL in the expanding corona. The fastest particles, electrons and ions, in the low-density region lead the expansion of the plasma. The electric field in the expanding DL accelerates the ions and causes the fast electrons to turn back into the target. Such DLs were observed experimentally (Eliezer and Ludmirsky 1983) and suggested theoretically by the prediction of 'rarefaction shock waves' for $T_h/T_c > 9.9$ (Bezzerides *et al.* 1978, Wickens *et al.* 1978, Diebold *et al.* 1987). A rarefaction shock occurs (Zeldovich and Raizer 1966) when the following unusual condition is satisfied: $d^2P/dV^2 < 0$, $V = 1/\rho$, $\rho = m_i n_i$ in a plasma and P is the pressure. In this case P is composed of two components: $P = n_c k_B T_h + n_h k_B T_h$, where n_h and n_c are the electron densities of the hot and cold plasmas respectively.

Electron transport in plasmas has been a major issue since the beginning of modern plasma physics (Spitzer and Härm 1953, Rosenbluth *et al.* 1957, Spitzer 1962, Braginskii 1965, Trubnikov 1965, Hinton and Hezeltine 1976, Stacey 1980, Nicholson 1983, Horton 1989, Hazeltine and Meiss 1992). The electron transport phenomena in laser-produced plasma have been extensively discussed in the literature (Haines 1980, 1989, Key 1980, 1983, 1991, Bobin 1985, Shvarts 1986, Galeev and Natanzon 1991, Yamanaka 1991, Bell 1995). In this chapter we discuss electron transport phenomena relevant to laser-produced plasma.

9.2 The Rocket Model

We now consider a planar steady-state ablation from a target, as shown schematically in figure 9.1. In this section it is assumed that the fluxes of mass, momentum and energy are constant and the equation of state of an ideal gas is used:

$$\begin{aligned} \text{flux of mass} &= \rho u \\ \text{flux of momentum} &= P + \rho u^2 \\ \text{flux of energy} &= \frac{\gamma}{\gamma - 1} Pu + \frac{1}{2}\rho u^3 + q + I \end{aligned} \tag{9.13}$$

where u is the plasma flow velocity, ρ is the density, P is the pressure, q is the electron heat flux, I is the absorbed laser energy flux (erg s^{-1} cm^{-2}) and γ is the ratio of the heat capacity at constant pressure (C_P) to heat capacity at

constant volume C_V. The following **ideal gas equations of state** are also available:

$$\begin{aligned}
\text{internal energy:} \quad & \varepsilon = C_V T = \left(\frac{1}{\gamma - 1}\right)\frac{P}{\rho} \\
\text{enthalpy:} \quad & h = C_P T = \left(\frac{\gamma}{\gamma - 1}\right)\frac{P}{\rho} \\
& \gamma = \frac{C_P}{C_V} = \frac{g+2}{g} \\
\text{isothermal } (T = \text{const.}) \text{ speed sound:} \quad & c_T = \sqrt{\frac{P}{\rho}} \\
\text{isentropic } (S = \text{const.}) \text{ speed sound:} \quad & c_S = \sqrt{\frac{\gamma P}{\rho}}
\end{aligned} \tag{9.14}$$

where g is the number of degrees of freedom of one particle. For a monoatomic gas $g = 3$ and $\gamma = \frac{5}{3}$. For electrons in the plasma $\gamma = \frac{5}{3}$, so that $\gamma/(\gamma - 1) = \frac{5}{2}$.

We now write six equations describing the flux conservation for mass, momentum and energy, according to (9.13), at the critical surface and at the ablation surface:

at the critical surface:

$$\begin{aligned}
& \rho_c u_c = \rho u \equiv \dot{m} \\
& \rho_c u_c^2 + P_c = \rho u^2 + P \\
& \dot{m}\left[\left(\frac{5}{2}\right)\frac{P_c}{\rho_c} + \left(\frac{1}{2}\right)u_c^2\right] + q_{out} = \dot{m}\left[\left(\frac{5}{2}\right)\frac{P}{\rho} + \left(\frac{1}{2}\right)u^2\right] + q_{in} + I \\
& q_{out} = \rho u_c^3 = \dot{m} u_c^2 \quad \text{(free streaming plasma)}
\end{aligned} \tag{9.15}$$

at the ablation surface:

$$\begin{aligned}
& \dot{m} = \rho u = \text{const.} \quad \text{('source' of plasma)} \\
& P_a = \rho u^2 + P \quad \text{(ablation pressure)} \\
& \dot{m}\left[\left(\frac{5}{2}\right)\frac{P}{\rho} + \left(\frac{1}{2}\right)u^2\right] + q_{in} = 0
\end{aligned}$$

where the quantities with the index c denote the variables at the critical surface from the corona side, while those without the index c denote the values between the corona and the ablation surface. Note that at the ablation surface $u = 0$ and $P = P_a$. Since in the corona the temperature is constant to a good approximation, it is conceivable that the plasma expands with the

isothermal speed of sound in the corona c_T given by

$$u_c = c_T = \sqrt{\frac{P}{\rho}}. \tag{9.16}$$

Using this relation together with the first two relations of (9.15) and the value of the ablation pressure (the sixth relation of (9.15)), one gets

$$P_a = 2\dot{m}c_T. \tag{9.17}$$

The third, the fourth and the last of equations (9.15) yield

$$I = 4\dot{m}c_T^2. \tag{9.18}$$

Using now the rocket equation for a one-dimensional plane geometry,

$$m(t)\frac{dv(t)}{dt} = P_a. \tag{9.19}$$

The mass $m(t)$ (g/cm^2) is accelerated to a velocity $v(t)$ at a time t by an ablation pressure P_a. The accelerated mass is defined by

$$m(t) = m_0 - \int_0^t \left(\frac{dm}{dt}\right) dt = m_0 - \dot{m}t \tag{9.20}$$

where it is assumed that the rate of plasma production is constant, i.e. $dm/dt =$ constant and m_0 is the initial mass. Substituting (9.17) and (9.20) into (9.19),

$$(m_0 - \dot{m}t)\frac{dv}{dt} = 2\dot{m}c_T \tag{9.21}$$

and integrating, the plasma rocket equation is obtained:

$$v(t) = 2c_T \ln\left(\frac{m_0}{m(t)}\right). \tag{9.22}$$

The hydrodynamic efficiency η_h is defined by

$$\eta_h = \frac{\frac{1}{2}m(t)v(t)^2}{I\tau} \tag{9.23}$$

where $\tau \approx \tau_L$ is the absorption time of the laser energy which is of the order of the laser pulse duration τ_L, I is the (time) average absorbed laser flux and $I \cdot \tau$ is the absorbed energy (erg/cm^2). Using equations (9.18), (9.20) and (9.22) into (9.23), one gets the hydrodynamic efficiency:

$$\eta_h = \frac{X(\ln X)^2}{2(1-X)}, \qquad X \equiv \frac{m(\tau)}{m_0}. \tag{9.24}$$

Note that for $X = 0.3$ the hydrodynamic efficiency is 30%, while for $X = 0.9$ the efficiency drops to 5%.

We now generalize the above analysis in order to estimate the ablation pressure necessary to accelerate a thin spherical shell to high velocities. The initial mass of this shell can be written as

$$m_0 = \rho_0 \Delta R_0 \tag{9.25}$$

where ρ_0 and ΔR_0 are the initial density and shell thickness accordingly. If during the acceleration period τ, of the order of the laser pulse duration, the shell radius R is much larger than its thickness ΔR, then for each segment of the shell one can use the plane geometry formulas, as derived above. Using (9.25) together with (9.17), (9.18), (9.23) and (9.24), the ablation pressure is

$$P_a = \left(\frac{X}{\eta_h}\right)\left(\frac{R_0}{4c_T\tau}\right)\left(\frac{\Delta R_0}{R_0}\right)[\rho_0 v(\tau)^2] \tag{9.26}$$

where $v(\tau)$ is the final (maximum) velocity of the accelerated shell, c_T (the isothermal sound velocity in the corona) is the exhaust velocity of the plasma causing the acceleration and $R_0/\Delta R_0$ is called the aspect ratio, limited (the maximum value) by hydrodynamic instabilities. From this equation one can see that for a given final shell velocity the required ablation pressure is inversely proportional to the hydrodynamic efficiency, and the larger the aspect ratio the less ablation pressure is needed. As an example, relevant to ICF, assuming $X/\eta_h \approx 0.5$, $R_0/(4c_T\tau) \approx 1$, $R_0/(\Delta R_0) = 10$, $\rho_0 = 0.2\,\mathrm{g/cm^3}$, one requires an ablation pressure of $P_a \approx 100\,\mathrm{Mbar}$ in order to achieve a shell velocity of $v \approx 10^8\,\mathrm{cm/s}$.

9.3 Relaxation Rates

In analysing a test particle, denoted by an index 1, moving with velocity $\mathbf{v}_1$ and interacting with a background plasma composed of particles, labelled 2, there are four relaxation rates τ of interest: the momentum loss or slowing down, the energy loss and two relaxation times related to transverse and parallel diffusion. In this section we only discuss the momentum loss and energy loss relaxation rates.

The relevant interactions discussed here are the Coulomb interaction between two charged particles (charges q_1 and q_2), described by the Rutherford cross section σ_{12} (see section 2.2). As in section 2.2, the impact parameter is denoted by b, $\mathbf{v}$ is the relative velocity between the colliding two particles (with indices 1 and 2), and the reduced mass is defined by

$$m_r = \frac{m_1 m_2}{m_1 + m_2} \tag{9.27}$$

CM and L label the centre of mass and the laboratory coordinates accordingly and θ is the scattering angle in the collision (see figure 9.2).

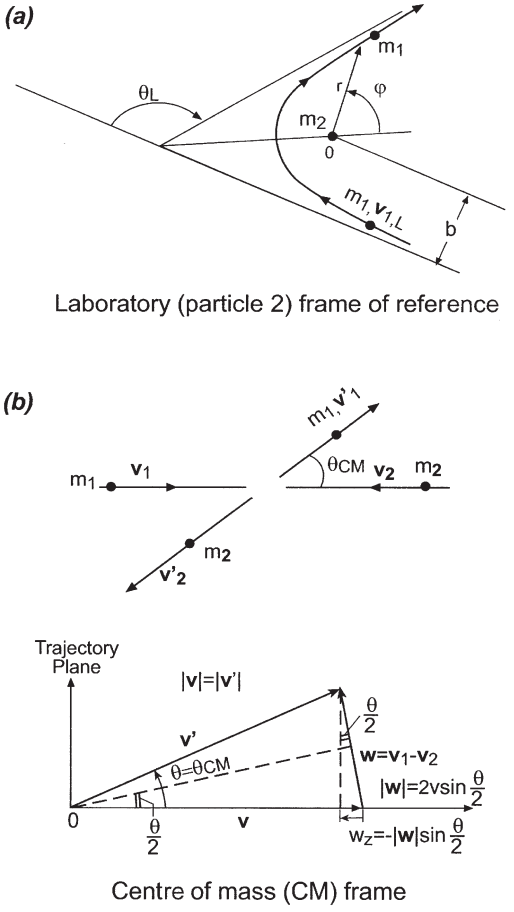

Figure 9.2. (a) Laboratory and (b) centre of mass (CM) frames of reference. In (a) the orbit is shown for a charged particle with mass m_1 scattered by a charged particle (with opposite charge) with mass m_2, positioned at O.

Conservation of momentum and energy of the Coulomb collision yields the scattering angle in the centre of mass (CM) system (in c.g.s. units):

$$\tan\left(\frac{\theta_{\mathrm{CM}}}{2}\right) = \frac{|q_1 q_2|}{m_{\mathrm{r}} v^2 b} \tag{9.28}$$

and the scattering angle of particle 1 in the laboratory frame is given by

$$\cot\theta_{\mathrm{L}} = \cot\theta_{\mathrm{CM}} + \frac{m_1}{m_2}\left(\frac{1}{\sin\theta_{\mathrm{CM}}}\right). \tag{9.29}$$

Since the collisions of interest are between the pairs electron–electron (ee), electron–ion (ei), ion–electron (ie) and ion–ion (ii), the following special cases are of interest:

$$\begin{aligned} m_1 \ll m_2\text{:} \quad & \theta_{\mathrm{L}} \approx \theta_{\mathrm{CM}} \\ m_1 = m_2\text{:} \quad & \theta_{\mathrm{L}} \approx \frac{\theta_{\mathrm{CM}}}{2} \\ m_1 \gg m_2\text{:} \quad & \theta_{\mathrm{L}} \approx \frac{m_2}{m_1} \sin\theta_{\mathrm{CM}}. \end{aligned} \tag{9.30}$$

All particles of type 1 incident into a ring between b and $b + \mathrm{d}b$ are scattered into angles θ_{CM} and $\theta_{\mathrm{CM}} + \mathrm{d}\theta_{\mathrm{CM}}$ in the CM frame of reference (or into angles θ_{L} and $\theta_{\mathrm{L}} + \mathrm{d}\theta_{\mathrm{L}}$ in the laboratory frame of reference). Therefore, the impact parameter b is related to the differential cross section $\mathrm{d}\sigma_{12}$ by

$$\mathrm{d}\sigma_{12}(\theta_{\mathrm{CM}}) = \sigma_{12}(\theta_{\mathrm{CM}})\,\mathrm{d}\Omega = \sigma_{12}(\theta_{\mathrm{CM}}) 2\pi \sin\theta_{\mathrm{CM}}\,\mathrm{d}\theta_{\mathrm{CM}} = 2\pi b\,\mathrm{d}b \tag{9.31}$$

where Ω is the solid angle and $\sigma(\theta_{\mathrm{CM}})$ is the Rutherford cross section (using (9.28)):

$$\sigma(\theta_{\mathrm{CM}}) = \frac{b\,\mathrm{d}b}{\sin\theta_{\mathrm{CM}}\,\mathrm{d}\theta_{\mathrm{CM}}} = \frac{(q_1 q_2)^2}{[2m_{\mathrm{r}} v^2 \sin^2(\theta_{\mathrm{CM}}/2)]^2}. \tag{9.32}$$

Since the angle of deflection increases with the decrease of the impact parameter (see (9.28)), the cross section that a particle is scattered at any angle larger than 90° is given by the impact parameter for $\theta = 90^\circ$:

$$\sigma_{12}(\theta_{\mathrm{CM}} \geq 90^\circ) = \pi b(90^\circ)^2 = \frac{\pi q_1^2 q_2^2}{m_{\mathrm{r}}^2 v^4} \tag{9.33}$$

where equation (9.28) has been used.

Equation (9.33) gives the cross section for a scattering angle larger than or equal to 90° in one collision. Now we calculate small-angle scattering that adds up to a large angle, say 90° deflection. We denote the small-angle scattering in the centre of mass frame by θ ($\theta \ll 1$). From equation (9.28),

$$\theta = \frac{2|q_1 q_2|}{m_{\mathrm{r}} v^2 b}. \tag{9.34}$$

The mean square deflection of a particle (called the test particle) that goes along a distance L in a plasma with a density of particles n_2 (here we calculate the deflection caused by particles of type 2) is

$$\begin{aligned} \theta_{\mathrm{CM}}^2 &= \sum \theta^2 = n_2 L \int_{\theta_{\min}}^{\theta_{\max}} \theta^2 \sigma_{12}(\theta) 2\pi \sin\theta\,\mathrm{d}\theta \\ &= \frac{18\pi n_2 L q_1^2 q_2^2}{m_{\mathrm{r}}^2 v^4} \int_{b_{\min}}^{b_{\max}} \frac{\mathrm{d}b}{b} = \frac{18\pi n_2 L q_1^2 q_2^2 \ln\Lambda}{m_{\mathrm{r}}^2 v^4} \end{aligned} \tag{9.35}$$

where the Coulomb cutoff coefficient is defined by the ratio of Debye length to the distance of closest approach (see section 2.2):

$$\Lambda = \frac{b_{\max}}{b_{\min}} = \left(\frac{3}{2\sqrt{\pi}}\right)\left(\frac{1}{q_1 q_2^2}\right)\left[\frac{(k_B T)^3}{n_2}\right]^{1/2}. \tag{9.36}$$

The following relation has been used between the relative velocity v and the temperature T:

$$\tfrac{1}{2} m_r v^2 = \tfrac{3}{2} k_B T. \tag{9.37}$$

The mean free path for large angle deflection, L_{90}, is obtained from (9.35) by substituting there $\theta_{CM}^2 = 1$, yielding the cross section σ_{90} for a large-angle scattering due to many small-angle deflections,

$$\begin{aligned} L_{90} &= \frac{m_r^2 v^4}{18\pi q_1^2 q_2^2 n_2 \ln\Lambda} = \frac{(k_B T)^2}{2\pi q_1^2 q_2^2 n_2 \ln\Lambda} \\ \sigma_{90} &= \frac{1}{n_2 L_{90}} = \frac{18\pi q_1^2 q_2^2 \ln\Lambda}{m_r^2 v^4} = \frac{2\pi q_1^2 q_2^2 \ln\Lambda}{(k_B T)^2} \end{aligned} \tag{9.38}$$

where (9.37) has been used. Note that the first of equations (9.38) is the equation given in (9.1) ($q_1 = -e$, $q_2 = Z$ and $Z n_2 = n_e$).

It is important to note that the probability (which is proportional to the cross section) of a large-angle scattering due to a single collision (in most plasmas) is significantly smaller than the probability of a large deflection caused by many small-angle scatterings:

$$\frac{\sigma_{90}}{\sigma(\theta_{CM} \geq 90^\circ)} = 8 \ln\Lambda. \tag{9.39}$$

Equation (9.39) is derived from equations (9.33) and (9.38). The factor of $8 \ln\Lambda$ is in the domain of 10–10^2 for most plasma systems discussed in this book. This fact is very important in analysing collision phenomena in plasmas.

The time required for large-angle deflection, in the CM system, is obtained from (9.38) and (9.37):

$$\tau_{90} = \frac{L_{90}}{v} = \left(\frac{3\sqrt{3}}{8\pi}\right)\frac{\sqrt{m_r}(k_B T)^{3/2}}{q_1^2 q_2^2 n_2 \ln\Lambda}. \tag{9.40}$$

We are interested in the large-angle deflection times in the laboratory frame of reference. Therefore, from equation (9.30), one gets that if $m_2 \geq m_1$ then the deflection in the laboratory system is comparable with that in the CM system, so that the calculated value of L_{90} in the CM system is the same

as in the laboratory system. Therefore, one can use the above formulae for e–e, e–i and i–i collisions. However, for i–e collisions (the test particle is the ion which is scattered by electrons) it follows from equation (9.30) that $\theta_L \sim (m_e/m_i)\theta_{CM}$, i.e. since m_e/m_i is about 1/2000 (for the hydrogen plasma) the test particle (the ion) must travel a 2000 times larger distance in order to undergo a large deflection in the laboratory frame. For the identical particle collisions the reduced mass is half the particle mass, and a factor of 2 was introduced since $\theta_L \approx \frac{1}{2}\theta_{CM}$ (see equation (9.30)).

From the above formalism (equation (9.40)) the following collision times for large-angle scattering, or equivalently the **momentum loss relaxation times** τ, are obtained (we drop the subscript 90), as seen in the laboratory frame of reference (note that **the first particle in the superscript is the test particle**):

$$\begin{aligned}
\tau^{ee} &= \left(\frac{3\sqrt{6}}{8}\right)\frac{\sqrt{m_e}(k_B T)^{3/2}}{\pi e^4 n_e \ln\Lambda} \\
&\approx 1.07\times 10^{-11}\left(\frac{10^{20}\,\mathrm{cm}^{-3}}{n_e}\right)\left(\frac{10}{\ln\Lambda}\right)\left(\frac{T_e}{1\,\mathrm{keV}}\right)^{3/2} \quad [\mathrm{s}] \\
\tau^{ii} &= \left(\frac{3\sqrt{6}}{8}\right)\frac{\sqrt{m_i}(k_B T)^{3/2}}{\pi Z^4 e^4 n_i \ln\Lambda} \\
\tau^{ei} &= \left(\frac{3\sqrt{3}}{8}\right)\frac{\sqrt{m_e}(k_B T)^{3/2}}{\pi Z^4 e^4 n_i \ln\Lambda} \\
\tau^{ie} &\approx \left(\frac{m_i}{m_e}\right)\tau^{ei}.
\end{aligned} \tag{9.41}$$

Assuming a neutral plasma, $n_e = Zn_i$ and the same temperature, one can get from the last equation the following order of the large-angle deflection collision times:

$$\tau^{ee} : \tau^{ei} : \tau^{ii} : \tau^{ie} \approx 1 : \frac{1}{Z\sqrt{2}} : \frac{1}{Z^3}\left(\frac{m_i}{m_e}\right)^{1/2} : \frac{1}{Z^3\sqrt{2}}\left(\frac{m_i}{m_e}\right). \tag{9.42}$$

The large-angle scattering collision time calculated here is an approximation of the momentum loss of the test particle. If a particle has an initial momentum in some direction, after scattering to a large angle the momentum in the initial direction is lost.

We now estimate the time required for a test particle to lose its energy. From momentum and energy conservation during a collision, a test particle 1, with energy E_1, is releasing energy ΔE_1 in the laboratory

frame according to the equation

$$\frac{\Delta E_1}{E_1} = \frac{4m_1m_2}{(m_1+m_2)^2}\sin^2\left(\frac{\theta_{\mathrm{CM}}}{2}\right). \tag{9.43}$$

The energy lost in multiple-scattering small-angle collisions can be calculated by substituting $\theta_{\mathrm{CM}} = 90^\circ$ in the last equation, yielding

$$\frac{\Delta E_1}{E_1} = \frac{2m_1m_2}{(m_1+m_2)^2}. \tag{9.44}$$

Therefore, in 90° collisions between identical particles, half of the initial energy is transferred by the test particle to the background particles. However, for electron–ion scattering only the fraction m_e/m_i of the initial energy of the test particle is transferred during 90° deflection. Denoting by τ_E **the energy relaxation time**, i.e. the time that $\Delta E_1/E_1 \approx 1$, one gets from equations (9.41), (9.42) and (9.44) (for $n_e = Zn_i$),

$$\begin{aligned}
\tau_E^{ee} &\approx \tau^{ee}\\
\tau_E^{ii} &\approx \tau^{ii} \approx \frac{1}{Z^3}\left(\frac{m_i}{m_e}\right)^{1/2}\tau^{ee}\\
\tau_E^{ei} &\approx \frac{1}{Z}\left(\frac{m_i}{m_e}\right)\tau^{ee}\\
\tau_E^{ie} &\approx \left(\frac{m_i}{m_e}\right)\tau^{ie} \approx \left(\frac{m_i}{m_e}\right)^2\tau^{ei}\\
\tau^{ee} : \tau_E^{ee} : \tau_E^{ii} : \tau_E^{ei} &\approx 1 : 1 : \frac{1}{Z^3}\left(\frac{m_i}{m_e}\right)^{1/2} : \frac{1}{Z}\left(\frac{m_i}{m_e}\right).
\end{aligned} \tag{9.45}$$

To conclude this analysis, it is important to note that the collision frequency ν^{12} for momentum loss and the collision frequency ν_E^{12} for the energy loss, where 1 denotes the test particle and 2 the background particles, are related to the relaxation times calculated above by

$$\nu^{12} = \frac{1}{\tau^{12}}, \qquad \nu_E^{12} = \frac{1}{\tau_E^{12}}. \tag{9.46}$$

The last of equations (9.45) show that electrons equilibrate, i.e. reach an equilibrium distribution (e.g. a Maxwell distribution of velocities), on a shorter time scale than the ions do by a factor of $Z^3(m_e/m_i)^{1/2}$. Moreover, the electrons reach equilibrium with the ions on a time scale longer by a factor $(1/Z)(m_i/m_e)$ than the electrons equilibrate with themselves. For example, in a typical corona of laser-produced plasma with an electron density $10^{20}\,\mathrm{cm}^{-3}$, an ion charge $Z = 10$, $m_i/m_e \approx 4 \times 10^4$ and an electron temperature 1 keV, $\ln\Lambda \approx 10$, one gets from equations (9.41) and (9.45)

that we can define an electron temperature after ~10 ps from the start of the laser–target interaction, an ion temperature after ~2 ps (note that for a hydrogen plasma this relaxation time changes to ~200 ps) and that the electron temperature is equal to the ion temperature after 40 ns. Thus, for most high-intensity laser pulses (0.1 ns to 10 ns) there is no equilibrium between the electrons and the ions in the corona. It is worth mentioning that for a solid state density plasma, $n_e \approx 10^{23}$, produced for example by a very short pulse duration (~100 fs), the above time scales are reduced by a factor of 1000 (assuming the same temperature). In this case the electrons will reach an equilibrium distribution with a temperature of 1 keV in about 10 fs.

The multiple small-angle scattering of the plasma introduces the **Coulomb logarithm ln Λ**, a factor included in the transport coefficients as well. $\ln \Lambda = b_{max}/b_{min}$ results from integration over the scattering angles θ, between large angles resulting from a small impact parameter b_{min} and small angles resulting from a large impact parameter b_{max}. The value of b_{max} is taken as the Debye shielding scale and is a function of electron velocity (i.e. temperature) and density. If the electrons move in a strong magnetic field, where the Larmor radius is smaller than the Debye length, then the Larmor radius should replace the value of b_{max}. However, this is seldom required in the laser-produced plasma. Last but not least, in dense and cold plasma the values of b_{max} and b_{min} are comparable and $\ln \Lambda$ may become negative, an unphysical result. This can happen when a large-angle deflection is more probable than the small-angle scattering. Such a plasma medium is the strongly-coupled plasma, where the electric potential energy is larger than the kinetic energy. In this case a value of $\ln \Lambda = 2$ is taken for practical calculations.

In conclusion, for plasmas where the small-angle scatterings are dominant, the Coulomb scattering of the plasma particles has a randomizing effect on the particle motion. Therefore, in this case, the electron drift motion may be described by diffusion or in the more general case by the Fokker–Planck equation.

9.4 The Fokker–Planck Equation

The electron energy transport can be described by the Boltzmann equation (see section 3.4):

$$\frac{\partial f}{\partial t} + \mathbf{v} \cdot \frac{\partial f}{\partial \mathbf{r}} + \frac{e\mathbf{E}}{m_e} \cdot \frac{\partial f}{\partial \mathbf{v}} = \left(\frac{\partial f}{\partial t}\right)_{coll} \tag{9.47}$$

where $f = f(\mathbf{r}, \mathbf{v}, t)$ is the electron density in phase space, $\mathbf{r} - \mathbf{v}$ space, $\mathbf{r}$ is the space coordinate and $\mathbf{v}$ is the particle velocity. $\mathbf{E}$ is the electrical field in the plasma and the magnetic field is neglected in (9.47). $(\partial f/\partial t)_{coll}$ is the collision term describing the scattering of electrons (by electrons and ions), as

described in the previous section. Assuming that the small-angle collisions are dominant, one can use the Fokker–Planck equation for the collision term.

The Fokker–Planck equation is derived in general by assuming a **Markov process**. If a measurable physical quantity develops in time in such a way that its 'future value' depends only on its 'present value', then the phenomenon describing this physical quantity is called a Markov process. In such a process the physical quantity changes in a random way. Let us take a physical variable X with measured values X_n, X_{n-1}, ..., X_1, X_0 at times $t_n > t_{n-1} > \cdots > t_1 > t_0$ respectively. The probability P to measure the value X_n, where the previous values were X_{n-1}, ..., X_1, X_0, in a Markov process is given by

$$P(X_n|X_{n-1}, \ldots, X_1, X_0) = P(X_n|X_{n-1}). \tag{9.48}$$

This equation describes the fact that the value X_n, measured at time t_n, depends only on its value X_{n-1} as measured at time t_{n-1}. A trivial example for a Markov process is the flipping of a coin. Then the number X_n of heads after n flips depends only on the number of heads X_{n-1} after $n-1$ flips, and not on all the history.

In analysing a continuous Markov process the situation is more complicated. If the physical phenomenon is described by a continuous function, then the existence of the derivatives contradicts the definition of the Markov process. For example, in this case X_{n+1} depends not only on X_n but also on the derivative $(\mathrm{d}X_n/\mathrm{d}t) = (X_n - X_{n-1})/\Delta t$, etc. Therefore, a Markov process may describe a continuous physical phenomenon only as an approximation. For example, in a Brownian motion the particle velocity undergoes a rapid variation due to each molecular collision, followed by a low-rate change due to the friction force. On a time scale of one collision the scattering is not Markovian. However, on a time scale of many collisions the Markov process is a very good approximation.

In plasma, due to the long-range Coulomb forces there are many small-angle scatterings causing large deflections (see previous section). The distribution function $f(v, t)$ is changing slowly on a time scale δt describing one (small-angle) collision. The Markov process may describe the changes on a time scale Δt, due to many small-angle collisions. In this case it is required that $\delta t \ll \Delta t$; however, Δt is small enough to define the variations and the derivatives of the physical quantities.

According to equation (9.48) for a Markov process the distribution function $f(v, t)$ is determined from the knowledge of $f(v - w, t)$, where $w = \Delta v$ is the change in velocity in the time interval Δt due to multiple small-angle collisions. It is assumed here that the distribution function in phase-space can be written $f(r, v, t) = n_0 f(v, t)$, where the spatial dependence is given by the constant n_0 (dimension cm^{-3}). The probability that a particle changes its velocity from v to $v + w$ is given by $P(v; w)$. If only

collisions are responsible to the change in $f(v,t)$, then one can write

$$\begin{aligned} f(\mathbf{v},t) &= \int P(\mathbf{v}-\mathbf{w};\mathbf{w}) f(\mathbf{v}-\mathbf{w}, t-\Delta t)\,\mathrm{d}^3 w \\ &\approx f(\mathbf{v},t)\int P(\mathbf{v};\mathbf{w})\,\mathrm{d}^3 w - \Delta t \frac{\partial f(\mathbf{v},t)}{\partial t}\int P(\mathbf{v};\mathbf{w})\,\mathrm{d}^3 w \\ &\quad - \int \sum_i w_i \frac{\partial}{\partial v_i}[P(\mathbf{v};\mathbf{w}) f(\mathbf{v},t)]\,\mathrm{d}^3 w \\ &\quad + \frac{1}{2}\int \sum_{i,j} w_i w_j \frac{\partial^2}{\partial v_i\,\partial v_j}[P(\mathbf{v};\mathbf{w}) f(\mathbf{v},t)] \end{aligned} \tag{9.49}$$

where a Taylor expansion has been made to second order, a good approximation for $\mathbf{w}$ small and Δt small. The indices i and j are the vector components in an orthogonal frame of reference. The integral of the probability function is one:

$$\int P(\mathbf{v};\mathbf{w})\,\mathrm{d}^3 w = 1 \tag{9.50}$$

and the rate of change of the first moment $\langle \mathbf{w} \rangle$ (dimension cm/s^2) and the second moments $\langle \mathbf{ww} \rangle$ (dimension cm^2/s^3) of $\mathbf{w}$ are

$$\begin{aligned} \langle w_i \rangle &= \frac{1}{\Delta t}\int P(\mathbf{v};\mathbf{w}) w_i\,\mathrm{d}^3 w \\ \langle w_i w_j \rangle &= \frac{1}{\Delta t}\int P(\mathbf{v};\mathbf{w}) w_i w_j\,\mathrm{d}^3 w. \end{aligned} \tag{9.51}$$

Substituting (9.50) and (9.51) into (9.49), one gets the **Fokker–Planck equation**

$$\left(\frac{\partial f}{\partial t}\right)_{\mathrm{coll}} = -\sum_i \frac{\partial}{\partial v_i}[\langle w_i \rangle f(\mathbf{v},t)] + \frac{1}{2}\sum_{i,j}\frac{\partial^2}{\partial v_i\,\partial v_j}[\langle w_i w_j \rangle f(\mathbf{v},t)]. \tag{9.52}$$

The first term on the right-hand side describes a 'drift', while the second term is the diffusion in the velocity space. In uniform plasma in thermal equilibrium the drift term 'pushes' the electrons to a zero velocity, but the electrons do not accumulate there because the diffusion term 'pushes' them away from the zero velocity.

The Fokker–Planck equation (9.52) can also be viewed as a continuity equation in the velocity space, with a density $f(\mathbf{v})$ and a current $\mathbf{J}(\mathbf{v})$:

$$\left(\frac{\partial f}{\partial t}\right)_{\mathrm{coll}} + \frac{\partial}{\partial \mathbf{v}} \cdot \mathbf{J}_{\mathrm{v}} = 0, \qquad \mathbf{J}_{\mathrm{v}} = \langle \mathbf{w} \rangle f - \frac{1}{2}\frac{\partial}{\partial \mathbf{v}} \cdot [\langle \mathbf{ww} \rangle f]. \tag{9.53}$$

As in the previous section, the test particles are denoted by index 1 and the background particles acquire index 2. The probability per unit time

($P\,\mathrm{d}^3v/\Delta t$) in equations (9.51) that a test particle, moving with relative velocity $\mathbf{v}_1 - \mathbf{v}_2$ relative to a background particle (moving with velocity $\mathbf{v}_2$), is scattered by the background particles, with a density $f_2\,\mathrm{d}^3v$, into the solid angle $\mathrm{d}\Omega$ is given by

$$\frac{P(\mathbf{v}_1;\mathbf{v}_2)\,\mathrm{d}^3\mathbf{v}_2}{\Delta t} = f_2(\mathbf{r}_2,\mathbf{v}_2,t)\sigma_{12}(v,\boldsymbol{\Omega})v\,\mathrm{d}^3\mathbf{v}_2\,\mathrm{d}\boldsymbol{\Omega}, \qquad v \equiv |\mathbf{v}_1 - \mathbf{v}_2| \tag{9.54}$$

where σ_{12} is the Rutherford cross section given in the CM frame by (9.32). The approximation $f(\mathbf{r},\mathbf{v},t) = n(\mathbf{r})f(\mathbf{v},t)$ is used, where $n(\mathbf{r})$ is the spatial density. $n(\mathbf{r})$ is omitted in the following analysis, since it cancels out in the Fokker–Planck equation (9.52). Note that the dimension of $f(\mathbf{r},\mathbf{v},t)$ is ($\mathrm{cm}^{-6}\,\mathrm{s}^3$), while the dimension of $f(\mathbf{v},t)$ is ($\mathrm{cm}^{-3}\,\mathrm{s}^3$).

Substituting (9.54) into (9.51), one has to calculate the averages

$$\begin{aligned}
\langle \mathbf{w}_1 \rangle &= \int \mathrm{d}^3v_2 \int \mathrm{d}\Omega\, \mathbf{w}_1 v\sigma(v,\boldsymbol{\Omega}) f_2(\mathbf{v}_2) \\
\langle \mathbf{w}_1\mathbf{w}_1 \rangle &= \int \mathrm{d}^3v_2 \int \mathrm{d}\Omega\, \mathbf{w}_1\mathbf{w}_1 v\sigma(v,\boldsymbol{\Omega}) f_2(\mathbf{v}_2) \\
\mathbf{w}_1 &= \mathbf{v}_1' - \mathbf{v}_1(\text{in lab. frame}) = \frac{m_2}{m_1+m_2}(\mathbf{v}' - \mathbf{v}) \equiv \frac{m_2}{m_1+m_2}\mathbf{w} \qquad (9.55)\\
&\left.\begin{aligned} \mathbf{v} &= \mathbf{v}_1 - \mathbf{v}_2 \\ \mathbf{v}' &= \mathbf{v}_1' - \mathbf{v}_2' \end{aligned}\right\} (\text{in CM frame}) \\
v &= |\mathbf{v}| = |\mathbf{v}'|
\end{aligned}$$

where primes denote the velocity value after the collision. The third equation of (9.55) is derived from the relation between the particle velocity in the laboratory frame and the particle velocity in the CM frame:

$$\begin{aligned}
\mathbf{v}_1(\text{lab}) &= \mathbf{v}_{\text{cm}} + \left(\frac{m_2}{m_1+m_2}\right)\mathbf{v} \\
\mathbf{v}_1'(\text{lab}) &= \mathbf{v}_{\text{cm}} + \left(\frac{m_2}{m_1+m_2}\right)\mathbf{v}' \\
\mathbf{v}_2(\text{lab}) &= \mathbf{v}_{\text{cm}} - \left(\frac{m_1}{m_1+m_2}\right)\mathbf{v} \\
\mathbf{v}_2'(\text{lab}) &= \mathbf{v}_{\text{cm}} - \left(\frac{m_1}{m_1+m_2}\right)\mathbf{v}'
\end{aligned} \tag{9.56}$$

where $\mathbf{v}_{\text{cm}}$ is the velocity of the centre of mass. The last equation of (9.55) is obtained by using in the centre of mass energy conservation ($\frac{1}{2}m_1v_1^2 + \frac{1}{2}m_2v_2^2 = \frac{1}{2}m_1v_1'^2 + \frac{1}{2}m_2v_2'^2$) and momentum conservation ($m_1\mathbf{v}_1 + m_2\mathbf{v}_2 = 0$; $m_1\mathbf{v}_1' + m_2\mathbf{v}_2' = 0$).

The change (in one collision) of the relative velocity $\mathbf{w}$ in the CM frame in Cartesian coordinates, where the z axis is chosen parallel to $\mathbf{v}$, is (see figure 9.2)

$$\begin{aligned} w_z &= -2v\sin^2\left(\frac{\theta}{2}\right) \\ w_x &= 2v\sin\left(\frac{\theta}{2}\right)\cos\left(\frac{\theta}{2}\right)\cos\phi \\ w_y &= 2v\sin\left(\frac{\theta}{2}\right)\cos\left(\frac{\theta}{2}\right)\sin\phi \\ \mathrm{d}\Omega &= \sin\theta\,\mathrm{d}\theta\,\mathrm{d}\phi. \end{aligned} \tag{9.57}$$

Using (9.57) and the Rutherford cross section (9.32) in equations (9.55), one gets

$$\begin{aligned} \langle \mathbf{w}_1 \rangle &= -\Gamma_{12}\left(1+\frac{m_1}{m_2}\right)\int \mathrm{d}^3 v_2 f_2(\mathbf{v}_2)\frac{\mathbf{v}_1-\mathbf{v}_2}{|\mathbf{v}_1-\mathbf{v}_2|^3} \\ \Gamma_{12} &\equiv \frac{4\pi q_1^2 q_2^2 \ln\Lambda}{m_1^2}. \end{aligned} \tag{9.58}$$

In obtaining this result the integral on $\mathrm{d}\Omega$ has been done. Thus, integrals with w_x and w_y yield zero (for the choice of reference in (9.57)), while with w_z one has (using (9.34) and (9.36))

$$\begin{aligned} \int \frac{\mathrm{d}\Omega}{\sin^4\left(\frac{\theta}{2}\right)} &= 2\pi\int \frac{\mathrm{d}\theta\sin\theta}{\sin^4\left(\frac{\theta}{2}\right)} = 2\pi\int_{\theta_{\min}}^{\theta_{\max}} \frac{\mathrm{d}\left(\frac{\theta}{2}\right)\cos\left(\frac{\theta}{2}\right)}{\sin\left(\frac{\theta}{2}\right)} \\ &= 2\pi\left[\ln\sin\left(\frac{\theta}{2}\right)\right]_{\theta_{\min}}^{\theta_{\max}} \approx 2\pi\left[\ln\left(\frac{\theta}{2}\right)\right]_{\theta_{\min}}^{\theta_{\max}} \\ &= 2\pi\ln\left(\frac{\theta_{\max}}{\theta_{\min}}\right) = 2\pi\ln\Lambda. \end{aligned} \tag{9.59}$$

Equation (9.58) can be written in a more convenient form by introducing the Rosenbluth potential $H(\mathbf{v})$, which satisfies a Poisson equation in the velocity space:

$$\begin{aligned} H_2(\mathbf{v}_1) &= \left(1+\frac{m_1}{m_2}\right)\int \mathrm{d}^3 v_2 \frac{f_2(\mathbf{v}_2)}{|\mathbf{v}_1-\mathbf{v}_2|} \\ \nabla_{\mathbf{v}}^2 H_2(\mathbf{v}_1) &= -4\pi\left(1+\frac{m_1}{m_2}\right) f_2(\mathbf{v}_1) \\ \langle \mathbf{w}_1 \rangle &= \Gamma_{12}\frac{\partial H_2(\mathbf{v}_1)}{\partial \mathbf{v}_1}. \end{aligned} \tag{9.60}$$

Using the differentiation laws,

$$\frac{\partial^2|\mathbf{v}_1-\mathbf{v}_2|}{\partial v_{1i}\,\partial v_{1j}}=\frac{\partial}{\partial v_{1i}}\left(\frac{v_{1j}}{|\mathbf{v}_1-\mathbf{v}_2|}\right)=\frac{\delta_{ij}}{|\mathbf{v}_1-\mathbf{v}_2|}-\frac{v_{1i}v_{1j}}{|\mathbf{v}_1-\mathbf{v}_2|^3} \tag{9.61}$$

and neglecting the integral terms not containing $\mathrm{d}\theta/\theta$ (considered to be small), one gets (i and j are the three components of an orthogonal frame of reference)

$$\begin{aligned} G_2(\mathbf{v}_1)&=\int \mathrm{d}^3v_2 f(\mathbf{v}_2)|\mathbf{v}_1-\mathbf{v}_2| \\ \nabla_{\mathrm{V}}^4 G_2(\mathbf{v}_1)&=-8\pi f_2(\mathbf{v}_1) \\ \langle w_{1i}w_{1j}\rangle&=\Gamma_{12}\frac{\partial^2 G_2}{\partial v_{1i}\,\partial v_{2j}}. \end{aligned} \tag{9.62}$$

Substituting (9.60) and (9.62) into (9.52), one gets the Fokker–Planck equation

$$\left(\frac{\partial f_\alpha(\mathbf{r},\mathbf{v},t)}{\partial t}\right)_{\mathrm{coll}}=\sum_\beta \Gamma_{\alpha\beta}\left[-\sum_{i=1}^{3}\frac{\partial}{\partial v_i}\left(f_\alpha(\mathbf{v},t)\frac{\partial H_\beta}{\partial v_i}\right)+\frac{1}{2}\sum_{i,j=1}^{3}\frac{\partial^2}{\partial v_i\,\partial v_j}\left(f_\alpha(\mathbf{v},t)\frac{\partial^2 G_\beta}{\partial v_i\,\partial v_j}\right)\right] \tag{9.63}$$

where f_α is the distribution of the α-th species of particles and the sum β on the right-hand side of (9.63) is over the collisions with the background particles (for the test particle α). The Rosenbluth potentials in (9.63) are defined according to (9.60) and (9.62):

$$H_\beta(\mathbf{v})=\left(1+\frac{m_\alpha}{m_\beta}\right)\int \mathrm{d}^3u\frac{f_\beta(\mathbf{u})}{|\mathbf{v}-\mathbf{u}|},\qquad G_\beta(v)=\int \mathrm{d}^3u|\mathbf{v}-\mathbf{u}|f_\beta(\mathbf{u}) \tag{9.64}$$

and the coupling constants $\Gamma_{\alpha\beta}$ are given in the approximation of equation (9.58) by

$$\Gamma_{\alpha\beta}=\frac{4\pi q_1^2 q_2^2 n_\alpha \ln\Lambda}{m_\alpha^2}. \tag{9.65}$$

The density of the α particles n_α has been included in (9.65) (in comparison with (9.58)) since the left-hand side of (9.63) describes the full distribution in phase space. This is necessary in order to substitute (9.63) (together with (9.64) and (9.65)) into the Boltzmann equation (9.47). The Boltzmann equation with the collisional term given in (9.63) is occasionally called the Fokker–Planck equation.

9.5 The Spitzer–Härm Conductivity

Knowledge of the time development of a fully ionized plasma due to collisions requires the simultaneous solution of the collisions of electrons with electrons, electrons with ions, ions with electrons and ions with ions. The general solution of these nonlinear integral-differential equations is not an easy task and can be done only with large computer resources. It is therefore very useful to look for simpler but approximate solutions that enable us to generate simple models of transport. The analytical models are very useful to comprehend the complicated phenomena of heat transfer in laser–plasma interaction.

For a distribution function depending on one space–one velocity coordinates x and v, and on the angle θ between the velocity and the spatial coordinate, $f = f(x, v, \cos\theta, t)$, the Fokker–Planck equation (9.63) can also be written as (Shkarofsky *et al.* 1966)

$$\left(\frac{\partial f}{\partial t}\right)_{\text{coll}} = \frac{1}{v}\frac{\partial}{\partial v}\left[v^2\left(\frac{D_{\|}}{2}\frac{\partial f}{\partial v} + Cf\right)\right] + \frac{D_{\perp}}{2v^2\sin\theta}\frac{\partial}{\partial\theta}\left(\sin\theta\frac{\partial f}{\partial\theta}\right) \tag{9.66}$$

where C (dimension (s^{-1})), $D_{\|}$ (dimension ($cm\,s^{-2}$)) and $D_{\perp}$ (dimension ($cm^2\,s^{-3}$)) are the coefficients of slowing down, diffusion in velocity space and diffusion in angular space respectively. These coefficients depend on the distribution function of the plasma electrons and ions. The angular diffusion term is dominated by electron–ion collisions, while the velocity diffusion term and the slowing down are more affected by electron–electron collisions. Therefore, for plasma with ion charge Z, the second term on the right-hand side of equation (9.66) is about Z times larger than the first term on the right-hand side of this equation (see equation (9.42), where the collision frequencies are proportional as $\tau_{\text{ee}}^{-1} : \tau_{\text{ei}}^{-1} = 1 : Z$).

If a plasma has a temperature gradient scale L_{T} much larger than the electron mean free path λ_{e}, $\lambda_{\text{e}} \ll L_{\text{T}}$ (λ_{e} and L_{T} are defined in (9.1) and (9.6)) and the distribution function has a weak angular dependence, then the electron distribution function can be expressed by the first two terms in a $\cos\theta$ perturbation expansion

$$f(x, v, \theta, t) = f_0(x, v, t) + f_1(x, v, t)\cos\theta \tag{9.67}$$

where f_0 and f_1 are the isotropic and the anisotropic components respectively. Since the large electron–ion collision frequency tends to maintain the distribution function almost isotropically, it is possible to neglect the higher-order terms in $\cos\theta$ in the expansion (9.67).

The isotropic component is assumed to be equal to the equilibrium Maxwellian distribution f_{M}:

$$f_0 = f_{\text{M}} = \frac{n_{\text{e}}}{(\pi)^{3/2}v_{\text{T}}^3}\exp\left(-\frac{v^2}{v_{\text{T}}^2}\right), \qquad f_1 \ll f_{\text{M}}, \qquad v_{\text{T}} \equiv \sqrt{\frac{2k_{\text{B}}T}{m_{\text{e}}}}. \tag{9.68}$$

The Boltzmann equation with the Fokker–Planck collision term has an analytic solution for the **Lorenz plasma**, i.e. ions with large Z, where f_1, the electric field E, $\partial f_M/\partial x$ and $\partial f_M/\partial t$ are small quantities (i.e. second-order terms or higher are neglected). Moreover, it is assumed that $\partial f_M/\partial t = 0$ and $\partial f_1/\partial t = 0$. In the Fokker–Planck equation (9.66) only the second term on the right-hand side contributes to a Lorenz plasma. Therefore, within those approximations, the Boltzmann equation (9.47) simplifies to

$$v\frac{\partial f_M}{\partial x} + \frac{eE}{m_e}\frac{\partial f_M}{\partial v} = -\frac{A}{v^3}f_1$$
$$A \equiv vD_\perp = \frac{8\pi Z n_e e^4 \ln\Lambda}{m_e} = \frac{v_T^3}{\tau_{ei}} = \frac{v_T^4}{\lambda_e} \tag{9.69}$$

where τ_{ei} is given in equation (9.41) and the electron mean free path λ_e equals L_{90} (for e–i collisions) in equation (9.40).

An additional equation is needed for the electric field E. Assuming charge neutrality in the plasma, which means that there is no electric current along the density gradient, gives the equation

$$J = \frac{4\pi e}{3}\int_0^\infty f_1 v^3\,dv = 0. \tag{9.70}$$

This model, the Lorentz model, is described mathematically by equations (9.68), (9.69) and (9.70). Substituting (9.68) into (9.69) and using

$$\frac{1}{n_e}\frac{\partial n_e}{\partial x} = \frac{1}{L_n}, \qquad \frac{1}{T}\frac{\partial T}{\partial x} = \frac{1}{L_T} \tag{9.71}$$

one gets

$$f_1 = -\frac{v^3}{A}\left(\frac{v}{L_n} - \frac{3v}{2L_T} + \frac{v^3}{v_T^2 L_T} - \frac{2eEv}{m_e v_T^2}\right)f_M. \tag{9.72}$$

Substituting f_1 from (9.72) into (9.70) and using

$$\int_0^\infty dv\, v^{2k+1}\exp\left(-\frac{v^2}{2v_T^2}\right) = \frac{k!}{2}(2v_T^2)^{k+1}, \quad k = 0, 1, 2, 3, \ldots \tag{9.73}$$

one gets an expression for the electric field (that cancels the current induced by the temperature gradient, see (9.4)):

$$\frac{2eE}{m_e v_T^2} = \frac{eE}{k_B T} = \left(\frac{1}{L_n} + \frac{5}{2L_T}\right). \tag{9.74}$$

This electric field is inserted into (9.72) to give the anisotropic electron distribution function f_1:

$$f_1 = \frac{n_e}{(\pi)^{3/2} A L_T v_T^3}\left(4v^4 - \frac{v^6}{v_T^2}\right)\exp\left(-\frac{v^2}{v_T^2}\right). \tag{9.75}$$

The heat flow is calculated by integrating in the velocity space the drifting electron distribution. The number (per cm^3) of drifting electrons with velocities between zero and v is given by $\frac{4}{3}\pi v^3 f_1$, and each electron carries an energy $\frac{1}{2}m_e v^2$. Therefore, the heat flux q is given by

$$q = \frac{2\pi m_e}{3}\int_0^\infty f_1 v^5\,\mathrm{d}v = \frac{m_e n_e}{3(\pi)^{1/2}AL_T v_T^3}\int_0^\infty \mathrm{d}v\left(4v^9 - \frac{v^{11}}{v_T^2}\right)\exp\left(-\frac{v^2}{v_T^2}\right). \quad (9.76)$$

After integrating (9.76) the heat flux is

$$q = -\left(\frac{4}{\sqrt{\pi}}\right)\frac{m_e n_e v_T^7}{AL_T} = -\left(\frac{12}{\sqrt{\pi}}\right)\lambda_e v_T n_e k_B \frac{\mathrm{d}T}{\mathrm{d}x} \quad (9.77)$$

where A was taken from equation (9.69), the relation between v_T and T is given in (9.68) and L_T was substituted from (9.71). The heat flux in this equation is the Lorentz limit of the Spitzer–Härm conductivity. The classical Spitzer–Härm conductivity has been analytically derived in agreement, up to a constant, with the coefficient κ in (9.2). Substituting the free-streaming flux from (9.7) into the flux (9.77), one gets

$$q \propto \left(\frac{\lambda_e}{L_T}\right)q_f \quad (9.78)$$

and for $\lambda_e/L_T \ll 1$ this is a reasonable result.

For $\lambda_e/L_T > 1$ (even for $\lambda_e/L_T > 0.1$ using the above numerical coefficients) the diffusion flux q is becoming larger than the free-streaming flux, which is absurd. In typical high-power laser-produced plasmas, between the critical surface and the ablation surface, the criterion $\lambda_e/L_T \ll 1$ is not satisfied. Therefore, the heat transport between the critical surface and the ablation surface cannot be described by the diffusion approximation, or by approximating the collision term in the Boltzmann equation by the Fokker–Planck equation. Another approach is needed in laser–plasma interactions in order to calculate how the energy is transported into the target. For this purpose the heat inhibition factor was introduced.

Another way to come to the same conclusion is to analyse f_1/f_M. Using equations (9.75), (9.68) and (9.69), this ratio is

$$\frac{f_1}{f_M} = \left(\frac{\lambda_e}{L_T}\right)\left(\frac{v}{v_T}\right)^4\left(4 - \left(\frac{v}{v_T}\right)^2\right). \quad (9.79)$$

This equation shows that f_1/f_M increases with λ_e/L_T and is equal to one for some value of the electron velocity v. However, the Spitzer–Härm approximation is valid only for $f_1/f_M \ll 1$. Between the ablation surface and the critical surface, L_T is chosen positive (i.e. $\mathrm{d}T/\mathrm{d}x > 0$); therefore, the positive x axis is pointing towards the laser radiation source (i.e. towards the vacuum) (see figure 9.1). The differential heat flux $q(v)$, which is is proportional to

$f_1 v^5$ (the integrand in (9.76)), is positive (flow towards the vacuum) if $f_1 > 0$ and negative when $f_1 < 0$. Since $f_1/f_M < 0$ for $v > 2v_T$ (f_M is always positive), all electrons with a velocity higher than $2v_T$ are transporting heat inside the target, while those electrons with $v < 2v_T$ are carrying energy from the ablation surface towards the corona. The reverse flow at low velocities is caused by the electric field and it is referred to in the literature as the 'return current'. The return current carries an equal but opposite current to that transported by the high-velocity electrons heating the target. This phenomenon ensures quasi-neutrality. The total heat flow is negative (see (9.77)); therefore, a net energy is transported into the target, so that the heat is predominantly carried by electrons with velocities between $2v_T$ and $3v_T$.

The total distribution function (9.67) can be written

$$f = f_M + f_1 \cos\theta = f_M \left[1 + \left(\frac{f_1}{f_M} \right) \frac{v_x}{v} \right]. \tag{9.80}$$

For particles moving into the target, $v_x/v = 1$, and therefore f becomes negative (an impossible situation) at $f_1/f_M < -1$. Analysing equation (9.79), one gets the unphysical situation, negative f, even for apparently a large temperature scale length such as $L_T/\lambda_e = 150$ if $v/v_T \approx 2.65$, a non-negligible region of energy transport into the target. It turns out that $L_T/\lambda_e > 10^3$ is required for the Spitzer–Härm approximation to be valid. Between the corona and the ablation surface this constraint is not usually satisfied. The steep temperature gradient in laser-produced plasmas requires, in general, a different formalism in order to explain the energy transport.

If there is a steep temperature gradient the electrons which have a long mean free path modify the local distribution function. This phenomenon is called non-local transport, since a large domain affects the heat transport. Because of the difficult problems of heat transport, between the corona and the ablation surface, a phenomenological approach is taken by using an effective inhibition factor in front of the free-streaming flow of electrons (see equation (9.8)).

In the next section a short discussion is given on the existence of hot electrons. In this case the physical phenomena are explained by two temperatures (or more), which in turn are derived from two (or more) Maxwellian electron distribution functions.

9.6 Hot Electrons

In laser-produced plasma the energy is absorbed by the electrons. When these electrons collide with the ions they are decelerated and emit x-ray radiation due to the bremsstrahlung effect. The logarithm of the energy spectrum of an x-ray when plotted as a function of the photon energy is a straight line if the electron distribution is Maxwellian. From the slope of this line the electron

temperature is deduced. This phenomenon is explained in the following paragraphs.

If there are two species of electrons then attempts are made to describe the electrons by two temperatures. Two temperatures imply two Maxwellian electron distributions, and the logarithm of the energy spectrum of x-ray when plotted as a function of the photon energy is described by a 'broken line'. From the slopes of the two lines the two temperatures can be deduced. It has been found experimentally that at laser intensities larger than $10^{15}\,\mathrm{W/cm^2}$, the x-ray emission from the laser-irradiated targets have an energy spectrum induced by a double Maxwellian electron distribution (Haines 1980).

The acceleration $a(t)$ of an electron while colliding with an ion, with charge Ze at a distance r, is given by the Coulomb force (c.g.s. units):

$$a(t) = \frac{Ze^2}{m_e r(t)^2}. \tag{9.81}$$

Classical electrodynamics shows that the accelerated electron radiates a power P:

$$P(t) = \frac{2e^2a^2}{3c^3} = \left(\frac{2Z^2e^6}{3m_e^2c^3}\right)\frac{1}{r^4} \tag{9.82}$$

where c is the speed of light and equation (9.81) has been used. Integrating over r and multiplying by the density numbers of the electron and the ion gives the total density power Q_b (erg/cm^3 s), emitted by bremsstrahlung:

$$Q_b = \frac{2Z^2e^6n_en_i}{3c^3m_e^2}\int_{r_{min}}^{\infty}\frac{4\pi r^2\,dr}{r^4} = \frac{8\pi Z^2e^6n_en_i}{3c^3m_e^2r_{min}}. \tag{9.83}$$

At r_{min} the classical approximation is no longer valid, since the uncertainty principle does not permit localization of the electron to a zero volume. As occasionally done in plasma physics, one takes the de Broglie scale length for r_{min} and relates the electron velocity to the temperature

$$r_{min} = \frac{\hbar}{m_e v}, \qquad v = \sqrt{\frac{k_B T}{m_e}}. \tag{9.84}$$

Substituting (9.84) into (9.83), the total power emitted per unit volume by the electrons, due to bremsstrahlung, is

$$Q_b = \left(\frac{16\pi^2Z^2e^6n_en_ik_B^{1/2}}{3c^3hm_e^{3/2}}\right)T_e^{1/2}. \tag{9.85}$$

In order to measure the electron temperature, a knowledge of the photon energy spectrum is required, rather than the total density power given in

this equation. For this purpose we analyse the energy ε emitted by one electron during the time it interacts with one ion. Equation (9.82) yields

$$\varepsilon = \int_{-\infty}^{+\infty} P\,\mathrm{d}t = \frac{2e^2}{3c^3}\int_{-\infty}^{+\infty} a(t)^2\,\mathrm{d}t \equiv \int_0^{\infty} P_\nu\,\mathrm{d}\nu \tag{9.86}$$

where P_ν is the radiated energy per unit frequency emitted (by one electron passing an ion) with a frequency ν. In classical mechanics the electron trajectory and its acceleration are calculated for the electron passing an ion, assuming that the energy loss of the electron is neglected (this approximation is correct for weak radiation). In a Coulomb interaction between two charges q_1 and q_2 with a reduced mass m_r, the trajectory $r(t)$ and the acceleration $a(t)$ are conveniently given as a function of a parameter α, the impact parameter b and the relative velocity v (see figure 9.2(a)):

$$\begin{aligned}
t &= \frac{1}{2}\left(\alpha + \frac{\alpha^3}{3}\right)\left[\frac{m_\mathrm{r}^2 b^3 v^3}{q_1^2 q_2^2}\right], \qquad r = \frac{1}{2}(1+\alpha^2)\left[\frac{m_\mathrm{r} b^2 v^2}{|q_1 q_2|}\right] \\
\cos\varphi &\equiv -\frac{1-\alpha^2}{1+\alpha^2}, \qquad \sin\varphi \equiv \frac{2\alpha}{1+\alpha^2} \\
a_\perp &= \frac{\mathrm{d}^2}{\mathrm{d}t^2}(r\sin\varphi) = \left[\frac{q_1 q_2}{m_\mathrm{r} b v^2}\right]^3 \left(\frac{v^2}{b}\right)\frac{8\alpha}{(1+\alpha^2)^3} \\
a_{\|} &= \frac{\mathrm{d}^2}{\mathrm{d}t^2}(r\cos\varphi) = -\left[\frac{q_1 q_2}{m_\mathrm{r} b v^2}\right]^3 \left(\frac{v^2}{b}\right)\frac{4(1-\alpha^2)}{(1+\alpha^2)^3} \\
a^2 &= a_\perp^2 + a_{\|}^2.
\end{aligned} \tag{9.87}$$

The solution $a(t)$ is substituted into (9.86) so that ε is calculated exactly (Miyamoto 1980). Here an estimate is given (Zeldovich and Raizer 1966, Haines 1980), which is correct within a constant of about 2, and the exact solution is quoted at the end of this calculation.

The time of interaction between the electron and the ion is of the order $\tau \approx b/v$. The dominant frequency in the Fourier transport is $2\pi\nu \approx 1/\tau \approx v/b$ (the dominant Fourier transport frequency usually satisfies $\omega\tau \approx 1$, where $\omega = 2\pi\nu$). Therefore, we can use these relations and (9.81) to obtain

$$\nu = \frac{v}{2\pi b}, \qquad \mathrm{d}\nu = -\frac{v\,\mathrm{d}b}{2\pi b^2} \tag{9.88}$$

$$\varepsilon = \left(\frac{2e^2a^2}{3c^3}\right)\tau = \left(\frac{2Z^2e^6}{3c^3m_\mathrm{e}^2}\right)\frac{1}{b^3 v}. \tag{9.89}$$

The electron with energy ε undergoes $n_\mathrm{i}\sigma(b)v$ collisions per unit time with ions in the impact parameter range b to $b + \mathrm{d}b$, where the cross section is

$\sigma_{ei}(b) = 2\pi b\,\mathrm{d}b$. Therefore, the energy radiated per unit time by an electron is

$$\begin{aligned}
\frac{\mathrm{d}E}{\mathrm{d}t} &= \int_{b_{\min}}^{\infty} \varepsilon n_i v 2\pi b\,\mathrm{d}b = \frac{4\pi Z^2 e^6 n_i}{3m_e^2 c^3}\int_{b_{\min}}^{\infty}\frac{\mathrm{d}b}{b^2} = \frac{8\pi^2 Z^2 e^6 n_i}{3m_e^2 c^3 v}\int_0^{\nu_{\max}}\mathrm{d}\nu \\
\frac{\mathrm{d}E}{\mathrm{d}t} &= \int_0^{\nu_{\max}} q_\nu\,\mathrm{d}\nu \\
q_\nu &\equiv \frac{8\pi^2 Z^2 e^6 n_i}{3m_e^2 c^3 v} \\
h\nu_{\max} &= \tfrac{1}{2}m_e v^2
\end{aligned} \tag{9.90}$$

where (9.88) is used and the photon energy ($h\nu$) cannot be larger than the kinetic energy of the electron. The power radiated per unit volume by the electrons is obtained by using (9.90):

$$\begin{aligned}
Q_b &\equiv \int \mathrm{d}\nu\, Q_\nu = \int \mathrm{d}\nu \int_{\sqrt{2h\nu/m_e}}^{\infty} q_\nu n_e f_M(v) 4\pi v^2\,\mathrm{d}v \\
f_M(v) &= \left(\frac{1}{\pi v_T^2}\right)^{3/2}\exp\left(-\frac{v^2}{v_T^2}\right) \\
v_T^2 &= \frac{2k_B T_e}{m_e} \\
Q_\nu &= \left(\frac{8\sqrt{2}}{3}\right)\frac{\pi^{3/2}Z^2 e^6 n_i n_e}{m_e^{3/2}c^3(k_B T_e)^{1/2}}\exp\left(-\frac{h\nu}{k_B T_e}\right).
\end{aligned} \tag{9.91}$$

An exact calculation yields $4/\sqrt{3} \approx 2.3$ times Q_ν of equation (9.91). The integral of (9.91) gives (9.85).

From equation (9.91) it is evident that a plot of $\ln[\mathrm{d}Q_b/\mathrm{d}(h\nu)]$ versus $h\nu$ yields a straight line, and from the slope it is easy to deduce the electron temperature. If the electron velocity distribution can be described not by one Maxwellian (as in the proof of (9.91)), but as a superposition of two Maxwellian distributions with two temperatures, then the integral of (9.91) yields

$$Q_\nu \propto \frac{n_c}{T_c^{1/2}}\exp\left(-\frac{h\nu}{k_B T_c}\right) + \frac{n_h}{T_h^{1/2}}\exp\left(-\frac{h\nu}{k_B T_h}\right) \tag{9.92}$$

where n_c and n_h are the spatial densities of the cold and hot electron species, while T_c and T_h are their respective temperatures. Such a spectrum was measured (Haines 1980) for neodymium laser pulses of the order of 1 ns and with intensity larger than $10^{15}\,\mathrm{W/cm^2}$ (see figure 9.3).

Energy transfer from electron plasma waves, nonlinear wave phenomena and resonance absorption can create the hot electrons. It appears that the

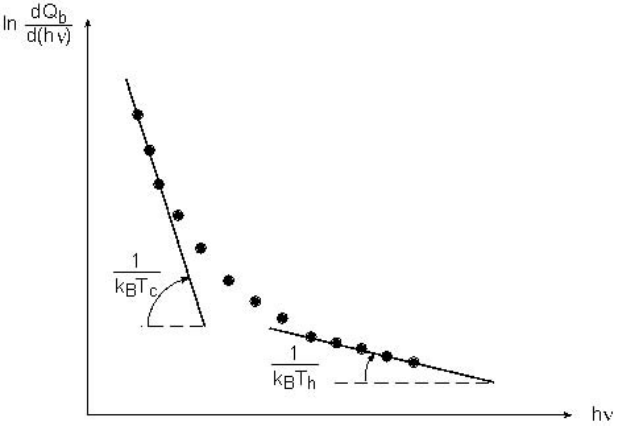

Figure 9.3. A typical x-ray spectrum induced by two electron temperatures.

dominant source of hot electrons is resonance absorption. It was found experimentally that the following scaling laws are satisfied for the hot electron temperature T_h:

$$T_h(\text{keV}) = 10\left(\frac{I_L\lambda_L^2}{10^{15}\,\text{W}\cdot\text{cm}^{-2}\,\mu\text{m}^2}\right)^{0.30\pm0.05} \quad \text{for } I_L\lambda_L^2 \geq 10^{15}\,\text{W}\cdot\text{cm}^{-2}\,\mu\text{m}^2$$

$$T_h(\text{keV}) = 10\left(\frac{I_L\lambda_L^2}{10^{15}\,\text{W}\cdot\text{cm}^{-2}\,\mu\text{m}^2}\right)^{2/3} \quad \text{for } I_L\lambda_L^2 \leq 10^{15}\,\text{W}\cdot\text{cm}^{-2}\,\mu\text{m}^2. \tag{9.93}$$

It is important to mention that with the femtosecond lasers, MeV electrons (and ions) have been measured for $I_L > 10^{19}\,\text{W/cm}^2$.

We conclude this section by showing that a very strange phenomenon can occur in thermodynamics for plasma with two temperatures. For a cold ion ($T_i = 0$) the ideal equation of state is

$$P = n_h k_B T_h + n_c k_B T_c. \tag{9.94}$$

For $T_h/T_c > 10$ one can obtain a (plasma) fluid which can satisfy

$$\left(\frac{\partial^2 P}{\partial V^2}\right)_S < 0, \qquad V = \frac{1}{\rho} = \frac{1}{m_i n_i} \tag{9.95}$$

where S is the entropy. A normal fluid cannot satisfy equation (9.95). However, two phase mixtures such as liquid and vapour can obey this equation. If (9.95) is satisfied then an unusual wave, called rarefaction shock wave, can exist (Zeldovich and Raizer 1966). As we shall see in the next chapter, in a shock wave the medium is compressed, while in a rarefaction wave the density of the medium is reduced. From this point of

view the rarefaction shock wave behaves like a rarefaction wave. However, while in a rarefaction wave the entropy S is conserved, in a shock wave the entropy increases, and in the rarefaction wave the entropy is decreasing: an unstable process.

In the following, we write the fluid equations for the plasma expanding into vacuum, where the plasma has two components of electrons (Bezzerides *et al.* 1978, Wickens *et al.* 1978). The continuity and the momentum equation for the ions moving without collisions in the electrostatic potential ϕ are

$$\frac{\partial n_\mathrm{i}}{\partial t}+\frac{\partial}{\partial x}(n_\mathrm{i}v_\mathrm{i})=0, \qquad m_\mathrm{i}\left(\frac{\partial v_\mathrm{i}}{\partial t}+v_\mathrm{i}\frac{\partial v_\mathrm{i}}{\partial x}\right)=-Ze\frac{\partial\phi}{\partial x}. \tag{9.96}$$

Neglecting the inertial term in both electronic fluids, the pressure of the hot and cold electrons are balanced by the potential force

$$\begin{aligned} en_\mathrm{c}\frac{\partial\phi}{\partial x}-k_\mathrm{B}T_\mathrm{c}\frac{\partial n_\mathrm{c}}{\partial x}=0 \Rightarrow n_\mathrm{c}=n_{\mathrm{c}0}\exp\left(\frac{e\phi}{k_\mathrm{B}T_\mathrm{c}}\right) \\ en_\mathrm{h}\frac{\partial\phi}{\partial x}-k_\mathrm{B}T_\mathrm{h}\frac{\partial n_\mathrm{h}}{\partial x}=0 \Rightarrow n_\mathrm{h}=n_{\mathrm{h}0}\exp\left(\frac{e\phi}{k_\mathrm{B}T_\mathrm{h}}\right). \end{aligned} \tag{9.97}$$

The temperatures T_c and T_h are assumed constants. Equations (9.96) and (9.97) are solved, together with the requirement of charge neutrality:

$$Zn_\mathrm{i}=n_\mathrm{c}+n_\mathrm{h}. \tag{9.98}$$

Using (9.94), (9.97) and (9.98), one can write the second equation of (9.96) in the following ways:

$$\begin{aligned} &\frac{\partial v_\mathrm{i}}{\partial t}+v_\mathrm{i}\frac{\partial v_\mathrm{i}}{\partial x}=-\frac{1}{n_\mathrm{i}m_\mathrm{i}}\frac{\partial P}{\partial x}=-\frac{1}{n_\mathrm{i}m_\mathrm{i}}\frac{\partial P}{\partial n_\mathrm{i}}\frac{\partial n_\mathrm{i}}{\partial x}=-c_\mathrm{S}(\phi)^2\frac{1}{n_\mathrm{i}}\frac{\partial n_\mathrm{i}}{\partial x} \\ &c_\mathrm{S}(\phi)^2=\frac{1}{m_\mathrm{i}}\frac{\partial P}{\partial n_\mathrm{i}}=\frac{1}{m_\mathrm{i}}\frac{\partial P}{\partial\phi}\left(\frac{\partial n_\mathrm{i}}{\partial\phi}\right)^{-1}=\frac{Z}{m_\mathrm{i}}\left[\frac{n_\mathrm{h}+n_\mathrm{c}}{(n_\mathrm{h}/k_\mathrm{B}T_\mathrm{h})+(n_\mathrm{c}/k_\mathrm{B}T_\mathrm{c})}\right]. \end{aligned} \tag{9.99}$$

We now look for a **self-similar solution**, like the one obtained in section 7.2, in analysing the plasma expansion into vacuum. The variables n_c, n_h, n_i, v_i and ϕ are functions of only one variable ξ:

$$\xi=\frac{x}{t}, \qquad \frac{\partial}{\partial x}=\frac{1}{t}\frac{\partial}{\partial\xi}, \qquad \frac{\partial}{\partial t}=-\frac{\xi}{t}\frac{\partial}{\partial\xi}. \tag{9.100}$$

Using these relations in the two equations of (9.96), where the second equation is taken from (9.99), one gets

$$\begin{pmatrix} v_\mathrm{i}-\xi & n_\mathrm{i} \\ c_\mathrm{s}^2/n_\mathrm{i} & v_\mathrm{i}-\xi \end{pmatrix}\begin{pmatrix} \mathrm{d}n_\mathrm{i}/\mathrm{d}\xi \\ \mathrm{d}v_\mathrm{i}/\mathrm{d}\xi \end{pmatrix}=\begin{pmatrix} 0 \\ 0 \end{pmatrix}. \tag{9.101}$$

Equations (9.101) have a solution only if the determinant of the matrix vanishes, implying

$$v_{\mathrm{i}} = c_{\mathrm{s}}(\phi) + \xi. \tag{9.102}$$

Substituting this relation into one of the equations of (9.101), one gets

$$n_{\mathrm{i}} \frac{\mathrm{d}v_{\mathrm{i}}}{\mathrm{d}\xi} + c_{\mathrm{s}}(\phi) \frac{\mathrm{d}n_{\mathrm{i}}}{\mathrm{d}\xi} = 0. \tag{9.103}$$

Using (9.97) and (9.98), with the boundary condition $\phi = 0$, $v = 0$ and $c_{\mathrm{s}} = c_0$ in the undisturbed plasma, one obtains after integrating (9.103) the following solution:

$$\begin{aligned} v_{\mathrm{i}} &= \left(\frac{1}{T_{\mathrm{c}}} - \frac{1}{T_{\mathrm{h}}}\right)^{-1} \left\{ \frac{c_{\mathrm{c}}}{T_{\mathrm{c}}} \ln \left[\left(\frac{c_{\mathrm{s}} - c_{\mathrm{c}}}{c_0 - c_{\mathrm{c}}} \right) \left(\frac{c_0 + c_{\mathrm{c}}}{c_{\mathrm{s}} + c_{\mathrm{c}}} \right) \right] \right. \\ &\qquad \left. + \frac{c_{\mathrm{h}}}{T_{\mathrm{h}}} \ln \left[\left(\frac{c_{\mathrm{h}} - c_0}{c_{\mathrm{h}} - c_{\mathrm{s}}} \right) \left(\frac{c_{\mathrm{h}} + c_{\mathrm{s}}}{c_{\mathrm{h}} + c_0} \right) \right] \right\} \\ c_{\mathrm{c}}^2 &\equiv \frac{Z k_{\mathrm{B}} T_{\mathrm{c}}}{m_{\mathrm{i}}}, \qquad c_{\mathrm{h}}^2 \equiv \frac{Z k_{\mathrm{B}} T_{\mathrm{h}}}{m_{\mathrm{i}}} \\ c_0^2 &= \left(\frac{Z}{m_{\mathrm{i}} k_{\mathrm{B}}} \right) \frac{n_{\mathrm{c}0} + n_{\mathrm{h}0}}{(n_{\mathrm{c}0}/T_{\mathrm{c}}) + (n_{\mathrm{h}0}/T_{\mathrm{h}})}. \end{aligned} \tag{9.104}$$

From (9.102) and (9.104) the solution of the potential $\phi(\xi)$ is obtained, implying for $T_{\mathrm{h}}/T_{\mathrm{c}} > 10$ a jump in the potential as shown schematically in figure 9.1 (the double layer).

The jump in the potential and the rarefaction shock wave are obtained if

$$\frac{\mathrm{d}^2 P}{\mathrm{d}V^2} = n_{\mathrm{i}}^3 m_{\mathrm{i}}^3 c_{\mathrm{s}}^2 \left(2 + \frac{\mathrm{d}c_{\mathrm{s}}^2}{\mathrm{d}\phi} \right) \leq 0. \tag{9.105}$$

Using (9.97) and (9.99) in this inequality, we get

$$\begin{aligned} &2 + \frac{\mathrm{d}c_{\mathrm{s}}^2}{\mathrm{d}\phi} \leq 0 \Rightarrow 2\beta^2 + \beta(6\alpha - 1 - \alpha^2) + 2\alpha^2 \leq 0 \\ &\alpha \equiv \frac{T_{\mathrm{h}}}{T_{\mathrm{c}}}, \qquad \beta \equiv \frac{n_{\mathrm{h}}}{n_{\mathrm{c}}}. \end{aligned} \tag{9.106}$$

This equation has a real solution for β only if

$$(6\alpha - 1 - \alpha^2)^2 - 16\alpha^2 \geq 0 \Rightarrow \alpha \equiv \frac{T_{\mathrm{h}}}{T_{\mathrm{c}}} \geq 5 + \sqrt{24} \approx 9.9. \tag{9.107}$$

In this domain of parameters the function $\phi(\xi)$ is not well defined, i.e. ϕ has three values for the same ξ, therefore the jump of ϕ (the singularity) is settled in this domain and a rarefaction wave is obtained.

Hot electrons is a peculiar and interesting phenomenon associated with high-power laser-produced plasmas. Sometimes this phenomenon is disturbing, like the preheating of solid targets for applications of shock waves, and sometimes it is a desirable effect, like in the creation of sources of high-energy x-rays.

9.7 Heat Waves

The local absorption of the laser energy is associated with the creation of a temperature gradient and a thermal flux to transport the absorbed energy. With the temperature gradient there are also pressure gradients that set the plasma into a 'fluid' motion. In most laser-produced plasmas the hydrodynamic energy transport substantially exceeds the heat conduction. However, in the interaction of very short laser pulses (of the order of 1 ps or less) with matter, the hydrodynamic motion does not have time to develop, and therefore in these cases the heat transport is dominant. Electrons or x-rays may serve as heat carriers (Ditmire *et al.* 1996, Fraenkel *et al.* 2000). For nonlinear transport coefficients, like the electron conductivity discussed in section 9.5, we expect that the energy transport is caused by a heat wave. Heat waves may also play an important role in inertial confinement fusion during the ignition process. In this section we shall formally show the solution for a one-dimensional geometry heat wave (Zeldovich and Raizer 1966, Krokhin 1971).

Let us consider the energy conservation equation:

$$\rho C_{\mathrm{V}} \frac{\partial T}{\partial t} = -\nabla \cdot (\mathbf{q}_{\mathrm{H}} - \mathbf{I}), \qquad \mathbf{q}_{\mathrm{H}} = -\kappa \nabla T, \qquad \kappa = BT^{\mathrm{n}}, \qquad \nabla \cdot \mathbf{I} \equiv W \tag{9.108}$$

where ρ is the density (g/cm^3), T is the temperature in Kelvin, $\mathbf{I}$ is the absorbed laser flux [erg/(time $\cdot$ cm^2)], $\mathbf{q}_{\mathrm{H}}$ is the heat flux [erg/(time $\cdot$ cm^2)], κ is the coefficient of thermal conductivity [erg/(cm $\cdot$ s $\cdot$ K)], W is the power density deposited by the laser [erg/(s $\cdot$ cm^3)], C_{V} is the specific heat at constant volume [erg/(g $\cdot$ K)], and B and n are constants. In one space dimension, chosen as x, and assuming a constant density ρ (a reasonable assumption for short laser pulse duration) and a constant C_{V}, equation (9.108) takes the form

$$\frac{\partial T}{\partial t} = \frac{\partial}{\partial x}\left(\chi \frac{\partial T}{\partial x}\right) + w, \qquad \chi = \frac{\kappa}{\rho C_{\mathrm{V}}}, \qquad w = \frac{W}{\rho C_{\mathrm{V}}}. \tag{9.109}$$

The coefficient χ is called the thermal diffusivity (cm^2/s) and can be expressed as

$$\chi = aT^n \tag{9.110}$$

where a is a constant.

If $n = 0$, i.e. a constant thermal diffusivity, then equation (9.109) is the simple diffusion equation. Assuming that the laser energy is deposited at $x = 0$ (e.g. all the energy is deposited at the critical surface located at $x = 0$) and at time $t = 0$ (i.e. a very short pulse duration), then

$$\frac{\partial T}{\partial t} = a\left(\frac{\partial^2 T}{\partial x^2}\right) + w, \qquad w = T_0 L\delta(x)\delta(t), \qquad T(x,0) = T_0 L\delta(x) \tag{9.111}$$

where $\delta(x)$ and $\delta(t)$ are the Dirac delta function

$$\int_{-L/2}^{L/2} \delta(x)\,\mathrm{d}x = 1, \qquad \int_{-\tau/2}^{\tau/2} \delta(t)\,\mathrm{d}t = 1 \tag{9.112}$$

and L is a scale length factor for the energy deposition and τ is the laser pulse duration. The solution of equation (9.111) is

$$T(x,t) = \frac{T_0 L}{(4\pi a t)^{1/2}} \exp\left(-\frac{x^2}{4at}\right). \tag{9.113}$$

Equation (9.113) is the solution of the linear heat transport equation (9.111). The nonlinear heat transport equation is

$$\frac{\partial T}{\partial t} = a\frac{\partial}{\partial x}\left(T^n \frac{\partial T}{\partial x}\right) + w. \tag{9.114}$$

For example, for electrons in plasma one can use equation (9.2) (proven in section 2.3), together with the C_V value of $\frac{3}{2}k_B$ per particle, to get

$$\left.\begin{aligned} \kappa &= \tfrac{1}{3}\lambda_e v_e n_e k_B \\ C_V &= \tfrac{3}{2}k_B\left(\frac{n_e}{\rho}\right) \end{aligned}\right\} \Rightarrow \chi = \frac{\kappa}{\rho C_V} = \frac{2}{9}\lambda_e v_e \propto T^{5/2} \tag{9.115}$$

where we have used equation (9.1), the electron mean free path $\lambda_e \approx T^2$, and the thermal speed of the electron $v_e \approx T^{1/2}$. Therefore, for the nonlinear electron heat transport in the plasma, $n = \frac{5}{2}$ in equation (9.114). In comparison, for radiation (x-rays) transport in a multiply-ionized plasma the power of T in this equation is in the domain ~4.5–5.5.

In some cases, like in a solid medium, C_V depends on temperature (C_V/particle equals $3k_B/2$ only for an ideal gas with three degrees of freedom). In this case equation (9.114) is not satisfied. When the specific heat is a function of the temperature, one can write for the energy E (erg/g),

$$E = \alpha T^k \Rightarrow T = \left(\frac{E}{\alpha}\right)^{1/k}, \qquad C_V = \left(\frac{\partial E}{\partial T}\right)_V = \alpha k T^{k-1} \tag{9.116}$$

where α is a constant (it can be a function of density ρ, but $V = 1/\rho$ is constant). In metals (see section 5.7), the electronic contribution to the equation of state is described by $k = 2$ to a good approximation (Eliezer *et al.* 1986). The coefficient α is given by the equation of state of the medium under consideration. Substituting (9.116) into (9.108) and using

$$\frac{\partial T}{\partial t} = \left(\frac{\partial E}{\partial T}\right)^{-1} \frac{\partial E}{\partial t} = \frac{1}{C_V} \frac{\partial E}{\partial t} \tag{9.117}$$

one gets the equation for the energy/mass E:

$$\frac{\partial E}{\partial t} = A \frac{\partial}{\partial t}\left(E^N \frac{\partial E}{\partial x}\right) + W, \qquad A \equiv \frac{B}{\rho k \alpha^{(n+1)/k}}, \qquad N \equiv \frac{n-k+1}{k}. \tag{9.118}$$

Equations (9.114) and (9.118) are identical from the mathematical point of view. If C_V is temperature-independent one has to solve equation (9.114), while if C_V depends on temperature then (9.118) has to be solved.

We now obtain an analytic solution (Zeldovich and Raizer 1966) of equation (9.114). The energy is deposited instantaneously at $t = 0$, at a plane positioned at $x = 0$. For $t > 0$ the heat propagates away from the $x = 0$ plane. The energy conservation is obtained by integrating equation (9.114) in space ($\int \mathrm{d}x$ from $-\infty$ to $+\infty$) and in time ($\int \mathrm{d}t$ from 0 to t). The first term on the right-hand side of the space integral of (9.114) vanishes, because $T(x = -\infty) = 0$ and $T(x = +\infty) = 0$. Therefore, the energy conservation implies the following equation:

$$\int_{-\infty}^{+\infty} T(x,t)\,\mathrm{d}x = \frac{1}{\rho C_V} \int I(t)\,\mathrm{d}t = \frac{\varepsilon}{\rho C_V} \equiv Q \tag{9.119}$$

where ε (erg/cm^2) is the deposited laser energy per unit area. The energy conservation (9.119) is satisfied, together with the heat conduction equation (9.114) for $t > 0$:

$$\frac{\partial T}{\partial t} = a \frac{\partial}{\partial x}\left(T^n \frac{\partial T}{\partial x}\right). \tag{9.120}$$

The energy deposition of the laser is instantaneous if the laser pulse duration is τ, if we are analysing times t much larger than τ ($t \gg \tau$). In this case the problem is defined only by two parameters: a [cm^2/(K^n · s)] and Q (K · cm), where K is Kelvin. There is only one way to describe the dimensions of temperature T and position x:

$$(x) = (aQ^n t)^{1/(n+2)}, \qquad (T) = \left(\frac{Q^2}{at}\right)^{1/(n+2)}. \tag{9.121}$$

Therefore, the measurable solution $T(x,t)$ cannot be a function of two variables x and t, but only of one dimensionless variable ξ that can be constructed from a, Q, x and t,

$$\xi = \frac{x}{(aQ^n t)^{1/(n+2)}} \tag{9.122}$$

and a coefficient which has the dimension of T. The general solution of equation (9.120) can be presented as

$$T(x,t) = \left(\frac{Q^2}{at}\right)^{1/(n+2)} f(\xi). \tag{9.123}$$

Substituting (9.123) into (9.120) and using (9.121) in order to take the derivatives

$$\frac{\partial f}{\partial t} = -\left(\frac{1}{n+2}\right)\left(\frac{\xi}{t}\right)\frac{\mathrm{d}f}{\mathrm{d}\xi}, \qquad \frac{\partial f}{\partial x} = \left(\frac{1}{aQ^n t}\right)^{1/(n+2)}\frac{\mathrm{d}f}{\mathrm{d}\xi} \tag{9.124}$$

one gets the ordinary differential equation for $f(\xi)$:

$$(n+2)\frac{\mathrm{d}}{\mathrm{d}\xi}\left(f^n\frac{\mathrm{d}f}{\mathrm{d}\xi}\right) + \xi\frac{\mathrm{d}f}{\mathrm{d}\xi} + f = 0. \tag{9.125}$$

This equation has to be solved subject to the boundary conditions

$$f(\xi = \infty) = 0, \qquad \frac{\mathrm{d}f}{\mathrm{d}\xi}(\xi = 0) = 0. \tag{9.126}$$

These boundary values are derived from $T(x = -\infty) = 0$ and $T(x = +\infty) = 0$, which are equivalent to $T(x = +\infty) = 0$ and $\partial T/\partial x(x = 0) = 0$. The second relation is the manifestation of the mirror symmetry $(x \leftrightarrow -x)$ about the plane $x = 0$.

A solution of equation (9.125) with the boundary condition (9.126) is

$$f(\xi) = \begin{cases} \left[\dfrac{n\xi_0^2}{2(n+2)}\right]^{1/n}\left[1 - \left(\dfrac{\xi}{\xi_0}\right)^2\right]^{1/n} & \text{for } \xi < \xi_0 \\ 0 & \text{for } \xi > \xi_0. \end{cases} \tag{9.127}$$

The constant ξ_0 is obtained by using the energy conservation (9.119), yielding

$$\int_{-\xi_0}^{+\xi_0} f(\xi)\,\mathrm{d}\xi = 1 \Rightarrow \xi_0 = \left[\frac{(n+2)}{n2^{n-1}\pi^{n/2}}\right]^{1/(n+2)}\left[\frac{\Gamma(1/2+1/n)}{\Gamma(1/n)}\right]^{n/(n+2)} \tag{9.128}$$

where Γ is the gamma function. Defining $x_f(t)$ as the front coordinate of the heat wave and $T_0(t)$ as the temperature at $x = 0$, the temperature $T(x, t)$ from (9.123) is given from (9.127) and (9.122):

$$\begin{aligned} T(x,t) &= T_0(t)\left(1 - \frac{x^2}{x_f(t)^2}\right)^{1/n} \\ x_f(t) &= \xi_0 (aQ^n t)^{1/(n+2)} \\ T_0(t) &= \left[\frac{n\xi_0^2}{2(n+2)}\right]^{1/n} \left(\frac{Q^2}{at}\right)^{1/(n+2)}. \end{aligned} \tag{9.129}$$

A typical temperature T as a function of x at a given time t is shown in figure 9.4.

The speed of propagation u_{hw} of the heat wave is defined by

$$u_{hw} = \frac{dx_f}{dt} = \left(\frac{\xi_0}{n+2}\right)(aQ^n)^{1/(n+2)} t^{-[(n+1)/(n+2)]}. \tag{9.130}$$

From equations (9.129) and (9.130), it appears that at $t = 0$ both the temperature and the heat wave velocity are singular ($\to \infty$). However, as was previously explained, the self-similar solution derived here is relevant only for times $t \gg \tau$, where τ is the laser pulse duration. Therefore, it might be convenient to write the solutions for T_0 and u in the form

$$\left.\begin{aligned} \frac{T_0(t)}{T_0(\tau)} &= \left(\frac{\tau}{t}\right)^{1/(n+2)} \\ \frac{u_{hw}(t)}{u_{hw}(\tau)} &= \left(\frac{\tau}{t}\right)^{(n+1)/(n+2)} \end{aligned}\right\} \quad \text{for } t \gg \tau. \tag{9.131}$$

In figure 9.4 the heat wave temperature space profile (at a time t), the flux and the cooling and heating domains are shown. Using the solution (9.129), one gets

$$\begin{aligned} T(x,t) &= T_0(t)\left(1 - \frac{x^2}{x_f^2}\right)^{1/n} \\ q_H(x,t) &= -BT^n \frac{dT}{dx} = \left(\frac{2BT_0^{n+1}}{x_f^2}\right)\left(1 - \frac{x^2}{x_f^2}\right)^{1/n} x \\ \rho C_V \frac{\partial T}{\partial t} &= -\frac{\partial q_H}{\partial x} = \left(\frac{2BT_0^{n+1}}{x_f^2}\right)\left(1 - \frac{x^2}{x_f^2}\right)^{-[(n-1)/n]} \left[\left(\frac{2+n}{n}\right)\frac{x^2}{x_f^2} - 1\right]. \end{aligned} \tag{9.132}$$

The heat flux q_H increases linearly, to a good approximation, from $x = 0$ to almost the front of the wave and drops very fast to zero at $x = x_f$. From the

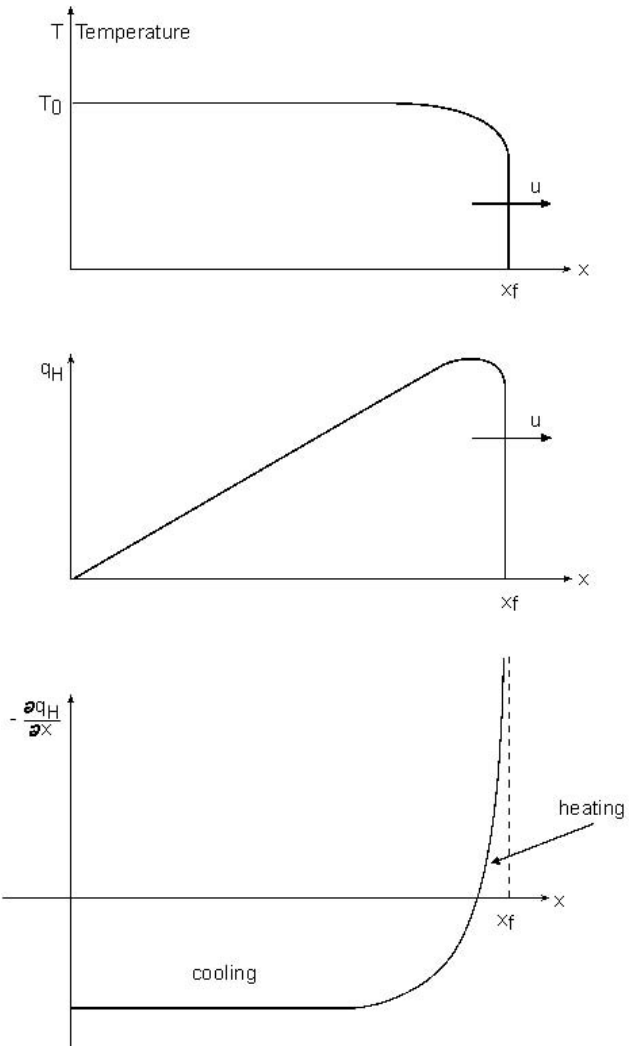

Figure 9.4. A schematic solution for a nonlinear heat wave.

last of equations (9.132), one notes that for $x/x_f < [n/(n+2)]^{1/2}$ the medium is cooled (i.e. the temperature decreases with time), while for $x/x_f > [n/(n+2)]^{1/2}$ the medium is heated. At $x/x_f = 1$ there is a singularity in the increase (in time) in temperature. However, the energy conservation ($\int T\,dx = \text{constant}$) is not violated, as required by this formalism. The main hot region is cooled almost uniformly and only the domain with the edge of the wave is heated very fast. The temperature near the wave front

can be described by the following approximation:

$$T(x,t) = T_0\left(1 - \frac{x^2}{x_f^2}\right)^{1/n} \approx T_0 2^{1/n}\left(1 - \frac{x}{x_f}\right)^{1/n} \quad \text{for } \frac{x}{x_f} \approx 1. \tag{9.133}$$

In laser–plasma interactions with very short laser pulses, the heat wave induced by the transport of x-rays may become more important than the heat wave created by electron transport (Ditmire *et al.* 1996, Fraenkel *et al.* 2000). We now give a short summary of the heat conduction by photons in a medium of thermal equilibrium between the electrons and the radiation.

The radiation heat flux is given by (see section 2.4)

$$\begin{aligned} \mathbf{q}_R &= -\frac{\lambda_R c}{3}\nabla U_p = -\kappa_R \nabla T \\ U_p &= \frac{4\sigma_{SB} T^4}{c} \\ \kappa_R &= \frac{16\sigma_{SB} T^3 \lambda_R}{3} \\ \lambda_R &= AT^j \quad \text{for } \rho = \text{const.} \end{aligned} \tag{9.134}$$

where T is the temperature of the electrons and the radiation; they are equal in thermal equilibrium. U_p is the radiation energy density (erg/cm^3), c is the speed of light, σ_{SB} is the Stefan–Boltzmann constant, ρ is the medium density and A and j are positive constants. λ_R is the radiation mean free path (the Rosseland mean free path) and for the equilibrium condition it is necessary that λ_R is smaller than the dimension of the medium. If the plasma is multiply ionized then j is in the domain of 1.5–2.5 (in λ_R given in equation (9.134)). In a fully ionized plasma the absorption and emission of the photons is by bremsstrahlung (i.e. electron–photon interaction in the presence of the ions) and in this case $j = \frac{7}{2}$ (Zeldovich and Raizer 1966):

$$\lambda_R(\text{bremsstrahlung}) = 4.8 \times 10^{24}\frac{T^{7/2}}{Z^2 n_i n_e} \quad [\text{cm}]. \tag{9.135}$$

Z is the charge of the ions, and n_i and n_e are the ion and electron densities respectively. For example, $Z = 1$, $Zn_i = n_e = 5 \times 10^{22}$ (appropriate for a femtosecond laser interacting with a deuterium plasma with solid density) and a temperature of 10^5 (about 10 eV), one gets a mean free path of about 6.1 μm.

The (Rosseland) mean free path for hydrogen-like plasma with a charge Z is given by

$$\lambda_R(\text{H-like}) \approx 8.7 \times 10^6 \frac{T^2}{Z^2 n_i} \quad [\text{cm}]. \tag{9.136}$$

In this case a comparison between the electron thermal conductivity (Spitzer–Härm conductivity κ_e—see sections 9.1 and 9.5) and the radiation

conductivity yields (Ditmire *et al*. 1996)

$$\frac{\kappa_{\mathrm{R}}}{\kappa_{\mathrm{e}}} \approx 5 \times 10^{18} \left(\frac{k_{\mathrm{B}} T}{\mathrm{eV}}\right)^{5/2} \left(\frac{\mathrm{cm}^{-3}}{n_{\mathrm{e}}}\right). \tag{9.137}$$

This relation implies that for a solid state density plasma $n_{\mathrm{e}} = Z n_{\mathrm{i}} = 10^{23}\,\mathrm{cm}^{-3}$, the radiation transport is more important than the electron heat transport for $k_{\mathrm{B}} T > 100\,\mathrm{eV}$.

Chapter 10

Shock Waves and Rarefaction Waves

10.1 A Perspective

The science of high pressure (Eliezer *et al.* 1986, Eliezer and Ricci 1991) is studied experimentally in the laboratory by using static and dynamic techniques. In static experiments the sample is squeezed between pistons or anvils. The conditions in these static experiments are limited by the strength of the construction materials. In the dynamic exdepends periments shock waves are created. Since the passage time of the shock is short in comparison with the disassembly time of the shocked sample, one can do shock wave research for any pressure that can be supplied by a driver, assuming that a proper diagnostic is available. In the scientific literature, the following shock-wave generators are discussed: a variety of guns (such as rail guns and a two-stage light–gas gun) that accelerate a foil to collide with a target, exploding foils, magnetic compression, chemical explosives, nuclear explosions and high-power lasers. The conventional high explosive and gun drivers can achieve pressures up to a few megabars.

The **dimension of pressure** is given by the scale defined by the pressure of one atmosphere at standard conditions $\approx$ **bar** $=$ **10^6 dyne/cm^2** (in c.g.s. units) $=$ **10^5 Pascal** (in m.k.s. units, Pascal $= \mathrm{N/m^2}$).

In 1974 the first direct observation of a laser-driven shock wave was reported (van Kessel and Sigel 1974). A planar solid hydrogen target (taken from a liquid-helium-cooled cryostat and inserted into an evacuated interaction chamber) was irradiated with a 10 J, 5 ns, Nd laser (1.06 μm wavelength) and the spatial development of the laser-driven shock wave was measured using high-speed photography. The estimated pressure in this pioneer experiment was 2 Mbar.

Twenty years after the first published experiment, the Nova laser from Livermore laboratories in the USA created a pressure of 750 ± 200 Mbar (Cauble *et al.* 1994). This was achieved in a collision between two gold foils, where the flyer (Au foil) was accelerated by a high-intensity x-ray flux created by the laser–plasma interaction.

The science of high pressure is usually analysed in a medium that has been compressed by a one-dimensional shock wave. For a one-dimensional shock wave traversing a known medium (density and temperature are known before the shock wave passes through), the density, pressure and energy of the shocked material are uniquely determined from the conservation of mass, momentum and energy, and the measurement of the shock and particle flow velocities.

The starting points in analysing the one-dimensional shock waves are the conservation laws of mass, momentum and energy in a fluid flow:

$$\begin{aligned} \frac{\partial \rho}{\partial t} &= -\frac{\partial}{\partial x}(\rho u) \\ \frac{\partial}{\partial t}(\rho u) &= -\frac{\partial}{\partial x}(P + \rho u^2) \\ \frac{\partial}{\partial t}\left(\rho E + \frac{1}{2}\rho u^2\right) &= -\frac{\partial}{\partial x}\left(\rho E u + P u + \frac{1}{2}\rho u^3\right). \end{aligned} \tag{10.1}$$

The usual notation is used, where x–t is space–time, ρ is the density, u is the flow velocity, P is the pressure and E is the internal energy per unit mass. In the previous chapter (section 9.7), in the discussion of heat waves, the fluid flow was neglected in favour of the heat flow. In this chapter we analyse a medium dominated by its flow and the disturbances that propagate with a speed of the order of the velocity of sound. In this case (unlike in section 9.7), the time of interest is in the domain where the heat wave velocity u_{hw} is much smaller than the sound velocity c_{s}. Furthermore, the laser pulse duration is not negligible. Therefore, to a good approximation one may assume that during the laser pulse duration a constant flux (the laser absorbed flux I) is supplied by the laser to the fluid at the boundary $x = 0$:

$$I = -\kappa\left(\frac{\partial T}{\partial x}\right)_{x=0} = -c_{\mathrm{V}}\rho a T^n\left(\frac{\partial T}{\partial x}\right)_{x=0} = \text{const.}, \qquad I \approx \frac{c_{\mathrm{V}}\rho a T_0^{n+1}}{x_{\mathrm{f}}} \tag{10.2}$$

where a is a constant, c_{V} is the heat capacity at constant volume and ρ is the density of the medium. x_{f} is the front position of the heat wave (see section 9.7) and T_0 is the temperature at the origin ($x = 0$), i.e. how far the heat wave front is from the origin $x = 0$ and how much the temperature increases there during the laser pulse duration.

The heat wave equation (energy conservation) can be approximated by

$$\rho c_{\mathrm{V}}\frac{\partial T}{\partial t} \approx \rho c_{\mathrm{V}}\frac{T_0}{t} \approx \frac{I}{x_{\mathrm{f}}}. \tag{10.3}$$

Solving equations (10.2) and (10.3) yields the order of magnitude solutions:

$$T_0 \approx \left(\frac{I}{\rho c_V}\right)^{2/(n+2)} a^{-1/(n+2)} t^{1/(n+2)}$$
$$x_f \approx \left(\frac{I}{\rho c_V}\right)^{n/(n+2)} a^{1/(n+2)} t^{(n+1)/(n+2)}. \tag{10.4}$$

These scaling laws can be derived by dimensional analysis. The problem under consideration is defined by two parameters: $[I/(\rho \cdot c_V)]$ with dimension $[\mathrm{cm} \cdot \mathrm{K/s}]$ and the diffusivity of the medium $\chi = aT^n$, defined by the coefficient a with dimension $[\mathrm{cm}^2/(\mathrm{K}^n \cdot \mathrm{s})]$. Therefore, the solution x_f scales as $[I/(\rho \cdot c_V)]^\alpha [a]^\beta [t]^\gamma = [\mathrm{cm}]$, yielding

$$\left(\frac{\mathrm{cm} \cdot \mathrm{K}}{\mathrm{s}}\right)^\alpha \left(\frac{\mathrm{cm}^2}{\mathrm{K}^n \cdot \mathrm{s}}\right)^\beta \mathrm{s}^\gamma = \mathrm{cm}^1$$
$$\Rightarrow \alpha + 2\beta = 1, \qquad \alpha - n\beta = 0, \qquad -\alpha - \beta + \gamma = 0$$
$$\Rightarrow \alpha = \frac{n}{n+2}, \qquad \beta = \frac{1}{n+2}, \qquad \gamma = \frac{n+1}{n+2}$$
$$\Rightarrow x_f \approx \left(\frac{I}{\rho c_V}\right)^{n/(n+2)} a^{1/(n+2)} t^{(n+1)/(n+2)}. \tag{10.5}$$

A similar procedure gives $T_0 = [I/(\rho \cdot c_V)]^\alpha [a]^\beta [t]^\gamma$, with $\alpha = 2/(n+2)$, $\beta = -1/(n+2)$ and $\gamma = 1/(n+2)$. This procedure justifies equations (10.4) as an order of magnitude solution, and implies that the exact solution is given by this equation up to a dimensionless constant, usually of the order 1.

According to equations (10.4), the heat wave velocity u_{hw} and the sound velocity c_s have a time dependence

$$u_{hw} = \frac{\mathrm{d}x_f}{\mathrm{d}t} \propto t^{-1/(n+2)}, \qquad c_s \propto T_0^{1/2} \propto t^{1/[2(n+2)]}. \tag{10.6}$$

From these equations one can see that the heat wave speed decreases with time, while the acoustic wave increases with time, so that the acoustic disturbance overtakes the thermal wave (see figure 10.1). An exact calculation of this problem (Babuel-Peyrissac *et al.* 1969) shows that for solid deuterium, with a density $0.2\,\mathrm{g/cm}^3$, and for an absorbed laser flux of $10^{15}\,\mathrm{W/cm}^2$, the sound wave overtakes the heat wave at 10 ps. From the above scaling laws it is evident that this time decreases for higher densities and lower absorbed laser intensity. Moreover, the inhibited thermal transport, as discussed in section 9.6, also reduces the time of heat-wave dominance. Therefore, in laser interaction with a solid target, the hydrodynamics effects predominate over the heat wave for laser pulse duration larger than 100 ps.

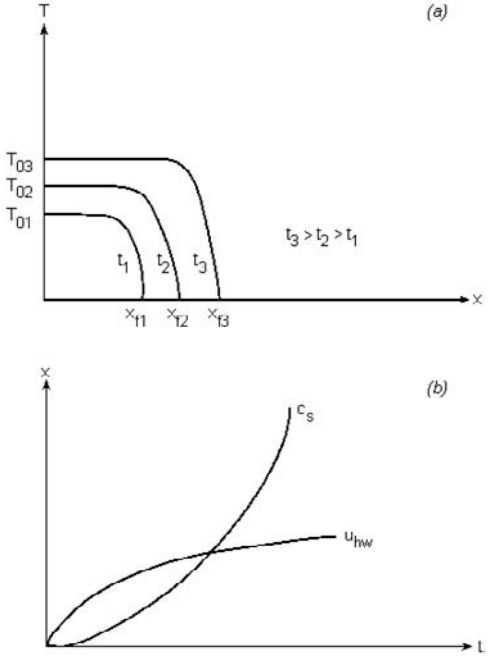

Figure 10.1. (a) Propagation of a heat wave during the laser pulse duration, where the laser absorbed flux is deposited at $x = 0$. (b) The positions of the heat wave front and the acoustic wave disturbance.

In sections 10.2 and 10.3 the sound wave and the rarefaction wave equations are given. The shock wave is discussed in sections 10.4 and 10.5. Section 10.6 analyses the constraints of a laser-induced shock wave for application in high-pressure physics. In sections 10.7 and 10.8 two possible applications of laser-induced shock waves and rarefaction waves are discussed.

In this chapter we consider only waves in one dimension with planar symmetry. In this case the variables describing the wave phenomena are functions only of the displacement x and the time t. The pressure P, the density ρ and the flow velocity u are, in general, functions of x and t.

10.2 Sound Waves

The physics of sound waves (Courant and Friedrichs 1976) is described by the motion of the fluid and the changes of density of the medium, caused by a pressure change. For an equilibrium pressure P_0 and density ρ_0, the

changes in pressure ΔP and density $\Delta\rho$ due to the existence of a sound wave are extremely small:

$$\begin{aligned} \rho &= \rho_0 + \Delta\rho, \qquad \frac{\Delta\rho}{\rho_0} \ll 1 \\ P &= P_0 + \Delta P, \qquad \frac{\Delta P}{P_0} \ll 1. \end{aligned} \tag{10.7}$$

It is now assumed that the undisturbed flow velocity is zero and the flow speed caused by the pressure disturbance is Δu, so that

$$u = u_0 + \Delta u, \qquad u_0 = 0, \qquad \frac{\Delta u}{c_s} \ll 1 \tag{10.8}$$

where c_s is the speed of sound. Using the small perturbations of (10.7) and (10.8), and neglecting second-order quantities in $\Delta\rho$, ΔP and u, the mass and momentum equations of (10.1) can be written in the form

$$\frac{\partial(\Delta\rho)}{\partial t} = -\rho_0 \frac{\partial u}{\partial x}, \qquad \rho_0 \frac{\partial u}{\partial t} = -\frac{\partial P}{\partial x}. \tag{10.9}$$

The motion in a sound wave is isentropic, $S(x) = \text{const.}$, therefore the change in the pressure is given by

$$\Delta P = \left(\frac{\partial P}{\partial \rho}\right)_S \Delta\rho \equiv c_s^2 \Delta\rho. \tag{10.10}$$

Differentiating the first equation of (10.9) with respect to time and the second equation with respect to space, adding the equations and using (10.10), one gets the wave equation

$$\frac{\partial^2(\Delta\rho)}{\partial t^2} - c_s^2 \frac{\partial^2(\Delta\rho)}{\partial x^2} = 0. \tag{10.11}$$

From this equation it is evident that c_s is the velocity of the $\Delta\rho$ disturbance, which is defined as the velocity of the sound wave. The pressure change ΔP and the flow velocity u satisfy a similar wave equation. Equation (10.11) has two families of solutions f and g:

$$\left.\begin{matrix} \Delta\rho \\ \Delta P \\ \Delta u \end{matrix}\right\} \approx f(x - c_s t) \quad \text{and} \quad g(x + c_s t) \tag{10.12}$$

where the speed of sound is

$$c_s = +\sqrt{\left(\frac{\partial P}{\partial \rho}\right)_S}. \tag{10.13}$$

The disturbances $f(x - c_s t)$ are moving in the positive x direction, while $g(x + c_s t)$ propagates in the negative x direction.

For a plasma satisfying an ideal equation of state, where the electron density $n_e = Zn_i$, Z is the ion charge and n_i is the ion density, and $T_e = T_i = T$ are the electron and ion temperatures, the pressure is given by

$$P = n_e k_B T_e + n_i k_B T_i = n_i (Z+1) k_B T = \frac{\rho}{m_i}(Z+1) k_B T \tag{10.14}$$

where m_i is the ion mass. An adiabatic process is described by

$$P = P_0 \left(\frac{\rho}{\rho_0}\right)^{\gamma}, \qquad \gamma = \frac{C_P}{C_V} \tag{10.15}$$

where C_P and C_V are the heat capacities at constant pressure and constant volume accordingly, and in a fully ionized plasma $\gamma = \frac{5}{3}$. The speed of sound for the ideal gas is

$$c_s = \left(\frac{\gamma P}{\rho}\right)^{1/2} = \left(\frac{\gamma (Z+1) k_B T}{m_i}\right)^{1/2}. \tag{10.16}$$

If the undisturbed gas is not stationary, then the flow stream carries the waves. A transformation from the coordinates moving with the flow (velocity u in the $+x$ direction) to the laboratory coordinates means that the sound wave is travelling with a velocity $u + c_s$ in the $+x$ direction and $u - c_s$ in the $-x$ direction. The curves in the x–t plane in the direction of propagation of small disturbances are called **characteristic curves**. For isentropic flow there are two families of characteristics described by

$$C_+: \quad \frac{dx}{dt} = u + c_s, \qquad C_-: \quad \frac{dx}{dt} = u - c_s \tag{10.17}$$

so that the physical quantities P and ρ do not change along these stream lines. There is also a characteristic curve C_0, where $dx/dt = u$, not discussed here. The $C_\pm$ characteristics are curved lines in the x–t plane because u and c_s are, in general, functions of x and t.

The equations of state describe any thermodynamic variable as a function of two other variables (assuming that the number of particles do not change). For example, the density $\rho = \rho(P, S)$ is a function of the pressure P and entropy S; therefore, for $S = \text{const.}$ one gets

$$\rho = \rho(P), \qquad \frac{\partial \rho}{\partial t} = \left(\frac{\partial \rho}{\partial P}\right)_S \frac{\partial P}{\partial t} = \frac{1}{c_s^2}\frac{\partial P}{\partial t}, \qquad \frac{\partial \rho}{\partial x} = \frac{1}{c_s^2}\frac{\partial P}{\partial x}. \tag{10.18}$$

Using these relations into the mass conservation and the momentum conservation given in (10.1), we get

$$\frac{1}{\rho c_s}\frac{\partial P}{\partial t} + \frac{u}{\rho c_s}\frac{\partial P}{\partial x} + c_s \frac{\partial u}{\partial x} = 0, \qquad \frac{\partial u}{\partial t} + u\frac{\partial u}{\partial x} + \frac{1}{\rho}\frac{\partial P}{\partial x} = 0. \tag{10.19}$$

Adding and subtracting these two relations yields

$$\left[\frac{\partial u}{\partial t}+(u+c_\mathrm{s})\frac{\partial u}{\partial x}\right]+\frac{1}{\rho c_\mathrm{s}}\left[\frac{\partial P}{\partial t}+(u+c_\mathrm{s})\frac{\partial P}{\partial x}\right]=0$$
$$\left[\frac{\partial u}{\partial t}+(u-c_\mathrm{s})\frac{\partial u}{\partial x}\right]-\frac{1}{\rho c_\mathrm{s}}\left[\frac{\partial P}{\partial t}+(u-c_\mathrm{s})\frac{\partial P}{\partial x}\right]=0. \tag{10.20}$$

The brackets [ ] in these equations are derivatives along the characteristics $C_\pm$. In order to comprehend this statement, we define a curve $x=y(t)$. The derivative of a function $F(x,t)$ along the curve $y(t)$ is given by

$$\left(\frac{\mathrm{d}F}{\mathrm{d}t}\right)_y=\frac{\partial F}{\partial t}+\frac{\partial F}{\partial x}\frac{\mathrm{d}x}{\mathrm{d}t}=\frac{\partial F}{\partial t}+y'\frac{\partial F}{\partial x}$$
$$\mathrm{d}F=\int\left(\frac{\mathrm{d}F}{\mathrm{d}t}\right)_y\mathrm{d}t,\qquad x=y(t),\qquad y'\equiv\frac{\mathrm{d}x}{\mathrm{d}t}. \tag{10.21}$$

For example, for the derivative of F along $x=$ constant one has $y'=0$, along a **stream line** $y'=u$, along the **characteristic** C_+ we have $y'=u+c_\mathrm{s}$, etc. Therefore, equations (10.20) and (10.21) can be rewritten as

$$\mathrm{d}J_+\equiv\mathrm{d}u+\frac{1}{\rho c_\mathrm{s}}\mathrm{d}P=0\quad\text{along } C_+\left(\frac{\mathrm{d}x}{\mathrm{d}t}=u+c_\mathrm{s}\right)$$
$$\mathrm{d}J_-\equiv\mathrm{d}u-\frac{1}{\rho c_\mathrm{s}}\mathrm{d}P=0\quad\text{along } C_-\left(\frac{\mathrm{d}x}{\mathrm{d}t}=u-c_\mathrm{s}\right). \tag{10.22}$$

These equations describe an isentropic flow in one dimension with planar symmetry. $\mathrm{d}J_\pm$ are total differentials and can be integrated:

$$J_+=u+\int\frac{\mathrm{d}P}{\rho c_\mathrm{s}}=u+\int\frac{c_\mathrm{s}\,\mathrm{d}\rho}{\rho},\qquad J_-=u-\int\frac{\mathrm{d}P}{\rho c_\mathrm{s}}=u-\int\frac{c_\mathrm{s}\,\mathrm{d}\rho}{\rho} \tag{10.23}$$

for the second relation on the right-hand side of these equations (10.10) has been used. J_+ and J_- are called **Riemann invariants** and are occasionally used to solve numerically the flow equations for (and only for) an isentropic process, since J_+ and J_- are constants along the characteristics C_+ and C_- respectively. For a non-isentropic flow the density and the speed of sound are functions of two variables, $\mathrm{d}J_+$ and $\mathrm{d}J_-$ are not total differentials, and therefore J_+ and J_- have no physical (or mathematical) meaning.

10.3 Rarefaction Waves

We now analyse the case where the pressure is suddenly dropped in an isentropic process, e.g. after the high-power laser is switched off and the ablation pressure drops. Another interesting case is after the laser-induced high-pressure wave has reached the back of a target and at the interface

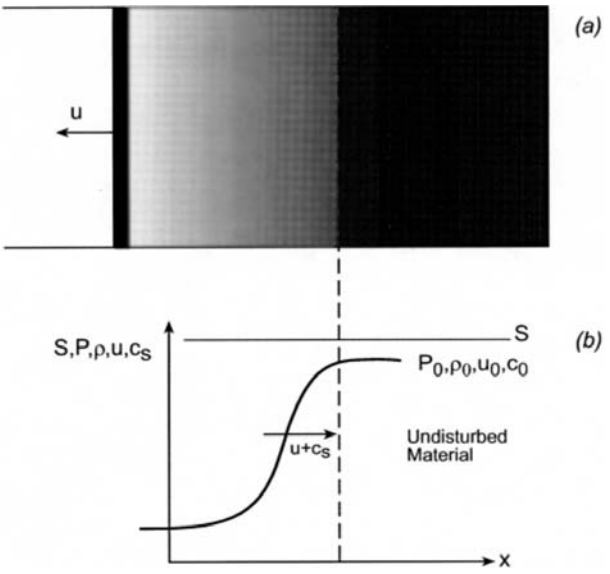

Figure 10.2. A forward moving rarefaction wave. The propagation velocity of the rarefaction wave at each point is $u + c_s$.

with the vacuum there is a sudden drop in pressure. In these cases, if one follows the variation in time for a given fluid element, one gets

$$\frac{D\rho}{Dt} < 0, \qquad \frac{DP}{Dt} < 0, \qquad \frac{D}{Dt} \equiv \frac{\partial}{\partial t} + u\frac{\partial}{\partial x}. \tag{10.24}$$

We consider the behaviour of a gas caused by a receding piston (figure 10.2a) in order to visualize the phenomenon of a rarefaction wave. In this figure the piston is moving in the $-x$ direction so that the gas is continually rarefied as it flows (in the $-x$ direction). The disturbance, called a rarefaction wave, is moving forward, in the $+x$ direction. One can consider the rarefaction wave to be represented by a sequence of jumps $\mathrm{d}\rho$, $\mathrm{d}P$, $\mathrm{d}u$, etc., so that we can use the Riemann invariant in order to solve the problem. The forward rarefaction wave moves into an undisturbed material defined by pressure P_0, density ρ_0, flow u_0 and the speed of sound c_{s_0}. Using (10.23) we get

$$u - u_0 = \int_{P_0}^{P} \frac{\mathrm{d}P}{\rho c_s} = \int_{\rho_0}^{\rho} \frac{c_s\,\mathrm{d}\rho}{\rho} \quad \text{rarefaction moving in } +x \text{ direction}$$

$$u - u_0 = -\int_{P_0}^{P} \frac{\mathrm{d}P}{\rho c_s} = -\int_{\rho_0}^{\rho} \frac{c_s\,\mathrm{d}\rho}{\rho} \quad \text{rarefaction moving in } -x \text{ direction.} \tag{10.25}$$

As an example we calculate some physical quantities for a rarefaction wave in an ideal gas. Since in a rarefaction wave the entropy is constant, one has the

following relation between the pressure, the density and the speed of sound (see equations (10.15) and (10.16)):

$$\frac{P}{P_0} = \left(\frac{\rho}{\rho_0}\right)^{\gamma}, \qquad \frac{c_s}{c_{s_0}} = \left(\frac{\rho}{\rho_0}\right)^{(\gamma-1)/2}. \tag{10.26}$$

Substituting (10.26) into (10.25) and doing the integral, one gets

$$u - u_0 = \int_{\rho_0}^{\rho} \frac{c_s \, d\rho}{\rho} = \int_{c_{s_0}}^{c_s} \frac{2 \, dc_s}{(\gamma - 1)} = \frac{2}{(\gamma - 1)}(c_s - c_{s_0})$$

$$\Rightarrow c_s = c_{s_0} + \tfrac{1}{2}(\gamma - 1)(u - u_0). \tag{10.27}$$

In this example the piston is moving in the $-x$ direction and at the gas–piston interface, and the gas velocity is the same as the piston velocity which has a negative value. The absolute value of the negative gas flow velocity is limited since the speed of sound is positive, i.e.

$$c_{s_0} + \tfrac{1}{2}(\gamma - 1)(u - u_0) \geq 0 \Rightarrow \frac{2c_{s_0}}{(\gamma - 1)} \geq -u + u_0 \geq -u = |u|. \tag{10.28}$$

From equation (10.27) it is evident that the speed of sound is decreased since u is negative. This implies, according to equations (10.26), that the density and the pressure are decreasing, as expressed mathematically in (10.24) and shown schematically in figure 10.2(b).

10.4 Shock Waves

The development of singularities, in the form of shock waves, in a wave profile due to the nonlinear nature of the conservation equations (10.1) has already been discussed by B. Riemann, W. J. M. Rankine and H. Hugoniot in the second half of the 19th century (1860–1890).

A shock wave is created in a medium that suffers a sudden impact (e.g. a collision between an accelerated foil and a target) or in a medium that releases large amounts of energy in a short period of time (e.g. high explosives). When a pulsed high-power laser interacts with matter, very hot plasma is created. This plasma exerts a high pressure on the surrounding material, leading to the formation of an intense shock wave, moving into the interior of the target. The momentum of the out-flowing plasma balances the momentum imparted to the compressed medium behind the shock front. The thermal pressure together with the momentum of the ablated material drives the shock wave.

It is convenient to analyse a shock wave by inspecting a gas compressed by a piston, moving into it with a constant velocity u. The medium has initially (the undisturbed medium) a density ρ_0 and a pressure P_0, and it is at rest, $u_0 = 0$. A shock wave starts moving into the material with a velocity

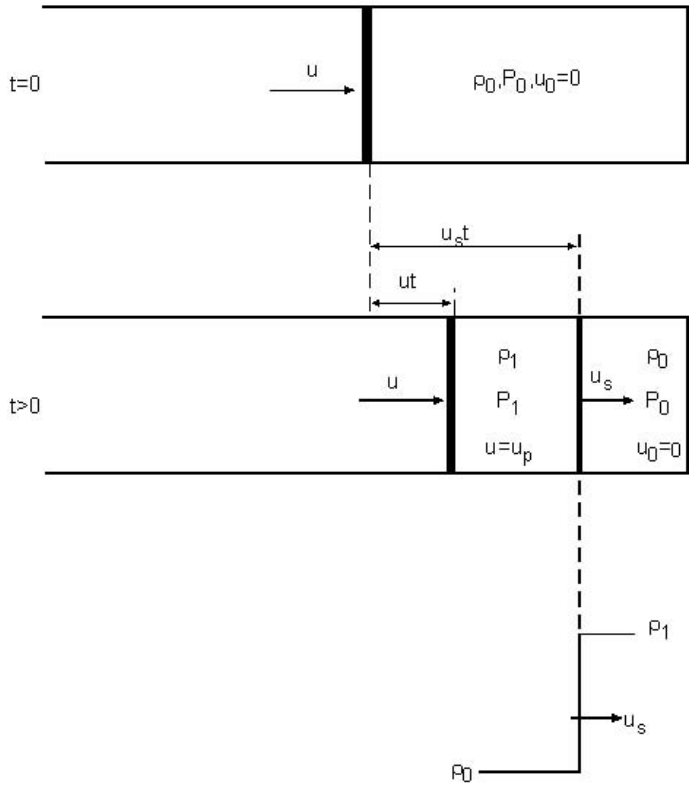

Figure 10.3. Shock wave created by the motion of a piston (the velocities are in the laboratory frame of reference). The subscript one denotes the unknown downstream variables, while the **upstream** variables (known initial condition) have a subscript zero.

denoted by u_s. Behind the shock front, the medium is compressed to a density ρ_1 and a pressure P_1. The gas flow velocity, denoted by u_p and usually called the particle velocity, in the compressed region is equal to the piston velocity, $u = u_p$. This case is schematically illustrated in figure 10.3. The initial mass before it is compressed, $\rho_0 A u_s t$ (A is the cross-sectional area of the tube), equals the mass after compression, $\rho_1 A(u_s - u_p t)$, implying the mass conservation law:

$$\rho_0 u_s = \rho_1 (u_s - u_p). \tag{10.29}$$

The momentum of the gas put into motion, $(\rho_0 A u_s t)u_p$, equals the impulse due to the pressure forces, $(P_1 - P_0)At$, yielding the momentum conservation law (or Newton's second law):

$$\rho_0 u_s u_p = P_1 - P_0. \tag{10.30}$$

The increase of internal energy E (energy/mass) and of kinetic energy per unit mass due to the piston-induced motion is $(\rho_0 A u_s t)(E_1 - E_0 + u_p^2/2)$. This increase in energy is supplied by the piston work, thus the energy conservation implies

$$\rho_0 u_s (E_1 - E_0 + \tfrac{1}{2} u_p^2) = P_1 u_p. \tag{10.31}$$

In the shock wave frame of reference, the undisturbed gas flows into the shock discontinuity with a velocity $v_0 = -u_s$ and leaves this discontinuity with a velocity $v_1 = -(u_s - u_p)$:

$$v_0 = -u_s, \qquad v_1 = -(u_s - u_p). \tag{10.32}$$

Substituting (10.32) into (10.29), (10.30) and (10.31), one gets the conservation laws of mass, momentum and energy, as seen from the shock-wave-front frame of reference:

$$\textbf{shock wave frame} \begin{cases} \rho_1 v_1 = \rho_0 v_0 \\ P_1 + \rho_1 v_1^2 = P_0 + \rho_0 v_0^2 \\ E_1 + \dfrac{P_1}{\rho_1} + \dfrac{v_1^2}{2} = E_0 + \dfrac{P_0}{\rho_0} + \dfrac{v_0^2}{2}. \end{cases} \tag{10.33}$$

These equations can be obtained more rigorously from the fluid equation (10.1) by integrating these equations over the shock wave layer. Assuming that the thickness of the shock wave front tends to zero, then for two points x_0 and x_1 lying on both sides of the shock discontinuity, one can write

$$\lim_{x_1 \to x_0} \int_{x_0}^{x_1} \frac{\partial}{\partial t} [\cdots] \, \mathrm{d}x = 0, \qquad \lim_{x_1 \to x_0} \int_{x_0}^{x_1} \frac{\partial}{\partial x} [\cdots] \, \mathrm{d}x = [\cdots]_{x_1} - [\cdots]_{x_0} \tag{10.34}$$

where $[\cdots]$ represent the different terms of equations (10.1). The procedure described in (10.34) yields the **jump conditions** in the shock wave frame of reference, as given by equations (10.33).

The jump conditions in the laboratory frame of reference are given in (10.29), (10.30) and (10.31) for a fluid initially at rest. In the more general case, the material is set in motion before the arrival of the shock wave (for example, by another shock wave). If the initial flow velocity is $u_0 \neq 0$, then the conservation laws (mass, momentum and energy) in the laboratory frame of reference (see figure 10.3) can be written

$$\textbf{laboratory frame} \begin{cases} \rho_0 (u_s - u_0) = \rho_1 (u_s - u_p) \\ \rho_0 (u_s - u_0)(u_p - u_0) = P_1 - P_0 \\ \rho_0 (u_s - u_0)(E_1 - E_0 + \tfrac{1}{2} u_p^2 - \tfrac{1}{2} u_0^2) = P_1 u_p - P_0 u_0. \end{cases} \tag{10.35}$$

Equations (10.34) or (10.35) are occasionally called the Rankine–Hugoniot relations. The Hugoniot relations are used to determine the state of the compressed solid behind the shock front. Assuming that the initial state is well defined and the quantities E_0, u_0, P_0 and ρ_0 are known, one has five unknowns E_1, u_p, P_1, ρ_1 and u_s with three equations (10.35). Usually the shock-wave velocity is measured experimentally, and if the equation of state is known (in this case one has four equations), $E = E(P, \rho)$, then the quantities of the compressed state can be calculated. If the equation of state is not known, then one has to measure experimentally two quantities of the shocked material, for example u_s and u_p, in order to solve the problem.

From the first two equations of (10.33) and using (10.32), the following general relations can be written:

$$\begin{aligned} &\frac{v_0}{v_1} = \frac{\rho_1}{\rho_0} \equiv \frac{V_0}{V_1}, \qquad V \equiv \frac{1}{\rho} \\ &v_0 = V_0 \left(\frac{P_1 - P_0}{V_0 - V_1} \right)^{1/2} = |u_s| \\ &v_1 = V_1 \left(\frac{P_1 - P_0}{V_0 - V_1} \right)^{1/2} \\ &v_0 - v_1 = [(P_1 - P_0)(V_0 - V_1)]^{1/2} = |u_p|. \end{aligned} \tag{10.36}$$

Substituting v_0 and v_1 from these relations into the third relation of (10.33), one gets

$$E_1(V_1, P_1) - E_0(V_0, P_0) = \tfrac{1}{2}(P_1 + P_0)(V_0 - V_1). \tag{10.37}$$

The thermodynamic relation $E(V, P)$ is the equation of state of the material under consideration, and assuming knowledge of this function, then equation (10.37), yields a graph (the notation of P_1 is changed to P_H and V_1 is V):

$$P_H = P_H(V; V_0, P_0). \tag{10.38}$$

This curve is known in literature as the Hugoniot curve. The Hugoniot curve, shown schematically in figure 10.4(a), is a two-parameter (V_0, P_0) family of curves, so that for each initial condition (V_0, P_0) there is a different curve. The Hugoniot curve is not a thermodynamic function, it does not show the pressure–volume (or density) trajectory of a shock wave development, but it is a plot of all possible final shocked (compressed) states for a given initial state (V_0, P_0). For example, the Hugoniot curve is different from the isentropic curves of the pressure $P_S(V, S)$, which describe the thermodynamic trajectory of pressure–volume (or density) for any given entropy S. In figure 10.4(a) two isentropes and one isotherm are also plotted schematically. It is interesting to note that for a given final pressure the compression is higher for an isentrope relative to the Hugoniot, and the isothermal compression is the highest.

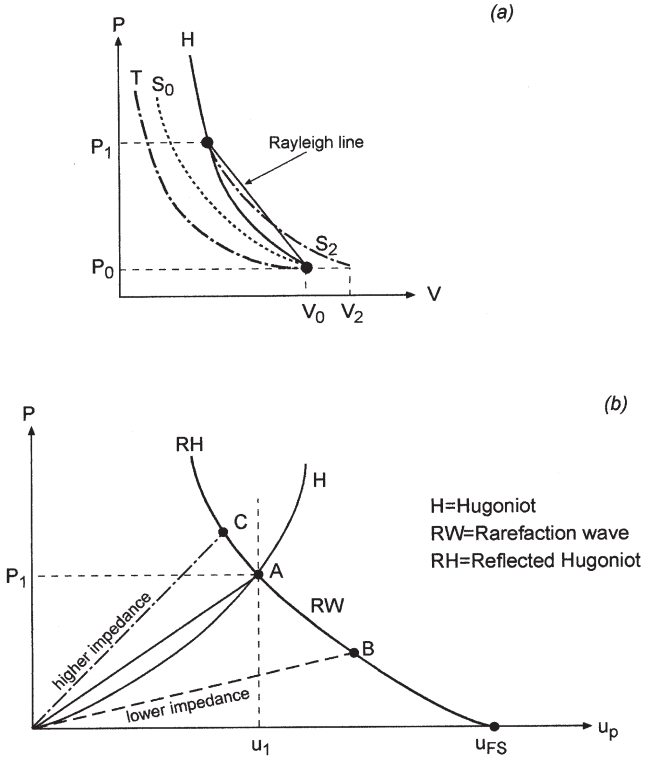

Figure 10.4. (a) The Hugoniot P–V curve, denoted by H, an isentrope S_0 and an isotherm, denoted by T, both starting like the Hugoniot at V_0, and an isentrope S_2 starting at the final shock pressure P_1. (b) The Hugoniot P–u_p curve. RW is the release wave (rarefaction wave), while RH is the reflected Hugoniot.

It is useful to consider the shock wave relations for an ideal gas with constant specific heats. In this case the equations of state are

$$E = C_V T = \frac{PV}{\gamma - 1}, \qquad S = C_V \ln(PV^\gamma) \tag{10.39}$$

where γ is defined in (10.15). Substituting (10.39) into (10.37), the Hugoniot curve for an ideal gas equation of state is obtained:

$$\frac{P_1}{P_0} = \frac{(\gamma+1)V_0 - (\gamma-1)V_1}{(\gamma+1)V_1 - (\gamma-1)V_0}. \tag{10.40}$$

From this equation it follows that the compression ratio $\rho_1/\rho_0 = V_0/V_1$ cannot increase above a certain value determined by γ. The pressure in the shocked ideal gas tends to infinity for the maximum possible compression,

given by

$$\frac{P_1}{P_0} \to \infty \Rightarrow \left(\frac{\rho_1}{\rho_0}\right)_{\max} = \left(\frac{V_0}{V_1}\right)_{\max} = \frac{\gamma+1}{\gamma-1}. \tag{10.41}$$

For example, the maximum compression caused by a planar shock wave in a medium with $\gamma = \frac{5}{3}$ is $4\rho_0$.

Using equation (10.16), for the speed of sound c_s, and equation (10.40), both for the ideal equation of state fluid, one obtains from (10.36):

$$\begin{aligned} M_0^2 &\equiv \left(\frac{u_s}{c_{s_0}}\right)^2 = \left(\frac{v_0}{c_{s_0}}\right)^2 = \frac{1}{2\gamma}\left[(\gamma-1) + (\gamma+1)\frac{P_1}{P_0}\right] > 1 \\ M_1^2 &\equiv \left(\frac{v_1}{c_{s_1}}\right)^2 = \frac{1}{2\gamma}\left[(\gamma-1) + (\gamma+1)\frac{P_0}{P_1}\right] < 1. \end{aligned} \tag{10.42}$$

The ratio M of the flow velocity to the sound velocity is known as the **Mach number**. In the limit of a weak shock wave, defined by $P_1 \approx P_0$, one has $M_1 \approx M_0 \approx 1$. However, equations (10.42) yield in general $M_1 < 1$ and $M_0 > 1$. The meaning of these relations is that in the shock frame of reference, the fluid flows into the shock front at a **supersonic velocity** ($M_0 > 1$) and flows out at a **subsonic velocity** ($M_1 < 1$). In the laboratory frame of reference, one has the well-known result that the shock wave propagates at a supersonic speed (with respect to the undisturbed medium), and at a subsonic speed with respect to the compressed material behind the shock. Although this phenomenon has been proven here for an ideal gas equation of state, this result is true for any medium, independent of the equation of state (Landau and Lifshitz 1987).

In a shock wave the entropy always increases. For example, in an ideal gas, equations (10.39) and (10.40) give the increase in entropy during a shock wave process:

$$\begin{aligned} S_1 - S_0 &= C_v \ln\left(\frac{P_1 V_1^\gamma}{P_0 V_0^\gamma}\right) \\ &= \left[\frac{P_0 V_0}{(\gamma-1)T_0}\right] \ln\left\{\left(\frac{P_1}{P_0}\right)\left[\frac{(\gamma-1)(P_1/P_0)+(\gamma+1)}{(\gamma+1)(P_1/P_0)+(\gamma-1)}\right]^\gamma\right\} > 0. \end{aligned} \tag{10.43}$$

The increase in entropy indicates that a shock wave is not a reversible process, but a dissipative phenomenon. The entropy jump of a medium compressed by shock wave increases with the strength of the shock wave (defined by the ratio P_1/P_0). The larger P_1/P_0, the larger is $S_1 - S_0 = \Delta S$. The value of ΔS is determined by the conservation laws (mass, momentum and energy) and by the equation of state. However, the mechanism of this change is described by viscosity and thermal conductivity (Zeldovich and Raizer 1966), not discussed in this book.

So far we have discussed a one-dimensional, steady-state shock wave passing through a gas or a fluid medium, with a thermal equilibrium ahead of and behind the shock wave front. When a shock wave is created in a solid material, one has to take into account the elastic–plastic properties of the target (Asay and Shahinpoor 1993). For shock waves with a pressure larger than 20 kbar, all the material strength properties are negligible and the solid target may be considered a liquid. Since we are interested in high pressures, larger than 20 kbar, the fluid jump equations (10.33) and (10.35) are relevant.

It was found experimentally (McQueen 1991) that for many solid materials, initially at rest, the following linear relation between the shock velocity u_s and the particle velocity u_p is valid to a very good approximation:

$$u_s = c_0 + \alpha u_p \tag{10.44}$$

where c_0 and α are constants. c_0 is the bulk sound speed at standard conditions. In table 10.1 the experimental values of c_0 and α are given (Steinberg 1996) for some elements that fit equation (10.44). ρ_0 is the initial density of the elements (with an atomic number Z). Equation (10.44) is occasionally called the (Hugoniot) equation of state.

Table 10.1. The experimental fit to $u_s = c_0 + \alpha u_p$ on the Hugoniot curve. u_s is the shock wave velocity, u_p is the particle flow velocity and ρ_0 is the initial density of the element with an atomic number Z.

	Element	Z	ρ_0 (g/cm^3)	c_0 (cm/μs)	α
Li	Lithium	3	0.534	0.477	1.066
Be	Beryllium (S200)	4	1.85	0.800	1.124
Mg	Magnesium	12	1.78	0.452	1.242
Al	Aluminium (6061-T6)	13	2.703	0.524	1.40
V	Vanadium	23	6.10	0.5077	1.201
Ni	Nickel	28	8.90	0.465	1.445
Cu	Copper	29	8.93	0.394	1.489
Zn	Zinc	30	7.139	0.303	1.55
Nb	Niobium	41	8.59	0.444	1.207
Mo	Molybdenum	42	10.2	0.5143	1.255
Ag	Silver	47	10.49	0.327	1.55
Cd	Cadmium	48	8.639	0.248	1.64
Sn	Tin	50	7.287	0.259	1.49
Ta	Tantalum	73	16.69	0.341	1.2
W	Tungsten	74	19.3	0.403	1.237
Pt	Platinum	78	21.44	0.364	1.54
Au	Gold	79	19.3	0.308	1.56
Th	Thorium	90	11.7	0.213	1.278
U	Uranium	92	19.05	0.248	1.53

It is convenient to describe the Hugoniot curve in the pressure–particle speed space, $P - u_p$. In particular, for the (10.44) equation of state, the Hugoniot is a parabola in this space (see figure 10.4(b)). When the shock wave reaches the back surface of the solid target, the free surface starts moving (into the vacuum or the surrounding atmosphere) with a velocity u_{FS} and a release wave, in the form of a rarefaction wave, is backscattered into the medium. Note that if the target is positioned in vacuum, then the pressure of the back surface (denoted in the literature as the **free surface**) is zero, a boundary value fixed by the vacuum. If an atmosphere surrounds the target, then a shock wave will run into this atmosphere. In our analysis we do not consider this effect and take $P = 0$ at the free surface. This approximation is justified for analysing the high-pressure shocked targets that are considered here.

If the target A is bounded by another solid target B (see figure 10.5(a)), then a shock wave passes from A into B and a wave is backscattered (into A). The **impedances** $Z = \rho_0 u_s$ of A and B are responsible for the character of this reflected wave. If $Z_A > Z_B$ then a rarefaction wave is backscattered (into A), while in the $Z_A < Z_B$ case a shock wave is backscattered at the interface between A and B. Note that in both cases a shock wave goes through (into medium B). These possibilities are shown schematically in figure 10.4(b). The main laser beam creates a shock wave. The Hugoniot of A is denoted by H, and point A describes the pressure and particle flow velocity of the shock wave (just) before reaching the interface between the targets. If $Z_A > Z_B$ then the lower impedance line (the line $P = Zu_p$) meets the rarefaction wave (RW) curve at point B, while point C describes the case $Z_A < Z_B$ (a higher impedance) where at the interface a shock wave is backscattered. The final pressure and final flow velocity (just) after the wave passes the interface is determined by point C for the higher impedance ($Z_B > Z_A$) and by point B for the lower impedance ($Z_B < Z_A$). This latter case is shown in detail in figure 10.5(b).

If the impedances of A and B are not very different, **impedance matching**, then to a very good approximation the RW curve in figure 10.5(b) and RH–RW curve in figure 10.4 are the mirror reflection (with respect to the vertical line at $u_1 = \text{constant}$) of the Hugoniot H curve. In this case, from figure 10.5(b), one has

$$\begin{aligned} Z &\equiv \rho_0 u_s \\ P_1 &= Z_A u_1 = \rho_{0A} u_{sA} u_1 \\ u_{sA} &= c_{0A} + \alpha_A u_1 \\ P_2 &= Z_B u_2 \\ \tan\theta = \frac{u_2 - u_1}{P_1 - P_2} &= \frac{u_1}{P_1} \Rightarrow \frac{P_2}{P_1} = \frac{2Z_B}{Z_A + Z_B} \approx \frac{2\rho_{0B} c_{0B}}{\rho_{0A} c_{0A} + \rho_{0B} c_{0B}} \end{aligned} \tag{10.45}$$

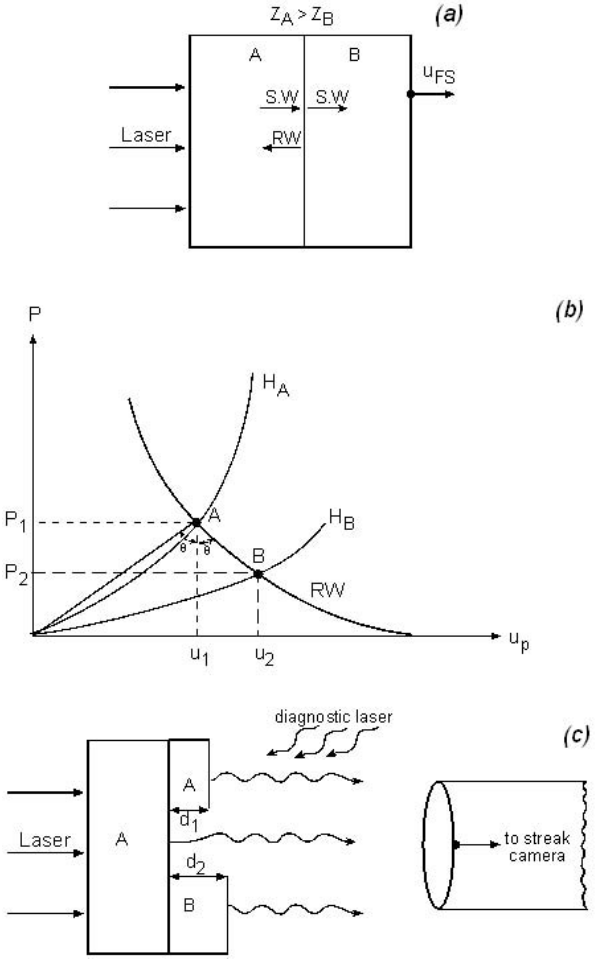

Figure 10.5. (a) A laser induces a shock wave into target A with impedance smaller than target B. A rarefaction wave (RW) is reflected at the interface A–B. (b) The Hugoniot curves H_A and H_B for shock waves in A and B. The reflected rarefaction wave (RW) is also shown. (c) A schematic setup for an impedance-matching experiment.

where the last approximate equality is for weak shock waves. A similar result is obtained in the case with higher impedance ($Z_B > Z_A$).

In figure 10.5(c) a schematic setup of an impedance-matching experiment is given. When a shock wave reaches the interface with the vacuum (or the surrounding atmosphere), it irradiates according to the temperature of the shock wave heated medium. Note that it is a very difficult task to calculate the temperature of the shocked medium from the measurement of this irradiation. If the shock wave temperature is high (about a few thousand

K), then the self-illumination may be large enough to be detected by a streak camera (or other appropriate optical collecting device with a fast information recording). If the detecting devices are not sensitive to the self-illumination then the measurement of a reflected (diagnostic) laser may be more useful, since the reflection changes significantly with the arrival of the shock wave. The shock wave velocities in A and B are directly measured in this way by recording the signal of shock breakthrough from the base of A, and from the external surfaces of the stepped targets. The time t_1 that the shock wave travels through a distance d_1 in A, and the time t_2 that the shock wave travels through a distance d_2 in B, yields the appropriate shock velocities in both targets. Since the initial densities are known, the impedances of A and B are directly measured. The equation of state of A is known and the Hugoniot of A is plotted. Using equations (10.45), P_1 is known (from the measurement of u_{sA}) and P_2 is directly calculated from the measurements of both impedances. In this way, the difficult task of measuring two parameters in the unknown (equation of state) material B is avoided.

As has been shown, it is quite straightforward to measure the shock-wave velocity (assuming that the shock wave is steady, one-dimensional and the measurement device is very accurate). It is also possible to measure indirectly the particle flow velocity by measuring the free-surface velocity. Accurate optical devices, called VISAR (velocity interferometer system for any reflector) and ORVIS (optically recording velocity interferometer system) (practically, very fast recording 'radar' devices in the optical spectrum), have been developed to measure accurately the free-surface velocity. After the shock wave reaches the back surface of the target, a release wave with the characteristics of a rarefaction wave is backscattered into the target. Since this isentrope is almost the mirror image of the Hugoniot (see figure 10.4(b); the 'mirror' is at $u_1 =$ constant), one gets

$$u_1 = \tfrac{1}{2} u_{FS}. \tag{10.46}$$

Therefore, the measurement of u_s and u_{FS} determines all the parameters in the compressed medium (assuming the initial state is accurately known).

The highest laser-induced pressures, $\sim 10^8$–10^9 atm, have been obtained during the collision of a target with an accelerating foil. This acceleration was achieved by laser-produced plasma, or by x-rays from a cavity produced by laser–plasma interactions. It is therefore now shown how the pressure is calculated in a planar collision between a flyer and a target.

The flyer has a known (i.e. measured experimentally) initial velocity before impact, u_f. The initial state before collision is for the target (B), $u_p = 0$ and $P = 0$, while for the flyer (A), $u_p = u_f$ and $P = 0$. Upon impact, a shock wave moves forward into B, and another shock wave goes into the flyer in the opposite direction. The pressure and the particle velocity are continuous at the target–flyer interface. Therefore, the particle velocity of the target changes from zero to u, while the particle velocity in the flyer

changes from u_f to u. Moreover, the pressure in the flyer plate A equals the pressure in the target plate B, and if the equations of state are known and given by (10.44), and the second equation of (10.35) is used to calculate the pressure, one gets

$$P_H = \rho_{0B} u(c_{0B} + \alpha_B u) = \rho_{0A}(u_f - u)[c_{0A} + \alpha_A(u_f - u)]. \tag{10.47}$$

This is a quadratic equation in u, with the following solution:

$$\begin{aligned} u &= \frac{-b - \sqrt{b^2 - 4ac}}{2a} \\ a &\equiv \rho_{0A}\alpha_A - \rho_{0B}\alpha_B \\ b &\equiv -(c_{0A}\rho_{0A} + c_{0B}\rho_{0B} + 2\rho_{0A}\alpha_A u_f) \\ c &\equiv (c_{0A}\rho_{0A} + \rho_{0A}\alpha_A u_f)u_f. \end{aligned} \tag{10.48}$$

Once the flow velocity is known, it is substituted into (10.47) to derive the pressure. If the equation of state of the target is not known, then it is necessary to measure the shock-wave velocity u_{sB} as explained above. In this case, the pressure equality in the flyer and the target yields

$$P_H = \rho_{0B} u_{sB} u = \rho_{0A}[c_{0A} + \alpha_A(u_f - u)](u_f - u). \tag{10.49}$$

Note that in this equation u_{sB} is known. The solution of this equation is

$$\begin{aligned} u &= u_f + w - \left[w^2 + \left(\frac{\rho_{0B}}{\rho_{0A}\alpha_A}\right)u_{sB}u_f\right]^{1/2} \\ w &\equiv \frac{1}{2\alpha_A}\left(c_{0A} + \frac{\rho_{0B}u_{sB}}{\rho_{0A}}\right). \end{aligned} \tag{10.50}$$

In these types of experiment it is occasionally convenient to measure the free-surface velocity of the target and to also study the dynamic strength of materials, as explained in section 10.8.

We end this section with a short comment on shock-wave stability. One can see from (10.26) that different disturbances of density travel with different velocities, so that the larger the density ρ the faster the wave travels. Therefore, an initial profile $\rho(x, 0)$ becomes distorted with time. This is true not only for the density but also for the pressure $P(x, 0)$, for the flow velocity $u(x, 0)$, etc. In this way a smooth function of these parameters will steepen in time due to the nonlinear effect of the wave propagation (higher amplitudes move faster). Therefore, a compression wave is steepened into a shock wave because in most solids the sound velocity is an increasing function of the pressure. In the laboratory frame of reference, the speed of a disturbance is the sum of the flow velocity and the sound velocity $(c_s + u)$. Therefore, a higher-pressure disturbance will catch up with the lower-pressure disturbance, causing a sharpening profile of the wave. In

reality there are also dissipative mechanisms such as viscosity and thermal transport. Therefore, the sharpening profile mechanism can only increase until the dissipative forces become significant, and they begin to cancel out the effect of increasing sound speed with pressure. When the sum of these opposing mechanisms cancels out, the wave profile no longer changes in time and it becomes a steady shock wave.

The dissipative phenomena are nonlinear functions of the strain rate (strain is the relative distortion of a solid $\sim \mathrm{d}l/l$ and the strain rate is the time derivative of the strain). Therefore, for very fast laser-induced phenomena, the rise-time of a shock wave is very small and it can be significantly less than 1 ns.

As already stated above, a disturbance moves at the speed $c_\mathrm{s} + u$ in a compression wave. Therefore, a disturbance behind the shock front cannot be slower than the shock velocity, because in this case it will not be able to catch the wave front, and the shock would decay (i.e. the shock is unstable to small disturbances behind it). Similarly, a small compressive disturbance ahead of the shock must move slower than the shock front in order not to create another shock wave. Thus the conditions for a stable shock wave can be summarized as

$$\frac{\mathrm{d}c_\mathrm{s}}{\mathrm{d}P} > 0, \qquad c_\mathrm{s} + u_\mathrm{p} \geq u_\mathrm{s}, \qquad u_\mathrm{s} > c_{\mathrm{s}_0}. \tag{10.51}$$

The first of these equations states that the speed of sound increases with increasing pressure. The second equation describes the fact that the shock wave is subsonic (Mach number smaller than one) with respect to the shocked medium. The last equation of (10.51) is the well-known phenomenon that a shock wave is supersonic (Mach number larger than one) with respect to the unshocked medium. Using equations (10.13) and (10.36),

$$c_\mathrm{s} = \sqrt{\left(\frac{\partial P}{\partial \rho}\right)_\mathrm{S}} = V\sqrt{-\left(\frac{\partial P}{\partial V}\right)_\mathrm{S}}, \qquad u_\mathrm{s} = V_0\sqrt{\frac{P_1 - P_0}{V_0 - V_1}} \tag{10.52}$$

one gets from the last of equations (10.51) the following shock stability criterion:

$$\frac{P_1 - P_0}{V_0 - V_1} > -\left(\frac{\partial P}{\partial V}\right)_{\mathrm{S},0}. \tag{10.53}$$

This inequality states that the slope of the Rayleigh line (figure 10.4(a)) is larger than the slope of the isentrope at the initial state. Similarly, one can show that the second of equations (10.51) yields the criterion that the Hugoniot at the final state (denoted by 1) must be steeper than the Rayleigh line:

$$\frac{P_1 - P_0}{V_0 - V_1} \leq -\left(\frac{\mathrm{d}P}{\mathrm{d}V}\right)_{\mathrm{H},1}. \tag{10.54}$$

It is important to point out that these criteria are not always satisfied. For example, the speed of sound of fused silica decreases with pressure in a domain of low pressures, so that in this case the shock wave is not stable. Moreover, in the regime of phase transitions (solid–solid due to change in symmetry or solid–liquid), the shock wave can split into two or more shock waves. However, in these cases the stability criteria can be satisfied for each individual shock wave.

10.5 Shock Waves in the Presence of Magnetic Fields

Megagauss magnetic fields are easily achieved in laser plasma interactions (see chapter 8). These large magnetic fields, which are created in the corona, have a large pressure:

$$P_{\mathrm{B}}(\mathrm{Mbar}) \approx 0.04[B(\mathrm{Mgauss})]^2. \tag{10.55}$$

The magnetic fields do not penetrate into the solid on the time scale of the shock-wave transient. Since we are mainly interested in the high pressures (∼Mbar) achieved in the solid target, it appears that the high magnetic fields in the corona do not play any important role. However, if shock waves are created in the corona, or between the critical surface and the ablation surface, then the magnetic pressure, the thermal pressure and the shock-wave pressure might be comparable:

$$\beta \equiv \frac{P_{\mathrm{T}}}{P_{\mathrm{B}}} \approx 4\left(\frac{n_{\mathrm{e}}}{10^{20}\,\mathrm{cm}^{-3}}\right)\left(\frac{T_{\mathrm{e}}}{\mathrm{keV}}\right)\left(\frac{\mathrm{MGauss}}{B}\right)^2. \tag{10.56}$$

For small magnetic fields, $\beta \gg 1$, the magnetic fields are not important. However, for $\beta \approx 1$ or smaller, a state that is possible to achieve with a few megagauss magnetic field, the creation of a shock wave requires the analysis of shock waves in the presence of a magnetic field.

Since the magnetic field has in general a direction not parallel to the shock-wave velocity, it is necessary to consider the directions normal and parallel to the shock-wave front (the discontinuity). In the following the shock-wave (front) frame of reference is used. The normal components to the shock front are denoted by a subscript 'n', while the tangential components (i.e. the components parallel to the shock-wave surface) have the subscript 't'. As in the previous section, the variables before the shock (upstream) and after the shock (downstream) get the subscript 0 and 1 respectively. In this case one has the following jump equations (across the shock-wave discontinuity):

(a) mass conservation;
(b) momentum conservation normal and parallel to the shock front;

(c) energy conservation; and
(d) continuity (over the shock front) of the normal magnetic induction field B_n and of the parallel electric field E_t.

We use the magneto-hydrodynamic equations (in Gaussian units) to derive conservation laws in the form

$$\begin{aligned}
&\frac{\partial}{\partial t}[X] + \nabla \cdot \Gamma = 0 \\
&\lim_{V \to 0} \iiint_V \frac{\partial}{\partial t}[X] = 0 \Rightarrow \iiint_V \nabla \cdot \Gamma \, \mathrm{d}V = \oiint_A \boldsymbol{\Gamma} \cdot \mathbf{n} \, \mathrm{d}A = 0 \\
&\Rightarrow (\boldsymbol{\Gamma}_0 - \boldsymbol{\Gamma}_1) \cdot \mathbf{n} \equiv [\boldsymbol{\Gamma} \cdot \mathbf{n}] = 0
\end{aligned} \tag{10.57}$$

where V is a volume containing the shock wave singularity, A is the area enclosing the volume V (Gauss divergence theorem) and $\mathbf{n}$ is a unit vector perpendicular to the area under consideration. The area A is taken as a small box surrounding the shock front, where the thickness of the box tends to zero (therefore V goes to zero). In this case only the two faces with directions $\mathbf{n}$ and $-\mathbf{n}$, on either side of the shock front, contribute to the integral. Γ_0 and Γ_1 are the values of Γ on either side of the shock surface (the discontinuity). The end result of the class of equations (10.57) is the jump conditions across the shock wave front.

The Maxwell equation, which describes the fact that there are no magnetic poles, gives immediately a jump condition:

$$\nabla \cdot \mathbf{B} = 0 \Rightarrow (\mathbf{B}_0 - \mathbf{B}_1) \cdot \mathbf{n} = 0 \Rightarrow B_{0n} = B_{1n}. \tag{10.58}$$

Another Maxwell equation, together with the zero Lorentz force ($\mathbf{E} + \mathbf{v} \times \mathbf{B}/c = 0$), yields

$$\begin{aligned}
&\frac{\partial \mathbf{B}}{\partial t} = -c\nabla \times \mathbf{E} = \nabla \times (\mathbf{v} \times \mathbf{B}) = \nabla \cdot (\mathbf{B}\mathbf{v} - \mathbf{v}\mathbf{B}) = 0 \\
&\Rightarrow [(\mathbf{B}\mathbf{v} - \mathbf{v}\mathbf{B}) \cdot \mathbf{n}] = 0 \Rightarrow [B_t v_n - v_t B_n] = 0 \\
&\Rightarrow B_{0t} v_{0n} - v_{0t} B_{0n} = B_{1t} v_{1n} - v_{1t} B_{1n}
\end{aligned} \tag{10.59}$$

a new jump condition. This equation is the continuity of the tangential component of the electric field (note that $\mathbf{E} = \mathbf{B} \times \mathbf{v}/c$ in the present approximation).

The mass conservation is directly derived in the usual form:

$$\frac{\partial \rho}{\partial t} + \nabla \cdot (\rho \mathbf{v}) = 0 \Rightarrow [\rho \mathbf{v} \cdot \mathbf{n}] = 0 \Rightarrow \rho_0 v_{0n} = \rho_1 v_{1n}. \tag{10.60}$$

The momentum jump conditions (two equations) are obtained from the following combined momentum and Maxwell equations:

$$\begin{aligned} &\rho\frac{\mathrm{d}\mathbf{v}}{\mathrm{d}t} = -\nabla P + \frac{1}{c}\mathbf{J}\times\mathbf{B} \\ &\nabla\times\mathbf{B} = \frac{4\pi}{c}\mathbf{J} \\ &\Rightarrow \rho\frac{\mathrm{d}\mathbf{v}}{\mathrm{d}t} = -\nabla P + \frac{1}{4\pi}(-\tfrac{1}{2}\nabla B^2 + \mathbf{B}\cdot\nabla\mathbf{B}). \end{aligned} \tag{10.61}$$

The following identities, derived by using (10.58) and (10.60),

$$\nabla\cdot(\rho\mathbf{v}\mathbf{v}) = \rho\mathbf{v}\cdot\nabla\mathbf{v} - \mathbf{v}\frac{\partial\rho}{\partial t} = \rho\frac{\mathrm{d}\mathbf{v}}{\mathrm{d}t} - \frac{\partial}{\partial t}(\rho\mathbf{v}), \qquad \nabla\cdot(\mathbf{B}\mathbf{B}) = \mathbf{B}\cdot\nabla\mathbf{B} \tag{10.62}$$

are used in (10.61) in order to derive the momentum equation in the following form (it is more convenient to use these identities in this new equation in order to derive (10.61)):

$$\frac{\partial}{\partial t}(\rho\mathbf{v}) + \nabla\cdot\left[\rho\mathbf{v}\mathbf{v} - \frac{1}{4\pi}\mathbf{B}\mathbf{B} + \mathbf{I}\left(P + \frac{B^2}{8\pi}\right)\right] = 0 \tag{10.63}$$

where $\mathbf{v}\mathbf{v}$ and $\mathbf{B}\mathbf{B}$ are tensors of the second rank (i.e. matrices with components $v_i v_j$, $B_i B_j$, $i,j = 1,2,3$ in Cartesian coordinates), and $\mathbf{I}$ is the unit matrix (with components $\delta_{ij} = 1$ for $i = j$ and zero for $i \neq j$, so that $\nabla\cdot(\mathbf{I}\psi) = \nabla\psi$). This equation is in the desired form of (10.57), yielding the momentum jump conditions:

$$\begin{aligned} &\left[\left(\rho\mathbf{v}\mathbf{v} - \frac{1}{4\pi}\mathbf{B}\mathbf{B}\right)\cdot\mathbf{n}\right] + \left[\left(P + \frac{B^2}{8\pi}\right)\mathbf{n}\right] = 0 \\ &\Rightarrow \begin{cases} \left[\rho v_\mathrm{n}^2 + P + \dfrac{B_\mathrm{t}^2}{8\pi}\right] = 0 \\ \left[\rho v_\mathrm{t} v_\mathrm{n} - \dfrac{B_\mathrm{t} B_\mathrm{n}}{4\pi}\right] = 0. \end{cases} \end{aligned} \tag{10.64}$$

The two relations were obtained for the normal and tangential components (the jump condition for B_n has been used in the first relation).

The last equation to be obtained is the energy relation. In section 3.1 (equation 3.19), the following energy conservation is derived:

$$\frac{\partial}{\partial t}\left[\rho\left(\varepsilon + \frac{1}{2}v^2\right)\right] + \nabla\cdot\left[\rho\mathbf{v}\left(\varepsilon + \frac{P}{\rho} + \frac{1}{2}v^2\right)\right] - \mathbf{E}\cdot\mathbf{J} = 0 \tag{10.65}$$

where the transport term and the external forces are neglected. The problem now is to write the Joule heating term in a format required by a conservation law (like the first two terms of (10.65)). Using $\mathbf{E}$ and $\mathbf{J}$ from equations (10.59)

and (10.61). the Joule heating term can be written in the following way:

$$-\mathbf{E}\cdot\mathbf{J}=\frac{1}{4\pi}[(\mathbf{v}\times\mathbf{B})\cdot\nabla\times\mathbf{B}]$$
$$=\frac{1}{4\pi}[\mathbf{B}\cdot(\mathbf{v}\cdot\nabla)\mathbf{B}-\mathbf{v}\cdot(\mathbf{B}\cdot\nabla)\mathbf{B}]. \tag{10.66}$$

Using (10.59) (multiplied by **B**) and vector algebra, the following identity is derived:

$$\frac{\mathrm{d}}{\mathrm{d}t}\left(\frac{B^2}{2}\right)=B^2\nabla\cdot\mathbf{v}-\mathbf{B}(\mathbf{B}\cdot\nabla)\mathbf{v}$$
$$\Rightarrow\frac{\partial}{\partial t}\left(\frac{B^2}{2}\right)=B^2\nabla\cdot\mathbf{v}-\mathbf{B}(\mathbf{B}\cdot\nabla)\mathbf{v}-\mathbf{v}\cdot\nabla\left(\frac{B^2}{2}\right). \tag{10.67}$$

Using the identity (10.67) in (10.66), we can write

$$-\mathbf{E}\cdot\mathbf{J}=\frac{\partial}{\partial t}\left(\frac{B^2}{8\pi}\right)+\frac{1}{4\pi}\nabla\cdot[B^2\mathbf{v}-(\mathbf{B}\cdot\mathbf{v})\mathbf{B}]. \tag{10.68}$$

We confirm this identity by an alternative derivation. The energy conservation of the electromagnetic field in a medium is (see Appendix A, equations (A.10) and (A.14), in Gaussian units)

$$\frac{\partial}{\partial t}\left(\frac{B^2}{8\pi}\right)+\nabla\cdot\left(\frac{c}{4\pi}\mathbf{E}\times\mathbf{B}\right)=-\mathbf{J}\cdot\mathbf{E} \tag{10.69}$$

where the $\mathbf{D}\cdot\mathbf{E}=\varepsilon E^2$ (ε is the dielectric coefficient) is neglected. This equation together with

$$\mathbf{E}+\frac{\mathbf{v}\times\mathbf{B}}{c}=0,\qquad(\mathbf{B}\times\mathbf{v})\times\mathbf{B}=B^2\mathbf{v}-(\mathbf{B}\cdot\mathbf{v})\mathbf{B} \tag{10.70}$$

yields equation (10.68).

Substituting (10.68) into (10.65) gives the energy equation in the desired form for the jump condition across the shock wave:

$$\frac{\partial}{\partial t}\left[\rho\left(\varepsilon+\frac{1}{2}v^2+\frac{B^2}{8\pi}\right)\right]+\nabla\cdot\left\{\rho\mathbf{v}\left(\varepsilon+\frac{P}{\rho}+\frac{1}{2}v^2\right)+\frac{1}{4\pi}[B^2\mathbf{v}-(\mathbf{B}\cdot\mathbf{v})\mathbf{B}]\right\}=0$$
$$\Rightarrow\left[\left\{\rho\mathbf{v}\left(\varepsilon+\frac{P}{\rho}+\frac{1}{2}v^2\right)+\frac{1}{4\pi}[B^2\mathbf{v}-(\mathbf{B}\cdot\mathbf{v})\mathbf{B}]\right\}\cdot\mathbf{n}\right]=0$$
$$\Rightarrow\left[\varepsilon+\frac{P}{\rho}+\frac{1}{2}(v_\mathrm{n}^2+v_\mathrm{t}^2)+\frac{B_\mathrm{t}^2}{4\pi\rho}-\frac{v_\mathrm{t}B_\mathrm{t}B_\mathrm{n}}{4\pi}\right]=0. \tag{10.71}$$

In summary, the jump equations derived above are: (10.58), (10.59), (10.60), (10.64) and (10.71). The shock-wave surface is at an angle θ relative to the magnetic induction **B**, i.e. the shock front propagates with an angle θ relative

to the magnetic induction **B**. The variables before the shock and after the shock in the shock-wave frame of reference are

$$\begin{aligned} &\textbf{upstream}: \quad \rho_0, P_0, E_0; v_{0\mathrm{n}}, v_{0\mathrm{t}}; B_{0\mathrm{n}} = B\cos\theta, B_{0\mathrm{t}} = B\sin\theta \\ &\textbf{downstream}: \quad \rho_1, P_1, E_1; v_{1\mathrm{n}}, v_{1\mathrm{t}}; B_{1\mathrm{n}}, B_{1\mathrm{t}} \end{aligned} \tag{10.72}$$

where $\rho = 1/V$ is the density, P is the pressure, E is the internal energy connected to the entropy and the density by the thermodynamic relation

$$\mathrm{d}E = T\,\mathrm{d}S - P\,\mathrm{d}V \tag{10.73}$$

and **v** is the medium velocity in the shock-wave frame of reference. As shown above, one has the following six jump conditions (Thompson 1962, Shkarofsky *et al.* 1966):

$$\begin{aligned} &(1) \quad \rho_0 v_{0\mathrm{n}} = \rho_1 v_{1\mathrm{n}} \\ &(2) \quad P_0 + \rho_0 v_{0\mathrm{n}}^2 + \frac{B_{0\mathrm{t}}^2}{8\pi} = P_1 + \rho_1 v_{1\mathrm{n}}^2 + \frac{B_{1\mathrm{t}}^2}{8\pi} \\ &(3) \quad \rho_0 v_{0\mathrm{n}} v_{0\mathrm{t}} - \frac{B_{0\mathrm{n}} B_{0\mathrm{t}}}{4\pi} = \rho_1 v_{1\mathrm{n}} v_{1\mathrm{t}} - \frac{B_{1\mathrm{n}} B_{1\mathrm{t}}}{4\pi} \\ &(4) \quad \frac{1}{2}(v_{0\mathrm{n}}^2 + v_{0\mathrm{t}}^2) + \varepsilon_0 + \frac{P_0}{\rho_0} + \frac{v_{0\mathrm{n}} B_{0\mathrm{t}}^2 - v_{0\mathrm{t}} B_{0\mathrm{n}} B_{0\mathrm{t}}}{4\pi\rho_0 v_{0\mathrm{n}}} \\ &\qquad = \frac{1}{2}(v_{1\mathrm{n}}^2 + v_{1\mathrm{t}}^2) + \varepsilon_1 + \frac{P_1}{\rho_1} + \frac{v_{1\mathrm{n}} B_{1\mathrm{t}}^2 - v_{1\mathrm{t}} B_{1\mathrm{n}} B_{1\mathrm{t}}}{4\pi\rho_1 v_{1\mathrm{n}}} \\ &(5) \quad B_{0\mathrm{n}} = B_{1\mathrm{n}} \\ &(6) \quad v_{0\mathrm{n}} B_{0\mathrm{t}} - v_{0\mathrm{t}} B_{0\mathrm{n}} = v_{1\mathrm{n}} B_{1\mathrm{t}} - v_{1\mathrm{t}} B_{1\mathrm{n}}. \end{aligned} \tag{10.74}$$

The first equation is the mass conservation, the second and third equations are the momentum conservation and the fourth equation is the energy conservation. The fifth equation is the continuity of the normal component of **B**, while the last equation is the continuity of the tangential component of the electric field (note that $\mathbf{E} = \mathbf{B} \times \mathbf{v}/c$). Assuming that the initial conditions are known, one has in (10.74) six equations with seven unknowns (see the downstream variables of (10.72)). Therefore, it is necessary to measure one parameter. For example, if the plasma satisfies the ideal gas equation of state, then a measurement of the temperature behind the shock wave gives the pressure.

10.6 The Study of High-Pressure Physics

The problems with laser-induced shock waves are the small size of the targets ($\sim$100 μm), the short laser pulse duration ($\sim$1 ns), the poor spatial uniformity

of a coherent electromagnetic pulse (the laser), and therefore the non-uniformity of the created pressure. All these difficulties have been addressed in the literature and the subject of laser-induced shock wave research has been developed significantly. The critical problems are summarized below and their possible solutions are discussed.

(a) The planarity (one-dimensional) of the shock wave regardless of the laser irradiance non-uniformity.
(b) Steady shock wave during the diagnostic measurements in spite of the laser short-pulse duration.
(c) Well-known initial conditions of the shocked medium. This is required to control (i.e. to avoid) the fast electron and x-ray preheating.
(d) Good accuracy ($\sim$1%) of the measurements.

The planarity of the shock wave is achieved by using optical smoothing techniques (Lehmberg and Obenschain 1983, Kato *et al*. 1984, Skupsky *et al*. 1989, Koenig *et al*. 1994, Batani *et al*. 1996). With these devices the laser is deposited in the target uniformly, within $\sim$2% of energy deposition. For example (Lehmberg and Obenschain 1983), one technique denoted as 'induced spatial incoherence' (ISI) consists of breaking each laser beam into a large number of beamlets by reflecting the beam off a large number of echelons. The size of each beamlet is chosen in such a way that its diffraction-limited spot size is about the target diameter. All of the beamlets are independently focused and overlapped on the target. Another technique (Kato *et al*. 1984) divides the beam into many elements that have a random phase shift. This is achieved by passing the laser beam through a phase plate with a randomly phase-shifted mask.

The focal spot of the laser beam on target has to be much larger than the target thickness in order to achieve a one-dimensional steady-state shock wave. In figure 10.6 one can see a schematic profile of a planar target with thickness d, irradiated by a laser with a focal spot area $= \pi R_L^2$. A lateral rarefaction wave enters the shocked area and reduces the pressure and density of the shocked area. This effect distorts the one-dimensional character of the wave, since the shock front is bent in such a way that for very large distances ($\gg d$) the shock-wave front becomes spherical. The rarefaction wave propagates toward the symmetry axis with the speed of sound c_s (in the shock-compressed area), which is larger than the shock-wave velocity u_s. Therefore, the good (i.e. undisturbed by the rarefaction wave) one-dimensional shock area $= \pi R_g^2$ is limited by

$$R_g = R_L - \left(\frac{d}{u_s}\right) c_s = R_L - d\tan\theta \leq R_L - d, \qquad A \equiv \pi R_L^2 \geq 10d^2 \quad (10.75)$$

where d/u_s is the time that the shock wave reaches the back surface. Therefore, in order to have a one-dimensional shock wave one requires that $R_g \approx d$, implying an $R_L \approx 2d$ at least, so that the laser focal spot area

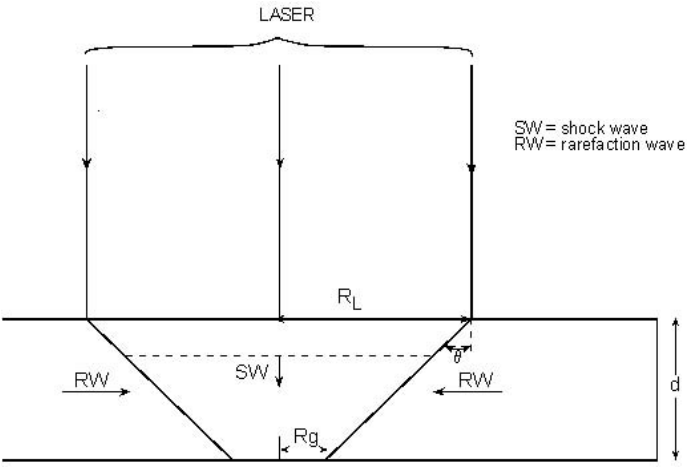

Figure 10.6. A planar target profile irradiated by a laser (the target thickness is d). The one-dimensional spot area $= \pi R_g^2$ (g for 'good') in comparison with the laser irradiation area $= \pi R_L^2$. RW and SW stand for rarefaction wave and shock wave respectively.

$A \approx 10d^2$. This constraint implies very large laser focal spots for thick targets.

The second constraint requires a steady shock wave, i.e. the shock velocity has to be constant as it traverses the target. In figure 10.7 one can see a schematic x–t (space–time) diagram of a laser-induced shock wave. A rarefaction wave (RW), initiated at a time $\Delta t \approx \tau_L$ (the laser pulse duration) after the end of the laser pulse, follows a shock wave (SW) into the target. It is necessary that the rarefaction wave does not overtake the shock wave at position $x = d$ (the back surface) during the measurement of the shock-wave velocity, implying $\tau_L > d/u_s$. For strong shocks, the shock velocity is of the order of the square root of the pressure (see (10.36) or (10.52)), therefore

$$\tau_L > \frac{d}{u_s} \propto \frac{d}{\sqrt{P}}. \tag{10.76}$$

Hot electrons can appear during the laser–plasma interaction (see section 9.6), causing preheating of the target. This preheats the target before the shock wave arrives, therefore 'spoiling' the initial conditions for the high-pressure experiment. Since it is not easy to measure accurately the temperature of the target due to this preheating, it is necessary to avoid preheating. By using shorter wavelengths (0.5 μm or less), the fast electron preheat is significantly reduced. It is therefore required that the target thickness d is larger than the hot electron mean free path λ_e. Using the scaling law for

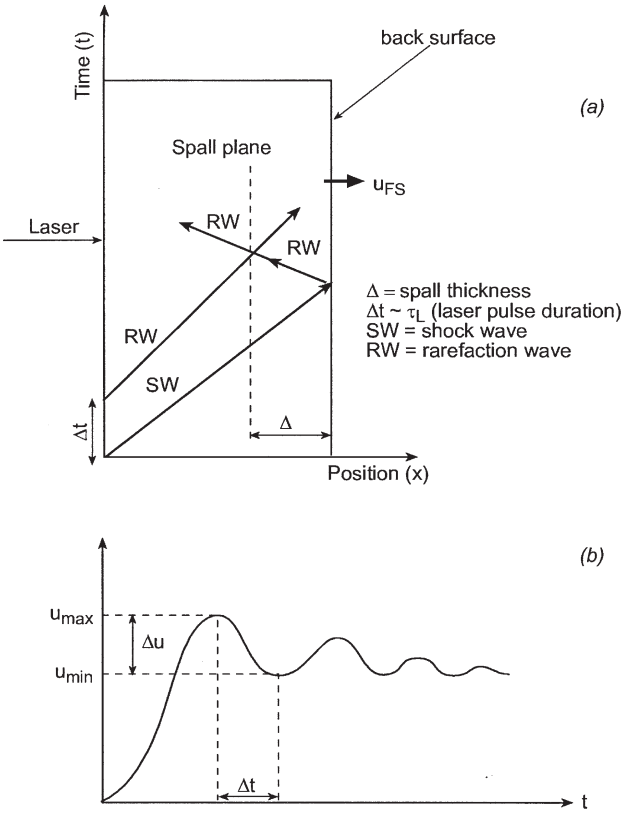

Figure 10.7. (a) *x–t* (space–time) diagram of a laser-induced shock wave. A rarefaction (RW), initiated after the end of the laser pulse, follows a shock wave (SW) into the target. After the shock wave reaches the back surface a rarefaction is reflected. A spall may be created at the intersection of the two rarefaction waves. (b) Typical free-surface velocity when a spall is created.

the hot electron temperature T_h (see equation (9.94)), one has

$$d \gg \lambda_e \propto T_h^2 \propto (I_L \lambda_L)^{0.6}. \tag{10.77}$$

Taking into account all of the constraints given by the relations (10.75), (10.76) and (10.77), and using the experimental scaling law

$$P \propto I_L^{0.8} \tag{10.78}$$

one gets the scaling of the laser energy W_L

$$W_L = I_L A \tau_L \propto I_L^{2.4} \propto P^3. \tag{10.79}$$

Therefore, in order to increase the one-dimensional shock-wave pressure by a factor two, it is necessary to increase the laser energy by an order of magnitude.

A more elegant and efficient way to overcome this problem is to accelerate a thin foil. The foil absorbs the laser, plasma is created (ablation) and the foil is accelerated as in a rocket. In this way, the flyer stores kinetic energy from the laser during the laser pulse duration (the acceleration time) and delivers it, in a shorter time during the collision with a target, in the form of thermal energy. The flyer is effectively shielding the target so that the target initial conditions are not changed by fast electrons or by laser-produced x-rays. For these reasons the laser-driven flyer can achieve much higher pressures on impact than the directly-laser-induced shock wave (Fabbro *et al.* 1986, Cauble *et al.* 1994).

The accuracy of measurements in the study of laser-induced high-pressure physics require diagnostics with a time resolution better than 100 ps, and occasionally better than 1 ps, and a spatial resolution of the order of few microns. The accurate measurements of shock-wave speed and particle-flow velocity are usually obtained with optical devices, including streak camera (Veeser *et al.* 1979, Cottet *et al.* 1985, Ng *et al.* 1987, Evans *et al.* 1996) and velocity interferometers (Moshe *et al.* 1996, Celliers *et al.* 1998).

10.7 Studies of Equations of State

The phenomena of shock-wave propagation through condensed matter are strongly related to the physics of the equations of state (Altshuler 1965, Eliezer *et al.* 1986, Eliezer and Ricci 1991, Bushman *et al.* 1993, Eliezer *et al.* 2002). Atoms in a solid state are attracted to each other at large distances and repel each other at short distances. At zero temperature and zero pressure the equilibrium is obtained at a specific volume V_{0c}, reached at the minimum of the (potential) energy. The atoms can be separated to a large distance by supplying the binding energy (also known as the cohesion energy) of the order of a few eV/atom, while compressing a condensed matter requires energy to overcome the repulsive forces.

Small pressures, of the order of 10^2 atm, can compress a gas to a few times its initial density. However, the compression of a metal by only 10% requires an external pressure (static or shock wave) of the order of 10^5 atm. This is evident from the values of the **compressibility** at standard conditions $\sim 10^{-6}$ atm^{-1}, where κ is defined by

$$\kappa_S = -\frac{1}{V}\left(\frac{\partial V}{\partial P}\right)_S. \tag{10.80}$$

Note that the **bulk modulus** B_S is the inverse of the compressibility, $B_S = 1/\kappa_S$.

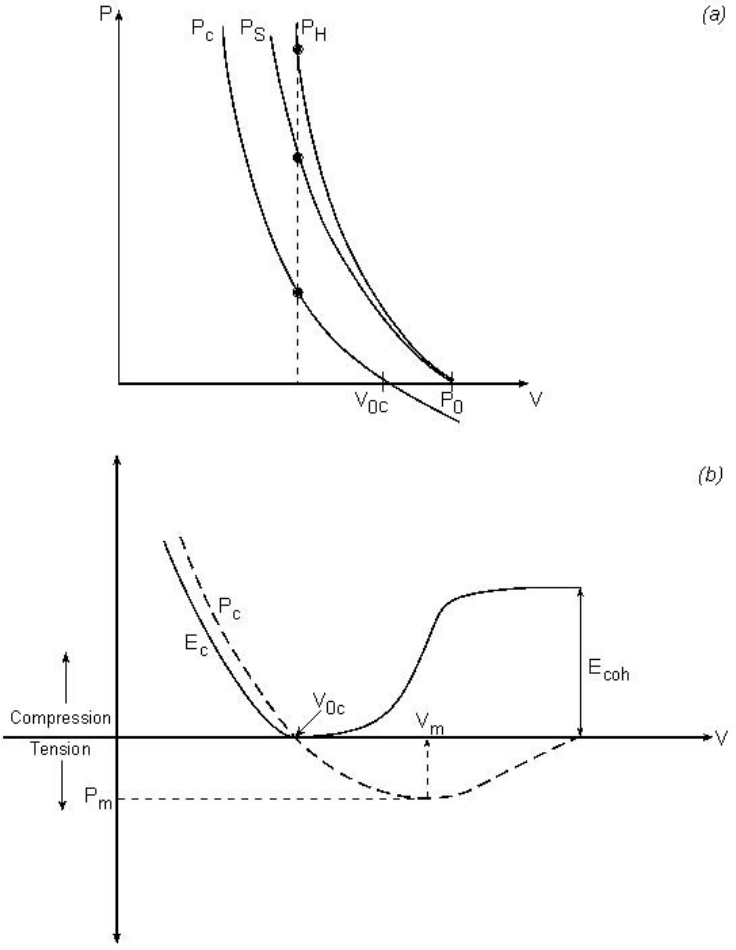

Figure 10.8. (a) The cold pressure P_c, the Hugoniot pressure P_H and the isentrope P_s. The initial conditions for P_H and P_s are $V_0 = 1/\rho_0$, $P_0 = 0$ and T_0 (room temperature). (b) A schematic presentation is given for the cold energy E_c and pressure P_c. The cohesion energy E_{coh} and the minimum pressure P_m, both at $T = 0$, are also shown. For $P_c > 0$ the solid is compressed, while for $P_c < 0$ a tension is applied on the medium.

The P–V diagram in figure 10.8(a) describes the Hugoniot curve $P_H(V)$ for the initial conditions V_0, T_0 and $P_0 = 0$. Note that the atmospheric pressure is negligibly small in comparison with the shock-wave pressures under consideration, so that $P_0 = 0$ or 1 atm are equivalent initial conditions for shock-wave experiments in solids. The difference in figure 10.8(a) at any particular value of V between the cold pressure P_c and the Hugoniot pressure P_H, is equal to the thermal pressure P_T that is caused by the shock wave.

Since P_T is positive, the cold pressure at room temperature is negative, $P_c(V_0) < 0$. In this figure the isentrope P_S that passes through the beginning of the Hugoniot is also shown, so that the mutual positions of P_H, P_S and P_c are illustrated.

The pressure and the internal energy of a material can be divided into two contributions:

(a) The temperature-independent term caused by the interaction forces between the atoms of the material. The appropriate pressure P_c and energy E_c are defined as 'cold pressure' and 'cold energy' respectively.
(b) The thermal term is usually divided into two parts: one part describes the motion of the atoms in the lattice, while the second part is due to the electron thermal motion.

P_a and E_a denote the thermal lattice pressure and energy respectively, and the appropriate electron contributions are P_e and E_e. Therefore, the equation of state is usually written in the following form:

$$\begin{aligned} P(V,T) &= P_c(V) + P_T(V,T) \\ P_T(V,T) &= P_a(V,T) + P_e(V,T) \\ E(V,T) &= E_c(V) + E_T(V,T) \\ E_T(V,T) &= E_a(V,T) + E_e(V,T). \end{aligned} \tag{10.81}$$

The thermodynamic relation relates the cold pressure and energy:

$$E_c(V) = -\int_{V_{0c}}^{V} P_c(V)\,\mathrm{d}V. \tag{10.82}$$

As usual, the potential energy is fixed up to a constant, and this constant has been chosen in such a way that $E_c(V_{0c}) = 0$. Note that $P_c(V_{0c}) = 0$ is the definition of V_{0c}. It has been found that to a good approximation, near the Hugoniot curve, the lattice thermal energy and pressure are related through the Gruneisen equation of state, and the energy is described by the Debye solid-state theory:

$$E_a = C_V(T - T_0) + E_0, \qquad P_a(V,T) = \frac{\gamma_a(V)}{V} E_a \tag{10.83}$$

where γ_a is the Gruneisen coefficient (assumed to be a function of V), C_V is the lattice specific heat at constant volume, T_0 is the initial temperature in the shock wave experiment, usually the room temperature, and E_0 is the internal energy at T_0, defined by

$$E_0 = \int_0^{T_0} C_V(T)\,\mathrm{d}T. \tag{10.84}$$

At room temperature and for slightly lower and higher temperatures, the specific heat C_V has the Dulong–Petit value

$$\begin{aligned} C_V &= \frac{3R}{\langle A\rangle}\left[\frac{\text{erg}}{\text{g}\cdot\text{deg}}\right] \\ R &= 8.314\times 10^7\left[\frac{\text{erg}}{\text{mol}\cdot\text{deg}}\right] \\ \langle A\rangle &= \text{average atomic weight}\left[\frac{\text{g}}{\text{mol}}\right]. \end{aligned} \tag{10.85}$$

For example, $\langle A\rangle$ for aluminium and copper is 27 and 63.55 respectively.

Assuming for the electron thermal part an equation of state similar to the Gruneisen equation of state for the lattice, one has

$$P_e = \frac{\gamma_e}{V}E_e. \tag{10.86}$$

To the first approximation, the thermal electron energy is taken from the free electron model,

$$E_e = \tfrac{1}{2}\beta T^2 \tag{10.87}$$

and β is related to the specific volume V by the thermodynamic relation,

$$\left(\frac{\partial E}{\partial V}\right)_T = T\left(\frac{\partial P}{\partial T}\right)_V - P. \tag{10.88}$$

Substituting (10.86) and (10.87) into (10.88) yields

$$\begin{aligned} \frac{\partial\beta}{\partial V} = \frac{\gamma_e\beta}{V} &\Rightarrow \beta = \gamma_e \exp\left(\int_{V_0}^{V}\frac{\gamma_e\,\mathrm{d}V}{V}\right) \\ \beta &= \beta_0\left(\frac{V}{V_0}\right)^{1/2} \quad \text{for } \gamma_e = 0.5. \end{aligned} \tag{10.89}$$

The value of $\gamma_e = 0.5$ is a good approximation for many metals up to shock-wave data of a few megabars pressure.

Combining equations (10.81), (10.82), (10.83), (10.86) and (10.89), one gets

$$\begin{aligned} P &= P_c + \frac{\gamma_a}{V}[C_V(T-T_0)+E_0] + \frac{1}{4}\left(\frac{\beta_0}{V_0}\right)\left(\frac{V_0}{V}\right)^{1/2}T^2 \\ E &= -\int^V P_c\,\mathrm{d}V + C_V(T-T_0) + E_0 + \frac{\beta_0}{2}\left(\frac{V}{V_0}\right)^{1/2}T^2. \end{aligned} \tag{10.90}$$

The cold pressure can be described by a polynomial in $(V_{0c}/V)^{1/3}$ in such a way that it fits the experimental values of the bulk modulus, the derivative of the bulk modulus at zero pressure, the cohesion energy and the Thomas–Fermi model (or modified models) at very high compressions.

Although the equations of state described in equations (10.90) have 10 parameters, they do not describe phase transitions, such as solid to solid with different symmetry or melting and evaporation. In order to describe these phenomena, many more parameters based on theoretical models and experimental data are required.

As explained in section 10.4, in a shock-wave experiment one can measure the shock-wave velocity (u_s) and the particle velocity (u_p). It has also been attempted to measure the temperature associated with a shock wave; however, the experimental data so far are not very accurate.

The shock-wave velocity is directly measured in a stepped target (velocity = measured step length/measured time difference) using an optical streak camera. The particle velocity is more difficult to measure, and u_p is deduced, for example, from impedance-matching experiments (see section 10.4) or by the optical measuring of the free-surface (i.e. back surface) velocity. The measured equation of state is given in the form of the linear u_s–u_p equation (10.44). The velocity measurements should have an accuracy of about 1%, in order to give good accuracy (~10%) in other variables such as pressure, energy, etc. It is important to point out that the linear u_s–u_p relation (equation (10.44) and table 10.1), is not always correct for all solid elements.

Sometimes a higher polynomial in u_p is necessary to fit the experimental data. For example (Steinberg 1996),

$$\begin{aligned}
\textbf{hafnium}: \quad & u_s(\text{cm}/\mu\text{s}) = 0.298 + 1.448u_p - 3.852\left(\frac{u_p}{u_s}\right)u_p + 7.0\left(\frac{u_p}{u_s}\right)^2 u_p \\
\textbf{lead}: \quad & u_s(\text{cm}/\mu\text{s}) = 0.2006 + 1.429u_p + 0.8506\left(\frac{u_p}{u_s}\right)u_p - 1.64\left(\frac{u_p}{u_s}\right)^2 u_p \\
\textbf{titanium}: \quad & u_s(\text{cm}/\mu\text{s}) = 0.502 + 1.536u_p - 5.138\left(\frac{u_p}{u_s}\right)u_p + 10.82\left(\frac{u_p}{u_s}\right)^2 u_p.
\end{aligned} \tag{10.91}$$

In the following part of this section, it is shown how one can study the thermodynamic equations of state in the neighbourhood of the Hugoniot from the measurements of the shock velocity and the particle velocity. For simplicity, the further discussion assumes the linear u_s–u_p relation (equation (10.44)), valid for many metals.

It is convenient to define the parameter η related to the compression ρ/ρ_0, in such a way that $\eta = 0$ for no compression and $\eta = 1$ for an

infinite ρ/ρ_0:

$$\eta \equiv 1 - \frac{V}{V_0} = 1 - \frac{\rho_0}{\rho}. \tag{10.92}$$

Using equations (10.36) and (10.44), the particle velocity and the shock velocity can be presented in the following way:

$$\left.\begin{aligned} \frac{u_\mathrm{p}}{u_\mathrm{s}} &= \frac{V_0 - V}{V_0} = \eta \\ u_\mathrm{s} &= c_0 + \alpha u_\mathrm{p} \end{aligned}\right\} \Rightarrow \begin{cases} u_\mathrm{p} = \dfrac{\eta c_0}{1 - \alpha\eta} \\ u_\mathrm{s} = \dfrac{c_0}{1 - \alpha\eta} \end{cases}. \tag{10.93}$$

Substituting these results into the Hugoniot pressure, one gets P_H as a function of V (or η), the experimentally measured quantities c_0 and α, and the initial condition V_0:

$$P_\mathrm{H} = \rho_0 u_\mathrm{s} u_\mathrm{p} = \frac{\eta c_0^2}{V_0(1-\alpha\eta)^2} = \frac{c_0^2(V_0 - V)}{[V_0 - \alpha(V_0 - V)]^2}. \tag{10.94}$$

It is interesting to point out that from this equation the maximum possible compression is obtained for an infinite P_H, implying

$$\frac{\rho_\mathrm{max}}{\rho_0} = \frac{\alpha}{\alpha - 1}. \tag{10.95}$$

For example (see table 10.1), α of aluminium equals 1.4, implying that in a shock wave the compression ρ/ρ_0 is smaller than 2.5.

The derivative of this pressure with respect to the specific volume V is

$$\begin{aligned} P'_\mathrm{H} \equiv \left(\frac{\mathrm{d}P}{\mathrm{d}V}\right)_\mathrm{H} &= \frac{\mathrm{d}P_\mathrm{H}}{\mathrm{d}V} = -\left(\frac{c_0}{V_0}\right)^2 \frac{1 + \alpha\eta}{(1-\alpha\eta)^3} \\ &= -c_0^2 \left\{ \frac{V_0 + \alpha(V_0 - V)}{[V_0 - \alpha(V_0 - V)]^3} \right\}. \end{aligned} \tag{10.96}$$

Using this relation, the bulk modulus on the Hugoniot, B_H, is obtained:

$$B_\mathrm{H} = -V\left(\frac{\mathrm{d}P}{\mathrm{d}V}\right)_\mathrm{H} \tag{10.97}$$

and its derivative with respect to the pressure can also be derived:

$$\begin{aligned} \left(\frac{\mathrm{d}B_\mathrm{H}}{\mathrm{d}P}\right)_\mathrm{H} &= \left(\frac{\mathrm{d}B_\mathrm{H}}{\mathrm{d}V}\right)_\mathrm{H} \left(\frac{\mathrm{d}V}{\mathrm{d}P}\right)_\mathrm{H} \\ &= -\left[\left(\frac{\mathrm{d}P}{\mathrm{d}V}\right)_\mathrm{H} + V\left(\frac{\mathrm{d}^2P}{\mathrm{d}V^2}\right)_\mathrm{H}\right] \frac{1}{(\mathrm{d}P/\mathrm{d}V)_\mathrm{H}} \\ &= -\left[1 + \frac{V(\mathrm{d}^2P/\mathrm{d}V^2)_\mathrm{H}}{(\mathrm{d}P/\mathrm{d}V)_\mathrm{H}}\right]. \end{aligned} \tag{10.98}$$

Experimentally one measures the bulk modulus at constant entropy and its derivative at $V = V_0$, $P = P_0 = 0$ (the shock wave initial condition). For the Hugoniot pressure and the isentrope P_S starting at $V = V_0$, $P = P_0 = 0$, the following relations are valid:

$$\left(\frac{dP_H}{dV}\right)_{P_0,V_0} = \left(\frac{dP_S}{dV}\right)_{P_0,V_0}, \qquad \left(\frac{d^2P_H}{dV^2}\right)_{P_0,V_0} = \left(\frac{d^2P_S}{dV^2}\right)_{P_0,V_0}. \tag{10.99}$$

From equations (10.96), (10.97), (10.98) and (10.99), the following important relations are derived:

$$\begin{aligned} B_H(P_0, V_0) &= B_S(P_0, V_0) = \frac{c_0^2}{V_0} = \rho_0 c_0^2 \\ B'_H(P_0, V_0) &= B'_S(P_0, V_0) = 4\alpha - 1. \end{aligned} \tag{10.100}$$

From shock-wave data (equation of state), one knows c_0 and α and therefore the bulk modulus and its pressure derivative. The last two physical quantities, B_S and $dB_S/dP = B'_S$, are very important in calculating the cold pressure P_c and energy E_c. B_S, of the order of 1 Mbar, can also be measured in static experiments thanks to the technological advances in reaching high pressures (up to a few megabars). However, it is difficult to measure B'_S in static experiments to a good accuracy since this quantity measures the curvature of the P–V curve. On the other hand, the shock-wave experiments in this domain of pressure are easily and accurately performed.

We now calculate the speed of sound:

$$c_s = \sqrt{\left(\frac{\partial P}{\partial \rho}\right)_S} = V\sqrt{-\left(\frac{\partial P}{\partial V}\right)_S} \equiv V\sqrt{-\frac{dP_S(V)}{dV}}. \tag{10.101}$$

For this purpose one needs the isentrope pressure curve $P_S(V)$, which can be calculated from the knowledge of the Hugoniot pressure $P_H(V)$ using the (ion) Gruneisen equation of state. In order to do so, the electron thermal contribution P_e should be neglected. For most of the solid materials, $P_e \ll P_a$ for pressures less than a few hundred kilobars. For example, we demonstrate this for aluminium at a shock-wave pressure of 580 kbar. At this Hugoniot point, the compression is 1.40 and the temperature is 1480 K. Using the following experimental data at standard conditions

$$\begin{aligned} \textbf{aluminium}: \quad V_0^{-1} &= \rho_0 = 2.70\ [\mathrm{g/cm^3}] \\ C_V &= 8.96 \times 10^6\ [\mathrm{erg/(g \cdot deg)}] \\ B_S &= 1.36 \times 10^{12}\ [\mathrm{dyne/cm^2}] = 1.36\ \mathrm{Mbar} \\ E_0 &= 10^7\ [\mathrm{erg/g}] \\ \gamma_a &= 2.09 \\ \beta_0 &= 500\ [\mathrm{erg/(g \cdot deg^2)}] \end{aligned} \tag{10.102}$$

we get from the equations of state (10.90):

$$\textbf{aluminium}: \quad \frac{V_0}{V} = \frac{\rho}{\rho_0} = 1.40, \quad T_{\mathrm{H}} = 1480\,\mathrm{K}, \quad P_{\mathrm{H}} = 580\,\mathrm{kbar}$$
$$\Rightarrow P_{\mathrm{c}} = 495.6\,\mathrm{kbar}, \quad P_{\mathrm{a}} = 83.5\,\mathrm{kbar}, \quad P_{\mathrm{e}} = 0.9\,\mathrm{kbar}. \tag{10.103}$$

From this example one can see that even in a shock wave with 580 kbar of pressure in aluminium, the electronic thermal part contributes about 0.15% to the total pressure. Therefore, in the following analysis the electronic thermal part is neglected.

The Gruneisen equation of state (see (10.83)) can be written in the form

$$P(V, E) = P_{\mathrm{c}}(V) + \frac{\gamma_{\mathrm{a}}(V)}{V}[E - E_{\mathrm{c}}(V)]. \tag{10.104}$$

Substituting $P = P_{\mathrm{H}}$ in this equation and subtracting it from P, one gets

$$P - P_{\mathrm{H}} = \frac{\gamma_{\mathrm{a}}}{V}(E - E_{\mathrm{H}}). \tag{10.105}$$

For $P = P_{\mathrm{S}}$, the derivative of (10.105) yields (after using $\mathrm{d}E_{\mathrm{S}}/\mathrm{d}V = -P_{\mathrm{S}}$)

$$P_{\mathrm{S}} = -\frac{\mathrm{d}E_{\mathrm{H}}}{\mathrm{d}V} + (P_{\mathrm{H}} - P_{\mathrm{S}})\frac{d}{\mathrm{d}V}\left(\frac{V}{\gamma_{\mathrm{a}}}\right) + \frac{V}{\gamma_{\mathrm{a}}}\left(\frac{\mathrm{d}P_{\mathrm{H}}}{\mathrm{d}V} - \frac{\mathrm{d}P_{\mathrm{S}}}{\mathrm{d}V}\right). \tag{10.106}$$

Taking the derivative of the Hugoniot energy relation (10.37) gives

$$\frac{\mathrm{d}E_{\mathrm{H}}}{\mathrm{d}V} = \left(\frac{V_0 - V}{2}\right)\frac{\mathrm{d}P_{\mathrm{H}}}{\mathrm{d}V} - \left(\frac{P_0 + P_{\mathrm{H}}}{2}\right). \tag{10.107}$$

Substituting (10.107) into (10.106) yields

$$\frac{\mathrm{d}P_{\mathrm{S}}}{\mathrm{d}V} = \left[1 - \frac{\gamma_{\mathrm{a}}}{2V}(V_0 - V)\right]\frac{\mathrm{d}P_{\mathrm{H}}}{\mathrm{d}V} + \frac{\gamma_{\mathrm{a}}}{2V}(P_0 + P_{\mathrm{H}}) + \frac{\gamma_{\mathrm{a}}}{V}(P_{\mathrm{H}} - P_{\mathrm{S}})\frac{\mathrm{d}}{\mathrm{d}V}\left(\frac{V}{\gamma_{\mathrm{a}}}\right) - P_{\mathrm{S}}\left(\frac{\gamma_{\mathrm{a}}}{V}\right). \tag{10.108}$$

Using equations (10.101) and (10.108) and defining the sound speed on the Hugoniot points, i.e. c_{H} is equal to c_{S} for $P_{\mathrm{S}} = P_{\mathrm{H}}$, one gets

$$c_{\mathrm{H}}^2 = \left(\frac{\gamma_{\mathrm{a}}V}{2}\right)P_{\mathrm{H}} + \left[\left(\frac{\gamma_{\mathrm{a}}V}{2}\right)(V_0 - V) - V^2\right]\frac{\mathrm{d}P_{\mathrm{H}}}{\mathrm{d}V}$$
$$c_{\mathrm{S}}^2 = c_{\mathrm{H}}^2 + \gamma_{\mathrm{a}}V(P_{\mathrm{S}} - P_{\mathrm{H}})\left[1 + \frac{\mathrm{d}}{\mathrm{d}V}\left(\frac{V}{\gamma_{\mathrm{a}}}\right)\right]. \tag{10.109}$$

In the second equation of (10.109), the speed of sound c_{S} is along the release isentrope off the Hugoniot (i.e. an isentrope starting after the shock-wave point with pressure P_{H}). See curve S_2 in figure 10.4(a). It was

found experimentally that the Gruneisen coefficient satisfies the relation

$$\frac{\gamma_a(V)}{V} = \frac{\gamma_0}{V_0} = \text{const.} \tag{10.110}$$

Using this relation in (10.109) yields the approximate relation

$$c_S^2 \approx c_H^2 + \gamma_0 \left(\frac{V^2}{V_0}\right)(P_S - P_H). \tag{10.111}$$

Substituting into (10.109) the equations (10.93), (10.94) and (10.96), one gets the sound speed on the Hugoniot points as a function of measured quantities, $\eta = u_p/u_s$, c_0 and α:

$$c_H = c_0 \frac{1-\eta}{(1-\alpha\eta)^{3/2}} \sqrt{\frac{\gamma_0\eta}{2}}(1 + \alpha\eta - \gamma_0\alpha\eta^2)^{1/2}. \tag{10.112}$$

From equation (10.111), or more accurately from (10.109), the Gruneisen parameter may be determined if the Hugoniot pressure and the speed of sound are measured experimentally. By placing a transparent material coupled to the target under consideration, the rarefaction overtakes the shock wave and reduces significantly the shock pressure. By measuring this phenomenon, the change in light radiance caused by the decrease in the shock pressure, the speed of sound in the shocked material can be measured.

10.8 Studies of Dynamic Strength of Materials

Spall is a dynamic fracture of materials, extensively studied in ballistic research (Rosenberg *et al*. 1983, Bushman *et al*. 1993). The term spall, as used in shock wave research, is defined as planar separation of material, parallel to the wave front as a result of dynamic tension perpendicular to this plane. The reflection of a shock-wave pulse from the rear surface (the free surface) of a target causes the appearance of a rarefaction wave into the target. Tension (i.e. negative pressure) is induced within the target by the crossing of two opposite rarefaction waves, one coming from the front surface due to the fall of the input pressure and the second due to reflection of the shock wave from the back surface (see figure 10.7(a)). If the magnitude and duration of this tension are sufficient then internal rupture, called spall, occurs. In this section we point out that this type of research can also be done with laser beams (Gilath *et al*. 1988, Eliezer *et al*. 1990, Boustie and Cottet 1991, Fortov *et al*. 1991, De Resseguier and Cottet 1995, Eliaz *et al*. 2000, Moshe *et al*. 2000).

Spall in ductile materials is controlled by localized plastic deformation around small voids that grow and coalesce to form the spall plane. In very fast phenomena and very high tension, as in high-power pulsed laser

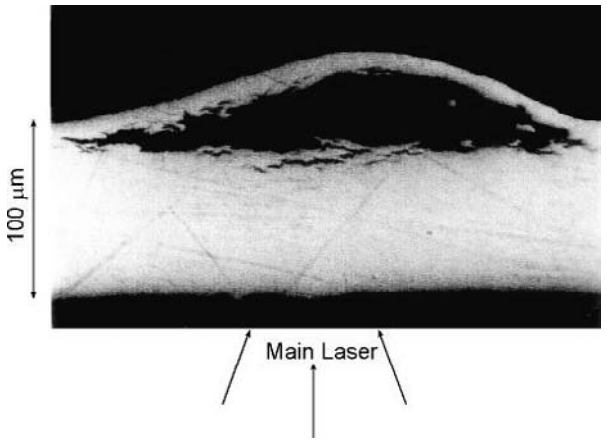

Figure 10.9. Cross section in an Al 6061 target after the spall creation.

interaction with a target, new voids are created due to fluctuations and also contribute to the spall formation. Spall in brittle materials takes place by dynamic crack propagation without large-scale plastic deformation. In this section we do not describe the physics of dynamic failure (Grady 1988, Dekel *et al*. 1998).

In figure 10.9 a cross section with a spall of an aluminium (6061) target, 100 μm thick, is shown. A laser-created shock wave in the aluminium target induced the spall. This typical metallurgical cross section was taken after the experiment was finished. The strain ε that has been formed at the spall area is defined by

$$\varepsilon(1\mathrm{D}) = \frac{\Delta l}{l}, \qquad \varepsilon(3\mathrm{D}) = \frac{\Delta V}{V} = -\frac{\Delta \rho}{\rho} \tag{10.113}$$

where Δl is the difference between the final and original lengths of the target in one dimension and l is the original length, while in three dimensions the strain is defined by the relative change in the volume. From the cross section of figure 10.9 one can measure directly the dynamic strain. One of the important parameters, for the different models describing the spall creation, is the strain rate

$$\dot{\varepsilon} = \frac{\mathrm{d}\varepsilon}{\mathrm{d}t}. \tag{10.114}$$

High-power short-pulse lasers have been used to create strain rates as high as $5 \times 10^8\ \mathrm{s}^{-1}$. When the shock wave reaches the back surface of the solid target, bounded by the vacuum (or the atmosphere), the free surface develops a velocity $u_{\mathrm{FS}}(t)$. This velocity is given by the sum of the particle flow velocity u_{p} and the rarefaction wave velocity U_{r}. The material velocity increase U_{r} is given by the Riemann integral along an isentrope from some point on the

Hugoniot (pressure P_H) to zero pressure (see equations (10.25) and (10.101)):

$$u_{FS} = u_p + U_r, \qquad U_r = \int_0^{P_H} \frac{dP}{\rho c_s} = \int_{\rho_0}^{\rho} \frac{c_s \, d\rho}{\rho} = \int_{V(P_H)}^{V(P=0)} \left(-\frac{dP_S}{dV} \right)^{1/2} dV. \tag{10.115}$$

The derivative dP_S/dV is given in equation (10.108), so that knowledge of P_S gives the value of U_r. Layers of the target adjacent to the free surface go into motion under the influence of the shock-wave transition from V_0, $P_0 = 0$ to V, P_H, and subsequent isentropic expansion in the reflected rarefaction wave from P_H, V to $P_0 = 0$, V_2 (see figure 10.4(a)), where $V_2 > V_0$. Although these two processes are not the same, it turns out that for $u_p \ll u_s$ one has, to a very good approximation,

$$u_p \approx U_r \Rightarrow u_{FS} \approx 2u_p. \tag{10.116}$$

It was found experimentally, for many materials, that this relation is very good (within 1%) up to shock-wave pressures of about 1 Mbar. Therefore, from the free-surface velocity measurements, one can calculate the particle flow velocity of the shock-wave compressed material. This free-surface velocity, together with the experimental measurement of the shock-wave velocity, might serve as the two necessary quantities, out of five (P_H, $V = 1/\rho$, E_H, u_s, u_p), to fix a point on the Hugoniot.

A typical free-surface velocity measurement, in the case of the creation of a spall, is given in figure 10.7(b). u_{max} (related to u_p in the above discussion) in this figure is the maximum free-surface velocity. At later times the free-surface velocity decreases to u_{min} until a second shock arrives from the spall, 'the new free surface'. When a rarefaction wave reaches the internal rupture of the target (the spall) a shock wave is reflected towards the free surface, causing an increase in the free-surface velocity. These reverberation phenomena are repeated until the free surface reaches an asymptotic constant velocity. The spall strength Σ, i.e. the negative pressure (tension) that a spall occurs, can be calculated using the Riemann invariants

$$\left.\begin{aligned} u(P=0, u=u_{min}) \equiv u_{min} &= u_0' - \int_{\Sigma}^{0} \frac{dP}{\rho c_s} \\ u(P=0, u=u_{max}) \equiv u_{max} &= u_0' + \int_{\Sigma}^{0} \frac{dP}{\rho c_s} \end{aligned}\right\} \Rightarrow \Delta u \equiv u_{max} - u_{min} = 2\int_{\Sigma}^{0} \frac{dP}{\rho c_s}. \tag{10.117}$$

Assuming that the negative pressure is not too large, then to a good approximation $\rho = \rho_0$ and $c_s = c_0$, implying that the spall strength is

$$\Sigma = -\frac{\rho_0 c_0 (u_{max} - u_{min})}{2} \equiv -\sigma_{spall}. \tag{10.118}$$

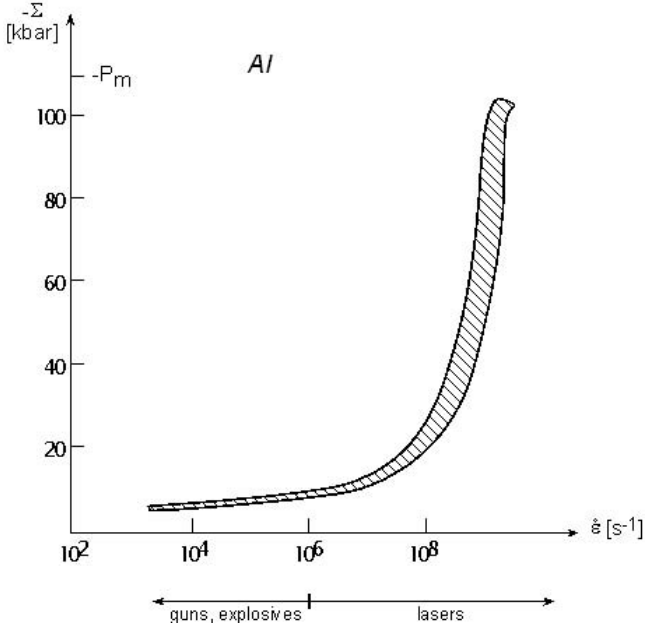

Figure 10.10. Experimental values of spall strength σ_{spall} as a function of the strain rate for aluminium. $-P_{\text{m}}$ is the maximum theoretical value of the spall strength (see figure 10.8(b)).

The minimum (i.e. the maximum absolute value) possible Σ is given by the equation of state, as shown in figure 10.8 by the value P_{m}.

The strain ε and the strain rate $\mathrm{d}\varepsilon/\mathrm{d}t$ can be approximated by

$$\varepsilon = \frac{u_{\text{p}}}{c_0}, \qquad \dot{\varepsilon} = \frac{\mathrm{d}\varepsilon}{\mathrm{d}t} = \frac{1}{2c_0}\frac{\mathrm{d}u_{\text{FS}}}{\mathrm{d}t} \approx \frac{1}{2c_0}\frac{\Delta u}{\Delta t} \tag{10.119}$$

where Δt is the time difference (see figure 10.7(b)) between the time measurements of $u_{\max}$ and $u_{\min}$. The experimental data of σ_{spall} as a function of the strain rate are summarized in figure 10.10 for aluminium targets. Up to about a strain rate of $10^6\,\text{s}^{-1}$, the strain creation methods are gun drivers of plates or high explosives, while the higher strain rates are achieved with high-power pulsed laser drivers. The minimum pressure, in the pressure-specific volume curve, gives the equation of state theoretical spall strength. As already mentioned above, in reality the theoretical value of spall is not achieved due to material defects. However, for extremely high strain rates, the theoretical values from the equations of state are expected, since the material defects do not have enough time to 'combine' and induce a spall, so that the inter-atomic forces dominate the strength of the material in this case. As can be seen from the isotherms of aluminium in figure 10.11, calculated with a semi-empirical wide range equation of state, the spall strength also depends on the temperature of the shocked target.

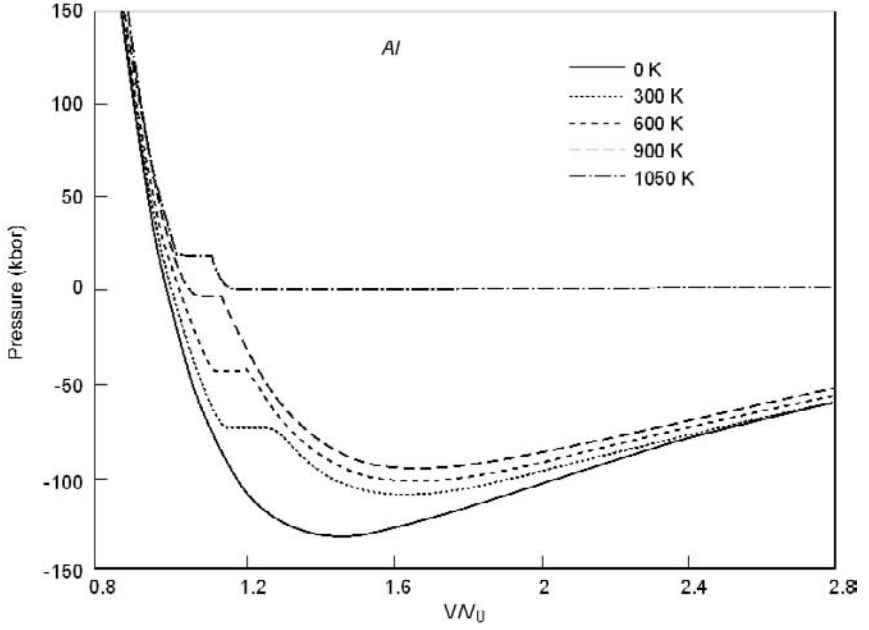

Figure 10.11. Isotherm of aluminium, calculated with a semi-empirical wide range equations of state.

Last, but not least, from the free-surface measurements the shock-wave pressure is known if the equation of state is available (equation (10.44)):

$$P_{\mathrm{H}} = \rho_0 u_{\mathrm{s}} u_{\mathrm{p}} \approx \rho_0 \left(c_0 + \alpha \frac{u_{\max}}{2} \right) \frac{u_{\max}}{2}. \tag{10.120}$$

From the analysis in this chapter, one can see that the high-power laser devices are successfully 'joining' the club of high-pressure physics.

Chapter 11

Hydrodynamic Instabilities

11.1 Background

The Rayleigh–Taylor (RT) instability occurs if a heavy fluid is supported by a light fluid in a gravitational field (Rayleigh 1883). Equivalently, one gets RT instability when a light fluid pushes and accelerates a heavy fluid (Taylor 1950) (see figure 11.1). In general, the RT instability occurs whenever a pressure gradient opposes a density gradient (∇P is in an opposite direction to $\nabla\rho$).

The hydrodynamic instabilities, and in particular the RT instability, have been reviewed in the literature (Chandrasekhar 1961, Drazin and Reid 1981, Kull 1991). Reviews on RT instabilities in laser–plasma interactions, with an emphasis on inertial confinement fusion (ICF), are also available (Bodner 1991, Gamaly 1993, Hoffman 1995).

A sinusoidal wave, with amplitude ξ, on the surface between the two RT unstable fluids will grow exponentially:

$$\xi = \xi_0 \exp(\gamma_0 t), \qquad \gamma_0 = \sqrt{Aka}, \qquad A \equiv \frac{\rho_H - \rho_L}{\rho_H + \rho_L}, \qquad k = \frac{2\pi}{\lambda} \tag{11.1}$$

where λ is the wavelength of the sinusoidal wave, a is the acceleration of the two fluids (or $a = g$ in the gravitational field, without acceleration), ρ_H and ρ_L are the densities of the heavier and the lighter fluids and A is the Atwood number. γ_0 is the classical value obtained by Rayleigh, more than a hundred years ago, for two fluids in contact in the gravitational field ($a = g$ in (11.1)).

For example, when a high-power laser interacts with a thin foil, plasma is created and accelerates the foil. In this case one has a low-density medium (the plasma) accelerating a high-density medium (the solid target); therefore, the acceleration is subject to RT instabilities. For a typical high-power laser acceleration of the order of $10^{15}\,\mathrm{cm/s^2}$ and a wavelength of the order of the foil thickness $\sim 100\,\mu\mathrm{m}$, one gets $\gamma_0 \approx 10^9\,\mathrm{s^{-1}}$, implying that the classical e-folding time is $1/\gamma_0 \approx 1\,\mathrm{ns}$.

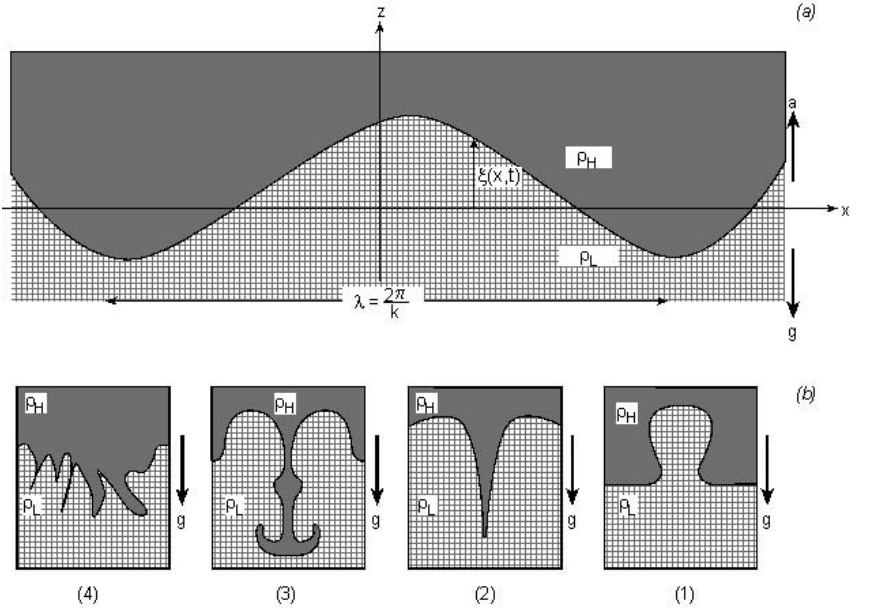

Figure 11.1. Rayleigh–Taylor (RT) instability in the presence of gravitation g (down) or acceleration a (up). The upper fluid density ρ_H is larger than the lower fluid density ρ_L. (a) A normal mode is shown. (b) Characteristic flow patterns in the evolution of RT instability: (1) a bubble formation penetrating the heavy fluid, (2) a spike entering a medium with very low density, (3) a spike formation with vortex motion, (4) intermixing between the fluids.

Another very important example is the acceleration of thin shells, subject to RT instabilities, in ICF. The use of shells in ICF, in comparison with solid spheres, has reduced significantly the peak laser power (and energy) required to ignite a target of a given mass. The following order of magnitude calculations demonstrate the importance of RT instabilities in ICF. The ablation pressure P_a, that accelerates the shell, is a function of the irradiating laser intensity I, which scales like $P_a \sim I^{2/3}$. For a shell with an initial radius R_0 and thickness ΔR_0, the implosion velocity v_f scales as $v_f^2 \sim P_a(R_0/\Delta R_0)$. The resulting stagnation pressure is $P_f \approx P_a(R_0/\Delta R_0)G$, where G is a radial convergence factor of the order of 100. The minimum energy for ignition scales as $1/P_f^2$. The ablation pressure for ICF pellets, expected to be about $P_a \approx 30\,\text{Mbar}$, has to increase to about $P_f \approx 100\,\text{Gbar}$, i.e. by a factor of 3000, implying an aspect ratio $R_0/\Delta R_0 \approx 30$. The larger the aspect ratio the higher the implosion pressure (P_f), implying a smaller laser energy ($\sim 1/P_f^2$). However, the magnitude of $R_0/\Delta R_0$ is limited by RT instabilities.

Since the beginning of the ICF programme, the RT instability has been a subject of uncertainties and controversies. Some scientists believe that an initial aspect ratio $R_0/\Delta R_0$ as high as 100 is 'safe' against RT instabilities, while others

were predicting that even an aspect ratio of 4 is going to 'destroy' the shell (before the desired high compression is achieved) by RT instabilities. The aspect ratio is a very important parameter for ICF since thicker pellets require a higher laser intensity to achieve the desired high pressure, and very high laser intensity could drive unacceptable plasma instabilities (see chapter 6). In addition, thicker shells require a larger amount of laser energy.

The RT instability can cause a disturbance to grow from extremely small amplitude to a level that can disrupt the flow completely. In the above examples it can break the accelerated foil or the shell before it reaches the desired final velocity.

The initial disturbance, called the 'seed', arises from limitations to fabricate a perfect plane (for foil acceleration) or a perfect spherical shell for ICF. Small perturbations caused by the roughness of the material structures, or by machining marks during the preparation of the target, are sources of instability seeds. Furthermore, the pattern of the laser intensity on the target can imprint a disturbance on an initially perfect smooth target. Since these types of disturbance are facts of reality, one has to calculate the constraints on the target smoothness and on the laser uniformity from the hydrodynamic instability theory.

Any initial perturbation can be described as an infinite series (e.g. a Fourier series) of normal modes (with wavelength $\lambda = L/j$, $j = 1, 2, 3, \ldots$). Any given mode is not growing to infinity by the RT instability, but is expected to saturate at a finite amplitude ($\sim\lambda/2$). On their route to saturation, perturbations with wavelength greater than the fluid thickness would destroy the flow (break the foil or the shell).

The shorter wavelength modes reach saturation before the longer wavelength modes (see equation (11.1), $\gamma_0 \sim (a/\lambda)^{1/2}$). After the shorter wavelength modes stop growing, they transfer their acquired energy to the longer wavelength disturbances, and the small disturbances are converted into larger structures. It turns out that these structures have the topology of bubbles and spikes. The lighter fluid penetrates the heavier fluid in the form of bubbles, and spikes of the heavier fluid enter the lighter fluid. Characteristic flow patterns in the evolution of RT instability are shown in figure 11.1(b), where a bubble formation penetrating the heavy fluid is shown together with possible spikes entering the lighter medium. A schematic spike formation with vortex motion and late intermixing between the fluids are also shown in this figure.

The saturation mechanism can be understood (Shvarts *et al.* 1995) by the existence of a nonlinear drag force:

$$F_{\mathrm{d}} \approx -\rho_{\mathrm{d}} S u^2. \tag{11.2}$$

The ambient fluid for bubbles is the heavy liquid and the ambient fluid for spikes is the light fluid; therefore, $\rho_{\mathrm{d}} = \rho_{\mathrm{H}}$ for bubbles and $\rho_{\mathrm{d}} = \rho_{\mathrm{L}}$ for spikes. S is the area and u the velocity of the bubbles or the spikes. Equating

the drag force with the buoyancy force for a disturbance with volume V,

$$F_b \approx (\rho_H - \rho_L)aV \tag{11.3}$$

one gets

$$u \approx \sqrt{a\lambda}, \qquad \text{amplitude} \approx \frac{u^2}{2a} = \frac{\lambda}{2}. \tag{11.4}$$

In order to get a feeling of the size of RT instability according to equation (11.1), we consider the shell uniformity requirement in ICF. According to this equation the shorter wavelengths have higher growth rates; therefore, one has to consider the shortest wavelength that will destroy the shell, about $\lambda \approx 3\Delta R_0$. The shell is first accelerated, then it expands at a constant velocity and finally it decelerates during the compression stages. The RT instabilities occur during the acceleration and during the deceleration phases, since in both cases ∇P is in an opposite direction to $\nabla\rho$. In this example we are interested in the RT instability during the acceleration phase. As an order of magnitude estimate, one can assume that the shell acceleration is constant until the shell is at a distance $R_0/2$ from the centre, $R_0/2 \approx \frac{1}{2}at^2$. Using this relation and $\lambda \approx 3\Delta R_0$, the growth of an initial amplitude ξ_0 for Atwood number ≈ 1 is, according to equation (11.1),

$$\frac{\xi}{\xi_0} = \exp\sqrt{\frac{2R_0}{\Delta R_0}}$$

$$\xi = \frac{\Delta R_0}{2} \approx 50\,\mu\text{m} \Rightarrow \begin{cases} \xi_0 \approx 3.6 \times 10^{-9}\,\text{cm} & \text{for } \dfrac{R_0}{\Delta R_0} = 100 \\ \xi_0 \approx 2.2 \times 10^{-6}\,\text{cm} & \text{for } \dfrac{R_0}{\Delta R_0} = 30. \end{cases} \tag{11.5}$$

Taking into account the pellet fabrication and the laser initial imprint on the shell surface, it seems that such initial smoothness is technologically impossible. Therefore, there must be some mechanism that reduces the RT instabilities significantly or all ICF schemes would fail.

Following the Landau–Lifshitz analysis (Landau and Lifshitz 1987) of a chemical burn front of a weak deflagration, it was suggested (Bodner 1974, Takabe *et al.* 1985) that the plasma ablation stabilizes the RT instability. The ablated material flows away from the target interface, creating the low-density corona that accelerates the target. The pressure increase from the target towards the corona gives the acceleration force. The ablation flow through the unstable region and the smoothing of temperature perturbations by the radiation flux can act to reduce the growth rate in the RT instability at the ablation surface. The ablation stabilization is explained by the fact that the disturbance is convected away from the interface before it grows. According to this stabilization, the growth rate of the RT instability is

effectively reduced to

$$\gamma = \alpha\sqrt{ka} - \beta k u_a, \qquad u_a = \frac{1}{\rho_{max}}\left(\frac{dm}{dt}\right), \qquad \alpha \approx 0.9, \quad \beta \approx 3 \tag{11.6}$$

where ρ_{max} is the peak density at the interface and dm/dt is the mass (per unit area) ablation rate. The ratio between the u_a term and the classical RT term for ICF plasmas is about 25% only, therefore this stabilization is not sufficient.

In analysing the RT instability it is required to consider the evolution of multimode perturbation. In spherical geometry the perturbation wave number is given by the angular momentum number l:

$$l = \frac{2\pi R}{\lambda}. \tag{11.7}$$

The growth rate for each mode is $\gamma_l = (al/R_0)^{1/2}$ and using the approximation $at^2 \sim R_0$, one gets

$$\gamma_l t \approx \sqrt{l}. \tag{11.8}$$

The nonlinear evolution of the RT instability, starting with a multimode initial perturbation (Gardner *et al.* 1988, Haan 1989, Dahlburg *et al.* 1995, Shvarts *et al.* 1995, Oron *et al.* 1998), was comprehensively studied using numerical simulations in two and three dimensions.

Other hydrodynamic instabilities of importance in laser–target interaction are the Richtmyer–Meshkov (RM) instability and the Kelvin–Helmholtz (KH) instability. The RM instability (Richtmyer 1960, Meshkov 1969) occurs when a shock wave passes through a corrugated interface between two fluids of different densities (see figure 11.2). This phenomenon is a limiting case of the RT instability, where the shock wave imparts an impulsive acceleration to the interface, so that the acceleration acts on the fluid during an infinitesimally short duration. As in the RT case under unstable conditions, small perturbations on the interface can grow into bubbles of light fluid penetrating the heavy fluid and spikes of heavy fluid entering into the light fluid.

The KH instability (Kelvin 1910, Chandrasekhar 1961, Brown and Roshko 1974, Melrose 1986) occurs when two fluids in contact have different flow velocities (in the direction parallel to the interface) across the interface. The classical example is the generation of water waves by wind blowing over the surface of the water. The gradient in the parallel velocity, referred to in the literature as 'velocity shear', can be unstable and produce vortices and turbulence, creating a mixing zone between the fluids. The KH instability can develop along the interface of 'climbing' bubbles and 'declining' spikes at the late stage of RT instability, when the shear velocity is large. A shear velocity is also generated in RM instability if the shock wave is crossing the interface not in a normal direction to the interface between the fluids.

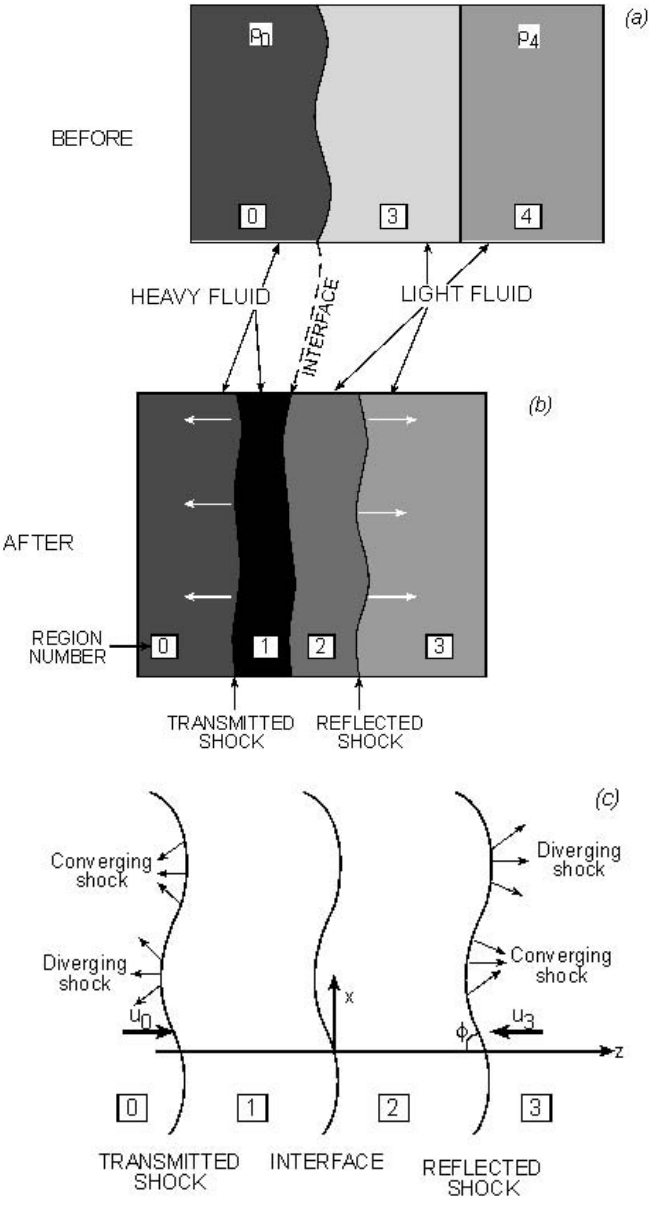

Figure 11.2. A presentation of the Richtmyer–Meshkov instability. A shock wave passes through a perturbed interface between two fluids, from the light to the heavy fluid. (a) Before the shock crosses the interface, (b) after the shock crosses the interface and (c) converging and diverging shocks at the shock wave surfaces.

In the following sections the RT, RM and KH instabilities are analysed. The RT instability is discussed in greater detail (the next four sections) than the other instabilities.

11.2 Rayleigh–Taylor Instability, Linear Analysis

The hydrodynamic equations describing the motion under consideration are the following mass and the momentum conservation equations:

$$\frac{\partial \rho}{\partial t} + \nabla \cdot (\rho \mathbf{v}) = 0, \qquad \rho \frac{\partial \mathbf{v}}{\partial t} + \rho(\mathbf{v} \cdot \nabla)\mathbf{v} = -\nabla P + \rho \mathbf{g} \tag{11.9}$$

where ρ is the fluid density, $\mathbf{v}$ is the flow velocity, P is the pressure and $\rho\mathbf{g}$ is the external force acting on the fluid (if there is an acceleration, then $\mathbf{a} = -\mathbf{g}$). The Cartesian coordinates with unit vectors $\hat{\mathbf{x}}$, $\hat{\mathbf{y}}$ and $\hat{\mathbf{z}}$ are used, and the gravitational field (or the acceleration) is perpendicular to the interface between the fluids

$$\mathbf{g} = -g\hat{\mathbf{z}}. \tag{11.10}$$

The instability is investigated here in the linear approximation (Chandrasekhar 1961, Hoffman 1995):

$$\begin{aligned} \rho &= \rho_0 + \rho_1, & \rho_0 &\gg \rho_1 \\ \mathbf{v} &= \mathbf{v}_0 + \mathbf{v}_1, & \mathbf{v}_0 &\gg \mathbf{v}_1 \\ P &= P_0 + P_1, & P_0 &\gg P_1. \end{aligned} \tag{11.11}$$

The variables with subscript 1 describe how a small perturbation grows in time. If the amplitude of the perturbation never returns to its initial value, then it is said that the flow is unstable with respect to the initial perturbation. Substituting (11.11) into equations (11.9), and neglecting higher orders than one (see section 2.5), yields the following equations to the zeroth order and the first order respectively:

$$\frac{\partial \rho_0}{\partial t} + \nabla \cdot (\rho_0 \mathbf{v}_0) = 0, \qquad \rho_0 \frac{\partial \mathbf{v}_0}{\partial t} + \rho_0(\mathbf{v}_0 \cdot \nabla)\mathbf{v}_0 = -\nabla P_0 + \rho_0 \mathbf{g} \tag{11.12}$$

$$\frac{\partial \rho_1}{\partial t} + \nabla \cdot (\rho_0 \mathbf{v}_1 + \rho_1 \mathbf{v}_0) = 0$$

$$\rho_1 \frac{\partial \mathbf{v}_0}{\partial t} + \rho_0 \frac{\partial \mathbf{v}_1}{\partial t} + \rho_0[(\mathbf{v}_1 \cdot \nabla)\mathbf{v}_0 + (\mathbf{v}_0 \cdot \nabla)\mathbf{v}_1] + \rho_1(\mathbf{v}_0 \cdot \nabla)\mathbf{v}_0 = -\nabla P_1 + \rho_1 \mathbf{g} \tag{11.13}$$

For the analysis of RT instability it is assumed that $\mathbf{v}_0 = 0$, so that the equations (11.13) for the perturbations are simplified to

$$\frac{\partial \rho_1}{\partial t} + \nabla \cdot (\rho_0 \mathbf{v}_1) = 0, \qquad \rho_0 \frac{\partial \mathbf{v}_1}{\partial t} + \nabla P_1 - \rho_1 \mathbf{g} = 0\,. \tag{11.14}$$

For an incompressible fluid the speed of sound equals infinity, so that communications by sound signal are instantaneous. Therefore, it is assumed that an incompressible flow is a reasonable assumption for flow velocities much smaller than the local speed of sound. In Lagrangian coordinates (see section 3.2) the density in this case does not change with time:

$$\frac{\mathrm{d}\rho}{\mathrm{d}t} = \frac{\partial \rho}{\partial t} + \mathbf{v} \cdot \nabla \rho = 0. \tag{11.15}$$

Using the linearization procedure in this equation, together with the first of equations (11.14), one gets the following two equations:

$$\nabla \cdot \mathbf{v}_1 = 0 \tag{11.16}$$

$$\frac{\partial \rho_1}{\partial t} + \mathbf{v}_1 \cdot \nabla \rho_0 = 0. \tag{11.17}$$

Instead of equations (11.14) we have to solve for the incompressible fluid the second equation of (11.14), together with equations (11.16) and (11.17). In our problem ρ_0 is constant in both fluids, and therefore the initial density changes only in the z direction, normal to the interface between the two fluids. This implies that $\partial\rho_0/\partial x = 0$, $\partial\rho_0/\partial y = 0$ and only at the interface $\partial\rho_0/\partial z \neq 0$. Writing these equations explicitly in Cartesian coordinates, one gets

$$\begin{aligned}
\rho_0 \frac{\partial v_{1x}}{\partial t} + \frac{\partial P_1}{\partial x} &= 0 \\
\rho_0 \frac{\partial v_{1y}}{\partial t} + \frac{\partial P_1}{\partial y} &= 0 \\
\rho_0 \frac{\partial v_{1z}}{\partial t} + \frac{\partial P_1}{\partial z} + \rho_1 g &= 0 \\
\frac{\partial \rho_1}{\partial t} + v_{1z} \frac{\partial \rho_0}{\partial z} &= 0 \\
\frac{\partial v_{1x}}{\partial x} + \frac{\partial v_{1y}}{\partial y} + \frac{\partial v_{1z}}{\partial z} &= 0
\end{aligned} \tag{11.18}$$

We have five equations with five unknowns, v_{1x}, v_{1y}, v_{1z}, P_1 and ρ_1. It is convenient to solve these equations after a Fourier transform in x–y, or equivalently the disturbance is analysed by its normal modes, with solutions depending on x, y and t in the following way:

$$\left.\begin{aligned}
\mathbf{v}_1(x, y, z, t) &= \mathbf{u}(z) \\
P_1(x, y, z, t) &= \delta P(z) \\
\rho_1(x, y, z, t) &= \delta\rho(z)
\end{aligned}\right\} \times \exp(\mathrm{i}k_x x + \mathrm{i}k_y y + \gamma t) \tag{11.19}$$

where k_x, k_y and γ are constants. Substituting (11.19) into equations (11.18) gives

$$\begin{aligned} \gamma\rho_0 u_x + \mathrm{i}k_x \delta P &= 0 \\ \gamma\rho_0 u_y + \mathrm{i}k_y \delta P &= 0 \\ \gamma\rho_0 u_z + \frac{\partial \delta P}{\partial z} + g\delta\rho &= 0 \\ u_z \frac{\mathrm{d}\rho_0}{\mathrm{d}z} + \gamma\delta\rho &= 0 \\ \mathrm{i}k_x u_x + \mathrm{i}k_y u_y + \frac{\partial u_z}{\partial z} &= 0. \end{aligned} \tag{11.20}$$

Multiplying the first equation by $\mathrm{i}k_x$, the second equation by $\mathrm{i}k_y$, adding these two new equations and solving with the last equation, one gets

$$\delta P(z) = -\left(\frac{\gamma\rho_0}{k^2}\right)\frac{\mathrm{d}u_z}{\mathrm{d}z} \tag{11.21}$$

where k is defined by

$$k^2 = k_x^2 + k_y^2. \tag{11.22}$$

Substituting $\delta\rho(z)$ from the fourth equation of (11.20), together with $\delta P(z)$ from (11.21) into the third equation of (11.20), one gets the following equation for u_z:

$$\frac{d}{\mathrm{d}z}\left(\rho_0 \frac{\mathrm{d}u_z}{\mathrm{d}z}\right) - \left[k^2\rho_0 - \left(\frac{k^2 g}{\gamma^2}\right)\frac{\mathrm{d}\rho_0}{\mathrm{d}z}\right]u_z = 0. \tag{11.23}$$

If the fluid is confined between two rigid planes at $+z_\mathrm{B}$ and $-z_\mathrm{B}$, then the boundary conditions are

$$u_z(\pm z_\mathrm{B}) = 0, \qquad \left(\frac{\mathrm{d}u_z}{\mathrm{d}z}\right)_{\pm z_\mathrm{B}} = 0. \tag{11.24}$$

We take in our following analysis $z_\mathrm{B} \to \infty$. Equation (11.23) is an eigenvalue equation, with u_z the eigenfunction and the term in $[\cdots]$ is the eigenvalue. Therefore, γ is fixed for any given values of $\rho_0(z)$, k and g.

The interface is the surface $z = 0$, and the density is assumed constant anywhere except between the fluids at $z = 0$. Therefore, for $z \neq 0$, equation (11.23) is given by

$$z \neq 0: \quad \frac{\partial^2 u_z(z)}{\partial z^2} - k^2 u_z(z) = 0 \tag{11.25}$$

and its general solution is

$$z \neq 0: \quad u_z(z) = \alpha\exp(kz) + \beta\exp(-kz). \tag{11.26}$$

Since u_z vanishes at the boundary, and the velocity is continuous at the interface (otherwise an infinite acceleration is needed for the fluid to cross the interface), one has the solution

$$u_z(z) = \begin{cases} w\exp(+kz) & \text{for } z < 0 \\ w\exp(-kz) & \text{for } z > 0. \end{cases} \tag{11.27}$$

Equation (11.23) is now integrated across the interface from $-\varepsilon$ to $+\varepsilon$, where ε is an infinitesimal element of z. Using (11.27) and denoting the density of the fluid above and below the interface by ρ_{up} and ρ_{down} accordingly (the direction up and down is determined by the direction of **g**), the integral gives

$$\begin{aligned} &\int_{-\varepsilon}^{+\varepsilon} \frac{\mathrm{d}}{\mathrm{d}z}\left(\rho_0 \frac{\partial u_z}{\partial z}\right)\mathrm{d}z - \int_{-\varepsilon}^{+\varepsilon} k^2\rho_0 u_z\,\mathrm{d}z + \int_{-\varepsilon}^{+\varepsilon} \frac{gk^2 u_z}{\gamma^2}\frac{\mathrm{d}\rho_0}{\mathrm{d}z}\,\mathrm{d}z = 0 \\ &\lim_{\varepsilon\to 0}\int_{-\varepsilon}^{+\varepsilon} \frac{\mathrm{d}}{\mathrm{d}z}F(z)\,\mathrm{d}z = \lim_{\varepsilon\to 0}\left[F(+\varepsilon) - F(-\varepsilon)\right] \equiv \Delta_0 F; \\ &\lim_{\varepsilon\to 0}\int_{-\varepsilon}^{+\varepsilon} G(z)\,\mathrm{d}z = 0, \qquad G(z) \text{ continuous at } z = 0 \\ &\Rightarrow kw\left[-(\rho_{\text{up}} + \rho_{\text{down}}) + \frac{gk}{\gamma^2}(\rho_{\text{up}} - \rho_{\text{down}})\right] = 0. \end{aligned} \tag{11.28}$$

The first integral gives the first term, the second integral vanishes and the third integral gives the second term. Using the solution of the last equation for the instability parameter γ and equation (11.19), the following result is obtained:

$$\begin{aligned} \gamma^2 &= Akg \\ A &\equiv \frac{\rho_{\text{up}} - \rho_{\text{down}}}{\rho_{\text{up}} + \rho_{\text{down}}} \\ v_z(x,y,z,t) &= \begin{cases} w\exp[\mathrm{i}(k_x x + k_y y)]\exp(+kz)\exp(\gamma t) & \text{for } z < 0 \\ w\exp[\mathrm{i}(k_x x + k_y y)]\exp(-kz)\exp(\gamma t) & \text{for } z > 0. \end{cases} \end{aligned} \tag{11.29}$$

The dimensionless parameter A is called the Atwood number. If $\rho_{\text{up}} > \rho_{\text{down}}$, then A is positive and therefore γ is a real number. In this case the perturbation grows exponentially and the interface is unstable. On the other hand, if $\rho_{\text{up}} < \rho_{\text{down}}$, then A is negative and therefore γ is an imaginary number, causing the interface and the physical quantities (e.g. pressure, v_z) to oscillate with a frequency of $(|A|kg)^{1/2}$. From the solutions (11.19) (see in particular (11.29)), one has that the physical variables oscillate in the x–y plane with a wavelength λ, related to the wave number k by

$$\lambda = \frac{2\pi}{k}, \qquad k = \sqrt{k_x^2 + k_y^2} \tag{11.30}$$

and the time dependence is given by $\exp(\gamma t)$.

11.3 Ablation-Surface Instability

The ablation-surface instability occurs when a laser is accelerating a solid foil or shell. In this case a high-pressure low-density plasma region is created from the ablated material that accelerates the foil, due to the expanding plasma (the rocket effect). During the acceleration the foil is subject to Rayleigh–Taylor instabilities since a low-density medium accelerates a high-density medium (for the high accelerations obtained here, the gravitation is not relevant).

Because energy is deposited at the interface between the foil (with a density ρ_{foil}) and the adjacent plasma (with a density ρ_{pl}), a velocity discontinuity is permitted at the interface together with the density jump. It is assumed that there is a sharp density jump, so that the density is described by a θ function:

$$\rho_0(z) = \rho_{\text{pl}}\theta(-z) + \rho_{\text{foil}}\theta(z), \qquad \theta(z) = \begin{cases} 1 & \text{for } z > 0 \\ 0 & \text{for } z < 0. \end{cases} \tag{11.31}$$

In the foil reference frame of coordinates (the foil is at rest in this frame), the ablated material moves in the $-\hat{\mathbf{z}}$ direction ($\hat{\mathbf{z}}$ is a unit vector in the z direction) with velocity v_{pl}:

$$\mathbf{v}_0 = -v_{\text{pl}}\theta(-z)\hat{\mathbf{z}} = \begin{cases} -v_{\text{pl}}\hat{\mathbf{z}} & \text{for } z < 0 \\ 0 & \text{for } z > 0. \end{cases} \tag{11.32}$$

The second equations of (11.12) and (11.13), without the gravitational term, can be combined in the following way:

$$\rho_0\left(\frac{\partial \mathbf{v}_1}{\partial t} + \mathbf{v}_1 \cdot \nabla \mathbf{v}_0 + \mathbf{v}_0 \cdot \nabla \mathbf{v}_1\right) = \frac{\rho_1}{\rho_0}\nabla P_0 - \nabla P_1. \tag{11.33}$$

These three equations, together with the last two equations of (11.20) (the incompressibility assumption), are the five equations with the five unknowns to be solved. Substituting (11.19) into these equations leads, in a similar way that equation (11.23) was obtained, to the following equation for the velocity $u_z(z)$:

$$\frac{\partial}{\partial z}\left(\rho_0 \frac{\partial u_z}{\partial z}\right) - \frac{k^2 \rho_0 v_{0z}}{\gamma}\frac{\partial u_z}{\partial z} - \left(k^2\rho_0 - \frac{ak^2}{\gamma^2}\frac{\partial \rho_0}{\partial z} + \frac{k^2\rho_0}{\gamma}\frac{\partial v_{0z}}{\partial z}\right)u_z = 0 \tag{11.34}$$

where the acceleration a is defined by

$$a \equiv -\left(\frac{1}{\rho_0}\right)\frac{\partial P_0}{\partial z}. \tag{11.35}$$

Equation (11.34) is now integrated across the interface from $-\varepsilon$ to $+\varepsilon$, where ε is an infinitesimal element of z. The density and the initial velocity are described by a θ function, and the derivative of these terms gives the Dirac

δ function since

$$\frac{\mathrm{d}\theta(z)}{\mathrm{d}z} = \delta(z). \tag{11.36}$$

The integral of the Dirac function over the segment, including the zero of the argument, is equal to one, while the integral of regular functions and the θ function from $-\varepsilon$ to $+\varepsilon$, where $\varepsilon \to 0$, is equal to zero. Therefore, the integrals of the second and third terms of (11.34) vanish, the integrals of the first and fourth terms (using (11.27)) are similar to the integrals of (11.28), and only the integral of the fifth term in (11.34) is new and is equal to

$$\int_{-\varepsilon}^{+\varepsilon} \frac{k^2\rho_0 u_z}{\gamma}\frac{\partial v_{0z}}{\partial z}\,\mathrm{d}z = \frac{k^2 w}{\gamma}\int_{-\varepsilon}^{+\varepsilon}\rho_0\frac{\partial v_{0z}}{\partial z}\,\mathrm{d}z = \frac{k^2 w}{\gamma}\left[\left(\frac{\rho_{\mathrm{pl}}+\rho_{\mathrm{foil}}}{2}\right)v_{\mathrm{pl}}\right]. \tag{11.37}$$

At the last step we have used the symmetry of δ ($\delta(z) = \delta(-z)$) and the identity

$$\int_{-\varepsilon}^{+\varepsilon}\theta(z)\delta(z)\,\mathrm{d}z = \frac{1}{2} \tag{11.38}$$

that can be easily verified from integrating by parts.

Therefore, the integral of (11.34) over the interface yields (using (11.38) and the integrals in (11.28))

$$kw\left[(\rho_{\mathrm{foil}}+\rho_{\mathrm{pl}}) - \frac{ak}{\gamma^2}(\rho_{\mathrm{foil}}-\rho_{\mathrm{pl}}) + \frac{k}{2\gamma}(\rho_{\mathrm{foil}}+\rho_{\mathrm{pl}})v_{\mathrm{pl}}\right] = 0. \tag{11.39}$$

Simplifying this equation gives

$$\gamma^2 + \left(\frac{kv_{\mathrm{pl}}}{2}\right)\gamma - akA = 0, \qquad A \equiv \frac{\rho_{\mathrm{foil}}-\rho_{\mathrm{pl}}}{\rho_{\mathrm{foil}}+\rho_{\mathrm{pl}}}. \tag{11.40}$$

The solution of this quadratic equation is

$$\begin{gathered}\gamma = -\frac{kv_{\mathrm{pl}}}{4} \pm \sqrt{\left(\frac{kv_{\mathrm{pl}}}{4}\right)^2 + Aka} \\ v_{\mathrm{pl}} \ll 4\sqrt{\frac{Aa}{k}} \Rightarrow \gamma \approx \sqrt{Aka} - \frac{kv_{\mathrm{pl}}}{4} + \cdots.\end{gathered} \tag{11.41}$$

From this result one can see that the ablation reduces (compare with equation (11.29) for $g = a$) the growth rate of the RT instability.

In deriving equation (11.41), many simplifying assumptions have been made. For example, the incompressibility assumption, the spatial extent and the density gradient of the plasma were neglected, the plasma heating was not taken into account, etc.

It is interesting to point out that a detailed numerical simulation of the ablation instability, taking all the above-mentioned effects into account

(Takabe *et al.* 1985) gives a fit described by equation (11.6). In comparison between this fit and equation (11.41): there are two main differences the constant $\frac{1}{4}$ is changed to about 3 and u_a is changed to v_{pl} ($(A)^{1/2} \approx 0.9$ is a good approximation for the plasma–solid interface). While v_{pl} is the plasma velocity far from the ablation surface, the u_a represents the mass ablation rate per unit area divided by the density of the ablation surface. Since $v_{pl} \gg u_a$, the numerical fit (11.6) and equation (11.41) seem not to be inconsistent. There is, however, a difference between the numerical fit (11.6) and equation (11.41), since in the above value of γ the approximation $kv_{pl}/4 \ll (Aka)^{1/2}$ has been made, while the numerical fit does not require this perturbation. Therefore, in analysing equation (11.6) it is permitted to introduce a cutoff wavenumber k_c, defined by

$$\gamma(k_c) = 0 \Rightarrow k_c = \left(\frac{\alpha}{\beta}\right)^2 \left(\frac{a}{u_a^2}\right), \qquad \lambda_c \equiv \frac{2\pi}{k_c}. \tag{11.42}$$

Equation (11.6) shows that for wavelength $\lambda < \lambda_c$ (i.e. $k > k_c$) the ablation is stable, and only the wavelengths higher than λ_c contribute to the ablation RT instability.

11.4 The Magnetic Field Effect

In high-power laser–plasma interactions very strong magnetic fields are created (see chapter 8). Megagauss magnetic fields (d.c.) were measured for moderate laser intensities. In this section it is shown that the magnetic field parallel to the accelerated interface between two fluids, where the heavier fluid is above the lighter fluid, stabilizes the RT instability.

The acceleration is assumed to be in the z direction, the interface between the fluids are in the x–y plane $z = 0$ and the fluids are incompressible plasmas with zero resistivity (= 1/electrical conductivity = $1/\sigma_E$). The linearization procedure, as in equation (11.11), is used in this analysis with a magnetic field (Gaussian units are used):

$$\mathbf{B} = \mathbf{B}_0 + \mathbf{B}_1, \qquad \mathbf{B}_0 = \textbf{const.}, \qquad \frac{|\mathbf{B}_1|}{|\mathbf{B}_0|} \ll 1. \tag{11.43}$$

The momentum equation is (see equations (3.10) and (3.11), where the electric field **E** is neglected relative to the **B** field)

$$\rho \frac{\partial \mathbf{v}}{\partial t} = -\nabla P + \frac{1}{c}(\mathbf{J} \times \mathbf{B}) \tag{11.44}$$

where **v** is the fluid velocity, ρ and P are density and pressure respectively, **J** is the electric current and c is the speed of light. Using the Maxwell equation,

$$\mathbf{J} = \left(\frac{c}{4\pi}\right) \nabla \times \mathbf{B}. \tag{11.45}$$

The linearized momentum equation can be written

$$\rho_0 \frac{\partial \mathbf{v}}{\partial t} = -\nabla P_1 - \frac{\mathbf{B}_0}{4\pi} \times (\nabla \times \mathbf{B}_1) - g\rho_1 \hat{\mathbf{z}}. \tag{11.46}$$

This equation has to be solved, together with the following linearized Maxwell equation for zero resistivity (see equation (8.33), with $1/\sigma_E = 0$):

$$\frac{\partial \mathbf{B}}{\partial t} = -c\nabla \times \mathbf{E} = \nabla \times (\mathbf{v} \times \mathbf{B}_0) \tag{11.47}$$

the mass conservation and the incompressibility requirement (equations (11.16) and (11.17)). In these approximations, the zero divergence of the magnetic field

$$\nabla \cdot \mathbf{B}_1 = 0 \tag{11.48}$$

is not an independent equation, since it is derived from equation (11.47).

In this problem there are eight independent equations, (11.46), (11.47), (11.16) and (11.17), with eight unknowns, ρ_1, P_1, $\mathbf{v}$ and $\mathbf{B}_1$. We shall write explicitly these equations for two cases:

1. The initial magnetic field is perpendicular (vertical) to the interface between the fluids, $\mathbf{B}_0 = B_0\hat{\mathbf{z}}$.
2. The initial magnetic field is parallel (horizontal) to the interface between the fluids, $\mathbf{B}_0 = B_0\hat{\mathbf{x}}$:

$$\begin{aligned}
\mathbf{B}_0 = B_0\hat{\mathbf{z}}: \quad & \rho_0 \frac{\partial v_x}{\partial t} = -\frac{\partial P_1}{\partial x} + \frac{B_0}{4\pi}\left(\frac{\partial B_{1x}}{\partial z} - \frac{\partial B_{1z}}{\partial x}\right) \\
& \rho_0 \frac{\partial v_y}{\partial t} = -\frac{\partial P_1}{\partial y} + \frac{B_0}{4\pi}\left(\frac{\partial B_{1y}}{\partial z} - \frac{\partial B_{1z}}{\partial y}\right) \\
& \rho_0 \frac{\partial v_z}{\partial t} = -\frac{\partial P_1}{\partial z} - g\rho_1 \\
& \frac{\partial \mathbf{B}_1}{\partial t} = B_0 \frac{\partial \mathbf{v}}{\partial z}, \qquad \nabla \cdot \mathbf{v} = 0, \qquad \frac{\partial \rho_1}{\partial t} + v_z \frac{\partial \rho_0}{\partial z} = 0
\end{aligned} \tag{11.49}$$

$$\begin{aligned}
\mathbf{B}_0 = B_0\hat{\mathbf{x}}: \quad & \rho_0 \frac{\partial v_x}{\partial t} = -\frac{\partial P_1}{\partial x} \\
& \rho_0 \frac{\partial v_y}{\partial t} = -\frac{\partial P_1}{\partial y} + \frac{B_0}{4\pi}\left(\frac{\partial B_{1y}}{\partial x} - \frac{\partial B_{1x}}{\partial y}\right) \\
& \rho_0 \frac{\partial v_z}{\partial t} = -\frac{\partial P_1}{\partial z} + \frac{B_0}{4\pi}\left(\frac{\partial B_{1z}}{\partial x} - \frac{\partial B_{1x}}{\partial z}\right) - g\rho_1 \\
& \frac{\partial \mathbf{B}_1}{\partial t} = B_0 \frac{\partial \mathbf{v}}{\partial x}, \qquad \nabla \cdot \mathbf{v} = 0, \qquad \frac{\partial \rho_1}{\partial t} + v_z \frac{\partial \rho_0}{\partial z} = 0.
\end{aligned} \tag{11.50}$$

As in the previous two sections, the following x–y–t dependence of the variables is assumed:

$$\left.\begin{aligned} \mathbf{v} &= \mathbf{u}(z) \\ \mathbf{B}_1 &= \delta\mathbf{B}(z) \\ P_1 &= \delta P(z) \\ \rho_1 &= \delta\rho(z) \end{aligned}\right\} \times \exp(\mathrm{i}k_x + \mathrm{i}k_y + \gamma t). \tag{11.51}$$

Substituting (11.51) into equations (11.49) and (11.50) yields, after algebraic manipulations, the following differential equations for the two cases under consideration:

$\mathbf{B} = B_0\hat{\mathbf{z}}$:

$$\left[\frac{\mathrm{d}}{\mathrm{d}z}\left(\rho_0\frac{\mathrm{d}}{\mathrm{d}z}\right) - \frac{B_0^2}{4\pi\gamma^2}\left(\frac{\mathrm{d}^2}{\mathrm{d}z^2} - k^2\right)\frac{\mathrm{d}^2}{\mathrm{d}z^2}\right]u_z(z) = \left[\rho_0 k^2 - \frac{gk^2}{\gamma^2}\left(\frac{\mathrm{d}\rho_0}{\mathrm{d}z}\right)\right]u_z(z). \tag{11.52}$$

$\mathbf{B} = B_0\hat{\mathbf{x}}$:

$$\left[\frac{\mathrm{d}}{\mathrm{d}z}\left(\rho_0\frac{\mathrm{d}}{\mathrm{d}z}\right) + \frac{B_0^2k_x^2}{4\pi\gamma^2}\left(\frac{\mathrm{d}^2}{\mathrm{d}z^2} - k^2\right)\right]u_z(z) = \left[\rho_0 k^2 - \frac{gk^2}{\gamma^2}\left(\frac{\mathrm{d}\rho_0}{\mathrm{d}z}\right)\right]u_z(z). \tag{11.53}$$

In laser–plasma interaction the horizontal magnetic field might play an important role in stabilizing the RT instabilities. In particular, if the large d.c. magnetic field (e.g. the vector product of the density gradient and the temperature gradient; see chapter 8), created in the corona, penetrates into the ablation surface then the ablation surface instability is significantly modified. Therefore, only equation (11.53) is further analysed in the following part of this section.

For $k_x = 0$, equation (11.53) is identical to equation (11.23), where no magnetic field is applied. Therefore, the disturbances that are independent of the coordinate along the direction of $\mathbf{B}_0$ (perpendicular to $\mathbf{g}$) are not affected by the existence of the magnetic field. In this case, $\mathbf{B}_0$ does not contribute to the development of the RT instability. In other words, the magnetic field in the x direction, which can stabilize the RT instabilities for wavelengths shorter than a critical value λ_c, does not stabilize any RT instability that develops along the y direction.

For $k_x \neq 0$. the RT instabilities in the hydromagnetic problem (equation (11.53)) are not identical to the RT instabilities in the hydrodynamic problem (equation (11.23)). We solve equation (11.53) for two uniform fluids separated at the surface $z = 0$, with a density distribution given by

$$\rho(z) = \rho_{\mathrm{up}}\theta(z) + \rho_{\mathrm{down}}\theta(-z). \tag{11.54}$$

At the horizontal boundary $z = 0$, the following continuity conditions must be satisfied:

$$\begin{aligned} &\lim_{\varepsilon \to 0} \{u_z(+\varepsilon) = u_z(-\varepsilon)\} \\ &\lim_{\varepsilon \to 0} \{B_z(+\varepsilon) = B_z(-\varepsilon)\}. \end{aligned} \tag{11.55}$$

The second equation follows from the first equation (or vice versa) by the use of (11.51) in the fourth equation of (11.50). The physical meaning of the first equation (11.55) is that there is not an infinite acceleration when a fluid element crosses the interface, while the second equation describes the fact that monopoles do not exist ($\nabla \cdot \mathbf{B} = 0$). Using the solution (11.27), which is also valid in this problem, one gets by integrating equation (11.53) along the interface (similar to the integrals in the previous two sections):

$$\gamma^2 = gk \left[\frac{\rho_{\text{up}} - \rho_{\text{down}}}{\rho_{\text{up}} + \rho_{\text{down}}} - \frac{B_0^2 k_x^2}{2\pi(\rho_{\text{up}} + \rho_{\text{down}})gk} \right]. \tag{11.56}$$

The angle ϕ between the k vector and the initial magnetic field (x axis), and the wavelength of a sinusoidal disturbance (a normal mode), are defined by

$$\cos\phi = \frac{k_x}{k} = \frac{k_x}{\sqrt{k_x^2 + k_y^2}}, \qquad \lambda = \frac{2\pi}{k}. \tag{11.57}$$

The stable modes, $\gamma^2 < 0$, are therefore satisfying

$$\lambda < \frac{B_0^2 \cos^2\phi}{g\Delta\rho} \equiv \lambda_{\text{c}}, \qquad \Delta\rho \equiv \rho_{\text{up}} - \rho_{\text{down}}. \tag{11.58}$$

For example, in laser plasma acceleration with $g \approx 10^{15}\,\text{cm/s}^2$, magnetic fields of the order of 10 MG, $\Delta\rho \approx 1\,\text{g/cm}^3$ and $\cos\phi \approx 0.5$, one gets stable modes for wavelengths smaller than 0.05 cm, a non-negligible dimension for high-intensity laser–plasma interactions.

It is interesting to see that if $\cos\phi \to 0$, then the hydromagnetic result (11.56) goes to the hydrodynamic result (11.29).

We end this section by pointing out that surface tension σ_{st} (dimension $\text{erg/cm}^2 = \text{dyne/cm}$) also stabilizes the RT instability (Chandrasekhar 1961). The hydrodynamic instability in this case gives a similar result to equation (11.56) with the substitution

$$\sigma_{\text{st}} \to \frac{B_0^2 \cos^2\phi}{2\pi k}, \qquad \gamma^2 = gk \left[\frac{\rho_{\text{up}} - \rho_{\text{down}}}{\rho_{\text{up}} + \rho_{\text{down}}} - \frac{k^2 \sigma_{\text{st}}}{g(\rho_{\text{up}} + \rho_{\text{down}})} \right]. \tag{11.59}$$

11.5 Bubbles from Rayleigh–Taylor Instability

It has been shown in section 11.2 that the amplitude of a sinusoidal perturbation increases exponentially with time in the RT instability. When the

amplitude becomes of the order of the wavelength ($>0.1\lambda$), then higher harmonics of the original perturbation appear in the disturbance. The interaction between the different modes results in the formation of bubbles, with the light fluid penetrating into the heavy fluid and spikes of heavy fluid falling into the light fluid. The full-time development of the RT instability has been discussed in the literature (Davies and Taylor 1950, Layzer 1955). In this section the asymptotic steady state of the bubble motion is considered (Hoffman 1995) using the potential flow theory.

For an incompressible irrotational fluid the flow velocity $\mathbf{v}(\mathbf{r}, t)$ satisfies the following equations:

$$\nabla \cdot \mathbf{v} = 0, \qquad \nabla \times \mathbf{v} = 0 \tag{11.60}$$

Using these equations and the identity $\nabla \times (\nabla\varphi) = 0$, one can define a velocity potential ϕ which obeys the Laplace equation:

$$\nabla^2\varphi = 0. \tag{11.61}$$

The Cartesian coordinates are chosen in such a way that the bubble moves in the z direction and the vector $\mathbf{k}$ ($k_x = k, k_y = 0$) is chosen in the x direction so that the y direction can be neglected. The bubble surface motion is analysed in the bubble centre of mass coordinates, where the Laplace equation takes the form

$$\frac{\partial^2\varphi}{\partial x^2} + \frac{\partial^2\varphi}{\partial z^2} = 0. \tag{11.62}$$

The following boundary conditions are appropriate for this problem:

$$v_x\left(x = \pm\frac{\lambda}{2}\right) = 0, \qquad v_z(z = +\infty) = -u\,. \tag{11.63}$$

The first equation describes an array of identical moving bubbles with a period of $\lambda = 2\pi/k$, or equivalently one bubble with a radius λ moving between two parallel frictionless walls at $x = \pm\lambda/2$. The second boundary condition is equivalent to the motion of a bubble with an asymptotic constant velocity u, or equivalently in the frame of reference of the bubble the flow is moving at $z =$ infinity with a velocity $-u$.

The solution of equation (11.62), subject to the boundary conditions (11.63), is

$$\begin{aligned} \varphi(x, z) &= -zu - \frac{\lambda}{2\pi}\sum_{n=1}^{\infty}\left(\frac{a_n}{n}\right)\exp\left(-\frac{2\pi n z}{\lambda}\right)\cos\left(\frac{2\pi n x}{\lambda}\right) \\ v_x &= \frac{\partial\varphi}{\partial x}, \qquad v_y = \frac{\partial\varphi}{\partial y}. \end{aligned} \tag{11.64}$$

It is convenient at this stage to introduce the concept of **streamlines** (Courant and Friedrichs 1948, Landau and Lifshitz 1987). The tangent to a streamline at any point on this line gives the direction of the velocity at that point as

determined by the differential equations $\mathrm{d}x/v_x = \mathrm{d}y/v_y = \mathrm{d}z/v_z$. In steady flow the streamlines are constant in time and coincide with the trajectories of the fluid particles. In this case a particle trajectory is given by a constant value of the stream function ψ, associated with the velocity potential by

$$\frac{\partial \psi}{\partial x} = \frac{\partial \varphi}{\partial z}, \qquad \frac{\partial \psi}{\partial z} = -\frac{\partial \varphi}{\partial x}. \tag{11.65}$$

The stream function that satisfies equations (11.64) and (11.65) is given by

$$\psi(x,z) = -xu - \frac{\lambda}{2\pi}\sum_{n=1}^{\infty}\left(\frac{a_n}{n}\right)\exp\left(-\frac{2\pi n z}{\lambda}\right)\sin\left(\frac{2\pi n x}{\lambda}\right). \tag{11.66}$$

At $z = +\infty$ the stream function equals $-xu$. Since in this model all the bubbles are identical, it is convenient to choose a trajectory

$$\psi(x,z) = 0. \tag{11.67}$$

Substituting (11.67) into (11.66) yields the equation that describes the surface of a bubble:

$$1 = \frac{\lambda}{2\pi x u}\sum_{n=1}^{\infty}\left(\frac{a_n}{n}\right)\exp\left(-\frac{2\pi n z}{\lambda}\right)\sin\left(\frac{2\pi n x}{\lambda}\right). \tag{11.68}$$

This equation has been solved (Davies and Taylor 1950) by using only the first term in the potential and in the streaming functions, i.e. $a_n \neq 0$ only for $n = 1$. Under this assumption the fluid flow velocity is

$$\begin{aligned} v_x &= a_1 \exp\left(-\frac{2\pi z}{\lambda}\right)\sin\left(\frac{2\pi x}{\lambda}\right) \\ v_z &= -u + a_1 \exp\left(-\frac{2\pi z}{\lambda}\right)\cos\left(\frac{2\pi x}{\lambda}\right) \end{aligned} \tag{11.69}$$

and the surface of the bubble is described by

$$a_1 \exp\left(-\frac{2\pi z}{\lambda}\right)\sin\left(\frac{2\pi x}{\lambda}\right) = \frac{2\pi x u}{\lambda}. \tag{11.70}$$

Choosing the coordinates in such a way that for $x = 0$ the peak of the bubble is at $z = 0$, then one has to solve equations (11.69) and (11.70) for

$$a_1 = u \tag{11.71}$$

in order to find the asymptotic velocity u.

For a steady flow ($\partial \mathbf{v}/\partial t = 0$), like the case under consideration, the momentum equation yields the famous **Bernoulli law** along a streamline:

$$\frac{1}{2}v^2 + \frac{P}{\rho} + gz = \text{const.} \tag{11.72}$$

In the present model it is assumed that the Atwood number $A \approx 1$, i.e. the upper fluid has a density much larger than the lower fluid. Therefore, it is

conceivable to assume a constant pressure within the lower density bubble at its border with the heavy fluid. On the other hand, the high-density fluid is in equilibrium with the bubble, and combining this with the assumption of constant density (incompressible fluid), one can rewrite Bernoulli's equation:

$$0 = \tfrac{1}{2}(v_x^2 + v_y^2) + gz \tag{11.73}$$

where the constant has been taken at zero since the peak at $z = 0$ of the bubble is a stagnation point with $v_x = v_y = 0$. Substituting (11.69) and (11.71), into (11.73) one gets

$$1 + \exp\left(-\frac{4\pi z}{\lambda}\right) - 2\exp\left(-\frac{2\pi z}{\lambda}\right)\cos\left(\frac{2\pi x}{\lambda}\right) + \frac{2gz}{u^2} = 0. \tag{11.74}$$

One has to solve the momentum equation, as expressed in equation (11.74), together with the bubble surface equation (11.70) (with $a_1 = u$), yielding the following equation for x:

$$\xi^2 \tan\xi - 2\xi\sin^2\xi + \tan\xi\sin^2\xi + \left(\frac{g\lambda}{\pi u^2}\right)\tan\xi\sin^2\xi\ln\left(\frac{\sin\xi}{\xi}\right) = 0 \tag{11.75}$$

$$\xi \equiv \frac{2\pi x}{\lambda}.$$

Except for $\xi = 0$ (i.e. $x = 0$), this equation has only one solution for a given value of $g\lambda/u^2$. In order to get the more general solution for all points on the bubble surface, one has to take into account the full expansions (or more terms) of equations (11.64) and (11.68). However, u can be obtained to a good approximation by solving equation (11.75) in the neighbourhood of $x = 0$ for different values of g, λ and u. For this purpose this equation is expanded in a series of ξ, yielding the following equation to the lowest relevant order (ξ^5):

$$\xi^5\left(1 - \frac{g\lambda}{6\pi u^2}\right) = 0 \tag{11.76}$$

with the following solution, for the asymptotic velocity of the bubble:

$$u = \sqrt{\frac{g\lambda}{6\pi}} \approx 0.2304\sqrt{g\lambda}. \tag{11.77}$$

As explained in section 11.1, equations (11.2), (11.3) and (11.4), this result is consistent with balancing the buoyancy force and the drag force acting on a rising bubble.

11.6 Richtmyer–Meshkov Instability

The Richtmyer–Meshkov (RM) instability is named after Robert D. Richtmyer, who suggested and also developed the theory of the instability,

and E. E. Meshkov, who proved experimentally the existence of this instability. The RM instability describes the behaviour of the interface between two fluids or gases, traversed by a shock wave. This interface is unstable when the shock wave crosses from the lighter to the heavier media and it is also unstable when the shock wave passes in the opposite direction. A schematic presentation of RM instability is given in figure 11.2. The shock wave imparts an impulsive acceleration to the interface, and as a result an interface disturbance grows initially linearly with time, it saturates, and it can develop into bubbles and spikes like in the RT instability.

We analyse two incompressible fluids with a disturbance of the interface given by

$$z(x,t) = \zeta(t)\exp(\mathrm{i}kx), \qquad k\zeta \ll 1 \tag{11.78}$$

where the real part of the right-hand side (i.e. $\cos kx$) is taken to describe the real z values. If the system is accelerated in the z direction with an acceleration $g(t)$, then the amplitude of the interface disturbance satisfies the equation:

$$\frac{\mathrm{d}^2\zeta(t)}{\mathrm{d}t^2} = kg(t)A\zeta(t), \qquad A \equiv \frac{\rho_{\mathrm{up}} - \rho_{\mathrm{down}}}{\rho_{\mathrm{up}} + \rho_{\mathrm{down}}}. \tag{11.79}$$

This equation is easily obtained from equations (11.29) in the two-dimensional space x–z. The fluid flow velocity solution derived in (11.29) satisfies

$$\frac{\partial^2 v_z}{\partial t^2} = \gamma^2 v_z, \qquad \gamma^2 = kgA \tag{11.80}$$

and therefore, if the displacement $\zeta(t)$ is defined by

$$\frac{\partial \zeta}{\partial t} = v_z \tag{11.81}$$

then equation (11.80) implies the validity of equation (11.79).

Denoting by U the increment of the velocity of an instantaneous impulse at $t = 0$,

$$g(t) = U\,\delta(t) \Rightarrow \int g(t)\,\mathrm{d}t = U \tag{11.82}$$

where $\delta(t)$ is the Dirac delta function, then equation (11.79) can be integrated to give

$$\begin{aligned} &\textbf{before impulse } (t<0): \quad \zeta = \zeta_0, \qquad \frac{\mathrm{d}\zeta}{\mathrm{d}t} = 0 \\ &\textbf{immediately after impulse}: \quad \zeta = \zeta_0, \qquad \frac{\mathrm{d}\zeta}{\mathrm{d}t} = kUA\zeta_0. \end{aligned} \tag{11.83}$$

As can be seen from this equation, after the impulse the amplitude ζ grows at a constant rate.

Table 11.1. The notation for the variables described in figure 11.2, in the case of weak shock waves: velocity $\mathbf{v} = (v_x, v_z)$, specific volume $V = 1/\rho$ where ρ is the fluid density, and pressure P. Note that $P_1 = P_2$.

The variable	Region 0 (heavy fluid)	Region 1 (heavy fluid)	Region 2 (light fluid)	Region 3 (light fluid)
Velocity $v_x(x,z,t)$	0	$u_{1,x}(z,t)\exp(\mathrm{i}kx)$	$u_{1,x}(z,t)\exp(\mathrm{i}kx)$	
Velocity $v_z(x,z,t)$	$u_0 > 0$	$u_{1,z}(z,t)\exp(\mathrm{i}kx)$	$u_{1,z}(z,t)\exp(\mathrm{i}kx)$	$u_3 < 0$
Specific volume $V(x,z,t) = 1/\rho$	V_0	$V_1 + \delta V(z,t)\exp(\mathrm{i}kx)$	$V_2 + \delta V(z,t)\exp(\mathrm{i}kx)$	V_3
Pressure $P(x,z,t)$	P_0	$P_1 + \delta P(z,t)\exp(\mathrm{i}kx)$	$P_2 + \delta P(z,t)\exp(\mathrm{i}kx)$	P_3

One of the basic assumptions for the correctness of (11.79) is that the medium is incompressible. For an impulsive acceleration, such as induced by a shock wave, this assumption is no longer valid and equation (11.79) cannot be used.

Following Richtmyer, we analyse the interface between two fluids (or gases) when a shock wave passes across a disturbed interface from the less dense to a denser medium. As described in figure 11.2, before and after the impulse, a planar shock wave passes a corrugated interface that causes the transmitted and the reflected shocks to also have corrugated surfaces. Before the arrival of the shock the medium is assumed to be at rest. Furthermore, the shock pressure behind the incident shock is assumed constant. In table 11.1 the notation is summarized for the fluid variables, described in figure 11.2. The notation of table 11.1 is given for weak shock waves, where

$$\frac{\delta V}{V_j} \ll 1, \quad j = 1,2, \qquad \frac{\delta P}{P_j} \ll 1, \quad j = 1,2 \tag{11.84}$$

and terms of the second order and higher in δP and δV are neglected. The fluid velocities are given in the frame of reference of the moving interface (after the shock wave has crossed the interface). In this system the mean position of the interface is $z = 0$, and the coordinates of the surfaces (1) between the fluids (the interface), (2) the transmitted shock wave and (3) the reflected shock wave are

$$\begin{aligned} \textbf{interface}: &\quad z = \zeta_0(t)\exp(\mathrm{i}kx) \\ \textbf{transmitted shock}: &\quad z = -w_1 t + \zeta_1(t)\exp(\mathrm{i}kx) \\ \textbf{reflected shock}: &\quad z = w_2 t + \zeta_2(t)\exp(\mathrm{i}kx) \end{aligned} \tag{11.85}$$

where w_1 and w_2 are the shock wave velocities in the interface frame of reference.

Since we are using the linear theory, one can take $\exp(\mathrm{i}kx)$ and $-\mathrm{i}\exp(\mathrm{i}kx)$ for $\cos kx$ and $\sin kx$ respectively. In general, complex functions are used with the meaning that at the last step the real values should be taken.

11.6.1 The differential equation for the pressure in regions 1 and 2

This analysis is a first-order perturbation theory with the small variables as given by (11.84) and also $u_{1,z} \ll w_1$ and w_2, and $\zeta_j k$ (for $j = 0, 1, 2) \ll 1$. For a weak shock wave (Zeldovich and Raizer 1966), the first-order perturbation theory gives the following relation between the pressure increase δP and the specific volume change δV (note that the notation of table 11.1 is used):

$$\delta P(z,t) = \left(\frac{\partial P}{\partial V}\right)_{\mathrm{S}} \delta V(z,t) = -\left(\frac{c_1^2}{V_1^2}\right)\delta V(z,t) \tag{11.86}$$

where c_1 is the speed of sound in the undisturbed medium of region 1 (the heavy fluid). This equation can be considered as the **equation of state** in our approximation.

The **mass conservation**, the first of equations (11.14), can be written as

$$\begin{aligned} &\frac{\partial}{\partial t}\left(\frac{1}{V_1+\delta V}\right) + \left(\frac{1}{V_1+\delta V}\right)\nabla\cdot\mathbf{v}(x,z,t) = 0 \\ &\Rightarrow V_1\left(iku_{1,x} + \frac{\partial u_{1,z}}{\partial z}\right) = \frac{\partial(\delta V)}{\partial t} = -\left(\frac{V_1^2}{c_1^2}\right)\frac{\partial(\delta P)}{\partial t} \end{aligned} \tag{11.87}$$

where at the last step equation (11.86) has been used.

The following two equations are obtained from the **momentum conservation**:

$$\begin{aligned} &\left(\frac{1}{V_1+\delta V}\right)\frac{\partial \mathbf{v}(x,z,t)}{\partial t} = -\nabla[P_1 + \delta P(z,t)\exp(\mathrm{i}kx)] \\ &\Rightarrow \begin{cases} \dfrac{1}{V_1}\dfrac{\partial u_{1,z}}{\partial t} = -\dfrac{\partial(\delta P)}{\partial z} \\ \dfrac{1}{V_1}\dfrac{\partial u_{1,x}}{\partial t} = -\mathrm{i}k\delta P. \end{cases} \end{aligned} \tag{11.88}$$

From equations (11.87) (one equation) and (11.88) (two equations), the following wave equation is derived for $\delta P(z,t)$ in region 1 (see figure 11.2), and similarly the second wave equation is obtained in region 2 with the substitution $c_1 \to c_2$:

$$\begin{aligned} &\frac{\partial^2}{\partial t^2}(\delta P) - c_1^2\left(\frac{\partial^2}{\partial z^2} - k^2\right)(\delta P) = 0 \\ &\frac{\partial^2}{\partial t^2}(\delta P) - c_2^2\left(\frac{\partial^2}{\partial z^2} - k^2\right)(\delta P) = 0. \end{aligned} \tag{11.89}$$

11.6.2 The boundary conditions on the interface

In order to solve equations (11.89) in regions 1 and 2, the equations at the boundaries of these domains have to be defined. Region 1 is defined between the interface (between the fluids) and the transmitted shock surfaces, while region 2 is between the interface and the reflected shock. The normal fluid velocities from both regions are equal at the interface, and therefore one can also write the acceleration continuity on the interface. Using the interface equation (11.85) and the momentum equation (11.88), the following boundary equations are derived by the requirement that the accelerations in the z direction, $\partial u_{1,z}/\partial t$ and $\partial u_{2,z}/\partial t$ are continuous:

$$\begin{aligned} \frac{\mathrm{d}^2\zeta_0(t)}{\mathrm{d}t^2} &= \left[-V_1\left(\frac{\partial(\delta P)}{\partial z}\right)\right]_{z=-0} \\ \left[V_1\left(\frac{\partial(\delta P)}{\partial z}\right)\right]_{z=-0} &= \left[V_2\left(\frac{\partial(\delta P)}{\partial z}\right)\right]_{z=+0}. \end{aligned} \tag{11.90}$$

The second equation is the needed boundary (at the interface) for the partial differential equation (11.89). The main objective of this problem is the study of the RM instability, and for this purpose the first of equations (11.90) gives the required information, i.e. the calculation of $\zeta_0(t)$.

In order to complete this problem the boundary conditions at the shock-wave surfaces are also needed.

11.6.3 The boundary conditions at the shock-wave surfaces

First, we use the Hugoniot relations (equations (10.36)) on the boundary of regions 2 and 3, at the reflected shock wave. One has to note that the initial conditions for the Hugoniot equations are those obtained at the final stage after the crossing of the first shock wave. In other words, the reflected shock enters a shocked medium. Moreover, area 3 has also been shocked before the present analysis is considered. However, for this domain the simple Hugoniot relations can be used, and P_3 and V_3 are easily calculated from the initial conditions of region 4, as shown in figure 11.2(a).

Therefore, the first and the fourth equations of (10.36) on the boundary of regions 2 and 3 can be written in the following way:

$$\begin{aligned} &\frac{w_2 + \dot{\zeta}_2(t)\exp(\mathrm{i}kx) - u_{1,z}(w_2t,t)\exp(\mathrm{i}kx)}{V_2 + \delta V(w_2t,t)\exp(\mathrm{i}kx)} \\ &\qquad = \frac{w_2 + \dot{\zeta}_2(t)\exp(\mathrm{i}kx) - u_3}{V_3} \\ &\frac{w_2 + \dot{\zeta}_2(t)\exp(\mathrm{i}kx) - u_3}{V_3} = \sqrt{\frac{P_2 + \delta P(w_2t,t)\exp(\mathrm{i}kx) - P_3}{V_3 - V_2 - \delta V(w_2t,t)\exp(\mathrm{i}kx)}} \end{aligned} \tag{11.91}$$

where the dot means time derivative and $P_2 = P_1$. The Hugoniot relations in the form of equations (10.36) are correct only for the velocity components perpendicular to the shock surface. Since the shock front is not a plane, one has to multiply the fluid velocities in these equations with the cosines of the angle between the velocity and the normal to the surface. However, since the angles are first-order variables, these cosines differ from unity by second-order quantities. Therefore, equations (11.91) are correct only to first order in perturbation theory, and by expanding these equations the following zeroth- and first-order equations are obtained respectively:

$$\frac{w_2}{V_2} = \frac{w_2 - u_3}{V_3}, \qquad \frac{w_2}{V_2} = \sqrt{\frac{P_2 - P_3}{V_3 - V_2}} \quad (\text{note: } P_2 = P_1) \tag{11.92}$$

$$\frac{1}{V_2}\left[\frac{d\zeta_2}{\mathrm{d}t} - u_{1,z}(w_2 t, t)\right] - \frac{w_2}{V_2^2}\delta V(w_2 t, t) = \frac{1}{2}\sqrt{\frac{P_2 - P_3}{V_3 - V_2}}\left[\frac{\delta P(w_2 t, t)}{P_2 - P_3} + \frac{\delta V(w_2 t, t)}{V_3 - V_2}\right] \tag{11.93}$$

$$\frac{1}{V_3}\frac{\mathrm{d}\zeta_2}{\mathrm{d}t} = \frac{1}{2}\sqrt{\frac{P_2 - P_3}{V_3 - V_2}}\left[\frac{\delta P(w_2 t, t)}{P_2 - P_3} + \frac{\delta V(w_2 t, t)}{V_3 - V_2}\right].$$

Inspecting the zeroth-order equations (11.92), one can easily recognize the Hugoniot jump conditions for planar one-dimensional waves. It turns out that our problem to zeroth order can be described by planar waves. The corrugation of the surfaces (interface and the shock waves) are described in this analysis by the first-order terms. Using the property that the Hugoniot pressure derivative with respect to the specific volume equals the isentrope derivative at the initial point on the Hugoniot (equation (10.99)), the first-order expansion of the Hugoniot pressure can be described by

$$\delta P(w_2 t, t) \equiv \delta P_2(t) = \left(\frac{\mathrm{d}\delta P_2}{\mathrm{d}V}\right)_{V_2}\delta V = \left(\frac{\mathrm{d}P_\mathrm{S}}{\mathrm{d}V}\right)_{V_2}\delta V = -\frac{c_2^2 \delta V}{(V_2 + \delta V)^2} \approx \frac{c_2^2 \delta V}{V_2^2} \tag{11.94}$$

where P_S is the isentropic pressure. Substituting this result into the second equation of (11.93) yields the following boundary condition:

$$\frac{\mathrm{d}\zeta_2(t)}{\mathrm{d}t} = \frac{1}{2}\left(\frac{V_3 V_2}{V_3 - V_2}\right)\left(\frac{c_2^2 - w_2^2}{c_2^2 w_2}\right)\delta P_2(t), \qquad \delta P_2(t) \equiv \delta P(z = w_2 t, t). \tag{11.95}$$

A similar procedure at the transmitted shock-wave surface yields a similar boundary relation:

$$\frac{\mathrm{d}\zeta_1(t)}{\mathrm{d}t} = \frac{1}{2}\left(\frac{V_0 V_1}{V_0 - V_1}\right)\left(\frac{c_1^2 - w_1^2}{c_1^2 w_1}\right)\delta P_1(t)$$
$$\delta P_1(t) \equiv \delta P(z = -w_1 t, t). \tag{11.96}$$

A second boundary value equation for the reflected shock-wave surface is obtained by the use of the first equation of (11.93). Substituting into this equation the relation between δP and δV at the shock front (equation (11.94)), and comparing the obtained value of $\mathrm{d}\zeta_2/\mathrm{d}t$ with that derived in (11.95), gives

$$u_{1,z}(w_2 t, t) = \frac{1}{2} V_2 \left(\frac{c_2^2 + w_2^2}{c_2^2 w_2}\right)\delta P_2(t). \tag{11.97}$$

By multiplying both sides of this equation with the total derivative, and describing the change in time of a moving fluid element on the shock surface, one gets

$$\left(\frac{\partial}{\partial t} + w_2 \frac{\partial}{\partial z}\right) u_{1,z}(z = w_2 t, t) = \frac{1}{2} V_2 \left(\frac{c_2^2 + w_2^2}{c_2^2 w_2}\right)\left(\frac{\partial}{\partial t} + w_2 \frac{\partial}{\partial z}\right)\delta P(z = w_2 t, t). \tag{11.98}$$

At this stage the mass and momentum equations (equations (11.87) and (11.88)) are necessary. However, before using these equations one has to calculate the x derivative of $u_{1,x}$.

The component of the fluid velocity $\mathbf{v}$, parallel to the shock surface, is continuous across this surface. Therefore, one can write to the first order in our perturbation theory (see figure 11.2(c)) (note $u_{1,x} = u_{2,x}$ and $u_{1,z} = u_{2,z}$):

$$u_{1,x}(w_2 t, t)\exp(\mathrm{i}kx) = u_3 \tan\phi$$
$$\tan\phi = \frac{\partial z}{\partial x} = \frac{\partial}{\partial x}[w_2 t + \zeta_2(t)\exp(\mathrm{i}kx)] = \mathrm{i}k\zeta_2(t)\exp(\mathrm{i}kx) \tag{11.99}$$
$$\Rightarrow \mathrm{i}k w_2 u_{1,x}(z = w_2 t, t) = -k^2 w_2 u_3 \zeta_2(t).$$

Adding this result to equation (11.98) and using the following mass and momentum equations for region 2 (similar to equations (11.87) and (11.88)):

$$\frac{\partial u_{1,z}}{\partial z} + \mathrm{i}k u_{1,x} = -\frac{V_2}{c_2^2}\frac{\partial \delta P}{\partial t}, \qquad -\mathrm{i}k\delta P = \frac{1}{V_2}\frac{\partial u_{1,x}}{\partial t} \tag{11.100}$$

one gets the following second boundary condition on the surface of the reflected shock wave:

$$\left(\frac{3}{2}w_2 + \frac{c_2^2}{2w_2}\right)\frac{\mathrm{d}}{\mathrm{d}t}(\delta P_2) = (w_2^2 - c_2^2)\frac{\partial}{\partial z}[\delta P(z = w_2 t, t)] + \frac{k^2 c_2^2 w_2 u_3}{V_2}\zeta_2(t). \tag{11.101}$$

A similar second boundary condition is given for the transmitted shock-wave surface:

$$\left(\frac{3}{2}w_1 + \frac{c_1^2}{2w_1}\right)\frac{\mathrm{d}}{\mathrm{d}t}(\delta P_1) = -(w_1^2 - c_1^2)\frac{\partial}{\partial z}[\delta P(z = -w_1 t, t)] + \frac{k^2 c_1^2 w_1 u_0}{V_1}\zeta_1(t). \tag{11.102}$$

The boundary conditions given in equations (11.101) and (11.102) describe the change in time of the shock-wave pressures. The first term on the right-hand side of these equations is the pressure gradient contribution behind the shock. The second term on the right-hand side of these equations describes the convergence or divergence of the shock-wave propagation due to the corrugation of the shock surfaces (see figure 11.2(c)).

In this analysis of the RM instability, we have discussed only the linear development of the flow using weak shock waves. The differential equations (11.89) are subject to the boundary equations described by equations (11.90), (11.95), (11.96), (11.101) and (11.102). It is evident that a proper solution of this problem requires the help of a computer. However, the solution of the complete nonlinear problem describing the full development of the RM instability needs two- and three-dimensional sophisticated numerical analysis.

11.7 Kelvin–Helmholtz Instability

The Kelvin–Helmholtz (KH) instability occurs (Kelvin (1910), Helmholtz (1881)) when two different layers of fluids are in relative motion, such as the generation of water waves by wind blowing over the surface of the water (see figure 11.3).

In laser–plasma interactions the KH instability may occur during the later stages of RT and RM instabilities, during the motion of the bubbles and the spikes. For example, the low-density bubbles move relative to the heavy fluid background with appropriate conditions to create KH instabilities.

The motion of an incompressible, inviscid (no viscosity) fluid streaming in the horizontal direction is now considered. The surface tension is neglected in this analysis, although it is straightforward to include this stabilizing effect. It is assumed that the streaming takes place in the x direction with a velocity U, where U is an arbitrary function of z. The fluid is accelerated in the z direction, or equivalently it moves in a potential described by the acceleration g (in the $-z$ direction). First-order perturbation is assumed with the following notation (see equation (11.11)):

1. The flow velocity is $\mathbf{v}(x, y, z, t) + U(z)\hat{\mathbf{x}}$, where the velocity components of $\mathbf{v} = (v_x, v_y, v_z)$ are first-order terms ($\mathbf{v}_0 = 0$ and $\mathbf{v}_1$ is denoted here by $\mathbf{v}$).
2. The fluid density is $\rho(x, y, z, t) = \rho_0(z) + \rho_1(x, y, z, t)$, where ρ_1 is a first-order term.

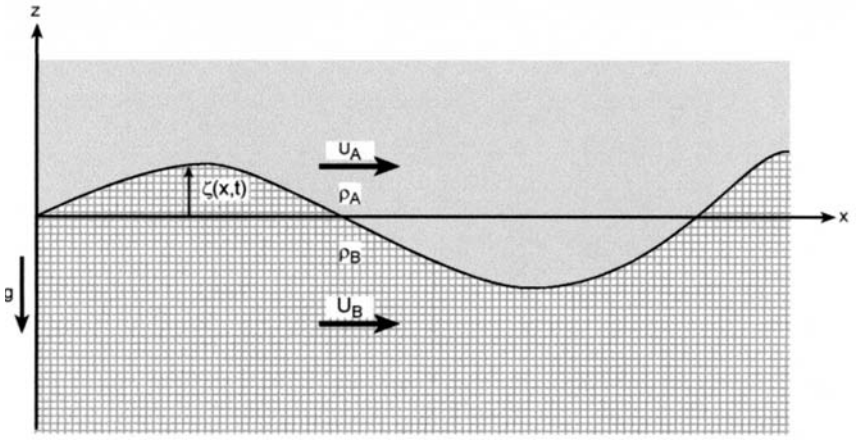

Figure 11.3. Two fluids A and B, with densities ρ_A and ρ_B, moving with different horizontal velocities U_A and U_B. The interface between the two media develops a disturbance with a wave number $k = 2\pi/\lambda$.

3. The pressure is $P = P_0 + P_1(x, y, z, t)$, with P_1 a first-order term.

The momentum conservation, mass conservation and the incompressible fluid assumption give five equations similar to those in (11.18). The following equations are derived by substituting $\mathbf{v}$ by $\mathbf{v} + \mathbf{U}$ in the conservation equations (11.9) and using a similar first-order perturbation theory, as has been done for example in section 11.2:

$$\begin{aligned}
\rho_0 \frac{\partial v_x}{\partial t} + \rho_0 U \frac{\partial v_x}{\partial x} + \rho_0 v_z \frac{\mathrm{d}U}{\mathrm{d}z} + \frac{\partial P_1}{\partial x} &= 0 \\
\rho_0 \frac{\partial v_y}{\partial t} + \rho_0 U \frac{\partial v_y}{\partial x} + \frac{\partial P_1}{\partial y} &= 0 \\
\rho_0 \frac{\partial v_z}{\partial t} + \rho_0 U \frac{\partial v_z}{\partial x} + \frac{\partial P_1}{\partial z} + g\rho_1 &= 0 \\
\frac{\partial \rho_1}{\partial t} + U \frac{\partial \rho_1}{\partial x} + v_z \frac{\mathrm{d}\rho_0}{\mathrm{d}z} &= 0 \\
\frac{\partial v_x}{\partial x} + \frac{\partial v_y}{\partial y} + \frac{\partial v_z}{\partial z} &= 0.
\end{aligned} \tag{11.103}$$

We assume that the interface between the fluids is initially at $z = 0$, the disturbance $\zeta(x, y, t)$ is in the z direction (also a first order perturbation term) and it obeys the following equation:

$$\frac{\partial \zeta}{\partial t} + U(z = \zeta)\frac{\partial \zeta}{\partial x} = v_z(z = \zeta). \tag{11.104}$$

This equation describes the velocity of the disturbance normal to the interface. Analysing the disturbance by its normal modes, one can look for the following solutions (note that here the time dependence is $\exp(\mathrm{i}\Gamma t)$, while in (11.19) it is $\exp(\gamma t)$):

$$\left.\begin{aligned}&\mathbf{v}(x,y,z,t)=\mathbf{u}(z)\\&\rho_1(x,y,z,t)=\delta\rho(z)\\&P_1(x,y,z,t)=\delta P(z)\\&\zeta(x,y,t)=\zeta_0\end{aligned}\right\}\times\exp[\mathrm{i}(k_x x+k_y y+\Gamma t)]. \tag{11.105}$$

Substituting (11.105) into equations (11.103) and (11.104), one gets accordingly

$$\begin{aligned}\mathrm{i}\rho_0(\Gamma+k_x U)u_x+\rho_0\left(\frac{\mathrm{d}U}{\mathrm{d}z}\right)u_z+\mathrm{i}k_x\delta P&=0\\ \mathrm{i}\rho_0(\Gamma+k_x U)u_y+\mathrm{i}k_y\delta P&=0\\ \mathrm{i}\rho_0(\Gamma+k_x U)u_z+\left(\frac{\mathrm{d}\delta P}{\mathrm{d}z}\right)+g\delta\rho&=0\\ \mathrm{i}(\Gamma+k_x U)\delta\rho+u_z\left(\frac{\mathrm{d}\rho_0}{\mathrm{d}z}\right)&=0\\ \mathrm{i}(k_x x+k_y y)+\left(\frac{\mathrm{d}u_z}{\mathrm{d}z}\right)&=0\end{aligned} \tag{11.106}$$

$$\mathrm{i}(\Gamma+k_x U_\zeta)\zeta_0=u_\zeta,\qquad U_\zeta\equiv U(z=\zeta),\qquad u_\zeta\equiv u(z=\zeta). \tag{11.107}$$

Similar to the algebra used to solve equations (11.20), the following differential equation is obtained for $u_z(z)$ by solving equations (11.106):

$$\begin{aligned}&\frac{\mathrm{d}}{\mathrm{d}z}\left\{\left[\rho_0(\Gamma+k_x U)\frac{\mathrm{d}}{\mathrm{d}z}\right]-\left[\rho_0 k_x\left(\frac{\mathrm{d}U}{\mathrm{d}z}\right)\right]\right\}u_z(z)\\ &\quad=\left[k^2\rho_0(\Gamma+k_x U)+\frac{gk^2}{(\Gamma+k_x U)}\left(\frac{\mathrm{d}\rho_0}{\mathrm{d}z}\right)\right]u_z(z).\end{aligned} \tag{11.108}$$

This differential equation is subject to boundary conditions such as that given in (11.24). Furthermore, from equation (11.107) it follows that

$$\frac{u_z(z=\zeta+0)}{\Gamma+k_x U(z=\zeta+0)}=\frac{u_z(z=\zeta-0)}{\Gamma+k_x U(z=\zeta-0)} \tag{11.109}$$

i.e. if one approaches the interface from below or from above, the same value of ζ_0 is obtained, or in other words, if U is continuous at the interface then u_z is also continuous there; however, if U is discontinuous, then the normal displacement on the interface at any point on the surface should be uniquely defined.

At this stage the 'jump' condition on the interface between the fluids is defined. For this purpose one has to integrate equation (11.108) across the

interface from $\zeta - \varepsilon$ to $\zeta + \varepsilon$ in the limit that ε goes to zero. As in (11.28), we define

$$\begin{aligned}
&\lim_{\varepsilon \to 0} \int_{\zeta-\varepsilon}^{\zeta+\varepsilon} \frac{\mathrm{d}}{\mathrm{d}z} F(z)\, \mathrm{d}z = \lim_{\varepsilon \to 0} [F(\zeta+\varepsilon) - F(\zeta-\varepsilon)] \equiv \Delta_\zeta \mathrm{F} \\
&\lim_{\varepsilon \to 0} \int_{\zeta-\varepsilon}^{\zeta+\varepsilon} G(z)\, \mathrm{d}z = 0, \qquad G(z) \text{ continuous at } z = \zeta \\
&\lim_{\varepsilon \to 0} \int_{\zeta-\varepsilon}^{\zeta+\varepsilon} \delta(z-\zeta)\, \mathrm{d}z = 1.
\end{aligned} \tag{11.110}$$

Integrating (11.108) and using (11.109) and (11.110), the following boundary condition (or as occasionally it is called, 'the jump' equation) is satisfied at the interface between the fluids:

$$\Delta_\zeta \left[\rho_0 (\Gamma + k_x U) \frac{\mathrm{d}u_z}{\mathrm{d}z} - \rho_0 k_x \left(\frac{\mathrm{d}U}{\mathrm{d}z} \right) u_z \right] = g k^2 \left(\frac{u_z}{\Gamma + k_x U} \right)_{z=\zeta} \Delta_\zeta \rho_0. \tag{11.111}$$

We calculate explicitly this equation for the following problem. Two uniform fluids, separated at the surface $z = 0$, have densities ρ_A and ρ_B (see figure 11.3). The upper fluid has a density ρ_A smaller than the lower fluid ρ_B, so that in this case we do not analyse the RT instability. Regarding the streaming, it is assumed that the upper fluid and the lower fluid stream have constant velocities U_A and U_B respectively.

Equation (11.108) for constant ρ_0 and U, i.e. anywhere except at the interface between the fluids, reduces to

$$\left(\frac{\mathrm{d}^2}{\mathrm{d}z^2} - k^2 \right) u_z(z) = 0. \tag{11.112}$$

The general solution of this equation is a linear combination of $\exp(kz)$ and $\exp(-kz)$. Taking into account that u_z vanishes at $\pm\infty$, and at $z = 0$ equation (11.109) must be satisfied, one obtains the solution

$$u_z(z) = \begin{cases} w(\Gamma + k_x U_\mathrm{B}) \exp(kz) & \text{for } z < 0 \\ w(\Gamma + k_x U_\mathrm{A}) \exp(-kz) & \text{for } z > 0. \end{cases} \tag{11.113}$$

Using (11.110), the jump relations relevant for this problem are

$$\begin{aligned}
\Delta_0 \left[\rho_0 (\Gamma + k_x U) \frac{\mathrm{d}u_z}{\mathrm{d}z} \right] &= k w [\rho_\mathrm{A} (\Gamma + k_x U_\mathrm{A})^2 + \rho_\mathrm{B} (\Gamma + k_x U_\mathrm{B})^2] \\
\Delta_0 \left[\rho_0 k_x \left(\frac{\mathrm{d}U}{\mathrm{d}z} \right) u_z \right] &= 0 \\
g k^2 \left(\frac{u_z}{\Gamma + k_x U} \right) \Delta_0(\rho_0) &= w g k^2 (\rho_\mathrm{A} - \rho_\mathrm{B}).
\end{aligned} \tag{11.114}$$

Substituting (11.114) into (11.111) yields the following quadratic equation in Γ:

$$\Gamma^2 + \frac{2k_x}{\rho_A + \rho_B}(\rho_A U_A + \rho_B U_B)\Gamma + \left[\frac{k_x^2}{\rho_A + \rho_B}(\rho_A U_A^2 + \rho_B U_B^2) - \frac{gk}{\rho_A + \rho_B}(\rho_B - \rho_A)\right] \tag{11.115}$$

with the solutions

$$\Gamma = -\frac{k_x}{\rho_A + \rho_B}(\rho_A U_A + \rho_B U_B) \pm \left[\frac{gk(\rho_B - \rho_A)}{\rho_A + \rho_B} - \frac{k_x^2 \rho_A \rho_B (U_B - U_A)^2}{(\rho_A + \rho_B)^2}\right]^{1/2}. \tag{11.116}$$

If the perturbations are perpendicular to the streaming, then the flow is stable:

$$k_x = 0: \quad \Gamma = \pm\sqrt{gk\left(\frac{\rho_B - \rho_A}{\rho_B + \rho_A}\right)}. \tag{11.117}$$

Since $\rho_B > \rho_A$, the solution of all perturbations behave like $\exp(i\Gamma t)$, Γ real, and therefore no instability.

If the perturbations are in any direction other than normal to the streaming, then instability occurs. Defining the angle θ between the vector $\mathbf{k}$ and the x axis, or more generally between the vectors $\mathbf{U}$ and $\mathbf{k}$,

$$\cos\theta = \frac{k_x}{k} = \frac{\mathbf{k}\cdot\mathbf{U}}{kU} \tag{11.118}$$

then instability occurs if Γ in equation (11.116) is complex, so that $\exp(i\Gamma t)$ increases exponentially. Instability exists when

$$k(U_B - U_A)^2 \cos^2\theta > g\left(\frac{\rho_B^2 - \rho_A^2}{\rho_B \rho_A}\right) \tag{11.119}$$

or equivalently the instability develops for any wave number k satisfying

$$k > k_{\min} \equiv g\left(\frac{\rho_B^2 - \rho_A^2}{\rho_B \rho_A}\right)\frac{1}{(U_B - U_A)^2 \cos^2\theta}. \tag{11.120}$$

It is interesting to point out that the KH instability occurs for any finite value of velocity jump across the interface, $U_B - U_A$, assuming that θ is not 90°. The stability of any static configuration becomes KH, unstable in the presence of a streaming difference (sharp gradient) across the interface of two fluids.

Appendix A

Maxwell Equations

It is here assumed that Maxwell equations are known and widely used, and therefore we only quote the differential equations (Jackson 1975, Knoepfel 2000) for completeness and for the use of notation. Both familiar systems of units, the m.k.s. (known as the **SI** units) and the c.g.s. (**Gaussian** units), are summarized. A prerequisite in plasma physics is to know and master both systems of units. For example, one of the most useful physical quantities is the laser flux energy I_L, which is usually given in **mixed units** [watt/cm^2]. In this book both systems of units are used in addition to the practical units, such as electronvolt (eV) for energy or temperature.

A.1 SI (m.k.s.) Units (International System of Units)

Maxwell equations are

$$\nabla \times \mathbf{E} = -\frac{\partial \mathbf{B}}{\partial t}, \qquad \nabla \times \mathbf{H} = \mathbf{J} + \frac{\partial \mathbf{D}}{\partial t}$$
$$\nabla \cdot \mathbf{D} = \rho_e, \qquad \nabla \cdot \mathbf{B} = 0. \tag{A.1}$$

The terminology for the five vectors and the one scalar in these Maxwell equations follow:

E is the **electric field strength** or electric intensity: units [Volt/m];
D is the electric flux density or electric induction or **displacement**: units [Coulomb/m^2];
H is the magnetic field strength or **magnetic intensity**: units [Ampere/m];
B is the magnetic flux density or **magnetic induction**: units [Tesla];
J is the the **free current density**: units [Ampere/m^2]; and
ρ_e is the **free electric charge density**: units [Coulomb/m^3].

Equations (A.1) (or in their integral form) are sometimes referred to by the names of the scientists who contributed a major part in the development of

these laws of nature. The first equation, **Faraday's law**; the second equation, the **Ampere–Maxwell law**; the third equation is **Gauss's law**, sometimes referred to as the **Poisson** equation; the fourth equation is the **Gauss–Faraday** law, which implies the absence of magnetic monopoles. In these equations $\mathbf{J}$ and ρ_e are considered as the sources of the electromagnetic fields $\mathbf{E}$, $\mathbf{D}$, $\mathbf{H}$ and $\mathbf{B}$. From the above Maxwell equations the **electric charge conservation** follows:

$$\frac{\partial \rho_e}{\partial t} + \nabla \cdot \mathbf{J} = 0. \tag{A.2}$$

In a plasma with ions and electrons,

$$\rho_e = e n_e + \sum_k q_k n_k, \qquad \mathbf{J} = e n_e v_e + \sum_k q_k n_k \mathbf{v}_k. \tag{A.3}$$

The different species of the ions are denoted by the index k, the charges and densities of the ions are q_k and n_k respectively, and v_k is their average velocities. e, n_e and v_e represent the charge, the density and the average velocity of the electrons respectively.

The **Lorentz law** gives the electromagnetic force applied on a particle with charge q:

$$\mathbf{F} = q(\mathbf{E} + \mathbf{v} \times \mathbf{B}). \tag{A.4}$$

In order to solve the Maxwell equations in a medium with sources, three more equations are required. These equations, known as the constitutive equations, are

$$\mathbf{D} = \tilde{\varepsilon}\mathbf{E} = \varepsilon_0 \varepsilon \mathbf{E} = \varepsilon_0 \mathbf{E} + \mathbf{P} \tag{A.5}$$

$$\mathbf{B} = \tilde{\mu}\mathbf{H} = \mu_0 \mu \mathbf{H} = \mu_0(\mathbf{H} + \mathbf{M}) \tag{A.6}$$

$$\mathbf{J} = \sigma_E \mathbf{E}. \tag{A.7}$$

The last equation is **Ohm's law**. $\varepsilon_0\varepsilon$ is the **dielectric constant** (sometimes called permittivity), $\varepsilon_0 = 8.8542 \times 10^{-12}$ [Farad/m], and is the dielectric constant in vacuum. $\mu_0\mu$ is the magnetic permeability, $\mu_0 = 4 \times 10^{-7}$ [Henry/m]. ε and μ are characterized by the medium and in general they can be functions of time, space, temperature, density, magnetic field, etc. For a non-isotropic medium ε and μ become tensors, and the problem might be quite complicated. $\mathbf{P}$ and $\mathbf{M}$, known as the electric and magnetic polarization vectors respectively, are two complementary convenient vectors to describe a medium.

The electromagnetic energy Q_{EM} in a volume Γ is given by

$$Q_{EM} = \int_\Gamma q_{EM}\, \mathrm{d}V = \frac{1}{2}\int_\Gamma (\mathbf{E}\cdot\mathbf{D} + \mathbf{H}\cdot\mathbf{B})\, \mathrm{d}V \quad \text{[Joules]}. \tag{A.8}$$

The electromagnetic energy density q_{EM} [Joules/m^3] and the flux of the electromagnetic energy (the Poynting vector) $\mathbf{I}_L$ in [Joules/(m^2 s)] are defined by

$$q_{EM} = \tfrac{1}{2}(\mathbf{E}\cdot\mathbf{D} + \mathbf{H}\cdot\mathbf{B}), \qquad \mathbf{I}_L = \mathbf{E} \times \mathbf{H}. \tag{A.9}$$

The following relation, also known as the **Poynting theorem**, gives the energy conservation for the electromagnetic field for a medium with continuous distribution of charge and current:

$$\frac{\partial q_{\mathrm{EM}}}{\partial t} + \nabla \cdot \mathbf{I}_{\mathrm{L}} = -\mathbf{J} \cdot \mathbf{E}. \tag{A.10}$$

This equation, derived from the Maxwell equations, is in the form of a continuity equation or a conservation law. The right-hand side of this equation is the total rate of doing work (per unit volume) by the electromagnetic fields. This term is easily understood by considering a particle with charge e moving with a velocity $\mathbf{v}$. The rate of doing work by the fields $\mathbf{E}$ and $\mathbf{B}$ is $e\mathbf{v} \cdot \mathbf{E}$. The magnetic field does not do work since $\mathbf{B}$ is perpendicular to $\mathbf{v}$. For a continuous charge distribution the $e\mathbf{v} \cdot \mathbf{E}$ changes into $\mathbf{J} \cdot \mathbf{E}$.

A.2 Gaussian (c.g.s.) Units

The Maxwell equations are given below in Gaussian units. The following conversion from SI to Gaussian units is made in writing the equations of electromagnetism:

$$\begin{array}{cc} \multicolumn{2}{c}{\textbf{SI} \rightarrow \textbf{Gaussian}} \\ \mathbf{E} \rightarrow \mathbf{E} & \varepsilon_0 \rightarrow 1/(4\pi) \\ \mathbf{D} \rightarrow \mathbf{D}/(4\pi) & \mu_0 \rightarrow 4\pi/c^2 \\ \mathbf{H} \rightarrow c\mathbf{H}/(4\pi) & \rho_{\mathrm{e}} \rightarrow \rho_{\mathrm{e}} \\ \mathbf{B} \rightarrow \mathbf{B}/c & \mathbf{J} \rightarrow \mathbf{J} \end{array} \tag{A.11}$$

where c is the speed of light and the Maxwell equations are

$$\begin{gathered} \nabla \times \mathbf{E} = -\frac{1}{c}\frac{\partial \mathbf{B}}{\partial t}, \qquad \nabla \times \mathbf{H} = \frac{4\pi}{c}\mathbf{J} + \frac{1}{c}\frac{\partial \mathbf{D}}{\partial t} \\ \nabla \cdot \mathbf{D} = 4\pi\rho_{\mathrm{e}}, \qquad \nabla \cdot \mathbf{B} = 0. \end{gathered} \tag{A.12}$$

The **Lorentz force** is

$$\mathbf{F} = q\left(\mathbf{E} + \frac{\mathbf{v} \times \mathbf{B}}{c}\right). \tag{A.13}$$

The electromagnetic energy density q_{EM} and the Poynting vector $\mathbf{I}_{\mathrm{L}}$ are given by

$$q_{\mathrm{EM}} = \frac{1}{8\pi}(\mathbf{E} \cdot \mathbf{D} + \mathbf{H} \cdot \mathbf{B}), \qquad \mathbf{I}_{\mathrm{L}} = \frac{c}{4\pi}(\mathbf{E} \times \mathbf{H}) \tag{A.14}$$

and with these definitions the Poynting theorem is identical to (A.10).

A useful conversion table between the SI units and the Gaussian units are given in table A.1.

Table A.1. Conversion between the SI and Gaussian units for the physical quantities related to the Maxwell equations.

Physical quantity	SI units	Conversion factor (CF), 1 SI = (CF) Gaussian	Gaussian units
Electric field, E	Volt/m	$10^{-4}/3$	statvolt/cm
Displacement, D	Coulomb/m^2	12×10^5	statcoulomb/cm^2
Magnetic intensity, H	Ampere/m	4×10^{-3}	Oersted
Magnetic induction, B	Tesla	10^4	Gauss
Charge, q	Coulomb	3×10^9	statcoulomb
Charge density, ρ_e	Coulomb/m^3	3×10^3	statcoulomb/cm^3
Current density, J	Ampere/m^2	3×10^5	statampere/cm^2
Energy, Q	Joule	10^7	erg
Energy flux, I_L	Watt/m^2	10^3	erg/(cm^2 s)
Energy density, q_{EM}	Joule/m^3	10	erg/cm^3
Permeability, $\mu\mu_0$ (μ dimensionless)	Henry/m	$10^7/(4\pi)$	–
Permittivity, $\varepsilon\varepsilon_0$ (ε dimensionless)	Farad/m	36×10^9	–

A.3 The Wave Equation

Using Maxwell equations, (A.1) and (A.12), for **constant** ε and μ, one gets the following wave equations for **E** and **H**:

SI units

$$\nabla^2\mathbf{E} - \frac{\varepsilon\mu}{c^2}\frac{\partial^2\mathbf{E}}{\partial t^2} - \nabla(\nabla\cdot\mathbf{E}) = \mu_0\mu\frac{\partial\mathbf{J}}{\partial t}$$
$$\nabla^2\mathbf{H} - \frac{\varepsilon\mu}{c^2}\frac{\partial^2\mathbf{H}}{\partial t^2} = \nabla\times\mathbf{J} \tag{A.15a}$$

Gaussian units

$$\nabla^2\mathbf{E} - \frac{\varepsilon\mu}{c^2}\frac{\partial^2\mathbf{E}}{\partial t^2} - \nabla(\nabla\cdot\mathbf{E}) = \frac{4\pi\mu}{c^2}\frac{\partial\mathbf{J}}{\partial t}$$
$$\nabla^2\mathbf{H} - \frac{\varepsilon\mu}{c^2}\frac{\partial^2\mathbf{H}}{\partial t^2} = \frac{4\pi}{c}\nabla\times\mathbf{J}. \tag{A.15b}$$

In deriving these equations the speed of light c was related to ε_0 and μ_0 by

$$c^2 = \frac{1}{\varepsilon_0\mu_0}. \tag{A.16}$$

Note that ε and μ are dimensionless.

A.4 Vector and Scalar Potentials

In some problems it is convenient to introduce a vector potential $\mathbf{A}$ and a scalar potential Φ defined by

$$\begin{array}{ll} \textbf{Gaussian units} & \textbf{SI units} \\ \mathbf{B} = \nabla \times \mathbf{A} & \mathbf{B} = \nabla \times \mathbf{A} \\ \mathbf{E} = -\nabla\Phi - \dfrac{1}{c}\dfrac{\partial \mathbf{A}}{\partial t} & \mathbf{E} = -\nabla\Phi - \dfrac{\partial \mathbf{A}}{\partial t}. \end{array} \tag{A.17}$$

The first and the fourth of Maxwell's equations (A.1) and (A.12) (i.e. the homogeneous equations) are satisfied identically, so that the potentials are determined by the other two (the inhomogeneous) equations. The inhomogeneous wave equations take the form

$$\begin{array}{ll} \textbf{Gaussian units} & \textbf{SI units} \\ \nabla^2\mathbf{A} - \dfrac{1}{c^2}\dfrac{\partial^2 \mathbf{A}}{\partial t^2} = -\dfrac{4\pi \mathbf{J}}{c} & \nabla^2\mathbf{A} - \dfrac{1}{c^2}\dfrac{\partial^2 \mathbf{A}}{\partial t^2} = -\mu_0 \mathbf{J} \\ \nabla^2\Phi - \dfrac{1}{c^2}\dfrac{\partial^2 \Phi}{\partial t^2} = -4\pi\rho_{\mathrm{e}} & \nabla^2\Phi - \dfrac{1}{c^2}\dfrac{\partial^2 \Phi}{\partial t^2} = -\dfrac{\rho_{\mathrm{e}}}{\varepsilon_0}. \end{array} \tag{A.18}$$

While the Maxwell equations are eight coupled first-order differential equations relating the electric and the magnetic fields, the 'potential equations' are four second-order differential equations coupled via the electromagnetic sources $\mathbf{J}$ and ρ_{e}.

The electromagnetic potentials are arbitrary up to a gauge. For example, one can change the potentials by the following transformation without changing the electric and magnetic fields (Gaussian units):

$$\mathbf{A} \to \mathbf{A}^* = \mathbf{A} + \nabla\Lambda, \qquad \Phi \to \Phi^* = \Phi - \frac{1}{c}\frac{\partial \Lambda}{\partial t} \tag{A.19}$$

where Λ is an arbitrary function of space and time. The electromagnetic fields, as defined by equations (A.17) (Gaussian units), are unchanged by the transformation (A.19). The meaning of this transformation is that we can choose the electromagnetic potentials $\mathbf{A}$ and Φ (without changing $\mathbf{E}$ and $\mathbf{B}$) in such a way that the following equation, called the **Lorentz gauge**, is satisfied:

$$\begin{array}{ll} \textbf{Gaussian units} & \textbf{SI units} \\ \nabla \cdot \mathbf{A} + \dfrac{1}{c}\dfrac{\partial \Phi}{\partial t} = 0 & \nabla \cdot \mathbf{A} + \dfrac{1}{c^2}\dfrac{\partial \Phi}{\partial t} = 0. \end{array} \tag{A.20}$$

Another useful gauge is the **Coulomb gauge** (in Gaussian and SI units):

$$\nabla \cdot \mathbf{A} = 0. \tag{A.21}$$

In Coulomb gauge the scalar potential satisfies the Poisson equation:

$$\nabla^2\Phi = -4\pi\rho_{\mathrm{e}} \quad \text{(Gaussian units)}, \qquad \nabla^2\Phi = -\frac{\rho_{\mathrm{e}}}{\varepsilon_0} \quad \text{(SI units)}. \tag{A.22}$$

The solution of (A.22) is (Gaussian units)

$$\Phi(\mathbf{r}, t) = \int \frac{\rho_e(\mathbf{r}', t)}{|\mathbf{r} - \mathbf{r}'|} \, d^3\mathbf{r}'. \tag{A.23}$$

The gauge (A.21) is called 'Coulomb gauge' because this implies that the solution for the scalar potential is the instantaneous Coulomb potential due to electrical charges ρ_e.

Appendix B

Prefixes

The following prefixes are used throughout the book.

Prefix	Symbol	Factor	Prefix	Symbol	Factor
zetta	Z	10^{21}	zepto	z	10^{-21}
exa	E	10^{18}	atto	a	10^{-18}
peta	P	10^{15}	femto	f	10^{-15}
tera	T	10^{12}	pico	p	10^{-12}
giga	G	10^{9}	nano	n	10^{-9}
mega	M	10^{6}	micro	μ	10^{-6}
kilo	k	10^{3}	milli	m	10^{-3}
hecto	h	10^{2}	centi	c	10^{-2}
deca	da	10	deci	d	10^{-1}

Appendix C

Vectors and Matrices

This appendix summarizes vector relations (Huba 1998, Woan 2000), used extensively in this book, and also few definitions related to matrix algebra applied in some chapters. Moreover, this appendix defines the notations for vectors and matrices used throughout the book.

C.1 Notation

scalars	$a, b, \ldots, A, B, \ldots$
vectors	$\mathbf{a}, \mathbf{b}, \ldots, \mathbf{A}, \mathbf{B}, \ldots$
unit vectors	$\hat{\mathbf{e}}_1, \hat{\mathbf{e}}_2, \hat{\mathbf{e}}_3, \hat{\mathbf{x}}, \hat{\mathbf{y}}, \hat{\mathbf{z}}, \ldots$
vector components	$a_j\,(j = 1, 2, 3), \ldots$
matrices	$\mathbf{a}, \mathbf{b}, \ldots, \mathbf{A}, \mathbf{B}, \ldots$ (similar notation for vectors and matrices)
matrix components	$a_{ij}\,(i = 1, \ldots, N; j = 1, \ldots, M)$ matrix has N lines and M columns
scalar product	$\mathbf{a} \cdot \mathbf{b}$
vector product	$\mathbf{a} \times \mathbf{b}$
gradient (operator)	∇
divergence	$\nabla\cdot$
rotor or curl	$\nabla\times$
Laplacian (operator)	∇^2

C.2 Coordinate System

A volume element $\mathrm{d}V$ and a line element $\mathrm{d}L$ are given by

$$\mathrm{d}V = h_1 h_2 h_3\,\mathrm{d}x_1\,\mathrm{d}x_2\,\mathrm{d}x_3, \qquad (\mathrm{d}L)^2 = \sum_{i=1}^{3} (h_i\,\mathrm{d}x_i)^2. \qquad \text{(C.1)}$$

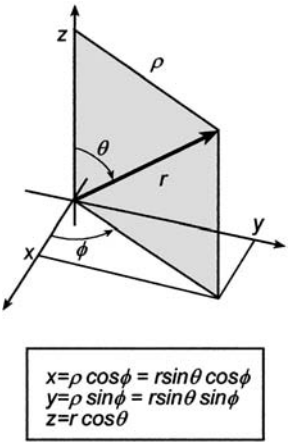

Figure C.1. Definition of the Cartesian, cylindrical and spherical coordinates.

In order to get the line element or the volume element for the Cartesian, cylindrical or spherical coordinate systems, one has to substitute h_i $(i = 1, 2, 3)$ and $\mathrm{d}x_i$ $(i = 1, 2, 3)$ from table C.1.

C.3 The Operator ∇

In the following definitions of the **gradient**, the **divergence**, the **curl** and the **Laplacian**, only the formulae for the general orthogonal coordinates are given. For the Cartesian, the cylindrical and the spherical coordinates, one has to substitute h_i $(i = 1, 2, 3)$ and x_i $(i = 1, 2, 3)$ from table C.1:

$$\nabla s = \frac{\hat{\mathbf{e}}_1}{h_1}\left(\frac{\partial s}{\partial x_1}\right) + \frac{\hat{\mathbf{e}}_2}{h_2}\left(\frac{\partial s}{\partial x_2}\right) + \frac{\hat{\mathbf{e}}_3}{h_3}\left(\frac{\partial s}{\partial x_3}\right) \tag{C.2}$$

Table C.1. Definition of a general orthogonal coordinate system and three examples: Cartesian coordinates, cylindrical coordinates and spherical coordinates.

Coordinate system	Cartesian	Cylindrical	Spherical	Any orthogonal coordinates
Unit vectors	$\hat{\mathbf{x}}, \hat{\mathbf{y}}, \hat{\mathbf{z}}$	$\hat{\boldsymbol{\rho}}, \hat{\boldsymbol{\varphi}}, \hat{\mathbf{z}}$	$\hat{\mathbf{r}}, \hat{\boldsymbol{\theta}}, \hat{\mathbf{z}}$	$\hat{\mathbf{e}}_1, \hat{\mathbf{e}}_2, \hat{\mathbf{e}}_3$
Point coordinates	(x, y, z)	(ρ, ϕ, z)	(r, θ, ϕ)	(x_1, x_2, x_3)
Metric elements	$h_1 = h_2 = 1,$ $h_3 = 1$	$h_1 = 1, h_2 = \rho,$ $h_3 = 1$	$h_1 = 1, h_2 = r,$ $h_3 = r\sin\theta$	(h_1, h_2, h_3)

$$\nabla \cdot \mathbf{v} = \frac{1}{h_1 h_2 h_3}\left[\frac{\partial}{\partial x_1}(v_1 h_2 h_3) + \frac{\partial}{\partial x_1}(v_2 h_3 h_1) + \frac{\partial}{\partial x_1}(v_3 h_1 h_2)\right] \tag{C.3}$$

$$\nabla \times \mathbf{v} = \frac{1}{h_1 h_2 h_3}\begin{vmatrix} \hat{\mathbf{e}}_1 h_1 & \hat{\mathbf{e}}_2 h_2 & \hat{\mathbf{e}}_3 h_3 \\ \partial/\partial x_1 & \partial/\partial x_2 & \partial/\partial x_3 \\ h_1 v_1 & h_2 v_2 & h_3 v_3 \end{vmatrix} \tag{C.4}$$

$$\begin{aligned}\nabla^2 s = {} & \frac{1}{h_1 h_2 h_3}\frac{\partial}{\partial x_1}\left[\left(\frac{h_2 h_3}{h_1}\right)\left(\frac{\partial s}{\partial x_1}\right)\right] + \frac{\partial}{\partial x_2}\left[\left(\frac{h_3 h_1}{h_2}\right)\left(\frac{\partial s}{\partial x_2}\right)\right] \\ & + \frac{\partial}{\partial x_3}\left[\left(\frac{h_1 h_2}{h_3}\right)\left(\frac{\partial s}{\partial x_3}\right)\right]\end{aligned} \tag{C.5}$$

where s is a scalar and $\mathbf{v}$ is a vector defined by its three orthogonal components v_1, v_2 and v_3. $|\cdots|$ denotes the determinant.

C.4 Vector and ∇ Identities

$$\begin{aligned}\mathbf{a}\cdot\mathbf{b} &= \mathbf{b}\cdot\mathbf{a} \\ \mathbf{a}\times\mathbf{b} &= -\mathbf{b}\times\mathbf{a} \\ \mathbf{a}\times(\mathbf{b}\times\mathbf{c}) &= (\mathbf{a}\cdot\mathbf{c})\mathbf{b} - (\mathbf{a}\cdot\mathbf{b})\mathbf{c} \\ (\mathbf{a}\times\mathbf{b})\cdot(\mathbf{c}\times\mathbf{d}) &= (\mathbf{a}\cdot\mathbf{c})(\mathbf{b}\cdot\mathbf{d}) - (\mathbf{a}\cdot\mathbf{d})(\mathbf{b}\cdot\mathbf{c}) \\ (\mathbf{a}\times\mathbf{b})\times(\mathbf{c}\times\mathbf{d}) &= (\mathbf{a}\times\mathbf{b}\cdot\mathbf{d})\mathbf{c} - (\mathbf{a}\times\mathbf{b}\cdot\mathbf{c})\mathbf{d}\end{aligned} \tag{C.6}$$

$$\begin{aligned}\nabla(st) &= s\nabla t + t\nabla s \\ \nabla\cdot(s\mathbf{v}) &= s\nabla\cdot\mathbf{v} + \mathbf{v}\cdot\nabla s \\ \nabla\times(s\mathbf{v}) &= s\nabla\times\mathbf{v} + (\nabla s)\times\mathbf{v}\end{aligned} \tag{C.7}$$

$$\begin{aligned}\nabla(\mathbf{a}\cdot\mathbf{b}) &= \mathbf{a}\times(\nabla\times\mathbf{b}) + (\mathbf{a}\cdot\nabla)\mathbf{b} + \mathbf{b}\times(\nabla\times\mathbf{a}) + (\mathbf{b}\cdot\nabla)\mathbf{a} \\ \nabla\cdot(\mathbf{a}\times\mathbf{b}) &= \mathbf{b}\cdot(\nabla\times\mathbf{a}) - \mathbf{a}\cdot(\nabla\times\mathbf{b}) \\ \nabla\times(\mathbf{a}\times\mathbf{b}) &= \mathbf{a}(\nabla\cdot\mathbf{b}) - \mathbf{b}(\nabla\cdot\mathbf{a}) + (\mathbf{b}\cdot\nabla)\mathbf{a} - (\mathbf{a}\cdot\nabla)\mathbf{b}\end{aligned} \tag{C.8}$$

$$\begin{aligned}\nabla\cdot(\nabla s) &= \nabla^2 s \\ \nabla\times(\nabla \mathrm{s}) &= \mathbf{0} \\ \nabla\cdot(\nabla\times\mathbf{v}) &= 0 \\ \nabla\times(\nabla\times\mathbf{v}) &= \nabla(\nabla\cdot\mathbf{v}) - \nabla^2\mathbf{v}.\end{aligned} \tag{C.9}$$

C.5 Integral Transformation

In equations (C.10) we use the notation: $V =$ volume, enclosed by a surface S, where the surface element (vector) is $\mathrm{d}\mathbf{S} = \mathbf{n}\,\mathrm{d}S$, $\mathbf{n}$ is the unit vector normal to the surface and pointing outwards from the volume V:

$$\begin{aligned}
\int_V \mathrm{d}V(\nabla f) &= \int_S \mathrm{d}S f \\
\int_V \mathrm{d}V(\nabla \cdot \mathbf{a}) &= \int_S \mathrm{d}\mathbf{S} \cdot \mathbf{a} \\
\int_V \mathrm{d}V(\nabla \times \mathbf{a}) &= \int_S \mathrm{d}\mathbf{S} \times \mathbf{a} \\
\int_V \mathrm{d}V[\nabla \cdot (f\nabla g)] &= \int_S \mathrm{d}\mathbf{S} \cdot (f\nabla g) \\
\int_V \mathrm{d}V(f\nabla^2 g - g\nabla^2 f) &= \int_S \mathrm{d}\mathbf{S} \cdot (f\nabla g - g\nabla f).
\end{aligned} \tag{C.10}$$

The second relation of (C.10) is called the Gauss divergence theorem, and the fourth and fifth equations are known as Green's first and second theorems.

In equation (C.11), S is an open surface encircled by the contour C, which has a line element (vector) $\mathrm{d}\mathbf{L}$:

$$\begin{aligned}
\int_S \mathrm{d}\mathbf{S} \times \nabla f &= \oint_C \mathrm{d}\mathbf{L} f \\
\int_S \mathrm{d}\mathbf{S} \cdot (\nabla \times \mathbf{a}) &= \oint_C \mathrm{d}\mathbf{L} \cdot \mathbf{a} \\
\int_S (\mathrm{d}\mathbf{S} \times \nabla) \times \mathbf{a} &= \oint_C \mathrm{d}\mathbf{L} \times \mathbf{a} \\
\int_S \mathrm{d}\mathbf{S} \cdot (\nabla f \times \nabla g) &= \oint_C f\,\mathrm{d}g = -\oint_C g\,\mathrm{d}f.
\end{aligned} \tag{C.11}$$

The second equation of (C.11) is known as Stoke's theorem.

C.6 Matrices

The definition of matrix $\mathbf{A}$, with elements a_{ij}, is given by

$$\mathbf{A} = \begin{pmatrix}
a_{11} & a_{12} & . & . & . & a_{1N} \\
a_{21} & a_{22} & . & . & . & a_{2N} \\
. & . & . & . & . & . \\
. & . & . & . & . & . \\
a_{M1} & a_{M2} & . & . & . & a_{MN}
\end{pmatrix} \tag{C.12}$$

where the matrix has M rows (lines) and N columns, i.e. $M \times N$ matrix, also denoted by (M, N).

The addition and multiplication of two matrices **A** and **B** are defined by

$$\begin{aligned} &\mathbf{A} + \mathbf{B} = \mathbf{C} \quad \text{if } a_{ij} + b_{ij} = c_{ij} \qquad [M_A = M_B, N_A = N_B] \\ &\mathbf{A} \cdot \mathbf{B} = \mathbf{C} \quad \text{if } \sum_k a_{ik} b_{kj} = c_{ij} \qquad [N_A = M_B] \end{aligned} \tag{C.13}$$

where a_{ij}, b_{ij} and c_{ij}, row number i and column number j, are all the elements of the matrices A, B and C respectively. In order to add two matrices it is necessary that their dimensions are equal, $M_A = M_B$, $N_A = N_B$. For multiplication it is necessary that the number of columns of the first matrix is equal to the number of rows of the second matrix. In this case, the dimension of C is $[M_C, N_C] = [M_A, N] \times [N, N_B] = [M_A, N_B]$.

For example, if $(M, N) = (3, 3)$ for one matrix, and $(M, N) = (3, 1)$ for the second matrix, then the matrix C is an $M = 3$, $N = 1$ matrix. By multiplying the dimensions of the matrices one satisfies the rule $(3, 3) \times (3, 1) = (3, 1)$. Note that the $(3, 1)$ matrix is actually a three-dimensional vector. More explicitly,

$$\begin{aligned} \mathbf{A} &= \begin{pmatrix} a_{11} & a_{12} & a_{13} \\ a_{21} & a_{22} & a_{23} \\ a_{31} & a_{23} & a_{33} \end{pmatrix} \\ \mathbf{B} &= \begin{pmatrix} b_{11} \\ b_{21} \\ b_{31} \end{pmatrix} \\ \mathbf{C} &= \begin{pmatrix} a_{11}b_{11} + a_{12}b_{21} + a_{13}b_{31} \\ a_{21}b_{11} + a_{22}b_{21} + a_{23}b_{31} \\ a_{31}b_{11} + a_{32}b_{21} + a_{33}b_{31} \end{pmatrix}. \end{aligned} \tag{C.14}$$

For **squared matrices**, i.e. $M = N$, the **trace** (tr **A**), the **determinant** (det **A**) and the **inverse matrix** ($\mathbf{A}^{-1}$) are occasionally used in this book; therefore, these quantities are now defined:

$$\operatorname{tr} \mathbf{A} = \sum_i a_{ii} \tag{C.15}$$

$$\det \mathbf{A} = \sum_i (-1)^{i+1} a_{i1} M_{i1} = \sum_i a_{i1} C_{i1}, \qquad C_{ij} = (-1)^{i+j} M_{ij} \tag{C.16}$$

where M_{ij} is the **minor of element** a_{ij} and C_{ij} is the **cofactor of the element** a_{ij}. M_{ij} is the determinant of the matrix that is left, an $[N-1, N-1]$ matrix, after deleting row number i and column number j of matrix $\mathbf{A}$.

The inverse matrix is defined by $\mathbf{A}^{-1}$:

$$\mathbf{A}^{-1}\mathbf{A} = \mathbf{A}\mathbf{A}^{-1} = \mathbf{1}, \qquad \det \mathbf{A} \neq 0 \tag{C.17}$$

where $\mathbf{1}$ is the unit matrix defined by: all diagonal elements ($a_{ii} = 1$) are equal to one and all off-diagonal elements vanish. Denoting the elements of $\mathbf{A}^{-1}$ by A^{-1}_{ij}, one has

$$A^{-1}_{ij} = \frac{C_{ji}}{\det \mathbf{A}} = \frac{(-1)^{i+j} M_{ji}}{\det \mathbf{A}} \tag{C.18}$$

where M_{ji} is the determinant of the matrix left after deleting row j and column i of matrix $\mathbf{A}$.

We end this appendix with an explicit example for a $[3, 3]$ matrix:

$$\mathbf{A} = \begin{pmatrix} a_{11} & a_{12} & a_{13} \\ a_{21} & a_{22} & a_{23} \\ a_{31} & a_{32} & a_{33} \end{pmatrix}$$

$$\operatorname{tr} \mathbf{A} = a_{11} + a_{22} + a_{33} \tag{C.19}$$

$$\det \mathbf{A} = a_{11}a_{22}a_{33} - a_{11}a_{23}a_{32} - a_{21}a_{12}a_{33} + a_{21}a_{13}a_{32} + a_{31}a_{12}a_{23} - a_{31}a_{13}a_{22}$$

$$\mathbf{A}^{-1} = \frac{1}{\det \mathbf{A}} \begin{pmatrix} a_{22}a_{33} - a_{23}a_{32} & a_{13}a_{32} - a_{12}a_{33} & a_{12}a_{23} - a_{13}a_{22} \\ a_{23}a_{31} - a_{21}a_{33} & a_{11}a_{33} - a_{13}a_{31} & a_{13}a_{21} - a_{11}a_{23} \\ a_{21}a_{32} - a_{22}a_{31} & a_{12}a_{31} - a_{11}a_{32} & a_{11}a_{22} - a_{12}a_{21} \end{pmatrix}.$$

Appendix D

A Note on the Maxwell Distribution

In thermal equilibrium the distribution function $f(\mathbf{r}, \mathbf{v})$, where $\mathbf{r}$ and $\mathbf{v}$ are the position and velocity coordinates of a particle, can be written

$$f(\mathbf{r}, \mathbf{v}) = f_0 \exp\left(-\frac{\varepsilon}{k_B T}\right) \tag{D.1}$$

where T is the temperature, k_B is the Boltzmann constant, and ε is the one-particle energy equal to the kinetic energy K plus the potential energy V:

$$\varepsilon = K + V = \tfrac{1}{2} m v^2 + V. \tag{D.2}$$

If the potential is a function only of the particle space-coordinate, then one can write

$$f(\mathbf{r}, \mathbf{v}) = f(\mathbf{r}) f(\mathbf{v}) = n(\mathbf{r}) C \exp\left(-\frac{m v^2}{2 k_B T}\right) \equiv n(\mathbf{r}) f_M(\mathbf{v}) \tag{D.3}$$

where $n(\mathbf{r})$ is the number of particles per unit volume at position $\mathbf{r}$, the velocity distribution f_M is called the Maxwell distribution, and it is convenient to write it in the form

$$f_M(v) = C \exp\left(-\frac{v^2}{v_T^2}\right), \qquad v_T^2 \equiv \frac{2 k_B T}{m} \tag{D.4}$$

and the following normalization is satisfied:

$$\int \mathrm{d}\mathbf{v} f_M(\mathbf{v}) = C \int \mathrm{d}\mathbf{v} \exp\left(-\frac{v^2}{v_T^2}\right) = 1$$

$$\mathrm{d}\mathbf{v} = \begin{cases} \mathrm{d}v & \text{in 1 dimension} \\ 2\pi v \, \mathrm{d}v & \text{in 2 dimensions} \\ 4\pi v^2 \, \mathrm{d}v & \text{in 3 dimensions.} \end{cases} \tag{D.5}$$

Note that v_T^2 in the Maxwell distribution (equation (D.4)) is by definition equal to $2k_BT/m$ (so that (D.1) is satisfied).

In three dimensions (velocity-space), the normalization yields

$$C\int_0^\infty \exp\left(-\frac{v^2}{v_T^2}\right)4\pi v^2\,\mathrm{d}v = 1 \Rightarrow C = \frac{1}{\pi^{3/2}v_T^3}. \tag{D.6}$$

The moments of the velocity $\langle v^n\rangle$ are defined by

$$\langle v^n\rangle \equiv \int v^n f_M\,\mathbf{dv}. \tag{D.7}$$

The following integrals are needed in order to calculate the moments defined by equation (D.7):

$$\begin{aligned} I_{2n} &\equiv \int_0^\infty v^{2n}\exp\left(-\frac{v^2}{v_T^2}\right)\mathrm{d}v = \frac{(2n-1)!!\sqrt{\pi}}{2^{n+1}}(v_T)^{2n+1} \quad n = 0,1,2,\ldots \\ I_{2n+1} &\equiv \int_0^\infty v^{2n+1}\exp\left(-\frac{v^2}{v_T^2}\right)\mathrm{d}v = \frac{n!}{2}(v_T)^{2n+2} \quad n = 0,1,2,\ldots \\ (2n-1)!! &\equiv 1\cdot 3\cdot 5\cdot\cdots\cdot(2n-1), \qquad (-1)!! = 1, \qquad (1)!! = 1, \text{etc.} \\ \mathrm{n}! &\equiv 1\cdot 2\cdot 3\cdot 4\cdot\cdots\cdot n. \end{aligned} \tag{D.8}$$

For example, in three dimensions

$$\begin{aligned} \langle v\rangle &= \frac{4\pi}{\pi^{3/2}v_T^3}\int_0^\infty v^3\exp\left(-\frac{v^2}{v_T^2}\right)\mathrm{d}v = \frac{2v_T}{\sqrt{\pi}} \\ \langle v^2\rangle &= \frac{4\pi}{\pi^{3/2}v_T^3}\int_0^\infty v^4\exp\left(-\frac{v^2}{v_T^2}\right)\mathrm{d}v = \frac{3v_T^2}{2} \equiv \frac{3k_BT}{m}. \end{aligned} \tag{D.9}$$

The second integral gives the well-known result

$$\tfrac{1}{2}m\langle v^2\rangle = \tfrac{3}{2}k_BT. \tag{D.10}$$

In one dimension,

$$\begin{aligned} f_M &= \frac{2}{\sqrt{\pi}v_T}\exp\left(-\frac{v^2}{v_T^2}\right) \\ \langle v\rangle &= \frac{2}{\sqrt{\pi}v_T}\int_0^\infty v\exp\left(-\frac{v^2}{v_T^2}\right)\mathrm{d}v = \frac{v_T}{\sqrt{\pi}} \\ \langle v^2\rangle &= \frac{2}{\sqrt{\pi}v_T}\int_0^\infty v^2\exp\left(-\frac{v^2}{v_T^2}\right)\mathrm{d}v = \frac{v_T^2}{2} \equiv \frac{k_BT}{m} \\ \tfrac{1}{2}m\langle v^2\rangle &= \tfrac{1}{2}k_BT. \end{aligned} \tag{D.11}$$

If averages are depending on 'directions', then in Cartesian and in spherical coordinates (velocity-space):

$$\mathrm{d}\mathbf{v} = \mathrm{d}v_x\,\mathrm{d}v_y\,\mathrm{d}v_z = v^2 \sin\theta\,\mathrm{d}\theta\,\mathrm{d}\varphi\,\mathrm{d}v. \tag{D.12}$$

For example, the first two moments of $\cos\theta$ (θ is the angle between the velocity vector $\mathbf{v}$ and the z axis) are

$$\begin{aligned}
\langle\cos\theta\rangle &= \frac{1}{\pi^{3/2}v_{\mathrm{T}}^3}\int_0^{\pi}\mathrm{d}\theta\sin\theta\int_0^{2\pi}\mathrm{d}\varphi\int_0^{\infty}\mathrm{d}v\,v^2\exp\left(-\frac{v^2}{v_{\mathrm{T}}^2}\right)\cos\theta \\
&= \frac{1}{2}\int_0^{\pi}\mathrm{d}\theta\sin\theta\cos\theta = 0 \\
\langle\cos^2\theta\rangle &= \frac{1}{\pi^{3/2}v_{\mathrm{T}}^3}\int_0^{\pi}\mathrm{d}\theta\sin\theta\int_0^{2\pi}\mathrm{d}\varphi\int_0^{\infty}\mathrm{d}v\,v^2\exp\left(-\frac{v^2}{v_{\mathrm{T}}^2}\right)\cos^2\theta \\
&= \frac{1}{2}\int_0^{\pi}\mathrm{d}\theta\sin\theta\cos^2\theta = \frac{1}{3}.
\end{aligned} \tag{D.13}$$

Similarly

$$\langle v_x^2\rangle = \langle v_y^2\rangle = \langle v_z^2\rangle = \tfrac{1}{3}\langle v^2\rangle. \tag{D.14}$$

The last result can also be obtained from symmetrical arguments (if the medium is symmetric by interchange of any two axes x, y and z). The v^n moments and the moments of the last two equations are frequently used in plasma transport phenomena (see section 2.3 and chapter 9).

Bibliography

Abramowitz M and Stegun I A eds 1964 *Handbook of Mathematical Functions with Formulas, Graphs and Mathematical Tables*, National Bureau of Standards Applied Mathematics Series, vol 55 (Washington, DC: US Government Printing Office)

Adam J C 1982 *Laser–Plasma Interaction* ed R Balian and J C Adam (Amsterdam: North-Holland)

Ahlstrom H G 1982 *Physics of Laser Fusion* (Springfield, VA: Livermore, US Technical Information Service)

Alfvén H 1988 *Laser Part. Beams* **6** 437

Allen P B 1987 *Phys. Rev. Lett.* **59** 1460

Altshuler L V 1965 *Sov. Phys. Usp.* **8** 52

Anisimov S I and Medvedev Yu V 1979 *Sov. Phys.-JETP* **49** 62

Anisimov S I, Kapeliovich B L and Perel'man T L 1974 *Sov. Phys.-JETP* **39** 375

Arad B, Eliezer S, Jackel S, Krumbein A, Lobenstein M, Salzmann D, Zmora H and Zweigenbaum S 1980 *Phys. Rev. Lett.* **44** 326

Asay R A and Shahinpoor M eds 1993 *High-Pressure Shock Compression of Solids* (New York: Springer)

Ashcroft N W and Mermin N D 1976 *Solid State Physics* (Fort Worth: Harcourt Brace College Publishers)

Ashcroft N W and Sturm K 1971 *Phys. Rev. B* **3** 1898

Babuel-Peyrissac J P, Fauquignon C and Floux F 1969 *Phys. Lett. A* **30** 290

Backus S, Durfee III C G, Murname M M and Kapteyn H C 1998 *Rev. Sci. Instrum.* **69** 1207

Baldis H A, Campbell E M and Kruer W L 1991 *Handbook of Plasma Physics* vol 3 *Physics of Laser Plasma* ed M N Rosenbluth, R Z Sagdeev, A Rubenchik and S Witkowski (Amsterdam: North-Holland) pp 361–434

Batani D, Bossi S, Benuzzi A, Koenig M, Faral B, Boudenne J M, Grandjouan N, Atzeni S and Temporal M 1996 *Laser Particle Beams* **14** 211

Bauche J, Bauche-Arnoult C and Klapish M 1988 *Physica Scripta* **37** 659

Bell A R 1986 *Laser Plasma Interaction 5* Proceedings of the 45th Scottish Universities Summer School in Physics, 1994, ed M B Hooper (Bristol: Institute of Physics Publishing) pp 139–68

Bernstein I B, Green J M and Kruskal M D 1957 *Phys. Rev.* **108** 546

Bezzerides B, Forslund D W and Lindman E L 1978 *Phys. Fluids* **21** 2179

Bhatnagar P L, Gross E P and Krook M 1954 *Phys. Rev.* **94** 511
Birdsall C K and Langdon A B 1985 *Plasma Physics via Computer Simulation* (New York: McGraw-Hill)
Bloembergen N 1999 *Rev. Mod. Phys.* **71** S283
Bobin J L 1985 *Phys. Rep.* **122** 173
Bodner S E 1974 *Phys. Rev. Lett.* **33** 367
——1991 *Handbook of Plasma Physics* vol 3 *Physics of Laser Plasma* ed M N Rosenbluth, R Z Sagdeev, A Rubenchik and S Witkowski (Amsterdam: North-Holland) pp 247–70
Bohm D 1949 *Characteristics of Electrical Discharges in Magnetic Fields* ed A Guthrie and R K Wakerlis (New York: McGraw-Hill) p 77
Bohm D, Burhop E H S and Massey H S W 1949 *Characteristics of Electrical Discharges in Magnetic Fields* ed A Guthrie and R K Waterling (New York: McGraw-Hill) p 13
Born M and Wolf E 1980 *Principles of Optics* 6th edn (Oxford: Pergamon)
Boussinesq J 1871 *Compte Rendus Acad. Sci. Paris* **72** 755
Boustie M and Cottet F 1991 *J. Appl. Phys.* **69** 7533
Boyd T J M and Cooke D 1988 *Phys. Fluids* **31** 651
Braginskii S I 1965 *Review of Plasma Physics* vol 1 ed M A Leontovich (New York: Consultants Bureau) pp 205–311
Briand J, Adrian V, El Tamer M, Gomes A, Quemener Y, Dinguirard J P and Kieffer J C 1983 *Phys. Rev. Lett.* **54** 38
Brown G L and Roshko A 1974 *J. Fluid Mech.* **64** 775
Brysk H 1975 *J. Phys.* **A8** 1260
Bushman A V, Kanel G I, Ni A L and Fortov V E 1993 *Intense Dynamic Loading of Condensed Matter* (Washington, DC: Taylor and Francis)
Cairns R A 1983 *Laser–Plasma Interaction 2* Proceedings of the 24th Scottish Universities Summer School in Physics, 1982, ed R A Cairns (Edinburgh: Scottish Universities Summer School in Physics Publications) pp 1–28
Cauble R, Phillion D W, Lee R W and Hoover T J 1994 *J. Quant. Spectrosc. Radiat. Transfer* **51** 433
Celliers P M, Collins G W, Da Silva L B, Gold D M and Cauble R 1998 *Appl. Phys. Lett.* **73** 1320
Chan C, Cho M H, Hershkowitz N and Intrator T 1984 *Phys. Rev. Lett.* **52** 1782
Chandrasekhar S 1961 *Hydrodynamic and Hydromagnetic Stability* (Oxford: Oxford University Press)
Chen F F 1974 *Laser Interaction and Related Plasma Phenomena* vol 3A ed H J Schwarz and H Hora (New York: Plenum) p 291
——1990 *Introduction to Plasma Physics* (New York: Plenum)
Clemmow P C and Dougherty J P 1969 *Electrodynamics of Particles and Plasmas* (Reading, MA: Addison-Wesley)
Cottet F, Hallouin M, Romain J P, Fabbro R, Faral B and Pepin H 1985 *Appl. Phys. Lett.* **47** 678
Courant R and Friedrichs K O 1948 *Supersonic Flow and Shock Waves* (New York: Interscience)
Cowan R D 1981 *The Theory of Atomic Structure and Spectra* (Berkeley: University of California Press) p 12
Crawford F S Jr *Waves; Berkeley Physics Course* vol 3 (New York: McGraw-Hill)

Crow J E, Auer P L and Allen J E 1975 *J. Plasma Phys.* **14** 65
Dahlburg J P, Fyfe D E, Gardner J H, Haan S W, Bodner S E and Doolen G D 1995 *Phys. Plasmas* **2** 2453
David F and Pellat R 1980 *Phys. Fluids* **23** 1682
Davies R M and Taylor G 1950 *Proc. Royal Soc. London A* **200** 375
Dawson J M 1962 *Phys. Fluids* **5** 445
——1968 *Advances in Plasma Physics* vol 1 ed A Simon and W Thompson (New York: Interscience) pp 1–66
Dawson J M and Lin A T 1974 Parametric instabilities in plasma, UCLA preprint PPG-191
Dederichs P H, Schober H R and Sellmyer D J 1981 *Landolt–Bornstein* 3rd edn, vol 13a (Berlin: Springer) p 11
Dekel E, Eliezer S, Henis Z, Moshe E, Ludmirsky A and Goldberg I B 1998 *J. Appl. Phys.* **84** 4851
DeMaria A J, Stetser D A and Heinan H 1966 *Appl. Phys. Lett.* **8** 174
Dendy R 1993 *Plasma Physics; an Introduction Course* (Cambridge: Cambridge University Press)
Denisov N G 1957 So*v. Phys.-JETP* **4** 544
De Resseguier T and Cottet F 1995 *J. Appl. Phys.* **77** 3756
Diebold D, Hershkovitz N and Eliezer S 1987 *Phys. Fluids* **30** 3308
Diels J C and Rudolph W 1996 *Ultrashort Laser Pulse Phenomena* (San Diego: Academic Press)
Ditmire T, Gumbrell E T, Smith R A, Mountford L and Hutchinson M H R 1996 *Phys. Rev. Lett.* **77** 498
Dragila R 1987 *Phys. Fluids* **30** 925
Drazin P G and Reid W H 1981 *Hydrodynamic Stability* (Cambridge: Cambridge University Press)
DuBois D F and Goldman M V 1965 *Phys. Rev. Lett.* **14** 544
Ehler A W 1975 *J. Appl. Phys.* **46** 2464
Eidmen K, Meyer-ter-Vehn J, Schlegel T and Huller S 2000 *Phys. Rev. E* **62** 1202
Einstein A 1917 *Phys. Z.* **18** 121
Eliaz N, Moshe E, Eliezer S and Eliezer D 2000 *Metall. Mater. Trans. A* **31** 1085
Eliezer S 1985 A stroll through the soliton theory, Institute for Fusion Studies preprint, IFSR 164, The University of Texas, Austin, TX
Eliezer S and Hora H 1989 *Phys. Reports* **172** 339–410
Eliezer S and Ludmirsky A 1983 *Laser Particle Beams* **1** 251
Eliezer S and Ricci R A eds 1991 *High Pressure Equations of State: Theory and Applications* (Amsterdam: North-Holland)
Eliezer S, Ghatak A and Hora H 1986 *An Introduction to Equations of State: Theory and Applications* (Cambridge: Cambridge University Press)
Eliezer S, Ghatak A, Hora H and Teller E 2002 *Fundamentals of Equations of State* (Singapore: World Scientific)
Eliezer S, Gilath I and Bar-Noy T 1990 *J. Appl. Phys.* **67** 715
Eliezer S, Hora H, Kolka E, Green F and Szichman H 1995 *Laser and Particle Beams* **13** 441
Eliezer S, Paiss Y and Strauss H 1992 *Phys. Lett. A* **164** 416
Elton R C 1990 *X-Ray Lasers* (Boston: Academic Press)
Evans A M, Freeman N J, Graham P, Horsfield C J, Rothman S D, Thomas B R and Tyrrell A J 1996 *Laser and Particle Beams* **14** 113

Evans R G 1986 *Laser–Plasma Interaction 3* Proceedings of the 29th Scottish Universities Summer School in Physics, 1985, ed M B Hooper (Edinburgh: Scottish Universities Summer School in Physics Publications) pp 266–78

Evely M D and Morales G J 1978 *Phys. Fluids* **21** 1997

Fabbro R, Faral B, Virmont J, Pepin H, Cottet F and Romain J P 1986 *Laser and Particle Beams* **4** 413

Fälthammer C G 1987 *Ann. Geophys.* **5A** 171

Fermi E, Pasta J and Ulam S 1955 Studies of Nonlinear Problems I, Los Alamos National Laboratory Report, LA1940

Fisher D, Fraenkel M, Henis Z, Moshe E and Eliezer S 2001 *Phys. Rev. E* **65** 016409-1

Forslund D W, Kindel J M, Lee K, Lindman E L and Morse R L 1975 *Phys. Rev.* **A11** 679

Fortov V E, Kostin V V and Eliezer S 1991 *J. Appl. Phys.* **70** 4524

Fraenkel M, Zigler A, Henis Z, Eliezer S and Andreev N E 2000 *Phys. Rev. E* **61** 1899

Friedberg J P, Mitchell R W, Morse R L and Rudinski L I 1972 *Phys. Rev. Lett.* **28** 795

Galeev A A and Natanzon A M 1991 *Handbook of Plasma Physics* vol 3 *Physics of Laser Plasma* ed M N Rosenbluth, R Z Sagdeev, A Rubenchik and S Witkowski (Amsterdam: North-Holland) pp 549–74

Gamaly E G 1993 *Nuclear Fusion by Inertial Confinement* ed G Velarde, Y Ronen and J M Martinez-Val (Boca Raton, FL: CRC Press) pp 321–49

Gantmakher V F and Levinson Y B 1987 *Carrier Scattering in Metals and Semiconductors* (Amsterdam: North-Holland)

Gardner C L, Glimm J, McBryan O, Menikoff R, Sharp D H and Zhang Q 1988 *Phys. Fluids* **31** 447

Gauthier J C 1989 *Laser–Plasma Interaction 4* Proceedings of the 35th Scottish Universities Summer School in Physics, 1988, ed M B Hooper (Edinburgh: Scottish Universities Summer School in Physics Publications) pp 105–38

Gibbon P and Forster E 1996 *Plasma Phys. Control Fusion* **38** 769

Gilath I, Eliezer S, Dariel M P and Kornblith L 1988 *Appl. Phys. Lett.* **52** 1128

Ginsburg V L 1961 *Propagation of Electromagnetic Waves in Plasmas* (New York: Gordon and Breach)

Glezer E N 1997 *Spectroscopy and Dynamics of Collective Excitations in Solids* ed DiBartolo (New York: Plenum) p 375

Goldston R J and Rutherford P H 1995 *Introduction to Plasma Physics* (Bristol: Institute of Physics)

Grady D E 1988 *J. Mech. Phys. Solids* **36** 353

Gray D R and Kilkenny J D 1980 *Plasma Phys.* **22** 81

Gurevich A and Pitaevski L P 1969 *Sov. Phys.-JETP* **29** 954

Gurevich A V, Pariiskaya L V and Pitaevski L P 1965 *Sov. Phys.-JETP* **22** 449

Gurevich A V, Pariiskaya L V and Pitaevski L P 1968 *Sov. Phys.-JETP* **27** 476

Haan S W 1989 *Phys. Rev.* A **40** 80

Haines M G 1980 *Laser Plasma Interaction 1* Proceedings of the 20th Scottish Universities Summer School in Physics, 1979, ed R A Cairns and J J Sanderson (Edinburgh: Scottish Universities Summer School in Physics Publications) pp 145–218

——1989 *Laser Plasma Interaction 4* Proceedings of the 35th Scottish Universities Summer School in Physics, 1988, ed M B Hooper (Edinburgh: Scottish Universities Summer School in Physics Publications) pp 139–70

——2001 *Phys. Rev. Lett.* **87** 135005-1
Hargrove L E, Fork R L and Pollack M A 1964 *Appl. Phys. Lett.* **5** 4
Hatakeyama R, Suzuki Y and Sato N 1983 *Phys. Rev. Lett.* **50** 1203
Hazeltine R D and Meiss J D 1992 *Plasma Confinement* Frontiers in Physics (Redwood City, CA: Addison-Wesley)
Hazeltine R D and Waelbroeck F 1998 *The Framework of Plasma Physics* (New York: Perseus Books)
Hellwarth R W 1961 *Advances in Quantum Electronics* ed J R Singer (New York: Columbia University Press) p 334
Helmholtz H 1881 *Ann. d. Phys. Chem.* **13** 385
Hershkowitz N 1985 *Space Sci. Rev.* **41** 351
Hinton F L and Hazeltine R D 1976 *Rev. Mod. Phys.* **48** 239
Hockney R W and Eastwood J W 1981 *Computer Simulation Using Particles* (New York: McGraw-Hill)
Hoffman N M 1995 *Laser Plasma Interaction 5* Proceedings of the 45th Scottish Universities Summer School in Physics, 1994, ed M B Hooper (Bristol: Institute of Physics Publishing) pp 105–37
Holzrichter J F 1980 *Laser Plasma Interaction 1* Proceedings of the 20th Scottish Universities Summer School in Physics, 1979, ed R A Cairns and J J Sanderson (Edinburgh: Scottish Universities Summer School in Physics Publications) pp 497–606
Hora H 1969 *Phys. Fluids* **12** 182
——1981 *Physics of Laser Driven Plasmas* (New York: Wiley)
——2000 *Laser Plasma Physics*, *Forces and the Nonlinearity Principle* (Bellingham, WA: SPIE Press)
Hora H, Lalousis P and Eliezer S 1984 *Phys. Rev. Lett.* **53** 1650
Horovitz Y, Eliezer S, Henis Z, Paiss Y, Moshe E, Ludmirsky A, Werdiger M, Arad B and Zigler A 1998 *Phys. Lett. A* **246** 329
Horovitz Y, Eliezer S, Ludmirsky A, Henis Z, Moshe E, Shpitalnik R and Arad B 1997 *Phys. Rev. Lett.* **78** 1707
Horton W 1989 *Phys. Rep.* **192** 1
Huba J D 1998 *NRL Plasma Formulary* (Washington, DC: Naval Research Laboratory Pub.)
Hughes T P 1980 *Laser Plasma Interaction 1* Proceedings of the 20th Scottish Universities Summer School in Physics, 1979, ed R A Cairns and J J Sanderson (Edinburgh: Scottish Universities Summer School in Physics Publications) pp 1–90
Ichimaru S 1994 *Statistical Plasma Physics* vol 1 *Basic Principles* vol 2 *Condensed Plasmas* (New York: Perseus Books)
Jackel S, Eliezer S and Zigler A 1981 *Phys. Rev. A* **24** 1601
Jackel S, Laluz R, Paiss Y, Szichman H, Arad B, Eliezer S, Gazit Y, Loebenstein H M and Zigler A 1982 *J. Phys. E* **15**, 255
Kaganov M I, Lifshitz I M and Tanatarov L V 1957 *Sov. Phys.-JETP* **4** 173
Kato Y, Mima K, Miyanaga N, Arinaga S, Kitagawa Y, Nakatsuka M and Yamanaka C 1984 *Phys. Rev. Lett.* **53** 1057
Kauffman R 1991 *Handbook of Plasma Physics* vol 3 *Physics of Laser Plasma* ed M N Rosenbluth, R Z Sagdeev, A Rubenchik and S Witkowski (Amsterdam: North-Holland) pp 111–62
Kaw P, Kruer W L, Liu C S and Nishikawa K 1976 *Advances in Plasma Physics* vol 6 ed A Simon and W B Thomson (New York: Wiley)
Kaw P, Schmidt G and Wilcox T 1973 *Phys. Fluids* **16** 1522

Kelvin, Lord 1910 *Mathematical and Physical Papers* iv *Hydrodynamics and General Dynamics* (Cambridge: Cambridge University Press)

Kentwell G W and Jones D A 1987 *Physics Reports* **145** 319

Key M H 1980 *Laser–Plasma Interaction 1* Proceedings of the 20th Scottish Universities Summer School in Physics, 1979, ed R A Cairns and J J Sanderson (Edinburgh: Scottish Universities Summer School in Physics Publications) pp 219–322

——1983 *Laser Plasma Interaction 2* Proceedings of the 24th Scottish Universities Summer School in Physics, 1982, ed R A Cairns (Edinburgh: Scottish Universities Summer School in Physics Publications) pp 107–28

——1991 *Handbook of Plasma Physics* vol 3 *Physics of Laser Plasma* ed M N Rosenbluth, R Z Sagdeev, A Rubenchik and S Witkowski (Amsterdam: North-Holland) pp 575–611

Key M H, Baumhacker H, Bigio I J, Bodner S, Brederlow G, Czuchlewski E, Fill E, Kirillov G A, Lehmberg R H, Obenschain S P, Offenberger A A, Owadano Y, Schroder C H, Shaw M J, Ueda K I, Volk R, Witkowski S and Witte K J 1995 *Energy from Inertial Fusion* ed W J Hogan (Vienna: IAEA Publication) pp 95–135

Koenig M, Faral B, Boudenne J M, Batani D, Benuzzi A and Bossi S 1994 *Phys. Rev. E* **50** R3314

Korteweg D J and de Vries G 1895 *Phil. Mag.* **39** 422

Krall N and Trivelpiece A 1973 *Principle of Plasma Physics* (New York: McGraw-Hill)

Krokhin O N 1971 *Physics of High Energy Density* ed P Caldirola and H Knoepfel (New York: Academic Press) pp 278–305

Kruer W L 1975 *Nucl. Technol.* **27** 216

——1988 *The Physics of Laser Plasma Interactions* (Redwood City, CA: Addison-Wesley)

Kull H J 1991 *Phys. Reports* **206** 197

Lalousis P 1983 PhD thesis, University of New South Wales, Australia

Lalousis P and Hora H 1983 *Laser Particle Beams* **1** 283

Landau L D 1946 *J. Phys. USSR* **10** 25

Landau L D and Lifshitz E M 1965 *Quantum Mechanics, Non-Relativistic Theory* (Oxford: Pergamon Press)

——1975 *Electrodynamics of Continuous Media* (Oxford: Pergamon Press)

——1987 *Fluid Mechanics* (Oxford: Pergamon Press)

Langdon B 1980 *Phys. Rev. Lett.* **44** 575

Langmuir I 1929 *Phys. Rev.* **33** 954

Larson A R 1974 Calculation of laser induced spall in aluminum targets, Los Alamos Laboratory Report LA-5619-MS

Layzer D 1955 *Astrophys. J.* **122** 1

Lehmberg R and Obenschain S 1983 *Opt. Comm.* **46** 1983

Lehner T 1994 *Physica Scripta* **49** 704

——2000 *Europhys. Lett.* **50** 480

Lifshitz E M and Pitaevskii L P 1981 *Physical Kinetics* (Oxford: Pergamon Press)

Liu C S and Tripathi V K 1995 *Interaction of Electromagnetic Waves with Electron Beams and Plasmas* (Singapore, World Scientific)

Ludmirsky A, Givon M, Eliezer S, Gazit Y, Jackel S, Krumbein A and Szichman H 1984 *Laser Particle Beams* **2** 2

Maiman T H 1960 *Nature* **187** 493

Max C 1976 *Phys. Fluids* **19** 84

McQueen R G 1991 *High Pressure Equations of State: Theory and Applications* ed S Eliezer and R A Ricci (Amsterdam: North-Holland)

Melrose D B 1986 *Instabilities in Space and Laboratory Plasmas* (Cambridge: Cambridge University Press)

Mendel C W and Olsen J N 1975 *Phys. Rev. Lett.* **34** 859

Meshkov E E 1969 *Fluid Dynamics* **4** 101

Mihalas D and Mihalas B W 1984 *Foundations of Radiation Hydrodynamics* (Oxford: Oxford University Press)

Milchberg H M and Freeman R R 1989 *J. Opt. Soc. Am. B* **6** 1351

Minguez E 1993 *Nuclear Fusion by Inertial Confinement* ed G Velarde, Y Ronen and J M Martinez-Val (Boca Raton, FL: CRC Press) pp 197–209

Miyamoto K 1980 *Plasma Physics for Nuclear Fusion* (Cambridge, MA: MIT Press)

Mocker H W and Collins R J 1965 *Appl. Phys. Lett.* **7** 270

Morales G J and Lee Y C 1977 *Phys. Fluids*, **20** 1135

More R M 1986 *Laser Plasma Interaction 3* Proceedings of the 29th Scottish Universities Summer School in Physics, 1985, ed M B Hooper (Edinburgh: Scottish Universities Summer School in Physics Publications) pp 157–214

——1991 *Handbook of Plasma Physics* vol 3 *Physics of Laser Plasma* ed M N Rosenbluth, R Z Sagdeev, A Rubenchik and S Witkowski (Amsterdam: North-Holland) pp 63–110

More R M, Zinamon Z, Warren K H, Falcone R and Murnane M 1988 *J. de Physique* **49** C7–43

Moshe E, Dekel E, Henis Z and Eliezer S 1996 *Appl. Phys. Lett.* **69** 1379

Moshe E, Eliezer S, Henis Z, Werdiger M, Dekel E, Horovitz Y, Maman S, Goldberg I B and Eliezer D 2000 *Appl. Phys. Lett.* **76** 1555

Mulser P and van Kessel C 1977 *Phys. Rev. Lett.* **38** 902

Nakai S, Andre M, Krupke W F, Mak A A, Soures J M and Yamanaka M 1995 *Energy from Inertial Fusion* ed W J Hogan (Vienna: IAEA Publication) pp 79–95

Ng A, Celliers P and Parfeniuk D 1987 *Phys. Rev. Lett.* **58** 214

Nicholson D 1983 *Introduction to Plasma Theory* (New York: Wiley)

Nishikawa K 1968 *J. Phys. Soc. Jap.* **24** 1152

Norreys P A, Santala M, Clark E, Zepf M, Watts I, Beg F N, Krushelnick K, Tatarakis M, Dangor A E, Fang X, Graham P, McCanny T, Singhal R P, Ledingham K W D, Cresswell A, Sanderson D C W, Magill J, Machasek A, Wark J S, Allott R, Kennedy B and Neely D 1999 *Phys. Plasmas* **6** 2150

Oron D, Alon U and Shvarts D 1998 *Phys. Plasmas* **5** 1467

Osborn R K 1972 *Phys. Rev. A* **5** 1660

Parks G K 1991 *Physics of Space Plasma*, *an Introduction* (Redwood City, CA: Addison-Wesley)

Pavlov V I 1979 *Sov. Phys. Usp.* **21** 171

Peierls R E 2001 *Quantum Theory of Solids* (Oxford: Clarendon Press)

Perry M D and Mourou G 1994 *Science* **264** 917

Perry M D, Pennington D, Stuart, B C, Tietbohl G, Britten J A, Brown C, Herman S, Golick B, Kartz M, Miller J, Powell H T, Vergino M and Yanovsky V 1999 *Opt. Lett.* **24** 160

Pert G J 1978 *Plasma Phys.* **20** 175

——1986 *Laser Plasma Interaction 4* Proceedings of the 35th Scottish Universities Summer School in Physics, 1985, ed M B Hooper (Edinburgh: Scottish Universities Summer School in Physics Publications) pp 193–211

Pomraning G C 1973 *The Equations of Radiation Hydrodynamics* (New York: Pergamon Press)

Raadu M A 1989 *Phys. Rep.* **178** 25
Rand S 1964 *Phys. Rev.* **136** B231
Raven A, Willi O and Rumsby T P 1978 *Phys. Rev. Lett.* **41** 554
Rayleigh, Lord 1876 *Phil. Mag.* **1** 257. Also *Scientific Papers* vol 1 (Cambridge: Cambridge University Press) pp 251–71
——1883 *Proc. London Math. Soc.* **14** 170
Richtmyer R D 1960 *Commun. Pure Appl. Math.* **13** 297
Robieux J 2000 *High Power Laser Interactions* (London: Intercept Pub.)
Rosen M D 1984 *Comm. Plasma Phys. Cont. Fusion* **8** 165
Rosenberg Z, Luttwak G, Yeshurun Y and Partom Y 1983 *J. Appl. Phys.* **54** 2147
Rosenbluth M N 1972 *Phys. Rev. Lett.* **29** 565
Rosenbluth M N, MacDonald W M and Judd D L 1957 *Phys Rev.* **107** 1
Russell J S 1844 *Reports on Waves* 14th Meeting of the British Association for the Advancement of Science (London: John Murray) pp 311–90
Saeki K, Iizuka S and Sato N 1980 *Phys. Rev. Lett.* **45** 1853
Salzmann D 1998 *Atomic Physics in Hot Plasmas* (Oxford: Oxford University Press)
Sargent III M, Scully M O and Lamb Jr W E 1974 *Laser Physics* (Reading, MA: Addison-Wesley)
Schlessinger L and Wright J 1979 *Phys. Rev.* **A20** 1934
Schmidt G 1966 *Physics of High Temperature Plasmas*, *An Introduction* (New York: Academic)
Sheng Z M and Meyer-ter-Vehn J 1996 *Phys. Rev.* **54** 1833
Shkarofsky I P, Jonston T W and Bachynski M P 1966 *The Particle Kinematics of Plasmas* (Reading, MA: Addison-Wesley)
Shvarts D 1986 *Laser Plasma Interaction 3* Proceedings of the 29th Scottish Universities Summer School in Physics, 1985, ed M B Hooper (Edinburgh: Scottish Universities Summer School in Physics Publications) pp 105–42
Shvarts D, Alon U, Ofer D, McCrory R L and Verdon C P 1995 *Phys. Plasmas* **2** 2465
Siegman A E 1986 *Lasers* (Mill Valley, CA: University Science Books)
Sigel R 1980 *Laser Plasma Interaction 1* Proceedings of the 20th Scottish Universities Summer School in Physics, 1979, ed R A Cairns and J J Sanderson (Edinburgh: Scottish Universities Summer School in Physics Publications) pp 661–710
Silin V P 1965 *Sov. Phys.-JETP* **20** 1510
——1965a *Sov. Phys.-JETP* **21** 1127
Skupsky S, Short R W, Kessler T, Craxton R S, Letzring S and Soures J M 1989 *J. Appl. Phys.* **66** 3456
Smith R A 1987 *Laser Particle Beams* **5** 381
Spence D E, Kean P N and Sibbett W 1991 *Opt. Lett.* **16** 42
Speziale T and Catto P 1977 *Phys. Fluids* **20** 1420
Spitzer L 1962 *Physics of Fully Ionized Gases* 2nd edn (New York: Interscience)
Spitzer L and Härm R 1953 *Phys. Rev.* **89** 977
Stamper J A 1991 *Laser Part. Beams* **9** 841
Stamper J A and Tidman D A 1973 *Phys. Fluids* **16** 2024
Stamper J A, Papadopoulos K, Sudan R N, Dean S O, McLean E A and Dawson J M 1971 *Phys. Rev. Lett.* **26** 1012
Steiger A D and Woods C H 1972 *Phys. Rev. A* **5** 1467
Steinberg D J 1996 *Equation of State and Strength Properties of Selected Materials* UCRL-MA-106439, Livermore, CA, USA

Stix T H 1992 *Waves in Plasmas* (New York: American Institute of Physics)
Strickland D and Mourou G 1985 *Opt. Commun.* **56** 219
Svelto O 1976 *Principle of Lasers* (New York: Plenum)
Tajima T 1989 *Computational Plasma Physics with Applications to Fusion and Astrophysics* Frontiers in Physics (Redwood City, CA: Addison-Wesley)
Takabe H, Mima K, Montierth L and Morse R L 1985 *Phys. Fluids* **28** 3676
Taylor G 1950 *Proc. Roy. Soc. A* **201** 192
Thompson W B 1962 *An Introduction to Plasma Physics* (Reading, MA: Addison-Wesley)
Thyagaranjan K and Ghatak A K 1981 *Lasers, Theory and Applications* (New York: Plenum)
Trainor R J, Shaner, J W, Auerbach J M and Holmes N C 1979 *Phys. Rev. Lett.* **42** 1154
Trubnikov B A 1965 *Review of Plasma Physics* vol 1 ed M A Leontovich (New York: Consultants Bureau) pp 105–204
van Kessel C G M and Sigel R 1974 *Phys. Rev. Lett.* **33** 1020
Veeser L R, Solem J C and Liebar A J 1979 *Appl. Phys. Lett.* **35** 761
Wang X W and Downer M C 1992 *Opt. Lett.* **17** 1450
Washimi H and Taniuti T 1966 *Phys. Rev. Lett.* **17** 996
Wharton K B, Hatchett S P, Wilks S C, Key M H, Moody J D, Yanovsky V, Offenberger A A, Hammel B A, Perry M D and Joshi C 1998 *Phys. Rev. Lett.* **81** 822
Wickens L M, Allen J E and Rumsby P T 1978 *Phys. Rev. Lett.* **41** 243
Woan G 2000 *The Cambridge Handbook of Physics Formulas* (Cambridge: Cambridge University Press)
Woo W, Estabrook K and DeGroot J S 1978 *Phys. Rev. Lett.* **40** 1094
Yamanaka C 1991 *Introduction to Laser Fusion* (London: Harwood Academic)
Zabusky N J and Kruskal M D 1965 *Phys. Rev. Lett.* **15** 240
Zeldovich Ya B and Raizer Yu P 1966 *Physics of Shock Waves and High-Temperature Hydrodynamic Phenomena* ed Hayes W D and R F Probstein (New York: Academic Press)
Zhou J P, Taft G, Huang C P, Murnane M M and Kaptyn H C 1994 *Opt. Lett.* **19**, 1149
Zinovev V E 1996 *Handbook of Thermophysical Properties of Metals at High Temperatures* (New York: Nova Science)

Index

ablation
  plasma 257
  steady-state 180
ablation (surface) instability 264, 265, 268
ablation pressure 177, 183, 219, 255
ablation rate 258
ablation rate, mass 266
ablation stabilization 257
ablation surface 43, 44, 45, 177, 179, 181, 197, 198, 233, 266, 268
absorbed laser energy 140
absorption 28, 31, 32, 43, 78, 87, 94, 95, 106, 108, 157, 169, 173, 174, 175, 180, 205
absorption coefficient 18, 29, 54, 74,76, 78, 79, 88, 90, 91, 96, 97, 98, 103, 160, 173
absorption coefficient, inverse bremsstrahlung 161, 162
absorption domain 43
acceleration continuity 276
acceleration of a thin foil 241
acoustic wave 73, 105, 106, 121, 215, 216
adiabatic exponent 38
adiabatic oscillations 70
adiabatic process 218
Airy function 84, 85, 86, 95
Alfvén dispersion relation 169
Alfvén wave 145, 168
Alfvén wave velocity 169
Ampere–Maxwell law 285
amplifier 7, 8, 9, 10, 12, 13
amplitude
  elastic 111
  off-resonance 116
  power absorption 111
amplitude of oscillations 112
amplitude of the wave 125
angle of deflection 185
angle of rotation 155, 156
angular diffusion 195
angular momentum 159, 258
angular momentum conservation 160, 161
anisotropic 195
anisotropic electron distribution 196
anvils 213
aspect ratio 183, 255
astrophysics 73, 143
asymptotic expansion 86
asymptotic steady state 270
atomic physics 3
Atwood number 254, 257, 263
averaging over the initial positions 114
Avogadro's number 56
axisymmetric beam 160

B integral 13
backscattered wave amplitude 123
backscatter electromagnetic wave 121
back surface velocity 245
ballistic research 249
band, conduction 103
bandwidth 11, 12
Bernoulli equation 272
BGK model 57
binding energy 241
black body radiation 2
Bloch-electron band 98
blow-off velocity 44
body forces 53
Boltzmann distribution 3, 16
Boltzmann equation 57, 58, 59, 60, 189, 194, 196, 197
Boltzmann–Vlasov equation 55

Bose–Einstein distribution 100
boundary conditions on the interface 276
boundary equation 276, 279
boundary value equation 278
bremsstrahlung 27, 28, 74, 198, 199, 211
bremsstrahlung, inverse 27, 28, 74, 76, 77, 78, 91, 98, 109
bremsstrahlung, nonlinear 78
brightness 6, 7, 27
Brillouin instability 40, 122
Brillouin zone 98, 100
brittle materials 250
broadening, collisional 5
broadening, Doppler 5
broadening, homogenous 5
broadening, inhomogeneous 5
broadening, line 4, 5
Brownian motion 190
bubble formation 255
bubble surface equation 272
bulk modulus 241, 245, 246, 247
bulk sound speed 227
buoyancy force 257, 272

Caviton 65, 141
cavity 1, 6, 9, 11, 133
centre of mass (CM) 20, 147, 183, 184, 185, 186, 192, 193
centre of mass energy 18
centre of mass velocity 60
characteristic curves 218
characteristics 230
charge collectors 141
charge fluctuation 35
charge neutrality 69, 80, 121, 136, 147, 148, 177, 196, 203
charge separation 118, 141
chemical explosives 213
chemical potential 101
chirped pulse amplification (CPA) 1, 12, 13
circularly polarized laser 154, 157, 159, 160
circular polarization, left-handed 165
circular polarization, right-handed 165, 166
closest approach 19, 21, 34, 75, 186
cloud in cell 63
coherence, spatial 6, 7
coherence, temporal 6
coherent oscillations of the electrons 123
cohesion energy 241, 242, 245
cold electron 177, 178, 203, 242, 243
cold (electrons) pressure 44, 242, 243, 245, 247
cold temperature 180
collision
  binary 34, 57
  direct 57, 62
  electron 94
  electron–electron 74, 99, 101, 104, 160, 179, 187, 195
  electron–ion 20, 22, 51, 54, 58, 74, 87, 94, 123, 187
  electron–phonon 99, 101, 104
  instantaneous 22
collision frequency 17, 19, 20, 23, 24, 41, 57, 76, 102, 118, 160,188, 195
collision frequency, effective 58, 94
collision frequency, electron 97, 99
collision frequency, electron–ion 21, 41, 78, 90, 91, 123, 173, 195
collision frequency, velocity-dependent 105
collision term 189, 190
collision times for large-scale scattering 187
collisional absorption 74
collisionless damping 40
collisionless energy exchange 114
collisions, large angle 62
collisions per unit time 200
compressibility 241
compression domain 43
compression wave 231, 232
compressor 13
conduction band 54, 55
conservation
  centre of mass energy 192
  charge 36, 147, 285
  electromagnetic field energy 286
  energy 47, 49, 50, 51, 53, 54, 60, 87, 99, 100, 102, 103, 115, 122, 143, 149, 184, 187, 205, 207, 208, 210, 214, 223, 234, 235, 236, 237
  mass 37, 47, 48, 58, 59, 146, 147, 207, 214, 217, 218, 222, 223, 233, 234, 237, 260, 267, 275, 278, 280
  momentum 37, 47, 48, 50, 51, 52, 53, 59, 60, 70, 71, 72, 89, 100, 115, 121, 122, 127, 135, 136, 145, 146, 162, 168, 169, 184, 192, 203, 214, 217, 218, 222, 233, 235, 237, 260, 266, 272, 275, 276, 280
  radiation energy 33
conservation equations 56, 280
conservation laws 47, 106, 107, 108, 226, 286
constitutive equations 285
continuity equation 42, 48, 53, 55, 58, 59, 70, 71, 119, 136, 147, 158, 203, 269, 286

continuity equation, for ions 135
continuity equation in the velocity space 191
continuity of the normal magnetic induction field 234, 237
continuity of the parallel electric field 234, 237
convection of the magnetic field 152
convection of the plasma fluid 149, 151
converging shocks 259
coordinates
  Cartesian 26, 56, 58, 81, 154, 163, 168, 193, 235, 260, 261, 270, 292, 299
  cylindrical 160, 161, 292
  Eulerian 51, 52, 53
  Lagrangian 51, 52, 53
  spherical 18, 20
coordinates moving with the flow 218
corona 43, 44, 55, 76, 136, 137, 143, 175, 178, 179, 180, 182, 188, 189, 198, 233, 257
correlation function 74
corrugated interface 258, 274, 277
corrugation of the shock surfaces 279
cosmic radiation 23
Coulomb collision 184
Coulomb cutoff coefficient 186
Coulomb gauge 288, 289
Coulomb logarithm 177, 189
Coulomb potential 289
Coulomb scattering 189
coupling energy 52
crack propagation 250
critical density 30, 44, 76, 77, 94, 80, 84, 106, 135, 173, 156, 157, 159
critical surface 43, 45, 83, 84, 85, 87, 92, 93, 94, 106, 133, 175, 176,177, 179, 181, 197, 206, 233
cross section 17, 18, 19, 21, 23, 24, 31, 34, 185, 186, 200
cross section, differential 19
cross section, inverse bremsstrahlung 32
cross section, photoelectric 32
cross section, Rutherford 19
cross section, total 18, 19, 20
cutoff 164, 165, 166
cutoff wavenumber 266
cyclotron frequency 164, 167

damping 87, 88, 93, 94, 109, 110, 115, 120, 123, 173
  collisional 109, 112, 124
  collisionless (see Landau damping) 109
  spatial 78
damping rate 116
damping rate, spatial 76
de Broglie scale length 199
de Broglie wavelength 21
Debye length 20, 33, 34, 35, 36, 64, 69, 75, 127, 129, 138, 145, 186
Debye length, electron 62
Debye shielding 35, 189
Debye solid-state theory 243
Debye sphere 35, 45, 58, 62
decay instability 107, 108, 109
deflagration 257
degrees of freedom 38, 55, 111, 206
delta function, Dirac 4, 34, 61, 114, 141, 206, 264, 265, 273
density
  background 121, 136
  high frequency 119
  low frequency 119
  momentum 121
  pump energy 117
  steep 91
density fluctuation, electron 115
density fluctuation, ion 115
density jump 264
density profile, linear 77, 84, 87, 89, 90, 95
density ripple 118
derivative of the bulk modulus 245
derivatives along the characteristics 219
detailed balance 32
dielectric 40, 41, 42, 66, 67, 154, 156
dielectric coefficient 173, 236, 285
dielectric function 40, 41, 42, 80, 87, 90, 93, 94, 97
dielectric function, complex 94
dielectric permittivity 96, 98
dielectric tensor 170
diffraction limited 7
diffusion 24, 26, 60, 189, 191
  anomalous 25
  Bohm 26
  classical 25
  parallel 183
  transverse 183
diffusion approximation 178, 197
diffusion coefficient 24, 25, 58
diffusion equation 24, 206
diffusion flux 197
diffusion in angular space 195
diffusion in velocity space 195
diffusion relaxation time 152
diffusivity 215

dimension
  1D 63
  1.5D 63
  2D 63
  2.5D 63
  3D 63
dimensional analysis 215
dispersion relation 39, 40, 42, 68, 69, 71, 72, 73, 75, 76, 89, 90, 99, 105, 106, 107, 108, 129, 155, 156, 162, 163, 164, 165, 166, 167, 169
dissipation 5, 94, 125, 129
dissipative forces 232
dissipative phenomenon 226
dissipative radiative processes 17
distribution, energy 31
distribution, isotropic 21
diverging shocks 259
Doppler effect 4
double layer (DL) 135, 138, 141, 143, 176, 180
downstream variables 222, 237
drag force 257, 272
drift velocity 58
driving force 105, 115
Drude model 22, 149
ductile materials 249
Dulong–Petit law 55
Dulong–Petit value 244
dynamo effect 144, 153

echelons 238
effective mass, electron 101
e-folding time 254
eigenfunction 262
eigenstate, energy 15
eigenstate, ion 27
eigenvalue 115
  imaginary 118
eigenvalue equation 262
eigenvalue frequency 112
Einstein coefficients 2, 3
electrical conductivity 22, 23, 24, 41, 96, 97, 98, 99, 102, 149, 151, 266
electrical conductivity coefficient 80, 148, 177
electrical discharges 5
electric charge separation 69, 70
electric current 22, 41, 61, 79, 155, 158, 159, 162, 177, 196, 266
electric displacement 284
electric field
  high-frequency 134
  low-frequency 134
electric field phase 113
electric field strength 284
electric induction 284
electric polarization 285
electric potential 137, 138
electric potential energy 189
electromagnetic backscattered wave 122
electromagnetic energy density 285, 286
electromagnetic field momentum 66
electromagnetic field, high frequency 65
electromagnetic field, scattered 121
electromagnetic force 49, 285
electromagnetic modes 8, 9
electromagnetic sources 41, 42, 288
electromagnetic wave decaying 115
electromagnetic wave equation 122
electron, bound 16, 27, 28
electron conduction 179, 180
electron conductivity 205
electron cyclotron frequency 154, 170
electron cyclotron wave 166, 167
electron distribution function 195, 197
electron drift motion 189
electron effective mass 102
electron energy transport 189
electron fluid 33, 50, 51
electron fluid velocity 127, 136
electron inertia 72, 168
electron–ion scattering 188
electron oscillation frequency 30, 72, 73
electron–phonon interaction 55
electron–photon interaction 211
electron plasma frequency 106, 115, 123, 163
electron plasma frequency in the dielectric 155
electron (plasma) wave 71, 91, 94, 105, 106, 107, 109, 112, 115, 116, 117, 201
electron plasma wave (see also plasmon) 36, 39, 69
electron pressure 127, 150
electrons, degenerate 45
electron temperature 50, 52, 95, 102, 106, 118, 121, 127, 136, 137, 199, 201, 218
electron thermal conduction 176, 211
electron thermal motion 243
electron trajectory 200
electron transport 179
electron velocity distribution 20
electron velocity distribution function 178, 201
electrostatic plasma wave, high frequency 105
electrostatic potential 33, 34, 140, 203

electrostatic wave 172, 173
elliptical rotation of the electric field 164
emissivity 31
energy
  kinetic 189, 223, 241, 297
  potential 297
  thermal 241
energy band 28
energy conservation rate 123
energy deposition depth 54
energy equation, electron 54
energy equation, ion 54
energy exchange, electron–ion 100
energy exchange, electron–phonon 100
energy flow 60
energy flux 123, 287
energy loss 183, 188, 200
energy radiated per unit time by an electron 201
energy rate exchange 114
energy relaxation time 188
energy relaxation, electron 104
energy relaxation, ion 104
energy transfer rate 99
energy transport 179, 205
energy, internal 223
enthalpy 181
entropy 38, 203, 218, 220, 224, 226, 237, 247
entropy jump 226
equation, for magnetic field 151
equation of motion 33, 60, 61, 68, 74, 154
equation of state 24, 26, 33, 35, 37, 45, 47, 50, 51, 52, 53, 55, 57, 70, 149, 180, 207, 224, 225, 226, 228, 230, 231, 237, 241, 244, 245, 247, 248, 252, 275
equation of state, (semi-empirical) wide range 252, 253
equilibrium distribution 178, 189
Eulerian mass 52
Eulerian position 52
Eulerian space derivative 52
Eulerian time derivative 52
excited state 15
expanding plasma into the vacuum 135
exploding foils 213
exponential profile 77
external energy deposition 50
external force 110, 235, 260
external potential 35
extraordinary (electromagnetic) wave 145, 162, 163, 164, 165, 172
extraordinary mode 171
Faraday effect 10, 144, 153, 157, 168
Faraday–Maxwell equation 161
Faraday's law 285
fast electron preheat 239
fast electrons 141, 177, 241
fast ions 140, 141
Fermi–Dirac distribution 45, 101
Fermi energy 55, 101
Fermi momentum 101
Fermi–Pasta–Ulam problem 126
Fermi surface 98
Fermi temperature 101, 104
Fermi velocity 101, 103
field envelope 12
filamentation 13, 65
filaments 180
finite-difference approach 62
first moment 191
first-order equations 70
first-order variations 70
flow patterns 256
fluctuation 127, 153, 250
fluid, electron 69, 146
fluid element 220
fluid equations 47, 50, 53, 55, 122, 203, 223
fluid equations of two temperatures 51
fluid equations, electron 118
fluid equations, ion 35, 118
fluid, ion 69, 146
fluid models 138
fluid particle 26, 48, 52
fluid-Poisson equations 127, 128, 129
fluids energy equations, two 51
fluid theory 55, 56
fluid variables 52
flux
  absorbed laser 182
  energy 180
  heat 23, 177, 197, 205, 209
  heat energy 52
  laser energy 144
  mass 180
  momentum 26, 180
flux conservation
  energy 181
  mass 181
  momentum 181
  particle 17, 23, 25
flux continuity 139
flux of the electromagnetic energy 285
foil reference frame of coordinates 264
Fokker–Planck collision 58, 196

Fokker–Planck equation 189, 190, 191, 192, 194, 195, 196, 197
force
  frictional drag 110
  inertial 151
  periodic external 112
  viscous 151
force per unit volume 66
forced harmonic oscillator 109
Fourier components 63
Fourier modes 128
Fourier transform 11, 110, 116, 119, 129, 163, 166, 168, 169, 261
Fourier transport 200
fracture, dynamic 249
frame of reference of the moving interface 274
free current density 284
free electric charge density 284
free electron model 244
free energy 14, 15
free-streaming flow of electrons 198
free streaming flux 178, 197
free streaming plasma 181
free streaming velocity 113
free surface 228, 251
free-surface velocity 230, 231, 240, 245, 251
frequency components, fast 119
frequency components, low 119
frequency electric fields, high 134
frequency electric fields, low 134
frequency modulation 11, 12
frequency, complex 40
full frequency width at half maximum 111
full width half maximum (FWHM) 4
fully ionized plasma 195, 218
fusion 59

gain 8, 10
gamma function 209
gauge 288
Gauss divergence theorem 234, 294
Gauss equation 70
Gauss–Faraday law 285
Gauss's law 285
Gauss' theorem 47, 49
Gaussian profile 5, 9, 152
Gaussian pulse 11
Gaussian shape 5
Gaussian velocity distribution 63
geometrical optics 89
geometry, cylindrical 162
geometry, plane 52, 135, 162, 182, 183
global neturality 138, 139
grating 13
gravitation 254, 255, 260, 264
gravitational force 49
Green's first and second theorem 294
Green's function 152
grid points 63
grid spacing 62, 63
ground state 15
group velocity 12, 39, 71
growth rate 118, 257, 258
growth rate of the backscattered wave amplitude 123
Gruneisen coefficient 243, 249
Gruneisen equation of state 234, 244, 247, 248
Gruneisen parameter 249
gun drivers of plates 252
gyro motion 35
gyroradius, electron 35

Hall effect 149
Hamiltonian 15, 56
harmonic driving force 110
harmonic motion 37, 110
harmonic oscillations 110
heat capacities at constant volume, electron 102
heat capacities at constant volume, ion 102, 103
heat capacities, constant pressure 180, 218
heat capacities, constant volume 24, 180, 181, 218
heat capacity 24
heat capacity, electron 54, 99
heat capacity, lattice 54
heat carriers 205
heat conduction 53, 205
heat conduction coefficient 152
heat conduction by photons 211
heat conduction equation 207
heat conductivity, electron 99, 101, 103
heat deposition 98
heat diffusion equation 151
heat flow 23, 176, 178, 197, 198, 214
heat flux, differential 197
heat transfer 195
heat transport 24, 51, 60, 178, 198, 205
heat transport, electron 212
heat transport equation 206
heat wave 7, 175, 205, 211, 214, 216
heat wave equation 214
heat wave front 216

heat wave temperature space profile 209
heat wave velocity 209, 214, 215
Helmholtz equation 96
high energy electrons 74
high energy ions 140
highest laser-induced pressure 230
high-frequency (electron) wave equation 120
high-frequency phenomena 144
high-Z atoms 28
homogeneous equations 288
homogeneous medium 66, 75, 77, 79, 80, 126
hot electrons 44, 45, 91, 177, 180, 198, 291, 202
hot electrons pressure 44
hot electron temperature 240
hot spots 180
Hugoniot 221, 225, 230, 232, 243, 245, 277
Hugoniot curve 224, 225, 228, 229, 242, 243
Hugoniot energy relation 248
Hugoniot equation of state 227
Hugoniot pressure 242, 246, 247, 249, 251
Hugoniot relations 224, 276, 277
hydrodynamic effects 215
hydrodynamic efficiency 182
hydrodynamic equations 37, 260
hydrodynamic expansion 96
hydrodynamic instabilities 45, 162, 183, 254, 256, 258, 269
hydrodynamic theory 36, 47
hydrogen-like atom 32
hydrogen-like model 16

ideal gas equation of state 145, 149, 150, 181, 218, 226
ignition 205, 255
impact parameter 19, 20, 75, 183, 185, 189, 200
impedance matching 228, 229, 245
implosion pressure 255
implosion velocity 255
imprint (a disturbance) 256
imprint, laser initial 257
impulsive acceleration 258, 273, 274
incoherence, spatial 238
incoherent 3
incompressibility assumption 265
incompressible fluid 26, 261, 270, 272, 273
incompressible plasma 266
index of refraction 29, 30, 153, 155, 164, 166
  complex 96
  extraordinary 171
  nonlinear 11, 13, 42
  ordinary 171
indices of refraction for right and left polarization 166
induced transition 3
induced emission 31
induced emission lifetime 3
inertia of the electron 127, 145
inertial confinement fusion (ICF) 6, 162, 175, 179, 183, 205, 254, 256, 257, 258
inertial term 203
inhibited thermal transport 215
inhibition factor 178, 197, 198
inhomogeneous equations 288
inhomogeneous plasma 68, 79
inhomogeneous system 120
inhomogeneous wave equation 288
initial value problem 127
instability seeds 256
inter-atomic forces 252
inter-band absorption 98
interface equation 276
intermixing 255, 256
internal energy 49, 181, 237, 243
intra-band absorption 98
inverse Faraday effect 145, 157, 159, 161, 162
inverse matrix 170
inviscid (no viscosity) 279
ion frequency 79
ion (plasma) wave 73, 105, 106, 107, 108, 109, 112, 115, 117, 129
ion-acoustic instability 40
ion acoustic phase velocity 129
ion acoustic wave 122, 126, 127
ion cyclotron frequency 169
ion density fluctuation 118
ion density perturbation 121
ion density wave amplitude 122
ion fluid 50, 51
ion force (momentum) 119
ion lattice 54
ion local temperature 33
ion oscillation frequency 72, 73
ion pressure 44
ion temperature 52, 102, 106, 121, 127, 136, 218
ionization 14, 15, 17, 31, 58, 74, 103, 106, 118
ionization energy 16
ionization potential 15
ion-plasma frequency 134
irreversible process 19

irreversible thermodynamics 178
irrotational fluid 270
isentrope (process) 38, 217, 219, 224, 225, 230, 242, 247, 250, 277
isentrope pressure 247
isentropic curves 224
isentropic expansion 251
isentropic flow 218, 219
isolator 7, 8, 10
isotherm 224, 252, 253
isothermal electron equation 71
isothermal speed of sound 137, 182, 183
isotropic 30, 31, 195
isotropic pressure 59

Joule heating 97, 235, 236
jump condition 223, 233, 234, 236, 237, 277, 281, 282
jump equations 227, 233
jump in the potential 204

KdV (Korteweg and De Vries) equation, 125, 126, 127, 131, 132
Kelvin–Helmholtz instability 40, 258, 260, 283
Kerr cell 1, 9
kinematic theory 47
kinematic viscosity 151, 152
kinetic energy of the electron 201
Kirchhoff's law 32

laboratory coordinates 183
laboratory frame (of reference) 20, 183, 184, 187, 192, 222, 223, 226, 231
Lagrangian coordinates 261
Landau damping 40, 63, 93, 109, 115, 117, 123, 124, 173
Langmuir wave 105
Laplace equation 270
Laplacian 292
large angle deflection 186
large angle scattering 186
large deflection 187, 190
large-scale deflection 189
Larmor angular frequency 179
Larmor radius 35, 189
laser
  CO_2 7
  gas 5, 7
  helium-neon 1
  iodine 7
  KrF 7
  megajoule 8
  neodymium glass 1, 7, 10, 141
  solid state 7
  Ti–sapphire 1, 7
  x-ray 175
laser diode 5, 10
laser divergence 6, 7
laser electric field amplitude 134
laser energy deposition 54
laser energy fluency 8
laser energy flux 134, 284
laser intensity profile 98
laser irradiance non-uniformity 238
laser pump 108
laser pump amplitude 121
laser radius 135
laser scattering 106
laser spot 135
laser uniformity 256
lateral rarefaction wave 238
lattice specific heat at constant volume 243
left-handed circular polarization (LHCP) 153, 154, 155
light amplification 6
line absorption 27, 28
line broadening 28
line emission 27, 28
line shape 5
line shape function 4
line shape, natural 4
line width, natural 6
linear analysis 260
linear differential equation 127
linear equations 119
linear momentum 160
linear polarized (laser) electric field 153, 155, 168
linear theory 275
linear trajectory 69
linearization procedure 38, 70, 72, 128, 166, 261, 266
linearized equations 119, 162
linearized Maxwell equation 267
linearized momentum equation 267
Liouville's theorem 55, 56
longitudinal phonon mode 100
longitudinal sound velocity 99
longitudinal wave 39, 76, 164
Lorentz equation 61, 68
Lorentz force 286
Lorentz gauge 288
Lorentzian profile 4, 5

Lorentzian pulse 11
Lorentz law 285
Lorenz plasma 196
low-frequency electric field 119
L-wave 168

Mach number 226, 232
macroinstabilities 39
macroscopic electric fields 134
macroscopic quantity 58
macroscopic scale length 151
magnetic compression 213
magnetic field
  axial 153, 158, 159, 161, 162
  diffusion of 151
  external 172
  steady-state (d.c.) 144, 150, 154, 155, 162, 163, 168, 169, 170, 171
  toroidal 144, 145, 146, 150, 153, 176
magnetic field amplitude, laser 144
magnetic field diffusion time 152
magnetic field generation 65
magnetic fluid 146
magnetic flux density 284
magnetic monopoles (poles) 234, 285
magnetic permeability 155, 285
magnetic polarization 285
magnetic pressure 233
magnetic Reynolds number 144, 151, 152, 153
magnetized plasma 162,173, 174, 179
magneto-hydrodynamic equations 144, 149
magneto-hydrodynamics 146
Markov process 190
matrix element 99, 100
maximum possible compression 246
maximum possible growth of the instability 120
Maxwell distribution 20, 45,55, 57, 62, 176, 177, 178, 188, 198, 199, 297, 298
Maxwell equations 36, 38, 41, 42, 47, 50, 61, 66, 67, 70, 75, 80, 91, 94, 144, 145, 146, 149, 154, 158, 162, 168, 169, 171, 234, 235, 266, 284, 285, 286, 287, 288
Maxwellian distribution, equilibrium 195
Maxwellian double electron distribution 199
mean decay time 111
mean free path 17, 18, 19, 24, 31, 34, 35, 178, 186, 198, 211
mean free path, electron 177, 196, 206, 240
mean free path for hydrogen-like plasma 211
mean squared velocity 63
melting temperature 101
metallurgical cross section 250
metric elements 292
microinstabilities 39
mirror symmetry 208
mixing zone between the fluids 258
mode locking 1, 9
molecular collision 190
moment (definition) 60
moment equation 58, 60
moment equation, zero 59
moment of velocity 298
momentum, electron 147
momentum exchange 60
momentum, ion 147, 148
momentum jump conditions 235
momentum loss 183, 187, 188
momentum loss-relaxation time 187
momentum of the gas 222
momentum relaxation rate, electron 99, 101, 102,103
momentum transfer 65
monoatomic gas 181
monochromatic wave 75, 96, 169
monopoles 269
motion
  high-frequency 118
  low frequency 118
  quasi-neutral 118
multimode perturbation 258
multiple Coulomb collisions 177
multiple scattering 188
multiple small-angle collisions 190
multiple small-angle scattering 189

Navier–Stokes equation 26
negative pressure (tension) 251
neutral plasma 187
neutralizing background 33
Newton equation for electrons 142
Newton's law 22, 37, 41, 48, 52, 63, 79, 112, 222
non-isotropic medium 285
nonlinear differential equation 127
nonlinear dispersion relation 129
nonlinear drag force 256
nonlinear effect 138, 231
nonlinear equations 116
nonlinear evolution of the RT instability 258
nonlinear force 65, 69
nonlinear heat wave 210
nonlinear induced magnetic field 159
nonlinear interaction 126

nonlinear integral-differential equations 195
nonlinear localized wave 126
nonlinear mass string (Fermi, Pasta and Ulam) 125
nonlinear phenomenon 105
nonlinear plasma effects 64
nonlinear polarizability 105
nonlinear transport coefficients 205
nonlinear wave 125
nonlinear wave phenomena 201
non-local transport 198
non-Maxwellian electron velocity distribution 140
non-uniformity of the laser beam 179
normal mode 255, 256, 261
Nova laser 213
nuclear reaction 7
number of degrees of freedom 181

Ohm heating 50
Ohm's law 22, 25, 148, 285
Ohm's law, generalized 25, 144, 146, 147, 149
Onsager relations 178
opacity 31
optical fibre 13
optical smoothing techniques 238
optical spectrum 3
ordinary (O-mode) wave 145, 162, 163, 165, 172
orthogonal frame of reference 191, 194
ORVIS (optically recording velocity interferometer system) 230
oscillating two-stream instability 118
oscillations
  critically damped 110
  forced 110, 111
  high-frequency 127, 136
  over-damped 110
  weakly damped 110
oscillator 7, 8, 9, 13
oscillator, forced harmonic 110
oscillator, harmonic 115
out-flowing plasma 221

parabolic initial density profile 141
parabolic laser profile 161
parametric (decay) instability 40, 65, 106, 105, 108, 109, 110, 115, 116, 118, 120
particle, charge collector 11
particle flow velocity 214, 228, 230, 241, 250, 251
particles, free-streaming 139
particle in cell (PIC) 61, 62
particle simulation code 47
particle simulations 61, 62
particle theory 47, 61
partition function 15
pellet, spherical 140
permeability 68, 287
permittivity 66, 285, 287
phase 6
phase plate 238
phase shift 88
phase space 55, 56, 57, 190, 194
phase space trajectory 56
phase transition, solid–solid 233
phase transitions 245
phase velocity 5, 39, 71, 74, 112, 124, 129, 164, 168
phonon 54, 100
phonon dispersion relation 100
phonon energy 103
phonon spectrum 99
photoelectric effect 27, 28
photoionization 27, 28
photon distribution function 29
photon energy spectrum 199
photon momentum 89
photon wave 107, 108
planar collision 230
planar symmetry 216, 219
planar waves 277
planarity 238
Planck function 30, 31
Planck's law 2, 16
plane-polarized light 153
plane wave 7, 168
plasma
  ideal 45
  neutral 139
  slab of 37
  strongly coupled 45, 189
  two component 127
plasma frequency 106, 118, 128, 145, 164
plasma expansion into vacuum 137, 203
plasma fluid 26
plasma frequency 37, 54, 62, 65
plasma heating 265
plasma instabilities 256
plasma lifetime 64
plasma neutrality 103
plasma oscillation 36, 37
plasma parameter 35
plasma–vacuum boundary 91

plasma–vacuum interface 82, 84, 85
plasma wave amplitude 40
plasmon 39, 71, 105, 106, 124
plastic deformation 249
Pockels cell 9
Pockels effect 10
Poisson equation 34, 36, 70, 71, 118, 119, 141, 193, 285
polarization force 49
polarization of the dielectric medium 155
polarization plane 10
polarization, p- 88, 91, 92, 93, 94, 95, 172, 173, 174
polarization, s- 88, 90, 95, 172
polarized electromagnetic field, linear 81, 82
polarized light, linear 10, 96
polarizer 10
ponderomotive force 65, 66, 67, 68, 69, 70, 71, 105, 118, 119, 134, 135, 133, 159
ponderomotive force, Landau–Lifshitz 65
ponderomotive pressure 72, 73
population inversion 6, 9
potential barrier 139
potential equations 288
potential force 203
potential jump 138
power density balance 115
power radiated by the electron 201
Poynting theorem 87, 286
Poynting vector 285, 286
preheating 44, 177, 205, 239
preheating, fast electron 238
preheating, x-ray 238
pre-pulse 11
pressure, ablation 45, 181, 182
pressure disturbance 217
pressure forces 222
pressure scale length 150
pressure tensor 26, 59, 60
probability density 55, 56
probability function 191
probability per unit time 19
propagation, electromagnetic field 74, 79, 87
pulse duration (FWHM) 98
pulse shape 8, 10, 11
pump (laser) energy flux 120
pump amplitude 120
pump frequency 118
pump wave 105, 121, 122
pumping laser 106

Q factor 9
Q switching 1
quadrupole 142
quantum mechanics 21
quantum solid state physics 98
quasi-momentum 100
quasi-neutrality 35, 72, 138, 139, 141, 145, 198
quiver velocity 45

radar 12, 230
radial convergence factor 255
radiation conductivity 27, 211, 212
radiation energy density 211
radiation energy transport 29
radiation field, equilibrium 30
radiation flux 257
radiation heat flux 211
radiation mean free path 211
radiation pressure 44, 68, 73, 77
radiation sources 6
radiation transport 29, 30, 212
radiative equilibrium 31
radiative recombination 27, 28
radiative transfer, equation of 29
rail guns 213
Raman instability 40
Raman scattering 144
random phase shift 238
random process 153
randomly phase-shifted mask 238
Rankine–Hugoniot relations 224
rarefaction shock wave 180, 202
rarefaction wave 137, 202, 204, 205, 213, 216, 219, 220, 225, 228, 229, 230, 238, 239, 240, 249
rarefaction wave velocity 250
rate equations 2, 3, 17
rate of change of the particle energy 113
rate of doing work 286
rate of gain 57
rate of growth 122
rate of plasma production 182
Rayleigh line 232
Rayleigh–Taylor (RT) instability 40, 45, 254, 255, 256, 257, 258, 260, 264, 265, 266, 268, 269, 270, 279, 282
recombination 17
reduced mass 20, 183, 187, 200
reduced momentum 100
reflected electric field 96
reflected electrons 139
reflected Hugoniot 225
reflected ions 139

reflected light, back 10
reflected shock 259, 274, 276, 278
reflection coefficient 96, 173
reflection, laser 89
reflectivity, laser 44
refractive index 5
relative velocity 20, 148, 183, 186
relativistic factor 45
relaxation time 22, 54, 189
release isentrope 248
release wave 225, 228, 230
repulsive forces 241
resonance 93, 94, 111, 112, 164, 165, 166, 173
resonance absorption 4, 91, 95, 109, 201, 202
resonance absorption in a magnetic plasma 145, 169
resonance absorption mechanism 172
resonance condition 117
resonance solution 112
resonant frequency 3, 123
resonant width 111
restoring force 37
return current 177, 198
return force 110
reverberation 251
reversible process 226
Reynolds number 151
Richtmyer–Meshkov (RM) instability 40, 258, 259, 260, 272, 273, 279
Riemann integral 250
Riemann invariants 219, 220, 251
right-handed circular polarization (RHCP) 153, 154, 155
right-hand rule 165
rocket effect 264
rocket equation for plasma 182
rocket model 180
Rogowski coils 143
Rosenbluth potential 193, 194
Rosseland mean free path 211
Rutherford cross section 183, 185, 192, 193
R-wave, 168

Saha equation 15, 16, 17, 23
saturation 256
scalar potential 288, 289
scale length 35, 62, 150
scale length factor for the energy deposition 206
scaling law 27, 202, 215, 240
scattering 29, 31
  backward 108
  elastic 19
  electron–phonon 99
  forward 108
  Rutherford 21
scattering angle 19, 20, 183, 184
scattering time of the electron 179
Schrödinger equation 82
screening 21, 33, 34, 45
screening scale length 33
sech-pulse 11
second harmonic generation 65
second moment 191
seed 256
self-focusing 11, 65
self-illumination 229, 330
self-oscillation 8
self-similar solution 137, 138, 203, 209
shape function 63
shell targets 175
shock discontinuity 223
shock frame of reference 226
shock front 222, 224, 237, 238, 277
shock stability criterion 232
shock surface (the discontinuity) 234, 236, 277
shock wave 7, 43, 45, 176, 202, 205, 213, 214, 216, 221, 222, 224, 225, 228, 230, 232, 233, 238, 240, 242, 243, 244, 245, 247, 248, 249, 251, 258, 259, 273, 274
shock wave convergence 279
shock wave divergence 279
shock wave frame of reference 223, 233, 237
shock wave front 227, 233
shock wave pressure 233, 279
shock wave singularity 234
shock wave stability 231
shock wave, steady-state 227
shock wave transient 233
shock wave velocity 224, 227, 230, 231, 232, 241, 245
shock wave, weak 226, 275, 279
single collision 186
single particle approach 68
singularities 172, 174, 221, 137, 157, 161, 205, 210
singularity, electric field 93, 94
skin depth 44, 54, 96, 97
slope of isentrope 232
small-angle collisions 185, 186, 188, 189, 190
solid–liquid phase transition 101
solitary wave 124, 125, 126, 131, 132, 133
solitary wave equation 127

soliton 127, 131, 132, 133
soliton equation 109
soliton solution 126, 129
sound speed (velocity) 106, 136, 137, 150, 215, 217, 218, 219, 221, 231, 232, 233, 238, 247, 249, 261, 275
sound speed on the Hugoniot points 249
sound velocity 214, 217
sound wave 216, 217, 218
source current 122
source, (external) energy 49, 53
source, external 51
source of plasma 181
sources of the electromagnetic fields 285
space perturbation 119
spall 240, 249, 250, 251
spall strength 251
spall thickness 240
spatial filter 10
spatial grid 61, 62
spatial modes, high frequency 63
specific heat 38, 206, 244
specific heat at constant pressure 38
specific heat at constant volume 38, 205
spectral distribution 2
spectral energy density scalar 30
spectral energy flux vector 30, 31
spectral energy flux, one sided 31
spectral radiation intensity 30
spectrometer 11
spectrum emission 11
speed sound, isentropic 181
speed sound, isothermal 181
spherical geometry 258
spherical shell 162, 183, 256
spikes 256, 258, 270, 273, 279
spins of the photons 159
Spitzer–Härm approximation 197, 198
Spitzer–Härm conductivity 195, 197
Spitzer–Härm (SH) theory 177, 178
spontaneous emission 2, 3, 31, 32
spontaneous emission lifetime 3
spontaneous transition, 3, 6
spring constant 110
stagnation point 272
stagnation pressure 255
standing wave 9
static electric field 65
static model 138, 140
steady flow 271
steady shock wave 232, 238, 239
steady state 25, 70, 110, 126, 148, 161
steady-state solution 112
Stefan–Boltzmann constant 31, 211
stimulated Brillouin instability 106, 107, 108, 109, 144
stimulated Brillouin scattering 106, 120, 121
stimulated Compton scattering 106
stimulated emission 1, 2, 3, 4
stimulated Raman instabilities 106, 107, 108, 109, 120, 124
Stokes (differential) equation 84, 88, 90
Stokes theorem 294
strain 232, 250, 252
strain rate 232, 250, 252
streak camera 229, 241, 245
streak camera, optical 11
streak camera, x-ray 11
stream function 271
stream line 218, 219, 270, 271
streaming velocity 135
strength of material 231, 249
stress 26
stress tensor 66
stretcher 13
strongly coupled parameter 45
subsonic 232
subsonic velocity 226
superposition 118, 164
superposition principle 127
supersonic 232
supersonic speed 226
supra-thermal electrons 180
supra-thermal (hot) temperature 140
surface expansion 96
surface forces 48, 49
surface tension 125, 269, 279
symmetry 245
  azimuthal 20
  cylindrical 52, 53
  plane 52, 53
  spherical 52, 53, 162
symmetry breaking 162

telescope 7, 10
temperature density scale length 178
temperature scale length 198
tension 242, 249
test particle 183, 185, 187, 188, 191, 192
theoretical spall strength 252
thermal (cold) temperature 140
thermal conduction 44, 175, 177
thermal conductivity 23, 24, 177, 226

thermal conductivity coefficient 25, 205
thermal diffusivity 205, 206
thermal distribution, electrons 78
thermal electron energy 244
thermal energy 78
thermal equilibrium 2, 3, 6, 14, 15, 30, 32, 191, 211, 227, 297
thermal flux 205
thermal flux of electrons 177
thermal lattice energy 243
thermal lattice pressure 243
thermal motion 123
thermal pressure 221, 233
thermal pressure, electron 72
thermal transport 232
thermal velocity 39, 63, 74, 178
thermal velocity, electron 78, 206
thermal wave 215
thermodynamic equilibrium 3, 5, 16
thermodynamic equilibrium, local (LTE) 16, 17, 20, 33, 47, 55, 61
thermodynamic equilibrium, non-local 55
thermodynamic function 224
thermodynamic relations 237, 243
thermodynamic state 14
thermodynamic trajectory 224
thermodynamics 66
thermodynamics for plasma with two temperatures 202
thermoelectric effect 177, 178
threshold energy 117
threshold laser field 117
threshold pumping 117, 120, 124
time average 111
time average over the fast oscillations 158
time of flight 141
toroidal direction 158
toroidal electric field 161
toroidal electron motion 161
toroidal electron velocity 160
torque 161
total derivative 48, 52
total differentials 219
total distribution function 198
total electric current 178
trace 295
trajectory of the fluid particles 271
transition probability 3, 100
transition, band–band 98
transitions, bound–bound 27
transitions, bound–free 27, 28
transitions, free–free 27, 28
transmitted electric field 96
transmitted shock wave 259, 274, 276, 278, 279
transport coefficient 3, 22, 27, 50, 189
transport domain 43
transport, energy 28, 43, 44, 45, 175
transport equation 31, 32, 33
transport of x-rays 211
transport phenomena 299
transverse wave 39, 76, 164
truncation 60
turbulence 258
two Maxwellian distribution 201
two stream plasma wave instability, 40
two-fluid model 141
two-fluid simulations 138
two-parameter family of curves 224
two-plasmon instability 40, 106
two-stage light-gas gun 213

Umklapp process 100
uncertainty principle 199
unit matrix 170, 235
unit vectors 292
unmagnetized plasma 163
upper hybrid frequency 164, 170
upstream variables 222

vector potentials 288
velocity distribution 20, 112, 113, 114, 297
velocity fluctuations 128
velocity jump 283
velocity potential 270, 271
velocity shear 258
velocity space 57, 191, 193, 197
Verdet constant 156
VISAR (velocity interferometer system for any reflector) 230
viscosity 26, 226, 232
viscosity, coefficient of 28
viscous fluid flow 152
Vlasov–Boltzmann equations 122
Vlasov equation 56, 57, 115, 138
volume force 48, 49, 50, 51, 145
vortex 255, 258
vortex motion 256

water wave 124
wave, damped 73
wave equation 126, 127, 275, 287, 154, 171
wave equation, electric field 80, 96
wave equation, electromagnetic (field) 79, 89, 90

wave equation, magnetic field 80, 83, 92
wave front 210, 232
wave modes in plasma 105
wave–particle interaction 109
wave propagation 126, 231
wave–wave instability 135
wave–wave interaction 106, 108, 109
Wiedemann and Franz law 24
WKB approximation 81, 82, 83, 90
WKB solution 93, 172
WKB validity condition 83

X-mode 163, 165, 166
x-ray flux 213
x-ray production 7
x-ray production, efficiency 29
x-ray propagation 176
x-ray radiation 27
x-ray, soft 29
x-ray sources 175

zero frequency 118
zero resistivity 266, 267